iJERGS International Journal of Engineering Research And General Science

Journal which deals with research, Innovation and Originality

International Journal Of Engineering Research and General Science

ISSN 2091 - 2730

Table of Content

CHIEF EDITOR BOARD

Message from Associate Editor In Chief

Let me first of all take this opportunity to wish all our readers a very happy, peaceful and prosperous year ahead.

This is the Third Issue of the Third Volume of International Journal of Engineering Research and General Science. A total of 275 research articles are published and I sincerely hope that each one of these provides some significant stimulation to a reasonable segment of our community of readers.

In this issue, we have focused mainly on the Innovation and Student works. We also welcome more research oriented ideas in our upcoming Issues.

Author's response for this issue was really inspiring for us. We received many papers from many countries in this issue than previous one but our technical team and editor members accepted very less number of research papers for the publication. We have provided editors feedback for every rejected as well as accepted paper so that authors can work out in the weakness more and we shall accept the paper in near future. We apologize for the inconvenient caused for rejected Authors but I hope our editor's feedback helps you discover more horizons for your research work.

I would like to take this opportunity to thank each and every writer for their contribution and would like to thank entire International Journal of Engineering Research and General Science (IJERGS) technical team and editor member for their hard work for the development of research in the world through IJERGS.

Last, but not the least my special thanks and gratitude needs to go to all our fellow friends and supporters. Your help is greatly appreciated. I hope our reader will find our papers educational and entertaining as well. Our team have done good job however, this issue may possibly have some drawbacks, and therefore, constructive suggestions for further improvement shall be warmly welcomed.

Er. Pragyan Bhattarai,

Associate Editor-in-Chief, P&R,

International Journal of Engineering Research and General Science

E-mail -Pragyan@ijergs.org

International Journal of Engineering Research and General Science Volume 3, Issue 3, Part-2 , May-June, 2015
ISSN 2091-2730

FPGA BASED N-BIT LFSR TO GENERATE RANDOM SEQUENCE NUMBER

Babitha P K, Thushara T, Dechakka M P
Assistant Professors
Dept. of ECE, Coorg Institute of Technology
E-mail Id: dechakka.mp@gmail.com

Abstract— LFSR based PN Sequence Generator technique is used for various cryptography applications and for designing encoder, decoder in different communication channel. It is more important to test and verify by implementing on any hardware for getting better efficient result. As FPGAs is used to implement any logical function for faster prototype development, it is necessary to implement the existing design of LFSR on FPGA to test and verify the simulated & synthesis result between different lengths. The total number of random state generated on LFSR depends on the feedback polynomial.

As it is simple counter so it can count maximum of 2^n -1 using maximum feedback polynomial. Here in this paper we implemented n -bit LFSR on FPGA by using VHDL to study the performance and analyze the behavior of randomness. The analysis is conceded out to find number of gates, memory and speed requirement in FPGA as the number of bits is increased. The comparative study of 8, 16 and n bit LFSR on FPGA is shown here to understand the on chip verification. Also the simulation problem for long bit LFSR on FPGA is presented.

Keywords— **LFSR, FPGA, PRNG, VHDL, FPGA, ASIC, RTL**

INTRODUCTION

For generating data encryption keys, random numbers are very much useful in the various applications such as communication channel, bank security, etc [1], [3]. it is used to design encoder and decoder for sending and receiving data in noisy communication channel. They have also been used aesthetically, for example in literature and music, and are of course ever popular for games and gambling [1]. When discussing single numbers, a random number is one that is drawn from a set of possible values, each of which is equally probable, i.e. a uniform distribution. Random number generator is a computational device to generate a sequence of numbers or that lack any pattern [2]-[5]. There are various methods for pseudo-random numbers are known [1], [3]. Most of them are based, on linear congruential equations [8], [9] and require a number of time consuming arithmetic operations. In contrast, the use of feedback shift registers permits very fast generation of binary sequences. Shift- register sequences of maximum length (m-sequences) are well suited to simulate truly random binary sequences [6], [7], [10]. With minimum length feedback polynomial 8, 16 and n-Bit LFSR based PRNG implemented on FPGA explain in [11], [12]. As we change the feedback polynomial the run-length as well randomness also changes. Here we have implemented n bit length sequences on FPGA using VHDL with maximum length feedback polynomial to understand the memory utilization and speed requirement. Also we have presented the comparison of performance analysis based on synthesis and simulation result as well identify the simulation problem for long bit LFSR. The target device we have used Xilinx Spartan 3S 1000 FPGA and XSA 3S1000 Board of Xess Corporation [17] and performed simulation and synthesis using Xilinx ISE 10.1 [18].

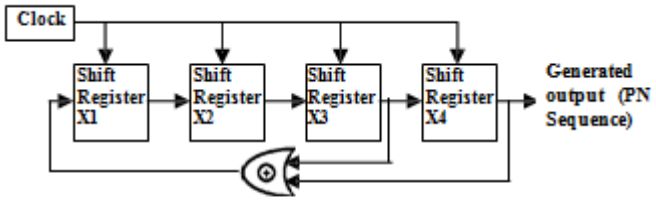

Figure 1. Basic block diagram of LFSR

FPGA is a predesigned reconfigurable IC [15]. It can be reconfigured any number of times according to the speciation of design. The FPGA configuration is generally defined using a hardware description language (HDL), similar to that used for an application-specific integrated circuit (ASIC) [14], [15]. The HDLs are VHDL and Verilog. We prefer VHDL for programming because of its widely in use [15], [16]. FPGAs can be used to implement any logical function that an ASIC can perform. Because of various advantages and rapid prototype development can possible, so FPGA is chosen here.

LINEAR FEEDBACK SHIFT REGISTER

LFSR is a shift register whose input bit is a linear function of its previous state. The most commonly used linear function of single bits is XOR. Thus, an LFSR is most often a shift register whose input bit is driven by the exclusive-or (XOR) of some bits of the overall shift register value. [1], [10]. The initial value of the LFSR is called the seed. Because the register has a finite number of possible states, it must eventually enter a repeating cycle. However, an LFSR with a well-chosen feedback function can produce a sequence of bits which appears random and which has a very long cycle. Applications of LFSRs include generating pseudo-random numbers, pseudo-noise sequences, fast digital counters, and whitening sequences. Both hardware and software implementations of LFSRs are common [11].

A. Implementation of LFSR based PRNG

Pseudo random number sequence generator is generated in VHDL according to the following circuit based on the concept of shift register.The bits in the LFSR state which influence the input are called taps. A maximum-length LFSR produces an m-sequence (i.e. it cycles through all possible 2^n -1 states within the shift register except the state where all bits are zero), unless it contains all zeros, in which case it will never change. The sequence of numbers generated by this method is random. The period of the sequence is (2^n - 1), where n is the number of shift registers used in the design. For 32 bit design the period is 4294967295. This is large enough for most of the practical application. The arrangement of taps for feedback in an LFSR can be expressed in finite field arithmetic as a polynomial mod 2. This means that the coefficients of the polynomial must be 1's or 0's. This is called the feedback polynomial or characteristic polynomial. For example, if the taps are at the 32^{nd}, 30^{th}, 11^{th} and 5^{th} bits, then the feedback polynomial is $X^{32} + X^{30} + X^{11} + X^5 + 1$

B. The rules for selecting feedback polynomial

The rules for selecting feedback polynomial are given in [11], [12]. The 'one' in the polynomial does not correspond to a tap it corresponds to the input to the first bit. The powers of the terms represent the tapped bits, counting from the left. The first and last bits are always connected as an input and output tap respectively. LFSR will only be maximum-length if the number of taps is even. There must be no common divisor to all taps.
Possible valid feedback polynomial and maximum length feedback polynomial [10], [13] for 8, 16 and 32 bit LFSR are given on table 1.

TABLE I. POSSIBLE AND MAXIMUM LENGTH POLYNOMIAL

Size of LFSR	Possible Feedback Polynomial	Maximum Length Feedback polynomial
8 Bit	$X^8 + X^7 + 1$, $X^8 + X^5 + 1$, $X^8 + X^7 + X^6 + X^5 + 1$, $X^8 + X^6 + X^4 + X^3 + X^2 + X^1 + 1$, etc	$X^{16} + X^{14} + X^{13} + X^{11} + 1$
16 Bit	$X^{16} + X^{15} + 1$, $X^{16} + X^{13} + X^{12} + X^9 + 1$, $X^{16} + X^{11} + X^{10} + X^7 + X^3 + X^1 + 1$, $X^{16} + X^{15} + X^{14} + X^{12} + X^7 + X^6 + + X^3 + X^2 + 1$, etc	$X^{16} + X^{14} + X^{13} + X^{11} + 1$
n Bit	$X^{32} + X^{31} + 1$, $X^{32} + X^{28} + X^{27} + X^9 + 1$, $X^{32} + X^{21} + X^{15} + X^{13} + X^{12} + X^{10} + + X^8 + X^4 + 1$, $X^{32} + X^{31} + X^{27} + X^{24} + X^{19} + X^{18} + + X^{17} + X^{14} + X^{13} + X^{11} + X^5 + X^4 + X^1$, etc	X^n+..... $X^{32} + X^{22} + X^2 + X^1 + 1$

SYNTHESIS AND SIMULATION

In this design, we describe the RTL-level of the LFSR pseudo-random number generator for 8-bit, 16-bit and n bit using VHDL language, and use the Xilinx's chip XC3S 1000
Sparta3 as the target chip. Then we synthesize, place and route on the Xilinx ISE platform. Finally we use ISE Simulator to do a timing simulation

A. Timing Simulation

The simulation waveform for 8-bit, 16-bit and n-bit are under the simulation clock frequency 371.747 MHz with 20 ns simulation clock period.

B. Design of 8-Bit LFSR

8-bit LFSR with maximum length feedback polynomial $X^8 + X^6 + X^5 + X^4 + 1$ generates $2^8 - 1 = 255$ random outputs, which is verified from the simulation waveform.

The circuit diagram for 8-bit LFSR with maximum length polynomial is shown in Fig. 2. In The timing simulation from 40 ns to 5140 ns. After this clock time the random output is repeating again.

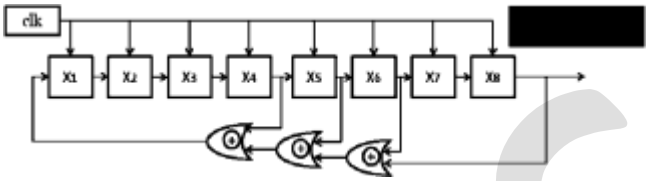

Figure 2. Circuit Diagram of 8- Bit LFSR with maximum length Feedback Polynomial $X^8 + X^6 + X^5 + X^4 + 1$

C. Design of 16-Bit LFSR

16-bit LFSR with maximum length feedback polynomial $X^{16} + X^{14} + X^{13} + X^{11} + 1$ generates $2^{16} - 1 = 65535$ random outputs, which is verified from the simulation waveform.

The circuit diagram for 16-bit LFSR with maximum length polynomial is shown in Fig. 3. In the timing simulation from 20 ns to 1310720 ns. It shows starting simulation and simulation at the end of cycle after which the sequence starts repeating again.

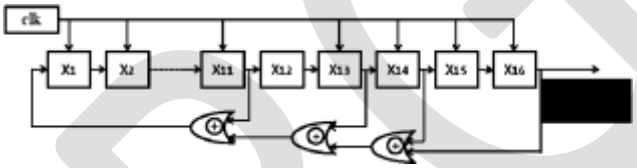

Figure 3. Circuit Diagram of 16- Bit LFSR with maximum length Feedback Polynomial $X^{16} + X^{14} + X^{13} + X^{11} + 1$

D. Design & Simulation of n-Bit LFSR

N-bit LFSR with maximum length feedback polynomial $X^n + X^{32} + X^{22} + X^1 + 1$ for which $2^n - 1 = 429,49,67,295$ random outputs, which is verified from the simulation waveform.

The circuit diagram for n-bit LFSR with maximum length polynomial is shown in Fig. 4. The timing simulation is shown in Fig. 7.a starting from 20 ns to 85899345920 ns (85.9 sec) and we can observe here the simulation is running for a long time to complete the sequence. In the Fig. 7.b a small zooming portion is shown and it can be observed the randomness behaviour for 32 bit LFSR from 30225 ns to 30500 ns. For 32 bit LFSR using Xilinx ISE 10.1 simulator, it is taking about 3 hour duration for simulating upto 1 sec time duration with 20 ns clock period. As the run length is very large which is 429,49,67,295 random states, so it is taking actual 85.9 sec to complete the sequence but practically simulate with ISE 10.1 is taking about 10-12 days.

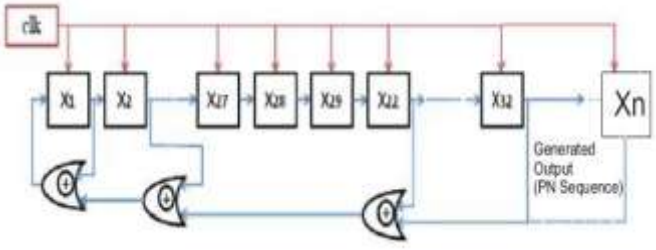

Figure 4. Circuit Diagram of n- Bit LFSR for maximum length Feedback Polynomial **X ^ n + … . X ^ 3 2 + X ^ 2 2 + X ^ 2 + X ^ 1 + 1**

E. Synthesis Result and comparison between 8, 16, n bit LFSR

The synthesis and simulation report for 8, 16 and 32 bit LFSR by using maximum length feedback polynomial are given in Table 2. Form the table we can find the total memory usage and simulation time of different length LFSR.

TABLE II. SIMULATION AND SYNTHESIS RESULT

Performance	8 Bit	16 Bit	n Bit
Time to complete the total states	40 ns to 5140 ns =5100 ns	20 ns to 1310720 ns = 1310.7 us	20 ns to 85899345920 ns = 85.9 sec
Total no. of Random States generating	255	65535	429,49,67,295
Clock	20 ns	20 ns	20 ns
Shift Register	08	16	32
Xor gate	01	01	01
Number of Slices	04	09	18
No. of Slice Flip Flops	08	16	32
No. of 4 i/p LUT	01	01	01
Total memory usage	185904 kb	185904 kb	185904 kb
GCLK	01	01	01
(Gate + Net) Delay	7.271 ns	7.271ns	7.271ns
Total pin	10	18	34

Synthesis report for the targeted device Xilinx Spartan 3S1000 FPGA

CONCLUSION

It is clearly found from the synthesis and simulation result that 8 bit 16 bit and n bit LFSR with maximum feedback polynomial can generate maximum random output. The n bit LFSR takes a lot of simulation time 85.9 sec with 20 ns clock period for generating 429,49,67,295 random output but practically it takes 10-12 days to complete the sequence by using Xlinx ISE 10.1 Simulator. So there is a simulation problem for long bit LFSR when it is targeting to FPGA for rapid prototyping development. Also we can find the memory utilization is same for all three LFSR. Definitely n bit LFSR with maximum length feedback polynomial will generate large sequence which is more secure than other but because of simulation difficulties modification in long bit LFSR is needed. In the practical use 8-bit and 16-bit LFSR is sufficient for different cryptographic applications.

REFERENCES:

[1] M. Luby, Pseudorandomness and Cryptographic Applications, Princeton University Press, 1996.

[2] Ding Jun, Li Na, Guo Yixiong, "A high-performance pseudo-random number generator based on FPGA" *2009 International Conference on Wireless Networks and Information Systems*.

[3] Jiang Hao, Li Zheying, "On the Production of Pseudo-random Numbers in Cryptography" in *Journal Of Changzhou Teachers College of Technology*, Vo1. 7 , No. 4, Dec. 2001.

[4] D. E. Knuth, "The Art of Computer Programming", Vol. 2: Seminumerical Algorithms. Reading, MA: Addison-Wesley, 1969.

[5] F. James, "A Review of Pseudo-random Number Generators," *Computer Physics Communications* 60, 1990.

[6] P. L'Ecuyer, "Random Numbers for Simulation," *Comm. ACM*, 33:10, 1990.

[7] Katti, R.S. Srinivasan, S.K., "Efficient hardware implementation of a new pseudo-random bit sequence generator" *IEEE International Symposium on Circuits and Systems, 2009. ISCAS 2009*.

[8] C. Li and B. Sun, "Using linear congruential generators for cryptographic purposes", *In Proceedings of the ISCA 20th International Conference on Computers and Their Applications*, pp. 13-18, March 2005.

[9] L'Ecuyer, Pierre, "Tables of Linear Congruential Generators of Different Sizes and Good Lattice Structure," *Mathematics of Computation*, Vol. 68, No. 225, 1999, Pages 249-260.

[10] Goresky, M. and Klapper, A.M. Fibonacci and Galois representations of feedback-with-carry shift registers, *IEEE Transactions on Information Theory*, Nov 2002, Volume**:** 48, On page(s): 2826 – 2836.

[11] Panda Amit K, Rajput P, Shukla B, "Design of Multi Bit LFSR PNRG and Performance comparison on FPGA using VHDL", *International Journal of Advances in Engineering & Technology (IJAET), Mar 2012*, Vol. 3, Issue 1, pp. 566-571.

[12] Sewak K, Rajput P, Panda Amit K, "FPGA Implementation of 16 bit BBS and LFSR PN Sequence Generator: *A Comparative Study*", In Proce. of the *IEEE Student Conference on Electrical, Electronics and Computer Sciences 2012*, 1-2 Mar 2012, NIT Bhopal, India.

[13] Efficient Shift Registers, LFSR Counters, and Long Pseudo-Random Sequence Generators, *Application Note*, Xilinx Inc.

[14] Jiang Hao, Li Zheying, "FPGA design flow based on a variety of EDA tools" in *Micro-computer information*,

2007(23)11-2:201-203.

[15] Brown S., Vranesic Z "Fundamental of Digital Logic Design with VHDL" McGraw Hill, 2nd Edition.

[16] Bhasker J, "*A VHDL Primer*", P T R Prentice Hall, Pages 1-2, 4-13, 28-30

International Journal of Engineering Research and General Science Volume 3, Issue 3, Part-2 , May-June, 2015
ISSN 2091-2730

SELECTIVE HARMONICS REDUCTION FOR PHASE LOCK LOOP UTILITY APPLICATION

Ramesh H R [1], Mahendra S M[2] & Guruprasad.A.M [3]

[1]Asst.prof., Dept. of ECE, CIT,Ponnampet-571216, Karnataka

mailtorameshhr@gmail.com, +91 8197296181

[2]Asst.prof., Dept. of ECE, CIT,Ponnampet-571216, Karnataka

mahendrasm1984@gmail.com, +91 9535058284

[3]Asst.prof., Dept. of ECE, CIT,Ponnampet-571216, Karnataka

guruprasad.cit@gmail.com, +91 9538656920

Abstract- The analysis and design of the phase-locked loop (PLL) system is presented for the phase tracking system of the single phase utility interface inverters Phase-locked loops (PLL) are widely used in power electronics equipment connected to the mains. The use of a square wave voltage-controlled oscillator instead of a sinusoidal one eliminates one multiplier, resulting in a simple PLL algorithm, suitable for low-cost processors. In spite of its simplicity, distorted grid voltages cause steady-state phase error. This project proposes the use of a modified square waveform obtained by the selective harmonics elimination (SHE) method to solve the phase error problem.

Key words: *selective harmonics elimination (SHE), phase-lock loop (PLL), power electronics*

1. Introduction

Coincides with invention of "coherent communication" (DeBellescize, 1932).The earliest widespread use of PLLs to the horizontal and vertical sweeps used in television, where a continuous clocking signal had to be synchronized with a periodic synch pulse (Wendt & Fredendall, 1943). PLLs critical to development of colour television (Richman, 1954).The first PLL IC arrived around 1965. This created an explosion in the use of PLLs. The first digital PLL appeared around 1970. This was of the classical digital PLL type. A few years later, the first all digital PLL appeared. The first laser appears in 1960. The first optical PLL arrives 4 years later. PLLs today:

- PLLs in every cell phone, television, radio, pager, computer, all telephony.
- The most prolific feedback system built by engineers.
- At low end: all software PLLs implement entire PLL functionality on sampled data.
- At high end: optical PLLs used in clock recovery for 160 Gbps data (OFC 2002).
- Boy band called: N'Sync

Phase-locked loop (PLL) is a feedback loop which locks two waveforms with same frequency but shifted in phase. The fundamental use of this loop is in comparing frequencies of two waveforms and then adjusting the frequency of the waveform in the loop to equal the input waveform frequency. A block diagram of the PLL is shown in Figure 1. The heart of the PLL is a phase comparator which along with a voltage controlled oscillator (VCO), a filter and an amplifier forms the loop. If the two frequencies are different the output of the phase comparator varies and changes the input to the VCO to make its output frequency equal to the input waveform frequency. The locking of the two frequencies is a nonlinear process but linear approximation can be used to analyze PLL dynamics.

Phase lock loops (PLLs) belong to a larger set of regulation systems. As an independent research and design field it started in the 1950s

The task of the PLLs is to maintain coherence between the input (reference) signal frequency, *f*i, and the respective output frequency, *f*o, via phase comparison. Another feature of PLLs is the filtering property, particularly with respect to the noise where its behavior recalls a very narrow low-pass arrangement that is not to be realized by other means.

Each PLL system is composed of four basic parts:

1. The reference generator (RG)

2. The phase detector (PD)

3. The low-pass filter *F*L *(f)* (in higher-order systems)

4. The voltage-controlled oscillator (VCO) and works as a feedback system shown in Fig. 1

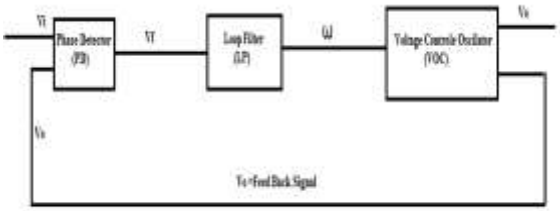

Fig1: Block diagram of PLL

.

Phase-locked loops (PLLs) are widely used in communication, control, automation, and instrumentation systems to achieve signal synchronization.

PLLs have found many applications in grid-connected power electronic devices:

1) To synchronize thyristor firing circuits.

2) To transform variables between stationary and synchronous rotating reference frames.

3) To compute power system disturbances in power quality monitoring systems.

4) To calculate reference signals for the internal control loops in uninterruptible power supplies dynamic voltage restorer's active filters and power converters used in distributed energy systems including wind and photovoltaic systems.

In these applications, the PLL detects the phase angle and frequency of the grid fundamental voltage. On the other hand, three-phase PLLs detect the positive sequence component, even for distorted and unbalanced grids.

2. SHE-PLL

Here we discuss about the SHE-PLL, if Vi and Vos have harmonics of the same order, they contribute to the dc component of *v*mult resulting in phase error. One solution for this problem consists of eliminating all the relevant harmonics that exist in the input voltage Vi from the VCO signal Vos. This new signal is called VoSHE and is obtained by means of the SHE algorithm.

The SHE waveform *vo*SHE is shown in Fig. 2, for $N = 5$ switching angles ($\alpha 1, \alpha 2, \alpha 3, \alpha 4, \alpha 5$) per quarter of VCO period T. The remaining switching instants are calculated by using the quarter- and half-wave symmetry of *vo*SHE shown in Fig3.3

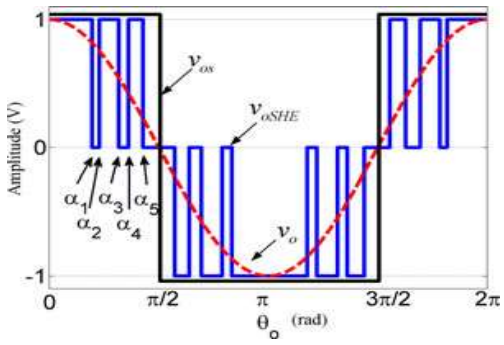

Fig 2; SHE proposed feedback signal, for N=5

The SHE waveform can be represented by a Fourier series according to

$$v_0 SHE = \frac{a_0}{2} + \sum_{n=1}^{\infty} a_n \cos(nw_0 t) + b_0 \sin(nw_0 t) \quad (1)$$

For the three-level voSHE waveform in Fig. 2, see the following.

1) The half-wave symmetry property results in a0 = 0: The quarter-wave symmetry property results in

$$a_n = \begin{cases} \frac{8}{T} \cdot \int_0^{T/4} v_{o\text{SHE}} \cos n\omega_o t \, dt, & n \text{ is odd} \\ 0, & n \text{ is even.} \end{cases} \quad (2)$$

2) The even-wave symmetry property of voSHE results in bn = 0 for all n:

According to [25], the quarter-wave coefficients are determined by

$$a_n = \frac{8}{2\pi} \cdot \left[\int_0^{\alpha_1} \cos n\theta_o \, d\theta_o + \int_{\alpha_2}^{\alpha_3} \cos n\theta_o \, d\theta_o + \int_{\alpha_4}^{\alpha_5} \cos n\theta_o \, d\theta_o \right] \quad (3)$$

$$a_n = \frac{4}{n\pi} \cdot (\sin n\alpha_1 - \sin n\alpha_2 + \sin n\alpha_3 - \sin n\alpha_4 + \sin n\alpha_5). \quad (4)$$

In this project, the values of ($\alpha 1, \alpha 2, \alpha 3, \alpha 4, \alpha 5$) are calculated by imposing $a1 = 1$, and $a3 = a5 = a7 = a9 = 0$in (11), resulting in

$$a_1 = \frac{4}{\pi} \cdot (\sin\alpha_1 - \sin\alpha_2 + \sin\alpha_3 - \sin\alpha_4 + \sin\alpha_5) = 1 \quad (4)$$

$$a_3 = \frac{4}{3\pi} \cdot (\sin 3\alpha_1 - \sin 3\alpha_2 + \sin 3\alpha_3 - \sin 3\alpha_4 + \sin 3\alpha_5) = 0 \quad (5)$$

$$a_5 = \frac{4}{5\pi} \cdot (\sin 5\alpha_1 - \sin 5\alpha_2 + \sin 5\alpha_3 - \sin 5\alpha_4 + \sin 5\alpha_5) = 0 \quad (6)$$

$$a_7 = \frac{4}{7\pi} \cdot (\sin 7\alpha_1 - \sin 7\alpha_2 + \sin 7\alpha_3 - \sin 7\alpha_4 + \sin 7\alpha_5) = 0 \quad (7)$$

$$a_9 = \frac{4}{9\pi} \cdot (\sin 9\alpha_1 - \sin 9\alpha_2 + \sin 9\alpha_3 - \sin 9\alpha_4 + \sin 9\alpha_5) = 0. \quad (8)$$

The numerical solution for the system of five nonlinear (4)–(8) is obtained using the Newton–Raphson method The starting point for the algorithm is obtained using the method presented in, resulting in $\alpha 1 = 25.58^\circ$, $\alpha 2 = 28.48^\circ$, $\alpha 3 = 48.49^\circ$, $\alpha 4 = 58.87^\circ$, and $\alpha 5 = 69.65^\circ$.The block diagram of the proposed SHE-PLL (see Fig.3) is similar to that of the square wave feedback. A slightly bigger lookup table compared to the square PLL is now required, since additional switching angles must be included. However, the SHE-PLL table will still be substantially smaller than what is required for generating a sinusoidal waveform.

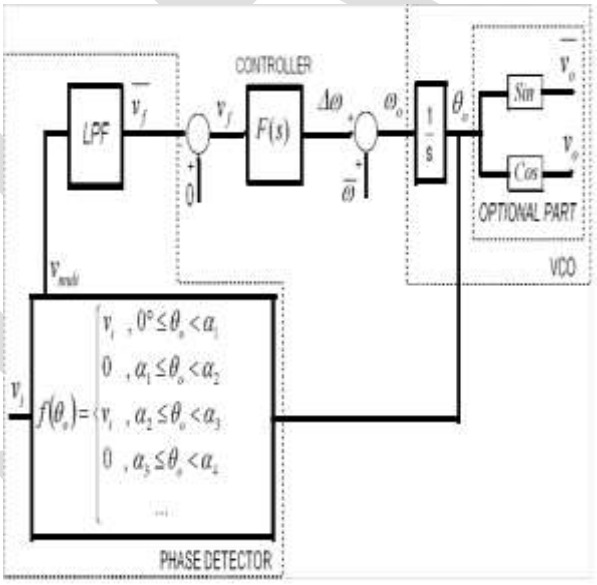

Fig3: Block Diagram of SHE-PLL Circuit of SHE-PLL

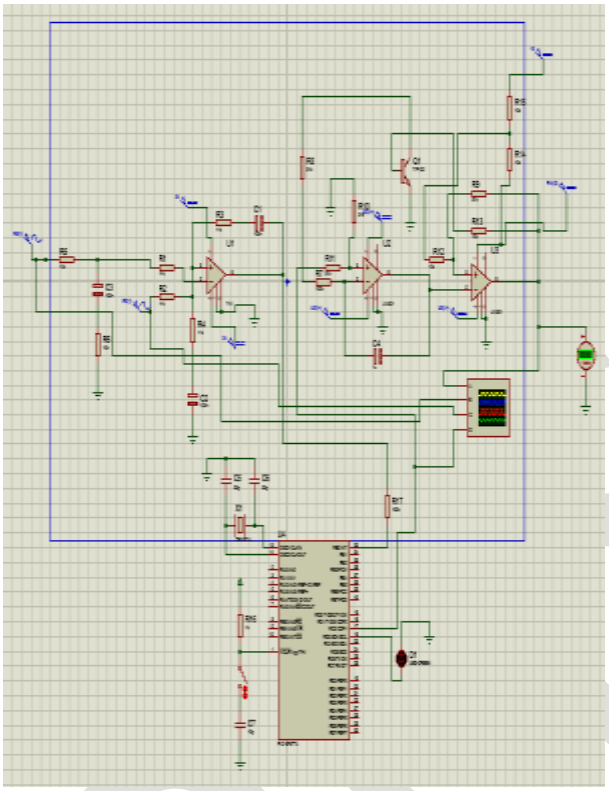

Fig4: Circuit of SHE-PLL

The fig4 shows the circuit of the SHE-PLL built using proteus software in the first part is the phase detector which detects the phase error of the two input signals and that is given to the controller here we are generating the pulse width modulated wave this width modulation was done by the values of the $\alpha 1$, $\alpha 2$, $\alpha 3$, $\alpha 4$, $\alpha 5$ the output of the controller is given to the VOC according to that we output signal VOC

3. RESULTS

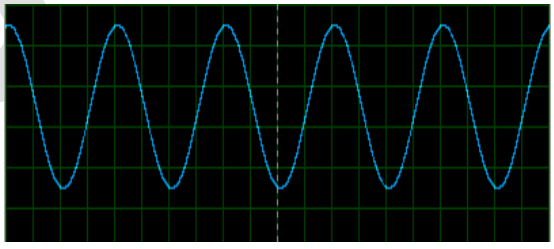

(a)

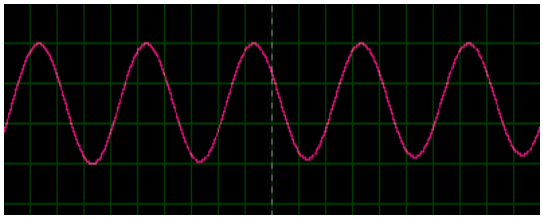

(b)

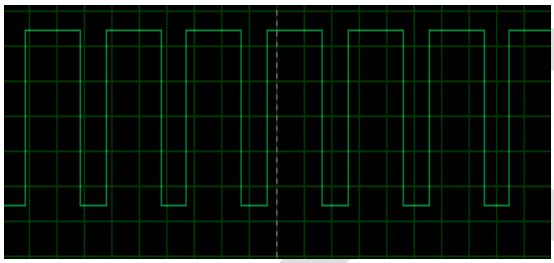

(c)

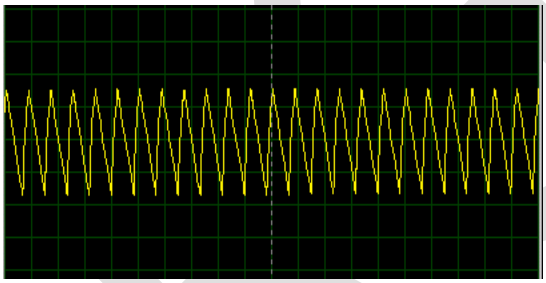

(d)

Fig 5: Simulation results :(a) input signal, (b) feedback signal, (c) SHE signal, (d) output of VOC.

4. CONCLUSION

This paper presented an implementation of a single-phase PLL based on a square wave feedback signal with SHE, suitable for power system applications. The use of a squared wave VCO simplifies the implementation of PLLs in FPGAs, DSPs, or microcontrollers, because the number of multiplications is reduced and the sine and cosine calculations may be eliminated for some applications. The SHE-PLL also eliminates the steady state phase error inherent to the square wave PLL when the input signal contains harmonics.

REFERENCES:

[1]. D. Jovcic, "Phase locked loop system for FACTS," IEEE Trans. Power Syst., vol. 18, no. 3, pp. 1116–1124, Aug. 2003.
[2]. H. Awad, J. Svensson, and M. J. Bollen, "Tuning software phase-locked loop for series-connected converters," IEEE Trans. Power Del., vol. 20, no. 1, pp. 300–308, Jan. 2005.
[3]. F. Blaabjerg, R. Teodorescu, M. Liserre, and A. V. Timbus, "Overview of control and grid synchronization for distributed power generation systems," IEEE Trans. Ind. Electron., vol. 53, no. 5, pp. 1398–1409, Oct. 2006.
[4]. A. Cataliotti, V. Cosentino, and S. Nuccio, "A phase-locked loop for the synchronization of power quality instruments in the presence of stationary and transient disturbances," IEEE Trans. Instrum. Meas., vol. 56, no. 6, pp. 2232–2239, Dec. 2007.
[5]. M. S. Padua, S. M. Deckmann, and F. P. Marafao, "Frequency-adjustable positive sequence detector for power conditioning applications," in Proc. IEEE 36th Power Electron. Spec. Conf., Jun. 2005, pp. 1928–1934.
[6]. R. M. Santos Filho, P. F. Seixas, P. C. Cortizo, L. A. B. Torres, and A. F. Souza, "Comparison of three single-phase PLL algorithms for UPS applications," IEEE Trans. Ind. Electron., vol. 55, no. 8, pp. 2923–2932, Aug. 2008.

[7]. M. Ciobotaru, V. G. Agelidis, R. Teodorescu, and F. Blaabjerg, "Accurate and less-disturbing active anti islanding method based on PLL for grid connected converters," IEEE Trans. Power Electron., vol. 25, no. 6, pp. 1576–1584, Jun. 2010.

[8]. F. Blaabjerg, P. Rodriguez, and M. Liserre, Grid Converters for Photovoltaic and Wind Power Systems. New York: Wiley, 2011, ch. 4.

[9]. V. Kaura and V. Blasko, "Operation of a phase locked loop system under distorted utility conditions," IEEE Trans. Ind. Appl., vol. 33, no. 1, pp. 58– 63, Jan./Feb. 1997

International Journal of Engineering Research and General Science Volume 3, Issue 3, Part-2 , May-June, 2015
ISSN 2091-2730

Collision Avoidance & Speed Control with Attendance Monitoring System

K. V. Karad, J. L. Rajput, Ankush Bhalaria

Asst. Professor,Department of Electronics and Telecommunication Engg.

SRES'College of Engineering, Kopargaon.

University of Pune, (M.S.) India.

karadkv@gmail.com, jaswantlr@gmail.com,ankush.bhalaria@gmail.com

Abstract— In today's world, there is a continuous need for automatic appliances with the increase in standard of living; there is a sense of urgency for developing circuits that would ease the complexity of life. Normally, this type of systems is useful in case of emergency areas where traffic is main concern & little carelessness may cause accident & death may occur. Now a days problem of traffic is much serious specially in the areas of schools as well as the places where crowd is more. A collision avoidance control system for a vehicle is provided which is designed to determine a target collision avoidance deceleration required for a system vehicle equipped with this system to bring a relative speed between the system vehicle and a target object into agreement with substantially zero without a physical collision with the target object and to determine a possibility of collision with the target object as a function of the target collision avoidance deceleration. This system is specially designed with the help of GSM & RFID for the school areas where chances of accidents are more.

Keywords— Collision avoidance, GSM, LPC 2148, RFID, speed control, Zigbee, DC motor.

1. INTRODUCTION

In today's world, increasing traffic is a major concern. The traffic police are inefficient to handle the traffic conditions. Today many people break the law by breaking the traffic rules. The traffic rules are broken often at the signals. People start moving ahead even though the signal is red and many culprits gat away since there is no police at the signal further such driving practice is an invitation for serious accidents. Same are the problems faced by different schools. Accidents are major concern for the school authorities as children are not always cross the roads properly. To solve all the above problems we have come up with an innovative soln. of anti-signal breaking system. Now days problem of traffic is much critical specially in the areas of schools as well as the places where crowd is more. In such cases, there is always requirement of collision free traffic with the control of speed. Because of advancement in technology, for every vehicle we have good driving speed & easily availability of vehicles adds the traffic.

As a result driving of a vehicle is quite difficult on the roads. This system is specially developed for the school places where most of the parents use their own vehicle for dropping their child at schools. Dropping & picking time of children is peak time, at this time traffic is more ,during this time chances of accident are more so to avoid this a system is designed with the help of GSM & RFID which will monitor the traffic by controlling the speed with the help of DC motor very well and avoid the collision.

2. NECESSITY

Now a days problem of traffic is much critical specially in the areas of schools as well as the places where crowd is more. In such cases, there is always requirement of collision free traffic with the control of speed. Because of advancement in technology, for every vehicle we have good driving speed & easily availability of vehicles adds the traffic as a result driving of a vehicle is quite difficult on the roads. This system is specially developed for the school places where most of the parents uses their own vehicle for dropping their child at schools. Dropping & picking time of children is peak time, at this time traffic is more ,during this time chances of accident are more so to avoid this a system is designed with the help of GSM & RFID which will monitor the traffic by controlling the speed with the help of DC motor very well and avoid the collision.

3. OBJECTIVES

Actually, this system has two objectives.

1. *Avoidance of collision & speed control.*
2. *Keeping the record of students by sending the message to their parents at what time they are entered or leave the school gate. In order to implement this system, GSM, RFID tag & RF Transceiver is required where as the speed of vehicle will be controlled by DC motor.*

4. LITERATURE SURVEY

A. Collision avoidance

The present invention relates generally to a collision avoidance control system which works to initiate collision avoidance action when the danger of possible collision with a target present ahead of a vehicle is encountered. Automotive collision monitor systems are known which work to estimate stopping distances of a system-equipped vehicle and a target preceding vehicle travelling ahead of the system-equipped vehicle and locations of the system-equipped vehicle and the target preceding vehicle after the elapse of a preset time to determine the danger of possible collision with the target preceding vehicle based on the stopping distances and the locations. For instance, Japanese Patent First Publication No. 08-132996 teaches such estimation of the stopping distances. Japanese Patent First Publication No. 05-181529 (corresponding to U.S. Pat. No. 5,473,538) teaches such estimation of locations of the system-equipped vehicle and the target preceding vehicle. It is, however, impossible for the above systems to determine the degree of deceleration to be produced in an automatic braking device of the system vehicle to avoid collision with the preceding vehicle based on the determination of the danger of possible collision. The systems, thus, need to perform an additional operation to determine a control variable to decelerate the system-equipped vehicle [1]. Japanese Patent First Publication No. 11-066495 teaches a collision avoidance control system which uses an inter vehicle distance between the system-equipped vehicle and the target preceding vehicle, a relative speed between the system-equipped vehicle and the target preceding vehicle, a minimum distance to be reserved between the system-equipped vehicle and the target preceding vehicle, acceleration of the target preceding vehicle, and a preset deceleration of the system-equipped vehicle to derive a quadratic function in terms of conditions required to avoid accidental collision with the target preceding vehicle and determines the possibility of the collision using a parabola, as represented by the quadratic function. Specifically, this system increases the preset deceleration of the system-equipped vehicle cyclically and determines the possibility of the collision based on the orientation of the parabola, an inclination of a straight segment of the parabola, coordinates of the straight segment of the parabola, and a predefined parabola determining equation in each cycle to bring a target deceleration used in deceleration control into agreement with a value of the preset deceleration when it is determined that there is almost no possibility of the collision.[1,2]

A collision avoidance control system comprising a travel control apparatus working to determine a target acceleration as functions of a distance to the target object and the relative speed and to decelerate or accelerate the system vehicle based on the target acceleration to control a travel condition of the system vehicle, and wherein the deceleration control activating threshold value is set greater than a maximum deceleration controllable by the travel control apparatus.

B. GSM

The GSM standard (Global System for Mobile Communications) for mobile telephony was introduced in the mid-1980s and is the European initiative for creating a new cellular radio interface. The GSM system uses a TDMA radio access system employed in 135 countries, operating in 200 KHz channels with eight users per channel. It is the most widely deployed digital network in the world today, used by 10.5 million people in more than 200 countries. GSM Bandwidth Allocation GSM can operate four distinct frequency bands: GSM 450: GSM 450 supports very large cells in the 450 MHz band. It was designed for countries with a low user density such as in Africa. It may also replace the original 1981 NMT 450 (Nordic Mobile Telephone) analog networks used in the 450 MHz band. NMT is a first generation wireless technology. [5] GSM 900: When speaking of GSM, the original GSM system was called GSM 900 because the original frequency band was represented by 900 MHz The GSM 1900 system has been added to the IS-136 D-AMPS (Digital Advanced Mobile Phone System) and IS-95 Code Division Multiple Access (CDMA) system both operated at the 1900 MHz band. The ITU (International Telecommunication Union) has allocated the GSM radio spectrum with the following bands: GSM 900: Uplink: 890–915 MHz Downlink: 935–960 MHz GSM 1800: Uplink: 1710–1785 MHz Downlink: 1805–1880 MHz GSM 1900: Uplink: 1850–1910 MHz Downlink: 1930–1990 MHz \

In the above, uplink designates connection from the mobile station to the base station and downlink denotes connection from the base station to the mobile station.

C. RFID

Radio Frequency Identification (RFID) is a technology for wireless information exchange over short distances. Even though the technology itself was invented about 50 years ago, recent development in the field of low cost RFID devices began to finally show its potential. The possibility of adding (minimal) computing capabilities to everyday's objects will support the development of ubiquitous computing in the near future. Applying RFID transponders to consumer goods will be common, creating an ever present computing environment spanning all parts of everyday's life. Today RFID commerce already constitutes a vital and ever expanding market. Judging by evidence from recent years, RFID industry will continue its rapid growth. In such a developing market security and privacy become increasingly important. An appropriate definition for security is a composite of the attributes confidentiality, integrity and availability (also called CIA).

5. SYSTEM DESIGN

Basically system is divided into two units.

1. Unit at the school gate

2. Unit on board the vehicle.

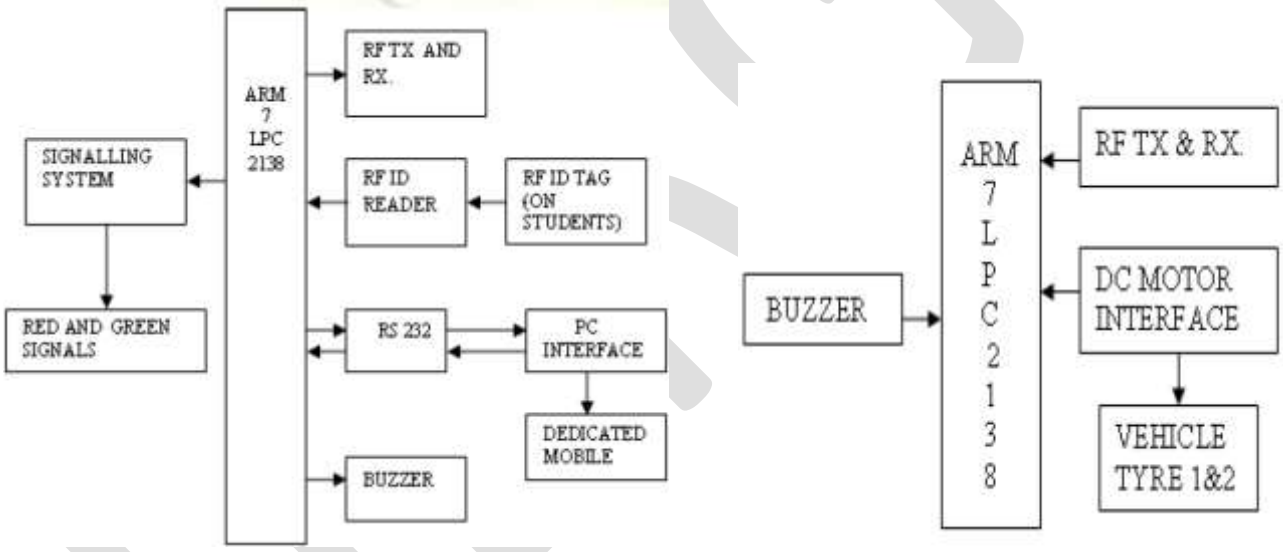

Fig. 1 Block Diagram of System

1. Unit at the school gate: Following are the different sections of this unit. RFID Reader unit**:** This unit is interfaced to the ARM and is situated at the gate of the school. All the students have the RFID tag with them. As soon as the student passes the front gate of the school the reader at the gate reads the RFID tag and sends this information to the PC. PC Unit: On board the PC we have a visual basic software .The PC after receiving the RF id tag information from the student compares it with the database of the students stored in the PC. It then sends a SMS to the concerned parents that the particular student has entered the school premises with in time of entry. Similarly this unit will send a SMS as soon as the student exits the school .In this way the parents get intimation during in time and out time of the respective student. Thus every parent will get a SMS that the student has reached the school in time. In case any parent doesn't get the SMS in time they can enquire about the student to the school. The SMS is sent using the dedicated mobile connected to the school PC using the AT commands. RF Transceiver unit**:** This unit senses if there are any vehicles in the close vicinity of the school. If any car approaches and there is no student at the gate then the ARM turns the signal to yellow indicating passing vehicle to slow down. If this unit senses a vehicle and also there is a student at the gate of the school ready to cross the road the ARM will immediately turn the signal to RED indicating to the vehicle to STOP. Also an RF indication is given to the passing vehicle about the status of the signal.

2. Unit on board the vehicle: This unit also has an RF Transceiver which sends an indication to the unit of the school informing about its presence. After this the Unit at the gate will send the indication about the status of the signal via the RF module which is received by the incoming vehicle. If the signal is RED then ARM will stop the vehicle using the DC motor speed control technique. If the signal is yellow then the ARM will reduce the speed to the safe limit automatically. After the student has passed the Vehicle can go on its way.

6. SYSTEM COMPONENTS

ARM7: The LPC2131/32/34/36/38 microcontrollers are based on a 16/32-bit ARM7TDMI-S CPU with real-time emulation and embedded trace support, that combine the microcontroller with 32 kB, 64 kB, 128 kB, 256 kB and 512 kB of embedded high-speed flash memory. A128-bit wide memory interface and a unique accelerator architecture enable 32-bit code execution at maximum clock rate. For critical code size applications, the alternative 16-bit Thumb mode reduces code by more than 30 % with minimal performance penalty. It is selected for the following reasons:

1. Two serial ports available
2. Cheap, easily available
3. Plenty guidance available
4. High level of computing possible.

TRANSMISSION MODULE XBEE protocol is used for wireless communication in between the ARM and the PC. 30 mtrs range, 2.4 GHz frequency XBee. Module is engineered to meet ZigBee/IEEE 802.15.4 standards and support the unique needs of low-cost, low-power wireless sensor networks. The modules require minimal power and provide reliable delivery of critical data between devices. The modules operate within the ISM 2.4 GHz frequency band and are pin-for-pin compatible with each other. RFID Tag The basic feature of an RFID system is the automatic identification of items. In its simplest form, such identification can be binary, e.g., paid or not paid, useful for alerting. Features 1. Frequency Band - HF 2. Common Frequency - 13.56 MHz. 3. Coupling - Inductive 4. Communication Range - 10 to 70 cm. 5. Data Rate - Low 6. Maturity - Established 7. Reader Cost - Medium

7. ADVANTAGES OF SYSTEM

- The system is easy to understand.
- Avoids the collision of vehicle by controlling the speed.
- Identification of student is easy as RFID tag is provided to each student.
- Easy to set up the system.
- Keeps the record of student's entrance or leaving time from school.

8. PARFORMANCE ANALYSIS

A. Analysis of Zigbee Transmitter and Receiver for Different Distances

TABLE I

ANALYSIS OF ZIGBEE TRANSMITTER AND RECEIVER

Sr. No.	Distance in Meter	Zigbee Analysis for receiver
1	5-10	The Zigbee receiver receives data from transmitter successfully.
2	11-21	The Zigbee receiver receives data from transmitter successfully.
3	22-25	The Zigbee receiver receives data sometimes.
4	25-30	No data received by Zigbee receiver from the transmitter

B. Performance of Ultrasonic sensor

TABLE II

ANALYSIS OF ULTRASONIC SENSOR FOR STOPPING DISTANCE.

Sr No.	Fixed Distance (in cm) A	Measured Stopping Distance (in cm) B	Stopped Distance(in cm) A-B
1	40	29.72	10.28
2	40	30.68	9.32
3	40	28.44	11.56
4	40	30.24	9.76
5	40	28.89	11.11
Avg.	**40**	**29.61**	**10.40**

C. Analysis for vehicle stopping time

TABLE III

ANALYSIS OF VEHICLE STOPPING TIME FOR THE RECEPTION OF SIGNAL

Sr No.	Measured Stopping Time (in sec)	Average Stopping Time (in sec)
1	8.88	8.99
2	9.48	
3	8.87	
4	8.51	
5	9.25	

D. Analysis of Vehicle Stopping Distance for the Reception of Signal

TABLE IV

ANALYSIS OF VEHICLE STOPPING DISTANCE

Sr No.	Measured Stopping Distance (in cm)	Average Distance (in cm)
1	50	**49.6**
2	48	
3	51	
4	48.5	
5	50.5	

9. RESULTS

Results for Detection of Card

A RFID Card (tag) which is provided to the student is read by the reader and card was as detected as buzzer beeps. So, the information like student's ID, Name, Year, Branch read by the card with In time during entrance in school premises.

Attendace Report Generation

To generate the attendance, date of that day is entered in report window. The GUI for attendance report generation is as shown.

Fig.3 GUI Result for Generating Attendance Report

Once the date entered in report window, attendance is generated in Excel sheet. The GUI window for attendance report generated is as shown.

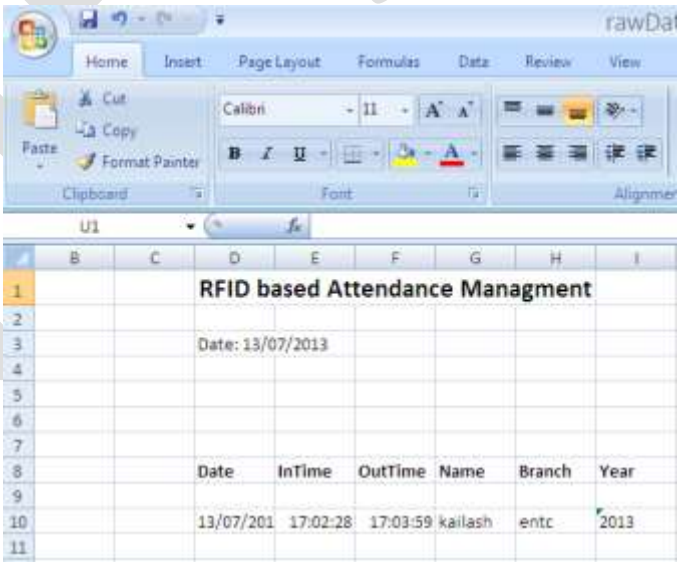

Fig. 4 GUI Result for Attendance Report

10. FUTURE SCOPE

Though, the system is well designed still it has limitation of distance or area coverage. This problem can be solved using the module of zigbee. For wireless transmission zigbee is the best solution that can replace existing RF Transceiver. In addition to this, signal indication i.e. RED & YELLOW signals may be replace wirelessly instead of wired.

CONCLUSION

The designed system gives the complete solution over the problem of traffic especially in case of school areas where parent's vehicle or private vehicles are coming for dropping or picking up their children or students. With the help of designed system speed of vehicle is kept in tolerable range by the indication of the signal so that traffic is neatly droved and ultimately vehicle collision is avoided which is leading to zero chances of accidents. The designed system is also intended for sending a message through a dedicated mobile to the student's parents by keeping record of their entrance or leaving time of school which makes parents tension free those who are not able to dropped or picked up from school. This system is also useful for especially in case of dummy students because the special RFID tag is provided to each student so without verifying the RFID tag students are not able to enter in the school campus. In short this system is very useful for controlling the speed of vehicle & ultimately avoidance of collision with in-out information of the student to their parents.

REFERENCES:

[1] B. Ulmer. 'VITA - An Autonomous Road Vehicle (ARV) for Collision Avoidance in Traffic'. In "Proc. of Int. Symp. on Intelligent Vehicles", Detroit June 92.
[2] Hyangjin Lee, Jeeyeon Kim, "Privacy threats and issues in mobile RFID " Korea Information Security Agency.
[3] Y. Bar-Shalom, X. Rong Li, T. Kirubarajan, Estimation with Applications to Tracking and Navigation. Wiley, 2001.
[4] F. Thomanek. et al."Multiple Object Recognition and Scene Interpretation forAutonomous Road Vehicle Guidance".
*[5] John Scourias, "Overview of the Global System for Mobile Communications",May 19,1995.
[6] Marc Langheinrich, "A Survey of RFID Privacy Approaches".
[7] Bernhard Riedl,Gernot Glouch,"A Comparative Literature Review on RFID security and Privacy".
[8] Kailash V. Karad, Girish A. Kulkarni "Gsm & Rfid Based Tx & Rx For Collision Avoidance & Speed Control", International Journal of Engineering Research and Applications (IJERA) ISSN: 2248-9622 www.ijera.com Vol. 3, Issue 1, January -February 2013, pp.898-902

International Journal of Engineering Research and General Science Volume 3, Issue 3, Part-2 , May-June, 2015
ISSN 2091-2730

Energy Optimization In Wireless Sensor Network Using Different Compression And Encrytion Techniques

Rakesh V

M.tech, Electronic and Communication
M.S.Ramiah Institute of Technology

Bengaluru, India

Rakeshvemu27@gmail.com

Sarala S M

Assistant Professor, Electronic and Communication

M.S.Ramiah Institute of Technology

Bengaluru, India

Saralasm@msrit.edu

Abstract- Wireless sensor networks(WSN) has been increased day by day to measure and monitor physical characteristics. It can implemented in the area where human cannot be reached. Each sensor node depends on power to do their activities. As the WSN has limited battery life time it's important to optimize power. There are many methods to optimize power in WSN. Here compression and encryption techniques are used for optimizing power in WSN. Here optimization means reducing the amount of energy consumption. If the input data is large then automatically the transmitters and receivers will take more amount of energy. So here by reducing the data size by compression and by sending an encrypted version of the compressed data, we are making the antennas to transmit and receive less amount of data than the actual data and also it will be more secured. At the receiving end by applying the decryption and reconstruction of the compressed data , we are able to recover the complete data. Then we will compare how much energy is optimized by different compression and encryption techniques.

Keywords – Sensor node, optimize, compression, encryption, battery, energy consumption

I. Introduction

Wireless sensor network (WSN) is most often set up in an ad-hoc mode by means of cheap small computational nodes distributed densely over a significant area. They consist of small power nodes with sensing, computational and wireless communicational capabilities that can be deployed deterministically or randomly over an area where the users wish to collect data. Typically, wireless sensor networks contain hundreds or thousands of identical sensor nodes. These sensor nodes have the ability to communicate with each other or directly to a base station. These sensor networks are highly distributed and the nodes are lightweight. A greater number of sensors will enable sensing over a large area. As the manufacturing of small of small, low cost sensors has been increasing technically and economically feasible, a large number of these networks can be networked to operate for variety of applications like military applications, disaster management, habitat monitoring, health monitoring, and home applications.

With the advent of ad hoc networks they can be distributed in remote site environments, so there is a focus on increasing the lifetime of sensor nodes though power transmission, power conservation and power management. Wireless sensor networks faces the problem

of energy constraints in terms of limited battery life time. Each node depends on energy for its activities. Failure one node can interrupt the entire system. So it is important to optimize energy. Energy optimization is the goal to reduce amount of energy required to provide for products and services. There are various approaches to improve energy efficiency. Reducing energy use reduced energy costs and may result in a financial cost saving to customers if the energy savings offset any additional costs of implementing an energy efficient technology.

In order to expand the working time of individual devices, it is frequent practice that some nodes will be deactivated, including radio transceiver. They remain in inactive state for the most of time and activated only to transmit or receive data from other nodes. Radio transceiver can operate in one out of three modes, which differ in the consumption of power necessary for proper operation: Active state-consumes more energy when transmitting or receiving, Idle state- consumes less energy, it is turned on and ready to change to data transmission or receiving, Sleep state- nodes shut down the radio to save energy. Steps can be taken to save energy are to schedule the state of nodes (active, idle, sleep), changing transmission range between nodes, using efficient routing and data collecting methods and avoiding the handling of unwanted data as in the case of over heading.

General block diagram of wireless sensor network is as shown below:

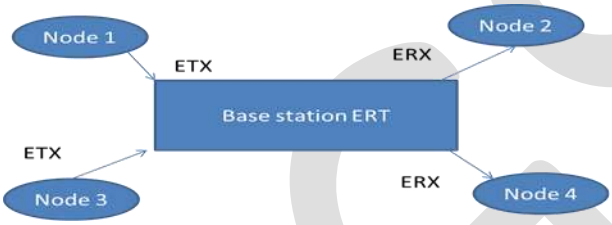

Figure 1: General block diagram of wireless sensor network

The above diagram consists of a wireless sensor networks consists of four nodes and one base station. These nodes are placed at different geographical locations. These nodes send data to base station and in turn also receive data from base station. Here base station is nothing but a router. When a wireless sensor network transmits a data to the base station or when a wireless sensor network receives a data from energy is utilized for accomplishing this task. Similarly energy is utilized by the base station to route the data. Suppose Node1 transmits the data to base station and let the energy utilized is ETX and Node2 receives the data from base station and the energy utilized is ERX. Similarly energy is also required by the base station to route the data and energy required for this purpose be ERT. Therefore total energy for overall process is the sum of all energies

T= ETX+ERT+ERX

Where T is total energy for overall task and ETX, ERT, ERX are the transmission energy, routing energy and receiving energy respectively.

The methods in which energy savings can be done are classified into two heads [1]:

Device level: Hardware component selection and their configuration to achieve low energy consumption in a wireless sensor node.

Network level: Choice of communication methods and protocols to minimize energy consumption.

In a sensor node there are four essential parts: processing unit, sensing unit, transceiver unit and power unit. Processing unit is a part of microcontroller unit which can read sensor data, perform some minimal computations and make a packet ready to transfer in wireless communication channel. In reality sensor unit is the medium for communicate between physical world and the conceptual world of processing unit. The senor unit is one of the vital part of wireless sensor mode, it sense and detect the physical state of environment and sends the data to processor. Processor manipulates data and decides where it has to promote or else transmit the data to base station. Sensor coverts energy forms one form to another form. In reality sensor act as the transducer where energy is converted into analog or digital. Sensor can be distinguished based on what kind of energy they detect or transfer to the system. A wireless sensor node can be built with different type of sensor, and different types of sensor use different amount of energy.

II. Methodology

In wireless sensor network the target is to optimize energy for transmission, routing and receiving of data. Here by using combination of various encryption and compression techniques energy can be optimized. If the input data is large nodes takes more energy to

transmit, so by reducing data size by compression techniques the transmitter consumes less energy and by encrypting the data network would be more secured.

In the proposed methodology, during transmission data is first encrypted and compressed using combination of various encryption and compression algorithms and at the receiver end reverse process is applied. The flow chart of the proposed methodology is shown below:

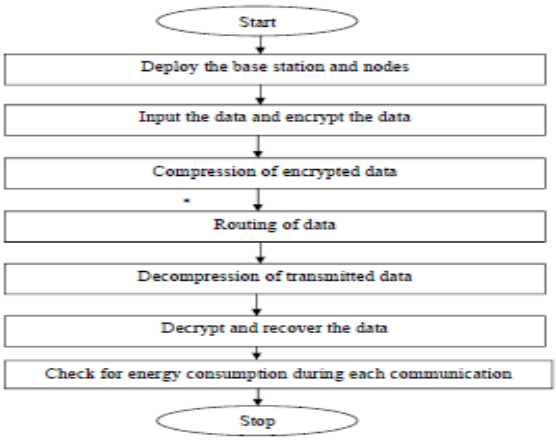

Figure 2: Flow chart of proposed methodology

III. Encryption Schemes Applied To Wireless Sensor Networks

In this approach the focus in on the energy efficiency of secure communication in wireless sensor networks. The encryption algorithms used are AES (Advanced encryption standard) and neural network based encryption/decryption. The input data used is image.

A. AES

AES is a symmetric block cipher where same key is used for both encryption and decryption. This standard specifies Rijnedael algorithm, a symmetric block cipher that can process data blocks of 128 bits, using cipher keys with lengths of 128, 192 and 256 bits. Here it consists of 10 rounds of processing for 128-bit keys, 12 rounds for 192-bit keys and 14 rounds for 256-bit keys. Except for the last round in each case, all other rounds are identical [12]. AES encryption algorithm is shown below:

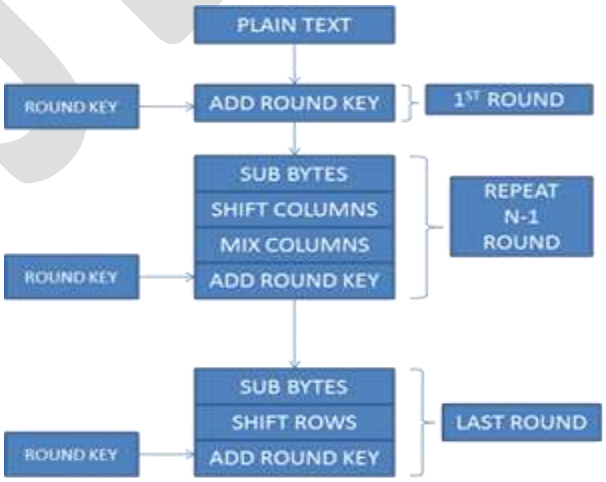

Figure 3: AES encryption algorithm

The input of AES algorithm is converted into 4*4 array, called state. Four transformations are performed for various operations on the state to calculate the output state. The transformations are add round key, sub bytes, shift rows and mix columns. Except for add round key each of these operations is invertible.

Sub bytes Transformation: This transformation is a non-linear byte substitution that operates independently on each byte of the state using a substitution table called S-box. This S-box is invertible. The S-box used in the sub bytes transformation is presented in hexadecimal form.

Shift Row Transformation: In this transformation, the bytes in the last three rows of the state are automatically shifted over a different number of states. The first row is not shifted. Second row is shifted left once, third row twice and last two three times it is shifted

Mix Columns Transformation: The mix columns transformation operates the state column by column, treating each column as a four term polynomial. The columns are considered as polynomials over GF (2^8) and multiplied modulo of x^4 +1 with a fixed polynomial a(x), given by a(x) = {3} x^3+ {1} x^2+ {1} x+ {2}. This can be written as multiplication matrix s'(x) = a(x) * s(x).

Add round key Transformation: In add round key transformation, a round key is added to the state by a simple bitwise XOR operation.

Key Expansion: The AES algorithm takes the cipher key and performs key expansion to generate a key schedule. The key expansion generates a total of Nb (block length i.e. 4) * (Nr (total number of rounds i.e. 10) +1) words. The algorithm requires an initial set of Nb words and each of the Nr rounds require Nb words of key data. The resulting key schedule consists of an array of 4-byte words, denoted $[w_i]$, where *i* is in the range of $0 \le i \le$ Nb (Nr + 1).

The expansion of the input key schedule proceeds according to pseudo code. It can be seen that for words in position that are multiple of Nk (length of expanded key), a transformation is applied to w[i- 1] prior to XOR , followed by a round constant which contains the values given by $[x^{i-1},\{00\},\{00\},\{00\}]$, with x^{i-1} being powers of *x* (*x* is denoted as {02}) in the field GF(2^8). Then consists of a cyclic shift of bytes in a word, followed by substitution using S-box. Then every following word, w [i], is equal to the XOR of previous word, w [i-1], and the word Nk position earlier, w [i-Nk].

B. Neural Network Based Encryption and Decryption

As the encryption standards such as AES, DES, RSA has been increased so neural network is another approach of encryption. Neural network plays important role in information security. Most of the algorithms used are generic, because of which the key exchange has become has prerequisite prior to data exchange [11]. Hence the strength of such encryption lies on the key length. In this encryption process it uses random substitution, and impurity addition creating more confusion to misguide the cryptanalyst. At receiving end, it uses artificial neural network to obtain the original data.

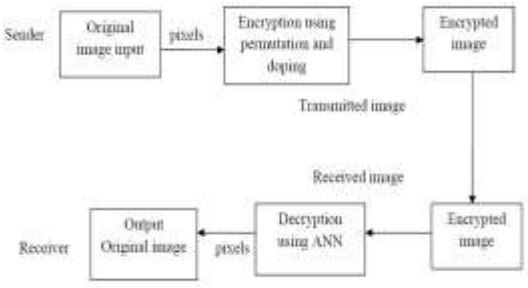

Figure 4: Block diagram of image transmission and reception

Artificial neural network: In general it is a highly interconnected, parallel distributed processing network with a large number of processing elements neurons. Each neuron is connected to other neurons by means of communication links each with associated weight. Typically, a neuron sends its activation as a signal to several other neurons. There are several architectures in which neurons can be connected. In this multilayer feedforward networks with backpropagation learning algorithm are used. It is made up of multiple layers. Architecture of this class consists of input and output layer also have one or more intermediate layers called hidden layers.

Here the neurons of one layer are connected to neurons of next layer and so on still the output layer. The hidden layer helps in performing useful intermediary computations before directing the input to the output. The training of a network by backpropagation involves three stages: the feed forward of input training pattern, the calculation and back propagation of associated error, and the adjustment of the weights. As the process converges, the final weights are stored in a file. After training, application of the network involves only the computations of the feedforward phase.

Encryption module: The image to be encrypted is read pixel by pixel and the transformation is done on these pixels using permutation, substitution, and impurity addition. Two levels of encryption are done to obtain high level encryption. The algorithm shown below does the necessary transformation.

Algorithm

First level encryption

Step 1: Get the pixel value of image file, [66] [01000010].

Step 2: Divide the pixel bytes into two parts (nibbles), [0100 0010].

Step3: Exchange the nibbles and concatenate to form byte, [00100100]

Step4: Calculate the impurity by XORing the original msb nibble and lsb nibble, [0110].

Step5: Shift the bits of impurity by 5 bits to the right [011000000] and EXOR with the step 3

[011100100] = [228].

Step6: Add impurity to the result obtained in step 5. The impurity chosen is 117

[117+228] = 345.

Step7: Continue step1 to step6 for all the pixels of image.

Addition of two columns:

Step8: Additional two columns are added and the value of 117 is added to first column and 627 to the second new column.

Second level encryption:

Step10: Add another level impurity to the resultant matrix obtained in step 8 such that impurity changes with respect to the position of the pixel

It is done in two levels because in the first level encryption all the pixels with same original value will have the same encrypted value and due to this intensity changes but the picture can be still visible. To overcome this second level encryption is done. During this impurity changes according to pixel position that means the pixel with same original value will have two different values after second level encryption.

Decryption module: At receiving end, decryption is achieved using an artificial neural network. The neural network is trained for standard mapping values and the weights are stored before applying input to it. The system is designed for three input layers- input, output and the hidden layer. The input and output layer has only one neuron, and the hidden layer has 695 neurons. Large numbers of neurons are essential for achieving high accuracy. The decryption process is achieved in three steps. During first stage, the impurity which was varying with respect to pixel is removed. In the second stage, the additional columns from the matrix which were added during encryption is deleted. During the third stage, the received image data and weights which are stored after training are used to simulate the network. The output of this stage is the recovered image.

IV. Compression Techniques Applied in Wireless Sensor Network

After encryption the following compression techniques are applied to the input. Compression means reducing the size if data so that it can save space while storing data and consume less energy while transmitting. There are two types of compression lossless compression and lossy compression. Lossless compression involve no loss of information. If data have been losslessly compressed, the original data can be recovered exactly from the compressed data. Lossy compression involves some loss of information. The data that have been compressed generally cannot be recovered or reconstructed exactly. Here lossless compression techniques and lossy compression is used. The lossless compression used is Huffman coding and Arithmetic coding.

I. Huffman Coding:

It is a lossless compression developed by David Huffman. It is an entropy encoding algorithm which uses variable length code table for encoding a source symbol. The variable length code has been derived in a particular way based on the estimated probability of occurrence for each possible value of the source symbol. It uses a specific method for choosing presentation for each symbol, resulting in prefix code. The Huffman coding can be constructed on two ideas: In an optimum code, the symbols that occur more frequently should have shorter codewords and the two symbols that occur least frequently will have same length.

II. Arithmetic coding:

It is a lossless compression based on the interval subdividing. In arithmetic coding source ensemble is represented by an interval between 0 and 1 on the real number line. Each symbol of the ensemble narrows this interval. As the interval becomes smaller, the number of bits needed to specify it grows. It assumes an explicit probabilistic model of the source. It uses the probabilities of the source messages to successively narrow the interval used to represent the interval less than low probability messages contribute fewer bits to the encoded ensemble.

III. Lossy Compression:

In a lossy compression the following steps are carried out. The first is that performs transform coding for the input data. The transform is done using discrete wavelet transform. It separates the high and low-frequency portions of a signal through the use of filters. Signal is passed through high & low pass filters and down sample by a factor of two. Multiple levels (scales) are made by repeating the filtering and decimation process on lowpass outputs. DWT is computed with a cascade of filtering followed by a factor 2 sub-sampling. The 2-D DWT is computed by successive low-pass and high-pass filtering of the image. By applying 2D DWT on an image, the image is decomposed into four subband LL, LH, HL, HH subband, corresponding to approximate, horizontal, vertical, and diagonal features respectively. The subband denoted by LL is approximately at half the original image. While the subband HL and LH contains the changes of images or edges along vertical and horizontal directions, respectively. The subband HH contains the detail in the high frequency of the image. LL subband is further decomposed into four subband. But as the level of decomposition is increased, there is a loss of resolution in the newly created subband. The first level of decomposition extracts finest resolution of details, the subband created in the second level of decomposition extract coarser details than the first one. Here Haar wavelet is used as it provides a simple and computationally efficient approach for analyzing the local aspects of a signal. Then next step is quantization, it converts a sequence of floating numbers to a sequence of integers. The simplest form is to round to the nearest integer. Another method is to multiply each number in by a constant k, and then round to the nearest integer. Next is entropy encoding here arithmetic encoding is used.

V. Routing and Energy Model

After compression the next step is routing of data it is done by LEACH (Low energy adaptive clustering hierarchy) protocol. It is a cluster cased routing protocol, which uses distributed cluster formation. LEACH randomly selects the cluster head based on the energy of the sensor node [5]. This is to form the sensor node based on the received signal strength and use cluster head as the routers to the base station. In LEACH, the cluster head gets the compressed data from the input sensor nodes. From cluster head it is passed to the base station. From base station it is transmitted to the other cluster head and then to the receiving node.

After routing of data the next important step is to calculate energy for transmission of data. Here we use first order radio model for wireless sensor networks. Here we have taken some assumptions for these networks. All sensors are within the wireless communication range when they communicate with each other or with the base station. Sensors should have homogeneous sensing,

computing and communication capabilities. Base station is located in the center of the sensor networks and it has infinity energy. Thus, to transmit a k-bit message a distance d, the energy consumed is:

$$E_{tx}(k,d) = k*E_{elect} + k*E_{amp}*d^2$$

Where E_{tx} is energy consumed for transmission, $E_{elect\ is}$ transmission and receiving energy and E_{amp} is amplifier energy.
After calculation of energy we compare the energy consumed by different combination of encryption and compression techniques.
Some of the considerations for calculating energy are as shown below:

Parameter	Value
Initial energy of each node	5 J
Transmission and Receiving energy (E_{elect})	50n J/bit
Amplifier energy (E_{amp})	0.0013pJ/bit/m^2
Type of distribution	Random
Energy level for node to be alive	0.009 J

Table 1: Energy model consideration for LEACH

IV. Results and Discussions

As mentioned earlier, before transmission of data to the networks it is encrypted using AES encryption and neural network based encryption/decryption and then using different compression techniques it is compressed. And then routing of data is done by LEACH protocol. Then energy is calculated for each combination and compared.

A. AES encryption results

The results of encryption and decryption are shown in below figure 4.1. The original size of image is 256*256*8. After encryption also it remains in same size so encryption here is just for security purpose.

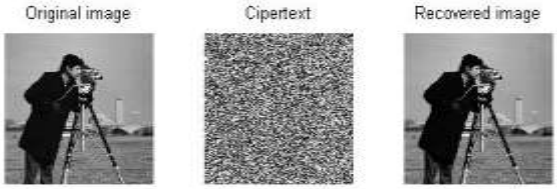

Figure 5: AES encryption and decryption

B. Neural network based encryption

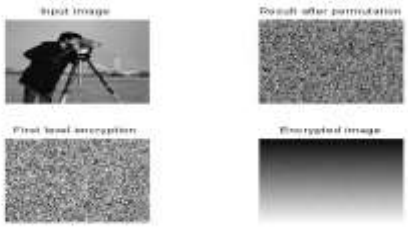

Figure 6: Output of Encryption

The encryption is done in two levels and decryption is done by using neural network

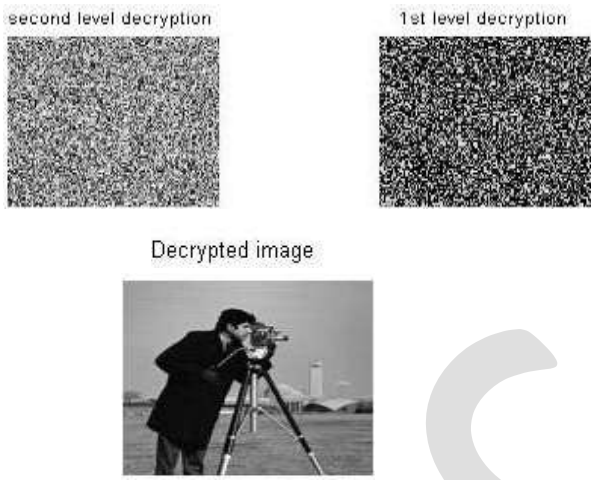

Figure 7: Output of Decryption

Energy consumed after encryption and compression results

Original Size of image	Transmission energy before compression	Energy consumed after Huffman compression	Energy consumed after arithmetic coding	Energy consumed after lossy compression
524288 bits	0.026739 J	0.023546 J	0.023430 J	0.00983 J

Table 2: Energy consumed by different compression techniques after encryption.

As we can see the above table the energy required for wireless sensor node to transmit the data for single time. After encryption the image size remains same. The energy consumption mainly depends on the size of data and distance between the nodes. As the data size is decreased the energy consumed will be less for wireless sensor network. For lossless compression the energy required is more but for lossy compressed data the energy required is less. The figure 8 gives the clear information about how many nodes are alive for how many rounds of communication.

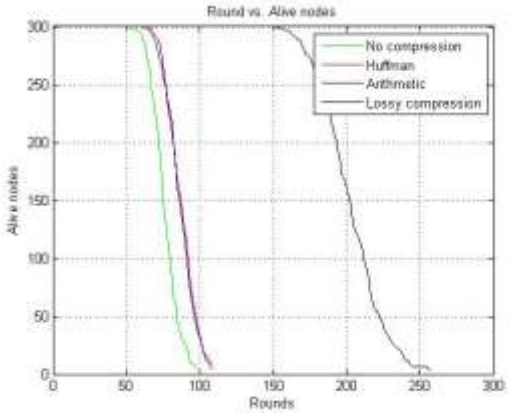

Figure 8: Number of rounds vs. number of alive nodes

V. Conclusion and Future work

In this project encryption is done so that the data will be more secured and to optimize energy various compression techniques and LEACH protocol has been applied. Here both lossless and lossy compression is done. We can see that more number of nodes is alive when the data is compressed. By these methods we can increase the life time of sensor nodes in wireless sensor network. There are many more issues to be resolved around energy management. By solving those we can reduce energy consumption of sensor nodes in wireless sensor networks. Particularly in the design of energy efficient protocol and its implementation has a significant scope.

REFERENCES:

[1]. Alba P.Sawlikar, Dr.Z.J.Khan & Dr.S.G.Akojwar "Power Optimization of Wireless Sensor Networks using Encryption and Compression Techniques" 2014 IEEE DOI 10.1109/ICESC.2014.43
[2]. C. M. Chao and Y. C. Chang "A power-efficient timing synchronization protocol for wireless sensor networks" Proc. Journal of Information Science and Engineering, pages 985-997.
[3]. IlkerDemirkol, CemErsoy, and FatihAlagöz, Bogazici University, "MAC Protocols For Wireless Networks: A Survey" IEEE Communications Magazine April 2006.
[4]. Kemal Akkaya and Mohamed Younis, "A Survey on Routing Protocols for Wireless Sensor Networks", Ad hoc Networks, vol. 3, no. 3, May 2005, pp. 325-349.
[5]. Rajashree.V.Biradar , S. R. Sawant , R. R. Mudholkar , V.C .Patil "Inter-Intra Cluster Multihop-LEACH Routing InSelf-Organizing Wireless Sensor Networks", International Journal of Research and Reviews in Computer Science (IJRRCS) Vol. 2, No. 1, March 2011
[6]. R. Ramanathan and R. Rosales-Hain, "Topology Control of Multihop Wireless Networks Using Transmission Power Adjustment," IEEE INFOCOM, 2000
[7]. J. M. Hellerstein and W. Wang, "Optimization of in-network data reduction," in DMSN Proceeedings of the 1st international workshop on Data management for sensor networks. NewYork, USA:ACM,2004, pp.40–47.
[8]. Energy-Efficient Data Acquisition in Wireless Sensor Networks Using Compressed Sensing" IEEE Conference, Date: 29-31 March 2011.
[9]. C.Karthik Sendhil Kumar, R.Sukumar and M.Nageswari "Sensors Lifetime Enhancement Techniques in Wireless Sensor Networks - A Critical Review"International Journal of Computer Science and Information Technology & Security (IJCSITS), ISSN: 2249-9555 Vol. 3, No.2, April 2013.
[10]. Oldewurtel, Frank and Mahonen, Petri, (2006) "Neural Wireless Sensor Networks", International Conference on Systems and Networks Communications, ICSNC '06, pp.28
[11]. Saraswathi.D.Joshi,V.R.Udupi & D.R.Joshi "A Image Encryption Decryption Using Advanced Encryption Standard" International Journal of Emerging Trends & Technology in Computer Science (IJETTCS) ISSN 2278- 6856 volume 3, Issue 3, May – June 2014
[12]. Y. Wang, G. Attebury, and B. Ramamurthy "A Survey of Security Issues in Wireless Sensor Networks" IEEE Communications Surveys & Tutorials, vol.8, no.2, pp. 2-23, 2006
[13]. Swati G Mavinkattimath and N S Sirdeshpande "Design and Implementation of a Private and Public Key Crypto Processor" IJEETC Vol. 2, No. 4, October 2013.
[14]. Neda Enami, Reza Askari Moghadam, Kourosh Dadashtabar & Mojtaba Hoseini "Neural Network Based Energy Efficiency In Wireless Sensor Networks: A Survey" IJCSES Vol.1, No.1, August 2010.
[15]. J S Rauthan and S Mishra "An improved Cluster Based Multi-hop Routing in Self- Organizing Wireless Sensor Networks" International Journal of Engineering Research & Technology (IJERT) Vol. 1 Issue 4, June – 2012

International Journal of Engineering Research and General Science Volume 3, Issue 3, Part-2 , May-June, 2015
ISSN 2091-2730

INTERLINE DYNAMIC VOLTAGE RESTORER FOR VOLTAGE SAG COMPENSATION USING SPWM TECHNIQUE

SMITHA SETHUMADHAVAN

smithamadhavan562@gmail.com

***ABSTRACT* :** The Dynamic voltage restorer [DVR], a custom power device has been used to protect sensitive loads from the effect of voltage sags /swells on the distribution feeder. The IDVR proposed in this paper provides a way to compensate the voltage sag caused in the power line. The main function is to inject the difference in voltage to the power line and thus maintain the load side voltage at the optimum value. This paper presents the modeling aspects of the IDVR system with the MLI working against voltage sags by simulation. The modelling and simulation of single phase IDVR using sinusoidal pulse width modualtion is presented.The digital simulation is carried out using MATLAB/SIMULINK. dc/dc converter is used to adjust the DC link voltage considering the amount of voltage sag so that the maximum possible output voltage levels are generated for a wide range of voltage sags.Closed loop control of voltage sag for simple IDVR system is modeled and simulated using MATLAB software.

Keywords- Powerquality, Interline Dynamic voltage Restorer[IDVR],Multilevel Inverter[MLI],Sinusoidal Pulse width modulation[SPWM],Total harmonic distortion[THD].

I. INTRODUCTION

A common characteristic of most electronics is that they are sensitive to voltage variations. Computers and other sensitive loads can lower their performance or even shutdown the process they are in control due to those variations. Voltage variations can be classified as disturbances that produce voltages below the nominal value, which are called voltage sags, and disturbances that produce voltages above the nominal value, which are called voltage swells.

Voltage sag is defined as a sudden reduction of supply voltage down 90% to 10% of nominal, followed by a recovery after a short period of time. Atypical duration of sag is 10ms to 1 minute. Voltage sag can cause loss of production in automated processes since voltage sag can trip a motor or cause its controller to malfunction. Voltage swell is defined as sudden increasing of supply voltage up 110% to180% in RMS voltage at the fundamental frequency with duration from 10ms to 1 minute. Switching off a large inductive load or energizing a large capacitor bank is atypical system event that causes swells. During power disturbances Dynamic Voltage Restorer (DVR) installed in front of a critical load will appropriately provide correction to that load only. Also DVR cannot provide compensation during full power interruptions. Voltage sag is a momentary decrease in RMS voltage lasting between half a cycle to a few seconds. It is generally caused by faults in the power system and is characterized by its magnitude and duration. Voltage sag magnitude is defined as the net RMS voltage during voltage sag, which is usually in per unit of the nominal voltage level. The voltage sag magnitude depends on various factors like the type of fault, the location of the fault and the fault impedance.

Voltage sag is most important power quality problems challenging the utility industry can be compensated and power is injected into the distribution system. By injecting voltage with a phase advance with respect to the sustained source-side voltage, reactive power can be utilized to help voltage restoration [1]. Dynamic Voltage Restorer, which consists of a set of series and shunt converters connected back-to-back, three series transformers, and a dc capacitor installed on the common dc link [3]. The Pulse-width modulation of Z-source inverter has recently been proposed as an alternative power conversion concept as they have both voltage buck and boost capabilities [4].The Z-source converter employs a unique X-shaped impedance network on its dc side for achieving both voltage-buck and boost capabilities this unique features that cannot be obtained in the traditional voltage-source and current-source converters. The proposed system is able to compensate long and significantly large voltage sags [2], [5] and [9].

Passivity-based dynamical feedback controllers can be derived for the indirect stabilization of the average output voltage. The derived controllers are based on a suitable stabilizing “damping injection” scheme [7]. Transformerless self-charging dynamic voltage restorer series compensation device used to mitigate voltage sags.

A detailed analysis on the control of the restorer for voltage sag mitigation and dc-link voltage regulation are presented [8]. Installation of the world's first Dynamic Voltage Restorer (DVR) on a major use. Utility system to protect a critical customer plant

load from power system voltage disturbances. The installed system at an automated yarn manufacturing and weaving factory provides protection from disturbances [10].

The modeling and simulation of ZSI based DVR is presented [11]and [13]. The modeling and simulation of IDVR is presented [12]and [15]. Simulation of MLI based DVR is presented in [16].In this paper the modeling and implementation of Multilevel inverter based dynamic voltage restorer for voltage sag compensation is presented. The simulation results are presented to show the effectiveness of the proposed control method.

II. INTERLINE DYNAMIC VOLTAGE RESTORER

The IDVR system consists of several DVRs in dif-ferent feeders, sharing a common DC-link. A two-line IDVR system shown in Fig.1 employs two DVRs are connected to two different feeders where one of the DVRs compensates for voltage swell/sag produced, the other DVR in IDVR system operates in power-flow control mode. The common capacitor connected between the two feeders act as the common DC suply.

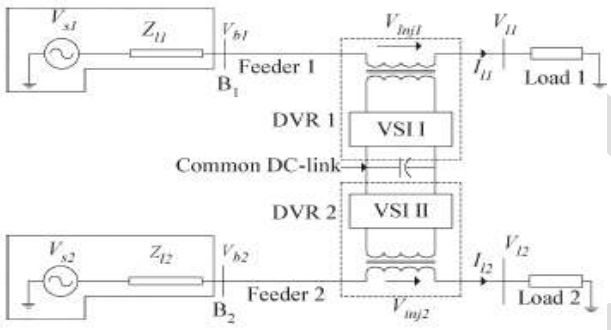

Fig.1. Schematic diagram of IDVR

Voltage swell/sag in a transmission system are likely to propagate to larger electrical distance than that in a distribution system. Due to these factors, the two feeders of the IDVR system in Fig.1 are considered to be connected to two different grid substations. It is assumed that the voltage distortion in Feeder1 would have a lesser impact on Feeder2. The upstream generation-transmission system is applied and the two feeders can be considered as two independent sources. These two voltage sources Vs1 and Vs2 are connected in series with the line impedances Zl1 and Zl2 which is in-turn connected to the buses B1 and B2 as in Fig. 1. The DVR is connected in series with the feeder and the DVRs across different feeders are connected by a common DC-link. The load across each feeder is connected in series to the DVR, where Vl1 and Vl2 are the voltages across the load.

The injection of an appropriate voltage needs a certain amount of real and reactive power which must be sup-plied by the DVR. Supply of real power is met by means of an energy storage facility connected in the DC-link. Large capacitors are used as a source of energy storage in most of the DVRs. Generally, capacitors are used to generate reactive power in an AC power system. However, in a DC system, capacitors can be used to store energy. When the energy is drawn from the energy storage capacitors, the capacitor terminal voltage decreases. Hence, large capacitors in the DC-link energy storage are needed to effectively mitigate voltage swell of large depths and long durations. The pulse can be generated using various modulation techniques. In this paper, the pulse for the switch is generated using SPWM.

III. VOLTAGE SAG COMPENSATION IN INTERLINE DYNAMIC VOLTAGE RESTORER USING SPWM TECHNIQUE

The IDVR system with two back-to-back connected DVR stations was implemented with a closed loop control of inverter switches. Fig.2 shows the Simulink model of the closed loop controlled IDVR.

The rectifier- inverter system is shown as a subsystem. The subsystem 1 consists of a full bridge inverter with a filter. Subsystem 2, shows the rectifier output voltage

The SPWM control technique is used to reduce the harmonic content in the output voltage. The driving sine pulses for the switches are shown in Fig.3.

Fig.4 (a) shows a 32.6 % voltage sag initiated at 300ms and it is kept until 600ms, with a total voltage sag du-ration of 300ms in low voltage feeder 1.

Fig.4 (b) and (c) show the voltage injected by the DVR 2 and the compensated load voltage respectively. Due to the presence of the IDVR, the load voltage remains constant throughout the voltage sag period.

Fig.5 shows the common DC link voltage waveform. Fig.6 shows the FFT analysis of the closed loop IDVR system for sag. The Total Harmonic Distortion (THD) value is 4.81%.

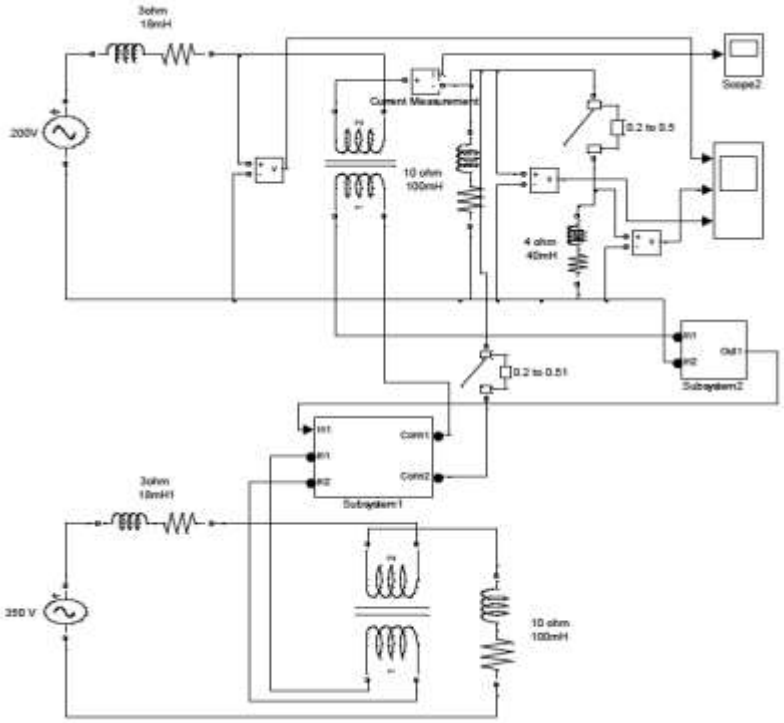

Fig.2 Simulation Circuit of IDVR

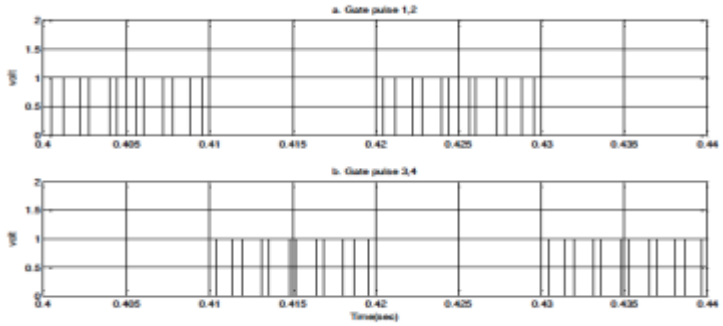

Fig.3 Driving pulses of inverter switches

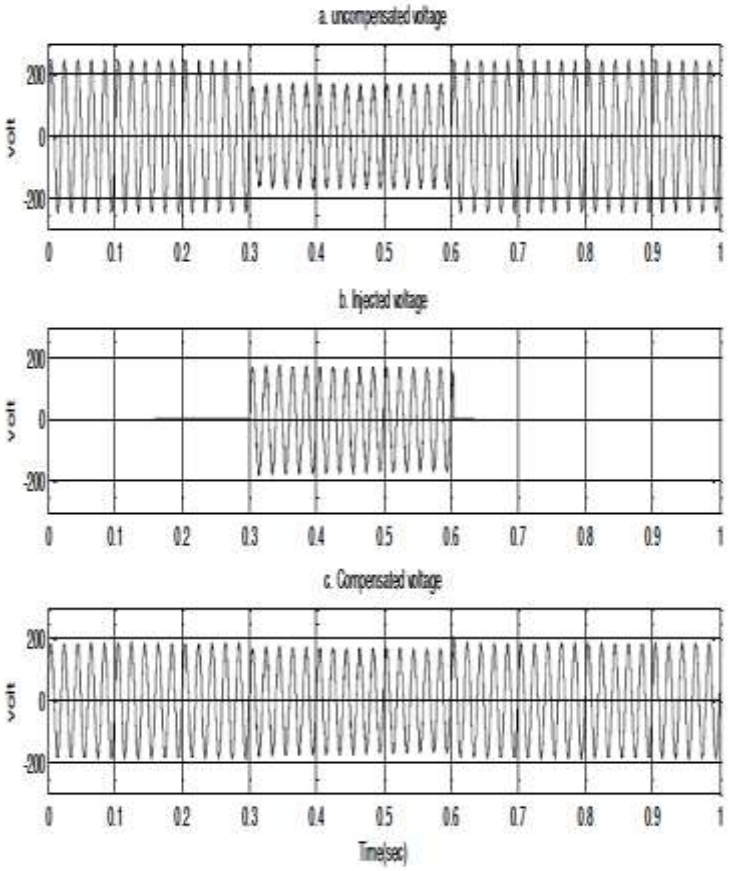

Fig.4 Response of IDVR to a voltage sag

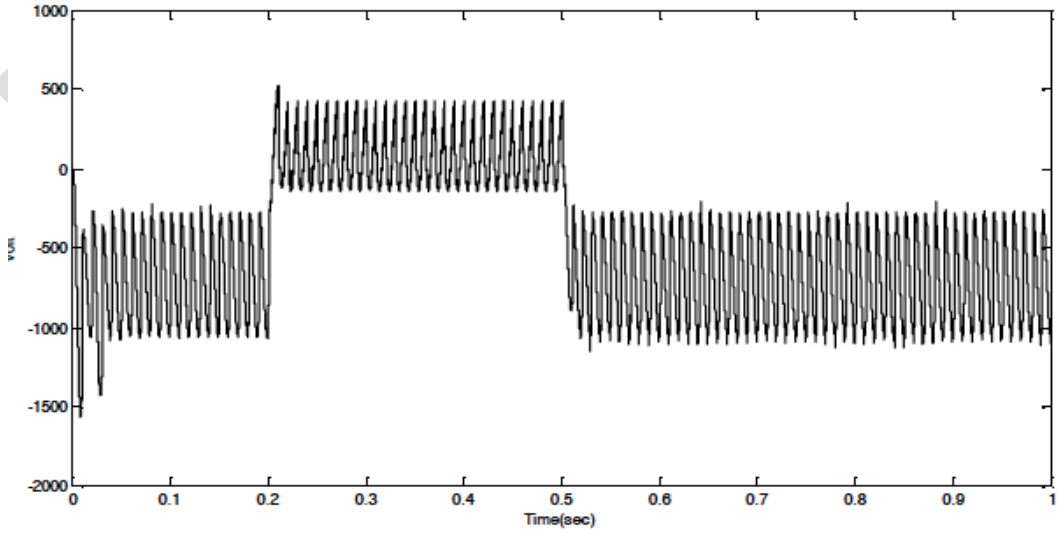

Fig.5 Common DC link voltage for sag

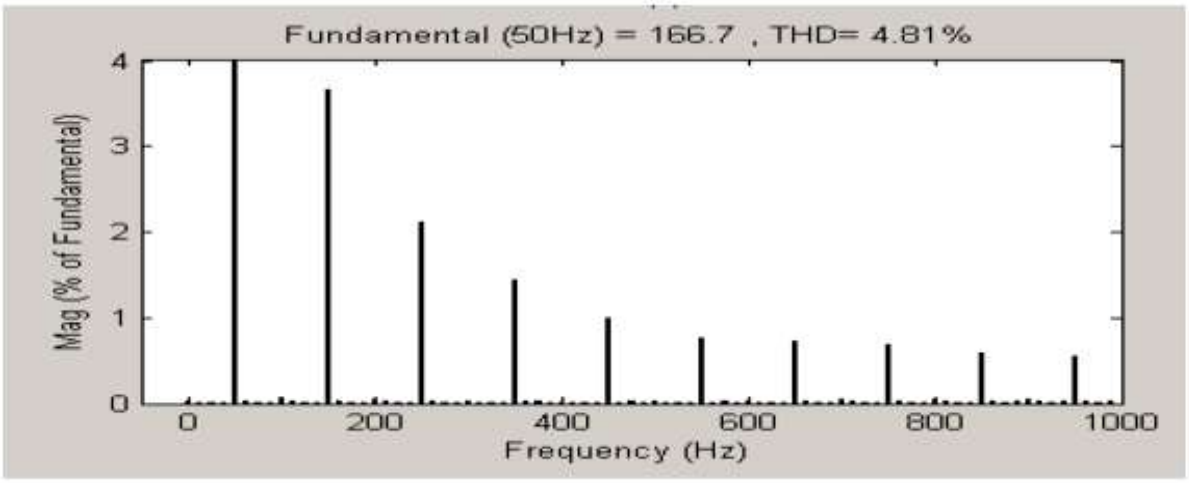

Fig.6 FFT analysis of IDVR for sag

IV. CONCLUSION

The simulink models of the closed loop controlled IDVR system with the H bridge inverter using SPWM technique for sag conditions are developed and the simulation results are presented The modelling and simulation of a IDVR system using MATLAB has been presented. IDVR is an effective custom power device for voltage sag mitigation. The impact of voltage sag on sensitive equipment is severe. Therefore, IDVR is considered to be an efficient solution due to its low cost, small size and fast response.The simulation results indicate that the implemented control strategy compensates for voltage sags with high accuracy. The results show that the control technique is simple and efficient method for voltage sag compensation.

REFERENCES:

Choi S. S, Li B. H, and Vilathgamuwa D. M (2000) "Dynamic voltage restoration with minimum energy injection," IEEE Trans. Power Systems, vol. 15, pp. 51-57.

Gajanayake C. J, Vilathgamuwa D. M, and Loh P. C (2005) "Small-signal and signal-flow-graph modeling of switched Z-source impedance network," IEEE Power Electronics Letters, vol. 3, pp. 111-116.

Jimichi T, Fujita H., and Akagi H. (2005) "Design and experimentation of a dynamic voltage restorer capable of significantly reducing an energystorage element," in Conf. Record Industry Applications Conference,14th IAS Annual Meeting..

Loh P. C, Vilathgamuwa D. M, Lai Y. S, Chua G. T, and Li Y (2004) "Pulse-width modulation of Z-source inverters," in Conf. Record IEEE Industry Applications Conference, 39th IAS Annual Meeting.

Peng F. Z. (2003) "Z-source inverter," IEEE Trans. Industry Applications, vol.39, pp. 504-510.

Samra N. A, Neft C, Sundaram A, and Malcolm W (1995) "The distribution system dynamic voltage restorer and its applications at industrial facilities with sensitive loads," in Proc. Power Conversion Intell. Motion Power Quality Long Beach, CA.

Sira-Ramirez H and Ortega R (1995) "Passivity-based controllers for the stabilization of DC-to-DC power converters," in Proc. 34th IEEE Conference on Decision and Control.

Sng E. K. K, Choi S. S, and Vilathgamuwa D. M (2004) "Analysis of series compensation and DC-link voltage controls of a transformerless selfcharging dynamic voltage restorer," IEEE Trans. Power Delivery, vol.19, pp. 1511-1518.

Torabzad S, Babaei E, Kalantari M (2010) "Z-Source Inverter based Dynamic Voltage Restorer" 1st Power Electronic & Drive Systems & Technologies Conference.

Woodley N. H, Morgan L, and Sundaram A (1999) "Experience with an inverter-based dynamic voltage restorer," IEEE Trans. Power Delivery, vol. 14, pp. 1181-1186.

Usha Rani P. and Rama Reddy S. (2011), 'Digital Simulation of an Interline Dynamic Voltage Restorer for Voltage Compensation', International conference on Computer, Communication and Electrical Technology ICCCET 2011, 18th& 19th March 2011, National College of Engineering, pp. 133-139 (IEEE Xplore 978-1-4244-9391-3/11)

Usha Rani P. and Rama Reddy S. (2011), 'Modeling and Simulation ZSI based DVR for voltage compensation', International conference on Computer, Communication and Electrical Technology ICCCET 2011, 18th& 19th March 2011, National College of Engineering, pp. 90-96 (IEEE Xplore 978-1-4244-9391-3/11)

Usha Rani P. and Rama Reddy S. (2011), 'Voltage sag / swell compensation in an interline dynamic voltage restorer', International conference on Emerging Trends in Electrical and Computer Technology, ICETECT 2011, 23rd& 24th March 2011, St. Xaviers Catholic College of Engineering, pp. 309-314 (IEEE Xplore 978-1-4244-7925-2/11)

Usha Rani P. and Rama Reddy S. (2011), 'Voltage sag / swell compensation using Z-source inverter based dynamic voltage restorer', International conference on Emerging Trends in Electrical and Computer Technology, ICETECT 2011, 23rd& 24th March 2011, St. Xaviers Catholic College of Engineering, pp. 268-273 (IEEE Xplore 978-1-4244-7925-2/11)

Usha Rani P (2013), 'Voltage Swell Compensation in an Interline Dynamic Voltage Restorer', Journal of Scientific and Industrial Research, -Accepted for publication-JSIR-5101-Ref.MSS/Rev/JSIR-5101 21.06.2013

Ebrahim Babaei and Mohammad Farhadi Kangarlu (2011)"A new scheme for MLI based DVR", International Conference on Electrical machines and systemsICEMS,PP1-6

International Journal of Engineering Research and General Science Volume 3, Issue 3, Part-2 , May-June, 2015
ISSN 2091-2730

A Z Source Half Bridge Converter for Electrochemical Power Supply

Reeto Jose K, Anisha Shivanandan, Vani Venugopal

PG Students (Power Electronics)Department of EEE, Vidya Academy Of Science And Technology Thrissur, Kerala, India

retokj@gmail.com

Abstract—One LC network is used for obtaining a power supply, which used as electrochemical power supply. Z source is connected in between the source and the load. It can generate various output voltage such as varied positive voltage or the negative voltage and varied time ratio between positive voltage and negative voltage. By using this type of power supply plating should be uniform and reduces the plating time. This converter is derived from the conventional half bridge converter. For getting this type of power supply duty of one switch is fixed as greater than 0.5. It can avoid the shoot through problem. Proposed converter is reduces the size, complexity and cost. It is more efficient than the other converters. Finally, the novel converter is simulated by using MATLAB/Simulink.

Keywords—LC network, shoot through, electro chemical supply, half bridge converter

INTRODUCTION

Conventional converters are voltage source and current source converters. In voltage source converters act as buck converter for dc-ac power conversion and act as boost converter for ac-dc power conversion. So additional boost converter is needed for desired output voltage. Thus system cost is increases and efficiency is reduces. Because of the presence of shoot through problem there is a chance for destroying the devices. In current source converter is act as boost inverter for dc-ac power conversion and act as buck converter for ac-dc power conversion. So additional boost converter is required for required output voltage. This will increases the system cost and reduces the efficiency. Shoot through problem will destroy the devices. The voltage source converter cannot be used as the current source and vice versa. Both the converters are vulnerable to EMI noise in terms of reliability[1],[5].In order to overcome these problems, introducing new topology is called as z source topology. It has unique impedance circuit to couple the converter main circuit to power source and the load. It has X shaped structure consist of two inductors and two capacitors. The shoot through zero state provides buck boost features to the inverter[6],[7].

Half bridge converter is consist of two switches which are connected in series.so there is a chance for shoot through problem which leads to breakdown of the switch. Large ripples making the system unstable. The novel converter is consist of Z source converter is placed in between the supply and the load. The novel converter solve the limited voltage problem and the unbalanced midpoint voltage problem. Conventional electro chemical supply is the dc supply[8]. The main disadvantage of using dc supply is first the electrode should be clean at the starting of plating, for that we have to reverse the supply. In order to get the smooth electroplating product current direction and the density should be varied according to the electroplating technology. Traditionally several cascaded circuit and the complex circuit is used for getting the multi output voltages[2],[8],[9],[10],[11].This increases the cost ,size and instability of the system.

PROPOSED CONVERTER

Proposed converter consisting of half bridge converter is placed in between the source and the load as shown in Fig.1. The source is either AC or DC. If AC supply is using, converted this into DC by an uncontrolled rectifier. The working principle of both is same. The diode D is used for preventing the current from back to the source[12]. The inductor is used in order to avoid strong current when the switches are in the shoot through mode.

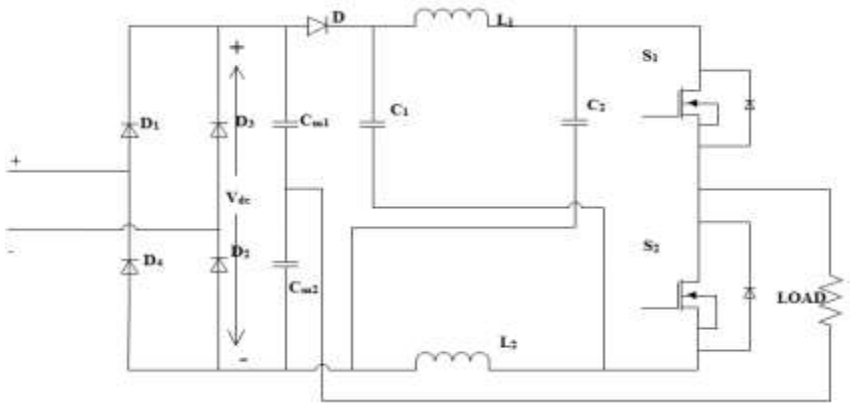

Figure 1. Proposed Converter

Some assumptions are considered for the working of the proposed converter.L_1=L_2,C_1=C_2=C_{m1}=C_{m2},All the components are ideal.

Here duties of switches are D_1 and D_2 by switches S_1 and S_2 respectively. D_1 =0.7and D_2=0.5

There are 3 modes of operations[3].

Mode 1:It is a shoot through state as shown in Fig.2. The capacitor C_1 and C_2 discharges the energy to the inductor. The diode D became reverse biased. According to the loop C_2-Load-C_{m2} the output voltage of the converter is taken as

$$V_0 = V_{c2} - V_{cm2} \qquad (1)$$

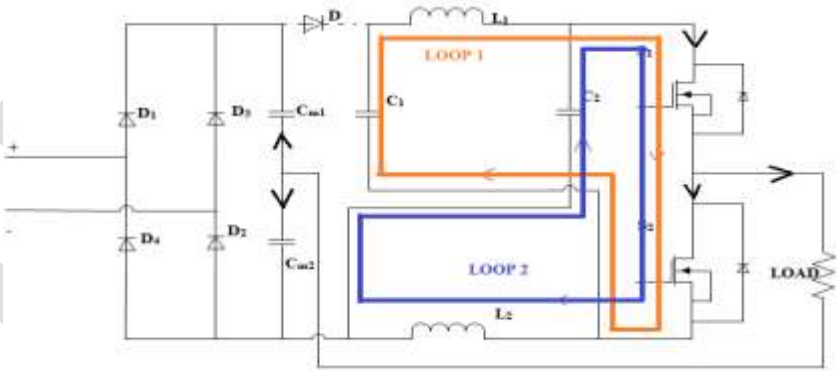

Figure 2. mode 1:S_1 and S_2 is ON

Mode 2:In loop 1,L_1 discharges the energy to C_2.

$$V_{L1} = V_{dc} - V_{c2} \qquad (2)$$

In loop 2 L_2 discharges the energy to C_1 as shown in Fig.3.

$$V_0 = V_{c2} - V_{cm2} \qquad (3)$$

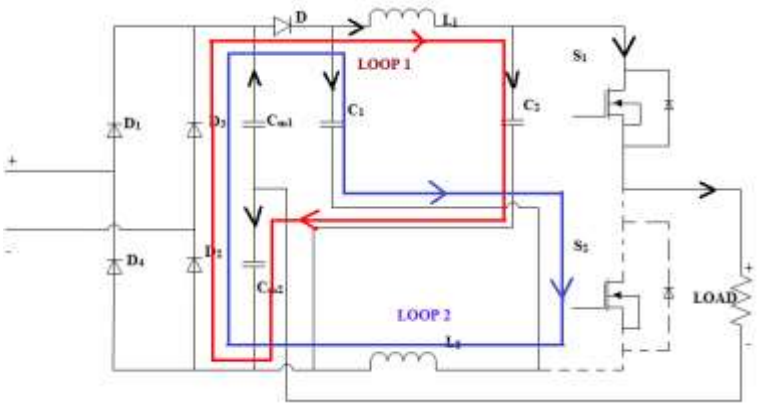

Figure 3. mode 2: S_1 ON and S_2 OFF

Mode 3:voltage across the C_2 is increases because L_1 discharges the energy to the C_2. voltage across the C_1 is increases because L_2 discharges the energy to the C_1.From the loop V_{in}-D-C_1-Load-C_{cm2},the output voltage is

$$V_0 = V_{in} - V_{c1} - V_{cm2} \qquad (4)$$

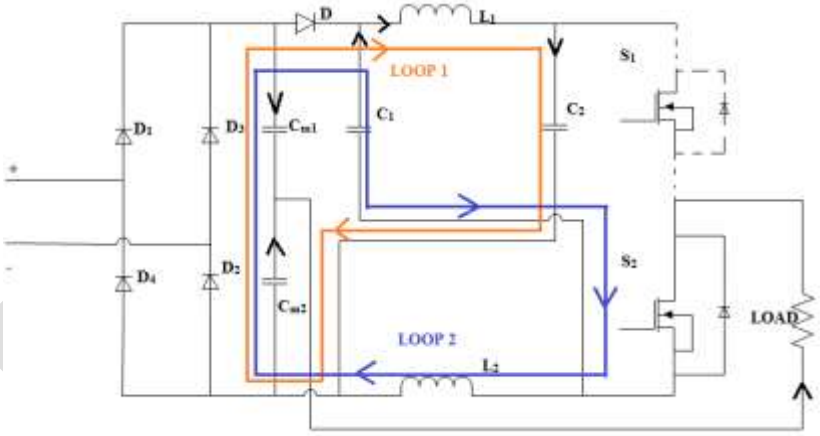

Figure 4. mode 3:S_1 OFF and S_2 ON

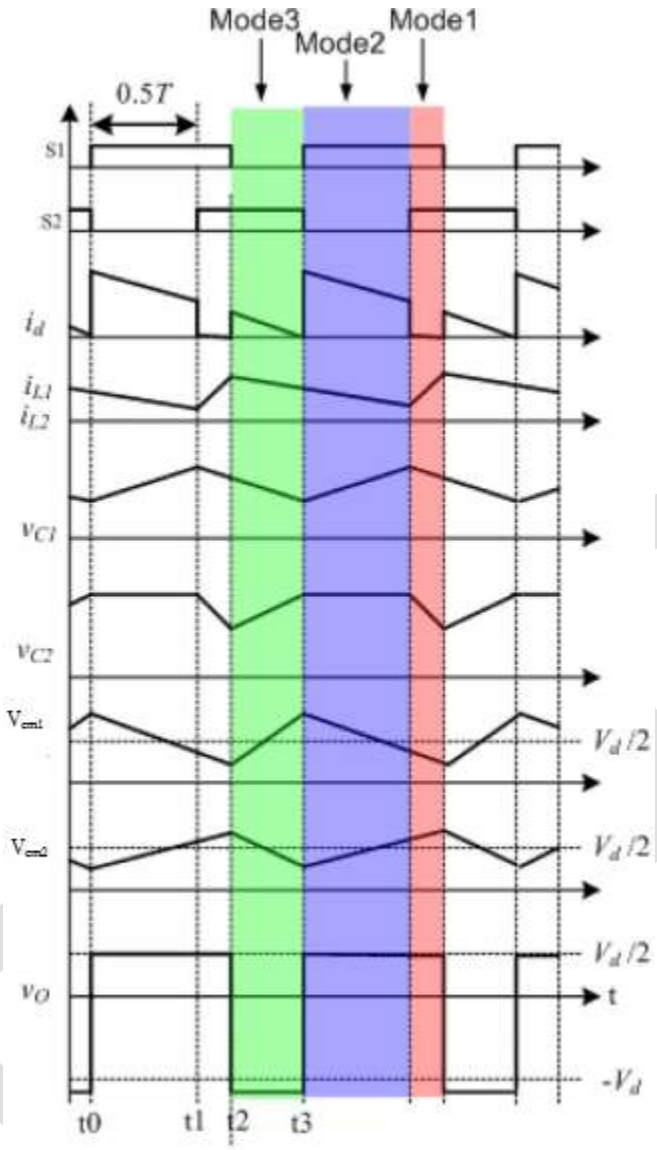

Figure 5. Waveforms of z source half bridge converter

PARAMETER DESIGN

In this section designing the inductance and the capacitance.

In the design section input is taken as the dc (V_{dc}) supply.

A. Design of the capacitor

Determine the voltage second characteristics of L_1,

$V_{c1}=V_{c2}=(2 – D_1 – D_2)V_d/(3 − (D=1 + D_2))$ (6)

$V_{cd2}= (2V_{c2}− V_d)D_1 – V_{c2} + V_d.$ (7)

Positive output voltage of the converter is obtained from the equation (3).

$V_p=\{(1 – D_1)V_d \}/\{3− 2(D_1 + D_2)\}$ (8)

Negative output voltage of the converter is

$V_n=− \{D_1V_d\}/\{3-2(D_1+D_2)\}$ (9)

From (6),(8) and (9)

When S_1 is on $V_{c2}=\{2-D_1-D_2\}V_0/\{1-D_1\}$ (10)

When S_2 is on and S_1 is off $V_{c2}=\{2-D_1-D_2\}V_0/\{-D_1\}$ (11)

The current through the I_{c2} and I_{L2} is $I_0/2$

Differential equation of the capacitor is

$C_2=I_{c2}dt/dvc_2$ (12)

$dt=\{D_1+D_2-1\}T$ (13)

$dvC2 = x_c\%V_{c2M}$ (14)

$X_c\%$ is the permitted fluctuation range.V_{c2M} is the maximum rated voltage of C_2.

Substituting equation (13) and (14) into (12)

$C_2 =\{Io(D_1 + D_2 - 1)T\}/\{2X_c\%V_{c2M}\}$

B. Design of the inductor

C. Differential equation of the inductance is

$V_{L2}=V_{L2}dt_L/di_{L2}$ (15)

$di_{L2}=X_L\%I_{L2}$ (16)

$V_{L2M}=V_{c2M}$ (17)

Substituting (13),(16) and (17) into (15) leads to

$L_2=\{_{2Vc2M}(D_1 + D_2 - 1)T\}/\{X_L\%I_0\}$

SIMULATION RESULT

Simulation parameters for the proposed converter and its values are given in the table 1.

Table 1. Simulation parameters and values

Parameters	Values
V_{in}	0.24
D_1,D_2	0.7T,0.5T

L_1,L_2	100µH
C_1,C_2,C_{m1},C_{m2}	470µF

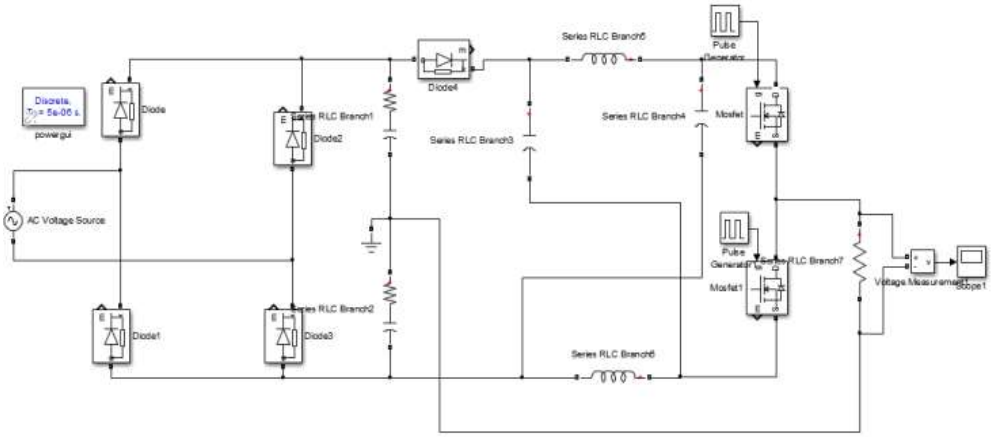

Figure 6. Simulation diagram of proposed converter

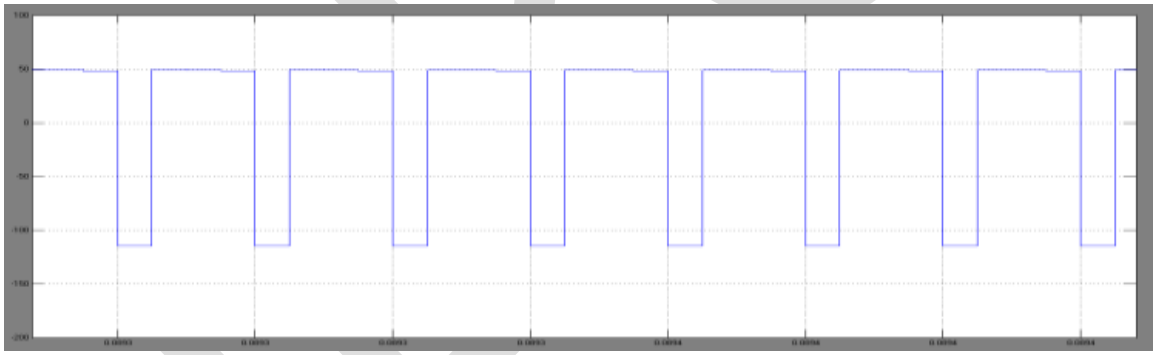

Figure 7. output waveform

CONCLUSION

The z source half bridge converter can be used for electrochemical supply when the duty of the switch S_1 is greater than 0.5T.Either dc or ac supply can be used as the input supply. By using this supply, get smooth electroplating product and plating time can be reduced. Novel converter is remove the all the drawbacks of conventional electrochemical supply. Efficiency and stability of the system is greater as compared to conventional one. The proposed converter is reduces the cost as the traditional one. Novel converter can solve the limited voltage problem.

REFERENCES:

[1] F. Z. Peng, "Z-source inverter," *IEEE Trans. Ind. Appl.*, vol. 39, no. 2,pp. 504–510, Mar./Apr. 2003. 1998.
[2] R. Caves. W.M Zhang,M.H Deng,Y.Q Pei and Z.A Wang,H. "Design and optimization of high current power supply for electrochemistry".in Proc.IPEC,2010,pp.86-91
[3] Guidong Zhang, Zhong Li, Bo Zhang,Dongyuan Qiu, Wenxun Xiao, and Wolfgang A. Halang "A Z-Source Half-Bridge Converter" IEEE Trans on industrial electronics,Vol. 61, no.3,March 2014.
[4] Muhammad H Rashid,Power Electronics,Devices, and Apllications, Third Edition.Pearson Publications.

[5] B. Zhao, Q. G. Yu, Z. W. Leng, and X. Y. Chen, "Switched Z-source isolated bidirectional DC–DC converter and its phase-shifting shoot through bivariate coordinated control strategy," *IEEE Trans. Ind. Electron.*, vol. 59, no. 12, pp. 4657–4670, Dec. 2012.
[6] Y. C. Hung, F. S. Shyu, C. J. Lin, and Y. S. Lai, "New voltage balance technique for capacitors of symmetrical half-bridge converter with current mode control," in *Proc. PEDS*, 2003, pp. 365–369.
[7] D. Boroyevich, D. Zhang, and P. Ning, "A shoot-through protection scheme for converters built with SiC JFETs," *IEEE Trans. Ind. Appl.*, vol. 46, no. 6, pp. 2495–2500, Nov./Dec. 2010.
[8] W. M. Zhang, M. H. Deng, Y. Q. Pei, and Z. A. Wang, "Design and optimization of high current power supply for electrochemistry," in *Proc. IPEC*, 2010, pp. 86–91.
[9] P. J. Stout and D. Zhang, "High-power magnetron Cu seed deposition on 3-D dual inlaid features," *IEEE Trans. Plasma Sci.*, vol. 30, no. 1, pp. 116- 117, Feb. 2002.
[10] X. Hu, Z. Y. Ling, X. H. He, and S. S. Chen, "Controlling transmission spectra of photonic crystals under electrochemical oxidization of aluminum," *J. Electrochem. Soc.*, vol. 156, no. 5, pp. C176–C179,2009.
[11] X. Hu, Z. Y. Ling, T. L. Sun, and X. H. He, "Tuning optical properties of photonic crystal of anodic alumina and the influence of electrodeposition,"*J. Electrochem. Soc.*, vol. 156, no. 11, pp. D521–D524, 2009.
[12] B. M. Ge, Q. Lei, W. Qian, and F. Z. Peang, "A family of Z-source matrix converters," *IEEE Trans. Ind. Electron.*, vol. 59, no. 1, pp. 35–46,Jan. 2012

International Journal of Engineering Research and General Science Volume 3, Issue 3, Part-2 , May-June, 2015
ISSN 2091-2730

A NOVEL APPROACH TO INCREASE CONFIDENTIALITY OF DATA USING PICTURE KEY ENCRYPTION

1Ishu Saini, 2Rajiv Mishra

1M. tech. student, CBS group of institution, Jhajjar, Haryana; isstranger77@gmail.com

2A.P. in CSE deptt, CBS group of institution, Jhajjar, Haryana; mishrarajiv99@gmail.com

Abstract— Diffie and Hellman first formulated key exchange algorithm. Man in the middle attack is major weakness of this algorithm. In this paper we propose PicPass protocol, picture is used as a password to make an agreement between two parties. The PicPass protocol having two function i.e. picture function as well as distortion function is used to make picture in a compact size and then it is sent to receiver. In this paper, a new technique is used i.e. picture is used as a password instead of text to authenticate key exchange between two parties so that they can communicate confidentially. It also gives practical solution against offline dictionary attacks by using both private and public key cryptography.

Keywords— Key Exchange, Protocol, Cryptography, Authentication, Confidential, Secret Picture , Covered Picture, Key Picture.

Introduction

Symmetric key cryptography is also called as secret key cryptography or private key cryptography.in this a single key is used for both encryption and decryption of messages between sender and receiver. It is also known as secret key as there is only single key between two of them and it must be kept secret to maintain the security of communication. Both parties must decide a single key and carry out transmission and it must not be known to others. At sender end the plain text get converted to cipher text using this key and reverse action is performed at another end. In this way original message is received by the receiver.[7]

But this algorithm suffers from a major problem of key exchange under the practical environment which is the agreement of key between the two parties? Two conventional solutions are handing over physically and over the courier. But these methods are totally irrelevant as the person could exchange message too via this and they are highly prone to attacks. A third way is to transmit the key over the same network along with acknowledgement from other side. But then, if it is intercepted by any intruder then the security breach occurs. Second problem is in case of broadcast we require a lot of key pairs and key ring gets very large. Also this problem is equally difficult as the same key is used for encryption and decryption per party.[1,4]

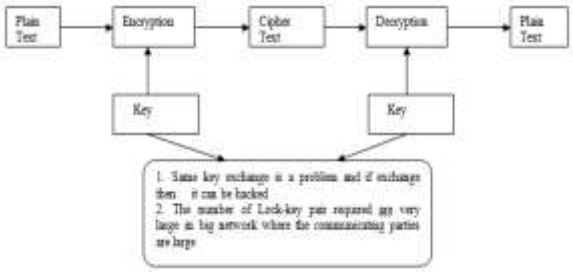

Figure 1 Key Exchange Problem [2]

Previous work: LDH proposed a key exchange protocol which is password based in which sender and receiver can authenticate one another to generate a very strong session key using a shared password over a medium which is not secure. A special function is used by having distortion and picture subroutines used as password in order to save password from offline dictionary attack. We used picture as password in place of text making it less exposed to attacks and hence more secure. Diffie and Hellman [6] first formulated

key exchange algorithm. Man in the middle attack is major weakness of this algorithm. In order to tackle this problem, another algorithm that uses text password for the agreement between two parties is proposed by Seo. [3] But again this algorithm (password) suffers another problem i.e. Offline dictionary attack. Secure protocol designing is still a major problem due to availability of offline dictionary attacks. Laih et. Al. suggested a key establishment protocol which is based on password in order to resolve the problem. The protocol is different from several others proposed protocols as it doesn't use public key and it uses special function $\varphi(r, s)=g(p(r, s))$,where g stands for distortion function, s is input argument which is random and p stands for picture function . In PicPass protocol, picture is used as a password to make an agreement between two parties. The PicPass protocol having two functions i.e. picture function as well as distortion function is used to make picture in a compact size and then it is sent to receiver.

II. Pic Pass Protocol

Encryption Steps:-

- Encryption of plain text that is to be send by the sender using encryption from secret picture which is actually sender's private key and thus generating cipher text using DES.
- Further, it will carry out the process on secret picture by the use of covered picture which is receiver's public key and thus encrypting with Rivers Shamir Adleman algorithm i.e. RSA.
- A digital envelope is sent to receiver having cipher text and picture so encrypted.

Decryption Steps:-

- Digital envelope will reach receiver's side.
- Digital envelope will be opened to get encrypted picture and decrypt using its own private key with RSA algorithm and receiver get secret picture.
- IP Filter would be applied to enable only authentic system to Decrypt the cipher text

  Jave code to validate IP would be as follow:

```
int flag=0;
try
{
Enumeration e = NetworkInterface. getNetworkInterfaces();
while(e.hasMoreElements())
{
NetworkInterface n = (NetworkInterface) e.nextElement();
   Enumeration ee = n.getInetAddresses();
   while (ee.hasMoreElements())
```

```
        {

    InetAddress i = (InetAddress) ee. nextElement();

        // System.out.println(i.getHostAddress());

        if(i.getHostAddress().equals("1.0.0.1"))

        flag=1;

       }}}

    catch(Exception e)

    {}

        if (flag==1)

        {

        //Decryption would be implemented

        }

        else

        {

        System.out.print("Invalid Ip");

        }}
```

- Cipher text will be changed using plane text using secret picture applying DES.
- Thus receiver will get the plain text.

III **ASSESSMENT BENEFITS**

The proposed protocol when implemented using java language is found to be protected from the above different attacks in the manner as:-

- **Offline Dictionary attack:-**The proposed protocol is safe from offline dictionary attack as we have not used any text or number key to encrypt and lock the plain text. We are using PNG images for our algorithm to take place and predicting of plain text from picture makes the life of a hacker uneasy as compared to let approach.[5]
- **Modification Attack:-** The protocol is safe from active attack because according to algorithm we have encrypted the data using picture and picture encryption increases the confidentiality of the original message a lot. The increase in confidentiality normally reduces the chance of modification attack.
- **Man-in Middle attack: -** The above protocol is safe from the man-in-middle attack as after the encryption. While comparing our Pic-Pass algorithm with other algorithm proposed earlier against various attacks the result is as displayed in the table 1.

	Replay Attack	Modification Attack	Offline Dictionary attack	Man-in middle attack
Diffie-Hellman Protocol	No	Yes	No	Yes
Seo-Sweeney Protocol	Yes	No	Yes	No
Tseng's Protocol	Yes	Yes	No	No
PicPass Protocol	No	No	No	No

Table 1 the Strength of the Protocols Against Some Known Attacks

IV Simulation results

When simulated in java programming language the proposed methodology i.e. Pic-Pass algorithm gives the following results (text encryption results for the similar simulation environment I also shown):

Size in bytes	Time1(Text Encryption)	Time2(Picture Encryption)
33776	31	110
39127	31	124
50593	47	125
65964	47	140
77334	78	125
139864	78	109
151642	78	105
160824	93	102
177543	93	99
188972	93	96
249876	101	96
280908	115	95
295408	140	93
307608	150	90
322567	160	88

Table 2 Time (ms) Taken by Text Encryption vs PicPass Encryption

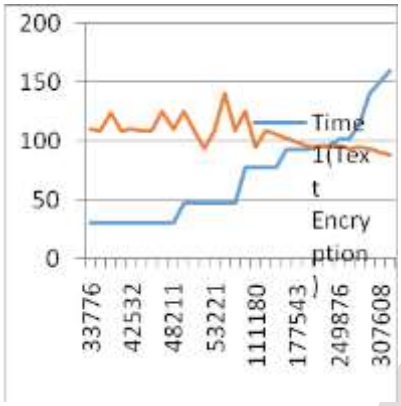

Figure 2 Analysis of Text Encryption vs PicPass Encryption

V. CONCLUSION AND FUTURE SCOPE

In this paper we proposed a new technique for authentication i.e. picture-password based key exchange algorithm instead of text password using both private and public key cryptography. This proposed protocols overcome the problem of offline dictionary attack from which Seo and Sweeny protocol suffers. After a certain calculation we can conclude that the PicPass algorithm is 55% better as compared to Text encryption. Moreover the simple text encryption/decryption suffers from the problems such as confidentiality, authentication and integrity i.e. the main attack is Man-in-Middle attack. But our proposed algorithm PicPass provides the solution of many attacks. The problem of key agreement is not fully solved. In particular, it has not yet been solved for two new users who want to communicate electronically. Some of the existing protocol solve the problem but not fully satisfactory.

REFERENCES:

1. David Pointcheval, *Password-based Authenticated Key Exchange.* (21-23 may 2012, Darmstadt, Germany)Springer-Verlag, LNCS 7293, pages 390-397.
2. David Pointcheval, Michel Abdalla, *Contributory Password-Authenticated Group Key Exchange with Join Capability*, (February 14-18, 2011, San Francisco, CA, USA), A. Kiayias Ed. Springer-Verlag, LNCS 6558, pages 142-160.
3. Seo, D.H., Sweeney, P., 1999, Simple authenticated key agreement algorithm, *Electronics. Letters* 35 (13) pp. 1073–1074.
4. [31] Diffie, W., Oorschot, P.C.V., Wiener, M.J., 1992, Authentication and authenticated key exchanges, *Des. Codes Cryptography*, 2, pp. 107-125
5. [32] Bellovin, S., Merritt, M., 1992, Encrypted key exchange: password-based protocols secure against dictionary attacks, in: *IEEE Symposium on Security and Privacy*, pp. 72–84.
6. [33] Diffie, W., Hellman, M.E., 1976, New directions in cryptography, *IEEE Trans.*, IT-22, (6), pp.644-654.
7. Crptography concepts, URL: http://en.wikipedia.org/wiki/private key crptography

International Journal of Engineering Research and General Science Volume 3, Issue 3, Part-2 , May-June, 2015
ISSN 2091-2730

A TAGUCHI APPROACH FOR OPTIMIZATION OF PROCESS PARAMETERES IN THERMOACOUSTIC REFRIGERATION

Shankar Kadam[1] Ravindra Edlabadkar[2] Dhnyanesh Kumbhar[3] Satish Kadam[4]

[1](M.Tech. Scholar, Mechanical Engineering Department, BVCOE, Pune, India
Email-id:kadamshankar16@gmail.com)

[2](M.Tech. Scholar, Mechanical Engineering Department, BVCOE,Pune, India
Email-id:dredlabadkar@gmail.com)

[3,4](Associate Professor, Mechanical Engineering Department, BVCOE,Pune, India
Email-id:dgkumbhar@bvucoep.edu.in)

Abstract- In TAR, pressure wave acoustic energy is converted into thermal energy, without any frictional energy losses. The objective of the study showcased here is to optimize the process parameters viz. stack position, stack material, frequency and acoustic wave type involved in TAR, using the Taguchi approach. An experimental set up is developed. Optimum combination is developed by the Taguchi approach over the results of experiments performed on the experimental set up. Optimized parameters given by the Taguchi approach are: stack position 150 mm, stack material glass fibre stack with capillary tube spacers, 350 Hz acoustic sine wave.

Keywords- TAR (TAR), Taguchi Approach, Process parameters, Stack, Acoustic wave frequency**.**

1. INTRODUCTION

Thermoacoustic refrigeration (TAR) is a technique of generating temperature difference across a thermoacoustic stack using acoustic energy, without the need of eco-sensitive refrigerants or use of moving parts. This heat pumping systems is beneficial over conventional systems. It uses environmentally safe working fluids, no seals, lubrication, frictional losses, facilitates cheap analogue control and design. TAR uses acoustic energy to generate cooling effect. It has sound source attached to an close ended resonator tube filled air, porous stack and two heat exchangers across the stack. The stack, the most vital component of TAR devices, is placed inside the resonator between pressure antinode and velocity antinode of the acoustic wave. The stack material should have low thermal conductivity and higher heat capacity than fluid, as it allows steady thermal gradient across the stack walls. The stack and resonator material should be strong enough and of low thermal conductivity to withstand higher pressure and prevent heat leakage.

The acoustic wave from an acoustic driver makes the gas resonant. The oscillating standing sound wave creates a temperature difference across the length of the stack because of compression and expansion of gas and facilitates heat exchange between fluid and stack[1]. The heat exchangers exchange heat with the surroundings at the cold and hot sides of the stack. The basic parameters affecting the performance of TAR are well under stood.[3]

Nsofor and Ali [2] studied the performance of TAR system of aluminum resonator tubing lined with plastic tubing by changing the frequency, load and pressure. Kartik M. Trivedi[6] studied the effect of thirteen various stack positions on performance of TAR. Thus it is inferred that stack positioning affects the temperature difference across stack ends. Mohammed Awwad Ali [4] undertook a 2D computational simulation of TAR. It identified the optimized parameters for TAR from the study.

Experiments were conducted by Giulio Allesina [5] varying the stack material, Stack geometry to analyze the performance of TAR. He used spiral and parallel stack geometries and conclude that parallel plate stack gives better result than the spiral stack, but parallel plate stack is difficult to manufacture.

The literature referred so far relates to the basic principles and performance augmentation of TAR and the authors came across no literature that specifies design of TAR using Taguchi approach. Therefore, the present study aims to find the optimum input parameters of standing wave TAR using air as a working fluid by Taguchi method. The most vital parameters influencing performance of TAR are frequency, stack position, stack material, and acoustic wave type. Using Taguchi method, the most productive optimum combination is obtained and investigated. The experimental setup of TAR has been developed using values generated from Taguchi for the desired output of temperature difference. Experiments are performed and the results are presented in this paper

2. EXPERIMENTAL SETUP

Figure 1 shows a schematic diagram of the TAR. It consists of an acoustic driver (speaker) which is connected to the resonator through a diverging conical adiabatic member (funnel). The stack is placed at appropriate position inside the resonator with two thermocouples across it for temperature measurement. These stacks forms different configurations and are made from Glass capillary tubes, Glass fibre with capillary spacers and Glass fibre with Nylon spacers. The capillary tubes and spacers are rolled into a bundle with outside diameter just abutting to inside diameter of the Glass resonator tube. The various configurations pertaining to stack material, stack position, frequency and type of acoustic wave are given in the table. Calibrated K type thermocouples and Digital Temperature Indicator are used to measure temperature at hot and cold end of the stack as well as atmospheric temperature. Electrical

power input to the speaker is measured using calibrated Ammeter and Voltmeter. The standard frequency generator is put to use and the pressure variations in the resonator tube at appropriate locations are measured using Pressure transducers.

2.1 Stack

The stack is used to convert acoustic power into heat, the amount of acoustic power that can be converted into heat depends on certain features of the stack like material properties, stack dimensions and the position of the stack in the resonator. Figure 2 shows a stack. The stack material should have a high heat capacity and low thermal Conductivity along resonator axis. The length is important for the temperature gradient. The length and cross-Sectional area of the stack determine how much the sound waves are intercepted. We have used three stack configurations viz. Glass capillary tube stacks, Glass fibre with nylon spacers and Glass fibre with glass capillary spacers. The thermal conductivity of the stack is taken as 1.25 W/mK. Figure 2 shows these different stacks.

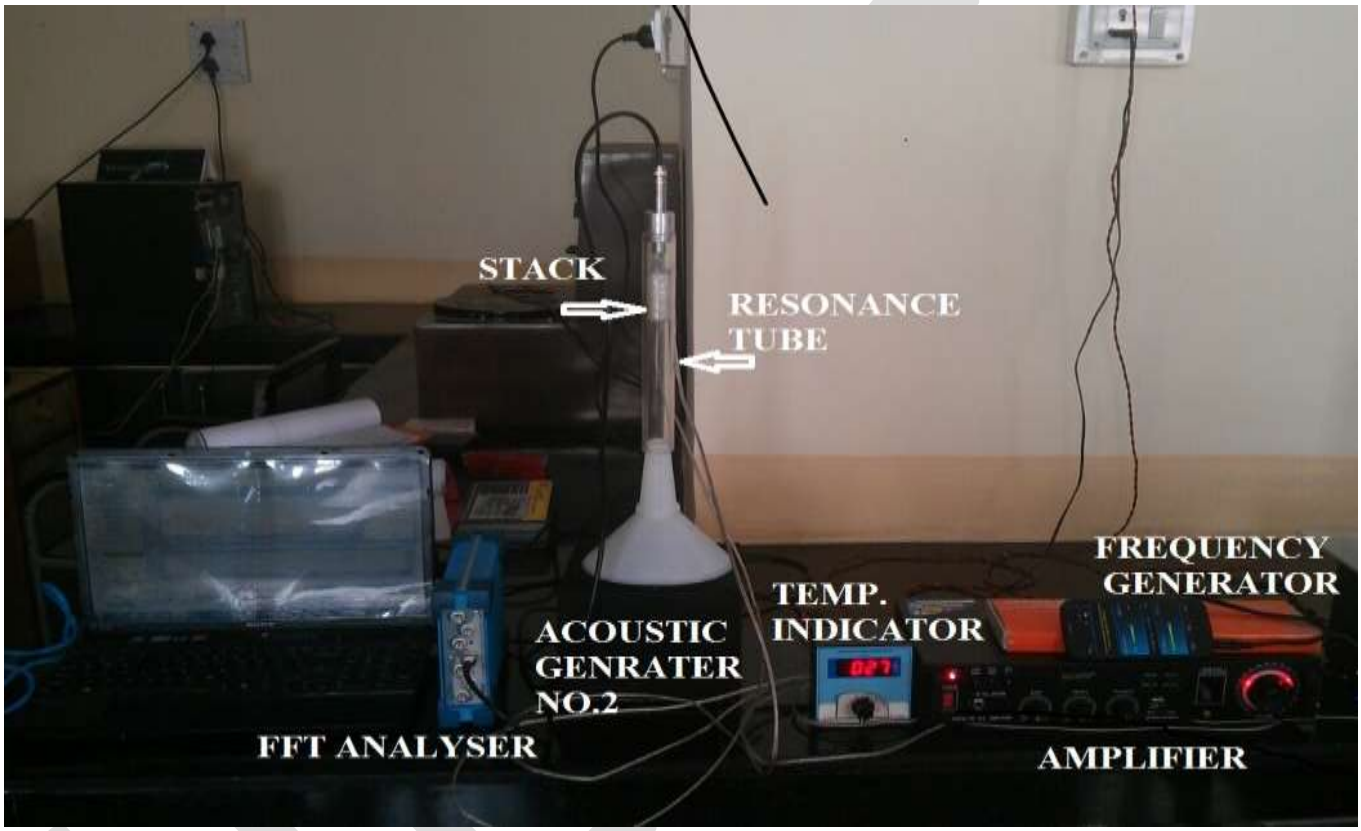

Figure 1: Experimental Set-up of TAR

Figure 2: Rolled Stack

2.2 Working Fluid

High mean fluid pressure, a high velocity of sound and a large cross-sectional area gives more thermo acoustic power. Hence generally, helium is used in thermo acoustic devices. But from low cost perspective, air at atmospheric pressure with low Prandlt number and low viscous losses is used as the working fluid.

2.3 Resonance Tube

The shape, length, weight and the losses are significant parameters in resonator design. Length of resonator is determined by the resonance frequency and minimal losses at the wall of the resonator. The length of resonator tube corresponds to quarter of the wavelength of the standing wave [1]:

Length of resonance tube,

L= v/4f ……[7,8]

Where,

Velocity of sound in air, v =340 m/s
Frequency of Sound wave, F=350 Hz

L= 340/(4*350)
= 0.242 m

Where, a is the speed of sound,

L is the length

and F is the resonance frequency

For the resonance frequency 350Hz, the length of resonant tube is set equal to 242 mm that corresponds to the quarter wavelength of the acoustic standing wave, the diameter of the resonator tube is set equal to 20mm. The acoustic resonator comprises of a straight acrylic tube of length 242 mm with internal diameter 20 mm and the thickness of the wall, 2.5mm. One end of the tube is attached to the small end of acrylic conical flask. At the other end of the resonator, an aluminum plug is placed which works as reflector wall and heat exchanger.

2.4 Acoustic Generator

Figure 3 shows acoustic generator with resonance tube. Acoustic driver supplies total acoustic power used by the refrigerator. The acoustic driver converts electric power into acoustic power. A loudspeaker with maximum power of 60 watts and 8Ω at the operating frequency of 350 Hz is selected as the acoustic driver for this study.

2.5 Measuring Instruments

Different process parameters viz. pressure, temperature, amperage, voltage are measured using calibrated instrumentation. The locations of measurements are selected judiciously and appropriately.

The pressure wave amplitude is measured using pressure transducer and FFT analyzer shown in figure 4. Calibrated K type thermocouples and calibrated digital temperature indicator are used to measure temperature of hot and cold end of the stack as well as atmospheric temperature. Electrical input to speaker is measured using calibrated 0-20 A, 600V Multimeter.

Figure 3: Resonator a top the acoustic generator

Figure 4: FFT Analyzer for pressure measurment

3. OPTIMIZATION APPROACH

Designs of experiments include the statistical tools used for process planning of experimentation and help collect appropriate data and subsequently minimize the number of experiments. Taguchi is one of such statistical tools, widely used in experimental designing to minimize the variation of noise factors and determine optimal parameters using Signal to Noise (SN) ratio graphs[10].

The aim of this work is to determined optimum parameters using Taguchi method, to get maximum temperature difference across two ends of the stack. Here three different types of quality characteristics are used viz. smaller is better, nominal is best and larger is better. In the experimentation, response is temperature difference across the stack ends for better performance of TAR. Performance of TAR is based on the temperature difference across stack, so we selected Larger the better quality characteristics for Taguchi analysis.

Table : 1 Parameters under investigation

Parameters	Level 1	Level 2	Level 3
Stack position (A)	100 mm	150 mm	190 mm
Stack Material (B)	Capillary tubes	Glass fiber with nylon spacers (GFW/TN)	Glass fiber with glass spacers (GFW/TC)
Frequency (C)	350 Hz	520 Hz	700 Hz
Wave type (D)	Sine	Square	Triangular

In design of experiment, four critical parameters selected are Stack position, Stack length, and Frequency and Wave type with three levels for each parameter. If full factorial analysis is undertaken, number of experiments required to be performed are 3^4=81[12]. To minimize this number Taguchi analysis is put to use. Obviously L_9 array has been selected for the analysis.

Table 2: Response of L_9 array

Test. No.	A	B	C	D	Response			SN ratio	Mean response
					1	2	3		
T_1	1	1	1	1	5	4	4	12.59	4.33
T_2	1	2	2	2	1	2	2	3.01	1.66
T_3	1	3	3	3	3	2	2	6.91	2.33
T_4	2	1	2	3	2	2	1	3.01	1.66
T_5	2	2	3	1	4	5	4	12.59	4.33
T_6	2	3	1	2	8	8	9	18.37	8.33
T_7	3	1	3	2	1	2	2	3.01	1.66
T_8	3	2	1	3	2	2	4	7.27	2.66
T_9	3	3	2	1	3	5	5	11.95	4.33

3.1 Signal to Noise Ratio

Larger the Better (SN) Ratio is used for non-availability of anticipated target value, and larger the value of the characteristic, higher is the temperature difference across the stack.

SN ratio is larger the better,

Find the value of SN ratio by using following formula

$$\text{S/N Ratio} = -10\log_{10}\left(\frac{1}{n}*\left(\sum\frac{1}{y^2}\right)\right)$$ ……(Minitab Start Guide)

SN ratio for trial 1,

$$T_1 = -10\log_{10}\left(\frac{1}{3}\sum\left(\frac{1}{5}\right)^2 + \left(\frac{1}{4}\right)^2 + \left(\frac{1}{4}\right)^2\right) = 12.59$$

Similarly, S/N ratio for T2 to T9 is calculated as shown in the table 2.

3.2 Predicted Taguchi Result

Predicted results of all full factorial design are determined using predicted Taguchi analysis in Minitab software. This predicted results show values of SN ratio and mean (response).It shows total 81 predicted results for 4 factor, 3 level design. Predicted results show that experiment number 46 has maximum predicted response of 8.78 K for A2B3C1D1 combination.

As per orthogonal array, nine experiments are performed. The results are fed as input parameter to Minitab software and same are analytically solved as well. The main effect plot for S/N ratio and mean effect plot for means are obtained which revealed optimum parameters with its level as shown in figure 5, for SN ratio and means.

3.2 Main effect plots

Main effect plots show severity of different levels of the factors on the response. The main effect is evident when the response varies with levels of the factors. The Minitab software is used for the analysis. figure 5 shows that Frequency has the most significant effect on SN ratio. This is evident as the 350Hz run gives higher SN ratios than 525Hz run and 700Hz. 525Hz and 700Hz runs have insignificant effect on SN ratio, as represented by the almost flat line in SN ratio plot. Stack position of 150mm has higher SN ratios than 100 mm and 190 mm stack positions.

Thus, maximum value of response in main effect plot for SN ratio and main effect plot for means helps select optimum combination A2-stack position=150mm, B3-stack material=glass fibre with capillary spacers, C1-Fequency=350Hz, D1-wave type = Sine wave. Taguchi method achieves this by two different ways. The first minimizes variability, and the other hits the target.

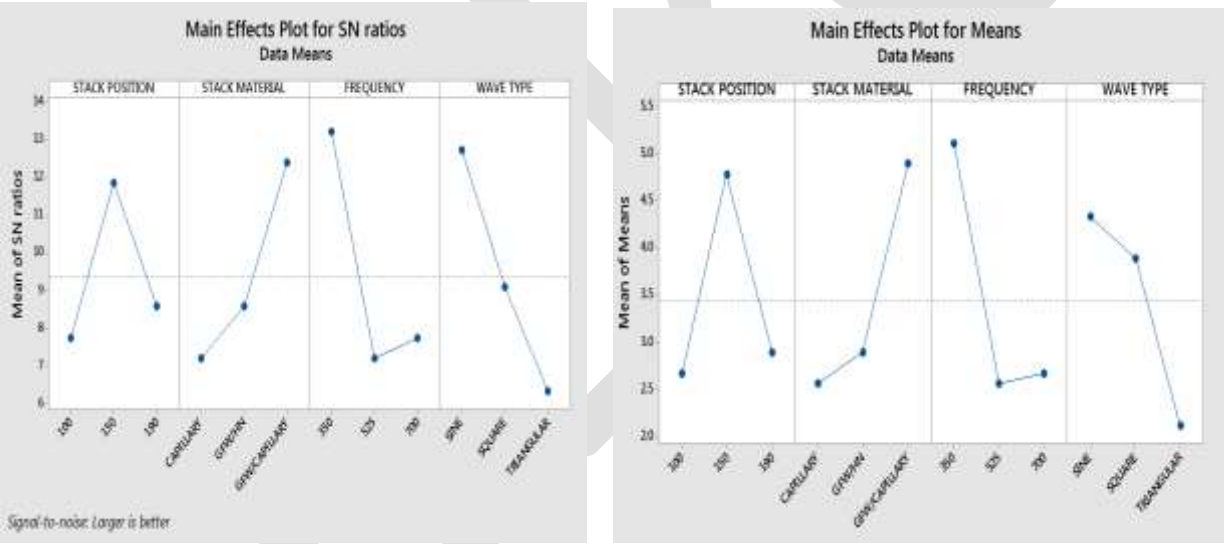

Figure 5: Main effect plot for SN ratios and means

3.3 Contour plots

Contour plots are used to explore the relationship between three variables at a time. Generally, there are two predictors and one response variable. Contour plots are useful for establishing desirable response values and operating conditions. Minitab plots the values for the x and y factors (predictors) on the x and y axes, while contour lines and colored bands represent the values for the z-factor (response).

Contour plot In Figure 6 shows that the maximum temperature difference occurs near 350 Hz and stack position 150 mm. The lowest temperature differences are found near 550 Hz and 130mm stack position. Contour plot represents functional relationship between stack materials and positions, on response. It is evident that stack material glass fibre with capillary tube spacers and 150mm stack position evokes maximum values of response (temperature difference). Counter plot portrays the effect of frequency and stack material, on response. 350 Hz frequency and glass fibre with capillary tube spacers stack material yields maximum values of response.

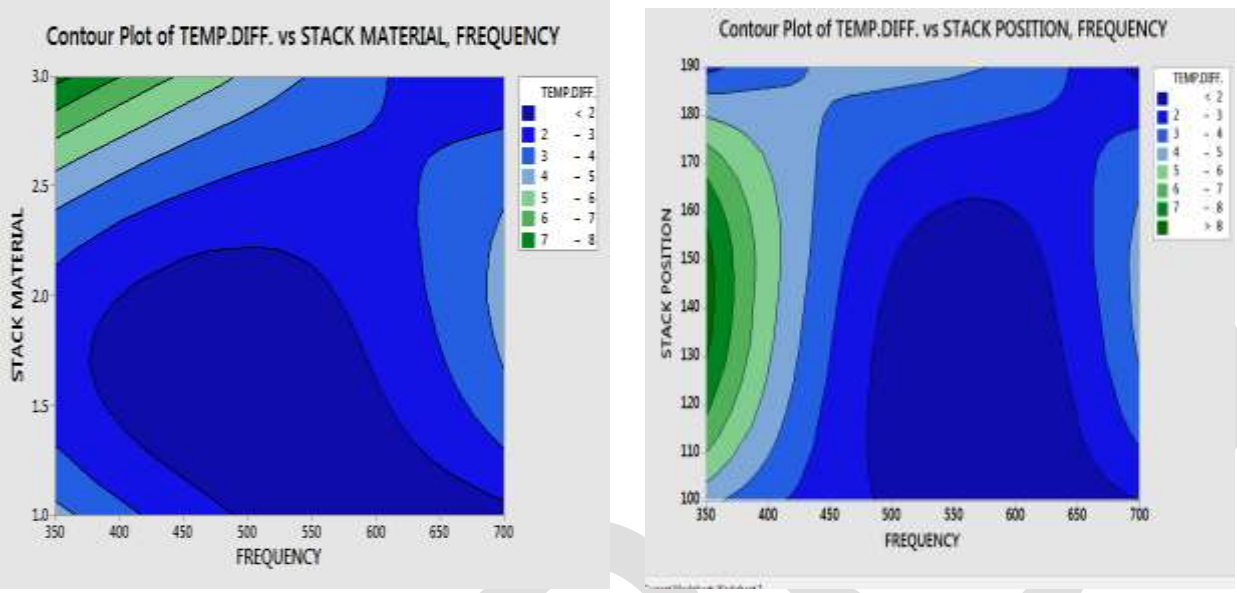

Figure 6: Contour plots of response (temperature difference)

4 ANOVA (Analysis of Variance)

Analysis of variance (ANOVA) is similar to regression and as such is used to investigate and model the relationship between a response variable and one or more predictor variables. Also it is used for multi-factorial study and precise analysis of data. Table 4 shows contribution ratio of individual factor. In figure 6 shows bar chart of all factors and its contribution ratio. Frequency has most contributing factor as compare with other factors.

ANOVA is used to investigate the significance and capability of the model. The ANOVA results of temperature difference across the stack, are presented in Table 4, which effectively represents the relationship between the response (temperature difference) and the significant input variables such as stack material, stack position, frequency and wave type. The mean squares are obtained by dividing the sum by the respective degrees of freedom. The F-value, is calculated by dividing the mean square of the concerned factor variations by variance of error. The F-values of parameter if greater than critical F value selected from F-distribution table, indicates that the factor is statistically significant at 95% of confidence level.

Table 4: ANOVA Table

source of variation	Sum of square	Dof	MS	F value	%P value
A	22.2963	2	11.15	21.49	18.16
B	26.74074	2	13.37	25.78	21.78
C	44.51852	2	22.26	42.92	36.27
D	19.85185	2	9.92	19.14	16.17
ERROR	9.33359	18	0.51		7.60
total	122.741	26	4.72		

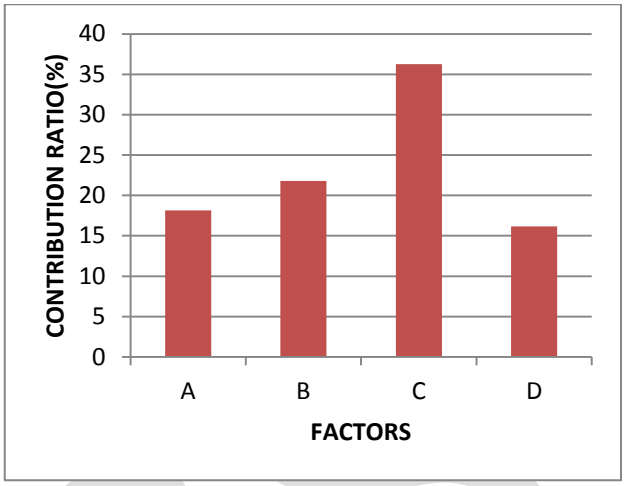

F_{18}^{2} (95%) = 3.55 ....From F-value table[11]

ANOVA table shows all values of F value in column, are greater than 3.55, so all factors are significant.

4.1 Verification Run

Predicted Taguchi analysis shows the predicted value of the Temperature difference as optimum value of Temperature difference of 8.78 K.

As per 95% CI = 8.78 K,

For validation of predicted results by Taguchi method, experiments with optimized parameters are to be undertaken.

The experiment for optimum combination of $A_2B_3C_1D_1$ (Stack position 150 mm, Stack material Glass fibre with capillary tube spacers, Frequency 350 Hz and Wave type Sine) produced Temperature difference of 10 K, in close agreement with predicted value.

5. CONCLUSIONS

Using the Taguchi approach, the effect of parameters viz. stack position, stack material, frequency and type of acoustic wave on the TAR performance, in terms of temperature difference has been studied and optimum parameter combination have been obtained.

From the ANOVA results, it is found that the frequency has most contributing factor influencing the performance of TAR.

Confirmation trial is performed for the Taguchi generated optimum combination and thus the predicted response is verified.

REFERENCES:

[1] Nsofor, E.C.(2009), "Experimental study on the performance of the thermoacoustic refrigerating system", Applied Thermal Engineering, 2672-2679.

[2] Hariharan, N.M., P. Sivashanmugam, and S. Kasthurirengan. (2013) "Optimization of TAR using response surface methodology", Journal of Hydrodynamics Ser B, 72-82.

[3] Mohammed Awwad Ali Al-Dabbas, (2013), "The Performance of the First Pilot TAR", Journal of Energy and Power Engineering, 2106-2114.

[4] Giulio Allesina, (2014), " An experimental analysis of a stand-alone standing-wave TAR" international journal of Energy and Environmental Engineering, vol.5/1/4.

[5] Kartik M.Trivedi (2014), "Effect of stack positioning on a temperature difference of thermo acoustic refrigerator" Indian journal of research, vol. No. 3, Issue No. 5, 2250-1991.

[6] Insu Paek, James E. Braun and Luc Mongeau, (2007), "Evaluation of standing-wave thermoacoustic cycles for cooling applications" International journal of refrigeration, 1059-1071.

[7] R. C. Dhuley and M.D. Atrey (2011), "Cooldown Measurements in a Standing Wave Thermoacousti Refrigerator", Indian Journal of Cryogenics, Vol.36, No.1-4, pp. 158-163.

[8] B. V. Kamble, B. T. Kuzhiveli, S. Kasthurirengan, Upendra Behera, K.V.Dinesh, Geeta Sen,M. V. N. Prasad (2011) "Performance characterization by Optimized Design of Thermoacoustic Prime Mover", Indian Journal of Cryogenics, Vol.36, No.1-4, pp. 37-41.

[9] Mehta S., Desai K., Naik H., Atrey M. (2013), " Investigations on performance improvement of standing wave type thermoacoustic prime mover using acoustic amplifier", Indian Journal of Cryogenics, Vol.38, No.1-4, pp.184-189.

[10] Sibel Gunes, Eyuphaqn Manay, (2011), " Taguchi approach for optimization of design parameters in a tube with coiled wire inserts" Applied Thermal Engineering, 2568-2577

[11] Stat Ease (2014)" Stat-Ease Handbook for Experimenters"

[12] J. Prasanna, L. Karunamoorthy, (2014), "Optimization of process parameters of small hole dry drilling inTi-6Al-4V using Taguchi", Measurement 48, 346-354

International Journal of Engineering Research and General Science Volume 3, Issue 3, Part-2 , May-June, 2015
ISSN 2091-2730

BOOST PWMCONTROL SCHEMEFOR A HALF BRIDGE LL RESONANT CONVERTERFORHOLD-UPSTATE OPERATION

B.HAREESH[1], N.SRAVANTHI[2]
PG Student [PE&ED], Dept. of EEE, SISTK, hareesh09212@gmail.com,India[1]
Associative professor, Dept. of EEE, SISTK, sravanthin918@gmail.com,Andhra Pradesh, India[2]

Abstract—In this paper, the proposed converter is predicated on a moiety-bridge LLC resonant converter structure and a single auxiliary switch is integrated at the primary side. The converter has two different operational characteristics. It shows the same operational characteristic with the conventional LLC resonant converters during nominal state. However, when ac line lost and the converter enters into the hold-up time state, which requires wide voltage gain changes,the control method of the proposed converter is transmuted to the PWM method utilizing the auxiliary switch. Since the proposed converter compensates wide voltage gain variation with PWM method of the auxiliary switch, the frequency variation range for the LLC resonant converter is highly reduced in the proposed converter. Therefore the transformer in the proposed converter can be designed at the optimal operating point and it results in decremented conduction loss of the magnetizing inductor current. Furthermore, the maximum voltage gain of the proposed converter is facilely incremented by elongating the obligation ratio of the auxiliary switch. It avails to decrement the link capacitance. To verify the efficacy of the proposed circuit, operational principle will be expounded and experimental results will be presented with following designation. 100 kHz of switching frequency, 250–400 V of input voltage range, 250 V of output voltage, and 75 W output potency.

Index Terms—Boost PWM control and zero voltage switching(ZVS), hold-up time, LLCresonant converter.

1.Introduction

In recent years, considerable researches have been performed for ac/dc converters to increment the puissance density and to amend the efficiency. These researches are mainly fixated on two-stage type ac/dc converter which includes a potency-factor rectification(PFC) stage besides output regulation circuit.

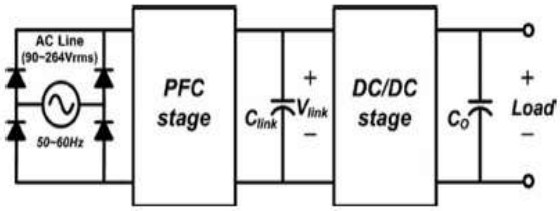

Fig. 1shows the structure of two-stage ac/dc converter.

The PFC stage is utilized to achieve unity power factor of the system and galvanic isolation and output voltage regulation characteristics are gratified by the dc/dc stage. In these two components, the dc/dc stage is regarded as the more critical part to ameliorate the efficiency of the system, because it converts high voltage input into variable load voltage/current output, which results in a consequential power loss. Furthermore, some designations require that the system.

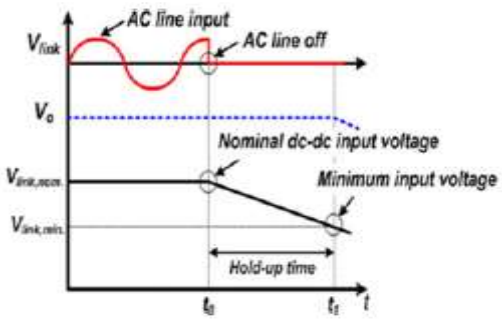

Fig. 2. Input voltage variation of dc/dc converter.

To maintain output voltage for a certain duration after loss of ac line voltage, called hold-up time (visually perceive Fig. 2), which make dc/dc converters have circumscribed efficiency and low power density .The hold-up duration is varied depends on designations ,from a few milliseconds to dozens of milliseconds.

During this time, a dc/dc converter is powered by the stored energy in link capacitors, so that the dc/dc converter should be designed to be able to compensate the wide input voltage range .Many approaches have been suggested for a high efficient dc/dc converter [1]–[3]. Among these approaches, LLC resonant converter [3] is culled as the most promising candidate in low power application, due to the zero voltage switching (ZVS)characteristic for the primary switches and no inversion-instauration quandary for the rectifier diodes .An LLC resonant converter shows the maximum efficiency in the nominal condition, when the converter is operated at the resonant frequency. However, the switching frequency becomes reduced and growing apart from the resonant switching point as the input voltage decreases. This frequency change becomes a considerable issue under a wide input variation condition .It makes LLC resonant converters have arduousness in magnetic design, and it withal decreases nominal efficiency of the converters. The dc conversion ratio of a conventional LLC resonant converter is represented as follows [3]–[5]. A number of different methods have been proposed to surmount this drawback of the LLC resonant converter [5]–[6].

Converter have low power density and incremented circuit intricacy .Boosting-up primary current is another method proposed in Fig.3 The converter applies zero voltage to the transformer utilizing the secondary auxiliary circuit and the primary current is build up during this period. Albeit higher voltage gain characteristic can be achieved with this method, the proposed converter requires many bulk components. Asymmetric PWM control scheme is proposed in Fig.4 [14]. This method increases voltage gain without utilizing any supplemental components, but with transmuting control scheme from frequency modulation(FM) to PWM control for the hold-up time operation. High voltage gain is achieved utilizing this method while maintaining high power density characteristic. However, the gain variation range is constrained in the converter (optically discern Fig3) and the maximum gain is tenacious by the resonant tank design.

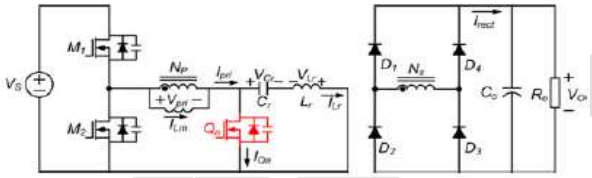

Fig. 3. Schematic diagram of the proposed converter.widely varied in the proposed converter operation, the converter

II. FEATURES OF THE PROPOSED CONVERTER

The circuit diagram of the proposed converter is represented in Fig. 3. It is predicated on the conventional HB LLC resonant converter and an auxiliary switch is integrated to the primary side of the converter. Fig. 8 shows the key operations of the proposed converter for the nominal state and for the hold-up state. In nominal state, the proposed converter is operated just identically tantamount to the conventional LLC resonant converter operated at the resonant switching frequency. The soft switching condition is intuited and no nonessential conduction loss is appeared in this operation. Therefore, the maximum efficiency is showed with the proposed converter during nominal state. When the converter enters into the hold-up state, the converter increases the voltage gain utilizing the auxiliary switch *Qa*. The resonant inductorcurrent is build up, while the auxiliary switch is conducted andit is transferred to load during off-state of the auxiliary switch.Therefore, higher voltage gain is easily achieved in the proposedconverter by increasing the duty ratio of *Qa*. The operationalcharacteristic is similar to the boost PWM operation.

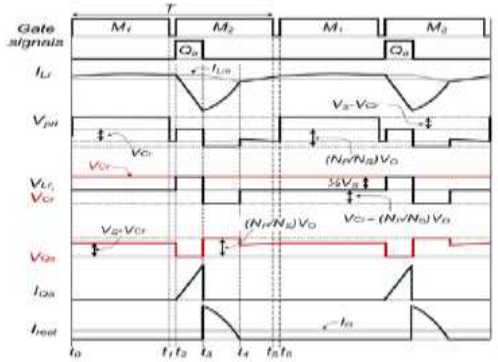

Fig. 4.Key waveforms of the proposed converter.

III. OPERATIONAL PRINCIPLES

Operations of the proposed converter are analyzed in this section.The operational principle for the nominal sate is the samewith that of the conventional *LLC* resonant converter operated atresonant frequency [7]–[10]. Thus, only the operation for holduptime is explained in this section. For the convenience of themode analysis, several assumptions are made as follows:

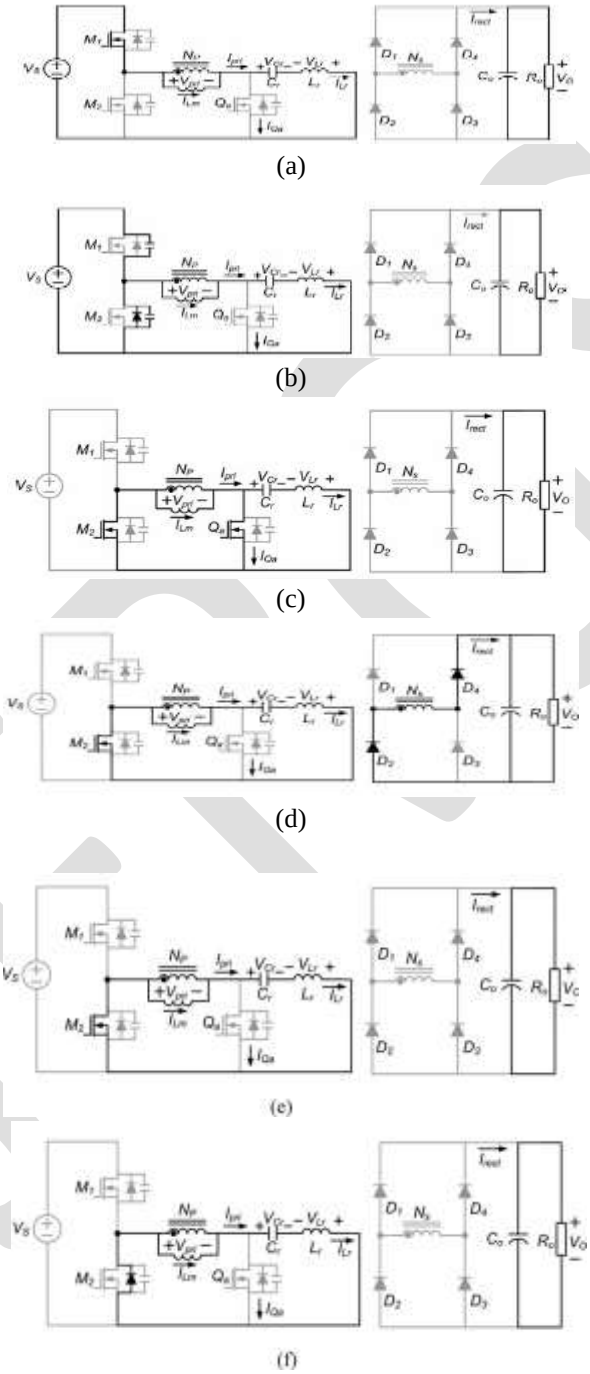

Fig. 5. Equivalent circuit of the proposed converter in hold-up state

A. Mode 1 (*t*0 −*t*1)*:* The switch*M*1 is conducted in this modeand resonant inductor current *I*Lr resonates with *Cr* and "*Lm* +*Lr*." The secondary side is disconnected from the primary sideand output energy is supplied with the output capacitor.

B. Mode 2 (*t*1−*t*2)*:* As *M*1 is turned OFF, the parasiticcapacitors of *M*1 and *M*2 start to be charged and discharged,respectively, in a resonant manner. Since the large magnetizinginductor energy is participated in this resonance, ZVS conditionof *M*2 is easily achieved.

C. Mode 3 (*t*2 −*t*3)*: Qa*and *M*2 is turned ON at *t*2. HBcapacitor voltage *V*Cr is applied to the resonant inductor *Lr*andresonant inductor current is linearly increased in this mode. It isexpressed as follows:

D. Mode 4 (*t*3−*t*4)*:* After the *Qa*switch is turned OFF, thebuilt-up resonant inductor current is transferred to the load side.Reflected output voltage is applied to magnetizing inductanceof the transformer and negative voltage,"*VCr*−(*NP*/*NS*)*VO*,"is found at the resonant inductor *Lr*.Therefore, the resonantinductor current decreases in this mode.

E. Mode 5 (*t*4−*t*5)When the resonant inductor currentreaches the magnetizing inductor current, *I*Lm, the secondaryside is disconnected from the primary side and resonance between*Cr* and"*Lm*+ *Lr*"appears in the converter.

F. Mode 6 (*t*5−*t*6)*: M*2 is turned OFF at *t*5 and the primary current flows through diode M2

IV. ANALYSIS AND DESIGN CONSIDERATION

In this section, key characteristics and design considerations of the proposed converter are presented and compared with the conventional LLC resonant converter. Generally, high capacitance design for a resonant capacitor and low inductance design for a resonant inductor are preferred in conventional LLC resonant converters for high power density and high efficiency, so that the capacitor voltage VCr is regarded as a constant value in this analysis for a more facile understanding of the proposed converter .Also the magnetizing inductor current, ILm, is considered as a constant value in this analysis during the switching period because the magnetizing inductor Lm is customarily designed to have very high inductance value compared to Lr , so that the current variation of ILm is neglected in conventional LLC converter operation

A. Voltage on the Resonant Capacitor

The voltage applied to the resonant capacitor *VCr*is used toderive the dc conversion ratio and current stress of the proposedconverter, and *VCr*can be achieved by using the simplified keywaveforms.Since each increment of resonant inductor currents Δ*i*Lr duringthe period of "*DQa*T" and "*DP* T" are the same, the duration"*DP* T" is achieved as follows:

$$\frac{V_{cr}}{L_r} D_{Qa} T = \frac{(nv_o - v_{cr}}{L_r} D_P \mathrm{T}$$

$$= \frac{L_r}{(nv_- v_{cr}} D_P \quad (1)$$

$$0.5\mathrm{T}(V_S - V_{cr}) = nv_0 D_P T + V_{cr}(0.5 - D_{Qa} - D_P)\mathrm{T}$$

(2)

$$V_{cr} = \frac{0.5v_0 - nV_0 D_P}{1 - D_{0a} - D_P} = \frac{nV_0 D_P}{D_{0a} + D_P} \quad (3)$$

Therefore, the resonant capacitor voltage can be representedas (5). It means the half of the input voltage is applied to theresonant capacitor during the hold-up state operation

$$V_{cr} = 0.5V_S \quad (4)$$

B. DC Conversion Ratio

The proposed converter has two different input–output voltage conversion ratios depending on its operational state. Fornominal state, it has the same operational characteristic with the conventional LLC resonant converter. Thus, voltage gain is affected by switching frequency, Fs , and the dc conversion ratio is expressed as

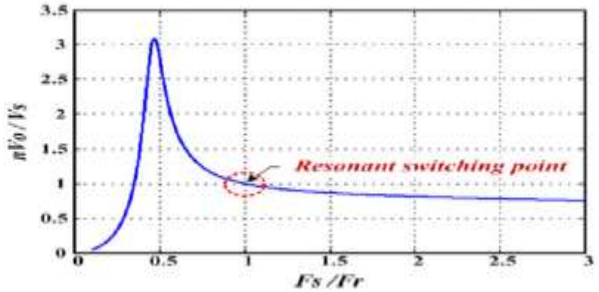

Fig. 6.Dc conversion ratio during nominal period
(at 75 W Specification).

At nominal state when the converter has fixed input voltagecondition, the proposed converter is operated at the resonant frequency Fr, and the switching frequency is ideally fine-tuned to the resonant frequency at any load condition. The cognation of voltage gain and switching frequency is depicted .A PWM method is adopted in the proposed converter to increment the voltage gain during hold-up state operation. Fig.8shows the key wave forms of the proposed converter during hold upstate operation. The shaded area AP

implicatively insinuates the total charge Q transferred from the input side to the secondary load side. Thus, output voltage can be derived by calculating the
area of AP , and total charge transferred to the load is represented as follows:

$Q = 0.5 * \frac{I_{PK} D_{PT}}{T} = \frac{V_0}{R_0} x \frac{1}{n}$(5)

Since *DP* T and *Ipk*values in (7) are calculated from thefollowing equations:

$$I_{PK} = \frac{V_{cr}}{L_r} D_{Qa} T \quad (6)$$

$$D_P T = \frac{V_{Cr}}{(nV_O - V_{Cr}} D_{Qa} T \quad (7)$$

The dc conversion ratio of the proposed converter in hold-upoperation is expressed as (10) and
As shown in Fig 13, the voltage gain in hold-up state isaffected by the duty ratio of*Qa*, and the gain is linearly increasedfollowed by the duty ratio.

C. Reduction of the Link Capacitor

After ac line lost, dc/dc converters are powered by energystored in link capacitors. Therefore, hold-up time condition andthe size of link capacitance are the major considerations

$\frac{1}{2} c_{link} X (v_{nom}^2 - v_{min}^2) \geq p_o t, t = hold - uptime$ (8)

Since the hold-up time condition and output power ratings aregiven specifications in the system, minimum link voltage is theonly one factor which affects the link capacitance design. Theequation for the link capacitance design.

$c_{link} \geq p_{0t} * \frac{2}{V_{nom}^2 - V_{min}^2}$ (9)

Since the dc conversion ratio of the proposed converter shows linear characteristic, reduction of link capacitor is easily achieved simply by increasing the maximum duty ratio of the auxiliary switch *Qa*. Size of capacitors is highly affected by the capacitances

D. Current Stress of Switches

The current stress of switches is a very paramount factor when designing the proposed converter. In nominal state, the current stresses of switches are identically tantamount with those of the conventional converters, but this condition is transmuted for the hold-uptime operation. Different from the conventional LLC resonant converter, the proposed converter shows boost PWM operation during the hold-up state. Thus, the peak value and RMS value of the resonant inductor current are varied depending on the obligation ratio of Qa . Withal, the dc offset current which is represented in the magnetizing inductor affects the current stress of the converter .The dc offset current is calculated utilizing current-second balance rule of the resonant capacitor Cr (optically discern). According to the current-second balance rule of the capacitor, sum of the total charge flows in and out of the resonant capacitor is zero. Therefore, the positive and the negative area in should be identically tantamount .The shaded area of each period, *ta−tbtb−tc*, *tc−td, td−te*,and *te−tf*are expressed as follows:
Shaded area of *ta−tb*

$\frac{1}{2} X \left(\frac{V_{cr}}{L_r} X I_{Lm} \right) * I_{Lm}$ (10)

E. Reduction of Conduction Loss in the NominalState

In conventional *LLC* resonant converters, the converter increasesvoltage gain by decreasing switching frequencies. Thus,the converter should be designed to be able to operate in wide range

Fig. 8. Maximum current stress of the primary switch (at 75WSpecification)

operational principle of the proposed converter in the nominal state is the same as that of the conventional *LLC* resonant converters.The converter is represented aswhere *ILmpk*is the peak value of magnetizing inductor current ,*t* dead is the dead time of the switches, and *C*oss represents the output capacitance of switches. The high magnetizing inductorcurrent results in conduction loss increases in the converter ,so that the magnetizing inductance should be designed to satisfyboth conditions, satisfying ZVS condition and minimizing conduction loss increases.

V. SIMULATION RESULTS

To verify the effectiveness of the proposed converter, prototypes of the proposed converter and the conventional *LLC* resonant converter are designed with following 75 W LED TV specifications:

1) input voltage range : 250 –400 V;
2) hold-up time : 60 ms;
3) output voltage : 250 V;
4) output power : 75 W (250 V/0.3 A);

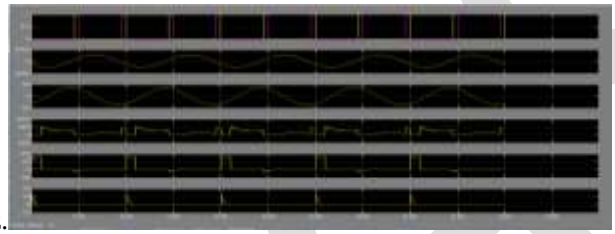

5) nominal switching frequency: 100 kHz.

Fig.7.Simulationwaveforms of the proposed converter operation at minimum input voltage. Nominal state,Hold-up state.

Also, the components used in both converters are the same except the auxiliary switch and the transformers. The auxiliary switch is newly added in the proposed converter. Although the proposed converter does not need any frequency changes for hold-up operation, the same transformer size is used in the experiment because of the dc offset current of the magnetizing Inductor. However, the transformer in the proposed converter can be designed to have higher magnetizing inductance to reduced he RMS value of magnetizing inductor current. Fig. 19shows the experimental waveforms of the proposed converter both in nominal state operation and hold-up state operation with the minimum input voltage condition (Vs =250 V).As expected, the proposed converter grows up its voltage gain by incrementing the obligation ratio of the auxiliary switch. When no PWM gate signal is applied to the auxiliary switch, the output voltage becomes153 V and it increments to 250 V for hold-up state operation with 20% obligation ratio of the auxiliary switch Qa .

The proposed converter shows boost PWM operation during hold-up state and the resonant inductor current is build up to −2.4 A while the auxiliary switch is conducted. The ZVS conditions are achieved in both converters. Since the proposed converter has higher magnetizing inductance, the RMS value and the peak value of the primary current, which is identically tantamount with the resonant inductor current in nominal state operation, is more minuscule in the proposed converter than those of the conventional converter replication is tested by transmuting the operational mode of the proposed converter under the same input voltage condition .Increased voltage gain is represented as the converter changes its operational modes from nominal operation condition to hold-up time operation condition.

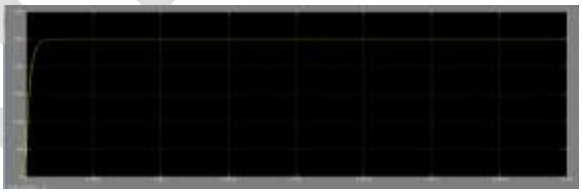

Fig. 9. Simulation waveforms of the proposed converter output voltage.

The proposed converter has higher efficiency over the entire load condition because the loss made by the primary current is reduced in the proposed converter .The efficiency difference becomes maximized at light load condition when the magnetizing inductor current takes up significant portion in the total primary current

VI. CONCLUSION

An incipient HB LLC resonant converter having boost PWM operation characteristic has been proposed. By adopting the PWM control method with an auxiliary switch, the proposed LLC resonant converter reduces its frequency variation range while maintaining the advantages of the conventional LLC resonant converters .Thus, high-K design with high Lm becomes enabled in the proposed converter. It makes the converter have low magnetizing inductor current which results in reduced conduction loss in the proposed converter. The characteristics of the proposed converter are verified with a 75 W prototype and it is compared with the LLC resonant

converter. Efficiency increase is represented in the proposed converter over the entire load condition from 0.86% efficiency amendment at full load condition to3.69% efficiency amelioration at 20% load condition. The efficiency results verifies that the efficacy of the proposed converter and the benefit of the proposed converter becomes maximized at light load condition when the magnetizing inductor current takes a sizably voluminous part in the total primary RMS current value .Consequently, the proposed converter is expected to find wide use for highefficient dc/dc converter having hold-up time requisites

REFERENCES:

[1] G. A. Karvelis,M. D.Manolarou, P. Malatestas, and S. N. Manias, "Analysisand design of non-dissipative active clamp for forward converters,"*IEE Proc., Electric Power Appl.*, vol. 148, pp. 419–424, Sep. 2001.

[2] J. C. P. Liu, N. K. Poon, B. M. H. Pong, and C. K. Tse, "Low output rippleDC-DC converter based on an overlapping dual asymmetric half-bridge topology," *IEEE Trans. Ind. Appl.*, vol. 22, no. 5, pp. 1956–1963, Sep.2007.

[3] R. Redl, N. O. Sokal, and L. Balogh, "A novel soft-switching full-bridgeDC/DC converter: Analysis, design considerations, and experimental resultsat 1.5 kW, 100 kHz," *IEEE Trans. Power Electron.*, vol. 6, no. 3,pp. 408–418, Jul. 1991.

[4] X Ruan and F Liu, "An improved ZVS PWM full-bridge converter withclamping diodes," in *Proc. IEEE Power Electro Spec Conf.* 2004,pp.1476–1481.

[5] M. Y. Kim, B. C. Kim, K. B. Park, and G. W. Moon, "LLC series resonantconverter with auxiliary hold-up time compensation circuit," in *Proc.IEEE* [6] B. C. Kim, K. B Park, and G. W. Moon, "Asymmetric PWM control scheme during hold-up time for LLC resonant converter," IEEE Trans. Ind. Electron., vol. 59, no. 7, pp. 2992–2997, Jul. 2012.

[7] I. H Cho, K. M. Cho, J. W. Kim, and G. W. Moon, "A new phase-shiftedfull-bridge converter with maximum duty operation for server power system,"*IEEE Trans. Power Electron.*, vol. 26, no. 12, pp. 3491–3500, Dec.2011.

[8] Y. K. Lo, C. Y. Lin, M. T. Hsieh, and C. Y. Lin, "Phase-Shifted full-bridgeseries-resonant DC-DC converters for wide load variations," *IEEE Trans.Ind.Electron.*, vol. 58, no. 6, pp. 2572–2575, Jun. 2011.

[9] B. Yang, P. Xu, and F. C. Lee, "Range winding for wideinput range frontend DC/DC converter,"in*Proc. IEEE Appl. Power Electron Conf. Expo.*,2001, pp. 476–479.

[10] G. Ivensky, S. Bronshtein, and A. Abramovitz, "Approximate analysis of resonant LLC DC-DC converter," *IEEE Trans. Power Electron.*,vol. 26,no. 11, pp. 3274–3284, Nov. 2011

International Journal of Engineering Research and General Science Volume 3, Issue 3, Part-2 , May-June, 2015
ISSN 2091-2730

Low Power and Area Single Edge Trigger D Flip Flop for Battery Operated Devices

R. D. Madankar

P.G. Scholar
Department of ECE
Government College of
Engineering, Amravati
madankar.rushikesh@gmail.com

A. M. Shah

Assistant Professor
Department of ECE
Government College of
Engineering, Amravati
mdamshah@gmail.com

Abstract - The devices such as laptop, mobile phones and personal digital assistants (PDA) require low power VLSI devices because these devices are operated on battery. The mobile devices require high speed and low power consumption for their long battery life. So power delay product plays vital role in designing of VLSI circuits. Flip flops are one of the most complex and power consuming component among the various building blocks in digital designs. Clocking network and flip flops consume about 30 to 70 % of total power in the system out of which 90 % is consumed by flip flop. So in this paper the designing of low power and area single edge triggered D flip flop is shown . This flip flop has reduce area and we are designing it by using various nanometer technologies.

Keywords - SET D flip flop, VLSI, lamada rule, single edge trigger, nanometer technology, clocking network, power dissipation and power budget.

INTRODUCTION

Flip-flops are the basic building block of the sequential circuits. They are used to store data, processed by combinational circuit and synchronization of operation at a given clock frequency. The flip flops are basic building block of the digital electronics systems used in computers and many other types of systems. Level trigger flip flop is also known as latch and this latch is mainly used as storage element. Other type of flip-flop is edge trigger. Flip-flop is edge trigger means their output changes at the rising or falling edge of clock (at positive or negative edge). Flip-Flop is an electronic circuit that stores the logical state of one or more data input signal with respect to edge of clock. They are also used in computational circuits to operate in selected sequences during recurring clock intervals to receive and maintain data for a short time period so that other circuits within a system can further process data. Data is stored in flip-flop at each rising and falling edge of clock signal so that it can be applied as inputs to other combinational or sequential circuits, the flip-flops that store data on rising or falling edge of clock are known as single edge triggered flip flops and the flip-flops that store data on both the rising and falling edge of a clock are called as double edge triggered flip-flops.

In many digital very large scale integration (VLSI) designs, the clock system there is clock distribution network and flip-flop, the flip flop is one of the most power consuming component. It approximately consume 30 to 70 % of the total system power, where 90 % of which is consumed by the flip-flops and the last branches of the clock distribution network that is driving the flip-flop . With the recent trend in frequency scaling and deep pipelining, this clocking system power is the major component in total power dissipation. For portable digital circuit the power budget is strictly limited, it is important to minimize the power consumption in both clock distribution networks and flip-flops. At high frequency operation in the timing budget, the latency of the flip-flops should be minimum. In modern VLSI technology it is necessary to reduce both power consumption and latency . The dual-edge triggering also reduce the power consumption in the clock distribution network but it increases complexity of the design and complexity of clock distribution network.

SET D FLIP FLOP DESIGN

Conventional 16-transistor SET D flip-flop operates either at positive edge or negative edge of the clock. For the proper operation of the flip-flop, the input value should be constant just before setup time (t_{setup}) and just after hold time (t_{hold}) of the triggering edge of the clock. The circuit in the fig.1. shows the conventional 16-transistor SET D flip-flop. This conventional SET D flip flop consist of master and slave section. The dashed vertical line separate master and slave sections . A PMOS transistor which is present in the feedback path as it leads to a more compact layout than using a NMOS transistor. The pass transistors can be replaced with transmission gates in high noise environment.

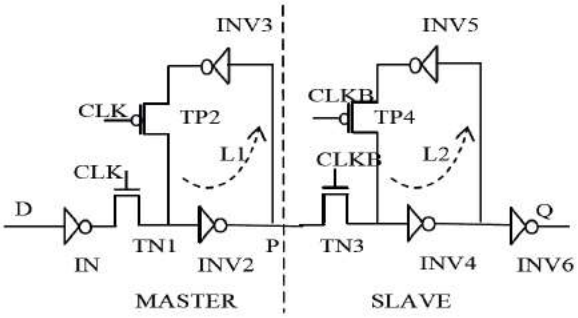

Figure 1) Conventional 16 transistor SET D flip flop

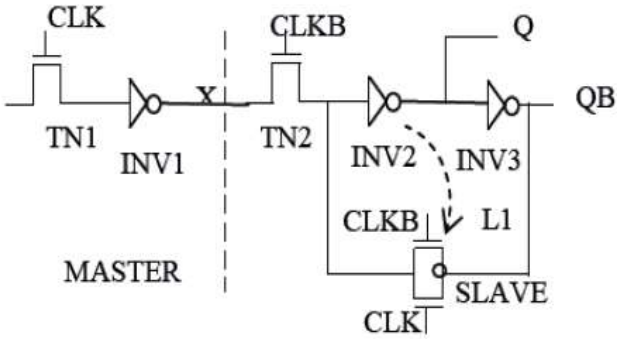

Figure 2) SET D flip flop using 10 transistor

The design of 10-transistor negative edge triggered SET D flip-flop is shown in fig.2. Here the feedback circuit of the master section is removed and in slave section feedback circuit consists of transmission gate. When clock is high , master latch is enable and the inverse of the data is stored to an intermediate node X. When the clock become LOW, the slave latch consisting of transistor TN2 and regenerative feedback circuit L1 becomes enable and produces data at the output Q and QB.

LAYOUT DESIGN OF SET D FLIP FLOP

To manufacture the physical mask layout of any circuit using a particular process it must follow some set of geometric constraints or rules, which are known as layout design rules. These layout design rules specify the minimum value of line widths for physical objects on-chip such as metal and poly-silicon interconnects or diffusion areas, minimum value of metal layer dimensions, and minimum value of separations between two such metal layer. If a metal line width is made too small then it is possible for the line to break during the fabrication process which result in an open circuit. When two lines are placed too close to each other in the layout then there may be formation of an unwanted short circuit by combining during or after the fabrication process.

The main objective of design rules is to achieve a high yield and reliability while using the smallest possible silicon area, to design any circuit with a particular technology. But there is a trade-off between higher yield which is obtained through conservative geometries and greater area efficiency, which is obtained through aggressive, high- density placement of various features on the chip.
In general the layout design rules notably increases the probability of fabricating a successful product with high yield.
The design rules are generally described in two ways
• Micron rules, in which the layout constraints such as minimum feature sizes and minimum allowable feature separations, are describe in terms of absolute dimensions in micrometers, or
• lambda rules, which specify the layout rules in terms of a single parameter (λ) and thus allow linear, proportional scaling of all geometrical constraints.

Lambda based layout design rules were originally designed to simplify the industry standard micron based design rules and to allow scaling capability for various technologies. It must be emphasized however that most of the submicron CMOS process design rules do not lend themselves to straightforward linear scaling. Therefore the use of lambda based design rules must be handled with caution in sub-micron geometries.

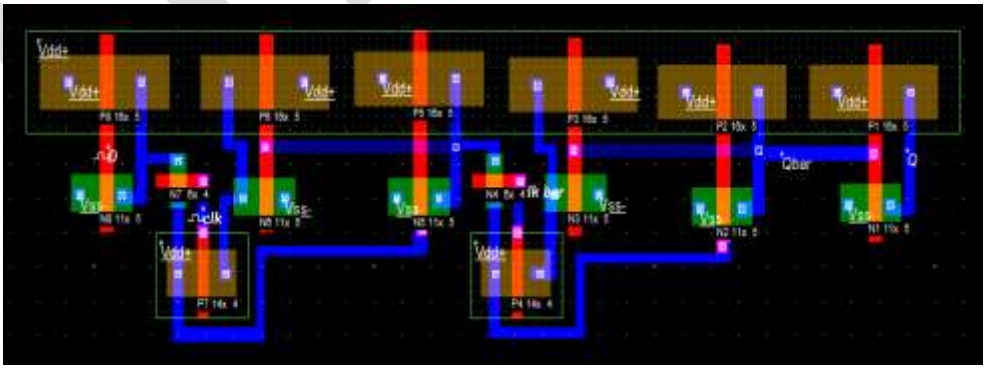

Figure 3) Layout design of conventional SET D flips flop

Device	Width	Length	Device	Width	Length
N1	11λ	5 λ	P1	16 λ	5 λ
N2	11 λ	5 λ	P2	16 λ	5 λ
N3	11 λ	5 λ	P3	16 λ	5 λ
N4	6 λ	4 λ	P4	14 λ	4 λ
N5	11 λ	5 λ	P5	16 λ	5 λ
N6	11 λ	5 λ	P6	16 λ	5 λ
N7	6 λ	4 λ	P7	14 λ	4 λ
N8	11 λ	5 λ	P8	16 λ	5 λ

Table 1) MOS size in conventional SET D flips flop

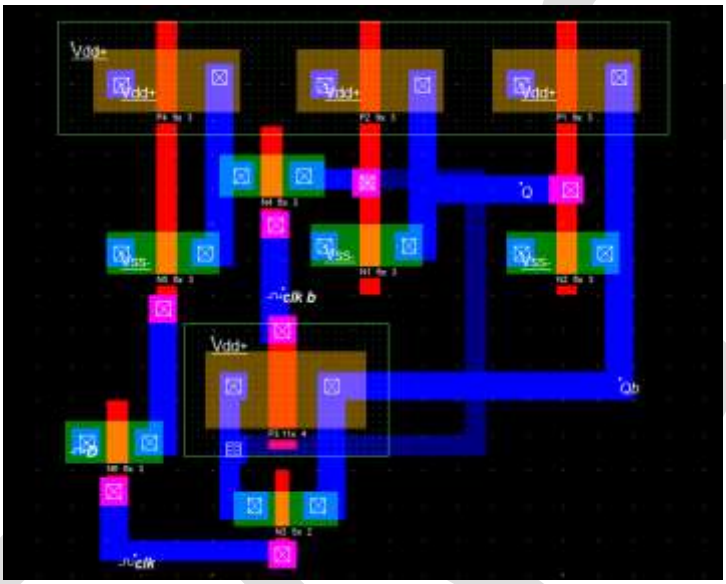

Figure 4) Layout design of ten transistors SET D flip flop

Device	Width	Length	Device	Width	Length
N1	6λ	3 λ	P1	9 λ	3 λ
N2	6 λ	3 λ	P2	9 λ	4 λ
N3	5 λ	2 λ	P3	11 λ	4 λ
N4	6 λ	3 λ	P4	9 λ	3λ
N5	6 λ	3 λ			
N6	6λ	3 λ			

Table 2) MOS size in ten transistors SET D flips flop

The value of lamada is changed with respect to nanometer technology. In 45 nm technology the value of lamada is 0.025 µm and in 32 nm its value is 0.015 µm. The fig.3. Shows the layout of conventional 16 transistors SET D flip flop with combine well. This Conventional 16- transistor SET D flip-flop operates at falling edge of the clock. For the proper operation of the flip-flop, the input value should be constant just before setup time (t_{setup}) and just after hold time (t_{hold}) of triggering edge of the clock. In this design PMOS P1,P2,P3,P5,P6 and P8 are provided with combine N well. The size of each MOS device is shown in table 1.
The fig.4. shows the layout of ten transistors SET D flip flop . In this design the feedback circuit of the master section is removed and in slave section feedback loop consists of transmission gate. In this design PMOS P1,P2 and P4 are provided . The size of each MOS device is shown in table 2.

SIMULATION

The above two layout designs are simulated using Microwind 3.5 tool in 45 nm and 32 nm process. The fig.5 shows the waveform of conventional 16 transistors SET D flip flop in 45 nm technology. The clock frequency is 1.08 GHz and for this frequency the power dissipation is 1.285 µW and maximum clock to Q rise time is 302 psec and fall time is 103 psec.

Figure 5) Waveform of conventional SET D flip flop

The fig.6 shows the waveform of ten transistors SET D flip flop in 45 nm technology. The clock frequency is 1.08 GHz and for this frequency the power dissipation is 4.644 µW and maximum clock to Q rise time is 82 psec and fall time is 83 psec.

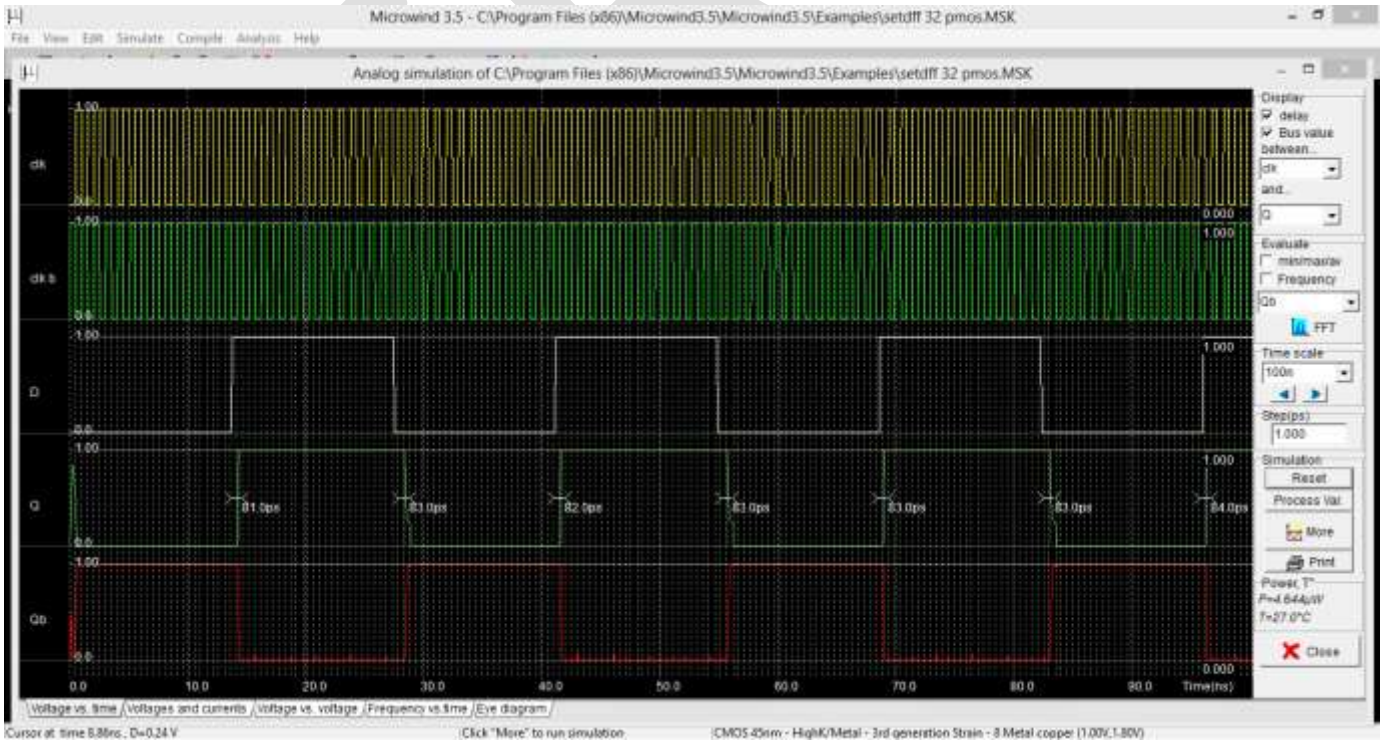

Figure 6) Waveform of ten transistors SET D flip flop

RESULT

As compared to conventional 16 transistors SET D flip flop area taken by ten transistors SET D flip flop is lowest in 32 nanometer technology than 45 nm technology but power consumed by conventional 16 transistors SET D flip flop is lowest in 32 nm technology than ten transistors SET D flip flop.

Design	45 nm	32 nm
Conventional 16 transistors SET D FF	12.1μm^2	9.8 μm^2
Ten transistors SET D FF	2.7 μm^2	2.2 μm^2

Table 3) Comparison of area

Design	45 nm	32 nm
Conventional 16 transistors SET D FF	1.282µW	1.266µW
Ten transistors SET D FF	4.644 µW	3.108 µW

Table 4) Comparison of power

ACKNOWLEDGMENT

I express my sense of gratitude and sincere regards to my guide A. M. Shah. I thank him for extending necessary help, providing facilities and time to time guidance in paper writing.

CONCLUSION

In low power applications , area and power consumption by the device are the main technological aspects to select a design over the other counterpart designs. The ten transistors SET D flip-flop shows better performance in terms of area and power dissipation over other design. This design is tested in 45nm and 32nm technology, thus it is also technology independent. The ten transistors SET D flip flop is used where the area requirement is minimum.

REFERENCES:

.

1. H. Kawaguchi and T. Sakurai, "A reduced clock-swing flip-flop (RCSFF) for 63% power reduction", IEEE J. Solid State Circuits, vol 33, no. 5, May 1998, pp. 807–811.
2. V. Stojanovic, V. G.Oklobdzija (1999) "Comparative Analysis of Master-Slave Latches and Flip-Flops for High Performance and Low-Power System",IEEE J. Solid-State Circuits, Vol.34,1999 pp. 536-548.
3. M.Sharma, K. Sharma,T. Sharma,Prof.B. P. Singh , N. Arora (2011) "SET D-Flip Flop Design for Portable Applications", IEEE, 2011, pp. 1-5
4. Hong Ting Lin, Yi Lin Chuang, Zong Han Yang, Tsung Yi Ho (2014) "Pulsed-Latch Utilization for Clock-Tree Power Optimization",IEEE Transactions On Very Large Scale Integration (VLSI) Systems, Vol. 22,2014 pp. 721-733
5. Myint Wai Phyu, Kangkang Fu, Wang Ling Goh, Kiat-Seng Yeo (2011) "Power- Efficient Explicit-Pulsed Dual-Edge Triggered Sense-Amplifier Flip-Flops",IEEE Transactions On Very Large Scale Integration (VLSI) Systems, Vol. 19, No. 1.
6. N.H. E. Weste and K. Eshraghian, Principles of CMOS VLSI Design: A System Perspective, 2nd ed. Reading MA: Addison-Wesley, 1993.
7. P. Akila(2012) "Designing Clock System Using Power Optimization Techniques in Flip flop",International Journal of Computer Applications Information Technology Vol. I,Issue II, September 2012 (ISSN: 2278-7720) pp. 60-64.
8. M. Sharma, Dr A. Noor, S. Tiwari, K. Singh (2009), "An Area and Power Efficient design of Single Edge Triggered D-Flip Flop", in Proc. IEEE International Conference on Advances in Recent Technologies in Communication and Computing, 2009, pp. 478-481.
9. Microwind 3.5 Users Guide, www.microwind.org
10. M. Sharma, K. G. Sharma,T. Sharma,Prof.B. P. Singh , N. Arora (2011), "Modified SET D Flip Flop for Low Power VLSI Application",IEEE (2011), pp. 1-5.
11. E. Sicard, S. M. Aziz (2010) "Introducing 45 nm technology in Microwind3", Microwind Application Note, 2010, pp. 1-16.
12. Tim Tuan, Arif Rahman, Satyaki Das, Steve Trimberger, Sean Kao (2007), "A 90-nm Low Power FPGA for Battery-Powered Applications",IEEE Transaction On Computer-Aided Design Of Integrated Circuits And System , Vol.26,no.2,February 2007, pp. 296-300.
13. E. Sicard, S. M. Aziz (2010), "Introducing 32 nm technology in Microwind3", Microwind Application Note,2010, pp. 1-16.
14. P. K. chakravarti1, R. Mehra (2015), "Layout design of D Flip Flop for Power and Area Reduction",International Journal of Scientific Research Engineering Technology (IJSRET), 14-15 March, 2015, pp. 154-158

International Journal of Engineering Research and General Science Volume 3, Issue 3, Part-2 , May-June, 2015
ISSN 2091-2730

Implementation of Truncated Multiplier for FIR Filter based on FPGA

Mr. A. D. Wankhade
P.G. Scholar
Department of ECE
Government College of
Engineering, Amravati
wankhadeakash9@gmail.com

Mr. S. S .Thorat
Assistant Professor
Department of ECE
Government College of
Engineering, Amravati
samratthorat@gmail.com

Abstract- Multiplication of two bits produces an output which is twice that of the original bit. It is usually needed to truncate the partial product bits to the required precision to reduce area cost. Fixed-width multipliers, a subset of truncated multipliers, compute only n-most significant bits (MSBs) of the 2n-bit product for n × n multiplication and use extra correction/compensation circuits to reduce truncation errors. Truncated multipliers provides significant improvements in area, delay, and power. The proposed method finally reduces the number of full adders and half adders during the tree reduction. The output is in the form of LSB and MSB. Finally the LSB part is compressed by using operations such as deletion, reduction, truncation, rounding and final addition because of which area is reduces.

In the proposed truncated multiplier design, introduces column-by-column reduction. In this design of truncated multiplier, to minimize the half adders in each column because the full adder has high compression rate when compared to HA. FPGAs reprogram ability and high degree of parallelism attracts them for DSP applications. The hardware description language VHDL is used to describe the design. The design is synthesized using Quartus-II software /Xilinx Project Navigator 13.1 software. Simulation is done using Modelsim. The design implementation is done on Altera DE board CYCLON-II family device EP2C35F672C6.

Keywords- Deletion, reduction, truncation, rounding, final addition, truncated multiplier, adaptive filter.

I. INTRODUCTION

The multiplier is an essential element of digital signal processing operations such as filtering and convolution. Most of the digital signal processing operations such as Discrete Cosine Transform (DCT) or Discrete Wavelet Transform (DWT) is accomplished by repetitive multiplication and addition. Hence the speed of these operations exclusively depends upon the speed of the multiplication operation being performed. It has been observed that the multiplier requires the longest delay among the basic operational blocks in a system; hence the critical path is predominantly determined by the multiplier.

Also, the standard multiplier has been observed to consume comparatively more area and power. Therefore a design which will reduce the consumed area or power or speed or any combination of the above three parameters is of research interest.

There is need of standard multiplier for DSP application such as filtering, convolution, and fast Fourier or discrete cosine transform. These operations for DSP application can be performed using truncated multiplier. Standard multiplier produces 2n bit output for n x n bit multiplication, whereas truncated multiplier gives n-bit output. This truncated multiplier follows steps such as delete non require bits, reduce the level, truncation, round up result using correction logic and final addition which offers precision improvement.

II. LITERATURE SURVEY

A faithfully rounded truncated multiplier design is presented where the maximum absolute error is guaranteed to be not more than 1 unit of least position. In there proposed method, they jointly considers the delete non require bits, reduce the level, truncation, round up result using correction logic and final addition of partial product bits in order to minimize the number of full adders and half adders during tree reduction. In this method efficiency of the proposed faithfully truncated multiplier with area saving rates of more than 30%. In addition, the truncated multiplier design also has smaller delay due to the smaller bit width in the final carry-propagate adder. The faithfully truncated multiplier has a total error of no more than 1 ulp and can be used in applications which need accurate result. By using this method we can be easily extended to signed or Booth multiplier design [1].

Low-cost finite impulse response (FIR) designs are presented using the concept of faithfully rounded truncated multipliers. They jointly consider the optimization of bit width and hardware resources without sacrificing the frequency response and output signal

precision. Non uniform coefficient quantization with proper filter order is proposed to minimize total area cost. Multiple constant multiplications-accumulations in a direct FIR Structure is implemented using an improved version of truncated multipliers. Compare to other FIR design approaches show that the proposed designs achieve the best area, delay and power results [2].

III. REDUCTION SCHEMES OF PARALLEL MULTIPLIERS

PP (partial product) generation produces partial product bits from the multiplicand and multiplier. PP reduction is used to compress the partial product bits to two. Finally the partial products bits are added by using carry propagate addition. Two famous reduction methods are available,

1. Dadda tree

2. Wallace tree

Dadda reduction performs the compression operation whenever it required. Wallace tree reduction always compresses the partial product bits.

In this proposed work standard parallel multiplier is design & truncated multiplier design, introduces column-by-column reduction. The result is obtained from standard parallel multiplier and truncated multiplier gives close result. Truncated multiplier minimizes the half adders in each column because the full adder has high compression rate when compared to HA.

A parallel tree multiplier design usually consists of three major steps, i.e PP generation, PP reduction, and final carry propagate addition. PP generation produces PP bits from the multiplicand and the multiplier. The goal of PP reduction is to compress the number of PPs to two, which is to be added for final addition. Wallace tree reduction manages to compress the PPs as early as possible, whereas Dadda reduction only performs compression whenever.

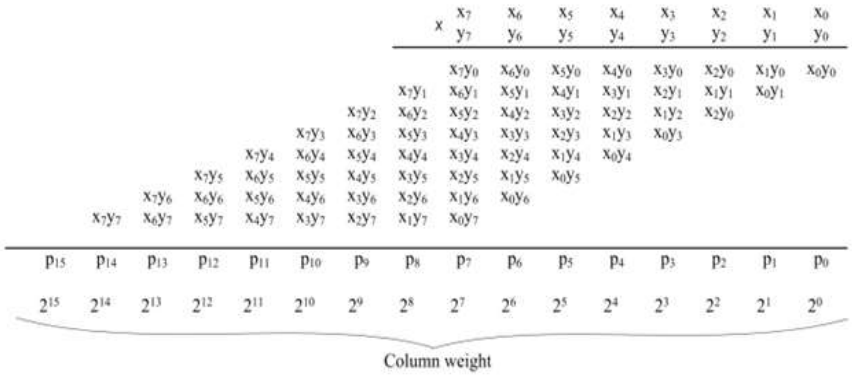

Fig. Standard parallel 8 x 8 bit multiplier

In this proposed work we first design standard parallel 8x8 multiplier which gives following result.

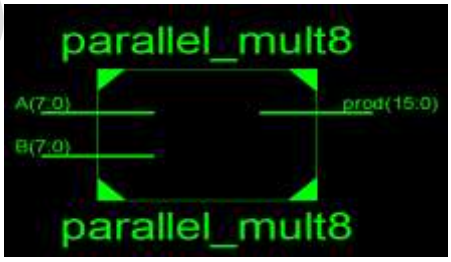

Fig. Block diagram of 8 x 8 parallel multiplier

Simulation result of standard parallel 8 x 8 bit multiplier is shown

/parallel_mult8/a	212	112	111	212
/parallel_mult8/b	140	112	60	140
/parallel_mult8/prod	29680	12544	6660	29680

This standard parallel 8x8 multiplier provides accurate result but requires large number of component to design by virtue of its area requirement is more. Also it requires more power and propagation delay. To reduce this requirement of area, power and delay we proposed truncated multiplier.

IV. PROPOSED TRUNCATED MULTIPLIER DESIGN

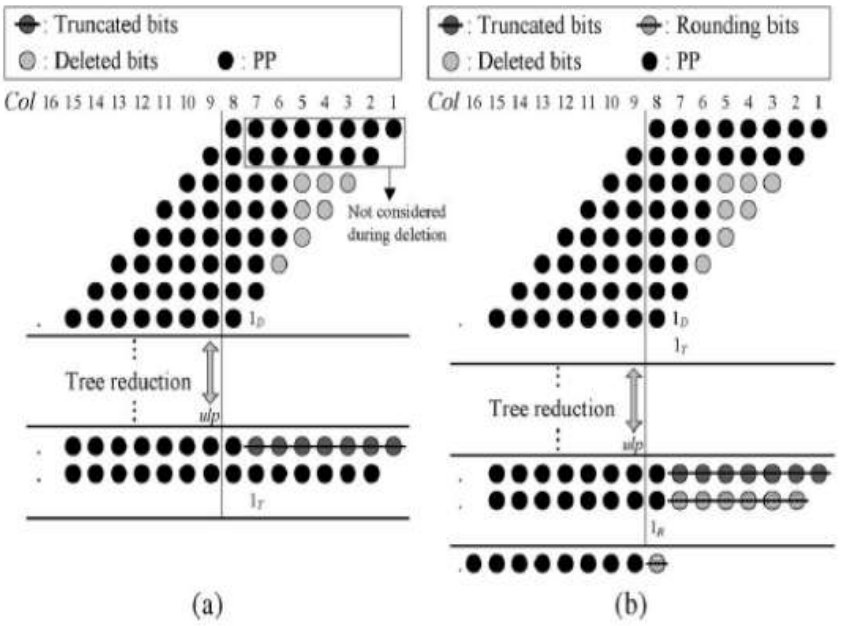

Fig. Proposed truncated multiplier design

For convenience, we assume 8 x 8 unsigned multiplication of two numbers. The objective of a good multiplier is to provide a better result, high speed and low power consuming chip. To save area requirement and power consumption of a VLSI design. In a truncated multiplier, number of the least significant columns of bits in the partial product matrix are not formed. Fig1. Show 8x8 truncated multiplication. (a) Deletion, reduction and truncation. (b) Deletion, reduction, truncation, rounding with correction logic and final addition.

PROPOSED ALGORITHM

In proposed architecture we multiply 8 x 8 bits, and the bits are reduced in step by step manner. Deletion is the first operation performed in Stage 1 to remove the PP bits, as long as the magnitude of the total deletion error is no more than 2^{-P-1}. Then numbers of stages are reduce the final bit width without increasing the error. Fig. shows proposed truncated multiplier. This reduces the area and power consumption of the multiplier [3]. For this we used Half Carry (HC), Full Carry (FC), Half Adder (HA), Full Adder (FA) logic to improve the result. Requirement of component for this truncated multiplier is less as compared to standard parallel multiplier; however it reduces the area required as well as delay and power. Following result is obtained for proposed 8 x 8 bit truncated multiplier which is approximately same as that of standard parallel multiplier with precision improvement.

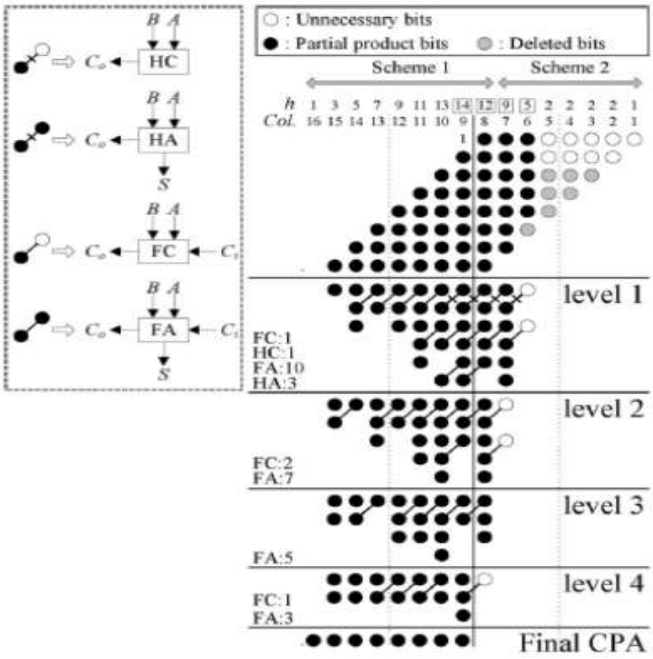

Fig. Proposed 8 x 8 bit truncated multiplier

The truncated multiplier for general M × N unsigned multiplication with a full product of M+N bits truncated to P bits. In other words, there are T = M + N – P bits truncated . First, perform deletion in stage 1 to remove the PP bits, as long as the magnitude of the total deletion error is not more. Bits[Col] represents the number of PP bits of column Col. Note that the first two rows of PP bits from column 1 to column T 1 are kept unchanged during the deletion process. Note that at column T + 1, we add a constant of which is the sum of the three constants (1_D, 1_T, and 1_R) in the aforementioned deletion, truncation, and rounding. In stage 2, for column Col, determine whether an HA is required or not (HA[Col] = true or false) and find the number of carry bits to the next column.

Furthermore, according to this experiments, it is observed that HAs should be used as early as possible in order to reduce the critical path delay because HAs have a smaller pin-to-pin delay compared with FAs. In stage 3, tree reduction is performed along with truncation and rounding. For the final two rows of PP bits from column 1 to column T − 1, there no need to generate these PP bits because they will be removed during the subsequent truncation and rounding processes. For example, in figure the two white dots at level 1 and the two white dots at level 2 are not generated during the compression with FAs or HAs. Thus, in this introduce two simplified versions of the FA and HA cells, i.e., full and half adders without the sum output bits. For column T, only need to generate the carry bit (to column T + 1) for the last FA compression because the sum output bit will be discarded during the rounding process. For example, the FA compression does not need to generate the white dot (the sum output bit) at level 4 of figure. Note that for column T + 1 to M + N, although it is adopted to determine whether an HA is needed or not, we actually do not compress the column height to one because this compression will cause ripple carry. Indeed, at the last level of the reduction process, some column, for example column i, has a height of three, and the remaining columns beyond this specific column, i.e., columns i +1, i + 2….., have a column height of two, as shown in level 4 of figure. Afterward, a final CPA performs the final summation. In the example in figure, the bit width of the final CPA is 7.

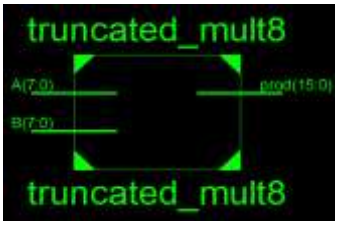

Fig. Block diagram of 8 x 8 bit truncated multiplier

Following simulations shows result of 8 x 8 truncated multiplier

This truncated multiplier is proposed multiplier for DSP applications. For this truncated multiplier there are different logic is applied such as deletion, reduction, truncation, rounding and final addition. It is providing multiplication of 8 × 8 bit which gives approximate result.

For FIR filter with standard 8 × 8 bit parallel multiplier

This simulation is for 2-Tap Adaptive FIR filter with standard parallel multiplier. From this it is clear that error continuously tending towards zero.

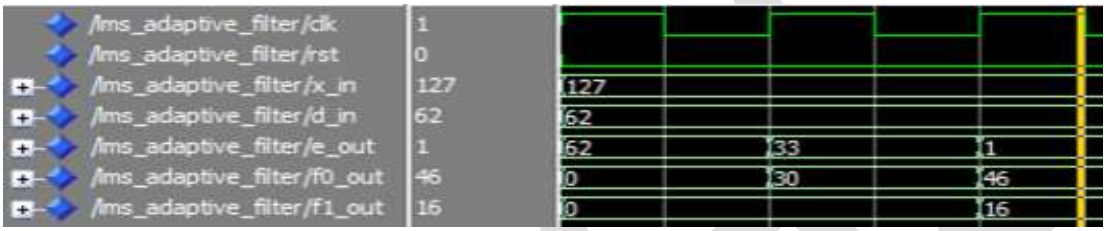

For FIR filter with 8 × 8 bit truncated multiplier

V. EXPERIMENTAL ANALYSIS

A) SYNTHESIS RESULT

For synthesis purpose we use Quartus-II software on hardware platform of Altera Cyclon-II family device EP2C35F672C6.

I. For Standard 8 × 8 bit parallel multiplier

For this standard 8 × 8 bit parallel multiplier requires more area as there is requirement of more number of logic elements.

Logic utilization	Used	Available	Utilization
Number of logic elements	189	33216	0.57%
Number of pins	32	475	6.7%

II. For 8 × 8 bit truncated multiplier

For this 8 × 8 bit truncated multiplier requires less area as there is need of less number logic elements which is comparatively less as compare to standard 8 × 8 bit parallel multiplier.

Logic utilization	Used	Available	Utilization

Number of logic elements	109	33216	0.328%
Number of pins	32	475	6.7%

This synthesis result shows the comparison between standard parallel multiplier and truncated multiplier on the basis of logic utilization.

III. For 2-Tap Adaptive FIR Filter with Standard 8 × 8 Bit Parallel Multiplier

Logic utilization	Used	Available	Utilization
Number of logic elements	758	33216	2.28%
Total logic registers	40	33216	----
Total pins	66	475	13.9%

IV. For 2-Tap Adaptive FIR filter with 8 × 8 Bit Truncated Multiplier

Logic utilization	Used	Available	Utilization
Number of logic elements	528	33216	1.58%
Total logic registers	88	33216	----
Total pins	66	475	13.9%

These synthesis result shows numbers of logic elements are required for 2-tap adaptive FIR filter with standard parallel multiplier is more as compared to truncated multiplier. It is concluded form this synthesis result area requirement is more as compare to truncated multiplier.

B) POWER ANALYSIS

In this power analysis result gives details of power dissipation for the different designs.

Power Analysis for Standard 8 × 8 Bit Parallel Multiplier

Core static thermal power dissipation	79.94mW
I/O thermal power dissipation	33.70mW
Total thermal power dissipation	113.64mW

Power Analysis for 8 × 8 Bit Truncated Multiplier

Core static thermal power dissipation	79.94mW
I/O thermal power dissipation	33.67mW
Total thermal power dissipation	113.61mW

Power Analysis for 2-Tap Adaptive Filter with Standard 8 × 8 Bit Parallel Multiplier

Core static thermal power dissipation	79.95mW
I/O thermal power dissipation	37.89mW
Total thermal power dissipation	117.84mW

Power Analysis For 2-Tap Adaptive FIR Filter with 8 × 8 Bit Truncated Multiplier

Core static thermal power dissipation	79.95mW
I/O thermal power dissipation	37.81mW
Total thermal power dissipation	117.76mW

It is concluded from this result power dissipation is more for standard multiplier as compare to truncated multiplier regarding 2-tap adaptive FIR filter.

C) TIMING ANALYSIS

Propagation delay for standard 8 × 8 bit parallel multiplier	22.412ns
Propagation delay for 8 × 8 bit truncated multiplier	19.366ns
Propagation delay for 2-Tap Adaptive FIR filter with standard parallel multiplier	21.56ns
Propagation delay for 2-Tap Adaptive FIR filter with truncated multiplier	9.79ns

D) COMPARATIVE ANALYSIS

There is need of more number of logic elements for implementing the design for standard 8 × 8 bit parallel multiplier as compare to truncated of multiplier. Also there is reduction in power dissipation and propagation delay for truncated multiplier. It is observed from the table, there is reduction in area, power and delay in truncated multiplier as compare to truncated multiplier.

Parameter	Parallel multiplier	Truncated multiplier	Filter with parallel multiplier	Filter with truncated multiplier
Design summary	LE 189/33216	109	758	528
Power analysis	Thermal Pd 113.64mW	113.61mW	117.84mW	117.76mW
Timing analysis	t_{pd}=22.412ns	19.366ns	21.56ns	9.79ns
No of HA, FA, HC, FC	8HA, 48FA	3HA,32FA, 1HC,4FC	more	less

ACKNOWLEDGMENT

I express my sincere gratitude to Mr. S. S. Thorat, Assistant Professor, Electronics Engineering Department, Government College of Engineering, Amravati, for extending his valuable insight for completion this work.

FUTURE SCOPE

Truncated multiplier can be effectively implemented in FIR filter structure. Conventional FIR filer performs ordinary multiplication of co-efficient and input without considers the length. Thus the structure can be made effective by replacing the existing multiplier with the proposed fixed width truncated multiplier for visible area reduction. It is nowadays used in PI temperature controller. Truncated multiplier is having more no of usages in that applications wherever truncation is possible to get approximate result. This truncated multiplier also applicable to any type of DSP applications where there is a need of multiplication process.

CONCLUSION

In this truncated multiplier, design is implemented by jointly considering the deletion, reduction, truncation, and final addition of PP bits. It is observed that the results of standard parallel multiplier and then compare this result with truncated multiplier which is approximately same. It is analyzed that area required for implementation of truncated multiplier reduces to large extent as compare to standard parallel multiplier. Also there is reduction in power dissipation and propagation delay. In this system final truncated multiplier satisfies the precision requirement.

REFERENCES

[1] Hou-Jen Ko and Shen-Fu Hsiao, "Design and Application of Faithfully Rounded and Truncated Multipliers With Combined Deletion, Reduction, Truncation, and Rounding", IEEE TRANSACTIONS on circuits and systems ii, Vol. 58, No. 5, May 2011, pp. 1-5.
[2] Shen-Fu Hsiao, Jun-Hong Zhang Jian, and Ming-Chih Chen, "Low-Cost FIR Filter Designs Based on Faithfully Rounded Truncated Multiple Constant Multiplication/Accumulation", IEEE TRANSACTIONS on circuits and systems, Vol. 60, No.5, May 2013, pp. 1-5.
[3] R. Devarani and C. S. Manikanandababu, "Design and implementation of truncated multipliers for precision improvement", International Conference on Computer Communication and Informatics (ICCCI-2013), Coimbatore, INDIA, Jan. 04 – 06, 2013.
[4] Nicola Petra, Member, IEEE, Davide De Caro, Senior Member, IEEE, Valeria Garofalo, Ettore Napoli, Antonio G. M. Strollo, Senior Member, IEEE, "Truncated Binary Multipliers With Variable Correction and Minimum Mean Square Error", IEEE TRANSACTIONS on circuits and systems, Vol. 57, No. 6, June 2010.
[5] Bindhya V, Marimuthu CN, "Design of Area Efficient FIR Filter Using Truncated Multiplier Technique for DSP Applications", Unique Journal of Engineering and Advanced Sciences 02(01), Jan-Mar 2014, pp. 10-13.

[6] P.Kavitha, R.Ramesh, "VLSI Implementation of Low-cost FIR Filter Structure Based on Improved Faithfully Rounded Truncated Multiplier", IRF International Conference, Chennai, 23rd March. 2014, pp. 1-5.
[7] Muhammad H. Rais, Member, IEEE and Syed M. Qasim, "FPGA Design and Implementation of Standard and Truncated 6x6-bit Multipliers", MASAUM Journal of Computing, Volume 1 Issue 2, September 2009.
[8] Verilog Hardware Description Language http://ece.niu.edu.tw/ chu/, pp. 17-85.
[9] Neha R. Laddha, "A Novel Approach For Displaying Data On LCD Directly From PC Using FPGA", International Journal of Emerging Science and Engineering(IJESE), April 2013, pp. 1-6.
[10] Volnei A. Pedroni, "Circuit Design with VHDL", MIT Press Cambridge , Massachusetts, 2004, pp. 1-173.
[11] DE2 Development and Education Board. Retrieved April 25, 2011, from altera: http: www.altera.com/education/univ/materials/boards/del/unv-del-board.html
[12] Altera, DE2 User Guide, October 2011, pp. 6-22.
[13] Suresh R.Rijal, Ms.Sharda G. Mungale, "Design and Implementation of 8 × 8 Truncated Multiplier on FPGA", International Journal of Scientific and Research Publications, Volume 3, Issue 3, March 2013, pp. 1-4.
[14] Andreas Thor Winther - s053010, "Testing and Analyzing Methods for Truncated Binary Multiplication", Finishing Bachelor Project Spring 2009, pp. 5-12.
[15] Jyotsna Yadav, Mukesh Kumar, Rohini Saxena, A. K. Jaiswal, "Performance Analysis of LMS Adaptive FIR Filter and RLS Adaptive FIR Filter for Noise Cancellation", Signal Image Processing : An International Journal (SIPIJ) Vol.4, No.3, June 2013

International Journal of Engineering Research and General Science Volume 3, Issue 3, Part-2 , May-June, 2015
ISSN 2091-2730

Efficient Implementation of Parallel Linear Phase FIR Digital Filters for Symmetric Convolution using Polyphase Decomposition

S. A. Takalkar, Student

Department of E&TC Engineering

Pune University, Pune

Smitatakalkar123@gmail.com

Y. D. Borole, Assistance Professor

Department of E&TC Engineering

Pune University, Pune

yogini.borole@raisoni.net

Abstract- This paper presents very efficient method that greatly reduces the consumption of hardware during design of FIR filters. Parallel processing together with linear phasing is a powerful technique which can be used to increase the throughput of the FIR filter or reduce the power consumption of the FIR filter. FIR filters are designed by exploiting the nature of symmetric coefficients. With the efficient usage of symmetric coefficients reduces the number of multipliers with increasing the number of adders, which does not affect the hardware cost to a great extent. Reduction in multiplier is advantageous with increase in certain number of because adders weight less in cost in terms of its silicon area and also the number of sub filter blocks remains fixed and does not increase along with the length of the FIR filter. With combination of fast FIR filtering and area reduction technique, a major reduction of multipliers is done. Overall, the proposed parallel FIR structures can lead to significant hardware savings for symmetric convolutions from the existing FFA parallel FIR filter, especially when the length of the filter is large

Keywords- Digital signal processing (DSP), fast finite-impulse response (FIR) algorithms (FFAs), parallel FIR, symmetric convolution, very large scale integration (VLSI)

I. INTRODUCTION

Digital audio, speech recognition, cable modems, radar, and high - definition television-these are but a few of the modern computer and communications applications rely on digital signal processing (DSP) and application-specific integrated circuits (ASICs). As industries constantly reinvent ASIC chips for lower power consumption and higher efficiency, there is a growing need in VLSI design methodologies for DSP. VLSI architecture theory and algorithms, addresses various architectures at the implementation level, and presents several approaches to analysis, estimation, and reduction of power consumption. to design high-speed, low-area, and low-power VLSI systems for a broad range of DSP applications. In some applications, FIR filters must be low-power or high speed supporting structures. For certain applications like video television broadcasts, higher order FIR filters are required. Design of these filters leads to hardware complexity and consumption of area and power. There are some techniques to reduce the complexity of the larger size filter blocks. In order to design these filters, polyphase decomposition is to be carried out where small-sized sub filter blocks are derived first and those sub-structures are cascaded or iterated to construct larger size filter blocks. This decomposition for FIR filter is used as a processing core to implement sub filters of proposed parallel FIR filters. Furthermore there have been papers proposing the FIR implementation using pipelining and parallel processing. Pipelining leads to increase in number of latches and system latency. Parallel processing increases the sampling rate by replicating the hardware. But parallel processing loses its advantage in practical implementation. Both the techniques reduce the power consumption to some extent. Considering the inefficiency of the above techniques, the basic nature of symmetric coefficients together with the polyphase decomposition is used in this paper to further reduce the amount of multipliers. This paper is organized as follows. A brief introduction is given in Section I , In Section II, the Introduction in Pipelining and Parallel Processing, In Section III Traditional FIR Algorithm and FFA, in section IV Proposed structure for symmetric convolution, Section V gives Proposed cascading scheme for FFA , Section VI conclusion And Section VII gives Acknowledgment.

II.PIPELINING AND PARALLEL PROCESSING

Pipelining transformation leads to a reduction in the critical path, which can be exploited to either increase the clock speed or sample speed or to reduce power consumption at same speed. In parallel processing, multiple outputs are computed in parallel in a clock period. Therefore, the effective sampling speed is increased by the level of parallelism. Similar to the pipelining, parallel processing

can also be used for reduction of power consumption. It is of interest to note that parallel processing and pipelining techniques are duals of each other, and if a computation can be pipelined, it can also be processed in parallel. Both techniques exploit concurrency available in the computation in different ways. While independent sets of computations are computed in an interleaved manner in a pipelined system, they are computed using duplicate hardware in parallel processing mode.

Designing a Parallel FIR System: Consider the 3-tap FIR filter described by, this system is a single-input single-output (SISO) system and is described by

$$y(n) = ax(n) + bx(n-1) + cx(n-2)$$

To obtain a parallel processing structure, the SISO system must be converted into a MIMO (multiple-input multiple-output) system. For example, the following set of equations describe a parallel system with 3 inputs per clock cycle (i.e., level of parallel processing $L = 3$).

$$y(3k) = ax(3k) + bx(3k-1) + cx(3k-2)$$

$$y(3k+1) = ax(3k+1) + bx(3k) + cxz(3k-1)$$

$$y(3k+2) = ax(3k+2) + bx(3k+1) + cx(3k)$$

Here k denotes the clock cycle. As can be seen, at the k-th clock cycle the 3 inputs $x(3k)$, $x(3k + 1)$ and $x(3k + 2)$ are processed and 3 samples are generated at the output. Parallel processing systems are also referred to as *block processing* systems and the number of inputs processed in a clock cycle is referred to as the *block size*. Because of the MIMO structure, placing a latch at any line.

III. TRADITIONAL FIR ALGORITHM AND FFA

A. Traditional FIR Algorithm

Assuming {x (n)} is an infinite-length input sequence and {h (i)} are the length-N FIR filter coefficients and {h (i)} are output sequence y(i) N-tap FIR filter which can be expressed in the general form as

$$y(n) = \sum_{i=0}^{N-1} h(i)x(n-i), \quad n = 0,1,2,...,\infty \qquad (1)$$

Traditional L- parallel FIR filter can be derived using polyphase decomposition as

$$\sum_{p=0}^{L-1} Y_p(z^L)z^{-p} = \sum_{q=0}^{L-1} X_q(z^L)z^{-q} \sum_{r=0}^{L-1} H_r(z^L)z^{-r} \qquad (2)$$

Where, $Xq = \sum_{k=0}^{\infty} z - kx(Lk + q)$,

$$Hr = \sum_{k-0}^{\left(\frac{N}{L}\right)-1} z - kx(Lk + r)$$

$$Yp = \sum_{k=0}^{\infty} z - kx(Lk + p)$$

For p, q, r = 0, 1, 2, 3, ……., L-1. From this FIR filtering equation, it shows that the traditional FIR will require L^2 – FIR sub filter blocks of length N/L for implementation.

$$Y_0 = H_0X_0 + z^{-2}H_1X_1$$

$$Y_1 = H_0X_1 + H_1X_0 \qquad (3)$$

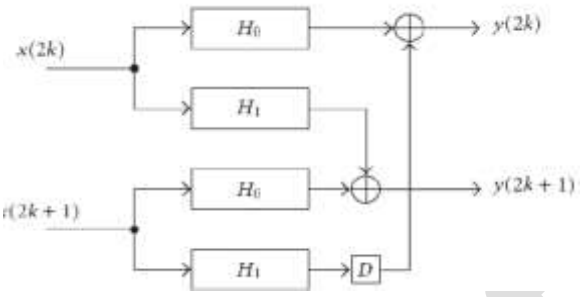

Figure1. Traditional 2-Parallel FIR Filter

B. Two parallel Fast FIR Algorithm

A two- parallel FIR filter can be expressed as

$$Y_0 = H_0X_0 + z^{-2}H_1X_1$$

$$Y_1 = (H_0 + H_1)(X_0 + X_1) - H_0X_0 - H_1X_1 \qquad (4)$$

For FFA with (4) require three FIR sub filter blocks of length N/2, one preprocessing and three post processing adders, and 3N/2 multipliers and 3(N/2-1)+ 4 adders, which reduces approximately one fourth over the traditional two- parallel filter hardware cost from (3). As implementation cost of a multiplier is greater than that of an adder, the cost to implement the parallel filtering structure can be approximated as being proportional to the number of multipliers required for the implementation. The hardware consumption of parallel fast FIR filter is 25% less when compared to traditional parallel FIR filters.

C. Three parallel Fast FIR Algorithm

A three-parallel FIR filter using FFA can be expressed as

$$Y_0 = H_0X_0 - z^{-3}H_2X_2 + z^{-3}\left(H_1 + H_2\right)\left(X_1 + X_2\right) - H_1X_1$$

$$Y_1 = \{(H_0 + H_1)(X_0 + X_1) - H_1X_1\} + (H_0X_0 - z^{-3}H_2X_2)$$

$$Y_2 = \{(H_0 + H_1 + H_2)(X_0 + X_1 + X_2)\}$$

$$- \{(H_0 + H_1)(X_0 + X_1) - H_1X_1\}$$

$$- \{(H_1 + H_2)(X_1 + X_2) - H_1X_1\} \qquad (5)$$

Above implementation requires six length N/3 FIR sub-filter blocks, three preprocessing and seven post processing adders, and three N multipliers and 2N+4 adders, which has reduced approximately one third over the traditional three-parallel filter hardware cost.

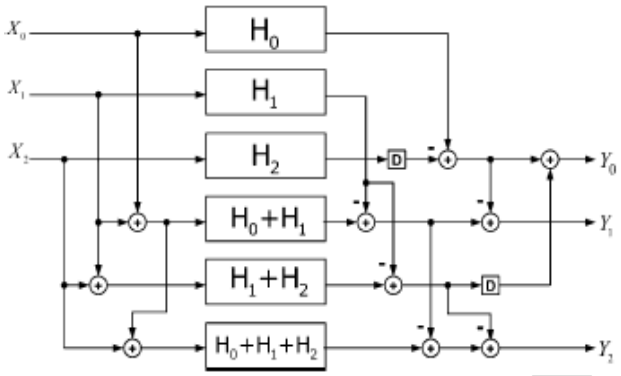

Figure2. Three-parallel FIR Filter implementation using FFA

IV. PROPOSED STRUCTURES FOR SYMMETRIC CONVOLUTIONS

The main idea is to create be low-power or high speed FIR filter. So it is necessary to manipulate the polyphase decomposition to earn as many sub filter blocks as possible exploiting the symmetry of coefficients.

A. Proposed Structure 3A, ((N mod) = 0)

For a set of symmetric coefficients in odd length N, when (N mod 3) equals zero,(8) can earn two more sub filter blocks containing symmetric coefficients than(7) This can be described with an example..

Example: - Consider a 27-tap FIR filter with a set of symmetric coefficients applying to the proposed two-parallel FIR filter.

{h(0),h(1),h(2),h(3),h(4),h(5),

h(6),h(7),h(8),h(9),…,h(26)}

where h(0)=h(26), h(1)=h(25), h(2)=h(24), h(3)=h(23), h(4)=h(22), h(5)=h(21),… ,h(12)=h(14), applying to the proposed two-parallel FIT filter structure , and the top two subfilter blocks will be as

$$H_0 \pm H2 = \{h(0) \pm h(2), h(3) \pm h(5),$$

$$h(6) \pm h(8), h(9) \pm h(7), \ldots h(18) \pm h(19)$$

$$h(20) \pm h(21), h(22) \pm h(23)\}$$

Where

$$h(0) \pm h(2) = \pm(h(24) \pm h(26))$$

$$h(3) \pm h(5) = \pm(h(21) \pm h(23))$$

$$h(6) \pm h(8) = \pm(h(18) \pm h(20))$$

$$h(9) \pm h(11) = \pm(h(15) \pm h(17)) \ldots \quad (6)$$

$$\begin{aligned}
Y_0 &= H_0X_0 + z^{-3} \times \{(H_1 + H_2)(X_1 + X_2) - H_1X_1 \\
&\quad - \Big((H_0 + H_2)(X_0 + X_2) - H_0X_0 \\
&\quad - \frac{1}{2}[(H_0 + H_2)(X_0 + X_2) \\
&\quad - (H_0 - H_2)(X_0 - X_2)]\Big)\} \\
Y_1 &= (H_0 + H_1 + H_2)(X_0 + X_1 + X_2) - (H_1 + H_2)(X_1 + X_2) \\
&\quad - (H_0 + H_2)(X_0 + X_2) \\
&\quad + \Big\{(H_0 + H_2)(X_0 + X_2) - \frac{1}{2} \\
&\quad \times [(H_0 + H_2)(X_0 + X_2) \\
&\quad - (H_0 - H_2)(X_0 - X_2)] - H_0X_0\Big\} \\
&\quad + z^{-3}\{(H_0 + H_2)(X_0 + X_2) \\
&\quad - (H_0 - H_2)(X_0 - X_2)] - H_0X_0\} \\
Y_2 &= H_1X_1 + \frac{1}{2} \times [(H_0 + H_2)(X_0 + X_2) \\
&\quad - (H_0 - H_2)(X_0 - X_2)]
\end{aligned}$$

(7)

Comparing with the existing FFA three-parallel FIR filter structure, the proposed structure leads to two more sub filter blocks, which contain symmetric coefficients. Hence for an N-tap three-parallel FIR filter , the proposed structure can save N/3 multipliers from the existing FFA structure.

B. **Proposed Structure 3B, ((N mod 3)=1)**

For a set of symmetric coefficients in odd length N, when(N mod 3) equals 1,such as N=25, the proposed structure 3B can earn one more sub filter block with symmetric coefficients over the existing FFA as shown in equ.(8) i.e., presented in

$$Y_0 = H_0X_0 + z^{-3} \times \{\frac{1}{2}[(H_1 + H_2)(X_1 + X_2) - (H_1 - H_2)(X_1 - X_2)]\}$$

$$Y_1 = (H_0 + H_1 + H_2)(X_0 + X_1 + X_2) - (H_1 + H_2)(X_1 + X_2) - (H_0 + H_1)(X_0 + X_1) + \left\{(H_1 + H_2)(X_1 + X_2) - \frac{1}{2} \times [(H_1 + H_2)(X_1 + X_2) - (H_1 - H_2)(X_1 - X_2)] - H_2X_2\right\} + Z^{-3}H_2X_2$$

$$Y_2 = (H_0 + H_1 + H_2)(X_0 + X_1 + X_2) - (H_1 + H_2)(X_1 + X_2) - (H_0 + H_1)(X_0 + X_1) + 2\left\{(H_1 + H_2)(X_1 + X_2) - \frac{1}{2} \times [(H_1 + H_2)(X_1 + X_2)] - H_2X_2\right\}$$

(8)

C. Proposed structure 3C, ((N mod 3) =2)

For a set of symmetric coefficients in odd length N, when (N mod 3) equals 2, such as N=23,the proposed structure 3C represented in (9),can earn one more sub filter block containing symmetric coefficients over the existing FF

$$Y_0 = \left\{\frac{1}{2}[(H_0 + H_1)(X_0 + X_1) + (H_0 - H_1)(X_0 - X_1)] - H_1X_1\right\} + z^{-2}H_1X_1$$

$$Y_1 = \frac{1}{2}[(H_0 + H_1)(X_0 + X_1) - (H_0 - H_1)(X_0 - X_1)] + z^{-3}H_2X_2$$

$$Y_2 = H_1X_1 + \{(H_0 + H_2)(X_0 + X_2) - \{(H_0 + H_1)(X_0 + X_1) - \frac{1}{2} \times [(H_0 + H_1)(X_0 + X_1) - (H_0 - H_1)(X_0 - X_1)] - H_1X_1\}\text{-}H_2X_2\}$$

(9)

Comparing with the existing FFA three-parallel FIR filter structure, the proposed structure leads to two more sub filter blocks, which contain symmetric coefficients. Hence for an N-tap three-parallel FIR filter , the proposed structure can save N/3 multipliers from the existing FFA structure.

V. PROPOSED CASCADING SCHME FOR FFA

In proposed cascading process, instead of applying the existing small-sized structured FFA's to every stage, interleaving of multiple various small-sized structures can be done to fully exploit the symmetry of coefficients. The cascading of FFA's is a straight-forward application. For example, a (m x m) FFA can be cascaded with a (n x n) FFA to produce (m x n) parallel filtering structure. The resulting filters will be of length $N/(m\,x\,n)$. During the cascading of the FFA's, it is important to keep track of both the number of multipliers and the number of adders required for the filtering structure.

MATHEMATICAL FORMULAE

The required number of multipliers for a L-parallel filter with symmetric coefficients of odd length N can be estimated by (11) and (12) as,

Case 1:

When $\frac{N}{\prod_{i=1}^{r} L_i}$ is even.

$$M = \frac{N}{\prod_{i=1}^{r} L_i}\left(\prod_{i=1}^{r} M_i - \frac{S}{2}\right). \quad (10)$$

Case 2:

When $\frac{N}{\prod_{i=1}^{r} L_i}$ is odd.

$$M = \frac{N}{\prod_{i=1}^{r} L_i}\prod_{i=1}^{r} M_i - \frac{S}{2}\left(\frac{N}{\prod_{i=1}^{r} L_i} - 1\right). \quad (11)$$

Li , is the small parallel block size such as (2 x 2) or (3 x 3) FFA.

r, is the number of FFAs used. Mr, is the number of sub filter blocks resulted from i-th FFA. S is the number of sub filter blocks containing symmetric coefficients. The number of the required adders in sub filter section can be given by

$$A_{sub} = \prod_{i=1}^{r} M_i \left(\frac{N}{\prod_{i=1}^{r} L_i} - 1\right). \quad (12)$$

A comparison between the proposed and the existing FFA structures for even symmetric coefficients with different length under different level of parallelism

VI. CONCLUSION

This paper has presented the new parallel linear-phase FIR structures which are highly beneficial to the symmetric convolutions of length. Multipliers play a major role in terms of area and power consumption in FIR implementation. Since multipliers out weight adders in hardware cost, it is economical to replace multipliers with adders. The proposed new parallel filter blocks exploit the nature of symmetric coefficients and further reduce the amount of multipliers with adders. However, the numbers of reduced multipliers increases along with the length of FIR filter whereas the number adders remain still. The Pipelining and parallel processing is including in this Paper.

VII. ACKNOWLEDGMENTS

First, I would like to thank my Project Guide Prof. Y.D.Borole for their guidance and interest. I also thank Head of Dept. Prof. A.D. Bhoi. I also thank them for all their patience throughout, in the cross-reviewing process which constitutes a rather difficult balancing act. Secondly, I would like to thank all the Staff Members of E&TC Dept. for providing me their admirable feedback and invaluable insights whenever I discussed my project with them.

REFERENCES:

[1] D. A. Parker and K. K. Parhi, "Low-area/power parallel FIR digital filter implementations, " *J. VLSI Signal Process. Syst.*, vol. 17, no. 1,pp. 75–92, 1997.

[2] J. G. Chung and K. K. Parhi, "Frequency-spectrum-based low-area low-power parallel FIR filter design," *EURASIP J. Appl. SignalProcess.*, vol. 2002, no. 9, pp. 444–453, 2002.

[3] K. K. Parhi, *VLSI Digital Signal Processing Systems: Design and Implementation*. New York: Wiley, 1999.

[4] Z.-J. Mou and P. Duhamel, "Short-length FIR filters and their use in fast nonrecursive filtering," *IEEE Trans. Signal Process.*, vol. 39, no.6, pp. 1322–1332, Jun. 1991.

[5] J. I. Acha, "Computational structures for fast implementation of L-path and L-block digital filters," *IEEE Trans. Circuit Syst.*, vol. 36, no. 6, pp. 805–812, Jun. 1989.

[6] C. Cheng and K. K. Parhi, "Hardware efficient fast parallel FIR filter structures based on iterated short convolution," *IEEE Trans. CircuitsSyst. I, Reg. Papers*, vol. 51, no. 8, pp. 1492–1500, Aug. 2004.

[7] C. Cheng and K. K. Parhi, "Further complexity reduction of parallel FIR filters," in *Proc. IEEE Int. Symp. Circuits Syst. (ISCAS 2005)*, Kobe, Japan, May 2005.

[8] C. Cheng and K. K. Parhi, "Low-cost parallel FIR structures with 2-stage parallelism," *IEEE Trans. Circuits Syst. I, Reg. Papers*, vol. 54, no. 2, pp. 280–290, Feb. 2007.

[9] I.-S. Lin and S. K. Mitra, "Overlapped block digital filtering," *IEEE Trans. Circuits Syst. II, Analog Digit. Signal Process*, vol. 43, no. 8,pp. 586–596, Aug. 1996.

[10] *"Design Compiler User Guide,"* ver. B-2008.09, Synopsys Inc., Sep.

[11]M. Potkonjak, M. B. Srivastava, and A. Chandrakasan. "Multiple Constant Multiplications: Efficient and Versatile Framework and Algorithms for Exploring Common Sub expression Elimination".In IEEE on C-ADvol. 15, no. 2, pp. 151-165, 1996

International Journal of Engineering Research and General Science Volume 3, Issue 3, Part-2 , May-June, 2015
ISSN 2091-2730

Design of Modified Carry Select Adder for Addition of More Than Two Numbers

Jasbir Kaur[1] and Lalit Sood[2]

Assistant Professor, ECE Department, PEC University of Technology, Chandigarh, India [1]

PG Scholar, Electronics (VLSI Design), PEC University of Technology, Chandigarh, India [2]

jasbirkaur@pec.ac.in[1] and lalitsood3@gmail.com[2]

Abstract— Due to rapidly growing system-on-chip industry, not only the faster units but also smaller area and less power has become a major design constraint for VLSI community. Further, demand for high speed is continuously increasing. In processors, most commonly used arithmetic operation is the addition operation. It is the adder delay that determines the maximum frequency of operation of the chip. Different topologies have been put forward, each providing trade-off between different performance parameters and as such no design is considered as superior. Carry select adder is considered to be best in terms of speed and provide compromise between ripple carry adder and carry look-ahead adder, but to a lesser extent at the cost of its area. In this paper, a modified carry select adder is designed that can add up to five 16-bit numbers with the help of compressors by following basic carry select addition procedure which is efficient to increase its speed of operation. This design is simulated using Cadence Tool.

Keywords— VLSI, High Speed, Ripple Carry Adder, Carry Look ahead Adder, Carry Select Adder, Modified Carry Select Adder, Cadence Tool.

I. INTRODUCTION

Due to the rapid growth of portable electronic component the low power arithmetic circuits become very important in VLSI industry. Multiplier-Accumulator (MAC) unit is the main building block in DSP processor. Full Adder is a part of the MAC unit can significantly affect the efficiency of whole system. Hence the reduction of power consumption of Full Adder circuit is necessary for low power application. Carry Select Adder are used for high speed application by reducing propagation delay. The basic operation Carry Select Adder (CSLA) is parallel computation. CSLA generates many carriers and partial sum [3]. The final sum and carry are selected by multiplexers (mux). Multiple pairs of Ripple Cary Adders (RCA) are used in CSLA structure. Hence, the CSLA is not area efficient.

This paper proposes the design of modified carry select adder which has two main features. One is this adder follows the basic procedure of carry select addition that increases speed of operation. Second is the compressors used for addition operate simultaneously and are independent of previous stage outputs that also contribute in increased speed of multiplication.

This paper is partitioned into six sections. Section II describes the conventional method for addition. Section III gives introduction to modified carry select adder. Section IV deals with design of modified carry select adder. Section V compares the results of proposed adder with conventional one. Conclusions and references follow.

II. CONVENTIONAL ADDER

The basic algorithm for addition of five numbers, *P*, *Q*, *R*, *S* and *T* makes use of the associative property of addition. That is, if 'Sum' can be written as sum of *P*, *Q*, *R*, *S* and *T*, then $Sum = P + Q + R + S + T$ can be written in a number of ways. Few examples are given below:

$Sum = (P + Q) + (R + S) + T;$

or

Sum = P + (Q + R) + (S +T);

or

Sum = (P + Q + R) + (S +T);

Or

… (a number of such combinations)

The terms on the right hand side can be readjusted and grouped together as per requirement. An addition algorithm finds a simple way to allow a simple calculation of the addends.

A bit-wise addition of five different 16-bit binary numbers using conventional method can be described with the help of Table 1. The schematic diagram for conventional adder is shown in Figure 1.

Table 1: Bit-wise addition of five 16-bit numbers using conventional method

Bits to be added	Sum	Carry[0]	Carry[1]
P[0],Q[0],R[0],S[0], T[0]	Sum[0]	$C_0[0]$	$C_0[1]$
P[1],Q[1],R[1],S[1], T[1],$C_0[0]$	Sum[1]	$C_1[0]$	$C_1[1]$
P[2],Q[2],R[2],S[2], T[2],$C_1[0]$,$C_0[1]$	Sum[2]	$C_2[0]$	$C_2[1]$
P[3],Q[3],R[3],S[3], T[3],$C_2[0]$,$C_1[1]$	Sum[3]	$C_3[0]$	$C_3[1]$
P[4],Q[4],R[4],S[4], T[4],$C_3[0]$,$C_2[1]$	Sum[4]	$C_4[0]$	$C_4[1]$
P[5],Q[5],R[5],S[5], T[5],$C_4[0]$,$C_3[1]$	Sum[5]	$C_5[0]$	$C_5[1]$
P[6],Q[6],R[6],S[6], T[6],$C_5[0]$,$C_4[1]$	Sum[6]	$C_6[0]$	$C_6[1]$
P[7],Q[7],R[7],S[7], T[7],$C_6[0]$,$C_5[1]$	Sum[7]	$C_7[0]$	$C_7[1]$
P[8],Q[8],R[8],S[8], T[8],$C_7[0]$,$C_6[1]$	Sum[8]	$C_8[0]$	$C_8[1]$
P[9],Q[9],R[9],S[9], T[9],$C_8[0]$,$C_7[1]$	Sum[9]	$C_9[0]$	$C_9[1]$
P[10],Q[10],R[10], S[10],T[10],$C_9[0]$, $C_8[1]$	Sum[10]	$C_{10}[0]$	$C_{10}[1]$
P[11],Q[11],R[11], S[11],T[11],$C_{10}[0]$, $C_9[1]$	Sum[11]	$C_{11}[0]$	$C_{11}[1]$
P[12],Q[12],R[12], S[12],T[12],$C_{11}[0]$, $C_{10}[1]$	Sum[12]	$C_{12}[0]$	$C_{12}[1]$

P[13],Q[13],R[13], S[13],T[13],C_{12}[0], C_{11}[1]	Sum[13]	C_{13}[0]	C_{13}[1]
P[14],Q[14],R[14], S[14],T[14],C_{13}[0], C_{12}[1]	Sum[14]	C_{14}[0]	C_{14}[1]
P[15],Q[15],R[15], S[15],T[15],C_{14}[0], C_{13}[1]	Sum[15]	C_{15}[0]	C_{15}[1]
C_{15}[0], C_{14}[1]	Sum[16]	C_{16}[0]	0
C_{16}[0], C_{15}[1]	Sum[17]	C_{17}[0]	0
Carry out	C_{17}[0]	0	0

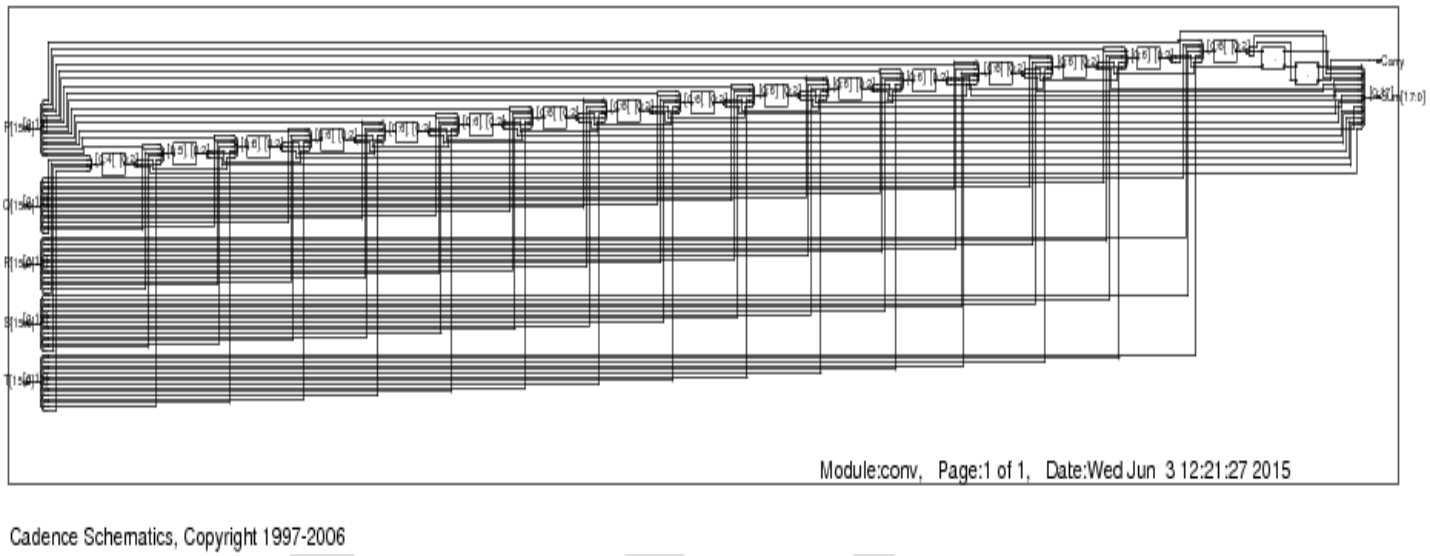

Figure 1: Schematic diagram of Conventional Adder

III. Introduction to Modified Carry Select Adder (MCS*l*A)

Modified Carry Select Adder is designed to add up to five 16-bit numbers. This MCS*l*A is made up of two components. First component is compressor that compresses five bits into two bits. Second component is carry select adder that generates the result by using ripple carry adders and multiplexers.

A. Compressor

For compressing five bits into two bits, two compressors are used. One is 3:2 compressor and another one is 5:3 compressor.

(i) 3:2 Compressor

3:2 Compressor is simply a full adder that adds three bits and generates two bit output as sum and carry [10]. The block diagram of 3:2 compressor is shown in Figure 2(a).

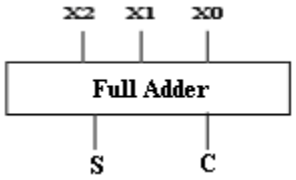

Figure 2(a): Block Diagram of 3:2 Compressor

(ii) 5:3 Compressor

5:3 Compressor is made up of two full adders and one half adder. It is designed to add five bits and generates final sum of three bits [8]. The block diagram of 5:3 compressor is shown in Figure 2(b).

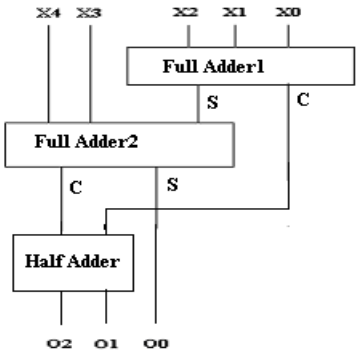

Figure 2(b): Block Diagram of 5:3 Compressor

B. Carry Select Adder

Carry Select Adder (CS*l*A) architecture consists of independent generation of sum and carry i.e., Cin=1 and Cin=0 are executed in parallel [6]. Depending upon Cin, the external multiplexers select the carry to be propagated to next stage. Further, based on the carry input, the sum will be selected. Hence, the delay is reduced. However, the structure is increased due to the complexity of multiplexers [4].The architecture of CS*l*A is shown in Figure 3.

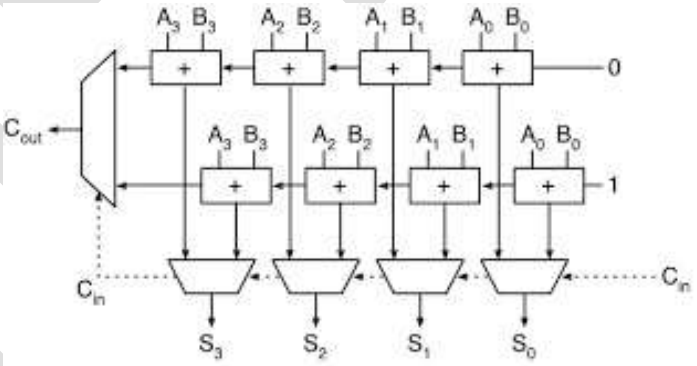

Figure 3: Block Diagram of CS*l*A

IV. Design of Modified Carry Select Adder

This MCS*l*A takes five 16-bit numbers P, Q, R, S and T as input and generates 18-bit sum and a carry. The architecture of MCS*l*A is shown step by step with the help of Figure 4(a), Figure 4(b), Figure 4(c), Figure 4(d) and Figure 4(e).

The schematic diagram for MCS*l*A is shown in Figure 5.

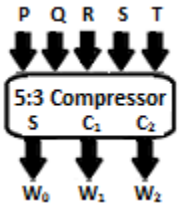

Figure 4(a): 16-bit 5:3 Compressor

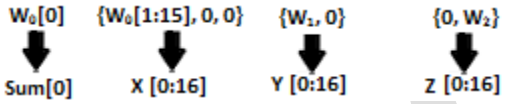

Figure 4(b): Rearrangement of bits

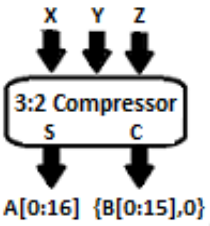

Figure 4(c): 17-bit 3:2 Compressor

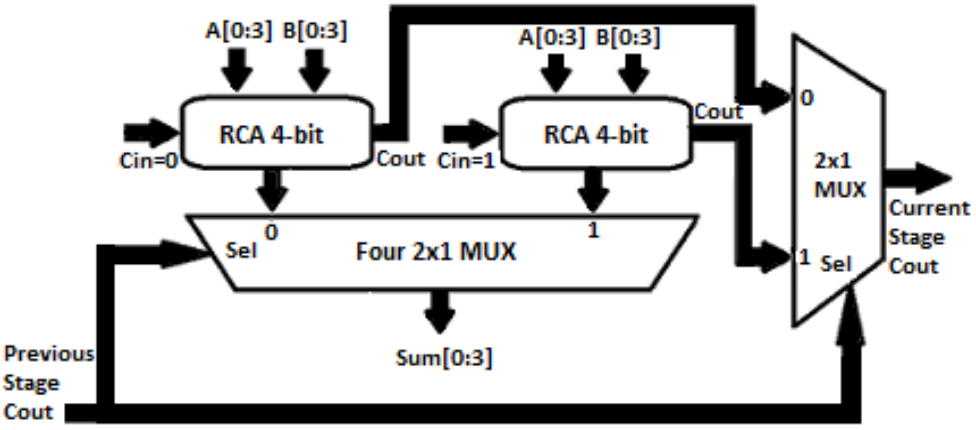

Figure 4(d): Basic Block of CS*l*A

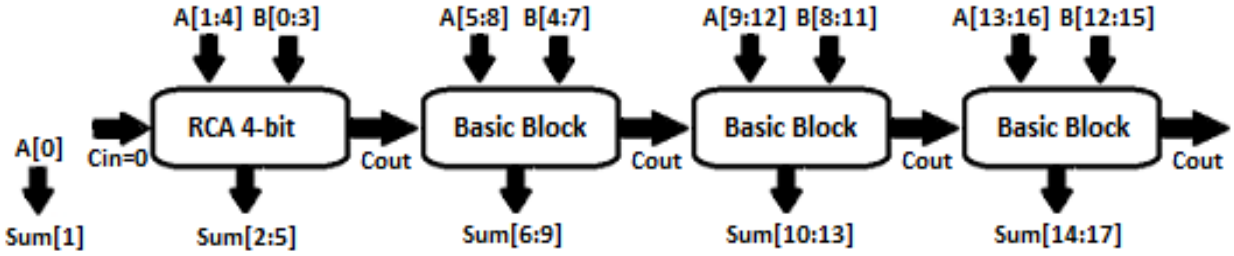

Figure 4(e): Block Diagram of CS*l*A

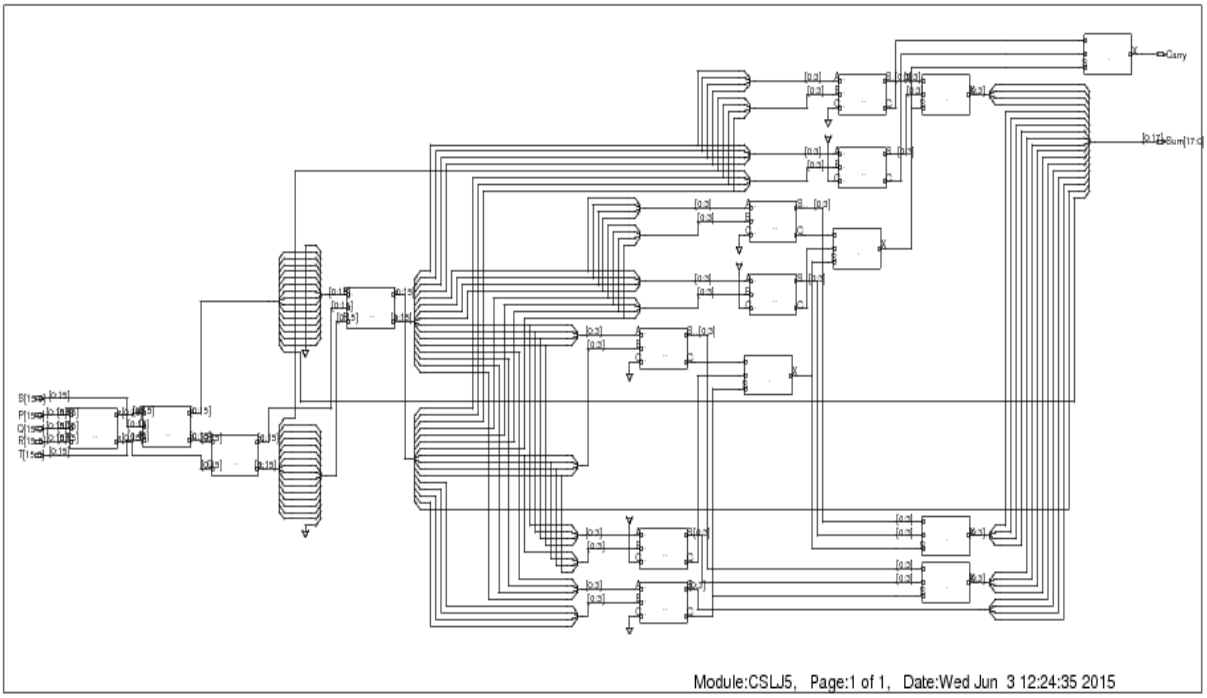

Figure 5: Schematic Diagram of MCS*l*A

V. Comparison

In this paper, the proposed modified carry select adder and conventional adder have been simulated using Cadence Tool. The comparison is done on the basis of basic parameters such as power consumption, speed of operation and area used. The comparative results of these two adders are shown in Table 2.

Table 2: Comparison between designed adder and conventional adder

Parameter	% increase/decrease for proposed adder as compared to conventional adder
Power	60.48% increased
Delay	82..66% decreased
Area	43.90% increased

VI. Conclusions

Different types of adder topologies are used for addition of binary numbers [1]. On comparing different adder topologies, it is found that carry select adder is the fastest one among other mostly used adders [2]. The carry select adder is modified to add up to five 16-bit numbers. This proposed adder is 82.66% faster than conventional adder. It can be used for high speed applications where area and power are not major issues.

REFERENCES:

[1] R.Uma, Vidya Vijayan, M.Mohanapriya, and Sharon Paul, "Area, Delay and Power Comparison of Adder Topologies", International Journal of VLSI Design & Communication Systems, vol.3, no.1, pp.153-168,Feb 2012.

[2] Jasbir Kaur, Lalit Sood, "Comparison Between Various Types of Adder Topologies", IJCST vnuno-ol.6, Issue 1, Jan-March 2015.

[3] Sarabdeep Singh, Dilip Kumar, "Design of Area and Power Efficient Modified Carry Select Adder", International Journal of Computer Applications, vol.33, no.3, pp.14-18,Nov 2011.

[4] Padma Devi, Ashima Girdher and Balwinder Singh, "Improved Carry Select Adder with Reduced Area and Low Power Consumption", International Journal of Computer Application,Vol 3.No.4, June 2010 .

[5] G.Shyam Kishore, "A Novel Full Adder with High Speed Low Area", 2nd National Conference on Information and Communication Technology (NCICT) 2011 Proceedings published in International Journal of Computer Applications® (IJCA).

[6] Romana Yousuf and Najeeb-ud-din,"Synthesis of Carry Select Adder in 65 nm FPGA", IEEE.

[7] J. Gu, C. Chang (2003), "Ultra low voltage low power 4-2 compressor for high speed multiplications", Proceedings of IEEE International Symposium on Circuits and Systems", Vol. 5, pp. 321-324.

[8] K. Prasad, K.K. Parhi (2001), "Low power 4-2 and 5-2 compressors", Proceedings of 35th Asilomar Conference on Signals, Systems and Computers, Vol. 1, pp. 129-133.

[9] C.-H. Chang, et. al., "Ultra low-voltage Low-Power CMOS 4-2 and 5-2 Compressors for Fast Arithmetic Circuits," Circuits and Systems I: Regular Papers, IEEE Transactions on, vol. 51, no. 10, pp. 1985 –1997, oct. 2004.

[10] S. Veeramachaneni, et. al. ,"Novel Architectures for High-Speed and Low-Power 3-2, 4-2 and 5-2 Compressors," in VLSI Design, 2007. Held jointly with 6th International Conference on Embedded Systems., 20th International Conference on, jan. 2007, pp. 324–329

International Journal of Engineering Research and General Science Volume 3, Issue 3, Part-2 , May-June, 2015
ISSN 2091-2730

Identification of Scene Text by Character Descriptor in Smart Mobile Devices

Devdas[1], Bhavana.S[2], Dr. Shubhangi D.C.[3]

Student, Department of computer science and engineering, VTU RO Kalaburagi, India[1]

Assistant professor, Department of computer science and engineering, VTU RO Kalaburagi, India[2]

Head of Department, Department of computer science and engineering, VTU RO Kalaburagi, India[3]

Email:Devd.bansode@gmail.com. Contact no: 8951781387

Abstract— Text data present in images and video contain useful information for automatic annotation, indexing, and structuring of images. Extraction of this information involves detection, localization, tracking, extraction, enhancement, and recognition of the text from a given image. However, variations of text due to differences in size, style, orientation, and alignment, as well as low image contrast and complex background make the problem of automatic text extraction extremely challenging. The main focus of this system is on two character recognition methods. In text detection, previously proposed algorithms are used to search for regions of text strings. Proposed system uses character descriptor which is effective to extract representative and discriminative text features for both recognition schemes. The local features descriptor HOG is compatible with all above key point detectors. Our method of scene text recognition from detected text regions is compatible with the application of mobile devices. A personal digital assistant (PDA) was chosen because it combines small-size, computational resources and low cost price. Three key technologies are necessary: text detection, optical character recognition and speech synthesis. The demo system gives us details of algorithm design and performance improvements of scene text extraction. It is able to detect text region of text strings from cluttered and recognize characters in the text regions.

Keywords— Scene text detection, scene text recognition, character descriptor, stroke configuration, text understanding, text retrieval mobile application.

1. INTRODUCTION

Text in the image contains useful information which helps to acquire the overall idea behind the image. Character extraction from image is important in many applications. It is a difficult task due to variations in character fonts, sizes, styles and text directions, and presence of complex backgrounds and variable light conditions. Several methods for text (or character) extraction from natural scenes have been proposed. If develop a method that extracts and recognizes those texts accurately in real time, then it can be applied to many important applications like document analysis, vehicle license plate extraction, text- based image indexing, etc. Camera-based applications on mobile phones are increasing rapidly. There can be valuable information in image. However, extraction of text from scene image is problematic due to factors such as variety of scale, orientation, font, style of character and complex background with multiple colors. Text Recognition in natural scene images is challenging than recognizing text from scans of printed pages, faxes and business cards. Modeling character structure is difficult due to high variability of geometry and appearance of characters natural image. To solve these problems text extraction is divided in two activities [9]: text detection and text recognition. Text detection localize region containing text characters [4]. Text recognition distinguishes different characters which are part of text word. We have presented two schemes text recognition process. First, a character recognizer to predict the category of a character in an image patch. Second, binary classifier which predicts existence of category. Two schemes of text recognition are compatible with applications related to scene text, which are text understanding and text retrieval. Text understanding acquires text information from natural scene to understand surrounding environment and objects, while text retrieval matches some stated user query against a set of free-text records. we design a discriminative character descriptor by combining several state-of-the-art feature detectors and descriptors[6].We model character structure at each character class by designing stroke configuration maps[5]. It involves 62 identity categories of text characters, including 10 digits [0-9] and 26 English letters in upper case [A-Z] and lower case [a-z]. An Android- based demo system is developed to show the effectiveness of our proposed method on scene text information extraction from nearby objects. Besides, previous work rarely presents the mobile implementation of scene text extraction, and we transplant our method into an Android-based platform. We propose an Android application that detects the text information within an image taken with a mobile phone camera, extracts it, recognizes it and translates it.

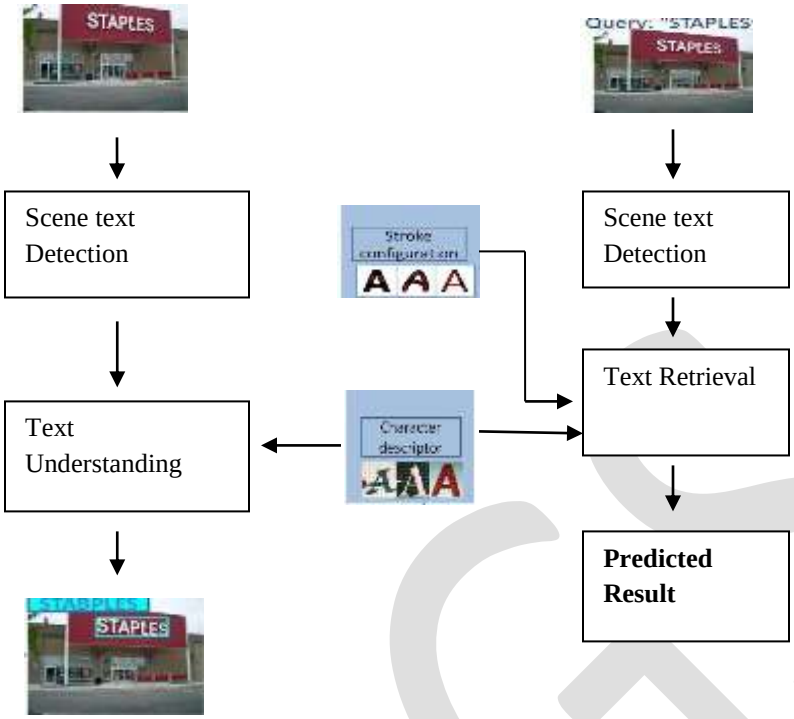

Fig. 1. The flowchart of our designed scene text extraction method

Objective of this system is the extraction of text from any image and then displaying its related information on the mobile screen. Main goal of this system is that if a person doesn't have or know any specific thing then he/she could get its information with the help of this android application**.**

In text extraction feature text is being extracted from the natural scene or an image. Here text extraction is done with the help of character description and stroke configuration [1]. Firstly the text will be detected, understood and then recognized. In searching process extracted text is being searched over net or in database. Here searching is done with the help of item ranking according to the item of interest. It basically derives meta data information about the item of interest by extending the user's given interest.

2. RELATED WORK

Our present a general review of previous work on scene text recognition respectively. Our observe that text characters from different categories are distinguished by boundary shape and skeleton structure, which plays an important role in designing character recognition algorithm. Extracting text from image is a difficult task. To perform this task various techniques have been implemented before. Cluster classification [1] is one of the techniques which have high accuracy in detecting text area and non-text area. There is new trend towards content based document image retrieval technique without going through OCR process [2].

There is another technique named as sliding window detection which has high accuracy of detecting text in natural scene. In Scale Invariant Feature Transform (SIFT), feature matching was adopted to recognize text characters in different languages, and a voting and geometric verification algorithm was presented to filter out false positive matches. SIFT reduces false positive rates by more than an order of magnitude relative to the best Haar wavelet based detector . Another source of information is found in the similarity and dissimilarity between pairs of characters. Weinman and Learned-Miller two characters which have nearly identical appearance have different labels [8].Text recognition system using above source of information have proved that two characters which have nearly identical appearance have different labels.

3. LAYOUT-BASED SCENE TEXT DETECTION

3.1 Layout Analysis of Color Decomposition

Test strings on signage boards consist of characters in uniform color and aligned arrangement. We can locate text information by extracting pixels with similar colors. A boundary clustering algorithm based on bigram color uniformity in our previous work [3]. Text boundaries on the border of text and its attachment surface are described by characteristic color-pairs, and we are able to extract text by distinguishing boundaries of characters and strings from those of background outliers based on color pairs. We then model color difference by a vector of color pair, which is obtained by cascading the RGB colors of text and attachment surfaces. Each boundary can be described by a color-pair, and we cluster the boundaries with similar color pairs into the sample layer. The boundaries of text characters are separated from those of background outliers.

3.2 Layout Analysis of Horizontal Alignment

In each color layer, we analyze geometrical properties of the boundaries to detect the existence of text characters. According to our observation, text information generally appears in text strings composed of several character members in similar sizes rather than single character, and text strings are normally in approximately horizontal alignment. This method involves following steps. Here we assume that length of signage and other text is enough to get benefit from repeatability of words while decoding. Here adjacent character grouping method is adopted from previous work [4]. For each connected component C we search for its siblings in similar size and vertical locations. When connected components C and C′ are grouped together as sibling components, their sibling sets will be updated according to their relative locations. When C is located on the left of C′, C′ will be added into the right-sibling set of C, which is simultaneously added into the left-sibling set of C′. For connected component C, if several siblings are obtained on its left and right, then we merge all these involved siblings into a region. This region contains a fragment of text string. To create sibling groups corresponding to complete text strings, we repeat above method to calculate all text string fragments in this color layer, and merge the string fragments with intersections.

4. STRUCTURE-BASED SCENE TEXT RECOGNITION

Our goal is to find the most likely word from this set of characters. We formulate this problem in an energy minimization framework, where the best energy solution represents the ground truth word we aim to find. The text retrieval schemes to verify whether a piece of text information exists in natural scene. In text retrieval, binary classifier distinguishes character class from other classes or background outliers. In text understanding character recognition is a multi-class classification problem. For each of the 62 character classes, we train a binary classifier to distinguish a character class from the other classes or non- text outliers. The specified character classes are defined as queried characters. In text retrieval, to better model character structure, we define stroke configuration for each character class based on specific partitions of character boundary and skeleton. In the text recognition technique as used the Optical Character Recognition (OCR) process is divided into following phases preprocessing, segmentation, feature extraction and classification. Fig 2. shows phases in classical OCR.

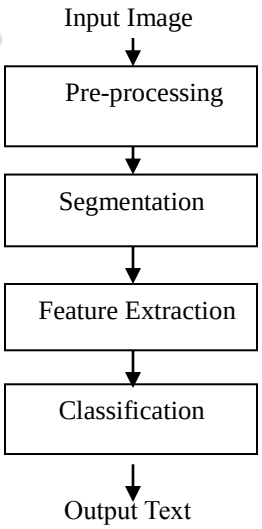

Fig .2.Optical Character Recognition

4.1 Character Descriptor

Four types of character descriptors are used to model character structure. Harris detector to extract key points from corners and junctions. MSER detector to extract key points from stroke components. Dense detector extracts key points uniformly. Random detector extracts present number of key points in a random pattern. By cascading BOW and GMM – based feature representations we get character descriptor as shown in figure 2 below. In GMM model the numbers and locations of key points from each patch should be identical. Therefore, it is only applied to the key points from DD and RD.

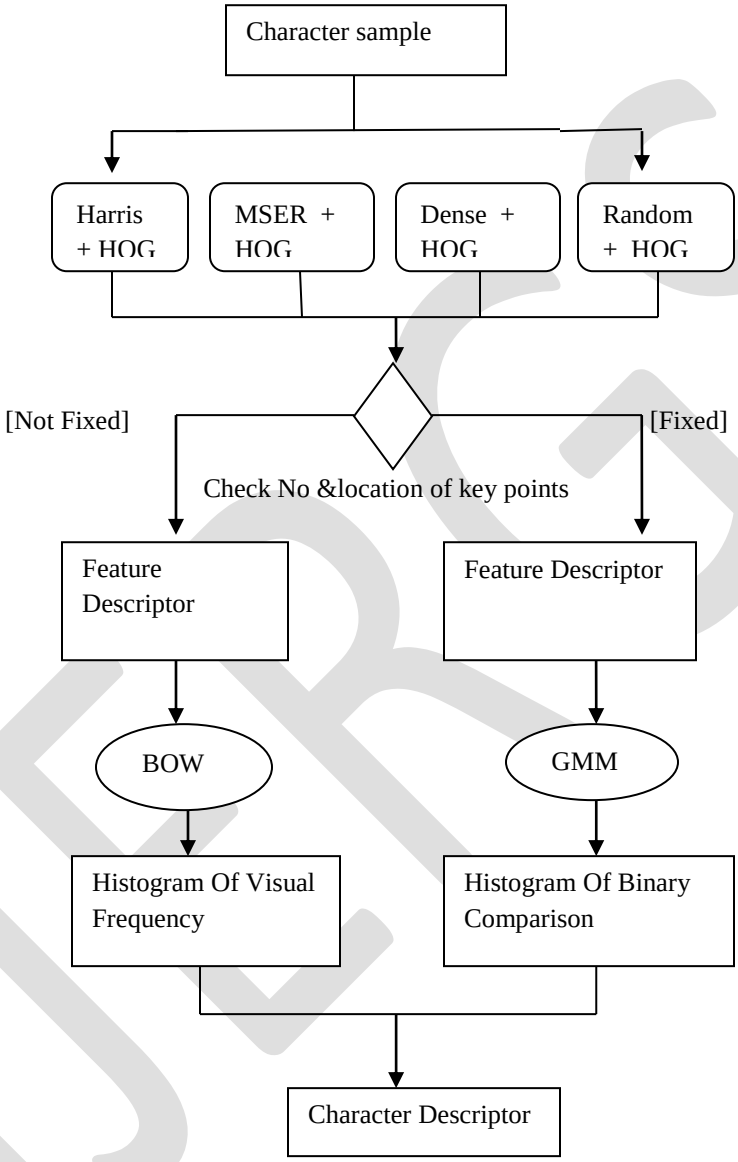

Fig.3. Flowchart of our proposed character descriptor.

Four feature detectors are able to cover almost all representative key points related to the character structure. At each of the extracted key points, the HOG(Histogram of Oriented Gradients) feature is calculated as an observed feature vector x in feature space. Each character patch is normalized into size 128 × 128, containing a complete character. In the process of feature quantization, the Bag-of-Words Model and Gaussian Mixture Model are employed to aggregate the extracted features. BOW model represent the frequency of word occurrence, but not their position. SIFT and SURE are not employed in our method because their performance on character recognition is low. Every character patch is normalized into size 128 × 128 containing complete character. In both models, character patch is mapped into characteristic histogram as feature representation.

4.1.1 BOW Model

The BOW representation is computationally efficient and resistant to intra-class variations. At first, k-means clustering is performed on HOG features extracted from training patches to build a vocabulary of visual words. Then feature coding and pooling are performed to map all HOG features from a character patch into a histogram of visual words. We adopt soft-assignment coding and average pooling schemes in the experiments. More other coding/pooling schemes will be tested in our future work.

At a character patch, the four detectors are applied to extract their respective key points, and then their corresponding HOG features are mapped into the respective vocabularies, obtaining four frequency histograms of visual words. Each histogram has 256 dimensions. Then we cascade the four histograms into BOW-based feature representation in 256 × 4 = 1024 dimensions.

4.1.2 Gaussian Mixture Model

The s-th($1 \leq s \leq K$)center is used as initial means μs of the s- th Gaussian in GMM. Then the initial weights ws and co- variances σs are calculated from the means. Next, an EM algorithm is used to obtain maximum likelihood estimate of the three parameters, weights, means, and co-variances of all the Gaussian mixture distributions. A likelihood vector from all Gaussians is represented by Eq. (1).

$$Px = (ws\ ps(x|\mu s,\ \sigma s\ ))|ks=1$$

$$=(w1\ p1(x|\mu 1,\ \sigma 1),w2\ p2(x|\mu 2,\sigma 2),\ .\ .\ .\ ,wK\ pK\ (x|\mu K,\ \sigma K\ ))\quad (1)$$

$$ps(x|\mu s,\ \sigma s\ ) = 1/\sigma\sqrt{2\pi}\exp(-1/2(x - \mu/\sigma)^2)$$

Where x denotes a HOG-based feature vector at a key point, Px denotes the likelihood vector of feature vector *x*, and $ps(x|\mu s,\sigma s)$ denotes the probability value of *x* at the s-th Gaussian. For likelihood Vectors (P*x*,P*y*), where

$$Px =(ws\ ps(x\ |\ \mu s,\sigma s\ ))|8s=1 \text{ and } Py =(ws\ ps(y\ |\ \mu s,\sigma s\ ))|8s=1$$

GMM- based feature representation by histogram of binary comparisons, as Eq. (2).

$$Fx,\ y =8\Sigma^{s-1}\ [2^{s-1}\ *(P^s\ ]$$
$$F = (Fx,\ y) \qquad (2)$$

$$P(^s) = 1 \quad ;\ \text{if } ws\ ps\ (x\ |\ \mu s,\sigma s) \geq \text{if } ws\ ps\ (y\ |\ \mu s,\sigma s), \text{ and}$$
$$P(^s) = 0 \quad ;\ \text{if } ws\ ps\ (y\ |\ \mu s,\sigma s\ ) > \text{if } ws\ ps\ (x\ |\ \mu s,\sigma s)$$

4.2 Character Stroke Configuration

In previously proposed method [7] stroke width consistency is used to detect scene text in complex background and achieve outstanding performance. Stroke is region bounded by two parallel boundary segments. Their orientation is regarded as stroke orientation and the distance between them is regarded as stroke width. The stroke configuration is estimated by synthesized characters generated from computer software. Character boundary and character skeleton are obtained by applying discrete contour evolution (DCE) [10] and skeleton pruning on the basis of DCE [11]. The accuracy of the skeleton position and stability of skeletons is guaranteed in this pruning method.DCE and skeleton pruning are invariant to deformation and scaling. Our estimate the stroke width and orientation on sample points of character boundary.

N points are sampled evenly from the polygon character boundary, with the polygon vertices reserved. In our experiment, we set N = 128. The number of points to be sampled on each side of the polygon boundary is proportional to its length. Secondly, stroke is contiguous part of an image that forms a band of a nearly constant width. We take b and its two neighboring sample points to fit a line when they are approximately collinear or else quadratic curve. Then the slope or tangent direction at b is used as stroke orientation. Characters are connected strokes with orientation. Thirdly, we calculate the skeleton-based stroke maps. At each boundary sample point, values of stroke width and orientation are compared with its neighboring points. Constituency of stroke width and orientation consistency 3 and π/8 respectively. Construct stroke section if sample points satisfy stroke related features. If not construct junction. These parameters are compatible with the synthesized character patches with size 128 × 128. While the other sample points, around

the intersections of neighboring strokes or the ends of strokes, compose junction sections of a character boundary.

4.2.1 Stroke Alignment Method

The basic structure of a character class can be described by the mean value of all stroke configurations from character samples of the class. Here, we estimate a mean value of stroke configuration so that it is able to handle various fonts, styles and sizes. Eq. (3) gives an objective function of stroke alignment.

$$E = \Sigma_i \, (D \, (\acute{S}, \, T_i \, (S_i)) + g(T_i)) \qquad (3)$$

$$D \, (Sm, Sn) = \sum_p \| Sm \, (p) - Sn \, (p) \|^2 \qquad (4)$$

D represents the distance between the stroke configurations of two character samples as Eq. (4), and $\acute{S}$ represents mean value of the stroke configuration s_i represents the transformation applied on the strokes of the i -th stroke configuration S_i.

5. RESULTS AND DISCUSSIONS

In what follows, we present a detailed evaluation of our method. We evaluate various components of the proposed approach to justify our choices. We compare our results with the best performing methods for the word recognition task.

Table -2: Accuracy rates of scene character recognition in ICDAR-2003 dataset compared with previously published results

ICDAR-2003 Dataset	AR
Ours	0.628
HOG+NN	0.515
SYNTH+FERNS	0.520
NATIVE+FERNS	0.640

Table -2: Accuracy Rates (AR) and False Positive Rates (FPR) of queried character classification in the three datasets

Dataset	AR	FPR
Char s 74K	0.726	0.078
Sign	0.868	0.0 75
ICDAR-2003	0.536	0.180

6. COMPARISON OF RESULTS

The experimental results in first Table show that our proposed descriptor outperforms the SYNTH+FERNS with AR 0.52 and comparable with NATIVE+FERNS having AR of 0.64.A character classifier is trained for each character class by using Chars74K samples, which is then evaluated over the three datasets to obtain the results. As shown in second table a character classifier is trained for each character class by using Chars74K samples, which is then evaluated over the three datasets to obtain the results.

7. CONCLUSION

Thus this paper achieves the objective of text extraction from image and displaying its information on android platform, w*ith the help of text extraction* algorithm.

It detects text regions from natural scene image/video, and recognizes text information from the detected text regions. Text understanding and text retrieval are respectively proposed to extract text information from surrounding environment. Character descriptor is effective to

extract representative and discriminative text features for both recognition schemes. To model text character structure for text retrieval scheme, we have designed a novel feature representation, stroke configuration map, based on boundary and skeleton. Quantitative experimental results demonstrate that proposed method of scene text recognition outperforms most existing methods.

REFERENCES:

1. Chucai Yi, "Scene Text Recognition in Mobile Applications by Character Descriptor and Structure Configuration,"IEEE Trans. Image Process., vol. 23, no. 7, July2014,pp.2972-2982**.**
2. D. L. Smith, J. Feild, and E. Learned-Miller, "Enforcing similarity constraints with integer programming for better scene text recognition," in Proc. IEEE Conf. Comput. Vis. Pattern Recognit., Jun. 2011,pp.73–80.
3. C. Yi and Y. Tian, "Localizing text in scene images by boundary clustering, stroke segmentation, and string fragment classification," IEEE Trans. Image Process., vol. 21, NO. 9, PP. 4256–4268, SEP. 2012.
4. C. Yi and Y. Tian, "Text string detection from natural scenes by structure-based partition and grouping," IEEE Trans. Image Process., vol. 20, no. 9, pp. 2594–2605, Sep. 2011.
5. N. Dalal and B. Triggs, "Histograms of oriented gradients for human detection," in Proc. IEEE Conf. Comput. Vis. Pattern Recognit., Jun. 2005, pp. 886–893.
6. T. de Campos, B. Babu, and M. Varma, "Character recognition in natural images," in Proc. VISAPP, 2009.
7. B. Epshtein, E. Ofek, and Y. Wexler. Detecting text in natural scenes with stroke width transform. In CVPR, 2010.
8. M. Everingham, L. Van Gool, C. K. I. Williams, J. Winn, and A. Zisserman. The pascal visual object classes (voc) challenge. IJCV, 2010.
9. V. Kolmogorov. Convergenttree-reweighted message passing for energy minimization. PAMI, 2006.
10. C. Colombo, A. D. Bimbo, and P. Pala, Semantics in Visual Information Retrieval, IEEE Multimedia, 6 (3) (1999) 38-53.
11. T. Sato, T. Kanade, E. K. Hughes, and M. A. Smith, Video OCR for Digital News Archive, Proc. of IEEE Workshop on Content based Access of Image and Video Databases, 1998, pp. 52-60.
12. Atsuo Yoshitaka and Tadao Ichikawa, A Survey on Content-based Retrieval for Multimedia Databases, IEEE Transactions on Knowledge and Data Engineering, 11 (1) (1999) 81-93.
13. W. Qi, L. Gu, H. Jiang, X. Chen, and H. Zhang, Integrating Visual, Audio, and Text Analysis for News Video, Proc. of IEEE International Conference on Image Processing, 2000, pp. 10-13.
14. H. D.Wactlar, T. Kanade, M. A. Smith, and S. M. Stevens, Intelligent Access to Digital Video: The Informedia Project, IEEE Computer, 29 (5) (1996) 46-52.
15. A.Gupta, Y. Verma, and C.V. Jawahar. Choosing linguistics over vision to describe images. In AAAI, 2012.
16. D. Hoiem, A. Efros, and M. Hebert. Closing the loop on scene interpretation. In CVPR, 2008.
17. Anand Mishra Karteek Alahari C. V. Jawahar. Top-down and bottom-up cues for scene text recognition. pages 1–3.
18. A. Mishra, K. Alahari, and C. V. Jawahar, "Top-down and bottom-up cues for scene text recognition," in Proc. IEEE Conf. Comput. Vis. Pattern Recognit., Jun. 2012, pp. 1063–6919.
19. S. Lu, L. Li, and C. L. Tan, "Document image retrieval through word shape coding," IEEE Trans. Pattern Anal. Mach. Intell., vol. 30, no. 11, pp. 1913– 1918, Nov. 2008

International Journal of Engineering Research and General Science Volume 3, Issue 3, Part-2 , May-June, 2015
ISSN 2091-2730

Special Sasakian Manifold with Induced Connection

L K Pandey

D S Institute of Technology & Management, Ghaziabad, U.P. - 201007

dr.pandeylk@rediffmail.com

Abstract—In 1960, S. Sasaki [7] dicussed on differentiable manifolds which are closely related to almost contact structure. Also in 1961, S. Sasaki and Y. Hatakeyama [8] discussed on differentiable manifolds with certain structures which are closely related to almost contact structure. In 1963, Y. Hatakeyama [1] discussed on differentiable manifolds with almost contact structures and in 2011, R. Nivas and A. Bajpai [5] studied on generalized Lorentzian Para-Sasakian manifolds. Hayden [2] introduced the idea of metric connection with torsion tensor in a Riemannian manifold. In 1980, R. S. Mishra and S. N. Pandey [3] discussed on quarter-symmetric metric F-connection. In 1992, Nirmala S. Agashe and Mangala R. Chafle [4] studied semi-symmetric non-metric connection in a Riemannian manifold. In this paper, generalized nearly Sasakian and generalized nearly special Sasakian manifolds have been introduced and some of their properties have been established with generalized Co-symplectic manifolds. Induced connection in a generalized special Sasakian manifold has also been studied.
.

Keywords—Generalized nearly Sasakian manifold, generalized nearly Special Sasakian manifold, generalized Co-symplectic manifolds and generalized semi-symmetric metric F-connection.

1. INTRODUCTION

An *n (=2m+1)* dimensional differentiable manifold M_n, on which there are defined covariant vector fields A_i,where $i =$ 3,4,5, …. $(n-1)$, the associated contravariant vector fields T_i, where $i = 3,4,5, \ldots . (n-1)$, a tensor field $F$of type (1, 1) and a metric tensor g, satisfying

(1.1) $F^2 = -I_n + \sum_{i=3}^{n-1} A_i \otimes T_i, \quad FT_i = 0, \quad A_i(T_i) = 1, \quad A_i(FX) = 0,$

Rank $F = n - i$

(1.2) $g(FX, FY) = g(X, Y) - \sum_{i=3}^{n-1} A_i(X) A_i(Y)$, where $A_i(X) = g(X, T_i), i = 3,4,5, \ldots . (n-1),$

$`F(X, Y) \overset{\text{def}}{=} g(FX, Y) = -`F(Y, X),$

Then M_n is called a generalized almost contact metric manifold (a generalized almost Grayan manifold) and the structure (F, T_i, A_i, g) is known as generalized almost contact metric structure [6].

Let D be a Riemannian connection on M_n, then we have [6]

(1.3) (a) $(D_X `F)(FY, Z) - (D_X `F)(Y, FZ) - \sum_{i=3}^{n-1} A_i(Y)(D_X A_i)(Z) - \sum_{i=3}^{n-1} A_i(Z)(D_X A_i)(Y) = 0$

(b) $(D_X `F)(FY, F^2 Z) = (D_X `F)(F^2 Y, FZ)$

A generalized almost contact metric manifold is called a generalized Sasakian manifold, if

(1.4) (a) $i(D_X F)(Y) + F^2 X \sum_{i=3}^{n-1} A_i(Y) + g(FX, FY) \sum_{i=3}^{n-1} T_i = 0 \Leftrightarrow$

(b) $i(D_X `F)(Y, Z) - g(FX, FZ) \sum_{i=3}^{n-1} A_i(Y) + g(FX, FY) \sum_{i=3}^{n-1} A_i(Z) = 0 \Leftrightarrow$

(c) $iD_X T_i = FX + T_i - \sum_{i=3}^{n-1} T_i,$

From which, we get

(1.5) (a) $i(D_X A_i)(FY) = g(FX, FY) \Leftrightarrow$

(b) $i(D_X A_i)(Y) - A_i(Y) + \sum_{i=3}^{n-1} A_i(Y) = `F(X,Y)$

A generalized almost contact metric manifold is called a generalized Special Sasakian manifold (a generalized S-Sasakian manifold), if

(1.6) (a) $i(D_X F)(Y) - FX \sum_{i=3}^{n-1} A_i(Y) + `F(X,Y) \sum_{i=3}^{n-1} T_i = 0 \Leftrightarrow$

(b) $i(D_X `F)(Y,Z) - `F(X,Z) \sum_{i=3}^{n-1} A_i(Y) + `F(X,Y) \sum_{i=3}^{n-1} A_i(Z) = 0 \Leftrightarrow$

(c) $iD_X T_i = F^2 X + T_i - \sum_{i=3}^{n-1} T_i$

From which, we get

(1.7) (a) $i(D_X A_i)(FY) = `F(X,Y) \Leftrightarrow$

(b) $i(D_X A_i)(Y) - A_i(Y) + \sum_{i=3}^{n-1} A_i(Y) = -g(FX, FY)$

A generalized almost contact metric manifold is called a generalized Co-symplectic manifold, if

(1.8) (a) $(D_X F)Y + \sum_{i=3}^{n-1} A_i(Y) F D_X T_i + \sum_{i=3}^{n-1} (D_X A_i)(FY) T_i = 0 \Leftrightarrow$

(b) $(D_X `F)(Y,Z) - \sum_{i=3}^{n-1} A_i(Y)(D_X A_i)(FZ) + \sum_{i=3}^{n-1} A_i(Z)(D_X A_i)(FY) = 0$

Therefore, a generalized Co-symplectic manifold will be a generalized Sasakian manifold, if

(1.9) (a) $i(D_X A_i)(FY) = g(FX, FY) \Leftrightarrow$ (b) $i(D_X A_i)(Y) - A_i(Y) + \sum_{i=3}^{n-1} A_i(Y) = `F(X,Y) \Leftrightarrow$

(c) $iD_X T_i = FX + T_i - \sum_{i=3}^{n-1} T_i$

And a generalized Co-symplectic manifold will be a generalized S-Sasakian manifold, if

(1.10) (a) $i(D_X A_i)(FY) = `F(X,Y) \Leftrightarrow$

(b) $i(D_X A_i)(Y) - A_i(Y) + \sum_{i=3}^{n-1} A_i(Y) = -g(FX, FY) \Leftrightarrow$ (c) $iD_X T_i = F^2 X + T_i - \sum_{i=3}^{n-1} T_i$

Nijenhuis tensor in a generalized almost contact metric manifold is given by

(1.11) $`N(X,Y,Z) = (D_{FX} `F)(Y,Z) - (D_{FY} `F)(X,Z) + (D_X `F)(Y,FZ) - (D_Y `F)(X,FZ)$

Where $`N(X,Y,Z) \stackrel{\text{def}}{=} g(N(X,Y),Z)$

2. GENERALIZED NEARLY SASAKIAN MANIFOLD

A generalized almost contact metric manifold is called a generalized nearly Sasakian manifold, if

(2.1) $i(D_X `F)(Y,Z) - \sum_{i=3}^{n-1} A_i(Y) g(FX, FZ) + \sum_{i=3}^{n-1} A_i(Z) g(FX, FY)$

$= i(D_Y `F)(Z,X) - \sum_{i=3}^{n-1} A_i(Z) g(FX, FY) + \sum_{i=3}^{n-1} A_i(X) g(FY, FZ)$

$= i(D_Z `F)(X,Y) - \sum_{i=3}^{n-1} A_i(X) g(FY, FZ) + \sum_{i=3}^{n-1} A_i(Y) g(FX, FZ)$

From which, we get

(2.2) (a) $i(D_X F)Y + i(D_Y F)X + \sum_{i=3}^{n-1} A_i(Y) F^2 X + \sum_{i=3}^{n-1} A_i(X) F^2 Y + 2 \sum_{i=3}^{n-1} T_i\, g(FX, FY) = 0 \Leftrightarrow$

(b) $i(D_X `F)(Y,Z) + i(D_Y `F)(X,Z) - \sum_{i=3}^{n-1} A_i(Y) g(FX, FZ) - \sum_{i=3}^{n-1} A_i(X) g(FY, FZ) +$

$2 \sum_{i=3}^{n-1} A_i(Z) g(FX, FY) = 0$

From which, we get

(2.3) (a) $i(D_X F)FY + i(D_{FY} F)X - \sum_{i=3}^{n-1} A_i(X) FY - 2 \sum_{i=3}^{n-1} T_i `F(X,Y) = 0 \Leftrightarrow$

(b) $i(D_X`F)(FY,Z) - i(D_{FY}`F)(Z,X) - \sum_{i=3}^{n-1} A_i(X)\,`F(Y,Z) - 2\sum_{i=3}^{n-1} A_i(Z)\,`F(X,Y) = 0$

(2.4) (a) $i(D_X F)F^2Y + i(D_{F^2Y}F)X - \sum_{i=3}^{n-1} A_i(X)F^2Y - 2\sum_{i=3}^{n-1} T_i\, g(FX,FY) = 0 \Leftrightarrow$

(b) $i(D_X`F)(F^2Y,Z) - i(D_{F^2Y}`F)(Z,X) + \sum_{i=3}^{n-1} A_i(X)g(FY,FZ) - 2\sum_{i=3}^{n-1} A_i(Z)g(FX,FY) = 0$

(2.5) (a) $(D_X F)Y + (D_Y F)X + \sum_{i=3}^{n-1} A_i(Y)\{FD_XT_i - (D_{T_i}F)X\} + \sum_{i=3}^{n-1} A_i(X)\{FD_YT_i - (D_{T_i}F)Y\} +$
$\sum_{i=3}^{n-1} T_i\{(D_XA_i)(FY) + (D_YA_i)(FX)\} = 0 \Leftrightarrow$

(b) $(D_X`F)(Y,Z) + (D_Y`F)(X,Z) - \sum_{i=3}^{n-1} A_i(Y)\{(D_XA_i)(FZ) - (D_{T_i}`F)(Z,X)\} -$
$\sum_{i=3}^{n-1} A_i(X)\{(D_YA_i)(FZ) + (D_{T_i}`F)(Y,Z)\} + \sum_{i=3}^{n-1} A_i(Z)\{(D_XA_i)(FY) + (D_YA_i)(FX)\} = 0$

Pre-multiplying X, Y, Z by F in (1.11) and using equations (2.1), (1.3) (b), we see that a generalized nearly Sasakian manifold will be completely integrable, if

(2.6) $(D_{\overline{X}}`F)\left(\overline{Y},\overline{\overline{Z}}\right) = (D_{\overline{Y}}`F)(\overline{X},\overline{\overline{Z}})$

3. GENERALIZED NEARLY SPECIAL SASAKIAN MANIFOLD

A generalized almost contact metric manifold is called a generalized nearly Special Sasakian manifold (a generalized nearly S-Sasakian manifold), if

(3.1) $i(D_X`F)(Y,Z) + \sum_{i=3}^{n-1} A_i(Y)`F(Z,X) + \sum_{i=3}^{n-1} A_i(Z)\,`F(X,Y)$

$= i(D_Y`F)(Z,X) + \sum_{i=3}^{n-1} A_i(Z)`F(X,Y) + \sum_{i=3}^{n-1} A_i(X)\,`F(Y,Z)$

$= i(D_Z`F)(X,Y) + \sum_{i=3}^{n-1} A_i(X)`F(Y,Z) + \sum_{i=3}^{n-1} A_i(Y)\,`F(Z,X)$

From which, we obtain

(3.2) (a) $i(D_X F)Y + i(D_Y F)X - \sum_{i=3}^{n-1} A_i(Y)FX - \sum_{i=3}^{n-1} A_i(X)FY = 0 \Leftrightarrow$

(b) $i(D_X`F)(Y,Z) + i(D_Y`F)(X,Z) + \sum_{i=3}^{n-1} A_i(Y)\,`F(Z,X) - \sum_{i=3}^{n-1} A_i(X)\,`F(Y,Z) = 0$

This gives

(3.3) (a) $i(D_X F)FY + i(D_{FY}F)X - \sum_{i=3}^{n-1} A_i(X)F^2Y = 0 \Leftrightarrow$

(b) $i(D_X`F)(FY,Z) - i(D_{FY}`F)(Z,X) + \sum_{i=3}^{n-1} A_i(X)g(FY,FZ) = 0$

(3.4) (a) $i(D_X F)F^2Y + i(D_{F^2Y}F)X + \sum_{i=3}^{n-1} A_i(X)FY = 0 \Leftrightarrow$

(b) $i(D_X`F)(F^2Y,Z) - i(D_{F^2Y}`F)(Z,X) + \sum_{i=3}^{n-1} A_i(X)`F(Y,Z) = 0$

(3.5) (a) $(D_X F)Y + (D_Y F)X + \sum_{i=3}^{n-1} A_i(Y)\{FD_XT_i - (D_{T_i}F)X\} + \sum_{i=3}^{n-1} A_i(X)\{FD_YT_i - (D_{T_i}F)Y\} = 0 \Leftrightarrow$

(b) $(D_X`F)(Y,Z) + (D_Y`F)(X,Z) - \sum_{i=3}^{n-1} A_i(Y)\{(D_XA_i)(FZ) - (D_{T_i}`F)(Z,X)\} -$
$\sum_{i=3}^{n-1} A_i(X)\{(D_YA_i)(FZ) + (D_{T_i}`F)(Y,Z)\} = 0$

Pre-multiplying X, Y, Z by F in (1.11) and using equations (3.1), (1.3) (b), we see that a generalized nearly S-Sasakian manifold will be completely integrable, if

(3.6) $(D_{\overline{X}}`F)\left(\overline{\overline{Y}},\overline{Z}\right) = (D_{\overline{Y}}`F)\left(\overline{\overline{X}},\overline{Z}\right)$

4. GENERALIZED NEARLY CO-SYMPLECTIC MANIFOLD

A generalized almost contact metric manifold is called a generalized nearly Co-symplectic manifold, if

(4.1) $(D_X`F)(Y,Z) - \sum_{i=3}^{n-1} A_i(Y)(D_X A_i)(FZ) + \sum_{i=3}^{n-1} A_i(Z)(D_X A_i)(FY)$

$= (D_Y`F)(Z,X) - \sum_{i=3}^{n-1} A_i(Z)(D_Y A_i)(FX) + \sum_{i=3}^{n-1} A_i(X)(D_Y A_i)(FZ)$

$= (D_Z`F)(X,Y) - \sum_{i=3}^{n-1} A_i(X)(D_Z A_i)(FY) + \sum_{i=3}^{n-1} A_i(Y)(D_Z A_i)(FX)$

Therefore, a generalized nearly Sasakian manifold will be a generalized nearly Co-symplectic manifold, if

(4.2) (a) $i(D_X A_i)(FY) = g(FX, FY) \Leftrightarrow$

(b) $i(D_X A_i)(Y) - A_i(Y) + \sum_{i=3}^{n-1} A_i(Y) = `F(X,Y) \Leftrightarrow$ (c) $iD_X T_i = FX + T_i - \sum_{i=3}^{n-1} T_i$

And a generalized nearly S-Sasakian manifold will be a generalized nearly Co-symplectic manifold, if

(4.3) (a) $i(D_X A_i)(FY) = `F(X,Y) \Leftrightarrow$

(b) $i(D_X A_i)(Y) - A_i(Y) + \sum_{i=3}^{n-1} A_i(Y) = -g(FX, FY) \Leftrightarrow$ (c) $iD_X T_i = F^2X + T_i - \sum_{i=3}^{n-1} T_i$

5. GENERALIZED INDUCED CONNECTION IN A GENERALIZED SPECIAL SASAKIAN MANIFOLD

Let M_{2m-1} be submanifold of M_{2m+1} and let $c : M_{2m-1} \to M_{2m+1}$ be the inclusion map such that

$$d \in M_{2m-1} \to cd \in M_{2m+1},$$

Where c induces a Jacobian map (linear transformation) $J : T'_{2m-1} \to T'_{2m+1}$.

T'_{2m-1} is tangent space to M_{2m-1} at point d and T'_{2m+1} is tangent space to M_{2m+1} at point cd such that

$$\hat{X} \text{ in } M_{2m-1} \text{ at } d \to J\hat{X} \text{ in } M_{2m+1} \text{ at } cd$$

Let $\tilde{g}$ be the induced metric tensor in M_{2m-1} , then

(5.1) $\tilde{g}(\hat{X}, \hat{Y}) = ((g(J\hat{X}, J\hat{Y}))b$

Semi- symmetric metric F-connection B in generalized special Sasakian manifold M_n is given by

(5.2) $iB_X Y = iD_X Y + \sum_{i=3}^{n-1} A_i(Y)X - \sum_{i=3}^{n-1} g(X,Y)T_i - 2\sum_{i=3}^{n-1} A_i(X)Y$

Where X and Y are arbitrary vector fields of M_{2m+1}. Let

(5.3) $T_i = Jt_i + \rho_i M + \sigma_i N$, where $i = 3,4,5, \ldots . (n-1)$.

Where t_i , $i = 3,4,5, \ldots . (n-1)$, are C^∞ vector fields in M_{2m-1}. M, N are unit normal vectors to M_{2m-1}.

Denoting by $\grave{D}$ the connection induced on the submanifold from D. Gauss equation is

(5.4) $D_{JX} J\hat{Y} = J(\grave{D}_X \hat{Y}) + p(\hat{X}, \hat{Y})M + q(\hat{X}, \hat{Y})N$

Where p and q are symmetric bilinear functions in M_{2m-1}. Also

(5.5) $B_{JX} J\hat{Y} = J(\grave{B}_X \hat{Y}) + h(\hat{X}, \hat{Y})M + k(\hat{X}, \hat{Y})N$,

Where $\grave{B}$ is the connection induced on the submanifold from B and h, k are symmetric bilinear functions in M_{2m-1}.

Inconsequence of (5.2), we have

(5.6) $iB_{JX}J\hat{Y} = iD_{JX}J\hat{Y} + \sum_{i=3}^{n-1} A_i(J\hat{Y})J\hat{X} - \sum_{i=3}^{n-1} g(J\hat{X},J\hat{Y})T_i - 2\sum_{i=3}^{n-1} A_i(J\hat{X})J\hat{Y}$

Using (5.4), (5.5) and (5.6), we have

(5.7)
$iJ(\grave{B}_X\hat{Y}) + ih(\hat{X},\hat{Y})M + ik(\hat{X},\hat{Y})N =$
$iJ(\grave{D}_X\hat{Y}) + ip(\hat{X},\hat{Y})M + iq(\hat{X},\hat{Y})N + \sum_{i=3}^{n-1} A_i(J\hat{Y})J\hat{X} - \sum_{i=3}^{n-1} g(J\hat{X},J\hat{Y})T_i -$
$2\sum_{i=3}^{n-1} A_i(J\hat{X})J\hat{Y}$
Using (5.3), we get

(5.8) $iJ(\grave{B}_X\hat{Y}) + ih(\hat{X},\hat{Y})M + ik(\hat{X},\hat{Y})N = iJ(\grave{D}_X\hat{Y}) + ip(\hat{X},\hat{Y})M + iq(\hat{X},\hat{Y})N + \sum_{i=3}^{n-1} a_i(\hat{Y})J\hat{X} -$

$$\sum_{i=3}^{n-1}(Jt_i + \rho_i M + \sigma_i N)\,\tilde{g}(\hat{X},\hat{Y}) - 2\sum_{i=3}^{n-1} a_i(\hat{X})J\hat{Y}$$

Where $\tilde{g}(\hat{Y},t_i) \stackrel{\text{def}}{=} a_i(\hat{Y})$

This implies

(5.9) $i\grave{B}_X\hat{Y} = i\grave{D}_X\hat{Y} + \sum_{i=3}^{n-1} a_i(\hat{Y})\hat{X} - \sum_{i=3}^{n-1} \tilde{g}(\hat{X},\hat{Y})t_i - 2\sum_{i=3}^{n-1} a_i(\hat{X})\hat{Y}$

Iff

(5.10) (a) $ih(\hat{X},\hat{Y}) = ip(\hat{X},\hat{Y}) - \sum_{i=3}^{n-1} \rho_i\tilde{g}(\hat{X},\hat{Y})$

(b) $ik(\hat{X},\hat{Y}) = iq(\hat{X},\hat{Y}) - \sum_{i=3}^{n-1} \sigma_i\tilde{g}(\hat{X},\hat{Y})$

Thus, we have

Theorem 5.1 The connection induced on a submanifold of a generalized special Sasakian manifold with a generalized Semi-symmetric metric F-connection with respect to unit normal vectors M and N is also generalized Semi- symmetric metric F-connection iff (5.10) holds.

REFERENCES:

[1] Hatakeyama, Y., "Some Notes on Differentiable Manifolds with almost contact structures", Tohoku Math. J. 2, pp. 176-181, 1963.
[2] Hayden, H. A., "Subspaces of a space with torsion", Proc. London Math. Soc., 34, pp. 27-50, 1932.
[3] Mishra, R. S. and Pandey,S. N., "On quarter-symmetric metric F-connection", Tensor, N.S., 34, pp. 1–7, 1980.
[4] Nirmala S. Agashe and Mangala R. Chafle, "A Semi-symmetric non-metric connection on a Riemmanian manifold", Indian J. pure appl. Math., 23(6), pp. 399-409, 1992.
[5] Nivas, R. and Bajpai, A., "Study of Generalized Lorentzian Para-Sasakian Manifolds", Journal of international Academy of Physical Sciences, Vol. 15 No.4, pp. 405-412, 2011.
[6] Pandey, L.K., "A note on generalized almost contact metric manifold" International General of Engineering Research and General Science, Vol. 3, Issue 3, pp. 709-712, 2015.
[7] Sasaki, S., "On Differentiable Manifolds with certain structures which are closely rerated to almost contact structure I", Tohoku Math. J., 12, pp. 459-476, 1960.
[8] Sasaki, S. and Hatakeyama, Y., "On Differentiable Manifolds with certain structures which are closely related to almost contact structure II", Tohoku Math. J., 13, pp. 281-294, 1961

International Journal of Engineering Research and General Science Volume 3, Issue 3, Part-2 , May-June, 2015
ISSN 2091-2730

THREE POINT BENDING OF ALUMINIUM MATRIX COMPOSITE PLATE PRODUCED BY STIR CASTING AND STATISTICAL ANALYSIS BY TAGUCHI METHOD

Shriyash S. Shinde, S. G. Kulkarni, S. S. Kulkarni

SKN Sinhgad College of Engineering, Pandharpur.

Abstract— Aluminium matrix composites (AMC's) are finding huge application in aerospace and automobile due their high performance, economic and environmental benefits owing to properties like reduced weight, low cost and high strength to weight ratio. Stir casting is one of the cheaper and conventional routes for manufacturing of particulate composites. Plates play a major role in modern day large size applications like aircraft, turbines and other structural components. The present investigation has been done to study effect of different input parameters namely aspect ratio, thickness and percentage reinforcement on three point bending. The three parameters i.e. aspect ratio (1, 1.5 and 2), thickness (3 mm, 6 mm and 9 mm), percentage reinforcement (4%, 8% and 12%) are used to produce plate samples by stir casting method. Statistical analysis is done by Taguchi method to study effect of these parameters.

Keywords— Aluminium matrix composite, plate, stir casting, aspect ratio, thickness, percentage reinforcement, Taguchi method.

INTRODUCTION

Modern day technology is growing at very rapid rate. It requires high performance materials with effective properties which conventional monolithic materials are unable to provide [1]. Composite materials are those formed by combining two or more materials on a macroscopic scale such that they have better engineering properties than the conventional materials [2]. Some of the properties that can be improved by forming a composite material are stiffness, strength, weight reduction, corrosion resistance, thermal properties, fatigue life, and wear resistance [3].

Aluminium and its alloys have attracted the most attention as matrix material in metal matrix composites [4]. In AMC one of the constituent is aluminum, which forms percolating network and is termed as matrix phase. The other constituent is embedded in this aluminum and serves as reinforcement [5]. In present wok production of AMC by stir casting method is done by taking aluminium alloy A356 as matrix material and alumina (Al_2O_3) as reinforcement. The present investigation has been done to study effect of different input parameters namely aspect ratio, thickness and percentage reinforcement on three point bending. The three parameters i.e. aspect ratio (1, 1.5 and 2), thickness (3 mm, 6 mm and 9 mm), percentage reinforcement (4%, 8% and 12%) are used to produce the plate samples. Statistical analysis is done by Taguchi method to study effect of these parameters.

MATRIX MATERIAL:

Aluminium alloy A356 is selected as matrix material for current experimentation. The various composition limits for A356 is,

Name of constituent	Cu max	Mg	Mn max	Si	Fe max	Zn max	Ti max	Other	Al
Percentage	0.25	2.25 to 0.45	0.35	6.5 to 7.5	0.6	0.35	0.25	0.05	Bal

Table 1. Composition of A356 [3].

Aluminium alloy A356 is ever more accepted in aircraft and automobile due to their high strength-to-weight ratio and its thixotropic structure. A356 based alloys have been developed with significant ductility, strength, elongation, hardness and toughness at room temperature in cast state [6].

REINFORCEMENT MATERIAL:

Reinforcement used in current work is Alumina. Alumina is used to increase the material strength, hardness & toughness. Aluminum oxide (alumina) possesses strong ionic inter atomic bonding giving rise to its desirable material characteristics. It has high hardness, excellent dielectric properties, refractoriness and good thermal properties which are applicable to wide range of applications [7].

COMPOSITE FABRICATION:

Stir casting is a liquid state method of composite materials fabrication, in which a dispersed phase (ceramic particles, short fibres) is mixed with a molten matrix metal by means of mechanical stirring. The liquid composite material is then cast by conventional casting methods and may also be processed by conventional Metal forming technologies [8]. In preparing aluminium matrix composites by stir casting method some of the factors that need considerable attention are as follows [9],

- To achieve uniform distribution of the reinforcement material
- To achieve wettability between the two main substances
- To minimize porosity in the cast metal matrix composite.

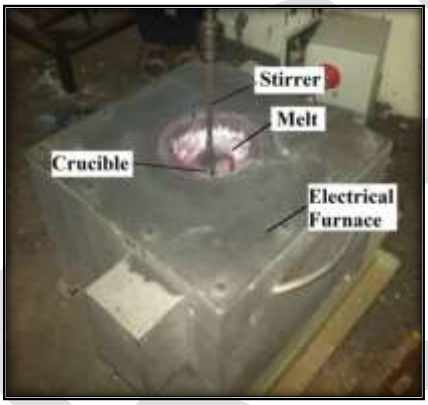

Fig 1. Stir casting setup.

The process of stir casting starts with placing an empty crucible in the furnace. The heater temperature is then gradually increased up to 800°C. Aluminium alloy is cleaned to remove dust particles, weighed and charged in the crucible for melting. Required quantities of reinforcement powder and magnesium powder are weighed on the weighing machine. Reinforcements are heated for 45 minutes at a temperature of 500°C. When matrix was in the semisolid stage condition at 650°C, one percentage by weight of pure magnesium powder is used as wetting agent. After five minutes the scum powder is added which forms a scum layer of impurity on liquid surface which to be removed. Heater temperature is then gradually increased to 800°C. At this heater temperature stirring is started and continued for five minutes. Stirring rpm is gradually increased from 0 to 300 RPM with the help of speed controller. Preheated reinforcements are added during five minutes of stirring. Reinforcements are poured manually with the help of conical hopper. The flow rate of reinforcements measured is 0.5 gram per second. Stirrer rpm is then gradually lowered to the zero. Then molten composite slurry is poured in the metallic mould without giving time for reinforcement to settle down at crucible bottom. Mould is preheated at 500°C temperature for one hour before pouring the molten slurry in the mould. This is necessary to maintain slurry in molten condition throughout the pouring. While pouring the slurry in mould the flow of the slurry is kept uniform to avoid trapping of gas, also distance between crucible and mould plays a vital role in quality of casting.

BEND TEST:

Three point bending tests are used to assess the strength of the composites by applying the force required to bend a plate. The data is often used to select materials for parts that will support loads without bending. Bend test is often used due to ease of the specimen preparation and testing [10]. For plate specimens three different parameters are considered as follows:

1. Aspect ratio: 1, 1.5 and 2.
2. Thicknesses: 3mm, 6mm and 9mm.
3. Reinforcement weight percentage: 4%, 8% and 12%.

The experimental design proposed by Taguchi involves use of orthogonal arrays to organize the parameters affecting the process and the levels at which they should be varied; it allows the collection of the necessary data to determine which factors are most affecting the product quality with a minimum amount of experimentation, hence it saves time and resources [13]. Knowing the number

of parameters and the number of levels, the proper orthogonal array can be selected. For this case L9 orthogonal array is selected from Array Selector. Aspect ratio, thickness of plates and percentage reinforcement are the three parameters with three levels are as follows,

Sr.No.	Aspect ratio	Thickness (mm)	Percentage Reinforcement
1	1	3	4
2	1	6	8
3	1	9	12
4	1.5	3	8
5	1.5	6	12
6	1.5	9	4
7	2	3	12
8	2	6	4
9	2	9	8

Table 2. Process parameters and levels.

Fig 2. Test setup for three point bending.

RESULT AND DISCUSSION:

The present investigation is to study deflection and load carrying capacity of composite plate. The deflection of plate should be minimum and load carrying capacity should be maximum. The parameters considered here are aspect ratio, thickness and percentage reinforcement. All the calculations are performed using Minitab software.

Analysis of signal of noise ratio:

The analysis for deflection of plate is carries out using smaller the better criteria and the same is expressed as,

S/N = -10*log10(sum(Y^2)/n).

Level	Aspect Ratio	Thickness	Percentage reinforcement
1	-9.816	-13.711	-9.018
2	-7.732	-7.816	-9.823
3	-8.412	-4.433	-7.120
Delta	2.084	9.278	2.703
Rank	3	1	2

Table 3. Response Table for S/N Ratios Smaller is better.

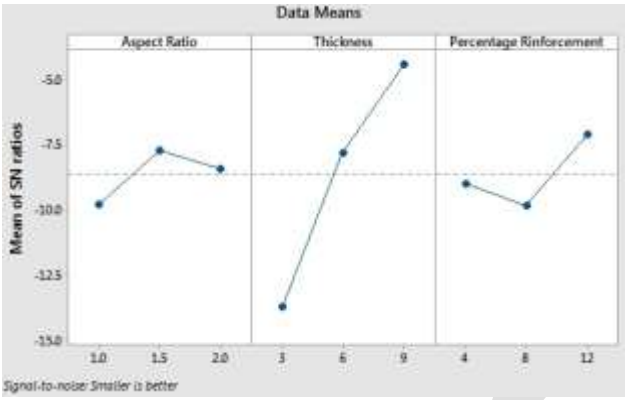

Fig 3. Main effect plot for SN ratios deflection.

The mean S/N ratio for each level of the three parameters is shown. The response table includes ranks based on Delta value. Rank 1 is assigned to the parameter with highest Delta value, rank 2 to second highest Delta value and so on. In this case thickness has the highest Delta value thus rank 1 is assigned to thickness. The effects of individual process parameters on the deflection of composite plate can be clearly seen. Maximum S/N ratio corresponds to minimum deflection and minimum S/N ratio corresponds to maximum deflection. It is observed that deflection of plate is minimum for aspect ratio 1.5, thickness 9mm and percentage reinforcement 12%.

The analysis for load carrying capacity of plate is carried out using larger the better criteria and the same is expressed as,

S/N (dB) = -10*log10(sum(1/Y^2)/n).

Level	Aspect Ratio	Thickness	Percentage reinforcement
1	81.87	79.80	81.05
2	80.96	80.29	80.54
3	80.14	82.88	81.39
Delta	1.73	3.08	0.85
Rank	2	1	3

Table 4. Response Table for Signal to Noise Ratios Larger is better.

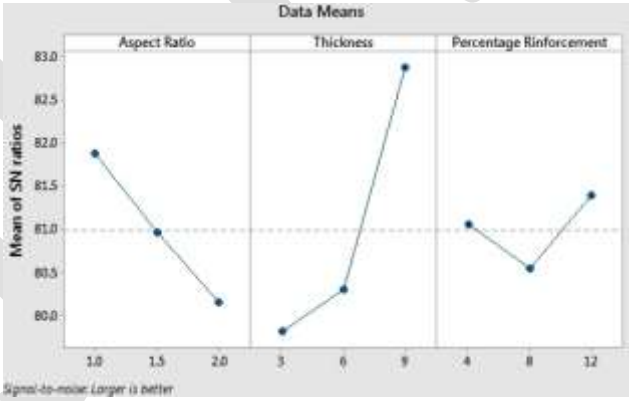

Fig 4. Main effect plot for SN ratios maximum force.

In this case also rank 1 is assigned to thickness. The effects of individual process parameters on the wear of the composite can be clearly seen. Maximum S/N ratio corresponds to maximum deflection and minimum S/N ratio corresponds to minimum deflection. It is observed that load carrying capacity of plate is maximum for aspect ratio 1, thickness 9 mm and percentage reinforcement 12%. In main effects plot the significance of each parameter can be judged by the inclination of plot. The parameter with highest inclination line has greater significance than the rest.

CONCLUSION:

1. AMC can be successfully manufactured by stir casting method at low cost. Uniform distribution of reinforcement, porosity and wettability of cast composite is greatly affected by process parameters.

2. The deflection and load carrying capacity of Al-Al_2O_3 aluminium matrix composite plate is studied by varying aspect ratio, thickness and percentage reinforcement using Taguchi orthogonal array. In main effects plots the significance of each parameter can be

judged by the inclination of plot. The parameter with highest inclination line has greater significance than the rest. From the main effects plot, it is seen that the parameter thickness is the most significant parameter while other parameters aspect ratio and percentage reinforcement are also significant parameters.

REFERENCES:

[1] A.M.S. Hamouda, S. Sulaiman, T.R Vijayaram, M. Sayuti, M.H.M. Ahmad "Processing and characterization of particulate reinforced aluminium silicon matrix composite" journal of Achievements in Materials and Manufacturing Engineering, volume 25, issue 2, December 2007.

[2] J. N. Reddy "Mechanics of Laminated Composite Plates and shells theory and analysis" CRC Press, Second Edition, 1997.

[3] S.G.Kulkarni, J.V. Meghnani, Achchhe Lal "Effect Of Fly Ash Hybrid On Mechanical Property And Density Of Aluminium 356 Alloy" Procedia Materials Science, Volume 5, pp. 746 – 754.

[4] M K SURAPPA "Aluminium matrix composites: Challenges and opportunities" Sadhana, Volume 28, Parts 1 & 2, pp. 319–334, February/April 2003.

[5] Rajeshkumar Gangaram Bhandare, Parshuram M. Sonawane "Preparation of Aluminium Matrix Composite by Using Stir Casting Method" International Journal of Engineering and Advanced Technology, Volume 3, Issue 2, December 2013.

[6] M. Karbalaei Akbari , O. Mirzaee, H.R. Baharvandi "Fabrication and study on mechanical properties and fracture behavior of nanometric Al2O3 particle-reinforced A356 composites focusing on the parameters of vortex method" Materials and Design, Volume 46, pp. 199–205, 2013.

[7] Hai Su, Wenli Gao, Zhaohui Feng, Zheng Lu " Processing, microstructure and tensile properties of nano-sized Al2O3 particle reinforced aluminum matrix composites" Materials and Design, Volume 36, pp. 590–596, 2012.

[8] Shashi Prakash Dwivedi, Satpal Sharma, Raghvendra Kumar Mishra "A356 Aluminum Alloy and applications- A Review" Advanced Materials Manufacturing & Characterization, Volume 4, Issue 2, 2014.

[9] Shubham Mathur1, Alok Barnawal "Effect of Process Parameter of Stir Casting on Metal Matrix Composites" International Journal of Science and Research, Volume 2 Issue 12, December 2013.

[10] Gui-Rong Yang, Wen-Ming Song, Jin-Jun Lu, Yuan Hao, Ying Ma (2008) Three-point bending behavior of surface composite Al2O3/Ni on bronze substrate produced by vacuum infiltration casting, journal of materials processing technology, volume 202, pp. 195–200, 2008.

[11]] Seung-Chul Lee, Seong-Taek Jeong, Jong-Nam Park, Sun jin Kim, Gyu-Jae Cho " A study on mechanical properties of carbon fiber reinforced plastics by three-point bending testing and transverse static response" journal of materials processing technology, volume 201, pp. 761–764.

[12] Shouvik Ghosh, Prasanta Sahoo, Goutam Sutradhar "Wear Behaviour of Al-SiCp Metal Matrix Composites and Optimization Using Taguchi Method and Grey Relational Analysis, Journal of Minerals and Materials Characterization and Engineering" Journal of Minerals and Materials Characterization and Engineering, Volume 11, pp.1085-1094, 2012.

[13] Lakhvir Singh, Baljinder Ram, Amandeep Singh "Optimization of process parameter for stir casted aluminium metal matrix composite using taguchi method" International Journal of Research in Engineering and Technology, Volume 2, Issue 8, August 2013

International Journal of Engineering Research and General Science Volume 3, Issue 3, Part-2 , May-June, 2015
ISSN 2091-2730

Efficient Malicious URL based on Feature Classification

Samridhi Sharma[1], Shabnam Parveen[2]

1. M.Tech Student, 2Assistant Professor, Computer Science & Engineering Department
JMIT, Radaur/Kurukshetra University, India

1. samridhisharma91@gmail.com

2 .er.shabnam786@gmail.com

9416333410

A**bstract**— Deceitful and malicious web sites pretense significant danger to desktop security, integrity and privacy. Malicious web pages that use drive-by download attacks or social engineering techniques to install unwanted software on a user's computer have become the main opportunity for the proliferation of malicious code. Detection of malicious URL has become difficult because of the phishing campaigns and the efforts to avoid blacklists. To look for malicious URL, the first step is usually to gather URLs that are live on the Internet. Then different algorithms are applied to detect malicious URL. This paper is about classifying URL based on features using machine learning techniques OneR, ZeroR, and Random Forest.

Keywords—. Machine Learning, Feature Extraction, Benign, Malicious, Web Pages, Classification Module, Attacks.

INTRODUCTION

The internet has become the medium of option for public to search for information, conduct business, and enjoy entertainment. At the same time, the internet turns out to be the most important stage used by miscreants to attack users. The most commonly used example is drive by download attack. In this attack, attackers insert different modes of attack in the web pages to which malicious URLs direct and once the victim clicks on a malicious URL, they are taken to that web page without notice. Then the attacker may steal any of the victim's information that is saved on the host computer, which may lead to grave financial loss. When malicious URLs are sent by friends, victims are more likely to click them. In addition to drive-by-download exploits, attackers also use social engineering to trick victims into installing or running un trusted software. As an example, consider a webpage that asks users to install a fake video player that is presumably necessary to show a video (when, in fact, it is a malware binary). Another example includes fake anti-virus programs. These programs are expanded by web pages that alert users into thinking that their machine is infected with malware, alluring them to download and execute an actual piece of malware as a remedy to the claimed infection. The web is growing rapidly and is a very large place, in which new pages (both begnin and malicious) are added at formidable place.

There has been lot of changes and phases in the history of malicious software since it has been exposed and detected in hosts and networks, preliminary from virus which is a self-Replicating adware but not self-transporting moving to worm, which is a self-replicating and self- transporting and going more for other. The figure of malware attack is increasing sharply with the rapid increase in complexity and interconnection of rising information systems. When the user clicks on the URL it is most likely to become a target. To prevent users from visiting such URL much may be malicious or contain illegal content, large amount of research generated by the security industry is done.

According to one study by the Gartner Group [McCall 2007], damage caused by the phishing in the United States is $3.2 billion loss in 2007, amid 3.6 million victims lessening for the attacks, a enormous raise from the 2.3 million the year previous to. Moore et al [Moore and Clayton 2007] provided details that the loss suffered by the consumers and businesses in 2007 in the US unaccompanied was about $2 billion.

A major percentage of those losses were basis by one mainly infamous group, called as the "rock phish gang" that uses toolkits to create a large number of unique phishing URLs, putting more pressure on the correctness and precision of blacklist-based anti-phishing techniques. New, previously unseen malicious executables, polymorphic malicious executables using encryption and metamorphic malicious executables adopting obfuscation techniques are more complex and difficult to detect. At present, most commonly used malware detection software make use of signature-based method and the heuristic based method to identify threats.

Signatures are strings of bytes which are short and exclusive to the programs. There use is to recognize scrupulous threats in executable files, records of boot, or memory. The disadvantage, this signature based method is not effective next to customized and unidentified malicious executables this is due to the signature extraction and generation process. Heuristic-based method is more complex than signature based detection techniques, the disadvantage of this method is that time consuming and still fails to detect new malicious executables.

The main outcomes of malicious content can be broadly grouped into the following three categories:

_ Phishing

_ Deceptive advertising

_ Computer infection for unauthorized use

A. Phishing

Phishing is an attack whereby an attacker tries to gain user's personal information by trying to trap the user into entering identifying and account information for a legitimate service. This method primarily targets financial and payment service sectors. Phishing attacks focusing on the economic and payment service sectors account for about 71% of the phishing attacks during that time, as indicated by the statistics.

B. Deceptive advertising

With this method of attack users are prompted to buy counter feit goods at low cost. The main example for this attack includes email spam advertising which will often show a pricelist as well as a URL to the web page where the goods may be purchased.

C. Computer infection for unauthorized use

The use of Botnets is done to exploits the machines by propagating when the user installs software. This can be done via many attack vectors, including that of drive-by downloads. When the user clicks on the link then the attacker exploits the user browser by installing the unwanted software in the background without the knowledge of user.

RELATED WORK

The presented work done on the detection of malicious URL can be broadly classified into three categories, specifically the blacklist based methods, the text based methods, and the URL based methods.

The *blacklist based methods* there are numerous blacklists existing which are a collection of malicious URLs and can be queried before visiting a page. The examples of backlists include Phish tank, Google Safe browsing, McAfee Site Advisor, Fortinet, URL lookup tool and WebsenseThreatSeeker Network. In order to have maintained blacklist variety of techniques are available such as honeypots, user feedbacks and crawlers. The advantage of blacklist method is it is accurate and simple and the disadvantage includes firstly the results produced are slow because of the direct verification process secondly it does not guarantee that every new Malicious URL will be in the backlist as it requires users to discover malicious URL.

The *text based methods* examine the text of the matching web page of a URL to detect whether the URL is malicious. The text provided by the Web pages for detection is very useful and of much consequence. For example, Provos et al. [1] discovered malicious URLs using features from the content of the equivalent URLs, such as the presence of definite javascript and whether iFrames are inappropriate. Moshchuk et al. [2] used the antispyware tools to examine downloaded trojan executables to identify malicious URLs. Byung-ik kim Km et al. [3] analyzes JavaScript density, frequency, entire JavaScript entropy, and entropy of each characteristic for the detection of malicious websites. The advantage of content based methods is when one has to perform an offline detection and

analysis; they are not competent of online detection. The disadvantage in online detection is that they often incur major latency, because examining and evaluate page text repeatedly costs much computation time and resource.

Most recently, the *URL based methods* use only the URL structures in detection URL Patterns are of much importance as with these patterns users can find the malicious actions. URL based features are now days used repeatedly to detect the malicious URL. McGrath and Gupta [4] they noticed disparity among normal URLs and phishing URLs in some features, such as the length of the URL, domain name length ,number of dots in URLs. With these features a classifier is build for phishing URL detection. Yadav et al. [5] analyzed additional features, which include the dissimilarity in bi-gram distribution of domain names between normal URLs and malicious ones. Their results conclude that normal URLs and malicious ones indeed have noticeable dissimilarity in the features extracted from URLs themselves alone. Le et al. [6] demonstrate that by using only the URL lexical features can maintain most of the performance in phishing URL detection. Kan and Thi[7] also worked on the lexical features of the URL only, but their work tries to group to normal URLs, such as news, business, and sports, instead of detecting malicious URLs from normal ones. Egan, S.et al, [8] concluded that the lightweight classifier is only slightly lower than that of fully-featured classification. They can define the normal behavior through static analysis of the browser behavior and compare with the browser behavior visiting a malicious web page, then determine whether a web page is malicious or not. Jian Cao et al., [9] have focused on forwarding based features along with URL and graph based features in order to train a detection model. They assess the arrangement employing concerning 100,000 early memos amassed from SinaWeibo, which is the biggest OSN website in China. Their study concludes that the forwarding base features are more effective than conventional features because of the high accuracy and low false positive rate HodaEldardiry et al.[10] has proposed a malicious insiders detection prototype which includes two types of activities blend-in anomalywhere malicious insiders try to behave similar to a group they do not belong. For this behavioral inconsistencies across these domains are observed which include logon, device, file, http, email sent and email received, and unusual change anomaly where malicious insiders exhibit changes in theirbehavior. Fusion algorithm is used to combine anomaly from multiple source of information

Hence this section presents the work done in the previous for the detection of malicious URL. The conclusion is most of the work done in this area in based on the URL features hence we will focus on the same.

CLASSIFICATION METHODS

This section briefly describes the various classification methods. As there are many classification algorithms but here we will describe only few of them. In machine learning there are two types supervised learning and unsupervised learning. Supervised learning presume that training examples are classified (labeled by class labels)Unsupervised learning focus on the examination of unclassified examples. In both cases, the objective is to build a *model* for the entire dataset, or to discover one or more patterns that hold for some part of the dataset.

Navie Bayes

It is generally used in spam filters. This method has been used form the ages in the information retrieval and text classification due to its probabilistic nature. The concept used in it is explanation the previous probability of each class, *P*(*Ci*),and the conditional probability of each feature value known the class, *P*(*aj*j*Ci*). It calculates approximately these measures by counting in training dataset the frequency of occurrence of the target class and of the feature values for all target class. Then, it uses the Baye's rule to calculate the latter probability of each target class; an unidentified instance is given which is returning prediction of the target class with the maximum such value:

C = argmax *Ci P*(*Ci*)□*jP*(*a jjCi*).

Support Vector Machine (SVM): SVMs are widely considered as recent models for binary classification of high dimensional data. They are trained to increase the edge of correct classification, and the resultant decision boundaries are vigorous to slight perturbations of the feature set, thus as long as a hedge beside over fitting. The better generalization capabilities of SVMs have been stand out by both theoretical studies and experimental successes. The decision rule in SVMs is given in terms of a kernel function K(x, x ') that calculate the resemblance between two feature vectors and non-negative coefficients $\{\alpha_i\}_{i=1}^{n}$ that point to which training examples lie close to the decision boundary. SVMs classify new examples by calculating their distance to the decision boundary. Up to a constant, this distance is given by:

$$H(x) = \sum_{i=0}^{n} a_i(2y_{i-1})K(x_i, x),$$

where the sum is over all training examples. The sign of this distance indicates the side of the decision boundary on which the example lies. In practice, the value of h(x) is threshold to predict a binary label for the feature vector x. SVMs are trained by first identifying a kernel function K(x, x ‘) and then computing the coefficients α_i that increase the margin of accurate classification on the training set. The necessary optimization can be devised as an example of quadratic programming, a predicament for which many efficient solvers have been developed.

Logistic Regression:

This is a straightforward parametric method for binary classification where examples are classified based on their distance from a hyper plane decision boundary. The decision rule is expressed in terms of the sigmoid function $\sigma(z) = [13]^{-1}$ which converts these distances into probabilities that feature vectors have positive or negative labels. The conditional probability that feature vector x has a positive label y= 1 is the following:

$P(y=1/x)=\sigma(w.x+b)$

EXPERIMENTS

1). DATA SET:The data set used in this research consisted of known malicious and known benign URLs. For malicious dataset, we obtained the data from Squidblacklist[11], a web service which provides lists of malicious URLS. Benign dataset was obtained from Alexa,[12] which is a web service that ranks web sites based on traffic generated. For example, web sites such Google and Facebook will be ranked higher in their list of websites compared those that are less frequented. Higher traffic generated web sites are less likely to be malicious because such sites are well preserved due to their fame among internet. The collected data was grouped into training with 460 instances and 534 attributes and testing data set. Training set is defined as a set of data used to discover potentially predictive relationships. The training set is used at the initial stage of the proposal to determine patterns or similarities between the different set of data obtained. The testing set is used to verify the set of patterns or similarities that was exposed during the training stage. The output of testing includes 220 malicious URL and 240 begnin URL.

2). FEATURE SELECTION

A. Host-based features: Host based features are those that require the use of exterior sources. The sources of information used in these features are WHOIS data, IP address information, and Domain Name properties which are briefly described as:

WHOIS data - It is the protocol through which query is made and responses are given by the database. It includes details when the domain is registered; expiration date registrars. With all this information available classifier can conclude how new the domain is and whether or not the domain belongs to an individual already associated with other malicious URLs.

IP address information - Each device in the computer network is assigned an IP address. It includes two features `host or network interface identification and location addressing. It is used to verify whether or not an IP address is in a blacklist. It includes the feature like hosting of the website and includes the IP address prefix and the AS number. This allows a specific ISP’s IP prefix to be flagged as malicious by the classifier. In addition to this it is associated geo location of the IP address.

Domain Name - It represents an Internet Protocol resource which includes host computer to access the Internet. Today the number of active domains reached 271 million.

B. Lexical features: These are the features of the URL that refer to the actual text of a URL and contain no outside information. These features are helpful as malicious URLs often “look” different than benign ones to experts. Features that fit in to this set consist of statistical information concerning lengths of features, tokens, numbers of delimiters and directory structure. This information is valuable as it is obfuscation resistant. To get the numerical statistic two terms are used firstly term frequency is the number of times a

word appear in document divided by total no of words in that document and secondly inverse document frequency defined as the logarithmic of total number of documents divided by the number of documents with term t in it.

C. Conclusion

Host-based features, lexical features or a combination of both, are then run through a classifier which will then present a forecast as to whether the URL is malign or benign. We represent this as 0 for malign and 1 as begnin.

3).Classifiers

In this section we have make the use of three supervised algorithms which are ZEROR, ONER, and Random Forest. As the URLs are collected they are then fragmented by the use of string to word vector convertor. After that we train the classifier and then test it .

A. ZERO R

ZeroR is the simplest association method that relies on the target and overlooks all its features. ZeroR classifier plainly predicts the popular group (class).Although there is no predictability manipulation in ZeroR, it is functional for delineating a baseline presentation as a benchmark for supplementary association methods.

B. ONER

OneR, also known as "One Rule", is a simple algorithm, yet accurate, This classification algorithm generates one rule for each predictor in the data set, and it then selects a rule with smallest total error as the "one rule". To create a rule for a predictor, The algorithm has to construct a frequency table for each predictor against the target class.

- Find Count of each value of target(class) in the dataset
- Calculate the most frequent class
- Make the rule allocate that class to this value of the predictors
- Find the total error of the rules for each predictor in the data
- Select the predictor with the smallest total error.
- Find the best predictor which possesses the smallest total error using OneR algorithm.

C. RANDOM FOREST

Random forests are an ensemble discovering method for association, regression and supplementary tasks, that work by constructing a multitude of decision trees at training period and outputting the class that is the mode of the classes (classification) or mean forecast (regression) of the individual trees. Random forests correct for decision trees' custom of over fitting to their training set.

The training algorithm for random forests applies the general technique of bootstrap aggregating, or bagging, to tree learners. Given a training set $X = x_1, \ldots, x_n$ with responses $Y = y_1, \ldots, y_n$, X_i Represents the input attributes, input URLs and Y represents the class {Malicious, Benign},

1. Split each URL according to their Latent features.
2. For each feature calculate frequency in each URL as Term Frequency
3. Create Feature Matrix $X_i^{"}$ by executing Inverse document Frequency for all urls
4. Classify Feature Matrix $X_i^{"}$ using Random Forest by
5. For $b = 1, \ldots, B$:
6. Sample, with replacement, n training examples from X, Y; call these $X_i^{"}$ Y_b.
7. Train a decision or regression tree f_b on $X_i^{"}$, Y_b.
8. After training, predictions for unseen samples x' can be made by averaging the predictions from all the individual regression trees on x':

$$\hat{f} = \frac{1}{B}\sum_{b=1}^{B} \hat{f}_b(x')$$

or by taking the majority vote in the case of decision trees.

RESULTS AND ANALYSIS

In our examinations, the classifier was trained and tested on comparable number of benign URLs as malicious URLs. The ratios of benign-to-malicious URLs do not differ considerably in training and testing. Such conditions can arise after the classifier is used in a disparate manner than it was trained. For example, presume that a established spam filter is utilized to remove URLs from dubious emails alongside product advertisements. With such URLs by now flagged, the aim of the classifier should shift to noticing phishing locations that do not continue in nearly the alike abundance as locations that merely vend spam-advertised products. The table below shows the result obtained for the classifying the URL for algorithms ZeroR, OneR, Random Forest.

Table1: Percentage of Correct and Incorrect URL

Classifier	Correct	Incorrect
ZERO R	52.17391304347826%	47.82608695652174%
ONER	54.56521739130435%	45.43478260869565%
RANDOM FOREST	91.52173913043478%	8.478260869565217%

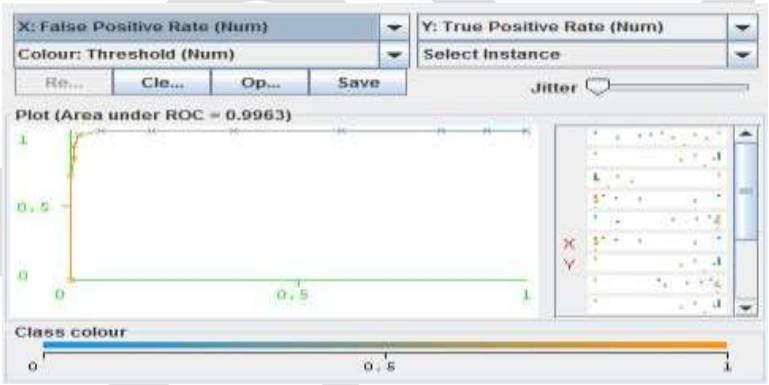

Fig1: Classification Results of Random Forest based Classifier showing ROC

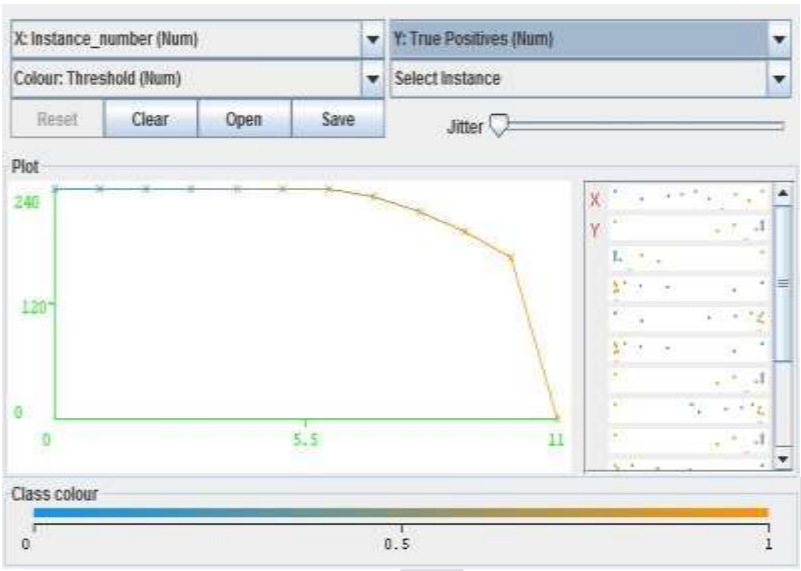

Fig 2: Classification Results of Random Forest based Classifier showing True Positive per instance

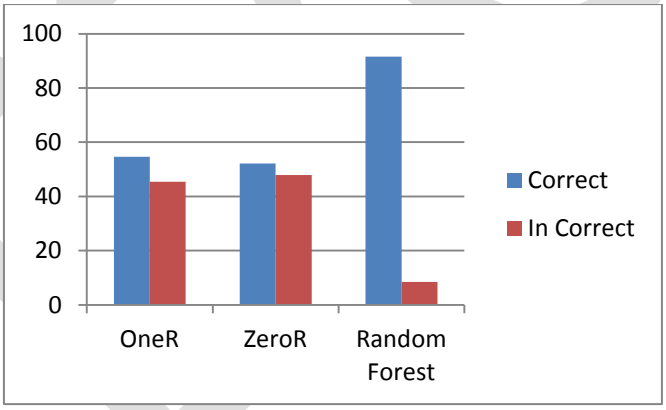

Fig 3: Graph showing the percentage for OneR, ZeroR and Random Forest**.**

CONCLUSION

This work presents the evaluation of three supervised contraption discovering models namely ZeroR, OneR and Random Forest for Malicious URL association, to notice URL as whichever malicious or not. All the supervised methods were trained and requested to a colossal number of URL's and manually tear into two classes. In a nutshell, Random forest based method display reassuring presentation alongside classification above 91% and Zero R and One R being 52% 54% respectively. As the number of URLs increased the accuracy rates for every single kind of contraption discovering ideal can be improved.In upcoming we will incorporate bit.ly like URL shortening in dataset for enhancing the finished association complexity. Enhancing presentation of Classifier can additionally be one more span of research. We will tolerate to enhance the scrutiny for discovering harmful malicious traffic and clustering clients infected by malware such as malicious bots, worms, virus and tolerating to vanquish weaknesses. We will additionally work on leading examination consolidated alongside a main IDS or malicious detection arrangements to assess the presentation of the method

REFERENCES:

[1]. Provos, N., Mavrommatis, P., Rajab, M.A., Monrose, F.: All your iframes point to us. In: Proceedings of the 17th Conference on Security Symposium, pp. 1–15. USENIX Association, Berkeley, CA, USA (2008)

[2]. Moshchuk, A., Bragin, T., Gribble, S.D., Levy, H.M.: A crawler-based study of spyware in the web. In: Proceedings of the Network and Distributed System Security Symposium (NDSS'06).The Internet Society, San Diego, California, USA (2006)

[3]. Byung-ik kim et. al Suspicious malicious website detection with strength analysis of a javascript obfuscation International journal of advanced Science and technology 2011

[4]. McGrath, D.K., Gupta, M.: Behind phishing: an examination of phisher modi operandi. In: Proceedings of the 1st Usenix Workshop on Large-Scale Exploits and Emergent Threats,pp. 4:1–4:8. USENIX Association, Berkeley, CA, USA (2008)

[5]. Yadav, S., Reddy, A.K.K., Reddy, A.N., Ranjan, S.: Detecting algorithmically generated malicious domain names. In: Proceedings of the 10th Annual Conference on Internet Measurement.IMC '10, pp. 48–61. ACM, New York, NY, USA (2010)

[6]. Le, A., Markopoulou, A., Faloutsos, M.: Phishdef: url names say it all. In: Proceedings of the 30thIEEE International Conference on Computer Communications, Joint Conference of the IEEEComputer and Communications Societies, pp. 191–195. IEEE, Shanghai, China (2011)

[7]. Kan, M.-Y., Thi, H.O.N.: Fast webpage classification using url features. In: Proceedings of the14th ACM International Conference on Information and Knowledge Management. CIKM '05,pp. 325–326.
ACM, New York, NY, USA (2005)

[8]. Egan, S. et al, in "An evaluation of lightweight classification methods for identifying malicious URLs" 2011

[9]. Jian Cao, Qiang Li, YuedeJi, Yukun He, and Dong Guo. *"Detection of Forwarding-Based Malicious URLs in Online Social* Networks." International Journal of Parallel Programming (2014): 1-18.

[10]. HodaEldardiry, Evgeniy Bart, Juan Liu, John Hanley, Bob Price, and Oliver Brdiczka. "Multi-domain informationfusion for insider threat detection." In Security and Privacy Workshops (SPW), 2013 IEEE, pp. 45-51. IEEE, 2013.

[11]. To get the mailicious URL http://www.squidblacklist.org/

[12]. To get the begnin URLhttp://www.alexa.com/topsites/global;1

International Journal of Engineering Research and General Science Volume 3, Issue 3, Part-2 , May-June, 2015
ISSN 2091-2730

CONTROL OF SOLAR PHOTOVOLTAIC (PV) POWER GENERATION IN GRID-CONNECTED AND ISLANDED MICROGRIDS

Hussain Basha Sh[1], Venkatesh p[2]

[1]PG Scholar, Dept of EEE, sree vidyanikethan engineering college (Autonomous) Tirupati, Andhra Pradesh, India.(email:hussain.sha@gmail.com). ph no 9494733600

Abstract— With the ever increasing demand of electricity, the requirement of green distributed energy resources and fast depletion of fossil fuel is increasing. Most common green distributed energy resources are Solar PV, Fuel Cell (FC), or Microturbines connected at the distribution voltage level. Most of the DERs are connected to the microgrids or utility grid with the help of power electronics interface. With the proper control of the inverter interface they are capable of producing both active and reactive power. This paper focuses on examination of the capability of the renewable energy based DERs, such as solar PV array and battery energy storage system (BESS) to provide voltage support in grid connected low-voltage microgrids and both voltage and frequency support in islanded microgrids. In addition to that an active and reactive (i.e., nonactive) power control is also provided by using solar PV functioning at MPPT and battery energy storage system for grid connected mode is also investigated. The control methods are carried out by using a Proportional and Integral (PI) controller. This paper also provides the balance between DC and AC sides of the inverter is also proposed and studied. The balance control method is also developed by using Proportional and Integral (PI) controller. Various case results are presented to validate the proposed methods. The simulation results, obtained in MATLAB/SIMULINK software, clearly prove the effectiveness of the proposed control methods.

Key words—Active and reactive power control, distributed energy resource (DER), distributed generation (DG), maximum power point tracking.

NOMENCLATURE

$v_t(t)$	Instantaneous PCC voltage
$V_t(t)$	Average PCC voltage
$v_c(t)$	Instantaneous inverter output voltage
$V_c(t)$	Average inverter output voltage
L_c	Coupling inductor
$P(t)$	Inverter average active power
$Q(t)$	Inverter average reactive power
$S(t)$	Inverter average apparent power
P_{MPPref}	Reference maximum power
α^*_1	Phase shift between $v_c(t)$ and $v_t(t)$
P_{Batt}	Actual injected battery active power
$P_{battref}$	Reference power to the battery
Q_{ref}	Average reactive power reference (Reactive load)
P_{ref}	Average active power reference (Active load)
Q_{actual}	Actual generated reactive power
P_{actual}	Actual generated active power
P_{actual}	Actual generated active power

INTRODUCTION

The microgrid is a collection of distributed generators or microresources, energy storage devices, and loads which operate as a single

and independent controllable system capable of providing both power and heat to the area of service [1]. The microresources that are incorporated in a microgrid are comprised of small units, less than 100 kW, provided with power electronics (PE) interface. Most common resources are Solar Photovoltaic (PV), Fuel Cell (FC), or microturbines connected at the distribution voltage level.

In a microgrid, the microsources and storage devices are connected to the feeders through the microsource controllers (MCs) and the coordination among the microsources is carried out by the central controller (CC) [2]. The microgrid is connected to the medium voltage level utility grid at the point of common coupling (PCC) through the circuit breakers. When a microgrid is connected to the grid, the operational control of voltage and frequency is done entirely by the grid; however, a microgrid still supplies the critical loads at PCC, thus, acting as a PQ bus. In islanded condition, a microgrid has to operate on its own, independent of the grid, to control the voltage and frequency of the microgrid and hence, acts like a PV (power-voltage) bus. The operation and management in both the modes is controlled and coordinated with the help of microsource controllers (MCs) at the local level and central controller (CCs) at the global level.

Similar to the traditional synchronous generator frequency control [3], the microgrid voltage and frequency control can also be performed using droop control methods [4]–[8]. The present work provides fast response characteristics for voltage and frequency control as compared to the secondary control considered in [8]. The analogy between inverter control and the synchronous generator control in an islanded microgrid is studied in detail in [9]. In the islanded mode, there is the necessity of having a reference voltage and frequency signals in the microgrid inverter control [10]. The operation and control of the inverter interface of renewable-based distributed energy resources (DERs), like Solar Photovoltaic (PV) in a microgrid, is a real challenge, especially when it comes to maintaining both microgrid voltage and freuency within an acceptable range. A voltage control method based on traditional droop control for voltage sag mitigation along with voltage ride through capability is proposed in [11]. A dynamic voltage regulation based on adaptive control is proposed in [12], [13]. However, there are not many research works performed on V-f or P-Q control using solar PV including MPPT control and battery storage in microgrids. In [14], frequency regulation with PV in microgrids is studied; however, this work does not consider the voltage control objective and lacks battery storage in the microgrid.

In [15], a small scale PV is considered in a grid-connected mode to control the active and reactive power of the system. Here, the control methods consider abc-dq0 transformation and vice versa which is avoided in the present paper. In [16], power modulation of solar PV generators with an electric double layer capacitor as energy storage is considered for frequency control. In [17], load frequency control is implemented in microgrid with PV and storage; however, this work also lacks the consideration of a voltage control objective. The voltage and frequency control with solar PV and battery in microgrid with an induction machine is investigated in [18]; however, this work does not explain the transfer mechanism of controls to consider the battery SOC constraint. In summary, the previous works in this topic either lack the incorporation of an energy storage component or the voltage control objective along with frequency control or the incorporation of control transition in different scenarios. The present work fulfills these gaps by considering all of these objectives.

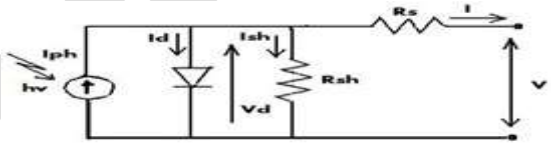

Fig. 1:. One diode equivalent circuit of Solar PV

II. SOLAR PV MODELING AND VALIDATION

The commonly accepted solar cell model is a one diode model [19]. This work uses the single diode model of the solar cell to model the Kyocera KC200GT solar array, which is shown in Fig. 1.

The I-V characteristics of a solar array, as shown in Fig. 2, are represented by (1).

$$I = I_{pv} - I_O\left(e^{\left(\frac{V+R_SI}{V_{therm}\alpha}\right)} - 1\right) - \frac{V+R_SI}{R_{sh}} \qquad 1$$

Where I_{pv} and I_0 are the photo current and the diode saturation currents respectively. The photocurrent of the PV array depends linearly on the solar irradiation and the cell temperature. Where I_{pv} and I_0 are the photo current and the diode saturation currents respectively. The photocurrent of the PV array depends linearly on the solar irradiation and the cell temperature. $V_{therm}(=N_skT/q)$ is the thermal voltage of the array, N_s being the cells connected in series for greater output voltage, K is the Boltzmann constant ($1.3806503X10^{-23}$ J/K), T is the temperature of the p-n junction of the diode q ($1.60217646 X 10^{-19}$) is the electron charge R_s and R_{sh} are the equivalent series and shunt resistances of the array respectively and a is the ideality factor usually chosen in the range $1a1.5$. Here a is taken as 1.

The photocurrent of the PV array depends linearly on the solar irradiance and the cell temperature, as shown by (2)

$$I_{pv} = \left(I_{pv,n} + K_I\Delta T\right)\frac{G}{G_n} \qquad (2)$$

Here, $I_{pv,n}$ is the photocurrent at the standard test condition (STC, 25^0C and 1000 W/m^2), K_I is the short circuit current/temperature coefficient, ΔT is the difference between the actual and nominal temperature in Kelvin, G is the irradiation on the device surface and G_n is the nominal radiation, both in W/m^2.

$I_{pv,n}$ can be calculated based on

$$I_{pv,n} = \frac{R_{sh}+R_s}{R_{sh}} I_{sc} \qquad (3)$$

Using these fundamental equations and parameters from the data sheet, the PV model is developed and verified with the panel datasheet. The I-V characteristics of KC200GT for different irradiance levels at the cell temperature of 25^0C and varying cell temperature for a constant irradiance level of 1000 W/m^2 as obtained from the simulation are shown in Figs. 2(a) and (b), respectively. The similarities of the I-V curves for different conditions with the corresponding curves in the KC200GT panel datasheet prove the validity of the developed solar panel model. The parameters of the PV panel under study are shown in Table I

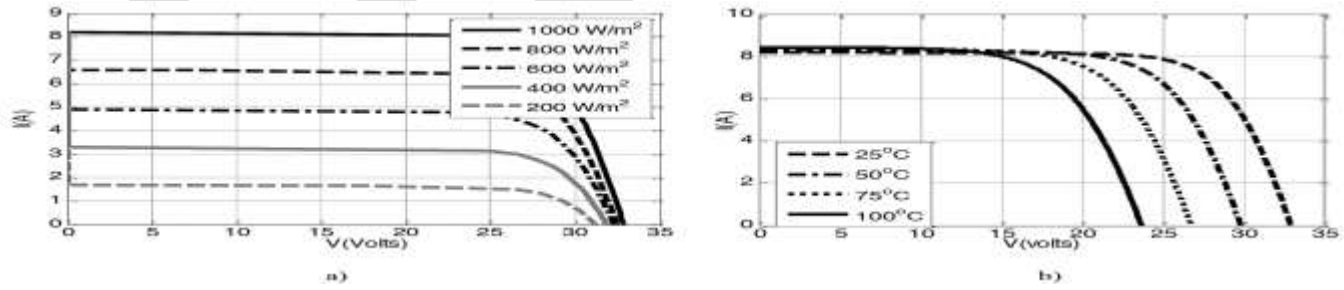

Fig. 2: The - characteristics of Kyocera KC200GT from simulation with (a) varying irradiance at a cell temperature of 25^0C and; (b) varying cell temperatureat 1000W/m^2

The PV system under study for the proposed V-f and P-Q control has 125 strings with each string having 4 series connected panels. The Maximum Power Point (MPP) for a single panel of KC200GT at 1000 W/m^2 and 25^0C (STC) is 200 W. Hence, the maximum power of the PV generator at STC is 125 X 4 X 200 =100kW. But the MPP varies according to the change in irradiance level and cell temperature.

Table 1:PV Panel Parameters at 1000 W/m^2 and 25^{0}C

Model	Kyocera KC200GT
PMPP	200W
VMPP	26.30V
IMPP	7.61A
VOC	32.90V
ISC	8.21A

III. PV SYSTEM CONFIGURATION AND SYSTEM DESCRIPTION

A. PV System Configuration

Fig. 3 shows the PV system configuration for V-f and P-Q control with PV operating at MPP including the battery storage backup. It is a two-stage configuration where a DC-DC boost converter is used for MPPT control. The system also considers a battery back-up in case of emergencies while maintaining the voltage and frequency of the microgrid or while trying to supply the critical loads.

A battery is connected in parallel to the PV to inject or absorb active power through a bidirectional DC-DC converter. When the battery is absorbing power, the converter operates in the buck mode and when battery is injecting power to the grid, it operates in the boost mode. The operation mode is maintained through the control signal provided to the converter switches.

The PV system is connected to the grid through a coupling inductor L_C. The coupling inductor filters out the ripples in the PV output current. The connection point is called the point of common coupling (PCC) and the PCC voltage is denoted as $v_c(t)$. The rest of the system in Fig. 3 denotes the IEEE 13-bus distribution feeder which is simplified as a substation with the feeder equivalent impedance, $R+jwL_S$. The PV source is connected to the DC link of the inverter with a capacitor C_{dc}. The PV is the active power source, and the capacitor is the reactive power source of the PV system.

According to the instantaneous power definitions for a balanced three-phase system consider $v_t(t)$ and $v_c(t)$ denote the instantaneous PCC voltage and the inverter output voltage (harmonics neglected) respectively,then the

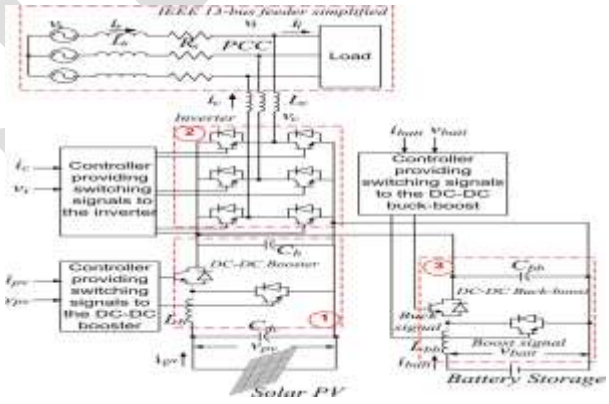

Fig. 3: System configuration of V-f control with solar PV generator operating at MPPT with a battery storage system.

average power of the PV denoted as P(t), the apparent power S(t) and the average reactive power Q(t) of the PV are as given by eqs.(4)-(6)[20]

$$P(t) = \frac{2}{T}\int_{t-\frac{T}{2}}^{t} v_{t(T)i_c(T)}dt = \frac{V_t(t)V_c(t)}{wL_c}\sin\alpha \tag{4}$$

$$S(t) = V_t(t)I_c(t) = \frac{v_t(t)}{\omega L_c}\sqrt{V_t(t)^2 + V_c(t)^2 - 2V_t(t)V_c(t)\cos\alpha} \tag{5}$$

$$Q(t) = \sqrt{S^2(t) - P^2(t)} = \frac{V_t(t)}{\omega L_c}(V_c(t)\cos\alpha - V_t(t)) \tag{6}$$

Here,α is the phase angle of $v_c(t)$relative to the PCC voltage. P(t) and Q(t) in (4) and (6) can be approximated by the first terms of the Taylor series if the angle α is small, as shown in (7) and (8):

$$P(t) \approx \frac{V_t(t)V_c(t)}{wL_c}\alpha \tag{7}$$

$$Q(t) \approx \frac{V_t(t)}{\omega L_c}(V_t(t) - V_c(t)) \tag{8}$$

B. Battery Modelling

In this paper, the battery model is taken from the MATLAB SimPower Systems library with appropriate parameters which will be used for the proposed V-f and P-Q controls. The detailed description about the battery model is given in [21].

It is assumed that the lead acid battery can be discharged up to SOC of 20% and can be charged up to SOC of 80%. The battery model in [21] is an analytical model with two equations representing the battery discharge and charge models. The battery discharge and charge model for a lead acid battery is given by eqs.(9) and (10), respectively.

$$\mathrm{V_{Batt}} = \mathrm{V_0} - \mathrm{R.i} - \mathrm{K}\frac{\mathrm{Q}}{\mathrm{Q-it}}(\mathrm{it} + \mathrm{t^*}) + \mathrm{Exp(t)} \tag{9}$$

$$\mathrm{V_{Batt}} = \mathrm{V_0} - \mathrm{R.i} - \left[\mathrm{K}\frac{\mathrm{Q}}{\mathrm{it-0.1Q}}\right]\mathrm{i^*} - \left[\mathrm{K}\frac{\mathrm{Q}}{\mathrm{Q-it}}\right].\mathrm{it} + \mathrm{Exp(t)} \tag{10}$$

where V_{batt} is the battery voltage (V), V_0 is the battery constant voltage (V), K is polarization constant (V/Ah) or polarization resistance Q is battery capacity (Ah), it=$\int i\,dt$ battery charge (Ah), A is exponential zone amplitude (V),B is exponential zone time constant inverse (Ah), R is the internal resistance is battery current (A), i and is filtered current (A).

The size of the battery is selected to provide a maximum backup power to compensate for the PV generation in the case of a very small or no irradiance level. In this work, the MPP of PV generator at STC is 100 kW. Hence, the battery is chosen to provide this amount of power for a maximum of 1 hour with an energy content of 100 kWh. The battery backup is considered for short duration applications like frequency control and supplying power to critical loads in the event of emergency situations One hour of battery backup is considered to be enough for other backup generators to take over the controls in the microgrid emergency situations.

C. Description Of IEEE 13-Bus Distribution Feeder

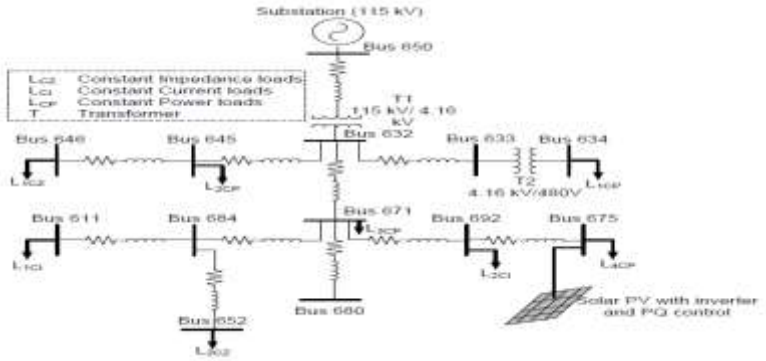

Fig. 4: IEEE-13 bus distribution feeder.

The diagram of the IEEE 13-bus distribution test system is shown in Fig. 4. It consists of a substation, 13 buses or nodes, 11 line sections, and 8 loads. The loads comprise of a combination of constant impedance, constant current, and constant power (ZIP) loads but most of them are constant power loads. The substation is at 115 kV and it is stepped down to 4.16 kV by a distribution transformer (T1). There is one more transformer (T2) which steps down 4.16 kV to 480 V. In the grid connected mode, the substation located at Bus 650 at 115 kV level is considered as a source. In an islanded microgrid case, a diesel generator connected at the same bus supplies the microgrid with a fixed amount of active power as referenced by the central controller (CC) of the microgrid.

IV. MPPT AND BATTERY INTEGRATED V-F AND P-Q CONTROL METHODS

MPPT and Battery Integrated V-f Control Method

The MPPT and battery integrated V-f control diagrams are shown in Figs. 5 and 6, respectively. The control comprises of one loop for MPPT control, two different loops for V-f control at the inverter side and another loop for battery power management.

The loop 1 in Fig. 5 is a MPPT control. The actual PV power output, P_{PV} is compared with the MPP reference, P_{MPPref} from the look up table 1 of irradiance versus MPP and this error is fed to a PI controller, PI_1 which outputs the duty cycle δ* for the DC-DC booster so that the array always operates at the referenced point by changing this duty cycle. The equation for this control loop is given by eq. (11). Here, Kp1and Ki1 are the controller proportional and integral gains respectively for this control loop.

$$\delta^* = K_{p1} * (P_{MPPref} - P_{PV}) + K_{i1} * \int_0^t (P_{MPPref} - P_{PV})\,dt \qquad (11)$$

Another feedback PI controller is used for voltage control at AC side. As shown in the control diagram in Fig. 5 (loop 2), the PCC voltage is measured and the rms value of is $v_t(t)$ calculated. Then, the rms value $V_t(t)$ is compared to a voltage reference $V_t(t)^*$ which could be a voltage specified by the utility, and the error is fed to a PI controller. The inverter output voltage is controlled so that it is in phase with the PCC voltage, and the magnitude of the inverter output voltage is controlled so that the PCC voltage is regulated at a given level $V_t(t)^*$. The control scheme can be specifically expressed as eq. (12).

$$v_{c1}^*(t) = v_t(t)\left[1 + K_{P2}(V_t^*(t) - V_t(t)) + K_{I2}\int_0^t\left((V_t^*(t) - V_t(t))dt\right)\right] \quad (12)$$

Where KP_2, KI_2 are the gain parameters of the PI controller2.

In eq. (12), 1 has been added to the right-hand side such that when there is no injection from the PV generator, the PV output voltage is exactly the same as the terminal voltage.

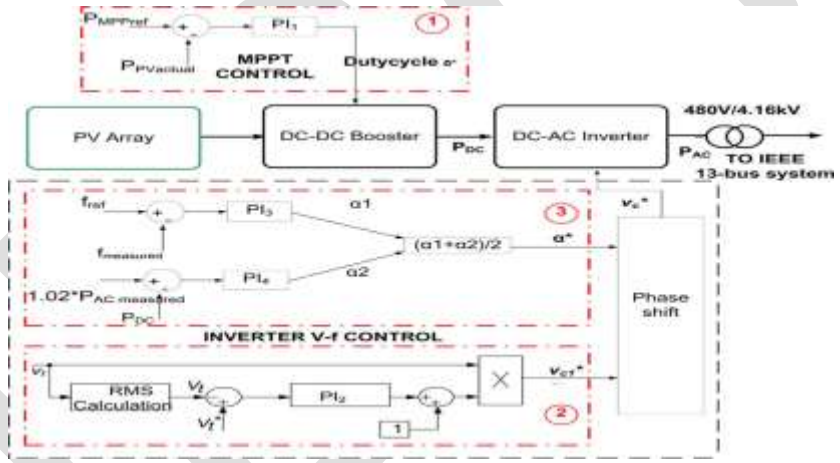

Fig. 5: Integrated Solar PV MPPT and V-f control diagram

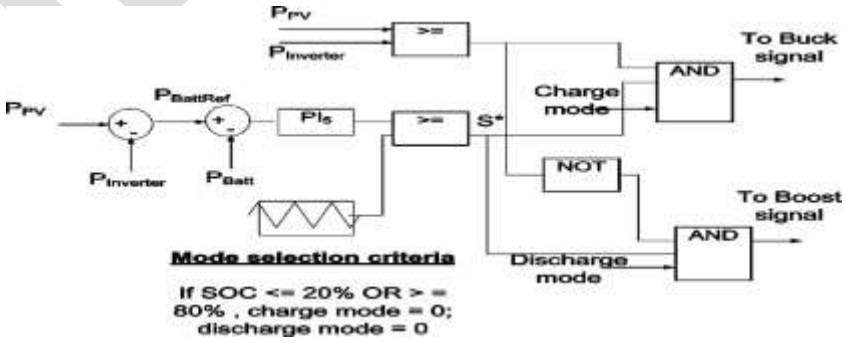

Fig. 6: Battery power control diagram.

The frequency control is carried out by controlling the active power output at the inverter side as shown in the outermost loop 3. The referenced microgrid frequency of 60 Hz is compared with the measured value, and this error is fed to the PI controller PI_3 that provides the phase shift contribution α_1^* so as to shift the voltage waveform in timescale. Thus, the active power injected will be enough to maintain the frequency at the nominal value 60 Hz. The equation for this control is given by eq. (13).

$$\alpha_1^* = K_{P3}(f_{ref} - f_{measured}) + K_{I3}\int_0^t (f_{ref} - f_{measured})dt \quad (13)$$

There is another controller PI_4 used in the same loop 3. This controller maintains the active power balance between the AC and DC side of the inverter. The reference signal for PI_4 is obtained from the dynamically changing active power injection from the inverter at the AC side as determined by the output of PI_3. Then, this measured AC side active power, PACmeasured is multiplied by a factor of 1.02 considering the efficiency of inverter as 98% such that the DC side active power is 102% of the AC side active power. The DC side active power is compared with this value of AC side power and the error is α_2^* fed to PI_4 to obtain the phase shift contribution from this loop is given by eq. (14).

$$\alpha_2^* = K_{P4}(1.02 * P_{AC} - P_{DC}) + K_{I4}\int_0^t (1.02 * P_{AC} - P_{DC})dt \quad (14)$$

The phase shift contributions from DC and AC sides, α_1^* and α_2^* are then averaged as given by eq. (15) to obtain the final phase shift, of the voltage waveform , v_{c1}^* which will then generate the voltage reference signal vc* for the inverter PWM.

$$\alpha^* = (\alpha_1^* + \alpha_2^*)/2 \quad (15)$$

Here, the reason behind considering phase shift contributions from both DC and AC side active power is to control the DC side voltage to achieve the desired value. By making α_1^* and α_2^* in a close range through the controller gains, it can be assured that the active power at the DC and AC sides is balanced. This, coupled with the voltage control loop, assures that the DC side voltage is maintained at the value desired by the AC side voltage.

The controls shown in the diagram of Fig. 5 and described above are also integrated with the battery power control shown in the diagram in Fig. 6. The battery is incorporated into the PV system configuration in order to supply or absorb active power to support the frequency control objective with the PV generator. If there is abundant solar power and the active power required for frequency control is less than PV MPP, then the battery will be charged; otherwise, if there is not enough solar power available or if the active power required for frequency control is more than maximum available power from PV, then the battery will supply the deficit power in order to follow the load and maintain the microgrid frequency at 60 Hz. Hence, the control method for the battery charge/discharge depending on this requirement is developed as shown in Fig. 6.

In Fig. 6, the reference power to the battery, $P_{Battref}$ is generated dynamically by subtracting the inverter active power injection, $P_{inverter}$ from the power generated by PV, P_{PV}. The controller comprises of a PI controller, PI_5 which receives the error signal obtained after subtracting the actual battery power, P_{batt} from the battery reference, $P_{Battref}$. The signal obtained from PI_5 is then compared with a triangular waveform of unity magnitude to generate the signal, S*. This is similar to common Pulse Width Modulation (PWM) in inverter controls. Kp_5 and KI_5 are the proportional and integral gains, respectively. The equation for this control is given by eq.(16).

$$S^* = K_{P5}(P_{Battref} - P_{Batt}) + K_{I5}\int_0^t (P_{Battref} - P_{Batt})dt \quad (16)$$

One more step is considered to differentiate the charging and discharging mode of the battery. This is undertaken by comparing PPV with Pinverter. If $P_{PV} >= P_{inverter}$, the battery is in charging mode, hence, the signal obtained from the PWM, S* and the result of this comparison is passed through a logical AND to generate a switching signal to activate the Buck mode of the DC-DC converter. If $P_{PV} >= P_{inverter}$ is false, (i.e., $P_{PV} < P_{inverter}$), the opposite of this signal and S* is passed through a logical AND to generate a switching signal to activate the boost mode of the DC-DC converter. Hence, with this control logic, the converter is capable of operating in both directions, therefore, effectively charging and discharging the battery whenever required.

B. Modification of V-f control to consider Battery State of Charge (SOC) constraint

When there is abundant solar irradiance available and the active power required for the microgrid frequency control is less than active power produced by solar PV generator at MPP i.e. $P_{fcontrol} < P_{PVMPP}$ and at the same time the battery SOC is 80%, then, the battery cannot be charged beyond this upper limit of SOC. In such case, decreasing the output power of solar PV generator would lead to underutilization of the solar resource. Hence, a global control mechanism is required in a microgrid which can transition the PV control from frequency control mode to constant power mode with power to be generated at P_{PVMPP}. Meanwhile, there should be a mechanism to allow any other generator of the microgrid to handle the frequency control problem. In the microgrid system under consideration, there is a diesel generator which can decrease its generation in order to match the PV generation increase. Hence, the power balance of the system will be maintained to eventually control the microgrid frequency.

Similarly, when the irradiance is low such that the maximum power from PV generator is not enough to maintain the microgrid frequency i.e. $P_{fcontrol} > P_{PVMPP}$ and at the same time, the battery SOC is 20%, then the battery will not be able to back up the PV generator and hence, the frequency control function needs to be transferred to other available generator if possible, in this case, a diesel generator. Again, a global control mechanism becomes an absolute necessity to allow the transition of PV generator control from frequency control mode to constant MPP mode and the transition of diesel generator control from constant active power mode to frequency control mode such that the frequency stability of the microgrid can be maintained.

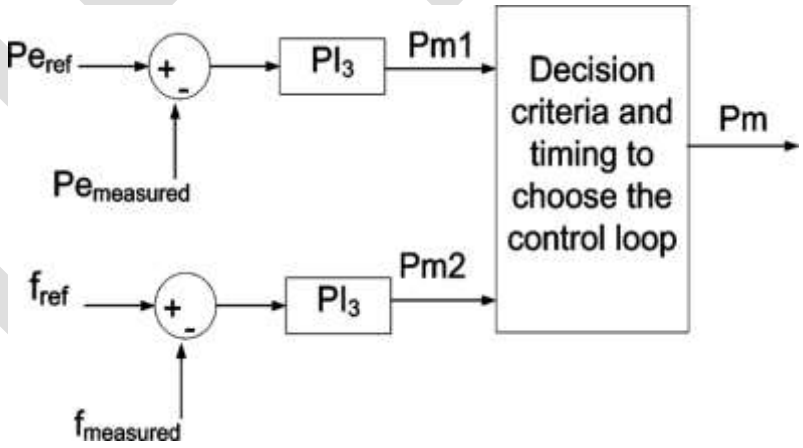

Fig. 7: Diesel generator control transition

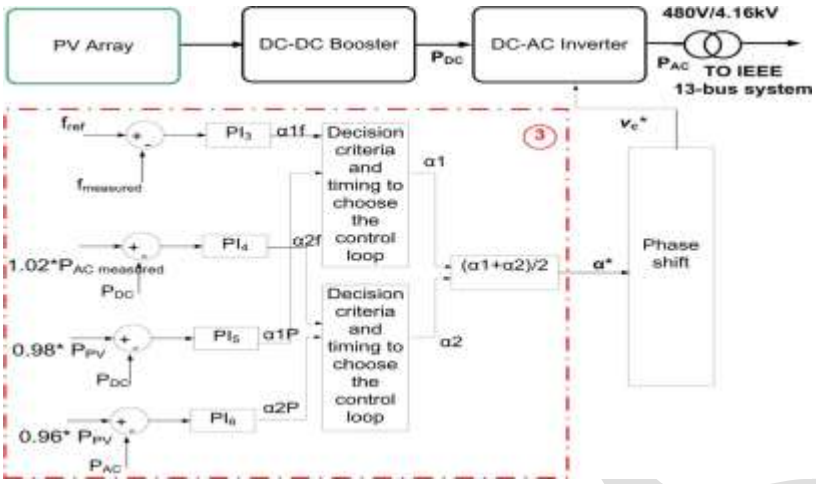

Fig. 8: Modification of PV inverter frequency control loop.

Fig. 6,7 and 8 shows the modifications of controls at different levels in the microgrid. Fig. 7 shows the transition of the diesel generator control from constant active power control to frequency control. Instead of considering the error between the reference electrical power and the measured electrical power to generate the mechanical power reference, the frequency error is considered in the controls. Fig. 8 shows the modification in V-f control loop of the PV inverter which includes the transition to another loop to take care of the constant active power control at MPP. The transition timing can be obtained from a separate module which compares active power generated from the PV generator with the inverter active power injection to maintain frequency and at the same time monitors the SOC of the battery and comes up with a time at which the controls should transition from one mode to the other. This logic, however, has not been implemented in the simulation. During the simulation process, the transition timing is heuristically selected as 1 sec so that the smoothness ın transfer of controls can be observed.

C. MPPT and Battery Integrated P-Q Control Method

This sub-section presents the proposed coordinated active and nonactive/reactive (P-Q) power control integrated with PV MPPT and battery controls. Either in grid connected or islanded mode, the microresources may be required to supply critical loads like hospitals, industries, etc. The proposed control strategy is applicable particularly for such cases. The MPPT control part for generating the duty cycle of a proper control for the DC-DC boost converter is the same as described in Section IV-A above and hence, will not be explained here. Thus, Fig. 9 shows the P-Q control blocks only, leaving behind the MPPT control block which is also present in the entire integrated control system. The P-Q control initially proposed in [22] and implemented in a larger system in [23] is converted to a more robust control with the integration of MPPT control and battery storage control in the present work.

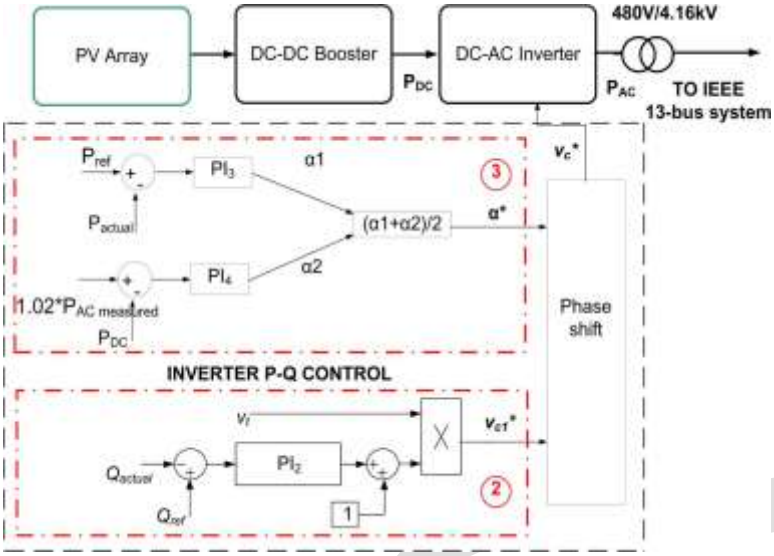

Fig. 9: Integrated Solar PV MPPT and PQ control diagram.

The inverter side P-Q control is slightly modified version of inverter V-f control. It is entirely based on the relationship of active and reactive power at PCC with inverter output phase and voltage magnitude as given by the (7) and (8), respectively. In Fig. 9 (loop 2), the measured reactive power injection at PCC is compared with the referenced reactive load and this error signal is passed to the PI controller,PI_2

Then, the term obtained is multiplied by the terminal voltage v_t to obtain the reference voltage v_{c1}^* which is in phase with v_t . The control loop 3 in Fig. 9 handles active power control through the controller,PI_3 to generate the phase shift contribution α_1^* and at the same time insure the active power balance between AC and DC sides through the controller,PI_4 . This is already explained in detail in Section V-A for V-f control. Thus, the equations for P-Q control are given by (17)–(20)

$$v_{c1}^* = (K_{P2}(Q_{ref} - Q_{actual}) + K_{I2}\int_0^t (Q_{ref} - Q_{actual})dt + 1)v_t \quad (17)$$

$$\alpha_1^* = K_{P3}(P_{ref} - P_{actual}) + K_{I3}\int_0^t (P_{ref} - P_{actual})dt \quad (18)$$

$$\alpha_2^* = K_{P4}(1.02 * P_{ACmeasured} - P_{DC}) + K_{I4}\int_0^t (1.02 * P_{ACmeasured} - P_{DC})dt \quad (19)$$

$$\alpha^* = (\alpha_1^* + \alpha_2^*)/2 \quad (20)$$

Equation (17) represents the reactive power control loop, (18) represents the active power control loop, and (19) ensures the active power balance between the DC and AC sides of the inverter. Equation (20) averages the phase shift contribution obtained from the

active power control at the AC and DC sides such that the active power control at AC side and power balance objectives are taken into account.

Table 2: Controller Gain Parameters For V-F Control (Case1)

MPPT Control Loop	K_{p1}	**6 X 10^{-8}**
	K_{i1}	**6 X 10^{-6}**
Voltage Control Loop	K_{p2}	**0.0004**
	K_{i2}	**0.005**
Frequency Control Loop	K_{p3}	**9.9 X 10^{-4}**
	K_{i3}	**5 X 10^{-3}**
P_{DC} Control Loop	K_{p4}	**0.8 X 10^{-9}**
	K_{i4}	**0.8 X 10^{-8}**
Battery Control Loop	K_{p5}	**1.5 X 10^{-8}**
	K_{i5}	**1.5 X 10^{-7}**

V. SIMULATION RESULTS AND DISCUSSIONS

This section presents the simulation results obtained with applications of the proposed control methods to the IEEE 13-bus distribution feeder. First, the results obtained from the coordinated V-f control are presented which is followed by the results from the coordinated P-Q control. In grid connected mode, the distribution feeder is considered to be supplied by a central generator with a substation at Bus 650 at 115 kV level and a PV generator at Bus 632. Hence, in an islanded case, the distribution feeder is supplied by a diesel generator and a PV connected at Buses 650 and 632, respectively.

A. Test of V-F Control in Microgrid Mode:

For the demonstration of the V-f control algorithm, two different irradiance cases are considered: Case 1 with irradiance 1000 W/m^2 and Case 2 with 750 W/m^2. The PI controller gain parameters for Case 1 are given in Table 2. The controller gains should be adjusted slightly for the change in irradiance.

While moving from the grid connected to microgrid mode, the diesel generator is controlled to generate a fixed amount of active power according to the command from the central controller. The diesel generator produces a fixed amount of 1.25 MW throughout the simulation period as shown in Fig. 10(a) and 11(a). It also shows the reactive power generated from the diesel generator.

In the islanded mode, the active power generated by the diesel generator is not enough to fulfill the power demand of the microgrid. Fig. 10(b) and Fig. 11(b) shows the microgrid frequency which initially dips to a value of 57.8 Hz due to the load-generation imbalance. The frequency control from the PV generator starts at 0.1 sec which quickly regulates the frequency back to 60 Hz in 0.2 sec. Fig. 10(c) and 11(c) shows the plot of the PCC voltage in p.u. It can be observed that voltage is also quickly regulated at 1 p.u.

after the control is started.

Fig. 10(d) and Fig. 11(d) shows the active and reactive power injection from the PV inverter which regulates the frequency and voltage of the microgrid. The active power injection from the inverter, which is required to maintain the frequency at 60 Hz in both cases, is around 80 kW.

However, there is a difference in the share of the PV generator and the battery energy storage while providing the required 80 kW to the microgrid. This is evident from Fig. 10(e) which shows the active power from the PV, the battery, and the inverter, respectively, for both cases.

In Case 1, solar irradiance is abundant at 1000 W/m^2 and hence, the PV generates the maximum power of 100 kW which is more than is required to maintain the microgrid frequency. The surplus 20 kW is used to charge the battery. The negative sign in battery power means that it is a charging phase, i.e., the battery absorbs power is shown in Fig. 10(e). In Case 2, PV generates only around 75 kW at MPP due to decreased irradiance. This is not sufficient to maintain the microgrid frequency at 60 Hz. Hence, the deficit power of around 5 kW is supplied by the battery as shown in Fig. 11(e). Here, the positive sign of battery power means that it injects active power into the microgrid

Fig. 10(f) and Fig. 11(f) shows the state of charge (SOC) of the lead acid battery considered for this study. Fig. 10(f) represents the SOC for Case 1 which shows that it gradually increases as the excess power is fed to charge the battery. The decreasing curve for Case 2 in Fig. 11(f) shows that the power is being extracted from the battery.

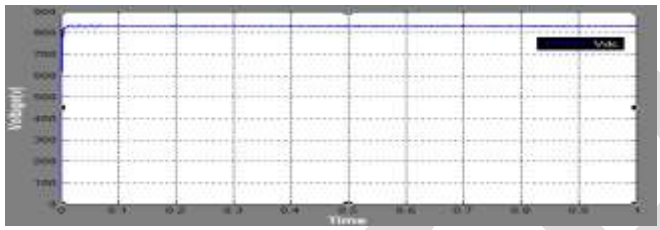

a

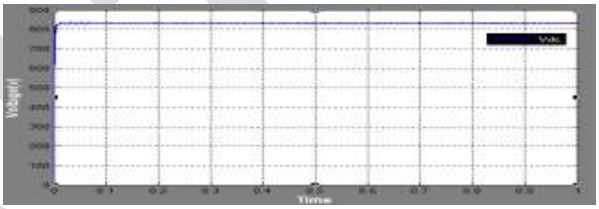

g

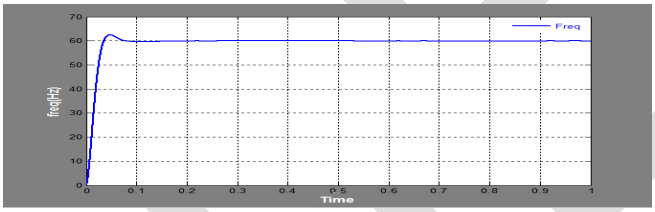

b

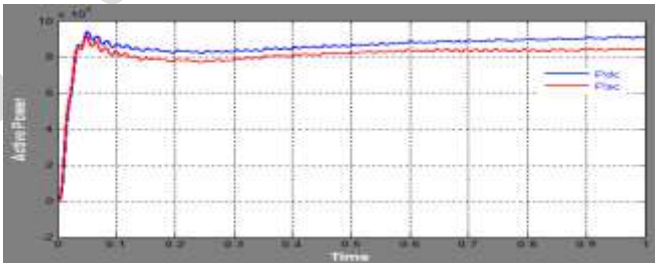

h

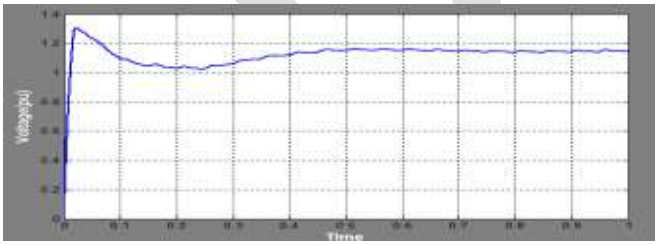

c

Fig. 10: Results of coordinated V-f control with solar PV including MPPT control and battery control (case I).

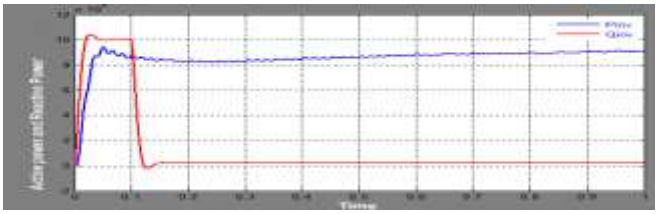

d

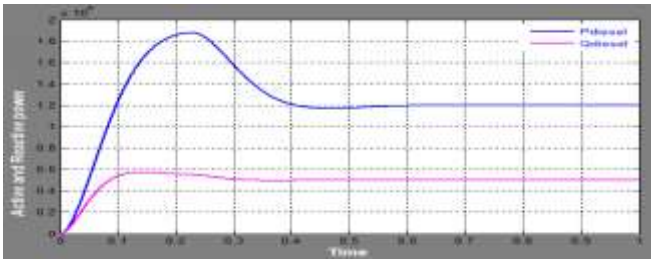

a

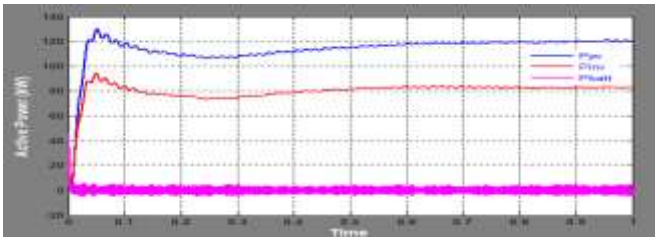

e

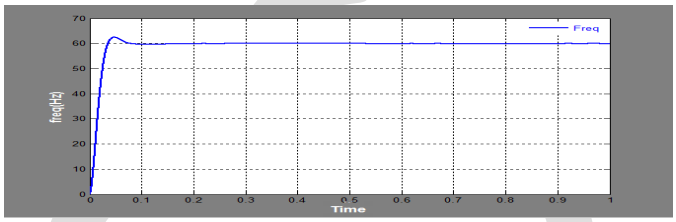

b

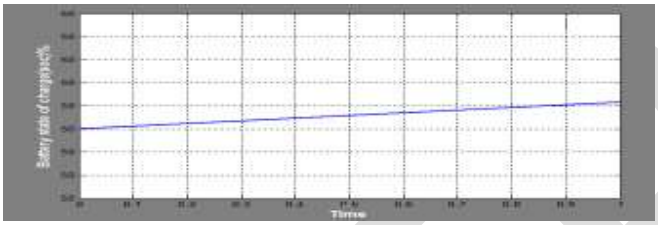

f

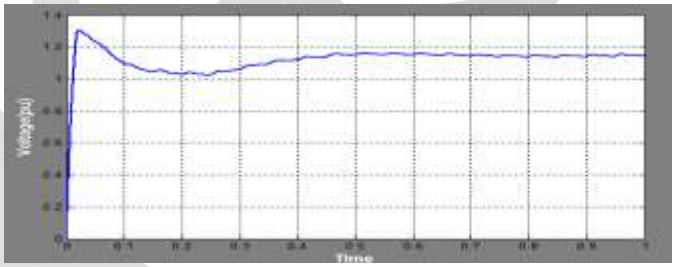

c

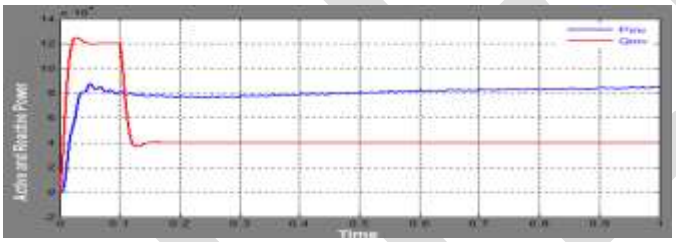

d

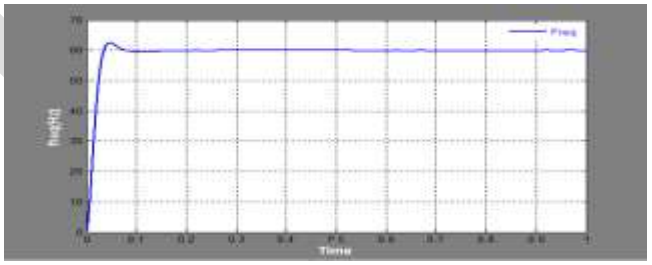

a

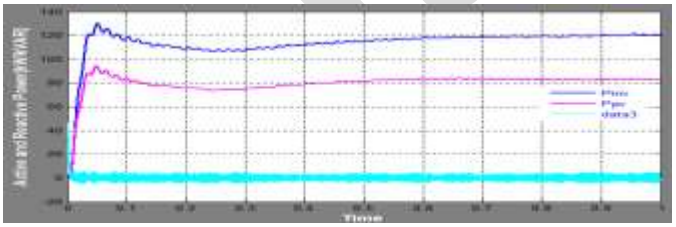

e

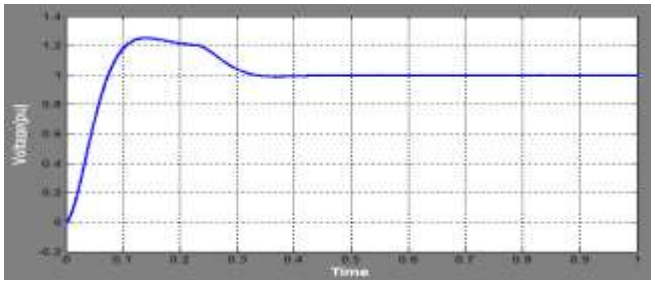

b

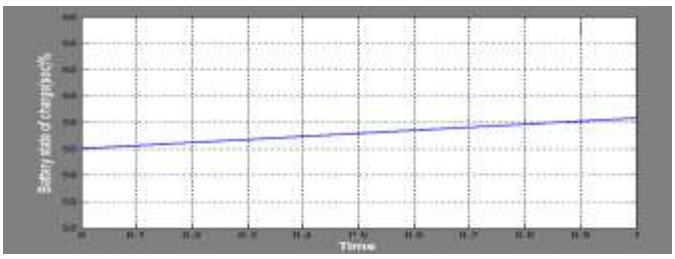

f

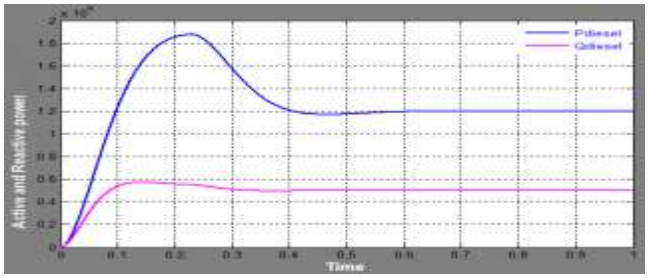

c

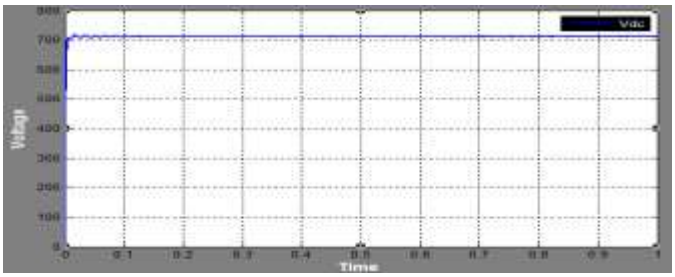

g

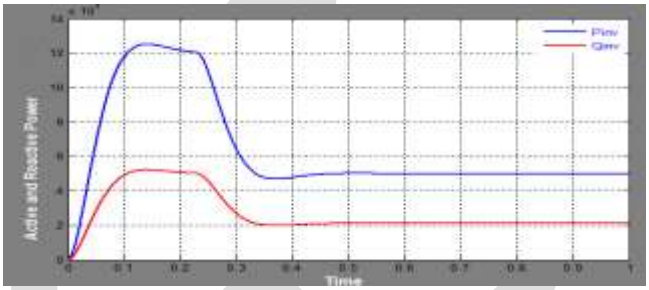

d

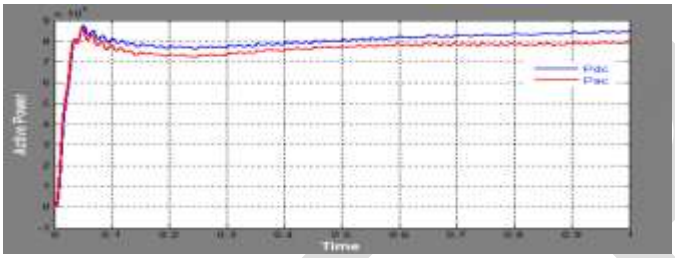

h

Fig. 11: Results of coordinated V-f control with solar

PV including MPPT control and battery control (case II)

Fig. 12: Results for V-f control of microgrid with diesel generato

Fig. 10(g) and Fig. 11(g) shows the DC voltage for both cases.It can be seen that the voltages are stably maintained at around 850 V and 550 V respectively for the two cases. Fig. 10(h) and Fig. 11(h) shows the active power at the DC and AC sides of the inverter for both cases. It is clear that DC active power is slightly higher than the AC side three phase average power. This accounts to some percentage (taken as 2% in the present work) of power losses between the DC and AC sides but the overall active power is balanced through controls. This power balance coupled with the AC side voltage control maintains the DC side voltage to a stable value which is the uniqueness of the proposed coordinated MPPT and inverter control.

Fig. 12(a) through (d) show the results obtained when the diesel generator is involved in the voltage and frequency regulation of the microgrid and the solar PV is controlled to dispatch constant active and reactive power. The V-f control of the diesel generator also starts at 0.1 sec just as in the case of the V-f control with PV generator and battery. Fig. 12(a) shows the frequency of the microgrid which shoots up in the beginning and then, gradually decreases and stays at 60 Hz in around 1 sec. It is clear from this figure that the diesel generator takes much longer time to recover the frequency than the PV and battery combination as discussed above. Fig. 12(b) shows the voltage plot of the microgrid. It is also clear that it takes around 1 sec for the voltage to settle down to 1 pu. Fig. 12(c) shows the power generated from the diesel generator and Fig. 12(d) shows the active and reactive power injection from the PV inverter which is operated at constant PQ mode. It takes about 1 sec for all the injections to stably reach the desired values. It is worth noting that the injection from the PV inverter is also affected by the oscillations in diesel generator output for the first few seconds

before reaching the steady state.

Hence, it is clearly verified that solar PV and battery without inertia can perform the V-f control for microgrid much faster than the diesel generator with inertial effect.

B. Test of V-F Control Showing Transition from Grid Connected to Islanded Microgrid Mode

A separate case study is carried out to show the dynamic characteristics of the proposed V-f and P-Q control algorithms while transitioning from the grid connected to microgrid structure. For this study, Case 1 of Section VI-A is considered in which the irradiance is at 1000 W/m^2. The bus 650 is connected to the substation in the grid connected mode and in the islanded case, the tie switch is opened at t=0.5 sec. The microgrid is then fed only by the diesel generator located at the same bus 650, and the PV generator and battery at bus 632. Fig. 13(a) shows the frequency of the system and voltage at PCC both in grid connected and islanded cases. It can be observed that the islanded microgrid frequency is quickly revived back to 60 Hz. A similar response can be observed in the voltage profile at PCC as shown in Fig. 13(b). This is due to the faster control characteristics of PV and battery integrated system involved in V-f control in islanded case.

Fig. 13(c) shows the active and reactive power injection from the PV inverter. The PV is controlled to a constant active power of around 50 kW and constant reactive powerof around 20 kVAR in a grid connected mode.Both active and reactive power injections from PV increase as the microgrid transitions to the islanded case in which PV is responsible for maintaining the microgrid frequency and voltage at PCC.

Fig. 13(d) shows the power injection at Bus 650 of the IEEE 13-bus system. The injection is from the substation in the grid connected mode.

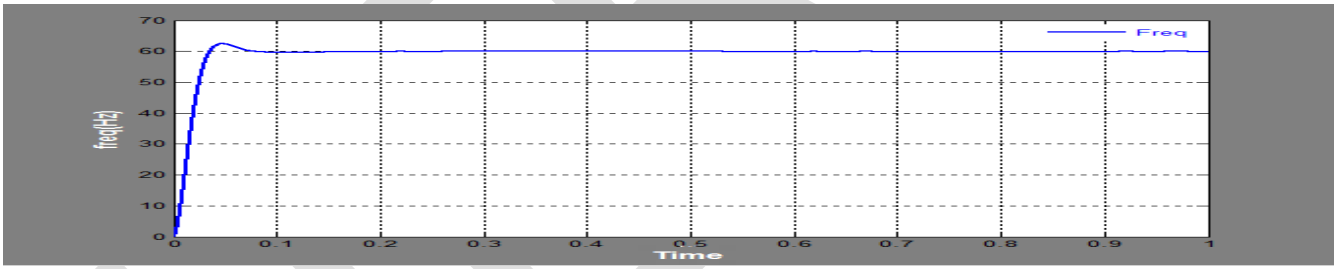

(a)

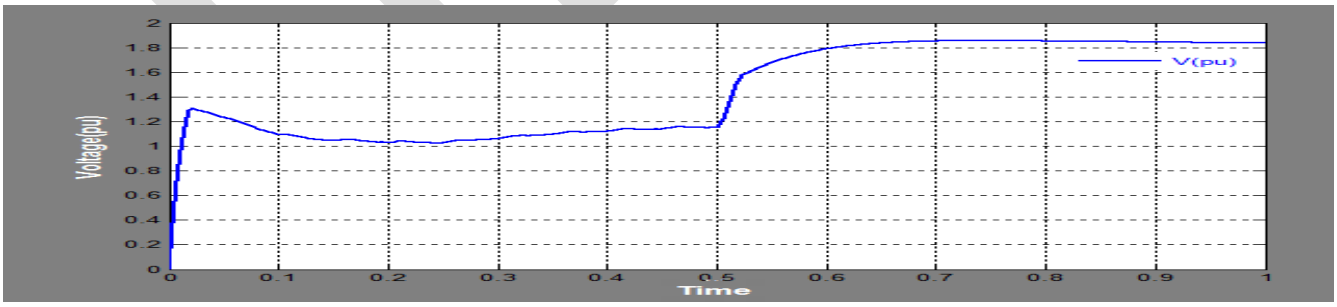

(b)

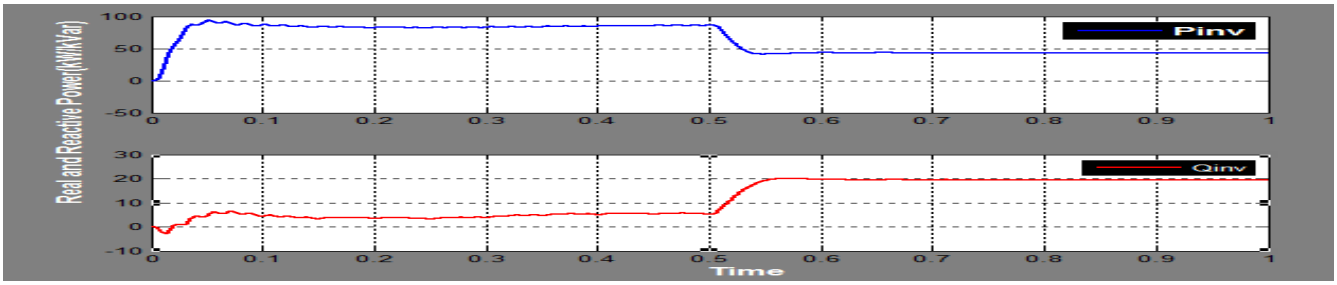

(c)

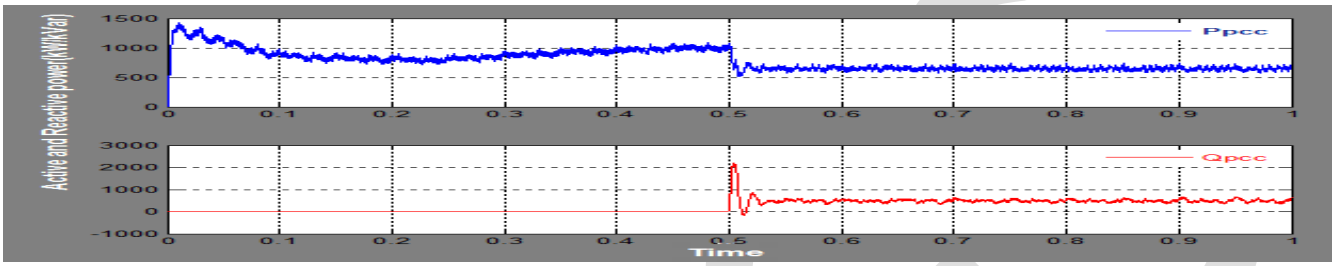

(d)

Fig. 13: Results of V-f control showing grid to microgrid transition.

In contrast, in islanded mode, the injection comes from the diesel generator which is maintained at a constant value of 1.25 MW. The results presented here clearly show the effectiveness of the V-f and P-Q control algorithms even when the microgrid transitions from the grid connected to the islanded mode.

D. Test of P-Q Control

The results of P-Q control with integrated MPPT and battery control is presented in Fig. 14 (a)–(f) for case 3 and in Fig. 15 (a)–(f) for case 4. Like V-f control, two different cases, namely Case 3 and Case 4, are considered for simulation validation of this control as well. Cases 3 and 4 are similar to Cases 1 and 2 with slight differences which are elaborated in the following paragraph. The controller gain parameters for Case 3 are given in Table 3. The parameters need to be readjusted slightly for Case 4.

Here, in Case 3, the critical active power load of a microgrid is less than the maximum available PV power (i.e.,Pref <=P_{PV}) , and in Case 4, Pref >P_{PV} . Hence, the disturbance for this part is the load changes which are very common in real operation. Moreover, since coordinated P-Q control method is to be validated, the load change is the most representative scenario to study the effectiveness of the proposed control. Hence, the solar irradiance is considered constant at 1000 W/m^2 for both cases. Fig. 14(a) and Fig. 15(a) shows the active and reactive power from the diesel generator. The diesel genset produces a constant active power of 1250 kW throughout the simulation period for both cases with a slight change in reactive power between the two cases. Fig. 14(b) and Fig. 15(b) shows the reference and actual active and reactive power of the PV inverter. The reference values of active power represent the critical loads of the microgrid as previously mentioned. The references of the active power for Cases 3 and 4 are 50 kW and 120 kW, respectively. Similarly, the references of the reactive power for Cases 3 and 4 are 20 kVAR and 70 kVAR, respectively. The references are chosen to demonstrate both charging and discharging processes of the backup battery energy storage system.

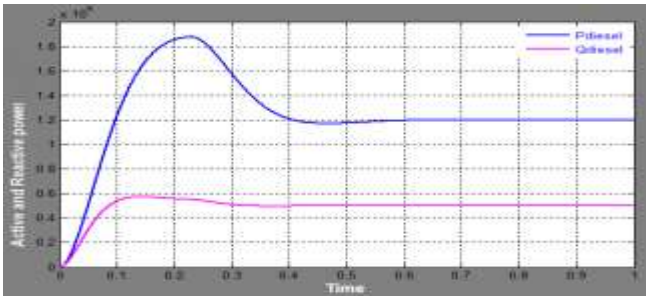

a

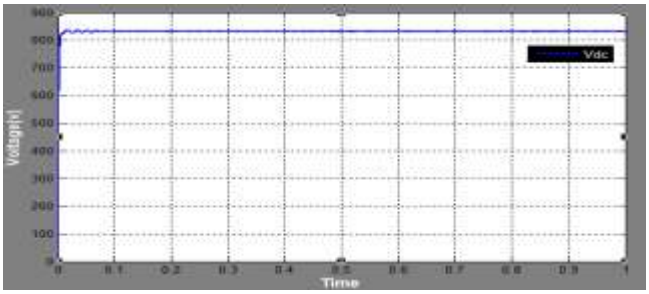

e

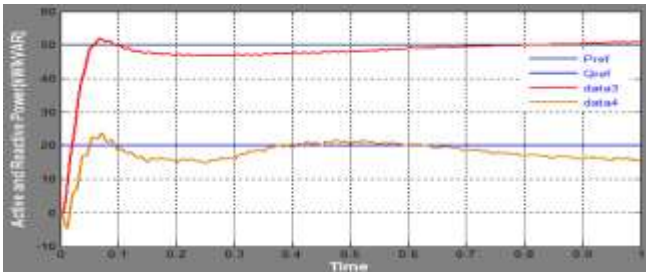

b

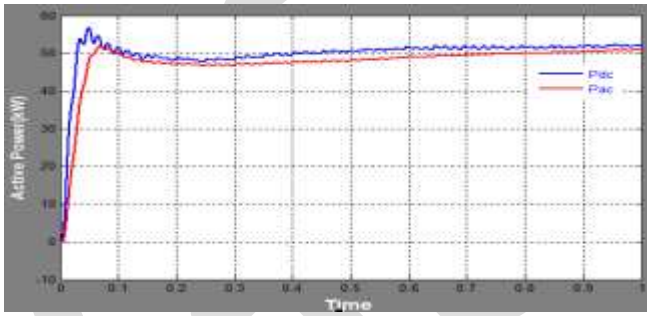

f

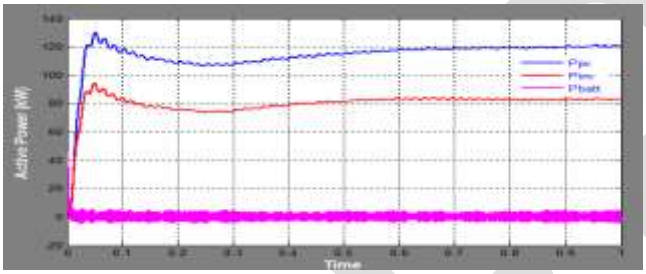

c

Fig. 14: Results of coordinated P-Q control with solar PV including MPPT control and battery control for case 3

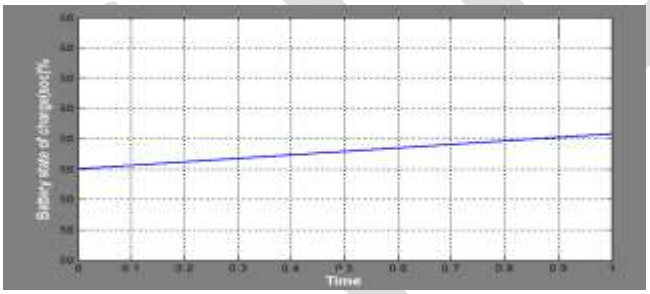

d

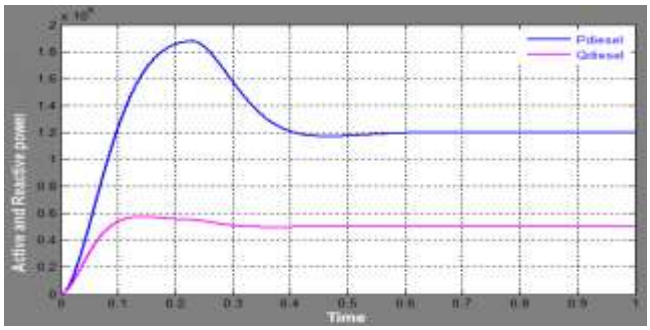

a

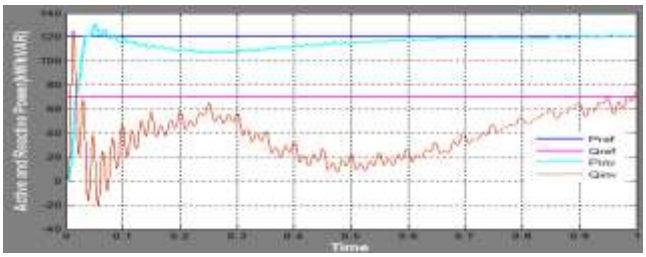

b

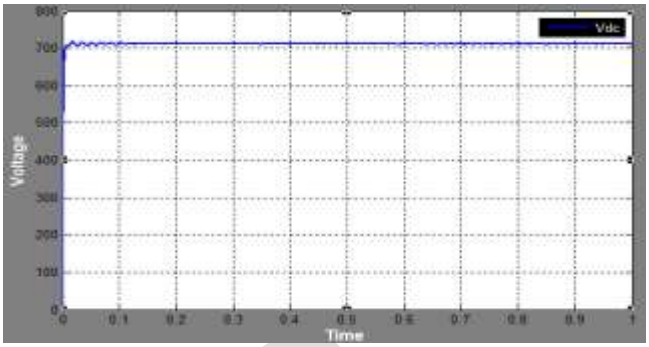

e

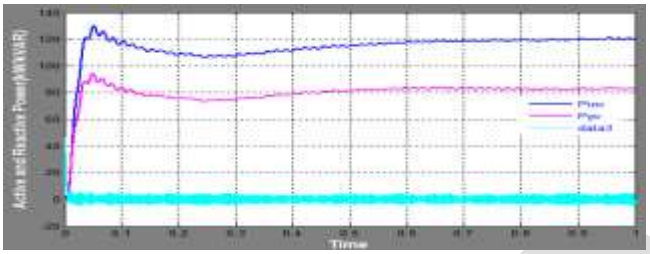

c

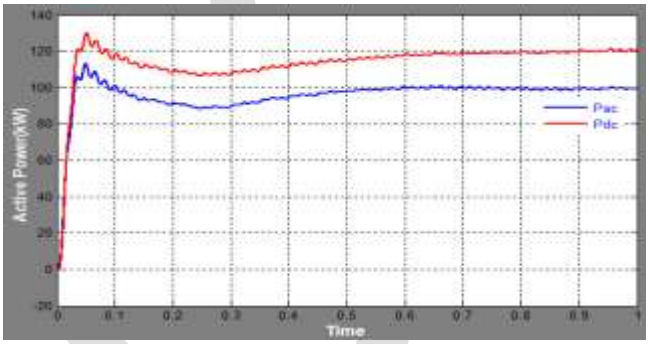

f

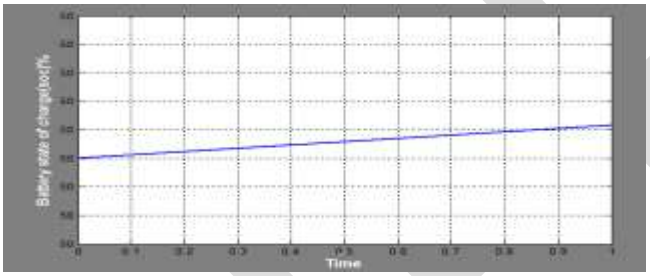

d

Fig. 15: Results of coordinated P-Q control with solar PV including MPPT control and battery control for case 4

It can be observed from Fig. 14(b) and Fig. 15(b) that the proposed coordinated controls are capable of serving the critical loads in as little as 1 seconds. Fig. 14(c) and Fig. 15(c) shows the plot of active power from the PV generator, the inverter injection, and the active power to and from the battery. In both cases, the power from PV is maintained constant at the MPP power of 100 kW through MPPT controls as shown in Fig. 14(c) and Fig. 15(c). The active power injection from the inverter is maintained at the reference values of 50 kW and 120 kW in Cases 3 and 4, respectively. These reference values are demanded by the critical loads. The generation from PV in Case 3 is more than the critical load by 50 kW. Thus, this surplus power is sent to charge the lead acid battery which is shown in (Pbatt Case3) Fig. 14(c). The negative sign of power from the battery shown in Fig. 15(c) shows that it is being charged.

For Case 4, the critical load is greater than the $PV_{generation}$ at MPP and the deficit power of 20 kW is supplied by the battery as shown by the (Pbatt Case4) curve in Fig. 15(c). As explained earlier, the positive sign of power from the battery shows that it is being discharged. Therefore, for Case 3, the power injection from the inverter comes only from the solar PV generator. However, in Case 4, the injection comes from PV and battery.

Fig. 14(d) and Fig. 15(d) shows the SOC of the battery. It is clear that the SOC changes occurs for Case 3 and Case 4 as expected because of the respective charging and discharging scenarios. It also validates the effectiveness of the battery control algorithm adopted in controlling the bidirectional power flow to and from the battery.

Fig. 14(e) and Fig. 15(e) shows the DC side voltage at the inverter input. It is stably maintained at around 820 V and 740 V for Cases 3 and 4, respectively. It validates the indirect control of the DC side voltage through the power balance between AC and DC sides of the inverter. Similarly, Fig. 14(f) and Fig. 15(f) shows the active power measured at the DC and AC sides of the inverter. Clearly, the DC side active power is slightly greater than the AC side power which means that the control algorithm also takes care of the efficiency of the inverter in the model. Hence, the effectiveness of the proposed coordinated P-Q control algorithm in microgrids is clearly demonstrated from the presented results.

ACKNOWLEDGEMENT

I am deeply indebted to my supervisor, **Mr. P.VENKATESH, *M.Tech. M.I.S.T.E.*, Assistant Professor, Department of Electrical and Electronics Engineering,** for his valuable guidance, constant encouragement and keen interest evinced throughout the course of my project work.

I express my deep sense of gratitude to **Dr. T.NAGESWAR PRASAD, *M.Tech., Ph.D.,*** Professor **and HOD, Department of Electrical and Electronics Engineering**, for his valuable guidance and constant encouragement given to me during this project work and the course.

I express my gratitude to our Principal **Dr. P.C. KRISHNAMACHARY** and the **Management** of SVEC for providing all the facilities and supporting in completing my project work successfully. I express my heartfelt thanks to all my **Teachers** in the department of **EEE** of Sree Vidyanikethan Engineering College for their moral support and good wishes.

Finally, I would like to express my sincere thanks to my parents, friends, one and all those who guided, inspired and helped me in completion of my project work.

CONCLUSION

The contribution of this paper can be summarized as follows:

- This paper proposes and presents coordinated strategies of V-f control and P-Q control, respectively, for microgrids with PV generator and battery storage.
- In the control strategies, the PV generator is operated at MPP, and the battery storage acts as a buffer in order to inject and absorb deficit or surplus power by using the charge/discharge cycle of the battery. The paper contributes in demonstrating the control strategies with effective coordination between inverter V-f (or P-Q) control, MPPT control, and energy storage control.
- The proposed control strategy also provides a smooth transition of PV side PQ control in grid connected mode to V-f control in islanded mode. This is the most essential feature required in the modern microgrid controllers.
- The proposed V-f control method shows a very satisfactory performance in reviving highly reduced voltage and frequency back to the nominal values in a matter of only 0.1 seconds. It is much faster than the diesel generator control which takes around 1 seconds to settle down. Hence, PV and battery installations might be applied effectively in restoring the microgrid frequency and the voltage at PCC after disturbances.
- Similarly, the proposed integrated and coordinated P-Q control algorithm can be effectively used in supplying some critical loads of a microgrid with solar PV and battery.

REFERENCES:

[1] Sarina Adhikari and Fangxing Li," Coordinated V-f and P-Q Control of Solar Photovoltaic Generators With MPPT and Battery Storage in Microgrids" in *Proc. IEEE Transactions On Smart Grid, vol. 5, no. 3, May 2014.*

[2] S. Chowdhury, S. P. Chowdhury, and P. Crossley, "Microgrids and ActiveDistribution Networks", IET Renewable Energy Series 6,2009.

[3] H. Saadat, *Power System Analysis*, 2nd ed. New York, NY, USA:Mc- Graw Hill, 2002.

[4] J. A. P. Lopes, C. L. Moreira, and A. G. Madureira, "Defining control strategies for MicroGrids islanded operation," *IEEE Trans. Power Syst.*, vol. 21, pp. 916–924, 2006.

[5] B. Awad, J.Wu, and N. Jenkins, "Control of distributed generation," *Electrotechn. Info.*, vol. 125/12, pp. 409–414,2008.

[6] J. C. Vasquez, J. M. Guerrero, E. Gregorio, P. Rodriguez, R. Teodorescu, and F.Blaabjerg, "Adaptive droop control applied to distributed generation inverters connected to the grid," in *Proc. 2008 IEEE ISIE*, pp. 2420–2425.

[7] H. Bevrani and S. Shokoohi, "An intelligent droop control for simultaneous voltage and frequency regulation in islanded microgrids," *IEEE Trans. Smart Grid*, vol. 4, no. 3, pp. 1505–1513, Sep. 2013.

[8] J. C. Vasquez, J. M. Guerrero, M. Savaghebi, and R. Teodorescu, "Modelling, analysis and design of stationary reference frame droop controlled parallel three-phase voltage source inverters," in *Proc. IEEE 8th ICPE & ECCE*, pp. 272–279,2011.

[9] T. L. Vandoorn, B. Meersman, J. D. M. De Kooning, and L. Vandevelde, "Analogy between conventional grid contro and islanded microgrid control based on a global DC-link voltage droop," *IEEE Trans. Power Delivery*, vol. 27, no. 3, pp. 1405–1414, Jul. 2012.

[10] H. Laaksonen, P. Saari, and R. Komulainen, "Voltage and frequency control of inverter based weak LV network microgrid," presented at the Int. Conf. Future Power Syst., Amsterdam, The Netherlands, Nov. 18, 2005.

[11] J. C. Vasquez, R. A. Mastromauro, J. M. Guerrero, and M. Liserre, "Voltage support provided by a droop-controlled multifunctional inverter," *IEEE Trans. Ind. Electron.*, vol. 56, pp. 4510–4519, 2009.

[12] H. Li, F. Li, Y. Xu, D. T. Rizy, and J. D. Kueck, "Adaptive voltage control with distributed energy resources: Algorithm, theoretical analysis, simulation and field test verification," *IEEE Trans. Power Syst.*, vol. 25, pp. 1638–1647, Aug. 2010.

[13] H. Li, F. Li, Y. Xu, D. T. Rizy, and S. Adhikari, "Autonomous and adaptive voltage control using multiple distributed energy resources," *IEEE Trans. Power Syst.*, vol. 28, no. 2, pp. 718–730, May 2013.

[14] L. D.Watson and J.W. Kimball, "Frequency regulation of a microgrid using solar power," in *Proc. 2011 IEEE APEC*, pp. 321–326.

[15] M. G. Molina and P. E. Mercado, "Modeling and control of grid-connected photovoltaic energy conversion system used as a dispersed generator," in *Proc. 2008 IEEE/PES Transm. Distrib. Conf. Expo.: Latin America*, pp. 1–8,2008.

[16] N. Kakimoto, S. Takayama, H. Satoh, and K. Nakamura, "Power modulation of photovoltaic generator for frequency control of power system," *IEEE Trans. Energy Conv.*, vol. 24, pp. 943–949, 2009.

[17] T. Ota, K. Mizuno, K. Yukita, H. Nakano, Y. Goto, and K. Ichiyanagi, "Study of load frequency control for a microgrid," in *Proc. 2007AUPEC Power Eng. Conf.*, pp. 1–6.

[18] L. Xu, Z. Miao, and L. Fan, "Coordinated control of a solar battery system in amicrogrid," in *Proc. 2012 IEEE/PES Transm. istrib. Conf. Expo. (T&D)*, pp. 1–7.

[19] M. G. Villalva, J. R. Gazoli, and E. R. Filho, "Comprehensive approach to modeling and simulation of photovoltaic arrays," *IEEE Trans. Power Electron.*, vol. 24, no. 5, pp. 1198–1208, 2009.

[20] Y. Xu, H. Li, D. T. Rizy, F. Li, and J. D. Kueck, "Instantaneous active and nonactive power control of distributed energy resources with a current limiter," in *Proc. IEEE Energy Conversion Congr. Expo.*, pp. 3855–3861,2010.

[21] O. Tremblay and L. A. Dessaint, "Experimental validation of a battery dynamic model for EV applications," *World Electric Vehicle J.*, vol. 3, 2009.

[22] Y. Xu, F. Li, D. T. Rizy, and J. D. Kueck, "Active and nonactive power control with distributed energy resources," in *Proc. 2008 40th North American Power Symp. NAPS'08*, pp. 1–7,2008.

[23] S. Adhikari *et al.*, "Utility-side voltage and PQ control with inverterbased photovoltaic systems," in *Proc. 18th World Congr. IFAC*,Milan, Italy, , pp. 6110–6116, Aug. 28–Sep. 2 2011.

International Journal of Engineering Research and General Science Volume 3, Issue 3, Part-2 , May-June, 2015
ISSN 2091-2730

AN OVERVIEW OF OUTLIER DETECTION IN WSN

Gaurav Goyal, Rajiv Munjal
M.tech. Student, CBS Group of Institutions, Jhajjar, Haryana;gauravgoyal.nrw@gmail.com;9953920564

Abstract- A wireless sensor network consist of large number of nodes that possesses very small battery life and data processing capabilities but these microelectronics system are capable of measuring physical and various environment related consequences like sound, pressure, motion, pollution causing agents etc. In this paper we will review the basics of wireless sensor network and outlier in the wireless sensor network. We will present various features of outliers like their types, how they are identified, various sources and degree of outliers. At last we will also present various challenges in detection of outlier in wireless sensor network.
Keywords: Wireless, Sensor Nodes, Outlier, Deployment, Clustering, Labeling, Outlier Identification**.**

I. INTRODUCTION

A wireless sensor network consist of large number of nodes that possesses very small battery life and data processing capabilities but these microelectronics system are capable of measuring physical and various environment related consequences like sound, pressure, motion, pollution causing agents etc. Wireless sensor network can be utilized in a wide variety of military applications such as war field monitoring and many more application like chemical spill prevention, heath care application, nuclear plants and traffic control etc. In surveillance applications, sensors are deployed in a certain field to detect and report events like presence, movement, or intrusion in the monitored area. Data collected by sensors are transmitted to a special node equipped with higher energy and processing capabilities called "Processing Node" (PN) or "sink". The processing node of wireless sensor network collect and compare data from various sources i.e. sensor nodes and thus extracting useful and meaningful information. In the architecture SNs are grouped into clusters controlled by a single command node. In wireless sensor network the sensor nodes are capable of doing only short distance communication which is radio based and responsible for detecting any target or event.
Every cluster has a entryway node that manages sensors in the cluster. Clusters can be formed based on many criteria such as communication range, number and type of sensors and geographical location. Sensors receive commands from and send readings to its gateway node, which processes these readings.[7,8]

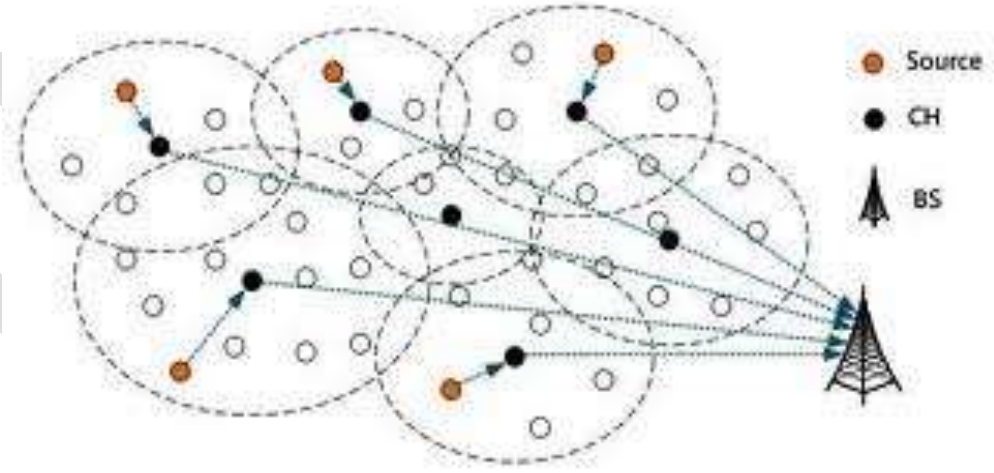

Figure 1: Sensor Network Architecture

Gateways can track events or targets using readings from sensors in any clusters as deemed by the command node. However, sensors that belong to a particular cluster are only accessible via the gateway of that cluster. Therefore, a gateway should be able to route sensor data to other gateways. Gateway nodes interface the command node with the sensor network via long haul communication links.
Outlier detection refers to the method of looking for problem in data of any event related to network in our case. These anomalous patterns are often referred to as outliers, anomalies, discordant observations, exceptions, faults, defects, aberrations, noise, errors, damage, surprise, novelty, peculiarities or contaminants in different application domains. In WSNs, outliers can be defined as, "those measurements that significantly deviate from the normal pattern of sensed data" [1]. This definition is based on the fact that in WSN

SNs are assigned to monitor the physical world and thus a pattern representing the normal behavior of sensed data may exist. Potential sources of outliers in data collected by WSNs include noise & errors, actual events, and malicious attacks.

II. TYPES OF OUTLIER

When the complete data is analyzed as per the central data approach by any central authority outliers can be identified properly and can be tackled appropriately at the corresponding station. When type of data is considered the outliers can be classified as local and global outliers:

Local Outliers: Taking the point that local outliers are recognized in wireless sensor network at individual sensor nodes, techniques for reducing communication overhead and maintaining scalability of network with proper determination of outliers is important. Many event detection applications, for example, vehicle following, surveillance and monitoring can be done using local outlier detection. Local outlier identification has two variations in wireless sensor network. One variation is that historical values are used for determining the wrong or faulty value in the given sensor network. Another option is adding historical reading of their own; where the value of neighbor is taken to determine the value is proper or not i.e. the anomaly is based on the feedback from the neighbor node. When compared with the second approach the first one lags as it doesn't provide that much accuracy and robustness in the detection of outliers.

Global Outliers: Global outliers are popular as they have global perspective and also they draw more attention as they focus on the complete characteristics of WSN instead of working locally like local outlier. On basis of different network architecture, different type of identification can be done on many nodes. All the data collected id transmitted to sink node in the centralized architecture. It delay the response time very much and cause a lot of communication overhead. Cluster head collect the data and identifies outlier in cluster based approach. It has better response time and energy consumption as compared to the former one.[10,12]

II. OUTLIER SOURCES AND HANDLING

There are three likely outlier sources in WSNs:

(a) Noise and errors which result in fault detection [1]

(b) Events which result in event detection [2].

(c) Malicious attacks which finally lead to intrusion detection.

Outlier handling is carried out by performing these three important steps:

Outlier labeling: Outlier labeling stands for detection of outlier from the given dataset it is performed with the help of various outlier detection algorithms.

Outlier Identification: Outlier identification deals with outlier detection as event or error or any kind of noice.

Outlier Accommodation: Once an observation is identified as a potential outlier, analysis should begin to determine whether an assignable cause can be found for the spurious result. If none of the reason can be found, a repetition can be suggested, the potential error node data should be backed up for future consequences. Robust statistical methods such as weighted least-squares regression minimize the effect of an outlier observation. Robust outlier detection techniques should be employed when the number of outliers is large, so that the resulting data distribution is not skewed, however non-robust techniques can be employed when the number of outliers is small.[11]

III. DEGREE OF OUTLIER

Outlier score recognizes the amount by which the sensor nodes reading diverges from the normal data reading. In wireless sensor network we have two scales for measuring the degree of being an outlier.

(a) Scalar: It is the outlier scale which divides the data measurement to determine whether it is normal or anomalous. This is actually zero one type of classification of data. This method neither differentiates between outliers, nor provides a ranked list of outliers.

(b) Outlier Score: In this a score is associated with outlier not only the classification of sensor reading as normal or anomalous. The score describe the degree of outlierness in the measurement of sensors.[3]

V. CHALLENGES OF OUTLIER DETECTION IN WSNs

Fetching out important information from given raw data is very tough job. [5] The complex design and data collected from sensor nodes are complex so it is difficult to determine outlier in it. Due to these reasons it is difficult to detect outlier in wireless sensor network:

- **Resource constraints**. The low quality and cheap sensor nodes have severe constraints in resources, like computational capacity, energy and communication bandwidth.

- **High communication cost.** In WSNs, radio communication consumes a big portion of energy not the computation in real. Computation cost for a sensor node is much lower than cost of radio communication [4].
- **Distributed streaming data.** Dynamic change can come in streaming data due to different streams. Additionally, the original distribution of data thus streamed cannot be known before receiving. Furthermore, direct computation of probabilities is difficult [6].
- **Dynamic network topology, frequent communication failures, mobility and heterogeneity of nodes**. A sensor network deployed in unattended environments over extended period of time is susceptible to dynamic network topology and frequent communication failures.
- **Large-scale deployment.** Deployed sensor networks can have massive size (up to hundreds or even thousands of SNs). The key challenge of traditional outlier detection techniques is to keep an extraordinary detection rate along with it keeping the rate of false alarm also was possible. This requires the construction of an accurate normal profile that represents the normal behavior of sensor data [5].
- **Identifying outlier sources.** The sensor network is expected to provide the raw data sensed from the physical world and also detect events occurred in the network. However, it is difficult to identify what has caused an outlier in sensor data due to the resource constraints and dynamic nature of WSNs.

Thus, the main challenge faced by outlier detection techniques for WSNs is to satisfy the mining accuracy requirements while maintaining the resource consumption of WSNs to a minimum. In other words the main question is how to process as much data as possible in a decentralized and online fashion while keeping the communication overhead, memory and computational cost low.[7]

VI. CONCLUSION & FUTURE SCOPE

In this paper we presented review the basics of wireless sensor network and outlier in the wireless sensor network. We also presented various features of outliers like their types, how they are identified, various sources and degree of outliers. At last, we represented various challenges in detection of outlier in wireless sensor network. More study can be carried out as review of types of outliers as further classification of local and global outliers. And, various algorithms can be implemented for detection of outliers in the wireless networks.

VII. REFERENCES

[1] Chandola, V., Banerjee, A. and Kumar, V., “Outlier detection: a survey”, Technical Report, University of Minnesota, 2007.

[2] S. Rajasegarar, C. Leckie, M. Palaniswami, and J. C. Bezdek, “Distributed anomaly detection in wireless sensor networks”, in Communication systems, 2006. ICCS 2006. 10th IEEE Singapore International Conference on, pp. 1 –5, October 2006.

[3] http://www.americanlaboratory.com/913-Technical-Articles/156961-Statistical-Outliers-in-the-Laboratory-Setting/

[4] S. Rajasegarar, J. C. Bezdek, C. Leckie, and M. Palaniswami, “Elliptical anomalies in wireless sensor networks,” ACM Trans. Sen. Netw., vol. 6, pp. 7:1–7:28, January 2010.

[5] D. J. Hill, B. S. Minsker, and E. Amir, “Real-time bayesian anomaly detection for environmental sensor data”, in proceedings of the 32nd conference of IAHR, 2011.

[6] S. Subramaniam, T. Palpanas, D. Papadopoulos, V. Kalogeraki, and D. Gunopulos, “Online outlier detection in sensor data using non-parametric models”, in proceedings of the 32nd international conference on Very large data bases, VLDB ’06, pp. 187–198, 2006.

[7] L. B. Oliveira, E. Habib, H. C. Wong, A. C. Ferreira, M. A. Vilaa and A. A. Loureiro, “Security of cluster-based communication protocols for wireless sensor networks” In 4th IEEE International Conference on Networking (ICN05), volume Lecture Notes in Computer Science, pages 449-458, Washington, DC, USA, 2005.

[8] W. Heinzelman, A. Chandrakasan and H. Balakrishnan,"Energy-Efficient Communication Protocol for Wireless Microsensor Networks", , January 2000.

[9] W. Heinzelman, “Application-specific protocol architectures for wireless networks”, Ph.D. thesis, Massachusetts Institute of Technology, 2000.

[10] Y. Zhang, N. Meratnia, and P. Havinga, “Outlier detection techniques for wireless sensor networks: A survey,” IEEE Communications Surveys & Tutorials, vol. 12, no. 2, pp. 159–170, 2010

[11] Z. Yang, N. Meratnia, and P. Havinga, “An online outlier detection technique for wireless sensor networks using unsupervised quarter-sphere support vector machine”, in Intelligent Sensors, Sensor Networks and Information. Processing, 2008, ISSNIP 2008. International Conference on, pp. 151 –156, December 2008.

[12] T. Kavitha, A. Chandra, "Wireless networks: a comparison and classification based on outlier detection methods "in CSEA 2012, vol. 4, special issue 1; 2013

International Journal of Engineering Research and General Science Volume 3, Issue 3, Part-2 , May-June, 2015
ISSN 2091-2730

Locus Discovery and Tracing System

G.Ranjithkumar, S.Gomathi, B.Kirthika.

Department of IT, Sri Krishna Arts and Science College,
ranjithkumar14mit016@skasc.ac.in,gomathisri@skasc.ac.in,kirthikab@skasc.ac.in and 8870323205

Abstract— Locus Discovery and Tracing System help us to find friends and family member's location with the help of Global Positioning System (GPS). The Location Based Service (LBS) is used to track the exact position of vehicle with the help of the GPS. Locus Discovery and Tracing System provide ability to track user's mobile device when user nearby location. This system uses mobile device, mapping service and repository system. The mobile device used to find location and send the pop up alert message to user. The repository used to store data about mobile user and map location. The mapping service is used to produce mapping data for mobile client and also web client. The nearby location is determined by the geographical area (geo-fence); the geographical area is divided into different types of zones. When user cross these one of the area the alert message is sent to user based upon zones (i.e. safe, risky, high risky).

Keywords— Discovery, Detection, Position, Location, Locus, GPS, LBS,

INTRODUCTION

The Global Positioning System (GPS) is a satellite-based navigation system that consists of 24 orbiting satellites, each of which makes two circuits around the Earth every 24 hours. These satellites transmit three bits of information – the satellite's number, its position in space, and the time the information is sent. These signals are picked up by the GPS receiver, which uses this information to calculate the distance between it and the GPS satellites. With signals from three or more satellites, a GPS receiver can triangulate its location on the ground (i.e., longitude and latitude) from the known position of the satellites. With four or more satellites, a GPS receiver can determine a 3D position (i.e., latitude, longitude, and elevation) [1].

Various GPS-based tracking systems have been successfully deployed and utilized in various applications such as fleet and vehicle location identification, and in route guidance. Recently, systems that integrate GPS and GSM technologies with Google earth to provide real-time data have also been proposed.

In today's world, child's safety is a major concern. It becomes difficult for the parents to keep track of their children all the time they are away from home. This application is of interest to the parents and police department to restrict the roaming of a mobile user to a predefined geographical boundary. If mobile user breaches this boundary, then a alert message containing mobile's current location is sent to register mobile phone numbers and email ids [2].

Tracking or detecting the position of people is very important for various reasons such as identifying the culprit, to notify friends about serious issues, to convey an important message etc. For this purpose, Global Positioning System (GPS) is being used widely. This paper proposes the Position Detection and Tracking system using Android which can be used to track friends and family members [3].GPS using following segments:

The Space segment: The space segment consists of 24 satellites circling the earth at 12,000 miles in altitude. This high altitude allows the signals to cover a greater area. The satellites are arranged in their orbits so a GPS receiver on earth can always receive a signal from at least four satellites at any given time. Each satellite transmits low radio signals with a unique code on different frequencies, allowing the GPS receiver to identify the signals. The main purpose of these coded signals is to allow for calculating travel time from the satellite to the GPS receiver. The travel time multiplied by the speed of light equals the distance from the satellite to the GPS receiver. Since these are low power signals and won't travel through solid objects, it is important to have a clear view of the sky.
The Control segment: The control segment tracks the satellites and then provides them with corrected orbital and time information. The control segment consists of four unmanned control stations and one master control station. The four unmanned stations receive data from the satellites and then send that information to the master control station where it is corrected and sent back to the GPS satellites.

The User segment: The user segment consists of the users and their GPS receivers. The number of simultaneous users is limitless [4]. In general, GPS receivers are composed of an antenna, tuned to the frequencies transmitted by the satellites, receiver-processors, and a highly stable clock (often a crystal oscillator). They may also include a display for providing location and speed information to the user. A receiver is often described by its number of channels: this signifies how many satellites it can monitor simultaneously [5].

The user segment uses GPS receivers shown below:

a)receiver integreted with phones

b)typical OEM GPS receiver

c) typical GPS receiver integreted with antenna

fig.1 GPS receivers

Location based Services can be classified in 2 categories they are following:

a) Public Safety / Emergency Services

The location of the client can be determined by the mobile carrier hence it finds great use during Emergency since it can be used during the emergency/health hazard to locate the mobile clients.

b) Consumer Services

Now days, smart phones like (Android, Blackberry and iPhone) provide a set of location based applications and services which helps the users to access the multiple services based on the user location.

- Maps Navigation-The users can use the Google Maps to get to the particular location or to trace the route between any two locations.
- Marketing /Advertising-Many corporate companies advertise their items based on the location of the clients. For Example –Sale in Shopping Mall near to your location.
- Location based Reminders-The phones can be used to set as the reminder based on the location [6].

Literature Review 1 :(Location Based Services using GPS On Mobile phone)

Ahemad Tutake, Abhijeet Tekawade, Ravindra Shinde, Mr. Sumit Hirve, Pranay Dhole are published paper on "Location Based Service using GPS on Mobile Phone" in International Journal of Innovative Research in Computer and Communication Engineering Vol-1, Issue -2.4. 2013.

This paper describes that the user's exact position can be track and find geographical location of the user. Location can be calculated using coordinates of geographic longitude, latitude. Location Based Services aimed to provide location based information for the users.

LBS used to find friends/family members location when they are nearby and send user location to the client. And also send alert message to the user through mobile phone. This will help to increase security for the woman.

This system uses the mobile station to retrieve the information about location with the coordinate values from server [7].

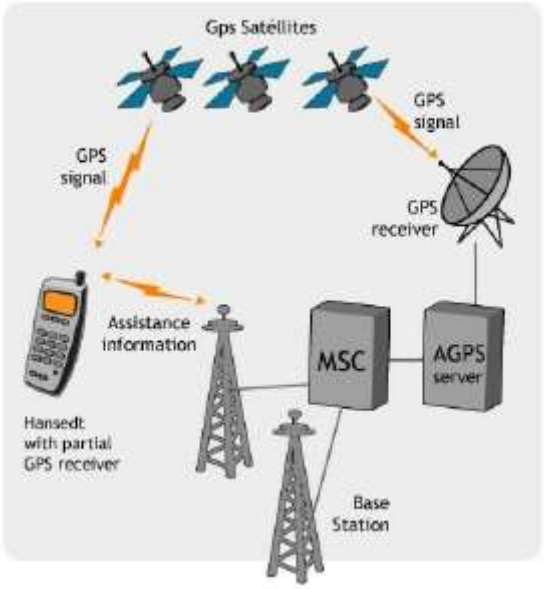

Fig.2 GPS working

Literature review 2(Mobile Tracking Application)

Purva Zalke, Radhika Kinage, Meenal Kulkarni, Jyotshna Kumari are published paper on "Mobile Tracking Application" in IJIRSET,Vol. 2, Issue 3.3.2013 Copyright to IJIRSET-617.

This paper describes about that the safety of child by using the mobile tracking application. This application involves only GPS enabled android mobile phones. Mobile tracking application stores the user's information and geo graphical areas. The geo graphical areas are divided into 3 zones (safe, risky, high risky).

Based upon these zones only user can identify the child whether he/his is safe or not and send different alert message for each zone. Radius of each zone can be setting up by the admin.

This application uses the GPS tracker to find the location and Google map is used to view the location everywhere; user can zoom in/ zoom out the location on the map.

The application can send message automatically only to user who are registered. This application used to discover the mobile location and if the location is outside the secured side means it will send alert message for corresponding zone to number which is registered by user.

In this application the GPS receiver uses two data such as almanac and ephemeris data. Almanac data used to store information about each satellite whereas ephemeris data used o store information about single satellite. This application includes methodology following: [8]

Step1. Install application.
Step2. Login
Step3. Enter phone number
Step4. Specify radius for each of the three zones
Step5. Select the Centre location on the map
Step6. Set the zones
Step7. The application checks for updates from the GPS at regular intervals
Step8. If the current location is outside the fence1 then send alert message1 go to step7
Step9. If the current location is outside the fence 2 then send alert message2 go to step7
Step10. If the current location is outside the fence3 then send alert message3 go to step7.

Literature Review 3(Location Tracking Of Nearest ATM Center Using GPS)

GUGAPRIYA A , KAVIYARASI S, VAITHEKI J. are published paper on Locus Tracking of Nearest ATM Center using GPS in) INTERNATIONAL JOURNAL OF INNOVATIVE TECHNOLOGY AND RESEARCH Volume No.1, Issue No.3,April-May 2013, 253–255.

This paper describes about tracking a nearest ATM center by using a Location Based Service on smart phones. Nowadays, the mobile devices are important one in the field of location based services. The mobile device is used in the field of banking service for fund transaction. M-banking service is more familiar in smart phones.

Location based service is used for real time information and to find the location. GPS is used to identify exact location of user and to navigate where u want to go for. In this paper author described that the GPS in mobile used for tracking ATM center. It can be done by integrate GPS receiver to the mobile.

GPS receiver calculates its location by measuring the distance of more satellites with the help of GIS. It shares the location information to the server. Using GPS chips user can identify any devices by integrate GPS chips to the devices. Example:-watch, car , etc..

In Location Based Service, GIS (Geographical Information Service) provides all functionalities of the LBS.

Google Maps are often used to view map location. Google Map is a part of GPS. GPS uses a MAP service for view map. It is often widely popular [9].

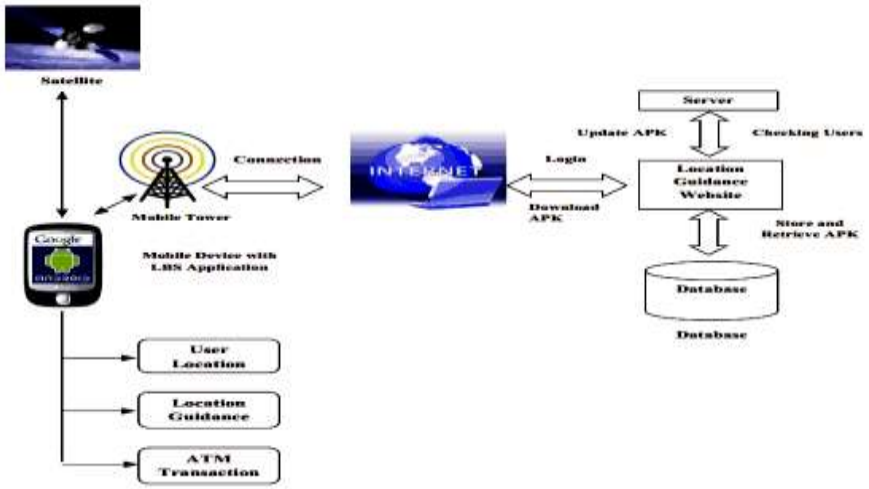

Fig.3 Tracking ATM center

The overview of GPS working on the Mobile (Android)

GPS-Global Positioning System

GPS is used to discover the exact spot of the portable device. Used to navigating from one place to another and discover time information of the user. It can be made up of three segments –

1) Space segment
2) Control segment
3) User segment

The space segment used to transmit one way signal that provides the GPS position and time information. And it consists of 24 satellites on the orbit.

The control segment used to upload or update the navigational & mapping data on satellite. The control segment switches the satellite.

The user segment consists of the mobile device that has GPS receiver to retrieve information from the satellite. And provides the diffused information, guess the 3-D position.

GPS receiver calculates its location by measuring the distance of more satellites with the use of GIS. It shares the location statistics to the GPS server. Using GPS chips user can identify any devices by integrate GPS chips to the devices. GPS receiver uses two data such as almanac and ephemeris facts. Almanac facts used to store statistics about each satellite whereas ephemeris facts used to store information about single satellite.

Android:

Android is an operating system based on a interface of java with Linux environment. Android-SDK used to develop application of android. It is developed for assistant numerous applications. It supports wireless application such as GPS, BLUETOOTH. It rehearses the 2-D and 3-D graphics [9].

Mobile station:

Mobile station is accompanying with the satellites that could be used to retrieve the statistics about coordinates using GPS and base station is used to track the locus from server base station of location database. Mobile station is interconnecting with the base station.

Mobile Tracking:

The mobile tracking is used to track the mobile phone of friends/family or users who are locate nearby. Mobile tracking used to implements the client server system by track the mobile phone. This system used to discover the nearest location for instance hotel, ATM. This system also tracks the device when moving. To locate the device at least it releases the roaming signal.

It uses the GPS to track the exact locus and send alert message to the user about the locus. The user can provide the alert message to friends if they nearby user location. GPS can be identified present statistics of location and if user travels to new place it can be updated.

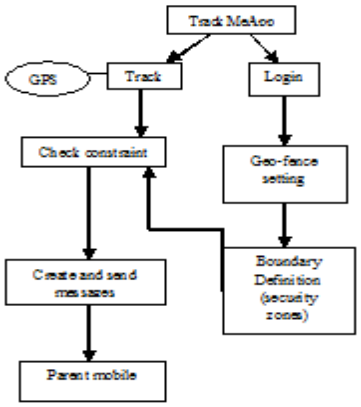

Fig.4 Block diagram of track me app

Mobile tracking application stocks the user's data and geo graphical regions. The geo graphical regions are separated into 3 ranges. Based upon these ranges only user can identify the child whether he/his is safe or not and send different alert message for each regions. Radius of every regions can be set up by the admin. This application uses the GPS tracker to find the location and google map is used to view the location everywhere; user can zoom in/ zoom out the location on the map [7].

Google Map

Google Maps are often used to view map location. Google Map is a part of GPS. GPS uses a MAP service for vision chart.

Fig 4.1 The three zones are mentioned below diagram

Location processing

Location processing used to process the location information and send to the user with the alert message. Ex, sent alert message with location to the parent about location of child.

Location Tracing

Location tracing used to track the location of user using GPS receiver. GPS receiver equipment integrates within the mobile [11].

Use of GPS

1) Woman security
2) Locate friends/family
3) Find location of child
4) Analysis of bus tracking
5) Tracking the car within nearby location
6) Detect the lost mobile
7) Track staff location
8) Detect accident zone.

System architecture

The Locus Discovery and Tracing System consists of the following six modules:

1) Mobile client.
2) Web client.
3) Repository.
4) Data (Documents, Audio, Video) sharing center.
5) Message Alert system for detection of Position of Friends.
6) Map service.

Mobile client

The mobile device used to find location and send the pop up alert message to user.

Repository

The repository can be used to stockpile records about mobile phone user and map location.

Mapping service

The mapping service is used to produce mapping data for mobile client and also web client.

Web client:

The repository information can be maintained and viewed in this section. The user improves the statistics of position from the web client on user mobile phone.

Alert system:

The SMS alert system used to discover the locus of our friend and family member

And update records to server. It directs spot modernize to the user when friends are within particular space.

Data sharing center:

Data sharing center used to sharing the data such as Audio, document, video, Image [10] etc...

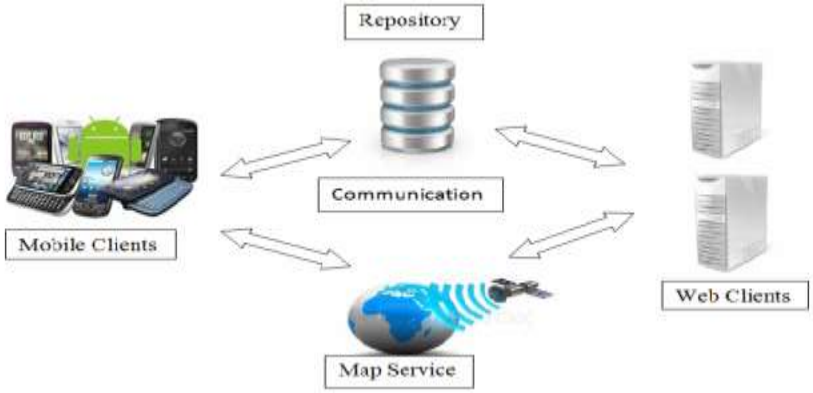

Fig 5 map service

LBS used for Location Tracking Through mobile phone:

LBS Application

Core LBS Features (Location Tracking, GIS Provider and Location Collection Services) to provide a consistent interface to LBS applications.

The LBS features(Locus tracking , Locus collection services and GIS provider) access to provide interface to application of LBS.

Location Tracing

Location tracing used to track the location of user using GPS handset. GPS receiver kit incorporates within the mobile.

This has functionality, which is following:

1. It stores the user's present and past locations.
2. It can be notify the user when user moving to other place.
3. It can be describing that which user is locating in which geo location.

GIS Provider

The GIS provider helps to determine the map information and information about the geographical coordinates. It is important component in LBS.

Location Collection Service

It is used to collecting the information such as latitude, longitude for a user.

To implement the LBS android using the following classes

1. Location Manager
2. Geo-coding
3. Google-Map
4. Location Provider

Location Manager

This class aids to keep all other component which is important to implement the LBS.

Location provider

Location provider used to describe the physical location and provide the location information to the all users [11].

Detect Accident using GPS and GSM

GPS is used for detecting the accident with the support of GSM. GPS uses GPS handset to discover accident location by calculating its speed. Accident can be discovered by use of sensors. After discovering the location it is send to GSM and GSM refers the data to the control unit, it has the GSM number to send data to reserve number which can be aid to call ambulance service.

Vehicle must have installed the GPS headset on its own. Server detects the nearest ambulance service and provide short route for the ambulance and also direct to hospital. Ambulance must have the GPS chip.

After this the traffic signal discovers the ambulance and alert roads to free way. When the near to the traffic it will automatically mark the signal as green by RF module [12].

CONCLUSION

In this paper, use of GPS user can detect the exact position and navigate user to destination location. It is often used to detect the accident using GPS with GSM and sensor network. To track the friends/family members when they are locate nearby residence of the user. If they trace nearby place then location is outline to the user. LBS can be sending the position data to the user and also send alert message to the user.

REFERENCES:

1) aqua.wisc.edu/cpr/Default.aspx?tabid=80

2) en.wikipedia.org/wiki/Global_Positioning_System

3) ijcsits.org/papers/vol4no32014/3vol4no3.pdf

4) ijiset.com/vol2/v2s5/IJISET_V2_I5_38.pdf

5) www.ijarcce.com/upload/2014/january/IJARCCE3B__A_unmesh_Location.pdf

6) www.ijarcce.com/upload/2014/january/IJARCCE3B__A_unmesh_Location.pdf

7) www.ijircce.com/upload/2013/april/18_V1204050_Mobile%20_H.pdf

8) www.ijitr.com/index.php/ojs/article/viewFile/87/pdf

9) www.ijirset.com/upload/march/15_Mobile%20Tracking.pdf

10) www.ijirset.com/upload/march/15_Mobile%20Tracking.pdf.

11) www.nhdfl.org/library/pdf/Forest%20Protection/Introduction%20to%20Global%20Positioning%20System.pdf

International Journal of Engineering Research and General Science Volume 3, Issue 3, Part-2 , May-June, 2015
ISSN 2091-2730

Performance Comparison Of Optical Amplifiers And their Hybrid Configurations In 8x10 Gbps WDM Based Optical Network

Upma, Poonam Singal

Deenbandhu Chhotu Ram University of Science and Technology , Murthal.

Upma14singh@gmail.com and Contact no.-09991839448

Abstract- Some conditions and requirements are not fulfilled by the individual amplifiers, so to accomplish various goals, hybrid configurations of amplifiers are designed. These hybrid amplifiers are composed with combination of (EDFA-SOA, RAMAN-EDFA, RAMAN-SOA) different amplifiers. In this paper we have investigated the performance of different amplifiers with 8 channel transmitter at data speed of 10 Gbits/s with constant attenuation value .2 dB/km. Performance is analyzed on the basis of Quality factor, eye opening, eye closure, jitter, bit error rate(BER).Different combinations provide better result that are suitable for efficient optical communication.

Keywords - Raman amplifier, semiconductor optical amplifier, erbium doper fiber, EDFA-SOA, RAMAN-SOA, RAMAN-EDFA, BER, WDM, hybrid amplifier optical fiber communication.

INTRODUCTION

Two major problems occur in the optical signal transmission are Attenuation and Dispersion. Power of signal is reduced during transmission is called attenuation. Pulse broadening and inter symbolic interference are major problems that causes dispersion. The growth of optical amplifiers permit a dramatic improvement in the efficiency of optical communication system [1]. Capacity increases is possible while reducing system cost, signal is degraded when transmitted over long distance. Earlier, it was accomplished with repeaters or we can say optoelectronic devices that convert optical signal into the electrical signal or vice versa. Evaluation of optical amplifiers eliminates the requirements of repeater or optoelectronic devices. Cost of system is also reduced by using optical amplifiers because there is no need of O-E OR E-O conversion. Optical amplifier is used in WDM system in which all the channel of transmitter are transmits simultaneously. Optical amplifiers are use plain after the transmitter and absolutely before the receiver for distortion free and efficient transmission of power.

Raman amplifiers are used to increase the capacity of fiber-optic networks, operates at the 1300 nm, 1400 nm for wavelength-division multiplexing or short-wavelength S-band[2]. As an example, using a cascade of -band lumped amplifiers, a 20-channel, OC-192 system is shown that propagates over 867 km of standard, single-mode fiber. Raman amplifiers provide a simple single platform for long-haul and ultralong-haul amplifier needs. Performance of augmented gain EDF amplifier systems by enhancing the stages of EDF amplifier & further by variation in pumping power on designed EDF amplifier system has been investigated [3] . It is investigated that signal to noise ratio and the noise figure can be find out by measuring the quality factor of amplified continuous wave signal modulated by external modulator [4].

Several technologies are used for the fabrication of Erbium-doped fiber [5].The semiconductor optical amplifier was able to transmit the signal from 69 to 112 kilometers. The main obstacle that limited the system performance was amplifier produced noise, that is very much greater than of the discrete Raman amplifier, which in turn has managed to extend transmission distance to 119 kilometers [6]. Performance of hybrid configuration has been analyzed with 16, 32 channel transmitter at data speed of 10Gbps [7]. SOA-EDFA showed good performance as it can travel max distance of 220,240,260 km at 16, 32 and 64 channels respectively. Also, RAMAN-EDFA showed a good performance as it has a high QUALITY FACTOR (24.27) and BER (1 X 10-40) at 16 channels [8].

The performance of optical amplifiers in DWDM system has been studied with different number channel of transmitter at channel spacing of 100 GHz [9-12]. We expend the investigation by comparing the performance of individual amplifier and their hybrid configuration. In this paper we have analyze the performance of RAMAN, EDFA, SOA, RAMAN-EDFA, RAMAN-SOA, EDFA-SOA various amplifiers with 8 channel of transmitter at data speed of 10Gbps and at attenuation 0.2dB/km.

SIMULATION SETUP

Simulation setup consist of total 10 blocks. In this, 8 channels are used to transmit with WDM in which all channel transmit the data simultaneously. Transmission speed used is 10 Gbps with channel spacing 50 GHz. Transmitter compound component made up of four components. (1) Data Source – Data source is used to generate the data in logical form with pseudo random sequence. (2) Modulator Drive – There are four types of modulator drivers in the simulation tool we have used. But in this investigation NRZ formatting is used. It is used to convert logical signal into the electrical signal. (3) CW Laser – CW Laser is used to generate laser beams equivalent to transmitter channels. In this case CW Laser generate 8 beams. (4) Amplitude Modulator – Amplitude modulator combine and modulates the signal coming from modulator drive and CW Laser and send it to transmission medium. Splitter is used to split the power to all output optical ports. Fiber is used with different lengths i.e. 10, 100, 200 km. The simulation set up is repeated for measuring the signal strength by utilizing various amplifiers i.e. EDFA, RAMAN, SOA, EDFA-SOA, RAMAN–EDFA, RAMAN-SOA using optical simulator. Performance of individual amplifiers and hybrid amplifiers are compares on the basis of Q factor, jitter, eye opening, eye closure, and BER.

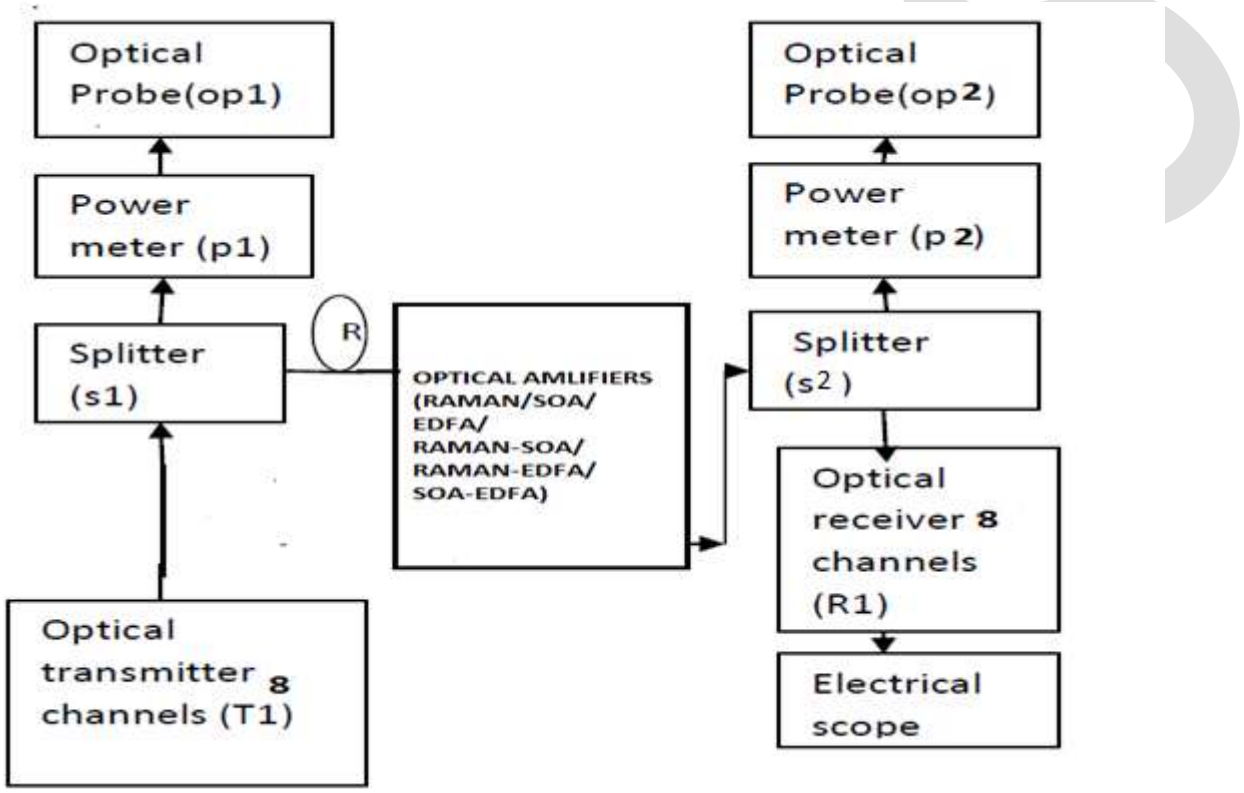

Fig. 1: Simulation Setup

RESULTS AND DICUSSION

WDM signal is transmitted at fixed attenuation and dispersion value of .2dB/km and 2 ps/nm/km respectively. Counter–propagating pump type is used for distributed Raman amplifier at operating temperature of 300 K with pump wavelength. EDFA is operates at wavelength range from 1250-1650 nm. EDFA having flat gain shape and fixed small signal gain of 25 dB. Various optical amplifiers has been compared for 8x10Gbps WDM system in term of received Q factor(dB), eye opening, eye closure(dB) and jitter(ns). In fig.2 variation in quality factor for different amplifier is 19.97 to 6.02(dB) for RAMAN, 15.24 to 6.02(dB) for EDFA, 14.73 to 6.02(dB) for SOA, 13.43 to 6.02(dB) for SOA-EDFA, 14.52 to 6.02(dB) for RAMAN-SOA, 19.92 to 6.02(dB) for RAMAN-EDFA. At 200km all amplifiers have almost same Q factor. The best Q factor is provided by RAMAN amplifier at 10 km of fiber length. At 100 km best Q factor is provided by RAMAN-EDFA.

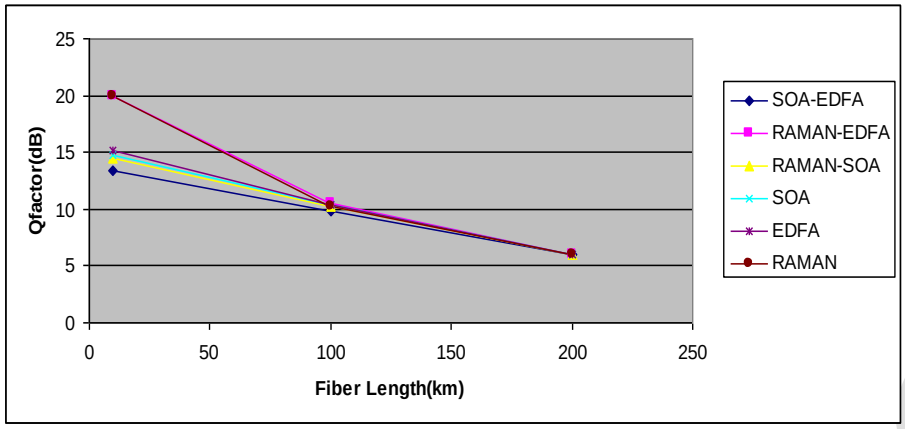

Fig 2: Q factor Vs fiber length

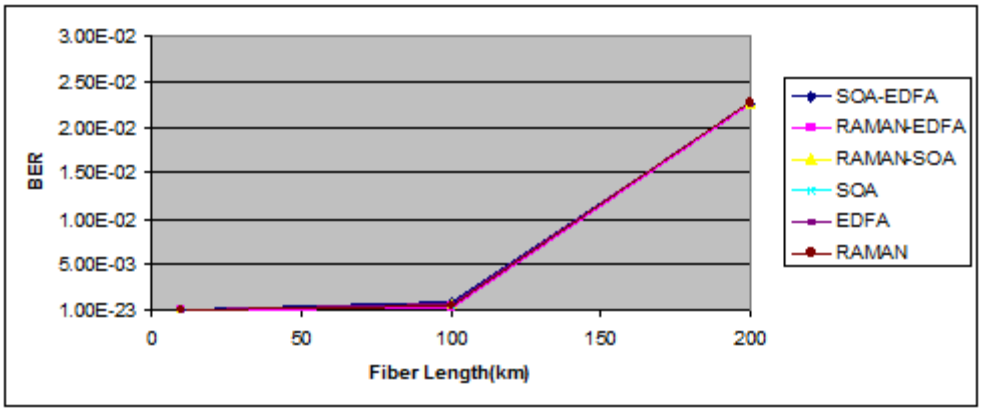

Fig 3: BER Vs fibre length

Figure 3 shows the graphical representation of BER Vs fiber length. Minimum BER is provided by RAMAN-EDFA so RAMAN-EDFA provide batter result. At 200km all the amplifiers have same BER i.e. .0227501 . SOA-EDFA provide highest BER as compare to all other amplifiers so it gives worst performance at all length.

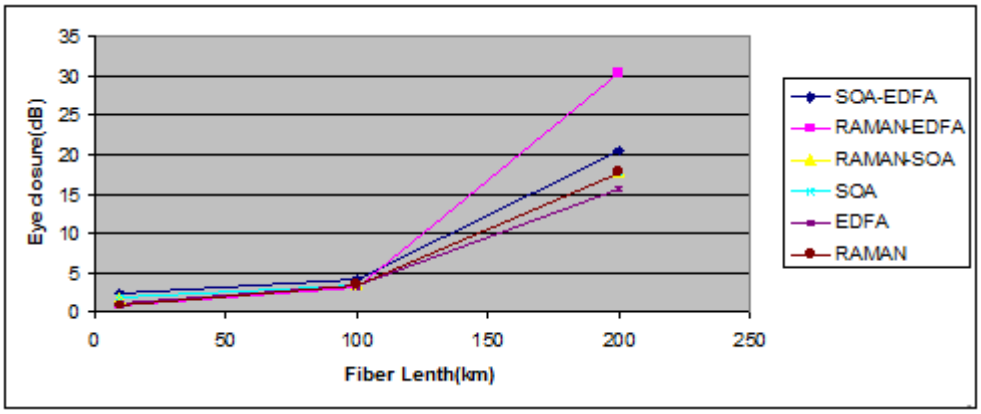

Fig 4: eye closure Vs fiber length.

The variation of eye closure in fig. 4 for various length of fiber is .84 to 17.77(dB) for RAMAN, .86 to 15.68 (dB) for EDFA, 1.75 to 17.73 (dB) for SOA, 1.81 to 17.74(dB) for RAMAN-SOA, .84 to 30.44(dB) for RAMAN-SOA, 2.31 to 20.47(dB) for SOA-EDFA. Eye closure increases with distance as shown in fig.4. Eye closure is maximum for RAMAN-EDFA and minimum for RAMAN-SOA.

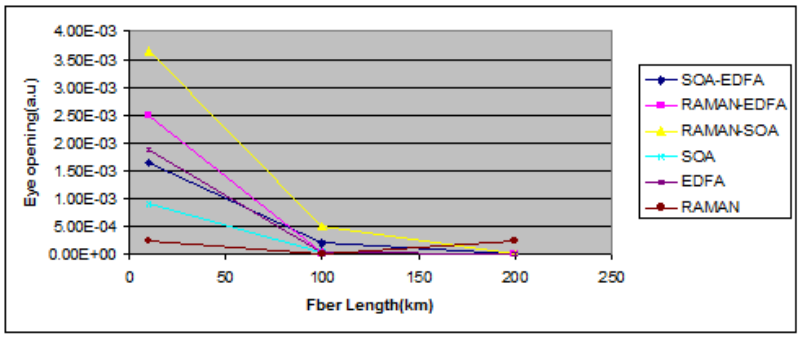

Fig 5: eye opening Vs fiber length

In figure 5. Eye opening vs. transmission distance is plotted. It is shown that eye opening decrease with distance. Larger eye opening means good quality of communication. Eye opening varies from 2.4 e-04 to 1.7e-009 for RAMAN, 1.88e-02 to 8.2e-009 for EDFA, 8.9 e-04 to 1.9e-008 for SOA, 3.6e-03 to 3.6e-007 for RAMAN-SOA, 2.5e-03 to 5.6e-010 for RAMAN-EDFA, 1.6e-03 to 1.00e-007 for SOA-EDFA. As shown in figure RAMAN-SOA provide highest eye opening as shown in figure 5 ,therefore it provide better result as compare to other amplifiers.

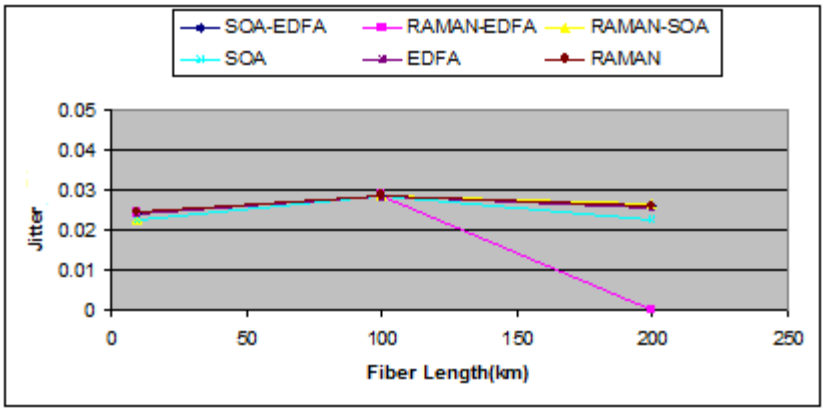

figure 6. Jitter vs. fiber length

In figure 6. Jitter vs. transmission distance is plotted. Jitter should be as small as possible. Lesser will be the jitter better will be the communication. Jitter is varies from .024 to .026 for RAMAN, .024 to .025 for EDFA, .0222 to .0227 for SOA, .0228 to .0227 for RAMAN-SOA, .024 to 5.6e-010 for RAMAN-SOA, .0237 to .0259 for SOA-EDFA. So as shown in graph value of jitter is minimum for RAMAN-EDFA . Therefore RAMAN-EDFA provide better performance as compare to other amplifiers in terms of jitter .

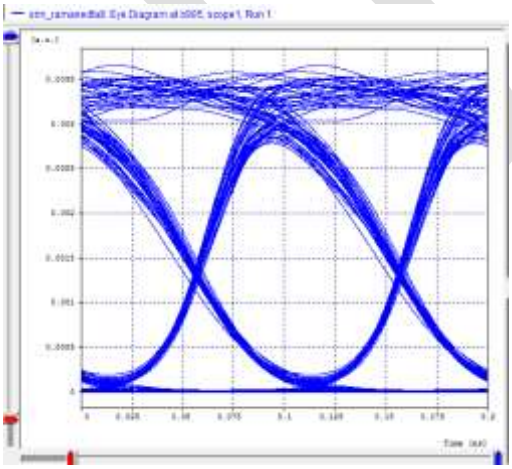

Fig 7: Eye diagram of RAMAN-EDFA at fiber length 10km.

CONCLUSION

We have designed and implemented hybrid optical amplifiers by using OptSim. We carried out simulation for different hybrid amplifier in the presence and absence of nonlinearities by varying the transmission distance and finding out most suitable among them. The performance of optical amplifiers was evaluated using the eye patterns, BER measurement, eye opening, eye closure ,jitter and Q factor. From this work it is concluded that RAMAN-EDFA gives best results than other amplifiers . RAMAN-EDFA gives highest Q factor 19.92(dB) ,smallest jitter (.0243) , minimum eye closure (.84694) but RAMAN-SOA provide largest eye opening (.00366) at 10 km.. From all these results we can say that RAMAN-EDFA provide best results among all these 6 amplifiers. So RAMAN-EDFA is promising alternative to RAMAN,EDFA,SOA,RAMAN-SOA and EDFA-SOA in optical fibre communication

REFERENCES:

[1] Govind P. Agarwal, "Fiber Optic Communication Systems", John Wiley &sons, Inc. Publication, 2003.
[2] M.N. Islam, Raman Amplifiers for Telecommunications. New York: Springer, 2004, pp. 331.
[3] Sunil Kumar Panjeta, Onkar ChanD, Danvir Mandal," Gain Optimization of EDF Optical Amplifier by Stages Enhancement and Variation in Input Pumping Power", International Journal of Scientific and Research Publications, Volume 2, Issue 11, November 2012 1 ISSN 2250-3153.
[4] Gyeong-ilKweon "Optical-Amplifier Noise- Figure Measurement by Q-Factor Analysis"Journal of the Korean Physical Society, Vol. 43, No. 5, pp. 714_721,November 2003.
[5] D.J.Digiovanni, D. P.Jablonowski, and M. F. Yan, " Advance in Fiber Design and Processing," Optical fiber Telecommunication, Vol. IIIA, edited by I.P. Kaminow and T. L. Koch, Academic Press,San Diego, Calif.,1997, pp. 63-91.
[6] S. Olonkins, V. Bobrovs, G. Ivanovs," Comparison of Semiconductor Optical Amplifier and Discrete Raman Amplifier Performance in DWDM Systems," Latvian Journal of Physics and Technical Sciences, ISSN 1392 – 1215 -2012. No. 7(123)
[7] Piyush Jain, Mr. Bipan Koushal, Shrija Jain," Performance Analysis of Different Hybrid Optical Amplifier Due to Varying Transmission Distance at 10 Gbps," International Journal of Emerging Technologies in Computational and Applied Sciences, 5(3), June-August 2013, pp. 246-250.
[8] Sameksha Bhaskar, M.L.Sharma, Ramandeep Kaur," Performance Comparison of Different Hybrid Amplifiers for Different numbers of channels," International Journal of Advanced Computer Science and Applications.
[9] Simranjit Singh, R.S. Kaler, "Hybrid optical amplifiers for 64 × 10 Gbps Dense Wavelength Division Multiplexed System"Optik Optics,vol.124 ,pp. 1311–1313, 2013
[10] Simranjit Singh, R.S. Kaler , "Performance Evaluation of 64 × 10 Gbps and 96 × 10 Gbps DWDM System with Hybrid Optical Amplifier for Different Modulation Formats"Optical optics,vol.123 ,pp. 2199–2203, 2012
[11] Simranjit Singh, R.S. Kaler,Amanpreet singh, "Performance evaluation of EDFA, RAMAN and SOA optical amplifier for WDM systems", Optik optics,vol.124 ,pp. 95-101, 2013
[12] Ramandeep Kaur, Rajneesh Randhawa, R.S. Kaler , "Performance Evaluation of Optical Amplifier for 16 × 10, 32 × 10 and 64 × 10 Gbps WDM system", Optik optics,vol.124 ,pp. 693-700, 20

International Journal of Engineering Research and General Science Volume 3, Issue 3, Part-2 , May-June, 2015
ISSN 2091-2730

Load Balancing in Cloud

Ms. Radha G. Dobale, Prof. R. P. Sonar
radha.dobale@gmail.com

Abstract- Proposed work states the load balancing concept in cloud. Instead of partitioning a file into a no. of chunks and balancing a load by migrating different chunks to different chunk servers, here a Load Balance Nearest Search Algorithm is presented to cope with the load imbalance problem. In this it migrates one user's one whole file into any one nearest node. Load is transferred from heavily loaded node to physically closed lightly loaded node. The proposed work strives to balance the loads of nodes and reduce the demanded movement cost with reduce spending on technology as much as possible.

Keywords- Load balancing, cloud, Load Balance Nearest Search Algorithm, chunks, threshold .

INTRODUCTION

Load balancing is essential for efficient operations in distributed environments. It means distributing the amount of work to do between different servers in order to get more work done in the same amount of time and serve clients faster [41].

The definition of cloud computing provided by National Institute of Standards and Technology (NIST) says that: "Cloud computing is a model for enabling convenient, on-demand network access to a shared pool of configurable computing resources (e.g., networks, servers, data storage, software applications and other computing services) that can be rapidly provisioned and released with minimal management effort or service provider interaction [42].
The main advantages of the cloud computing are the following:

- There is no need to download or install specific software
- The cost is low or even free, in some cases;
- If the client computer crashes, there is almost nothing lost because everything is stored into the cloud
- There is no need to update the local system when some new fix packs are released
- Cloud computing can be used on clients having minimal hardware requirements like mobile phones or PDAs;
- The problem of licensing different software packages is moved to the data center level
- No costs (or very small ones) for hardware upgrades;
- The users are not dependent by their personal computer because they can use any other device having an Internet connection and minimum software requirements.

LITERATURE REVIEW

Many algorithms have been proposed previously for load balancing. Some of those algorithms are as follows.

Paper [1] proposed load rebalancing for distributed file systems in clouds which is comparable with the existing centralized approach and considerably outperforms the prior distributed algorithm in terms of load imbalance factor, movement cost, and algorithmic overhead. A load rebalancing algorithm is used to reallocate file chunks such that the chunks can be distributed to the system as uniformly as possible while reducing the movement cost as much as possible. Here, the movement cost is defined as the number of chunks migrated to balance the loads of the chunk servers.

A proximity-aware load balancing scheme is discussed by using the concept of virtual servers. The goals of this scheme are not only to ensure fair load distribution over nodes proportional to their capacities, but also to minimize the load balancing cost by transferring loads between heavily loaded nodes and lightly loaded nodes in a proximity-aware fashion. This ensures a fair load distribution among nodes i.e. nodes carry loads proportional to their capacities [2].

In [3], a histogram manager maintains a histogram that reflects a global view of the distribution of the load in the system, and a load-balancing manager that redistributes the load whenever the node becomes overloaded or underloaded. Advantage of this paper is that it reduces the cost of constructing histogram, reduce the cost of maintaining histogram and reduce the cost of updating histogram.

Paper [4] mainly concerns with the load balancing of cloud datacenters to improve efficiency of the host machine and minimize number of active host machine to support green computing concept. Author introduces a threshold based Dynamic compares and balance algorithm (DCABA) for cloud server optimization. This paper has shown the applicability of load balancing and server consolidation techniques to obtain measurable improvements in server workload management and minimize the cost of cloud services.

In [5], load balancing of nodes in cloud using Ant Colony Optimization algorithm described the example of an ant that how ant care for every node they visit and record their data for future decision making. This efficiently distributes the load among the nodes such that the ants never encounter a dead end for movements to nodes for building an optimum solution set.

A Load Balancing Ant Colony Optimization algorithm in [6], found the optimal resource allocation for each task in the dynamic cloud system. LBACO algorithm is to balance the entire system load while trying to minimizing the make span of a given tasks set.

The analysis of three contemporary algorithms in [7] namely Round Robin, Equally Spread Current Execution Load (ESCE), Throttled Load Balancing in cloud analyst tool to resolve the issue of cloud load balancing as a preparation phase for new load balancing technique. This helps to enhance the overall cloud performance. This paper proposed a new VM load balancing algorithm: Weighted Signature based Load Balancing (WSLB) algorithm proposed to minimize the users response time.

A hybrid control strategy for load balancing in [8] presents the storage node cluster redistributes the load in its local range. On the other hand the system applies the overlapping structure to distribute the load to the global storage nodes by batch iteration approach. The local applies the centralized control strategy to quickly redistribute the load.

In [9], author proposes some common load-balancing tactics, which include: round-robin, weighted round-robin, least-connection, weighted least connection and shortest expected delay. Round-robin dispatches workloads to servers with an even occurrence. Resource-fit best dispatches a workload to the most resourceful server at a moment in the farm.

In [10], authors ensure that one chunk of a file and its two copies are stored in three different chunk servers at the same time. A load rebalancing algorithm not only achieves load balancing but also ensures the high reliability of the system.

The Central Load Balancer (CLB) in [11], is connected to all users and virtual machines present in cloud data center through Data center Controller. Load balancing helps to achieve a high user satisfaction and resource utilization ratio by ensuring an efficient and fair allocation of every computing resource, minimizing resource consumption, implementing fail-over, enabling scalability, avoiding bottlenecks and over-provisioning etc. The Central Load Balancer (CLB) manages load distribution among various virtual machines and assigns load corresponding to their priority and states. In this way this technique efficiently shares the load of user requests among various virtual machines.

In [12], authors proposed a comparative study between the three load balancing architectures in cloud computing: centralized, decentralized and hierarchical load balancers. Among the critical factor that affects the performance of a load balancer is its architecture which can be decentralized, centralized or hierarchical.

A novel decentralized load balancing architecture, called tldlb (two-level decentralized load balancer). Advantage of this is decentralized architecture for providing scalability and high availability capabilities to service more cloud users. This proposed a novel neural network-based load balancing algorithm, nn-dwrr, to distribute incoming requests to appropriate VMs [13].

In paper [14], The Benefits of Estimated Global Information in DHT Load Balancing reduces the network traffic induced by load balancing while achieving a better load balance than standard algorithms. Load balancing algorithms have two goals: (a) improving the load distribution fairness and (b) minimizing the data moved around for achieving the first goal. This shows the benefits of adding global estimates for both, active and passive load balancing algorithms.

The basic idea of hierarchical strategy in [15] is to divide processors into independent autonomous groups and to organize the groups in a hierarchy, thereby decentralizing the load balancing task. This deal with scalability challenges of load balancing at very large scale reduces the time and memory required for load balancing.

In [16], Cygnus has an ability to make load balancing decisions based on application defined load metrics, dynamically (re)configure load balancing strategies at run-time. Cygnus provides a framework for integrating strategies such as Round Robin, Random, Least Loaded, and Load Minimum to help increase overall system scalability.

In [17], authors focused on dynamical discrete-time load balancing in distributed systems in the presence of time delays with the double load-balancing strategy the overall completion time is further reduced in comparison to the single load balancing case. Load-transfer delays are negligible and the time required to implement the load balancing policy is also negligible so the best performance is obtained.

A new threshold load balancing method for workstations [18], decides a periodic time to perform load balancing. It performs load balancing with a long fixed period regardless of what the value of the average idle-time to avoid the load balancing overheads

In [19], parallel hybrid dataflow architecture is a scalable dynamic load balancing circuit for the proposed architecture and performance analysis. Here focus was on presenting the framework of the proposed HDCA system, the modeling, design, and performance of a “basic” and then “modular” (scalable) dynamic load balancing circuit for a HDCA type computer system.

Some of the algorithms about load balancing for distributed file system have been proposed previously. These are as follows.

Load rebalancing algorithm in [20], implemented so that central node should not overload. The implementation is done in Hadoop distributed file system. As apache Hadoop is used, security issues are arises. To solve security issues and to increase security, Kerberos authentication protocol is implemented to handle multiple nodes. As Hadoop’s use and demand grew in the network, handle big data security became critical, so that authentication mechanism Kerberos is used.

In [21], authors illustrate and define the load rebalancing problem in cloud DFSs. They advocate file systems in clouds shall incorporate decentralized load rebalancing algorithms to eliminate the performance bottleneck and the single point of failure.

In order to avoid the system burden caused by duplicate data in [22] proposes novel data center management architecture: Index Name Server (INS), which integrates deduplication and access point selection optimization techniques to enhance the performance of the cloud storage system. INS improves the efficiency of the cloud storage system. The proposed INS data center management mechanism omits the scanning procedure of traditional backup and decreases the backup cost and establish efficient backup of all schemes and methods.

In [23], it combined with greedy algorithm; the scheme provides a better load balancing algorithm for different load cases (CLB). CLB algorithm utilizes entropy and the scope of invalid cache invalid as the evaluation basis of load balancing effect. Authors proposed effect of load balancing and the scope of invalid cache. Cache-invalidation-scope model is established to improve the effect of load balancing.

In [24], authors proposed two novel brownout-aware load balancing algorithms. To test their practical applicability, they extended the popular lighted web server and load-balancer, thus obtaining a production-ready implementation. This paper presents a novel approach for improving resilience, the ability to hide failures, in cloud services using a combination of brownout and load-balancing algorithms.

A load balanced co-location algorithm in [25] is incorporated into CoHadoop++ which balance the load in cluster through optimal selection of data nodes based their load. CoHadoop++ ensures that the fault tolerance property of Hadoop is not compromised, when excluding nodes from the node selection policy.

In [26], a novel data partitioning and selective replication method utilizes the temporal information in prior workloads to predict future query patterns. This approach performs partitioning and replication simultaneously to reduce the number of servers processing queries while respecting load balancing and I/O load constraints under replication.

Policy-based security framework in [27] is highly evolving and dynamic for securely outsourcing enterprise data and computations. Instead of using several storage nodes or several computation nodes in the same CSP, multiple CSPs can be used for to increase reliability of the whole system.

Cost Minimization for Big Data Processing in Geo-Distributed Data Centers deals with big data processing in geo-distributed data centers jointly consider data placement, task assignment and data flow routing in a systematical way. This paper jointly studies the data placement, task assignment, data center resizing and routing to minimize the overall operational cost in large-scale geo-distributed data centers for big data applications [28].

As stated in [29], Chord maintains its routing information as nodes join and leave the system. Valuable for cooperative file sharing, time-shared available storage systems, and distributed indices for document and service discovery, and large-scale distributed computing platforms.

In [30], author proposed a new model for distributed load balancing allocation of virtual machine in cloud data center using the TOPSIS find the most suitable PM in the data center for the migrated VMs. Each node in the data center runs a module of the VM monitor which observes the local resource usages of the node.

In [31], authors discussed the future of content distribution among mobile devices forming mobile clouds. The future of mobile clouds is in novel in order to boost cooperation among users and connect people over the shared content.

In [32], with SDN, program the virtual switches at the physical servers so as to meet all those requirements, without demanding special hardware in the network. The abstraction of the SDN provides a logically centralized location where network configuration and control can be performed easily, while maintaining the scalability of the solution.

A framework for designing energy efficient cloud computing services over non-bypass IP/WDM core networks in [33] replicate content into multiple clouds based on content popularity yields 43% total saving in power consumption compared to power un-aware centralized content delivery.

In [34], author's asynchrony introduces security challenges which prevent information leakage not only through access patterns but also through timing of I/O events. Also proposes various practical optimizations which are key to achieving high performance and techniques for a data center to dynamically scale up a distributed ORAM.

PiCsMu in [35] aggregates multiple Cloud storage services, provides enhanced privacy and offers a distributed file sharing system. The work is to show the feasibility to store arbitrary data in different Cloud services for private use and/or for file sharing.

Software defined radio-based architecture that addresses problems and can be implemented on a cloud of general purpose computing platforms. Cloud-RAN can be implemented on general purpose processor and an off-the shelf software-defined radio front-end connected over commodity LAN network [36].

Objective of [37] is to maximize the system throughput, for which first proposes a novel admission cost model then devise efficient control algorithms and finally conduct experiments on proposed algorithms. It developed novel admission control algorithms through proposing novel admission cost model to model different resource consumptions.

The major purpose of [38] was to examine the cloud services pricing schemes and how they can improve previous pricing models by expanding the consumer set with time inconsistent behavior. A simple model of hyperbolic discounting function improved by including a more sophisticated form of hyperbolic discounting function where the model has impact of network externalities on consumers' utility function.

The Future of Cloud-Based Entertainment is about the future of cloud-based entertainment. Major portions of personal time and experience are being rendered, stored, or mediated in the cloud. Augmented reality can follow you on display surfaces throughout the home, such as walls, windows, mirrors, appliances, tablets, and tables [39].

Power Metering for Virtual Machine in Cloud Computing Challenges and Opportunities [40] makes a comprehensive investigation in issues regarding VM power metering, including server models, sampling, V=M power metering methods and the accuracy of the methods. Investigation regarding issues of VM power metering focused on estimating VM power at the software level, tools for information collection, modeling methods, and estimation.

PROBLEM FORMULATION

Analysis

In this stage an in-depth analysis is performed to obtain a detailed understanding of the business needs as defined in the business case and scope documents.

By analyzing previous algorithms where files and nodes can be created, deleted and appended. This results in load imbalance in distributed file system. To solve this issue I have developed logic on logical platform.

Problem Definition

The aim is to develop an approach for load balancing in cloud. A load balancing algorithm is proposed to cope with the load imbalance problem. Instead of partitioning a file into a no. of chunks and balancing a load by migrating different chunks to different chunk servers, the Load Balance Nearest Node Search Algorithm migrate one user's one whole file into any one nearest node. For this, the time complexity of manipulating of hash addresses to keep track of these file chunks are avoided. By doing this, it eliminates previous time consuming procedure.

Higher capacity nodes carry more loads. Load is transferred from heavily loaded node to physically closed lightly loaded node. This method balances the load when it reaches to threshold/control line only. Where it treats the overloaded portion above the threshold line and underloaded portion as below the load control line i.e. threshold line.

[Step 1- step 5: Load Balance Nearest Node Search Algorithm]

Step 1: For i=1 till i<=5 do i++
If nearest node's load is below the threshold line and Node remaining storage capacity >= User trying to upload file capacity
Then upload file. Go to step 11.

Step 2: For i=1 till i<=5 do i++
If nearest node remaining storage capacity >= User trying to upload file capacity
Then upload file. Go to step 11.

Step 3: X=Total no of nodes in cloud
For i=6 till i<=X do i++
If Empty nodes available and Node storage capacity >= User trying to upload file capacity
Then upload file. Go to step 11.

Step 4: For i=6 till i<=X do i++
If nearest node remaining storage capacity >= User trying to upload file capacity
Then upload file.

Step 5: Exit

RESULT

The proposed approach is working as an infrastructure-as-a-service in cloud experimental environment. It balances loads of nodes while uploading a file by redirecting requests of various users according to their current location to physically closed lightly loaded node by calculating shortest distance among all available nodes using Load Balance Nearest Node Search Algorithm which checks respective node's threshold by which propose system reduces the demanded movement cost. As user can access cloud service of file storage i.e. uploading a file and downloading a file from any location, system verify the steps of algorithm and store a file for valid user. If the same user accesses the storage-as-a-service from different location and or different cloud client then again it will check the steps of algorithm and according to current location his different files will distribute to different nodes. As per user request, the file get upload on shortest distance node by redirecting to respective node location.

If we host the servers at various locations then the same proposed approach will be applicable. The node path which differentiates between proposed approach and real time cloud. Here, as we are using a cloud environment logically, in logical environment, file get uploaded to respective node directory by directory path where in real time environment file will get redirected to actual server only by its IP address instead of directory path.

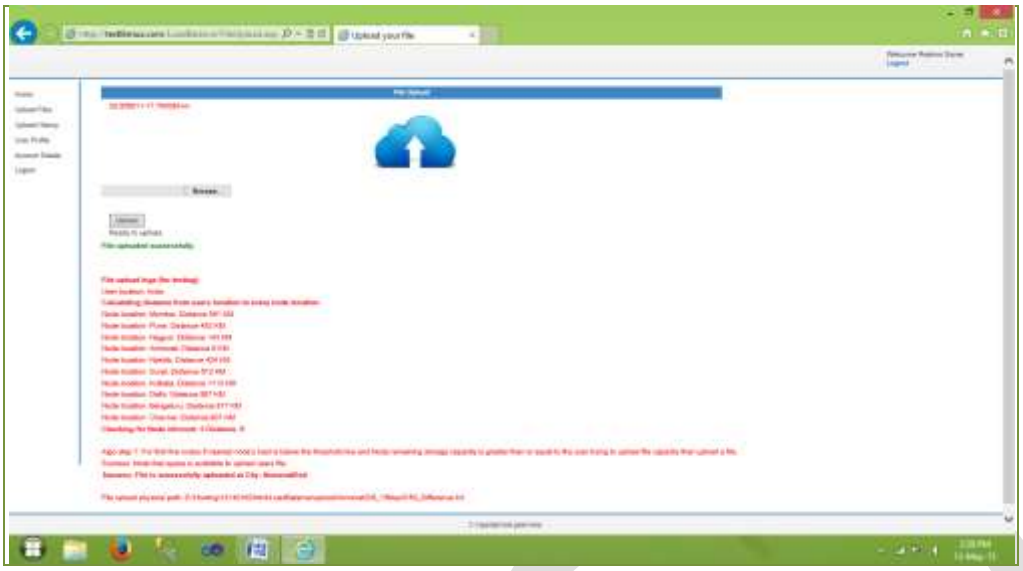

Screenshot 1: Upload a file from system1

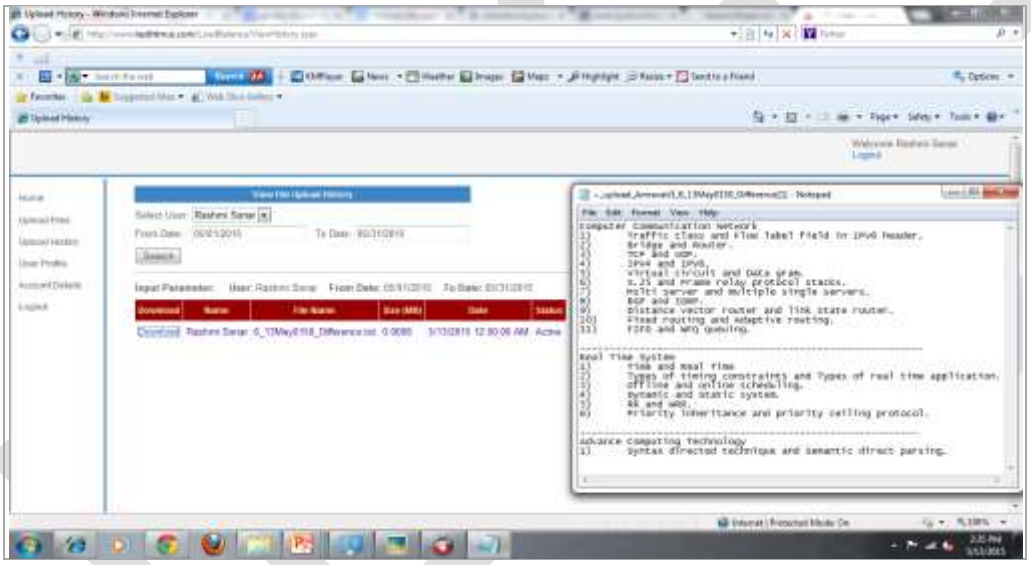

Screenshot 2: Download a file from system2

EXPERIMENTAL DISCUSSION & RESULT

For first five nodes if nearest node's load is below the threshold line and Node remaining storage capacity is greater than or equal to the user trying to upload file capacity then upload a file.

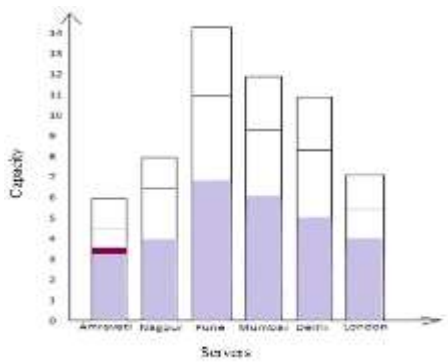

Fig 1: Load balanced when uploads a file below threshold

For first five nodes if nearest node remaining storage capacity greater than or equal to the user trying to upload file capacity then upload a file.

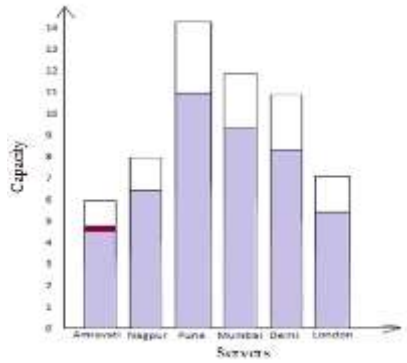

Fig 2: Load balanced when uploads a file above threshold

From all rest nodes if empty node available and node's storage capacity is greater than or equal to the user trying to upload file capacity then upload a file.

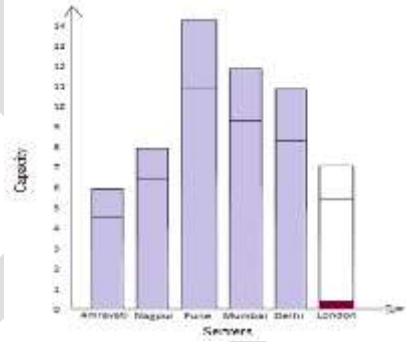

Fig 3: Load balanced on empty node

From all rest nodes if nearest node remaining storage capacity is greater than or equal to the user trying to upload file capacity then upload a file.

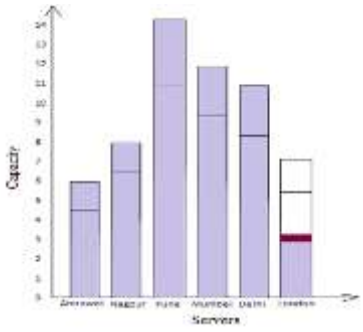

Fig 4: Load balanced on nearest node

Following table shows the difference between existing approach and proposed approach:

Sr. No.	Existing approach	Proposed approach
1.	Cloud partitions a file into a large no. of disjointed and fixed-sized pieces	Load Balance Nearest Node Search algorithm migrates one user's one whole file into any one nearest node.
2.	File chunks are not distributed as uniformly as possible among the nodes.	Removed the concept of file chunks.
3.	Manipulate hash addresses to keep track of file chunks	Time complexity of manipulating of hash addresses to keep track of file chunks are avoided
4.	Time consuming procedure.	Performance improved approach.
5.	Periodically checks for balancing a load.	Balances the load by comparing to threshold/control line only.

Table 1: Difference between existing approach and proposed approach

CONCLUSION

The proposed work strives to balance the loads of nodes by Load Balance Nearest Node Search algorithm which migrates one user file into any one nearest node. This is a performance improved approach which reduces the demanded movement cost as much as possible, maximized the throughput and minimized the response time. In experimental platform, we have implemented web based application where load is balanced for logical cloud.

FUTURE SCOPE

Energy efficiency has become one of the most active topics in large scale of data center or cloud computing environment today. In future work, we can create a group of the nodes which are underutilized by 25% and computing load in a single server which should be less than 75% or specified threshold control line for Green Computing.

REFERENCES:

[1] Hung-Chang Hsiao, Hsueh-Yi Chung, Haiying Shen, Yu-Chang Chao, "Load Rebalancing for Distributed File Systems in Clouds", Parallel and Distributed Systems, IEEE Transactions, June 2012, Volume:24 , Issue: 5, Pages:951-962.

[2] Yingw u Zhu and Yiming Hu, "Efficient, Proximity-Aware Load Balancing for DHT Based P2P Systems" Parallel and Distributed Systems, IEEE Transaction, Aril 2005, Volume:16, Issue:4, Pages: 349-361.

[3] Quang Hieu Vu, Member, IEEE, Beng Chin Ooi, Martin Rinard, and Kian-Lee Tan, "Histogram-Based Global Load Balancing in Structured Peer to Peer Systems", Knowledge and Data Engineering, IEEE Transaction,April 2009, Volume:21, Issue:4, Pages:595-608.

[4] Yatendra Sahu, Yatendra Sahu, Rajeev Kumar Gupta, "Cloud Server Optimization with Load Balancing and Green Computing Techniques Using Dynamic Compare and Balance Algorithm", Computational Intelligence and Communication Networks (CICN), 2013 5th International Conference, Sept 2013, Pages:527-531.

[5] Kumar Nishant, Pratik Sharma, Vishal Krishna, Chhavi Gupta and Kuwar Pratap Singh, Nitin and Ravi Rastogi, "Load Balancing of Nodes in Cloud Using Ant Colony Optimization", Computer Modelling and Simulation (UKSim), 2012 UKSim 14th International Conference, March 2012, Pages:3-8.

[6] Kun Li, Gaochao Xu, Guangyu Zhao, Yushuang Dong, Dan Wang, "Cloud Task scheduling based on Load Balancing Ant Colony Optimization", Chinagrid Conference (ChinaGrid), 2011 Sixth Annual, August 2011, Pages:3-9.

[7] Mr. M. Ajit, Ms. G. Vidya, "VM Level Load Balancing in Cloud Environment", Computing, Communications and Networking Technologies (ICCCNT),2013 Fourth International Conference, July 2013, Pages:1-5.

[8] Yilim Lu, Jian Zhang, Shaochun Wu and Shujuan Zhang,"A Hybrid Dynamic Load Balancing Approach for Cloud Storage", Industrial Control and Electronics Engineering (ICICEE), 2012 International Conference, August 2012, Pages:1332-1335.

[9] Rich Lee, Bingchiang Jeng, "Load-Balancing Tactics in Cloud", Cyber-Enabled Distributed Computing and Knowledge Discovery (CyberC), 2011 International Conference, Oct 2011, Pages:447-454 .

[10] Wenqiu Zeng, Ying Li, Jian Wu, Qingqing Zhong, Qi Zhang, " Load rebalancing in Large-Scale Distributed File System", Information Science and Engineering (ICISE), 2009 1st International Conference, Dec 2009, Pages:265-269.

[11] Gulshan Soni, Mala Kalra, "A Novel Approach for Load Balancing in Cloud Data Center", Advance Computing Conference (IACC), 2014 IEEE International, Feb 2014, Pages:807-812.

[12] Ektemal Al-Rayis, Heba Kurdi, "Performance Analysis of Load Balancing Architectures in Cloud Computing", Modelling Symposium (EMS), 2013 European, Nov 2013, Pages: 520-524.

[13] Chung-Cheng Li and Kuochen Wang, "An SLA aware load balancing scheme for cloud datacenters", Information Networking (ICOIN), 2014 International Conference, Feb 2014, Pages:58-63.

[14] Nico Kruber,Mikael H¨ogqvist,Zuse-Institut Berlin,Takustr. Thorsten Schutt, "The Benefits of Estimated Global Information in DHT Load Balancing", Cluster, Cloud and Grid Computing (CCGrid), 2011 11th IEEE/ACM International Symposium, May 2011, Pages:382-391 .

[15] Gengbin Zheng, Esteban Meneses, Abhinav Bhatel´e and Laxmikant V. Kale, "Hierarchical Load Balancing for Charm++ Applications on Large Supercomputers", Paralle processing workshops (ICPPW), 2010 39th International conference, Sept 2010, Pages: 436-444.

[16] Jaiganesh Balasubramanian, Douglas C. Schmidt, Lawrence Dowdy, and Ossama Othman, "Evaluating the Performance of Middleware Load Balancing Strategies", Enterprise Distributed Object Computing Conference, 2004. EDOC 2004. Proceedings Eighth IEEE International, Sept 2004, Pages:135-146.

[17] S. Dhakal, B. S. Paskaleva, M. M. Hayat, E. Schamiloglu, C. T. Abdallah , "Dynamical Discrete-Time Load Balancing in Distributed Systems in the presence of time delays", Decision and Control, 2003. Proceedings. 42nd IEEE Conference, Dec 2003, Volume:5, Pages:5128-5134.

[18] Hye-Seon Maeng, Hyoun-Su Lee, Tack-Don Han, Sung-Bong Yang, Shin-Dug Kim, "Dynamic Load Balancing of Iterative Data Parallel Problems on a workstation clustering", High Performance Computing on the Information Superhighway, 1997. HPC Asia '97, Aril 1997, Pages: 563 - 567.

[19] J. Robert Heath, Saivenkatesh Ramamoorthy, Charles E. Stroud and Andrew D. Hurt, "Modeling, Design, and Performance Analysis of a Parallel Hybrid DataCommand Driven Architecture System and Its Scalable Dynamic Load Balancing Circuit" Circuits and Systems II: Analog and Digital Signal Processing, IEEE Transactions,Jan 1997, Volume:44 , Issue: 1, Pages: 22-40.

[20] Ms. Vidya N. Chiwande, Prof. Animesh R. Tayal, "An Approach to Balance the Load with Security for Distributed File System in Cloud", Electronic Systems, Signal Processing and Computing Technologies (ICESC), 2014 International Conference, Jan 2014, Pages:267-270.

[21] Hsueh-Yi Chung, Che-Wei Chang,Hung-Chang Hsiao,Yu-Chang Chao, "The Load Rebalancing Problem in Distributed File systems", Cluster Computing (CLUSTER), 2012 IEEE International Conference, Sept 2012, Pages:117-125.

[22] Tin-Yu Wu, Wei-Tsong Lee, Yu-San Lin, Yih-Sin Lin, Hung- Lin Chan, Jhih-Siang Huang, "Dynamic Load Balancing Mechanism based on Cload Storage", Computing, Communications and Applications Conference, Jan 2012, Pages:102-106.

[23] Tao Wang, Xin Lv, Fang Yang, Wenhuan Zhou, Rongzhi Qi, HuaiZhi Su, "A load balancing scheme for distributed key-value caching system in cloud environment", Distributed Computing and Applications to Business, Engineering and Science (DCABES), 2014 13th International Symposium, Nov 2014, Pages:63-67.

[24] Cristian Klein, Alessandro Vittorio Papadopoulos, Manfred Dellkrantz, Jonas Durango, Martina Maggio, Karl-Erik Arzen, Francisco Hernandez-Rodriguez, Erik Elmroth, "Improving Cloud Service Resilience using Brownout-Aware Load-Balancing", Reliable Distributed Systems (SRDS), 2014 IEEE 33rd International Symposium, Oct 2014, Pages:31-40.

[25] Nishanth S, Radhikaa B, Ragavendar T J, Chitra Babu, and Prabavathy B, "CoHadoop++ A Load Balanced Data Colocation in Radoop Distributed File System", Advanced Computing (ICoAC), 2013 Fifth International Conference, Dec 2013, Pages: 100-105.

[26] Ata Turk, R. Oguz Selvitopi, Hakan Ferhatosmanoglu & Cevdet Aykanat, "Temporal Workload-Aware Replicated Partitioning for Social Networks", IEEE, Nov 2014, Vol: 26, Issue: 11, Pages: 2832-2845.

[27] Sourya Joyee De & Asim K. Pal, "A Policy-based Security Framework for Storage and Computation on Enterprise Data in the Cloud", IEEE, Jan 2014, Pages: 4986-4997.

[28] Lin Gu, Deze Zeng, Peng Li & Song Guo, "Cost Minimization for Big Data Processing in Geo-Distributed Data Centers", IEEE, Sept 2014, Pages: 314-323.

[29] Ion Stoica, Robert Morris, David Liben-Nowell, David R. Karger, M. Frans Kaashoek, Frank Dabek, and Hari Balakrishnan, "Chord A Scalable Peer to Peer Lookup Protocol For Internet Applications", Networking, IEEE/ACM Transaction, Feb 2003, Volume:11, Issue:1, Pages:17-30.

[30] Fei Ma, Feng Liu and Zhen Liu,"Distributed Load Balancing Allocation of Virtual Machine in Cloud Data Center", Software Engineering and Service Science (ICSESS), 2012 IEEE 3rd International Conference, June 2012, Pages: 20-23.

[31] Morten V. Pedersen and Frank H. P. Fitzek, "Mobile Clouds: The New Content Distribution Platform", IEEE, May 2012, Vol: 100, Pages: 1400-1403.

[32] Rogerio V. Nunes, Raphael L. Pontes & Dorgival Guedes, "Virtualized Network Isolation Using Software Defined Networks", IEEE, Oct 2013, Pages: 683-686.

[33] Ahmed Q. Lawey, Taisir E. H. El-Gorashi, and Jaafar M. H. Elmirghani, "Distributed Energy Efficient Clouds Over Core Networks", IEEE, April 2014, Vol: 32, Issue: 7, Pages: 1261-1281.

[34] Emil Stefanov and Elaine Shi, "ObliviStore: High Performance Oblivious Cloud Storage", IEEE, May 2013, Pages: 253-267.

[35] Guilherme Sperb Machado, Thomas Bocek, Michael Ammann, Burkhard Stiller, "A Cloud Storage Overlay to Aggregate Heterogeneous Cloud Services", IEEE, Oct 2013, Pages: 597-605.

[36] Yihenew Dagne Beyene, Riku Jantti & Kalle Ruttik," Cloud-RAN Architecture for Indoor DAS", IEEE, Sept 2014, Pages: 1205-1212.

[37] Qiufen Xiay, Weifa Liangy and Wenzheng Xuf, "Throughput Maximization for Online Request Admissions in Mobile Cloudlets", IEEE, Oct 2013, Pages: 589-596.

[38] Tayfun Keskin & Nazim Taskin, "A pricing model for cloud computing service", IEEE, Jan 2014, Pages: 699-707.

[39] Kilroy Hughes, "The Future of Cloud-Based Entertainment", IEEE, May 2012, Vol: 100, Pages: 1391-1394.

[40] Chonglin Gu, Hejiao Huang & Xiaohua Jia, "Power Metering for Virtual Machine in Cloud Computing_Challenges and Opportunities", IEEE, Sept 2014, Vol: 2, Pages: 1106-1116.

[41] http://en.wikipedia.org/wiki/Distributed_file_system_for_cloud

[42] http://www.nist.gov/itl/csd/cloud-102511.cfm

International Journal of Engineering Research and General Science Volume 3, Issue 3, Part-2 , May-June, 2015
ISSN 2091-2730

Automated Detection of Acute Lymphocytic Leukemia-A survey

Sulaja Sanal
Dept. of Computer Science & Engg.
Sree Buddha College of Engg. for Women.
Pathanamthitta, Kerala, INDIA
sulajasanal.07@gmail.com
+919400923731

Abstract— ALL is the most common type of leukemia in children. It is fatal if left untreated. The early detection of ALL is an important factor for the proper treatment. The manual checking of blood smear is time consuming and depends on the operator's ability. Hence automated techniques are introduced to enhance the performance. In this paper different automated method used for the detection of ALL is described.

Keywords— ALL, K means clustering, GVF snake, Otsu's thresholding, Zack algorithm, image preprocessing, CIELAB.

INTRODUCTION

Acute Lymphocytic Leukemia (ALL) is a cancer of the white blood cells. It is characterized by the overproduction and continuous multiplication of immature white blood cells in the bone marrow. It is also known as Acute Lymphoblastic Leukemia. ALL is a fast-growing cancer and it is fatal if left untreated, due to its rapid spread into the bloodstream and other vital organs [1]. But the diagnosis of this disease is very difficult because the symptoms are very similar to flu and other common diseases such as pain in joints and bones, tiredness, weakness etc. Blood test such as full blood count, and liver function test should do if the above mentioned symptoms are present. But this diagnosis only depends on the operator's skill. ALL is mostly seen in children.

The automatic detection of Acute Lymphocytic Leukemia from blood microscopic images generally avoids the problems of manual testing of blood smear and also increases the accuracy. It reduces the computational time and thus increases the efficiency. Automated Acute Lymphocytic Leukemia detection consists of the following steps:-

1. Image preprocessing
2. WBC identification
3. Nuclei extraction
4. Feature selection
5. Classification

The images that are produced by the digital microscope are normally in RGB color space. But these images are difficult to segment because of the change in quality due to the variation in illumination, camera settings etc. Hence the images are converted to CIE L*a*b color space images in [2].

The main advantages of this step are

- It reduces memory requirements.
- Increases the computational time.

Segmentation is used in image processing to extract the desired portion of the image for further processing. In this WBCs are extracted to check whether it is cancerous or not. For this, K-means clustering algorithm is used. It is the most popular unsupervised learning algorithm and was published in 1955. The selection of total number of clusters is an important step while using K-means clustering algorithm. In this 3 clusters are selected and that corresponds to nucleus, background and other blood cells such as erythrocytes and leukocyte's cytoplasm. But while using this algorithm, sometimes the edges of some nuclei were obtained instead of the whole nuclei. This problem can be avoided by using some morphological filtering methods such as

- Edge enhancement by Sobel operator.
- Canny edge detector to obtain continuous edge.
- Dilation to connect separated points of the membrane.
- Hole filling to fill the internal holes of the connected element having largest area.

The next step after getting the nuclei is feature extraction. Transforming the input data into a set of features is called feature extraction. Feature selection is an important step because it influences the performance of the classifier. In [2] four different types of features are used.

1. Texture features such as homogeneity, energy, contrast and correlation. Local Binary Pattern (LBP) is used for texture classification.
2. Color features such as mean, standard deviation and nucleus energy.
3. Shape features such as area, perimeter, compactness, major axis, minor axis, eccentricity, form factor, elongation and solidity.
4. Hausdroff dimension (HD) is an additional feature used in [2].

The main advantage of [2] is that the system is applied to complete blood smear images containing multiple nuclei. Many other systems process only sub images and it requires more computational time and memory. Two new features, such as cell energy and Hausdorff dimension (HD), have been used. The result is then compared with the results of the existing models.

In [3], the same procedure such as identification of WBC, extraction of nuclei from that, feature extraction and classification are done, but the methods for doing these steps are different from that used in [3]. The main difference is that, in [3] the leukocytes are separated as sub images from the whole image at first and then identifies the nucleus from the sub images and it classifies the presence of leukemia using neural network. In [3], there are five main modules.

1. Single cell selector module :- It enhances the image first and then identifies single cell
2. White cell identifier module :- It selects WBCs present in the image by separating them from other components
3. Lymphocyte identifier module :- It is used to recognize a lymphocyte with respect to other selected WBCs
4. Feature extraction module: - It takes the image coming from lymphocyte identifier module as input and produces a set of morphological indexes as output. It mainly consists of 3 steps.
    a. Lymphocyte membrane selection: - This can be achieved by using the techniques sobel enhancement, adaptive canny edge detection, structured image dilation, hole filling, structured image erosion.
    b. Nucleus and cytoplasm selection: - Otsu's method is the threshold used in this to segment the nucleus from the cytoplasm in the cell image.
    c. Feature extraction:- The feature set used in this are area, perimeter, Convex Area, Solidity, Major Axis Length, Orientation, Filled Area and Eccentricity
5. Classification module: - It processes the morphological indexes and will classify whether it is cancerous or not.

In [4] ALL-IDB is the image database used for getting the blood microscopic images for processing [5]. WBC identification in [4] consists of several phases.

1. Conversion from RGB to CMYK color model

    This conversion is made because leukocytes are more contrasted in Y component of CMYK color model, because the yellow color is present in all elements except leukocytes.

2. Histogram equalization or contrast stretching operations

    In order to make the segmentation easier, redistribution of image grey level is necessary. For that histogram equalization is used.

3. Segmentation by threshold using Zack algorithm

    Many threshold techniques are present. In this, threshold value based on triangle method or Zack algorithm is used.

4. Background removal operation.

    Background removal processes do not produce a clean result for the whole image. To clean up the image, area opening is used to delete all the objects with size smaller than the structuring element, which are circular in shape. Then the size is calculated based on the average size of the objects in the image.

5. Identification and separation of grouped leukocytes

This phase mainly consist of 2 steps.

a. Agglomerate identification through roundness analysis- Roundness is defined as the measure of circularity that avoids local irregularity. If roundness equals 1, then it is a circular object and less than 1 indicates deviation from circularity.

b. Watershed segmentation operation- It is used to separate adjacent leukocytes.

6. Image cleaning
   This method is used to remove all non-leukocytes and the leukocytes located on the edge of the image, which prevent errors in the later stages of the analysis process. Solidity is the feature used for image cleaning. It calculates the density of an object. If solidity value is 1, then it indicates a solid object, and if value less than 1, it indicates an object with irregular boundary.

7. Feature extraction
   The shape descriptors such as area, perimeter, major axis, minor axis and orientation are used as feature set in [4]. These are used to calculate elongation, rectangularity, compactness, convexity, roundness and the solidity.

The main disadvantage of shape feature is that they are more susceptible to errors in segmentation. For reducing these errors, shape descriptors are used together with regional descriptors.

1. Classification

For classification, SVM [6] is used. To evaluate the performance of SVM model the results is compared with k-Nearest Neighbor (k-NN) using the Euclidean distance measure with different values of k.

WBCs with giant nuclei are the main symptom of leukemia. But it is not sufficient to prove this disease and also other symptoms must be investigated. Another symptom of leukemia is the existence of nucleolus in nucleus. In [7] to diagnose this symptom and to discriminate between nucleoli and chromatins, curvelet transform [8] is used. It is a multi-resolution transform for detecting 2D singularities in images.

At first the image is separated into R G and B components. The median filter is then applied to R and G components. Then enhance the image using histogram equalization and Luv color transform. Then nuclei are extracted using K-means clustering algorithm. Then curvelet transform is applied on extracted nuclei and the coefficients are modified, and finally reconstruct a new image is used to extract the candidate locations of chromatins and nucleoli. For extracting the candidate zone of nucleolus feature based on the gradient of saturation channel is used. The method is applied on 100 microscopic images. The main advantage of [7] is that it also considers the nucleolus in addition to the nuclei for ALL detection.

Based on a new segmentation framework, WBCs are segmented into nucleus and cytoplasm in [9]. Twenty microscopic blood images were tested in this. At first the RGB images are converted to grey scale images. All further operations are performed in this grey scale image. Then nuclei of leukocytes are extracted by using Gradient Vector Flow (GVF) Snake model (active contours). Snakes are deformable curves that can move and change the shapes to deform to boundaries of objects in an image. Then nucleus is extracted and hole filling is done to enhance the image. In order to get the cytoplasm, the nucleus is subtracted from the grey scale image. But the image should not be clean. In order to enhance the image, Zack thresholding techniques are used. The nucleus segmentation part is based on morphological analysis, and the cytoplasm segmentation is based on pixel-intensity thresholding. The results show that the proposed method is able to yield 92% accuracy for nucleus segmentation and 78% for cytoplasm segmentation.

In [10], automated detection and sub classification of Acute Lymphocytic Leukemia using image processing and machine learning is used. In this, both supervised and unsupervised frameworks are used for segmentation of nucleus and cytoplasm. These methods are based on neural networks, feature space clustering and Markov random field modeling.

The morphological components of normal and malignant lymphocyte may differ. To automatically recognize ALL from blood samples, morphological, textual and color features are extracted from the segmented nucleus and cytoplasm.

In this, the sub classification of ALL is done based on French-American-British criteria. According to this, two methodologies based on morphology and phenotype is used. This includes segmentation, nucleus and cytoplasm extraction and classification. An improved scheme is also proposed to determine the origin of blast cells. Then an ensemble of decision tree is used to map the extracted features into either lymphoid or myeloid.

In [11], the ALL detection is performed based on fuzzy logic and neural network. 17 main features based on size, shape and color are extracted from the segmented nucleus and then these features are used for the distinction between normal and cancerous cell. The Multi-Layer Perceptron network trained by Scaled Conjugate Gradient (SCG) back propagation algorithm [12] and Fuzzy

network is used to classify the segmented regions into two classes either normal or abnormal. The result shows that the MLP network trained using SCG algorithm is able to achieve an acceptable classification performance compared to the Fuzzy network.

CONCLUSION

Automated detection of ALL minimizes the overhead of manual blood smear processing. The efficiency also increases by using the automated techniques. Many new techniques are introduced in this field for enhancement and among that image processing techniques are most popular nowadays. Some of the image processing techniques for the automated detection of ALL are studied in this paper.

REFERENCES:

[1] K. Breden, T. Schorr, J B Schorr, "Blood", Colliers Encyclopaedia, Vol. 4, 1978.
[2] Sos Agaian, Senior Member, IEEE, Monica Madhukar, and Anthony T. Chronopoulos, Senior Member, IEEE, "Automated Screening System for Acute Myelogenous Leukemia Detection in Blood Microscopic Images"IEEE SYSTEMS JOURNAL, 2014.
[3] F. Scotti, "Automatic morphological analysis for acute leukemia identification in peripheral blood microscope images," in Proc. CIMSA, 2005,pp.96–101.
[4] Lorenzo Putzu, Giovanni Caocci, Cecilia Di Ruberto "Leukocyte classification for leukemia detection using imageprocessing techniques",Artificial Intelligence in Medicine.2014.
[5] Donida Labati R, Piuri V, Scotti F.,"ALL-IDB: the acute lymphoblastic leukemia image Database for image processing in: Macq Benot, Schelkens Peter, editors".Proceedings of the 18th IEEE ICIP international conference on image processing,September 11–14. Brussels, Belgium: IEEE Publisher; 2011. p. 2045–8.
[6] Hsu, C-W, Chang C-C, Lin C-J, "A practical guide to support vector classification. Available from: http://www.csie.ntu.edu.tw/cjlin/papers/guide/guide.pdf".
[7] Ramin Soltanzadeh, Hossein Rabbani, and Ardeshir Talebi ″ Extraction of Nucleolus Candidate Zone in White Blood Cells of Peripheral Blood Smear Images Using Curvelet Transform,″ Hindawi Publishing Corporation Computational and Mathematical Methods in Medicine, 2012.
[8] O. Tuzel, L. Yang, P. Meer, and D. J. Foran, "Classificationof hematologic malignancies using texton signatures," PatternAnalysis and Applications, vol. 10, no. 4, pp. 277–290, 2007.
[9] Farnoosh Sadeghian, Zainina Seman, Abdul Rahman Ramli, Badrul Hisham Abdul Kahar, and M-Iqbal Saripan, "A Framework for White Blood Cell Segmentation in Microscopic Blood Images Using Digital Image Processing", Biological Procedures Online, Volume 11, Number 1, 2009.
[10] Subrajeet Mohapatra,"Hematological Image Analysis for Acute Lymphoblastic Leukemia Detection and Classification", Department of Electrical Engineering, National Institute of Technology Rourkela.
[11] Nurul Hazwani Abd Halim1, Mohd Yusoff Mashor, Aimi Salihah Abdul Nasir and Rosline Hassan," Performance Comparison between Multilayer Perceptron and Fuzzy ARTMAP Networks for Acute Leukemia Detection", International Journal of Research and Reviews in Computer Science (IJRRCS) Vol. 2, No. 5, October 2011, ISSN: 2079-2557.
[12] M. F. Moller, ―A Scaled Conjugate Gradient Algorithm for Fast Supervised Learning," Neural Networks, vol. 6(4), pp. 525–533, 1993

International Journal of Engineering Research and General Science Volume 3, Issue 3, Part-2 , May-June, 2015
ISSN 2091-2730

Continuous Water Quality Monitoring System for Water Resources at Remote Places

M N Barabde, S R Danve

MITCOE,Pune; mithilabarabde@gmail.com; 7709443655

Abstract—The current water quality monitoring system is a manual system with tedious process and is very time consuming. Thus to overcome the problems caused by the manual monitoring, a real time water quality monitoring system for water resources at remote places is proposed. The system architecture consists of data monitoring nodes, a base station and a remote station. All these stations are connected using wireless communication link. The data from nodes is send to the base station consisting of ARM controller designed for special compact space application. Data collected by the base station such as pH, turbidity, conductivity, etc is sent to the remote monitoring station. Data collected at the remote site can be displayed in visual format on a server PC with the help of MATLAB. This approach brings several advantages over current monitoring systems in terms of cost, portability, and applicability.

Keywords— Continuous monitoring, real time, wireless sensor network, pH sensor, turbidity sensor, conductivity sensor, zigbee technology.

INTRODUCTION

Water quality monitoring is an essential question in the whole world today. At present, for remote checking, satellite is generally used to screen the water quality for waterways, lakes, oceans and seas. In any case, satellites just offer a full scale perspective of the water quality. When it comes to a specific locale of interest, the precision of the satellite surveillance may not meet our prerequisites. With the advancement of correspondence innovation and sensor innovation [1][2], particularly the idea of remote sensor system and Cyber-Physical System (CPS), numerous endeavors have been made toward building new water quality observation advancements taking into account remote sensors conveyed submerged. Sensors have been produced for submerged environment that have the capacity to gather precisely a few water quality parameters, for example, temperature, chemical substances, pH, turbidity and so forth. These sensors can be outfitted with enhanced correspondence capacity, for occasion, transmitting information. Utilizing remote correspondence system, it is presently possible to arrange sensors as an independent sensor organize that gives ceaseless, exact water quality measures in moderately huge water body, for example, lakes. Submerged sensors system can serve as a promising and a reciprocal methodology with satellite surveillance for an exact remote detecting of water quality.

In this paper we describe the design of Wireless Sensor Network (WSN) that helps to monitor the quality of water with the help of information sensed by the sensors immersed in water, so as to keep the water resource within a standard described for domestic usage and to be able to take necessary actions to restore the health of the degraded water body. Using different sensors, this system can collect various parameters from water, such as temperature, pH, oxygen density, turbidity and so on. The rapid development of wireless sensor network (WSN) technology provides a novel approach to real-time data acquisition, transmission and processing. The clients can get ongoing water quality information from faraway. In a system of this kind, there are several nodes, a base station and a remote monitoring station. Each node contains a group of sensors and the nodes are circulated in distinctive water bodies. Data collected by sensor nodes is sent to the base station via WSN channel then to the remote monitoring station. The remote monitoring station is usually a PC with Graphic User Interface (GUI) for users to evaluate water quality data. The recorded data can be evaluated using various simulation tools for future correspondence and actions.

LITERATURE SURVEY

Central Water Commission (CWC) monitors water quality [3][4], by collecting samples from representative locations within the processing & distribution system. These samples are analyzed at the well equipped laboratories. At these laboratories samples from raw water, filter water and treated water are taken for analysis. The estimation of water parameters like turbidity, pH, dissolved oxygen, etc is done with the help of meters. So the disadvantages [5] of this existing system are that; there is no continuous and remote monitoring, human resource is required, less reliable, no monitoring at the source of waters i.e. no on field monitoring and the frequency of testing is very low. Due to these disadvantages of the existing system it is required to develop a system that will allow real time and continuous monitoring of water quality [7].

Thus various advanced technologies for monitoring water quality have been proposed in the recent years. In [8] the structure of the wireless sensor networking in which a number of sensor nodes are located in a lake is proposed. A much smaller number of UAVs also

watch the lake and they are controlled by the central monitoring station (CMS). The sensor nodes and UAVs are both movable whereas the CMS is fixed. The CMS collects the information from the sensors and process them. In [9] a framework for monitoring water quality by incorporating bacterial contamination of water for open water bodies using WSN (consisting of sensors for sensing parameters of interest), UV Light to probe the contamination of water and Fluorescence as a monitoring tool is proposed. [10] presents a web based wireless sensor network [1], [2] for monitoring water pollution by means of Zigbee and WiMax technologies. This system would have a local Zigbee network that will be capable of measuring various water quality parameters, a WiMax network and web based monitoring with the help of a controlling computer. The system is intended to collect and process information, thus making decisions in real time via a remote web server. The data is directed through the Zigbee gateway from sensor nodes to the web server by means of a WiMax network, thus permitting users to distantly monitor the water quality from their place instead of gathering data from the scene. Experimental results revels that the system is capable of monitoring water pollution in real time [12].

PROPOSED SYSTEM

The main aim here is to develop a system for continuous monitoring of water quality at remote places using wireless sensor networks with low power consumption, low cost and high detection accuracy. pH, conductivity, turbidity level, etc are the parameters that are analyzed to improve the water quality. Following are the objectives of idea implementation [11]:

- To measure water parameters such as pH, dissolved oxygen, turbidity, conductivity, etc using available sensors at remote place.
- To collect data from various sensor nodes and send it to base station by wireless channel.
- To simulate and analyze quality parameters for quality control. (Graphical and numerical record using MATLAB)
- To send SMS to an authorized person automatically when water quality detected does not match the preset standards, so that, necessary actions can be taken.

(A) HARDWARE DESIGN

The proposed water quality monitoring system based on WSN can be divided into three parts:

- Data monitoring nodes
- Data base station
- Remote monitoring center

(a) Data Monitoring Nodes

Figure 1 illustrates the data monitoring nodes which consist of a number of sensors (pH, turbidity, dissolved oxygen, conductivity, etc), signal conditioning circuit, a controller and RF module. The data sensed by the sensor will be passed through a signal conditioning circuit in order to manipulate the analog signal in such a way that it meets the requirements of the next stage for further processing. Then the manipulated data will be given to the controller. The inbuilt ADC will convert the analog signal to digital signal for further processing. With the help of the RF module the manipulated sensed data will be sending to the data base station as shown in figure 1.

(b) Data Base Station

The data from all the nodes is collected at the data base station as shown in figure 2. The data from each node is collected one after another i.e. using time multiplexing. This obtained data is displayed on a LCD display. Also, this data is forwarded to the remote monitoring station via zigbee module.

(c) Remote Monitoring Center

The remote monitoring station consists of a zigbee module which will receive the data sent by the data base station. This data will be fed to a server PC consisting of Graphic User Interface (GUI) via serial communication as shown in figure 3. The obtained data will be represented graphically with the help of MATLAB and will be saved for further reference. Also the obtained data is compared with the standard values of the water parameters. If the obtained water parameters do not match the preset values then SMS will be sending to an authorized person in order to take preventive measures.

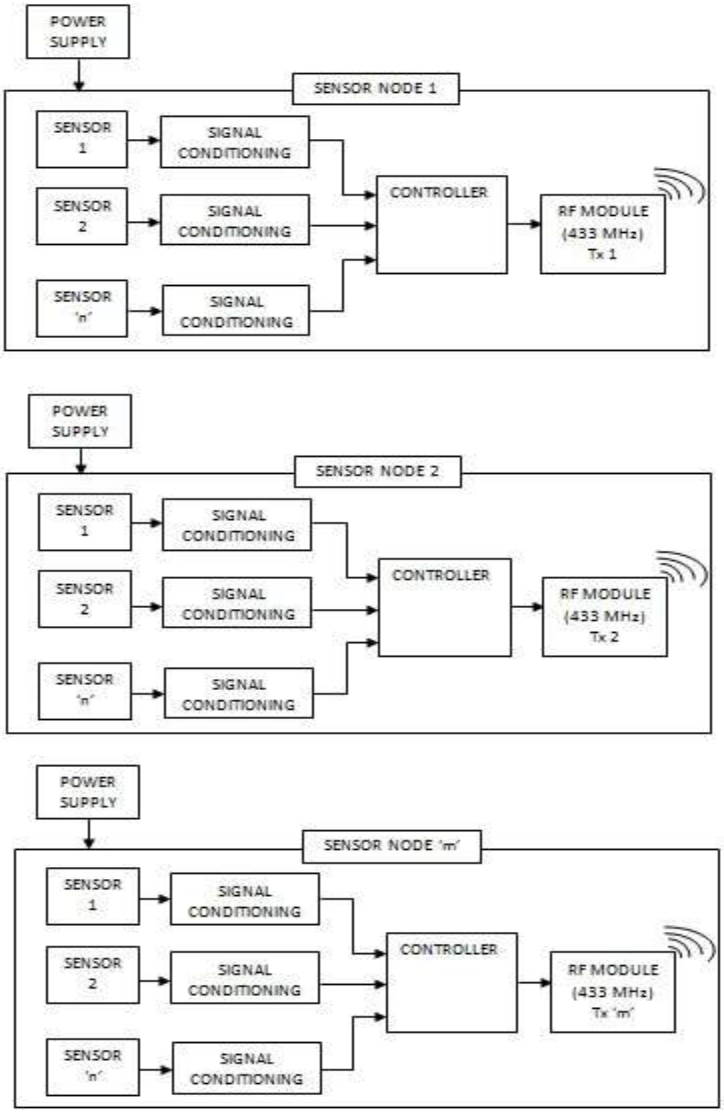

Figure 1: Data Monitoring Nodes

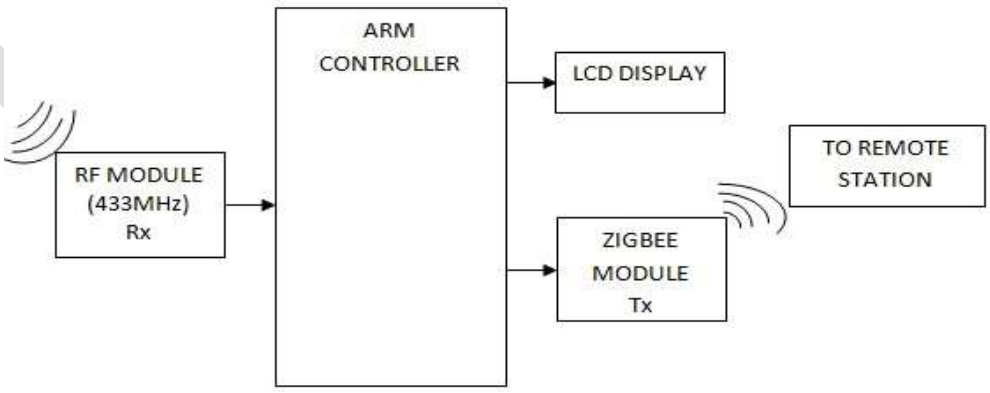

Figure 2: Data Base Station

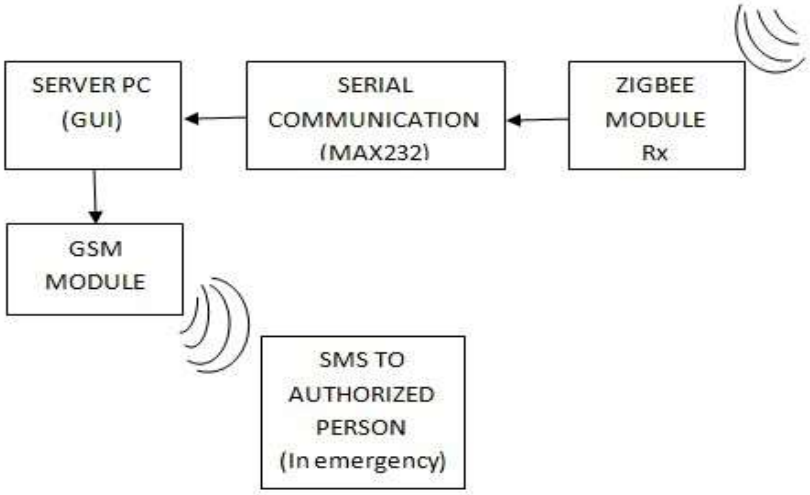

Figure 3: Remote Monitoring Station

(A) SOFTWARE DESIGN

Software design approach for water quality monitoring system is based on three parts, first is PIC programming, ARM programming and GUI design in MATLAB.

PIC programming is done in MPLAB IDE version 8.92 and ARM programming is done in Keil uVision4 IDE software. Embedded C is used as the programming language.

The GUI platform is successfully developed using the MATLAB software which is able to interact with the hardware at the remote monitoring station. The layout design of the front end of the GUI is shown in figure 4.

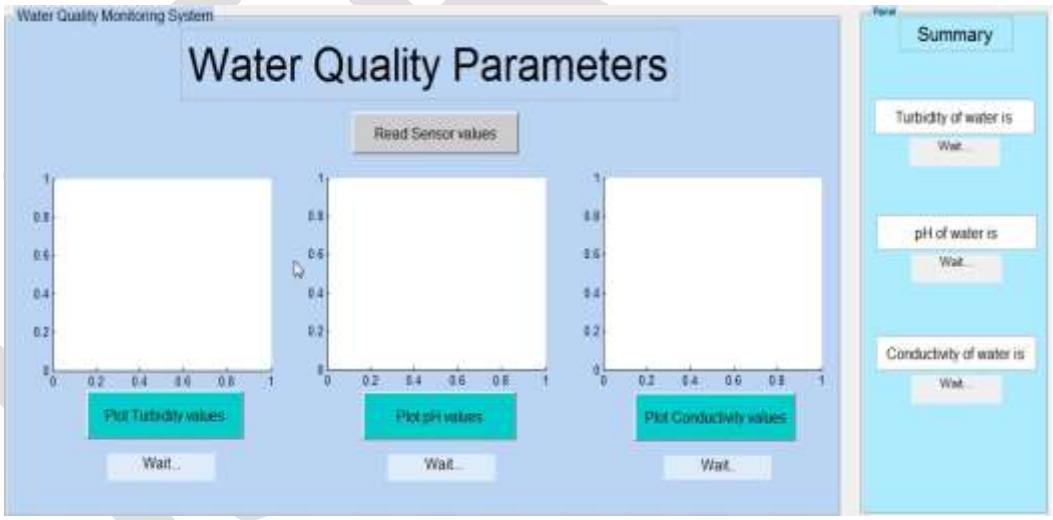

Figure 4: Layout design of the front end of the GUI

Once the sensor node is turned on, the conductivity, pH and turbidity sensors immersed in water start sensing the respective data. A push button named “Read sensor values” is provided for reading the conductivity, pH and turbidity values. Once the user clicks on this push button of the panel the zigbee transceiver on the receiver side sends a signal to the zigbee transmitter on the transmitter side demanding the corresponding data values to be sent. The push buttons named “Plot turbidity values”, “Plot pH values” and “Plot conductivity values” plots the different values that are obtained at the receiver side. Once the values are plotted, it is inherently saved and stored in MS Excel Database. These values are also displayed in the textbox continuously, shown in Fig.4.

RESULTS

The graphical user interface using MATLAB, displaying results is shown in figure 5.

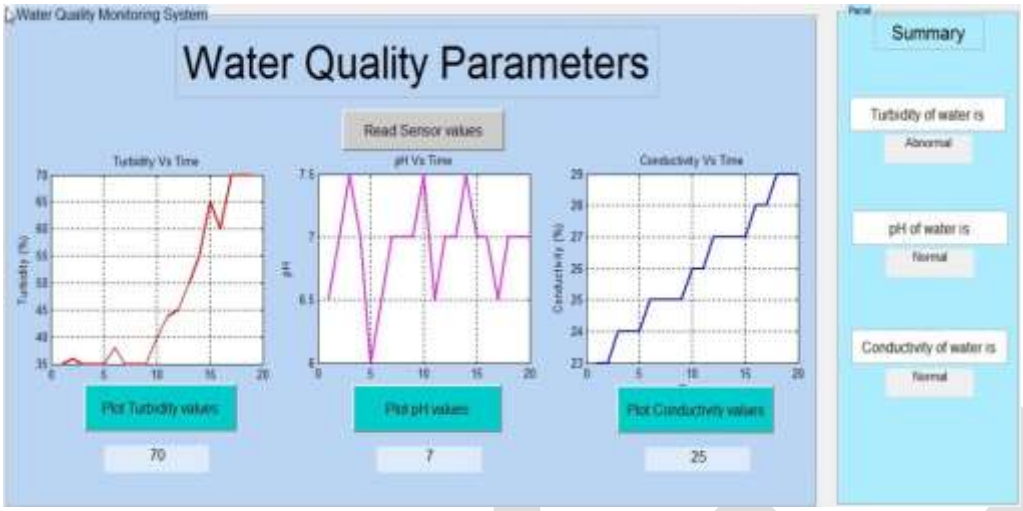

Figure 5: Snapshot of GUI of results displayed on PC.

From prior testing, a threshold value (range of values) is defined for the monitoring of pH, turbidity and conductivity of water. Depending on whether the average of the values obtained is less than or greater than the defined threshold, we get to know whether the water is acidic or basic, conductivity is high or low, is the water pure or impure and hence if it is suitable or not for the specific purpose.

CONCLUSION

The project addresses about developing an efficient wireless sensor network (WSN) based water quality monitoring system, which examines "water quality", an important factor as far as, irrigation, domestic purposes, industries, etc are concerned. Overall the proposed implementation of high power Zigbee based WSN for water quality monitoring system offering low power consumption and low cost is presented. Another important fact of this system is the easy installation of the system where the base station can be placed at the local residence close to the target area and the monitoring task can be done by any person with minimal training at the beginning of the system installation.

REFERENCES

[1] Ian F. Akyildiz, Weilian Su, Yogesh Sankarasubramaniam, and Erdal Cayirci Georgia Institute of Technology, "A Survey on Sensor Networks", *IEEE Communications Magazine*, August 2002

[2] Daniele Puccinelli and Martin Haenggi, "Wireless Sensor Networks: Applications and Challenges of Ubiquitous Sensing", *IEEE circuits and systems magazine*, IEEE 2005.

[3] Report on Water Quality Monitoring "Hot Spots" in Rivers of India (Central Water Commission, New Delhi), *Aug, 2011*

[4] "Guidelines for Water Quality Monitoring Central", Central Pollution Control Board, 2007-2008

[5] "Water Quality and field test kits essential knowledge and guidelines", National Council for Science and Technology Communication, 2013.

[6] "Planning of water-quality Monitoring systems", Technical Report Series No. 3
[Online] Available:
www.wmo.int/pages/hwrp/publications/Technical_report_series/TRNo3water_quality_monitoring_systems.pdf

[7] Uniform Drinking Water Quality Monitoring Protocol. [Online] Available: www.mdws.gov.in

[8] Li Zhenan, Wang Kai, Liu Bo, "Sensor-Network based Intelligent Water Quality Monitoring and Control", *International Journal of Advanced Research in Computer Engineering Technology,* Volume 2, Issue 4, April 2013.

[9] Julius Okache, Barry Haggett and Tahmina Ajmal, "Wireless Sensor Networks For Water Monitoring", *International Journal of Digital Information and Wireless Communications (IJDIWC),* vol. 4315, pp. 349360, November 2012.

[10] Steven Silva, Hoang N ghia Nguyen, Valentina Tiporlini and Kamal Alameh, "Web Based Water Quality Monitoring with Sensor Network: Employing ZigBee and WiMax Technologies", *IEEE Conference on Local Computer Networks,* IEEE 2011.

[11] Turkane Satish, Kulkarni Amruta, "Solar Powered Water Quality Monitoring system using wireless Sensor Network", *IEEE Conference on Automation, Computing, Communication, Control and Compressed sensing,* IEEE, 2013, pp. 281-285.

[12] M N Barabde, S R Danve, "A Review on Water Quality Monitoring System", *International Journal of VLSI and Embedded Systems-IJVES,* Vol 06, Article 03543; March 2015, pp. 1475-1479

International Journal of Engineering Research and General Science Volume 3, Issue 3, Part-2 , May-June, 2015
ISSN 2091-2730

Performance Evaluation of TCP Reno, SACK And FACK Over WIMAX

Kirti Sapra

Kurukshetra University(AICTE), kirtisapra91@yahoo.com, 8427825059

Abstract— This thesis mainly aims in the improvement of the congestion control mechanism over mobile WIMAX. Here, TCP sender side mechanisms are used to handle higher load, random packet loss and re transmission timeouts in high delay networks such a way as to keep the maximum size of congestion window, while keeping the control over congestion and re transmission at a minimal level. The TCP mechanisms are used against TCP Reno, TCP SACK and TCP FACK to see how they fair against congestion and higher offered load. Four network parameters are used to find out the best protocol for congestion control: throughput, average end to end delay, PDR & routing Load.

The base station node has been overloaded with 30 mobile nodes which will be sending their data at the same time. This will cause congestion at the network and above four parameters will be measured by using TCP congestion control mechanisms. NS2 simulator has been used as the simulation tool because of the ease of use of the graphical interface provided. The simulated graphs have been used to compare the performance of three TCP protocols used for simulation against four network parameters.

Keywords— TCP, Reno, SACK, FACK, NAM, NS2, Throughput, Average End To End Delay, Packet Delivery ratio

INTRODUCTION

Broadband wireless access (BWA) is a candidate for the next-generation wireless communication technology. Universal Interoperability for Microwave Access (WiMAX) is the organization behind interoperability and testing for the IEEE 802.16 spec[1]. Standard TCP congestion control mechanism is based on the reduction of its congestion window after a packet loss [2]. Even though such behavior works fairly well in the wired networks, where packets losses are mostly always caused by link congestion, it comes out rather ineffective when used for data transport in WiMAX networks. In the wireless environment the viable reasons of packet loss include fading, temporary detachments, and handovers. Even when some losses are recompensed in Data Link Layer, a part of them appears in Transport Layer for high Bit Error Rates. TCP New Reno improperly translates the causes of packet loss as congestion and consequently reduces its congestion window, thus exhibiting significant throughput degradation in these conditions. Another phenomenon which extremely affects performance of TCP is the network dissymmetry.

A network is assumed to be asymmetric when its characteristics in one direction greatly affect its performance in the other [3]. Asymmetry interrupts the smooth flow of ACKs in the reverse direction of traffic and subsequently the TCP ACK clocking mechanism of the TCP sender, causing expiration of timer , and continuous retransmissions, although, the packets may have correctly reached the receiver. In addition, frequent ACK delays result in timeout augments, hence, causing less protocol response to packet losses. There are several forms of dissymmetry, e.g. bandwidth , access , delay and packet loss. All packets are ingrained in WiMAX networks, especially in best-effort class of service, where TCP typically operates, due to difference of traffic among Subscriber Stations (SSs) and because the SS needs to receive a grant by the Base Station (BS) before sending any data [4].

Bandwidth dissymmetry is also very often in WiMAX networks when TDD is used. In TDD, the ratio of transmission b/w downlink and uplink direction can be adaptive & may cause starvation of bandwidth in the uplink, which in turn affect the regular flow of ACKs. A lot of research has been made to aim at suggesting different ways to improve the efficiency of TCP in wireless networks. Although, there are not pervasive comparative studies of TCP performance in WiMAX networks. In this work, we evaluate some representative TCP congestion control schemes under various traffic scenarios, which include single and multiple TCP flows through WiMAX networks in the presence of wireless channel errors, network asymmetries and various level of link congestion. The target is to find out the best performing TCP schemes and to suggest ways for further improvements.

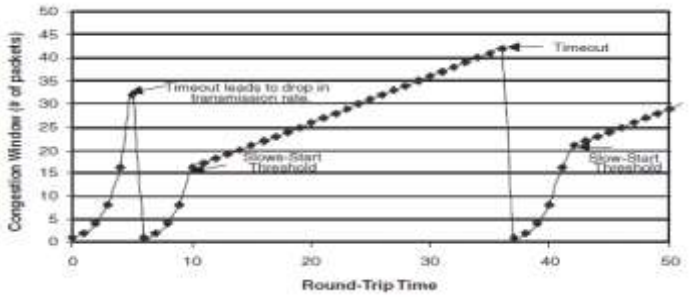

Figure 1 TCP congestion control

LITERATURE REVIEW

TCP Reno

It retains the basic principle of Tahoe, but uses the logic of duplicate acknowledgements (dupacks) to trigger Fast Retransmit. After 3 dupacks, TCP Reno takes it as a sign of segment lost and retransmit the packet immediately and enter Fast Recovery. In Fast Recovery, ssthresh and cwnd is set to half the value of current cwnd. For each subsequent dupack, increase cwnd by one and transmit a new segment if the new value permits it. TCP Reno cannot detect multiple packet loss within the same window [7].

TCP Sack

It is an extension of TCP RENO and it works around the problems face by TCP RENO, mainly detection of multiple lost packets, and re-transmission of more than one packet lost per RTT. SACK maintains the slow-start and fast retransmission of parts of RENO. It also has the crude grained timeout of Tahoe to fall back on, in case a packet loss does not get detected by the modified algorithm. SACK algorithm allows a TCP receiver to acknowledge out-of-order segments selectively rather than cumulatively by acknowledging the last correctly in order received segment [5]. If there are no such segments outstanding then it sends a new packet. Thus more than one segment lost can be sent in one RTT.

TCP Fack

It is a special algorithm that works on top of the SACK options, and is adapted at congestion controlling. FACK algorithm uses provided information from SACK to add more precise control to the injection of data into the network during recovery – this is achieved by explicitly measuring the total number of bytes of data outstanding in the network [6]. FACK decouples congestion control from data recovery thereby attaining more precise control over the data flow in the network. The main idea of FACK algorithm is to acknowledge the most forward selective acknowledgment sequence number as a sign that all the previous acknowledged segments were lost. This observation allows improving resumption of losses significantly.

SIMULATION ENVIRONMENT

In this section we will present the test setup used for comparing the above TCP mechanisms. The traffic scenarios were implemented in network simulator-2 as shown in figure 2. Network Simulator-2 (NS-2) is an open source, discrete event network simulator [8]. Table 1 shows the most important WiMAX and traffic parameters used in our simulations.

Channel type	Wireless Channel
Radio Propagation Model	Two Way Ground
Network Interface Type	OFDM
MAC Type	Mac 802.16
Antenna Model	Omni Antenna
No. Of Subscriber Nodes	30
Routing Protocol	OLSR

Table 1 Simulation Parameters

A detail simulation model based on NS-2 has been used in the interpretation, and in order to perfectly evaluate the effect of out-of-order packet while some of the TCP variants. The source-destination pairs are spread instant over the network. The data generator is FTP. Mobility models were created for the simulations using 30 nodes as shown in figure, and this model was set in such a way that

first all the 30 nodes were provided Then all the nodes move within their boundary by setting their final destination and the speed that each node move with. All the simulations are run for 200 simulated seconds. Different mobile and identical traffic scenarios have been used across the protocol to collect fair results.

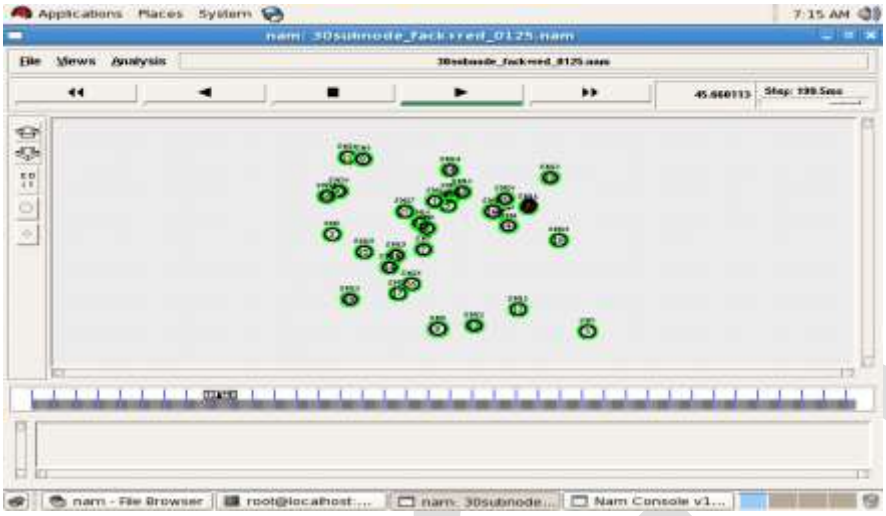

Figure 2 Nam animation trace with node deployment

SIMULATION RESULTS

In this section we present our simulation scenarios in WiMAX and consider the results obtained. With the help of graphs, the simulation has been figured out for various TCP variants based on higher offered load network scenario based on cyclic prefixes using NS-2.

Packet Delivery Ratio (PDR) :

Figure 3 shows the packet delivery ratio for TCP Reno TCP-Sack, TCP-Fack and TCP-Fack+RED when the cyclic prefix is varied. Simulation results shows that TCP-Fack gives higher performance when the value of cyclic prefix decreases. It is observed that the packet delivery ratio of TCP FACK over OLSR under higher offered load is better than both TCP-Reno and TCP-Sack.

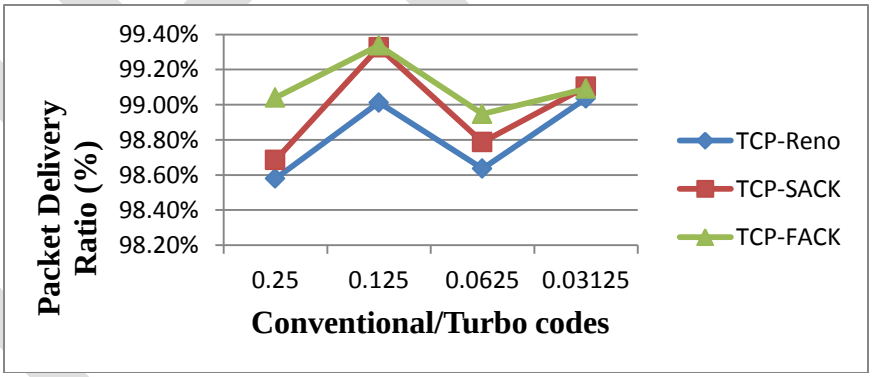

Figure 3 Packet Delivery Ratio

Throughput

The figure 4 shows the impact of mean speed on the throughput. It is observed that the throughput of TCP-FACK+ RED is better than other two TCP variants i.e TCP-Reno and TCP-Sack.

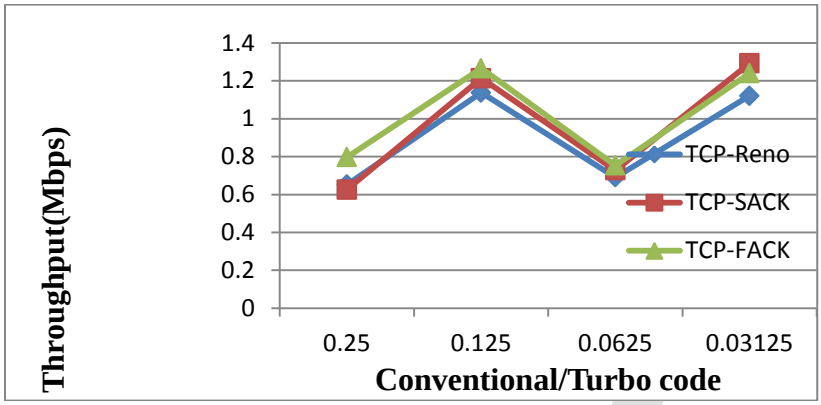

Figure 4 Throughput

Average Delay

The figure 5 showing the end-to-end delay when the number of source destination pairs are maximum.
OLSR protocol uses the route cache which many a times contains stale routes, as a result delay is comparatively higher. As the load on base station increases the delay increases. The end to end delay of TCP-FACK is higher than other TCP-variants i.e TCP-Reno and TCP-Sack.

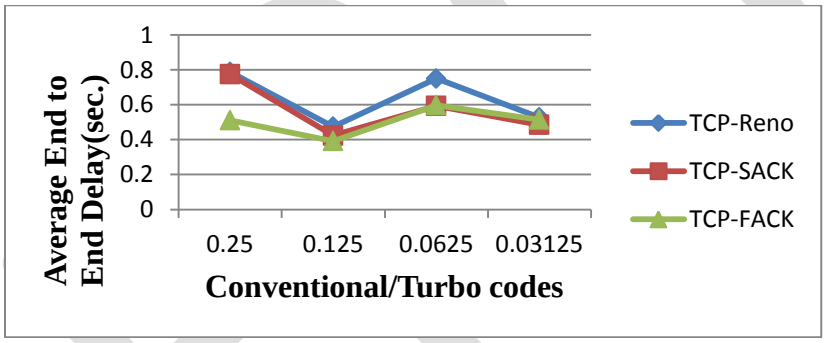

Figure5 Average End to End Delay

Routing Load

The figure 6 shows the impact of cyclic prefix on the routing load. It is noticed that the routing load of TCP-FACK outperforms TCP-Reno and TCP-Sack variants. When cyclic prefix is kept at lower value then the value of routing load is lower as cyclic prefix increases routing load increases.

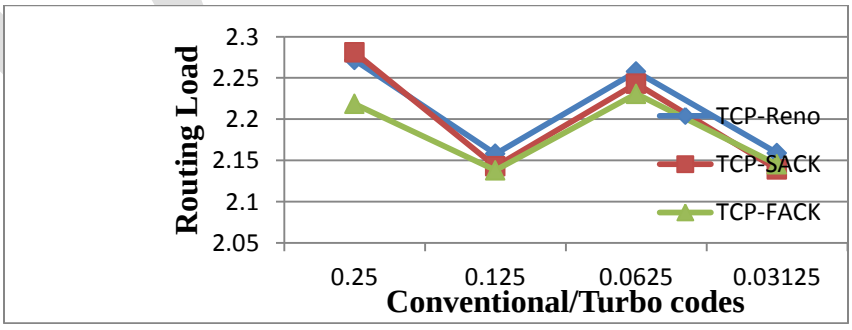

Figure6 Routing Load

CONCLUSION

It is a well known fact that TCP can experience significant performance degradation during hand-off, if multiple packet droppings, packet re-ordering or exorbitant hand-off delays occur. We have shown that the reaction on packet droppings and re-ordering is very much related to the implemented TCP version. Different TCP versions react with different types of behavior. In addition, from the perspective of transport layer, we believe that TCP will be on top of the routing protocols for reliable data transmission.

We simulated and compared the performance of various TCP algorithms viz. TCP-Reno, TCP-Sack, TCP-Fack in WiMax network by taking into account the condition of high offered load, irregular losses and retransmission timeouts that how it would affects the performance in wimax environment. We have seen that congestion and high offered load affect on TCP variants in a quite different way, Among three TCP variants, FACK outperforms other two. Since TCP has its variants, namely TCP-Reno, TCP-SACK and TCP-FACK, we performed the comparison of TCP-Reno, TCP-SACK, and TCP-FACK over OLSR under higher offered load. In summary, from the view of throughput, TCP-FACK outperforms other TCP variants. On the basis of the results obtained from simulation graphs and some trials in the literature, we can develop a bandwidth estimation technique to improve TCP-FACK performance over WiMAX environment, which is our interesting future work.

REFERENCES:

[1] IEEE Standard for Local and metropolitan area networks Part 16:*AirInterface for fixed broadband wireless access systems*, Oct. 2004.

[2] V. Jacobson, "Congestion Avoidance and Control," *in Proc.SIGCOMM'88, Standford, CA, pp.314-329.*

[3] H. Balakrishnan, V. Padmanabhan, R.H. Katz, "The effects of Asymmetry on TCP performance," *in Proc. Third ACM/IEEE Mobicom Conference, Budapest, Hungary*, Sept. 1997.

[4] A. Eshete, A. Arcia, D. Ros, Y. Jiang, "Impact of WiMAX network asymmetry on TCP," *Proc. of the 2009 IEEE Conf. on Wireless Comms & Networking Conference, p.1706-1711, Budapest*, 2009.

[5] Subedi, L., Najiminaini, M. and Trajkovic, L. (2009), "Performance E Evaluation of TCP Tahoe, Reno, Reno with SACK, and NewReno Using OPNET Modeler", Proceeding of International Conference on Methods and models in Computer Science IEEE.

[6] Francis, B., Narasimhan, V., Nayak, A. and Stojmenovic, I. (2012), "Techniques for Enhancing TCP Performance in Wireless Networks", International Conference on Distributed Computing Systems Workshops IEEE, DOI 10.1109/ICDCSW, pp. 222-230.

[7] Mathis, M. and Mahdavi, J. (1996), "Forward Acknowledgment: Refining TCP Congestion Control", Copyright 1996 by Association for Computing Machinery Inc ACM To appear in Computer Communication Review a publication of ACM SIGCOMM volume 2.number 4.

[8] Khan, A. U. R., Bilal, S. M. and Othman, M., "A Performance Comparison of Network Simulators for Wireless Networks", pp. 1-6.

[9] C. Chen, H. Wang, XinWang, M. Li, A.O. Lim, "*A Novel Receiver-aided Scheme for Improv-ing TCP Performance in Multihop Wireless Networks*", in Proc. of Int. Conference on Communications and Mobile Computing, pp. 272–277, 2009.

[10] Ruhani Ab Rahman ," *Performance Analysis of Routing Protocol in WiMAX Network*", IEEE International Conference on System Engineering and Technology,2011.

[11] Tarik Anouari ,"*Performance Analysis of VoIP Traffic in WiMAX using various Service Classes*", International Journal of Computer Applications ,Volume 52– No.20, August 2012.

[12]Vikram Mehta ,"*Performance Analysis of QoS Parameters for Wimax Networks*", International Journal of Engineering and Innovative Technology, Volume 1, Issue 5, May 2012

International Journal of Engineering Research and General Science Volume 3, Issue 3, Part-2 , May-June, 2015
ISSN 2091-2730

Smart Wireless Data-logger

Ashwin Y. Ankar[1], Dr. Pradeep B. Dahikar[2], Dr. Ashish K. Rewatkar [3]

[1] G H Raisoni Institute of Information Technology, Nagpur, Maharashtra, India.
***e-mail:** ashwin.ankar@gmail.com, **Contact No.** +91 9923 402 125
[2]Kamla Nehru Mahavidyalaya, Sakkardara Square, Nagpur, Maharashtra, India.
***e-mail:** pbdahikarns@rediffmail.com
[3] Nuva College of Engineering & Technology, Kalmeshwar, Nagpur, Maharashtra, India.
***e-mail:** ashishrewatkar@gmail.com

Abstract — This Paper proposed a portable wireless data acquisition system for temperature in real time process dynamics. Process variables (like temperature, pressure, flow, level) vary with time in certain applications and this variation should be recorded so that a control action can take place at a defined set point This paper proposes an embedded platform for a sensor having a network interface using the ZigBee protocol, that is specially designed for the sensors network. The ZigBee protocol is a wireless technology developed as an open global standard to address the unique needs of low-cost, low power, wireless sensors network .This wireless data logger senses and monitors the variations in the local temperature thereby transmits the data within the range to an assigned embedded processor based server. Received temperature is displayed on a local liquid crystal display (LCD) on assigned server and simultaneously on a computer.

Index Terms—Temperature Sensor, Embedded Controller, ZigBee Protocol, Control Algorithm.

1] INTRODUCTION

The smart logger is the convergence of the sensing features of a sensor with the intelligence and decision making abilities of a micro system. They have been successfully deployed in many industrial applications such as maintenance, monitoring, control, security, etc. Free from the hassles of any ordinary sensor system, it has its advantages in terms of portability, reliability, flexibility and robustness. Temperature is recorded using a temperature tag at user defined time intervals. The temperature tag can be programmed so that when the memory is full it either stops further recording or continues recording by overwriting the earliest of the previously recorded data [1][2].

The sensed temperature is transmitted through ZigBee module. On receiving end temperature is received through another ZigBee module and displayed on a local LCD display. Each acquisition of temperature is compared with a user defined set point. If this value exceeds the set point a control signal goes to a final control element or a buzzer. This temperature data is also communicated to the COM port of a Personal Computer (PC). Every time a temperature data is transmitted and received it is entered into a log, that is maintained in a PC connected via serial port and the plotting of the recorded temperature variations is also carried out simultaneously. The temperature log is maintained in the PC until the power supply to the microcontroller is reset.

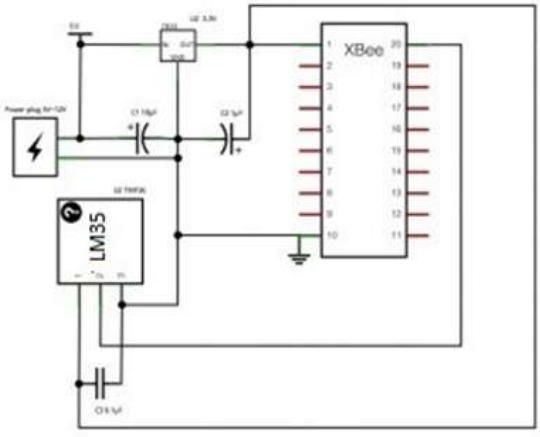

Fig 1 interfacing LM35 with Xbee

We have used the LM 35 interfaced with XBee module shown in Fig. 1 with a range of 0 to 150^{o}C. The temperature value is sensed and is then fed to the input ZigBee trans-receiver which transmits this temperature data to another ZigBee trans-Receiver located within a 10 m radius with minimum noise .The wireless technology, IEEE 802.14.5, that is used to implement our work enables broad-

based deployment of wireless networks with low-cost, low-power solutions. Most RF applications require battery power, so the lower the output power, better the durability. The proposed data logger can also be used for other process variables like pressure, flow, humidity and level like existing models [3][4]. The main functions of proposed temperature data logger are:

1) Continuous temperature monitoring.
2) Comparison with the set point.
3) To generate manipulating signal to the final control element.
4) A peer to peer and multipoint network can be established by configuring each module to operate as end device.
5) To transmit the data to remote display (PC or PDA).

Since this temperature data logger is equipped with 8 bit Microcontroller and ZigBee modules, it can be networked with same data loggers for other process variables in specific control applications [5].

The organization of the paper is as follows: In section 2, we discuss the proposed design that also presents the block diagram for our proposed system. Detailed circuit description is provided for each block used in this section. We have used the LM 35 interfaced with XBee module shown in Fig. 1 with a range of 0 to 150^{o}C. The temperature value is sensed and is then fed to the input ZigBee trans-receiver which transmits this temperature data to another ZigBee trans-Receiver located within a 10 m radius with minimum noise .The wireless technology, IEEE 802.14.5, that is used to implement our work enables broad-based deployment of wireless networks with low-cost, low-power solutions. Most RF applications require battery power, so the lower the output power, better the durability. The proposed data logger can also be used for other process variables like pressure, flow, humidity and level like existing models [3][4]. The main functions of proposed temperature data logger are:

1) Continuous temperature monitoring.
2) Comparison with the set point.
3) To generate manipulating signal to the final control element.
4) A peer to peer and multipoint network can be established by configuring each module to operate as end device.
5) To transmit the data to remote display (PC or PDA).

Since this temperature data logger is equipped with 8 bit Microcontroller and ZigBee modules, it can be networked with same data loggers for other process variables in specific control applications [5].

The organization of the paper is as follows: In section 2, we discuss the proposed design that also presents the block diagram for our proposed system. Detailed circuit description is provided for each block used in this section. Finally, some conclusions are offered in section 3

II) PROPOSED WORK

This work is divided into the following modules: first is the LM35-DZ temperature sensor, interfaced with ZigBee transreceiver Fig. 2.

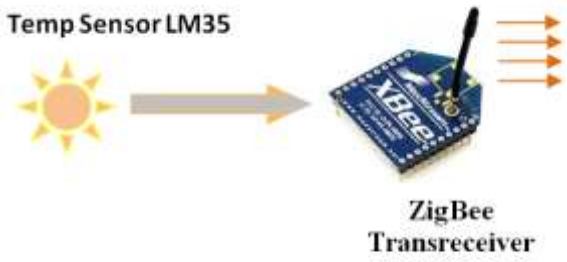

Fig 2 Transmitting End Block

Second is the ZigBee transreceiver present at both the transmitting and receiving end, providing the wireless interface to the controllers.

The final module is microcontroller at the receiving end interfaced with a MAX 232, an LCD and a DB9 connector as shown in Fig.3.

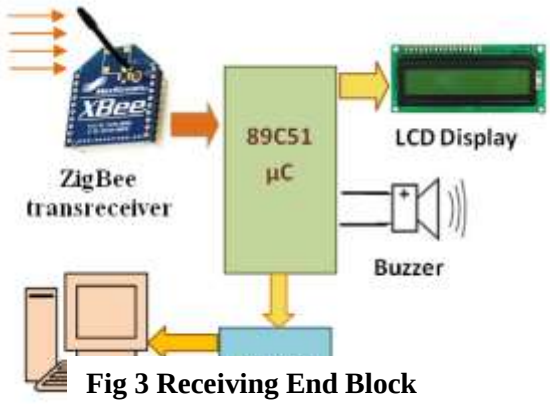

Fig 3 Receiving End Block

a) LM35-DZ Temperature sensor

The LM35 series are precision integrated-circuit temperature sensors, whose output voltage is linearly proportional to the Celsius (Centigrade) temperature. The LM35 thus has an advantage over linear temperature sensors calibrated in Kelvin, as the user is not required to subtract a large constant voltage from its output to obtain convenient Centigrade scaling. It can be used with single power supplies, or with plus and minus supplies. As it draws only 60 µA from its supply, it has very low self-heating, less than 0.1°C in still air. The LM35 is rated to operate over a 0° to +100°C temperature range.

b) ZigBee /IEEE 802.15.4 Modules

ZigBee or XBee Modules were engineered to meet IEEE 802.15.4 standards and support the unique needs of low-cost, low-power wireless sensor networks. The modules require minimal power and provide reliable delivery of data between devices. The modules operate within the ISM 2.4 GHz frequency band and are pin-for-pin compatible with each other. XBee/XBee-PRO RF Modules were engineered mount into a socket and therefore do not require any soldering when mounting them to a board.

Features

1) High Performance, Low Cost:
- XBee•Indoor/Urban: up to 100' (30 m)
- Outdoor line-of-sight: upto 300' (100 m)
- Transmit Power: 1 mW (0 dBm)
- Receiver Sensitivity: -92 dBm

2) Low Power Module:
- XBee•TX Current: 45 mA (@3.3 V)
- RX Current: 50 mA (@3.3 V)
- ower-down Current: < 10 µA

Advantages

1) Low duty cycle - Provides long battery life
2) Low latency
3) Support for multiple network topologies: Static, dynamic, star and mesh
4) Direct Sequence Spread Spectrum (DSSS)
5) Up to 65,000 nodes on a network
6) 128-bit AES encryption – Provides secure connections between devices
7) Collision avoidance
8) Link quality indication
9) Clear channel assessment
10) Retries and acknowledgements
11) Support for guaranteed time slots and packet freshness

c) MAX 232 (Communication Interface)

RS-232 (Fig. 4.) was created for one purpose, to interface between Data Terminal Equipment (DTE) and Data Communications Equipment (DCE) employing serial binary data interchange. So as stated the DTE is the terminal or computer and the DCE is the modem or other communications device. RS 232 is the most widely used serial I/O interfacing standard. In RS 232, a 1 is represented

by -3 to -25 v. while a 0 bit is +3 to + 25 v, making -3 to +3 undefined. For this reason, to connect any RS 232 to a microcontroller system we must use voltage converters such as MAX 232 to convert the TTL logic levels to the RS 232 voltage level, and vice versa. This chip is used when interfacing micro controller with PC to check the Baud rate and changes the voltage level because micro controller is TTL compatible whereas PC is CMOS compatible.

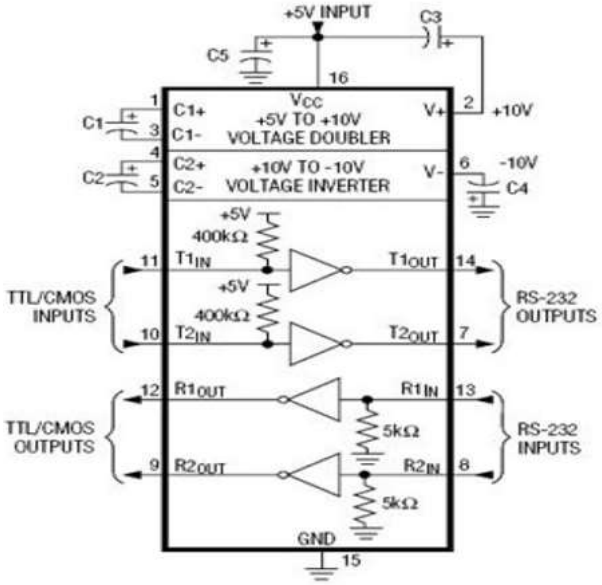

Fig 4 Operating Circuit of MAX 232

III) Hardware Circuitry (Transmitter/ Receiver)

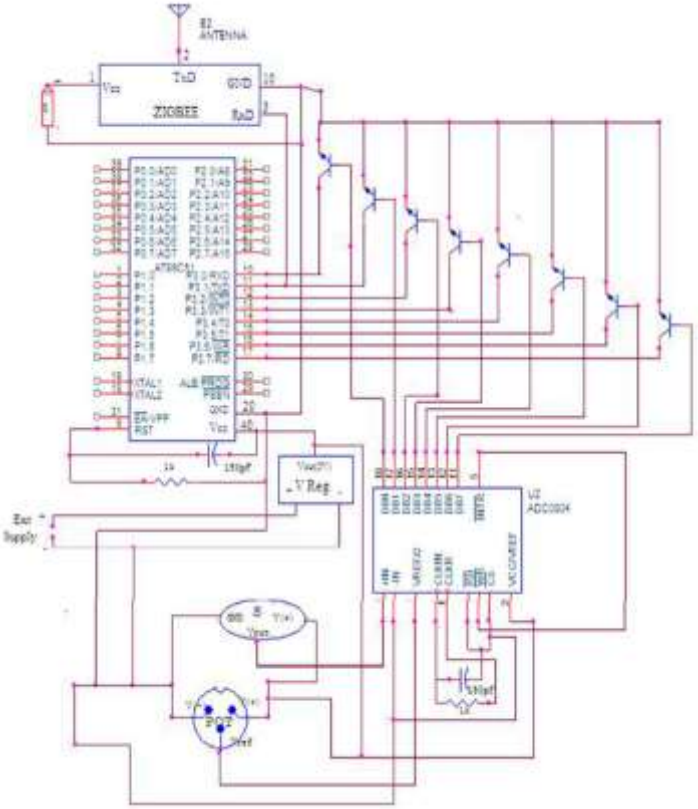

Fig 5 Transmitter

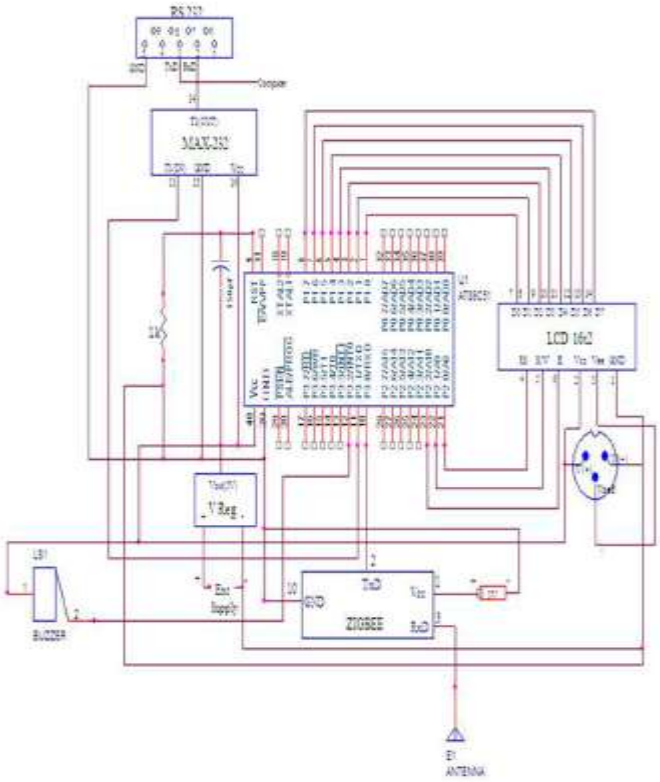

Fig 6 Receiver

IV) CONCLUSION AND FUTURE SCOPES

The proposed temperature logger can be used in the following applications:

1) The remote areas where battery power consumption is major issue.
2) The process industries where the physical channel between sensor and display unit is not possible.
3) Long range error free wireless transmission in sensor networks
4) Mining, Agriculture, Defense and biomedical applications

The future scope of this work is:

1) It can be used to make a network of clusters consisting of sensors in real time control applications
2) Compatible with different network protocols
3) A memory database can be built by using on chip memory as well as remotely connected PC through wireless link.

REFERENCES:

[1] Radek Kuchta, Radimir Vrba, "Wireless and Wired Temperature Data System", IEEE – ICONS,07 pp 49-53.

[2] Crowley, K. Frisby, J. Edwards, S. Murphy, S. Roantree, M. Diamond,"Wireless temperature logging technology for the fishing industry", IEEE - ICSENS.2004 pp 571-574. Vol (2).

[3] Wireless Sensor Networks: Technology, Protocols, and Applications by Kazem Sohraby, Daniel Minoli, and Taieb Znati (Hardcover - April 6, 2007).

[4] Ahonen T, Virrankoski R, and Elmusrati M.,.Greenhouse Monitoring with Wireless Sensor Network.Mechtronic and Embedded Systems and Applications. IEEE/ASME International Conference 1-4244-2368-2/08/IEEE, 2008

[5] Al adwan, Ibrahim, Munaf SN, . The Use of ZigBee Wireless Network for Monitoring and Controlling Greenhouse Climate., International Journal of Engineering and Advanced Technology (IJEAT) ISSN: 2249 . 8958, Volume-2, 2012

[6] Anjar Rinaldi, .Rancang Bangun Sistem Monitoring Parameter Lingkungan Mikro Pada Rumah Kaca (*Greenhouse*) Berbasis Internet., [skripsi], Bogor (ID) :Institut Pertanian Bogor, 2006

[7] Chusnul Arif, .Sistem Monitoring Pertumbuhan Tanaman dan Lingkungan Mikro di dalam Greenhouse Menggunakan Field Server., [skripsi], Bogor (ID) : Institut Pertanian Bogor, 2009

[8] Haryono, .Pedoman Umum Adaptasi Perubahan Iklim Sektor Pertanian., adan Penelitian dan Pengembangan Pertanian Kementrian Pertanian, 2011

International Journal of Engineering Research and General Science Volume 3, Issue 3, Part-2 , May-June, 2015
ISSN 2091-2730

Sensorized Glove for Rehabilitation Purpose

Priti D. Nandnikar, Dr. Manoj S. Nagmode

MITCOE PUNE, priti.nandnikar@gmail.com , 7709455860

Abstract— In human life they utilize hands for taking care of any task, so people are gifted users of their hands. They utilize them to hold and control things and to connect with pretty much clear gestural and non-verbal communication. These days' scientists are attempting to gain from the biology for research. As the developing actuation technologies and mechanical detecting empower the development of better mechatronic frameworks, as a result of this there has been a developing enthusiasm for research field. Application arenas are like robotics, entertainment, sign language understanding, medical field etc. In any case to appreciate hand developments and associations, scientists oblige suitable sensing/detecting system, similar to glove based system for information accomplishment. Lamentably a large portion of these system are either expensive solutions for lab utilization, or a few low value arrangements are insufficient, and both grade to be troublesome and hinder the characteristic hand developments. So in this paper we are presenting a moderate system. This system will be helpful in medial field for doctors and also for users. This system will sense the position of hand fingers and will send this data to the doctor utilizing wireless communication. For sensing the position of fingers we have utilized flex sensors, which is only a little strip. This system will be significant in rehabilitation process.

Keywords— Rehabilitation, signal conditioning, Degrees of Freedom, wireless communication, data acquisition, flex sensors, Graphical User Interface.

INTRODUCTION

Human uses the capacity to control and move things with hands to execute all sort of tasks [1]. This capacity has been case of study by scientific community. Researchers search for knowledge through analysis of hand trajectories to handle things and man-machine correspondence for motion acknowledgment. This data is then used to imprecise the standard activities and mechanized activities in gestural cooperation with social robots [2]. Moreover with the development of fields like military, overwhelming industry, physiotherapy, medicine and sports, arrangements are crucial to give robots the capacity to do precision activities like movement recognition, supported surgery, slashes recuperation and even to superior training.

These days we are helping to a change of temperaments. General keyword and mouse are being exchanged by different sorts of information equipment. For instance in Xbox utilizes the Kinect to catch humman movement and submit it to acknowledgment, iPad uses fingers to touch the screen or in Wii that we utilize Wiimote to create movement that is caught by the accelerometer and then converted into commands. However these arrangements don't offer reactions like the stimulus that we get when we interface with real objects. Accordingly in the previous 30 years, various advances were created to help researchers to proceed with their studies [3]. Those innovations are named as data glove based system. They are basically gloves instrumented with sensors used to perform data attainment. However all the presented technologies have a few liabilities since none satisfy the accompanying necessities like good resolution, parallel data acquisition, low cost and wireless communication.

Notice that a glove based system is defined as a collection of electronic sensors to be used for hand data attainment, processing and a provision for the sensors which can be worn on hand. Generally glove is a cloth glove where sensors will be sewn or stuck. Below Fig.1. shows a depicted human hand parts like fingers, wrist, back and palm. Fig.2. shows the bones of human hand which has different hand joints. Human hand is characterized for having Degrees of Freedom (DoF) to define hand motions. During the execution of movements each Finger joint has 1 DoF for the Proximal Interphalangeal (PIP) and Distal Interphalangeal (DIP), 2 DoF for the Metacarpophalangeal (MCP) and 3 DoF for the Trapeziometacarpal (TMCP). A glove prepared with one sensor per DoF may seem to be the most apparent design choice.

LITERATURE SURVEY

The first glove base system was produced amid the 70s. From that point forward some glove based systems have been proposed. This glove based system protypes were created at Massachusetts Institute of Technology (MIT) and were assigned as MIT-LED and Digital Entry Data Glove. In 1977 Thomas de Fanti and Daniel Sandin built up the Sayre glove model in Rich Sayre proposal. This glove was made utilizing light as source that is directed through exible tube, mounted along every finger, that as photocell to quantify light varieties. Right on time in the 80s MIT added to another version that utilized a LED system which was camera-based to track body movement in real time processing [4]. Later in 1983, Gary Crimes created and patented the Digital Entry Data Glove that had sensors installed on material to recognize if thumb is touching any piece of the hand or fingers, measure the thumbs joint exion, hand tilt and the twisting /exing of the lower arm [5].

Fig.1. Human hand parts.

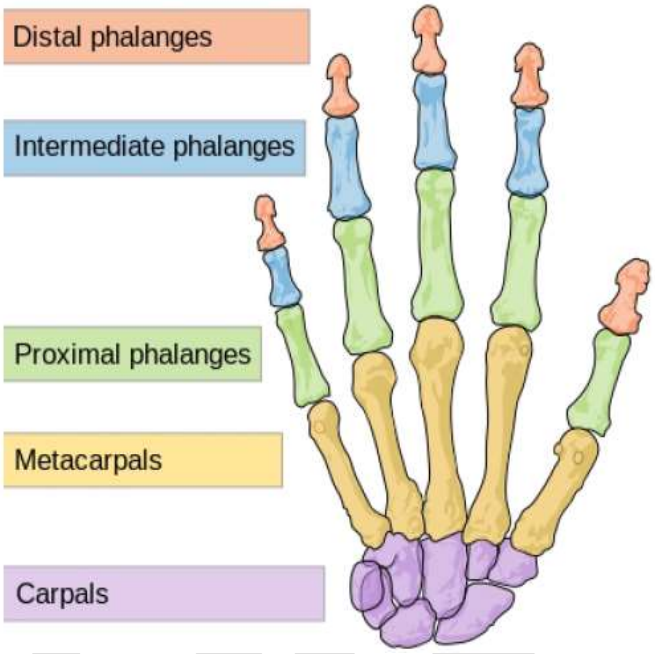

Fig.2. Bones of the human hand.

Zimmermam built up a data glove utilizing exible plastic tubes and detectors installed on a material to catch joint points. Late in 1987, Visual Programming Language Research, Inc. showed up with another adaptation utilizing fiber optics. This new form came outfitted with 5 to 15 sensors to gauge exion, abduction and adduction [6]. In 1989 Mattel Toy Company produced a minimal effort control gadget, the Power Glove, for the Nintendo video games. This glove has utilized resistive ink imprinted on flexible plastic bends which takes after the movements of every finger to quantify the general flexion of the fingers [7]. Nissho Electronics in 1995 developed and commercialized the Super Glove. This glove came with 10 to 16 sensors and used resistive ink printed on boards sewn on the glove cloth [8]. In 2002 Super Glove was updated for Power Glove, the P5 Glove [9].

The data gloves then improved using the force sensors. Which are widely used in many applications such as virtual reality applications, robotics, telecheric applications, and biomechanics. This new data glove will have all information of finger position as well as the force the fingers apply on an object. The force sensor was made of a steel plate substrate where the commercial strain gauges are attached [10].

In [11], they had an aim to create and test an arrangement of five virtual activities on top of a system, which is intended for the determination and restoration of patients with hand debilitations. They have actualized assignment arranged activities taking into account entrenched and basic activities, specifically the Jebsen Test of Hand Function and the Box and Block Test. These incorporate moving a container, masterminding squares, exploring a labyrinth, preparing with a dumbbell, and getting a handle on an elastic ball. In [12], they have introduced a wearable detecting glove with installed heterocore fiber-optic nerve sensors that identify finger flexion to accomplish unconstrained hand movement observing. This wearable detecting glove innovation has gone for decreasing the quantity of sensors for minimal effort and long haul observing without aggravating characteristic action. The hetero-core sensor components are situated on the back of the hand with the goal that they are not influenced by irregular wrinkles in the glove at the joints. Accordingly, the hetero-core flexion sensor after adjustment is equipped for distinguishing the joint edges of the fingers paying little heed to contrasts close by size, and the hetero-core detecting procedure empowers the detecting glove to be built with a base number of sensor focuses.

Artificial Neural Network (ANN) can be utilized for aligning the sensors on the Cyber Glove. There are three principle purposes behind picking ANNs for the adjustment of the CyberGlove. To begin with, ANNs have been effectively sought the alignments of numerous frameworks in a wide range of designing fields. Second, they have seen that there are some immediate and reliable connections between the human-hands portion size and the reporter sensors readings through the test. Third, once the last NNs are found for every sensor, the era of alignment information for any new subject is straightforward and quick [13]. The glove system can also use for the speechless person. In [14], it described an electronic talking glove, intended to encourage a simple correspondence through incorporated discourse for the advantage of speechless patients. Gestures of fingers of a client of this glove will be changed over into incorporated discourse to pass on a perceptible message to others, for instance in a discriminating correspondence with specialists. The glove is inside furnished with different flex sensors that are comprised of "curve delicate resistance components". This project is a helpful device for discourse hindered and halfway deadened patients which fill the correspondence hole between patients, specialists and relatives. As it is compact, obliges low power working on a solitary lithium-particle rechargeable battery and having less weight and strong gives understanding freedom to convey it anyplace at their will.

The glove system which is useful in restoration is given in [15]. This paper concentrates on mulling over and actualizing a framework for measuring the finger position of one hand with the point of offering criticism to the restoration framework. It comprises of a glove where sensors are mounted suitably designed and joined with an electronic molding and obtaining unit. The data in regards to the position is then sent to a remote framework. The goal of this paper is to give a sensorized glove to observing the recovery exercises of the hand. In [16] Giancarlo Orengo et.al introduced another system. In this system the sensor and their extracted models were connected to register the human knee revolution amid a stride cycle, either at moderate pace for a mobile example at 5 km/h, and at high velocity for a running example of a sprinter at 10 m/s, lastly the finger joint pivots at their most extreme precise speed. This was defeated a twofold reason: from one hand, to evaluate the model ability to foresee the sensor execution, following human body fragment turns at diverse velocity, without the need of estimation; from the other hand, to recuperate progressively the genuine sensor pivot from its resistance estimation, particularly in rapid applications, where its reaction is misshaped.

PROPOSED SYSTEM

This proposed system concentrates on study and execution of a system for measuring the finger position of hand with the point of offering solace to do the activity and to the recovery treatment. It comprises of a glove where sensors are mounted suitably arranged and associated with an electronic conditioning circuit. The data in regards to the position is then sent to a receiving section, means PC, utilizing the wireless communication. The proposed block diagram for transmitting section and receiving section is given in Fig.3. and Fig.4. respectively.

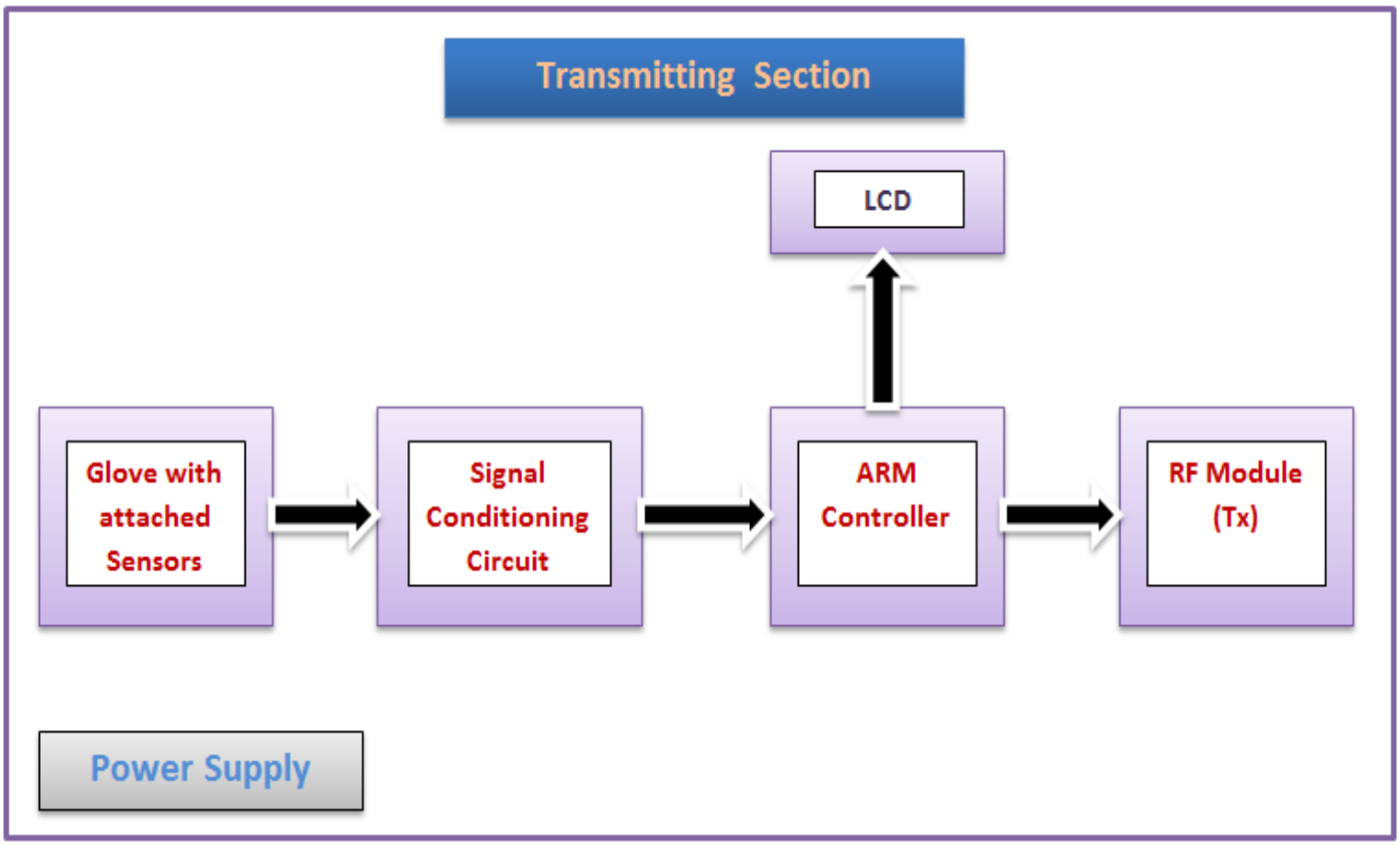

Fig.3. Proposed block diagram of transmitting section.

The system is made out of a transmitting section and a receiving section. The transmitting section is the transduction system and comprises of a glove including 5 flex sensors (one for every finger and number of sensors may change) joined with a microcontroller through front-end hardware. The management of the sensor estimation is allotted to the ARM microcontroller that performs a few capacities: interfacing and conditioning of signals from the sensor block and information transmission. Amid the operation, the receiving section which is comprised of a beneficiary and a PC, changes over, records, and showcases the got measures of joint deflection. In the transmitting section, we have sensors which are attached with the glove. From these sensors we will get output in the form of resistance. In the signal conditioning circuit we will convert this resistance into voltage using voltage divider circuit. The interfacing and conditioning of signals will be done by controller. The output of the controller is then transmitted using the RF module which operates on 433 MHz frequency. The finger movements are detected or not will be displayed on LCD on transmitter side. In this system 16X2 LCD is used. The transmitted data will be received using RF module in receiving section. The received data will be displayed on PC using any MATLAB software.

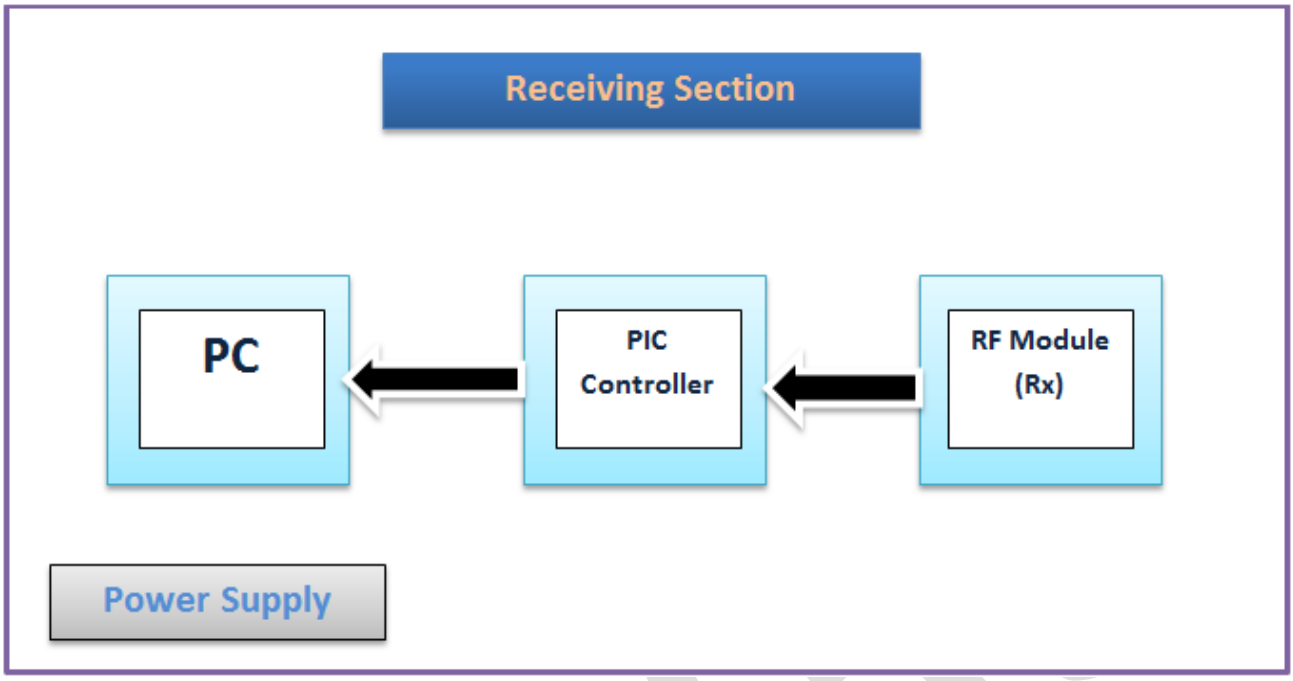

Fig.4. Proposed block diagram of receiving section.

The ARM7 means LPC2148 is used for the processing of the data. As it is 32-bit microcontroller it is very useful in this system. On the receiver side PIC16F877A is used. The flex sensor bends and flexes physically with motion device. The flat resistance (at 0° angle) of this sensor is 10KΩ and when its bend at 90° angle then its resistance will be 50KΩ. It has a power rating of 0.5 Watts continuous. The temperature ranges from -35°C to +80°C. The signal conditioning circuit in transmitting section is shown in below Fig.5.

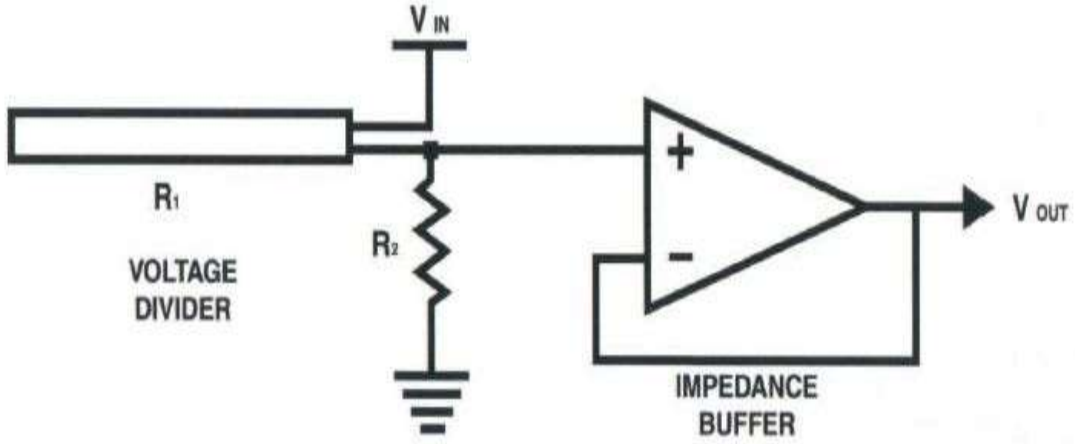

Fig.5. Signal conditioning circuit

The R_1 resistor is nothing but the variable resistance of flex sensor. This resistor is connected serially to R_2 resistor,which is a fix value resistor. Using this circuit the flex sensors output, variable resistance, is converted into the voltag. Each sensor requires its separate voltage divider circuit. The impedance buffer is, a single sided operational amplifier, utilized with these sensors because the low bias current of the op amp reduces error due to source impedance of the flex sensor as voltage divider. Suggested operation amps are the LM358 or LM324.

RESULT

For displaying the data from RF module receiver on PC we have used the MATLAB software. Using this MATLAB software we created a Graphical User Interface (GUI). This GUI is shown in below Fig.6. As shown in figure 5, this GUI shows the angle of each finger in the form of degree.

Fig.6. Result on PC using GUI.

CONCLUSION

In this paper, a new system for measuring the position of the fingers is proposed. This system will detect and measure the position of the fingers using flex sensors and it will be displayed on PC using suitable software. The application of this system is in biomedical field. This system will be useful for trauma, stroke patients to do exercise. It will have ability to perform the exercise at home which will reduce cost and difficulties of transport to hospital.

REFERENCES:

[1] D. R. Faria, R. Martins, and J. Dias "Human Reach-to-Grasp Generalization Strategies: A Bayesian Approach" in Workshop: Understanding the Human Hand for Advancing Robotic Manipulation, 2009
[2] D. R. Faria, H. Aliakbarpour, and J. Dias "Grasping Movements Recognition in 3d Space Using a Bayesian Approach" in Proceedings of the ICAR 2009 - 14th International Conference on Advanced Robotics, 2009
[3] L. Dipietro, A. M. Sabatini, and P. Dario "A Survey of Glove-Based Systems and their Applications" IEEE Transactions on Systems, Man, and Cybernetics—Part C: Applications and Reviews, vol. 38, no. 4, July 2008
[4] D. J. Sturman and D. Zeltzer "A Survey of Glove-Based Input" IEEE Comput. Graph. Appl., vol. 14, no. 1, pp. 3039, 1994
[5] G. Grimes "Digital Data Entry Glove Interface Device" U.S. Patent 4 414 537, AT&T Bell Lab., Murray Hill, NJ, 1983
[6] T. G. Zimmerman "A Hand Gesture Interface Devices" Proc. Humman Factors in Computing Systems and Graphics Interface, ACM Press, New York, pp. 189-192, 1987
[7] D. L. Gardner "The Power Glove" Des. News, vol. 45, pp. 63–68, 1989
[8] J. J. LaViola "A Survey of Hand Posture and Gesture Recognition Techniques and Technology" Brown Univ., Providence, RI, Tech. Rep. CS-99-11, 1999
[9] [Online].Available: http://www.essentialreality.com
[10] Kostas Tarchanidis and John Lygouras "Data Glove with a Force Sensor" IEEE transactions on instrumentation and measurement, vol. 52, no. 3, 2003
[11] Atif Alamri, Mohamad Eid, Rosa Iglesias, Shervin Shirmohammadi and Abdulmotaleb El Saddik "Haptic Virtual Rehabilitation Exercises for Poststroke Diagnosis" IEEE transaction on instrumentation and measurement, vol. 57, no. 9, September 2008
[12] Michiko Nishiyama and Kazuhiro Watanabe "Wearable Sensing Glove with Embedded Hetero-Core Fiber-Optic Nerves for Unconstrained Hand Motion Capture" IEEE transactions on instrumentation and measurement, vol. 58, no. 12, December 2009
[13] Jilin Zhou, François Malric, and Shervin Shirmohammadi "A New Hand-Measurement Method to Simplify Calibration in CyberGlove-Based Virtual Rehabilitation" IEEE transactions on instrumentation and measurement, vol. 59, no. 10, October 2010

[14] Syed Faiz Ahmed, Syed Muhammad Baber Ali and Sh. Saqib Munawwar Qureshi "Electronic Speaking Glove for Speechless Patients, A Tongue to a Dumb" IEEE Conference on Sustainable Utilization and Development in Engineering and Technology, 20 21 November 2010

[15] Michela Borghetti, Emilio Sardini, and Mauro Serpelloni "Sensorized Glove for Measuring Hand Finger Flexion for Rehabilitation Purposes" IEEE transactions on instrumentation and measurement, vol. 62, no. 12, December 2013

[16] Giancarlo Orengo, Antonino Lagati, and Giovanni Saggio "Modeling Wearable Bend Sensor Behavior for Human Motion Capture" IEEE sensors journal, vol. 14, no. 7, July 2014

International Journal of Engineering Research and General Science Volume 3, Issue 3, Part-2 , May-June, 2015
ISSN 2091-2730

AN OVERVIEW OF COMPARISON BETWWEEN 2-DIMENSIONAL AND 3-DIMENSIONAL SOLAR CELL ARRANGEMENTS

[1] NEELAM RAWAT, [2] POOJA SINGH

[1] M.Tech Student Govind Ballavh Pant University of Agriculture and Technology
email id-neelamrawat3049@gmail.com
contact no. 8755363712

Abstract— People all over the world are being aware of harmful effects of burning of fossil fuels for different uses especially electricity generation at present time. And this is the reason people are looking forward to the use of renewable energy sources especially solar energy as sun is not going to run out. In this paper our focus is on differentiating the ways of generation of electricity in different dimensions using solar energy.

Keywords— 2-D, 3-D, Solar energy, Solar Photo-voltaic, Solar Power Tree (SPT), Fibonacci, Phyllotaxy

INTRODUCTION

At the present time people are being aware of the importance of use of renewable energy sources in which solar energy resource is playing a crucial role. Initially for the most efficient use of solar energy solar panels as made of crystalline Si are mounted on rooftop of houses at some tilt angle as well as laid on some hut-like structure. This complete arrangement can be treated as 2-D structure which takes a lot of space and also have other drawbacks and to remove them solar panels are arranged in a 3-D structure and termed as Solar tree which use solar energy most efficiently per installation area. Solar power can be harnessed in different ways as via solar thermal technology, passive solar heating, PV cells etc. Among all these technologies, PV technology is simple, less costly and efficient comparatively. While comparing conventional PV modules installed on inclined hut-like structure with respect to Solar tree design one can treat conventional PV modules as 2-D structure and Solar tree as 3-D structure as in solar tree solar panels are installed in different azimuth and collect solar energy from different direction. Although both technologies include combination of solar panels in which they are arranged differently.

HISTORY OF PV MODULE

Solar power technology is not a recent technology. In mid 1800 solar power plants were developed to heat water so that steam can be generated for driving different machines. In 1839 **Alexander Edmond Becquerel** claimed that "shining light on an electrode submerged in a conductive solution would create an electric current" but he could not explain the effect. This was explained only after in 1905 when **Albert Einstein** published a paper on Photoelectric effect according to which many metals emit electrons when light shines upon them. In 1873 **Willoughby Smith** discovered the photoconductivity of Selenium while testing materials for underwater telegraph cables. In 1883 **Charles Fritt** made the first selenium solar cell but their efficiency of conversion was less than 1% and hence, they were not very practical. Research on Selenium PV continued for next several decades but they were not efficient enough to be put to widespread use. Over 100 years later, in 1941 **Russell Ohl** invented the solar cell, shortly after the invention of transistor. Si solar cell invented by Russell Ohl was 1% efficient but was not in practical use. In 1953 **Gerald Pearson**, **Calvin fuller** and **Daryl Chapin** discovered the Si solar cell. They showed in their research that by adding suitable impurities to Si, efficiency of solar cell improved. This cell was efficient enough to run small electrical devices. After some improvements in their design they combined together several solar cells and named this design Solar battery which is also known as solar panel. Conversion efficiency (converting solar energy into electricity) of these solar cells was 6%. In 1953 first solar cells were available commercially.

CONSTRUCTION AND WORKING OF SOLAR CELL

Solar cell is usually made of silicon. In crystalline form Si behaves like a semiconductor and hence is a poor conductor of electricity. To improve its conductivity pentavalent and trivalent impurities are added. This process of adding impurities is called doping. By adding trivalent and pentavalent impurities to Si, p-type and n-type Si is formed which have free electrons and holes respectively. When p-type and n-type Si comes into contact electrons move towards the p-side and come into contact with holes. After some time an equilibrium state is reached and electric field across the junction separates these two sides. When solar light hits solar cell, electron-hole pairs break apart due to its energy. Electric field across the junction doesn't allow free electrons to move towards the n-side. And

when an external path is provided electrons flow through this path and meet the holes in p-side. Flow of electrons through external path result into current and electric field across the junction causes voltage. Power is obtained using values of voltage and current. This overall phenomenon is called Photovoltaic effect. PV modules are made by connecting several individual cells together to achieve useful levels of voltage and current. To generate electricity at a large scale several pv modules are arranged in series and parallel combination resulting into a PV array.

TYPES OF SOLAR PANEL

There are different types of solar panel as follows:

(1) Crystalline solar panel

(i) monocrystalline
(ii) polycrystalline
(iii) string-ribbon

(2) Thin –film solar panel

(i) Amorphous-Si
(ii) Cadmium telluride
(iii) Copper indium gallium selenide
(iv) Organic photovoltaic cell

Crystalline Si forms the basis of mono and polycrystalline Si solar cells. **Monocrystalline** solar cells are also called single crystalline Si. These solar cells are made out of cylindrical Si ingots. To optimize performance and lower costs of a single monocrystalline solar cell, four sides are cut out of the cylindrical ingots to make silicon wafers.

Advantages:

- Monocrystalline solar panels have the highest efficiency rates (21.5% till April 2013) since they are made out of the highest-grade silicon.
- Monocrystalline silicon solar panels are space-efficient and also produce upto four times the amount of electricity as thin-film solar panels.
- Monocrystalline solar panels live the longest.
- At low light condition perform better than same rated poly-crystalline solar panels.

Disadvantages:

- Monocrystalline solar panels are the most expensive.
- If the solar panel is partially covered with shade, dirt or snow, the entire circuit can break down.
- During the process of production of monocrystalline Si through Czochralski process, a significant amount of Si ends up as a waste.

Polycrystalline Si solar panels were introduced in 1981 commercially. Unlike monocrystalline solar cells these cells are perfectly rectangular with no rounded edges.

Advantages:

- The amount of waste Si is less comparatively.

Disadvantages:

- Efficiency of polycrystalline solar panels is 13-16% due to lower Si purity.
- Lower space efficiency.

String ribbon solar panels are also made out of polycrystalline Si. String Ribbon is the name of a manufacturing technology that produces a form of polycrystalline silicon.

Advantages:

- The manufacturing of these solar panels only uses half the amount Si as monocrystalline manufacturing and this contributes to lower cost.

Disadvantages:

- The manufacturing of String Ribbon solar panels is significantly more energy extensive and more costly.
- Efficiency is at best on par with the low-end polycrystalline solar panels at around 13-14%.In research laboratories, researchers have pushed the efficiency of String Ribbon solar cells as high as 18.3%.

- String Ribbon solar panels have the lowest space-efficiency among crystalline based solar panels.

Thin-film solar cells are also known as thin –film photovoltaic cells. Depositing one or several thin layers of photovoltaic materials on substrate is the main gist of how thin film solar cells are manufactured. Depending on the technology, thin-film module prototypes have reached efficiencies between 7–13% and production modules operate at about 9%. Future module efficiencies are expected to climb close to the about 10–16%. Solar panels based on Amorphous silicon, Cadmium telluride and Copper indium gallium selenide are currently the only thin-film technologies that are commercially available on the market.

Advantages:

- Monocrystalline solar panels have the highest efficiency rates (21.5% till April 2013) since they are made out of the highest-grade silicon.
- Monocrystalline silicon solar panels are space-efficient and also produce upto four times the amount of electricity as thin-film solar panels.
- Monocrystalline solar panels live the longest.
- At low light condition perform better than same rated poly-crystalline solar panels.

Disadvantages:

- Monocrystalline solar panels are the most expensive.
- If the solar panel is partially covered with shade, dirt or snow, the entire circuit can break down.

Amorphous-Si solar cells have only been used for small scale applications such as in pocket calculators due to low output of electrical power but recent innovations have made them more attractive for some large applications too. With a manufacturing technique called "stacking", several layers of amorphous silicon solar cells can be combined, which results in higher efficiency rates (typically around 6-8%). Only 1% of the silicon used in crystalline silicon solar cells is required in amorphous silicon solar cells. On the other hand, stacking is expensive. **Cadmium telluride** is the only thin film solar panel technology that has surpassed the cost-efficiency of crystalline silicon solar panels in a significant portion of the market (multi-kilowatt systems). The efficiency of solar panels based on cadmium telluride usually operates in the range 9-11%. **FIRST SOLAR** has installed over 5 gigawatts (GW) of cadmium telluride thin-film solar panels worldwide. The same company holds the world record for CdTe PV module efficiency of 20.4% in February 2014. **Copper indium gallium selenide** solar cells have showed the most potential in terms of efficiency as compared to other thin film technologies. These solar cells contain less amounts of the toxic material cadmium that is found in CdTe solar cells. Commercial production of flexible CIGS solar panels was started in Germany in 2011.The efficiency rates for CIGS solar panels typically operate in the range 10-12 %. Swiss researchers have claimed a new world record efficiency of 18.7% for flexible copper indium gallium (di) selenide solar cells on plastics.

On comparing all types of solar cells it can be concluded that monocrystalline solar cells are the most space efficient but also more expensive while the thin film solar cells are less costly but the least efficient.

NEED FOR NEW INVENTION

Generally in solar power generation system PV panels are erected under the sun so that the surface of panel gets the maximum insolation of the day being laid at an angle. For more power in kilowatts it is required to have suitable structure over the landed area in an open space to hold the solar panels therefore hut like permanent fixed structure are made. But these structures require large area of land surface in acres for housing the panels to generate power in MW. And land is already a burning crisis in most of the countries. Again most of the agriculture areas are in need of electricity but are far away from the conventional power plants. And it would be uncountable loss if land is used for other purposes than agriculture. Hence, using vast land, for capturing solar power would never be cost effective and viable for human being. Hence there is a need of such design which can absorb solar radiation without occupying much surface area. Design should be capable of absorbing maximum solar power by providing maximum solar surface along with utilizing minimum land.

SOLAR POWER TREE

Here comes the idea of a Solar power tree a new invention of installing PV modules on a tall pole like structure with leaf like branches surrounding it following a pattern of spiraling Phyllotaxy as found in a natural tree. Solar tree is a revolutionary urban lighting concept as it satisfies all environmental, social, cultural and aesthetic demands. It represents solar energy technology in an artistic way.

HISTORY OF SOLAR TRE

In 1998 a number of sculptural structures incorporating solar photovoltaic cells had been erected among which a solar tree of capacity 7KW was presented by Gleisdorf, Austria. After that **Ross Lovegrove** designed a solar tree based on shape of coconut tree. His tree design consisted of steel pipes of height 5.5meter supporting a light bubble in which 38 solar cells of 38watt capacity each was connected to a 12v hidden battery system. And 1 watt Led's of different color was installed on tip of bubble. In this design the solar tree panels charged batteries during the day and at dusk it automatically switched on its Led's. The internal control was used to regulate amount of light produced according to the availability of charge left in batteries. In 2007 Lovegrove received Vogue Traveler Ecology Prize for his work with Solar Tree. **Milos Milisavljevic (2010)**, founder of 'The Strawberry Energy' a Serbian company, invented a solar tree specifically to charge mobile devices and installed it in the main park of Obrenovac municipality, Serbia. Its main parts were solar panels, rechargeable batteries which could make tree function for 14 days without sunshine, 16 cords for different type of mobile devices and small electronics which maintained balance between produced and consumed energy. **Asai Yuji** and **Toshiaki Yachi (2010)** presented a research paper in which they proposed a design of solar PV modules assembled three-dimensional structure which enabled more efficient conversion of limited amount of solar light using low cost solar cells. The proposed PV modules were tree shaped. Using simulation method they showed that these modules produce more electricity as compared to panels arranged in a conventional way. This solar tree design maximizes power generation per installation area and uses the solar energy effectively. **Aidan Dwyer (2011)** proposed a solar tree design during his research on the patterns of natural trees. He found that leaves and branches follow a specific pattern due to which they avoid shade from each other and find maximum sun exposure. This pattern is termed as Fibonacci pattern which was first discovered by Leonardo of Pisano while solving a math puzzle. Aidan's tree was based on this pattern and he claimed that this solar tree was more efficient as compared to conventional panel of same rating. **Marco Bernardi. *et al.* (2012)** proposed a paper in which they formulated the problem of PV based power generation in three-dimensions. This paper showed that 3DPV structures (Solar tree) could be realized practically and could improve solar energy generation as compared to flat panel. They concluded that 3DPV structures could use more number of hours per day for solar energy generation as well as might be enabled the design of sunlight concentrators using mirror. **V. Avdic. (2013)** proposed a paper which elaborated the possibility of building a solar tree in Sarajevo. Goal of this project was to achieve satisfying outcome which include multifunctional role (street light, mobile, laptop charging etc.), durability, aesthetically, economical and ecological acceptable. And to harness solar energy in an optimum manner various designs of solar tree are being proposed and solar tree has become a field of great research.

CONSTRUCTION AND WORKING OF SOLAR PANEL

Main important parts solar tree include in its design are Solar Panels, Batteries, LEDs, Batteries, Long Tower and Stems for connecting solar panels. Batteries are charged during the day and at dusk LEDs are automatically switched on and indicate how much energy is left. Batteries are used to store the energy so that it can be used in the night time and also during cloudy days.

ADVANCED SOLAR TREE

Fibonacci sequence: - Leonardo of Pisano developed the Fibonacci sequence that is given by Fn=Fn-1 + Fn-2. In this pattern next number in sequence is the result of sum of two previous numbers. In this sequence ratio of each number to its previous number settles to a value called Golden Ratio and is equal to 1.618034. This type of sequence is found in Oak tree, Elm tree, Almond tree etc. A naturalist Charles Bonnet observed that plants sprout their branches and leaves in a Fibonacci pattern such that leaves above do not hide below leaves and each gets a good share of sunlight. This whole arrangement is termed as Phyllotaxis and can be shown in fig. (a).

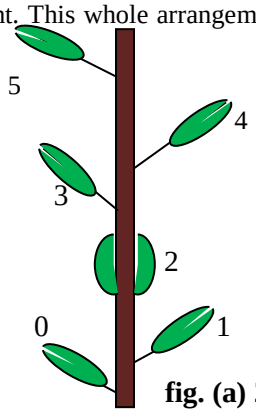

fig. (a) 2/5 phyllotaxis

Design of Advanced Solar Tree: - Design of this Solar Tree is based on the design of Oak tree. It is called advanced because as compared to other design this design is more efficient as solar panels used in this follow Fibonacci pattern. On the Oak tree Fibonacci

pattern is 2/5 which means that spirals cover 5 branches to spiral two times around the trunk to complete one pattern. Following this pattern Solar Panels are placed in different directions and thus receive solar energy during whole day time. This pattern places each Solar Panel in an optimum position so that each panel can receive maximum solar energy and also avoid shade from each other. Fibonacci pattern collects more sunlight when sun is at low angle and is extremely useful in winter season and in extreme latitudes.

SOLAR TREE IS BETTER THAN CONVENTIONAL PV TECHNOLOGY

Solar tree is better than conventional pv technology in several manners as it requires less land comparatively (requires 1% land as compared to conventional method). Solar tree can generate electricity very efficiently due to spiral phyllotaxis technique (one stem at each node) resulting into Fibonacci pattern. Solar tree also can collect energy from wind by making stems of tree flexible so that they can rotate in any direction and can produce electricity by shaking themselves. Solar tree uses the maximum hour of sunlight during whole day time comparatively as solar panels used in this capture sunlight in different directions. There are so many other advantages which proof solar tree is better than conventional pv technology to capture sunlight.

Disadvantages of Solar tree:-

- Installation cost is high.
- Hazards to eyesight from solar reflectors as well as may cause hazards to birds and insects.

CONCLUSION

As Solar PV technology for generating electricity is conventional as compared to Solar Power Tree technology hence it is widely adopted but solar power tree is a new method of generating electricity in more efficient way and it also overcomes the drawbacks of conventional method. It is the best option for generating maximum electricity using minimal land.

REFERENCES:

[1] Albert Einstein " On a heuristic point of view concerning the production and transformation of light, Annalen der Physik 17:132-148, 1905

[2] G.Pearson & J.Bardeen "Electrical properties of pure Silicon and Silicon containing alloys containing Boron and Phosphorus" , Phys Rev, vol.75: 865-83, 1949

[3] Stephen Douady and Yves Couder " Phyllotaxis as a physical self organized growth process", Physical review letter, vol.68, no.13: 2098-2101, March 30th, 1992

[4] Stephen Douady and Yves Couder "Phyllotaxis as a self organized growth process", Growth patterns in physical science and biology NATO ASI SERIES vol.304, New-York, Springer-US. pp. 341-352, 1993

[5] Adler,D.Barabe and R.V.Jean " A history of the study of phyllotaxis", Annals of Botany 80: 231-244, 1997

[6] T.Jenkins "A brief history of semiconductors", Phys Educ, vol.40,no.5: 430-439, 2005

[7] Vesselinka Petrova-Koch, Rudolf Hezel, Adolf Goetzberger "High efficient low cost Photovoltaic: Recent developments", Springer. pp. 1, ISBN-number 978-3-540-79358-8, 2009

[8] Lenling Zeng and Guozhao Wang " Modeling golden section in plants", Progress in natural science, vol.19, no.2: 255-260, 2009

[9] Asai Yuji and Toshiaki Yachi "A novel photovoltaic module assembled three-dimensional", 35th photovoltaic specialist conference (PVSC), Honolulu, HL, IEEE. pp. 002811-002816, June 20th-25th ,2010

[10] Marco Bernardi, Nicola Ferralis, Jin H. Wan, Rachelle Villalon and Jeffrey C. Grossman " Solar energy generation in three dimensions", Energy and environmental science, (5):6880-6884, March 8th ,2012

[11] S.N.Maity "Development of Solar Power Tree- An innovation that uses up very less land and yet generates much more energy from the sun rays by SPV method". Journal of Environmental Technology, 2: 59-69, 2013

[12] Anna Grigas "The Fibonacci Sequence: Its history, significance and manifestation in nature", Thesis, Graduation Honors program Liberty University, United States, 334p, 2013

[13] American physical society, US, APS News, This Month in Physics History, Bell labs demonstrate the first silicon solar cell. vol.18, no.4, April 2009. www.aps.org

International Journal of Engineering Research and General Science Volume 3, Issue 3, Part-2 , May-June, 2015
ISSN 2091-2730

SELECTION OF SUITABLE AREA FOR AUTOMOBILE MANUFAFCTURING HUB IN ANDHRA PRADESH STATE

Sreenivasulu Reddy .A [1], Venkataramaiah .P [2], Ram Madhav .K [3]

Department of Mechanical Engineering, S.V University, Tirupati, Andhra Pradesh, India.

E-mail: seetharamadasubcm@gmail.com [1]; pvramaiah@gmail.com [2]; kram.madhav@gmail.com [3]

Abstract—This paper presents the selection of suitable area for automobile manufacturing hub by considering several criteria's such as location, land, labour, raw materials, manufacturing resources, transport, social and environmental conditions [2]. Analytical Hierarchy Process is employed for the selection procedure in finding a best area to establish an automobile manufacturing hub by taking four potential locations in Andhra Pradesh state namely Kurnool, Vijayawada, Nellore and Visakhapatnam. It is found that Nellore is the suitable location for establishing an automobile hub. The ranking evaluation will provide good guidance for the location selection of automobile manufacturing hub to the any industrialist.

Keywords— Automobile Hub, AHP, Eigen vectors, Consistency Index, Consistency Ratio, Random Consistency Indices

(1) INTRODUCTION

An industrial hubs refers to a geographically proximate group of interconnected industries and related governmental institutions in a particular locational area. It is an outstanding location which provides direct road and rail access to main transportation networks [3]. It is an area zoned and planned for the purpose of industrial development and to specifically promote sectors such as information technology and information technology enabled services, biotechnology, agro, marine, food processing, tourism, textiles and automotive industries. Connections among different hubs are provided through industrial corridors [4].

Fig. 1.1. Andhra Pradesh State

For Example, Andhra Pradesh state have potential industrial benefits and it is the market brimming with opportunities like, plenty of natural resources, second largest mineral store house of India, large scale of agriculture and horticulture production, second longest

coastal corridor in India 972 kms, excellent infrastructure facilities, greenfield seaports and best power plants [5]. The A P government provides many special economic zones based on tax free industrial zones. It is the fastest growing base for IT and telecom sectors. A P state is the largest producer of cotton, vaccine, bulk drugs, paper, iron, steel, cement and food processing industries. Recent developments of Andhra Pradesh state, a need arises extensively to promote industrial investments. This paper is to provide suitable location for automobile industrial hub in Andhra Pradesh state.

(2) TYPES OF INDUSTRIAL HUBS:

Generally Industrial hubs are classified into two types, namely general purpose industrial hubs and functional industrial hubs.

2.1. General Purpose Industrial hubs

In this type of industrial hubs, different types of industries are encouraged except hazardous and highly polluting industries. The bulk of industries belong to this category.

2.2. Functional Industrial hubs

In this type of industrial hubs, only homogenous type of industries are encouraged. For example, only computer software industries are allotted in Hi-tech city at Hyderabad.

Industrial hubs having benefits like attractive business climate, accelerated investments in the state, increased infrastructure projects, increased economic growth, reduce regional disparities, attracts domestic as well as foreign investors, provides employment generation in the state and increases exports [5].

(3) FLOW CHART FOR SELECTION METHODOLOGY

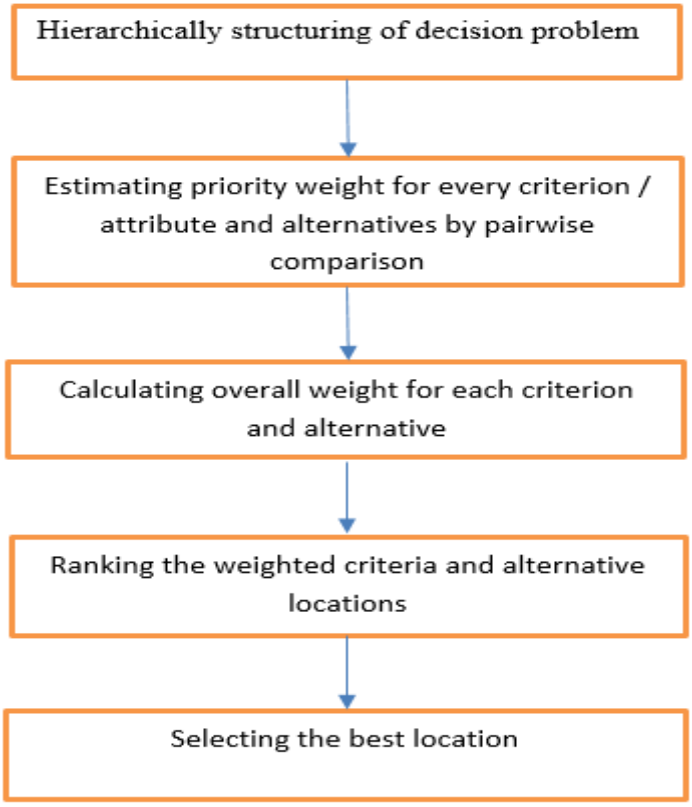

Fig. 3.1. Flow chart

(4) PROBLEM DESCRIPTION

It involves building the AHP hierarchy model. The developed AHP model, based on the identified criteria, contains four levels: such as the goal, the criteria's, sub-criteria's and generation of alternatives. Fig. 4.1 shows an illustrative four-level hierarchy for the industrial hub location selection. The goal is to select the suitable location in Andhra Pradesh for the automobile industrial hub. It is identified in the first level. The second, third and fourth level comprises of 8 criteria's, 24 sub-criteria's and 4 locational alternatives respectively as shown in the Fig. 4.1.

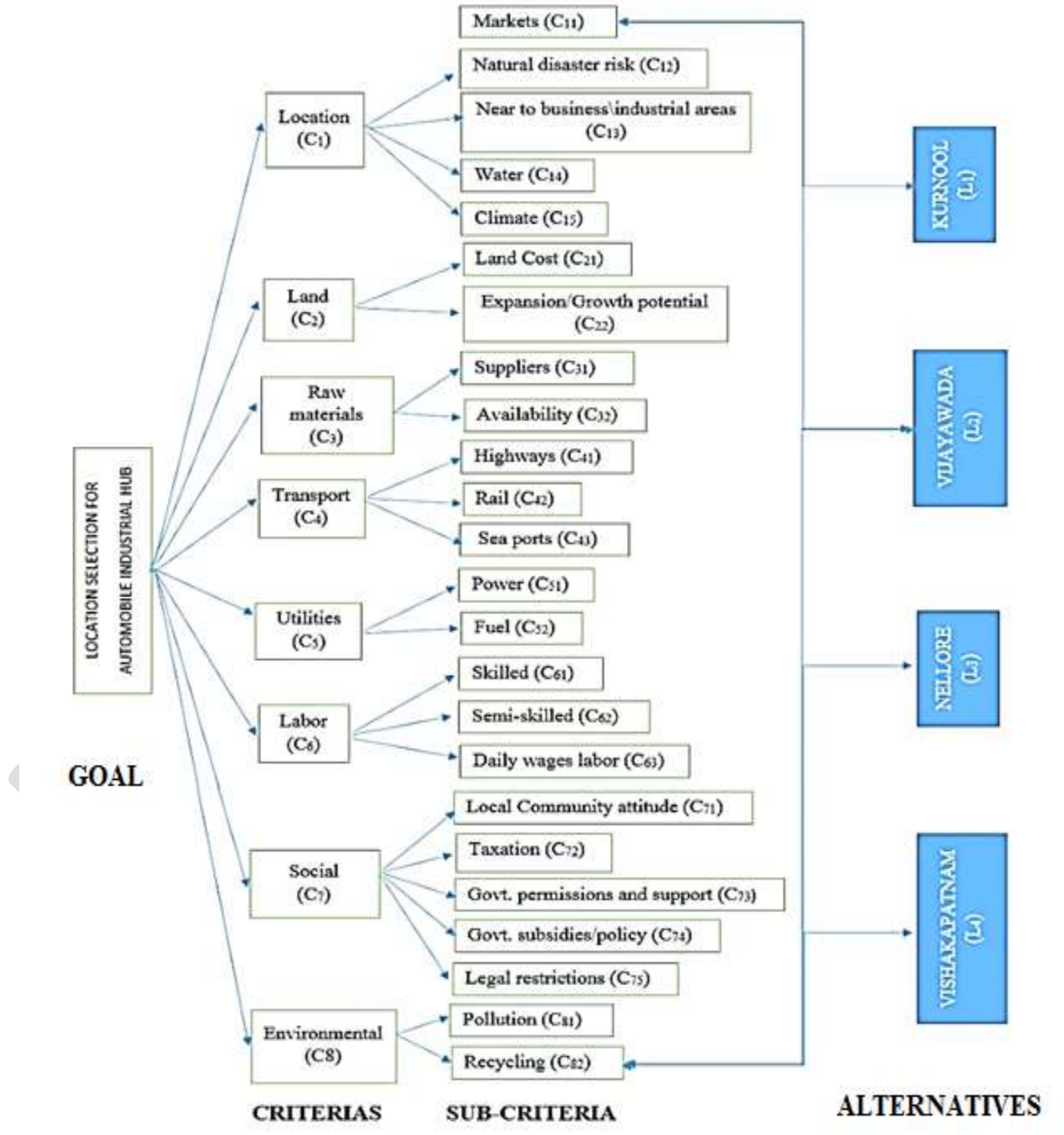

Fig. 4.1. Levels of parameters for automobile industry

4.2. Evaluating the Alternatives with Respect to Criteria's:

Step 1: Formulation of pair wise comparison matrix of criteria using AHP measurement scale is shown in Table 4.1.

Table 4.1. AHP measurement scale

Intensity of importance	Definition	Explanation
1	Equally preferred	Two activities contribute equally to the Objective
3	Moderately preferred	Experience and judgment slightly favor one activity over another
5	Moderately Strongly preferred	Experience and judgment strongly favor one activity over another
7	Very strongly preferred	An activity is favored very strongly over another; its dominance demonstrated in Practice.
9	Very strong and Extremely preferred	The evidence favoring one activity over another is of the highest possible order of affirmation
2,4,6,8	For compromise between the values	Sometimes one needs to interpolate a compromise judgment numerically because there is no good word to describe it
1/3,1/5,1/7,1/9	Reciprocals of the above quantities	If activity 'i' has one of the above quantity assigned to it when compared with activity `j' then j has reciprocal value when compared with 'i'

Table 4.2. Comparison Matrix of Criteria:

CRITERIA	C_1	C_2	C_3	C_4	C_5	C_6	C_7	C_8	Priority vector (PV)
C_1	1	2	2	2	2	2	2	2	0.2129
C_2	1/2	1	2	2	1	2	2	2	0.1679
C_3	1/2	1/2	1	1	2	2	2	2	0.1414
C_4	1/2	1/2	1	1	2	1	1	1	0.1087
C_5	1/2	1	1/2	½	1	1	2	1	0.1029
C_6	1/2	1/2	1/2	1	1	1	1	1	0.0890
C_7	1/2	1/2	1/2	1	1/2	1	1	2	0.0935
C_8	1/2	1/2	1/2	1	1	1	1/2	1	0.0836
COLUMN TOTAL (T_i)	4.50	6.50	8.00	9.50	10.50	11.00	11.50	12.00	

Step 2: Eigen vectors (E.V) are computed for the above matrix to obtain good approximation of priorities using geometric mean method. This is done by multiplying the elements in each row and taking their *n*th root. Where n is number of criteria.

E.V for $C_1 = \sqrt[8]{(1 \times 2 \times 2 \times 2 \times 2 \times 2 \times 2 \times 2)} = 1.8340$

(Similarly calculate the Eigen Vectors values up to C_8)

TOTAL (sum of E.V values) = 1.8340 + 1.4142 + 1.2968 + 0.9170 + 0.8408 + 0.7711 + 0.7711 + 0.7071 = 8.5521

Calculation of Priority Values (P.V) $= \frac{\text{Eigen vector value}}{\text{Total sum of Eigen Vectors}}$

P.V for $C_1 = \frac{1.8340}{8.5521} = 0.2144$

(Similarly calculate the Priority Values up to C_8)

Step 3: Calculation of Principal Eigen value multiplying the column totals with the respective P.V of each row and then adding the results to obtain Principal Eigen value where

T_i = column totals $P.V_i$ = priority vector of each criteria

$\lambda_{max} = \sum_{i=1}^{n} Ti \times P.V_i$

$= 4.50\times0.2144 + 6.50\times0.1653 + 8\times0.1516 + 9.50\times0.1072 + 10.50\times0.0983 + 11\times0.0901 + 11.50\times0.0901 + 12\times0.0826$

$= 8.3210$

Step 4: Calculation of Consistency Index (C.I) Then consistency index is calculated using following equation we get

Table 4.3. Random Consistency Table

Size of matrix	1	2	3	4	5	6	7	8	9	10
Random consistency index	0	0	0.58	0.9	1.12	1.24	1.32	1.41	1.45	1.49

$$C.I = \frac{(\lambda_{max} - n)}{n-1} = \frac{(8.3210 - 8)}{(8-1)} = 0.045$$

Step 5: Random Consistency Indices (R.I) is then determined for each of the square matrices using formula from the Table 4.3. R.I = 1.41

Step 6: Calculation of Consistency Ratio (C.R)

C.R is obtained by dividing CI with R I for the same size matrix and the random consistency number is chosen from Tables. In this case R.I is 1.41 as the size of matrix is eight. The value of C.R should be around 10% to be acceptable.

$$C.R = \frac{C\,I}{R\,I} = \frac{0.045}{1.41}$$

Hence the C.R is less than 10%; therefore the pair wise comparison matrix is acceptable and the weightages for output responses as follows.

Step 7: Pairwise comparison matrices (D_i =1, 2 . . . n) for each criteria's are constructed. AHP scale is used to assign weight to these matrices. The P.V values, Principal Eigen values, C.I and R.I are then computed using the same logic as in steps 5 and 6.

Comparison Matrix of Sub-Criteria's:

Table 4.4. Comparison Matrix for Location Sub-Criteria

C_1	C_{11}	C_{12}	C_{13}	C_{14}	C_{15}	(PV)
C_{11}	1	5	3	2	3	0.308
C_{12}	1/5	1	1/2	1/5	1/3	0.065
C_{13}	1/3	2	1	¼	1/2	0.111
C_{14}	½	5	4	1	2	0.332
C_{15}	1/3	3	2	1/2	1	0.18
TOTAL	2.36	16	10.56	3.95	6.83	

Table 4.5. Comparison Matrix for Land Sub-Criteria

C_2	C_{21}	C_{22}	P V
C_{21}	1	7	0.8750
C_{22}	1/7	1	0.1250
TOTAL	1.1429	8	

Table 4.6. Comparison Matrix for Raw Material Sub-Criteria

C_3	C_{31}	C_{32}	P V
C_{31}	1	5	0.8333
C_{32}	1/5	1	0.1667
TOTAL	1.2	6	

(Similarly calculate comparison matrices between all the criteria's and sub-criteria's i.e. C_4, C_5, C_6, C_7 and C_8 using Table 4.1)

Comparison Matrix between Locations

Table- 4.7 comparison matrix between c_{12} and location

C_{11}	L_1	L_2	L_3	L_4	P V
L_1	1	1/4	1/3	1/8	0.0750
L_2	4	1	1/3	1/2	0.1945
L_3	3	3	1	1	0.3640
L_4	5	2	1	1	0.3625
TOTAL	13	6.25	2.6667	2.7	

Table 4.8. Comparison Matrix between C_{12} and Locations

C_{12}	L_1	L_2	L_3	L_4	P V
L_1	1	2	1	3	0.3472
L_2	1/2	1	1/3	1	0.1423
L_3	1	3	1	3	0.3829
L_4	1/3	1	1/3	1	0.1276
TOTAL	2.8333	7	2.6667	8	

Table 4.9. Global Matrix

CRITERIA	P V	SUB CRITERIA	P V	L_1	L_2	L_3	L_4
C_1	0.2129	C_{11}	0.308	0.0790	0.1945	0.3640	0.3625
		C_{12}	0.065	0.3472	0.1423	0.3829	0.1276
		C_{13}	0.111	0.0967	0.2516	0.5549	0.0967
		C_{14}	0.332	0.1896	0.0893	0.2328	0.4883
		C_{15}	0.180	0.1838	0.0485	0.3637	0.4040
C_2	0.1679	C_{21}	0.8750	0.1475	0.0611	0.4113	0.3800
		C_{22}	0.1250	0.1140	0.2734	0.3846	0.2280
C_3	0.1414	C_{31}	0.8333	0.3151	0.0648	0.2676	0.3522
		C_{32}	0.1667	0.1514	0.0789	0.5162	0.2535
C_4	0.1087	C_{41}	0.2395	0.2420	0.3690	0.1554	0.2336
		C_{42}	0.6232	0.2505	0.4214	0.2014	0.1260
		C_{43}	0.1373	0.1306	0.4495	0.1691	0.2508
C_5	0.1029	C_{51}	0.9000	0.0790	0.1945	0.3640	0.3625
		C_{52}	0.1000	0.2166	0.4786	0.1083	0.1966
C_6	0.0890	C_{61}	0.6333	0.1584	0.4775	0.2544	0.1097
		C_{62}	0.2605	0.0996	0.5021	0.2296	0.1687
		C_{63}	0.1062	0.3359	0.2734	0.1487	0.2421
C_7	0.0935	C_{71}	0.5028	0.1175	0.4288	0.2644	0.1894
		C_{72}	0.2602	0.0485	0.1631	0.5554	0.2330
		C_{73}	0.1344	0.14419	0.10013	0.58874	0.16693
		C_{74}	0.0678	0.48498	0.08019	0.2875	0.14726
		C_{75}	0.034	0.1109	0.4642	0.1205	0.3042
C_8	0.0836	C_{81}	0.8000	0.5368	0.1013	0.1049	0.2568
		C_{82}	0.2000	0.6311	0.1046	0.0849	0.1792
TOTAL WEIGHTAGE				0.2171	0.2421	0.2964	0.2439

(Similarly calculate comparison matrices between all the sub-criteria's and locations i.e. C_{13}, C_{14} and soon

Table 4.10. Priority Order

LOCATIONS		WEIGHT	RANK
L_1	(Kurnool)	21.7	4
L_2	(Vijayawada)	24.2	3
L_3	(Nellore)	29.6	1
L_4	(Vishakhapatnam)	24.3	2

up to C_{82} using Table 4.1. all the calculated P.V values are tabulated in the global matrix and summarised to find the final weightage of locations)

From Table 4.10 The highest total weight of the location (L_3) shows that it is the best location out of all considered locations i.e., Nellore is the suitable location to make it as automobile hub in the state of Andhra Pradesh.

(6) CONCLUSIONS

AHP is used to identify the suitable area for automobile manufacturing hub in Andhra Pradesh state. The ranking order of the locations are Nellore, Vishakhapatnam, Vijayawada and Kurnool. It is observed from the results that Nellore is the best suitable location for an automobile manufacturing hub with highest weightage of 0.2964. This work will give a clear view for domestic and foreign investors to select a suitable area in Andhra Pradesh state. This work is useful to attract MNC's (Multinational Companies) and Local automobile industries to establish companies.

(7) REFERENCES

[1]. Tahriri F. and Osman M. R. "AHP approach for supplier evaluation and selection in steel manufacturing company", (2008) Pp. 2-3
[2]. Sriniketha .D "Plant location selection by using MCDM methods" 2248-9622, Vol. 4, Issue 12 (Part 1), December 2014, Pp. 4-5.
[3]. Saaty T. L. "How to Make a Decision: The Analytic Hierarchy Process", vol.2 no.1 1990, Pp. 12-19.
[4]. Tuzmen semih & Sipahi seyhan "A Multi-Criteria Factor Evaluation Model for Gas Station Site Selection" Volume 2, Number 1 July 2011, Pp.14-19.
[5]. Mehmet akalin, gulden turhan, azize sahin "The Application of AHP Approach for Evaluating Location Selection Elements for Retail Store: A Case of Clothing Store" vol.2 no.4, ISSN: 2147-4478, 2013, Pp. 47-56.
[6]. Hamid ebadi, roozbeh shad, mohamad javad valadanzoej, alireza vafaeinezhad "Evaluation of Indexing Overlay, Fuzzy Logic and Genetic Algorithm Methods for Industrial Estates Site Selection in GIS Environment."1993, Pp 18-15.
[7]. Theo K. Dijkstra "The Extraction of Weights from Pairwise Comparison Matrices." vol.2 no.5, April 6, 2010, Pp. 4-5.
[8]. Eylem Koçand Hasan Arda Burhan "An Application of Analytic Hierarchy Process (AHP) in a Real World Problem of Store Location Selection" vol. 5, no.1, 2015, Pp. 41-50.
[9]. Sihle mkhize and lindokuhle sibiya "Industrial Economic Hubs & Special Economic Zones" vol.2 no.12, 30 April 2013, Pp. 12-14.
[10]. Melvin Alexander, Social Security Administration, Baltimore, "MD Decision-Making using the Analytic Hierarchy Process (AHP) and SAS/IML" vol.2 no.3, 2012, Pp. 25-28.
[11]. Dalalah D, Al-oqla F and Hayajneh M. "Application of The Analytic Hierarchy Process (AHP) In Multi- Criteria Analysis of the Selection of Cranes" vol.2 no.3 2010, Pp. 45-51.
[12]. Ajith Abraham "AHP-Based Micro and Small Enterprises' Cluster Identification" vol.2 no.4, 2003, Pp 3-4.
[13]. Locating Urban Transit Hubs: A Multi-criteria Model and Case Study in China vol.2 no.12, 2011, Pp 4-10.
[14]. Mehrdad Hadipour and Maryam Kishani "Environmental Location Planning Of Industrial Zones Using AHP and GIS in Arak City, Iran" vol.2

no.4, August 2014, Pp. 12-14.

[15]. Athakorn Kengpol, Piya Rontlaong, Markku Tuominen "A Decision Support System for Selection of Solar Power Plant Locations by Applying Fuzzy AHP and TOPSIS: An Empirical Study" vol.2 no.4, September 2013, Pp. 7-9.

[16]. Davood Feiz, Hamidreza Tazikeh Miandareh and Mahdi Rohollahi "Identification of Industrial Clusters in Golestan Province Iran (Case: Industrial Estates of Golestan Province, Iran)" Vol. 3 Issue 6, June 2014, Pp. 4-5.

[17].Dalalah, D., AL-Oqla, F., and Hayajneh, M. (2010) "Application of the Analytic Hierarchy Process (AHP) in Multi-Criteria Analysis of the Selection of Cranes" Jordan Journal of Mechanical and Industrial Engineering, Pp. 567 – 578.

[18]. Chan, F. T. S., Kumar, N. (2007) "Global supplier development considering risk factors using fuzzy extended AHP-based Approach" International Journal of Management Science, Pp. 417-431.

International Journal of Engineering Research and General Science Volume 3, Issue 3, Part-2 , May-June, 2015
ISSN 2091-2730

Mobile Charger Based on Radiation Recycle Technology

Abhijeet Daigavane, Prof Kishor G. Sawarkar

MCT's Rajiv Gandhi Institute of Technology, Mumbai India

E-mail- abhijeet.daigavane@gmail.com

Contact No- +91-7709170976

Abstract— The invention comprises of conserving the energy by means of the simple yet, ingenious circuit .The power wasted in the transmission of the Electromagnetic signals is not judiciously used and is hence, wasted. And so, with the help of this circuit and the unique multiband antenna electricity can be generated from the signal radiations present in the atmosphere.
In addition to that, minimizing the radiations using array of such circuits can protect the areas hit by the ill effects of the signal radiations.

Keywords— Radiation, electricity generation, multiband antenna, voltage standing wave ratio.

INTRODUCTION

With the boom in the telecom industry, the atmosphere contains more signal radiations than the oxygen! But not all the frequency modulated radiated signal is used by the operator. Much of the power remains unused and is hence, wasted. In this project using the simple yet ingenious circuit, the Fm radiated signal present in the atmosphere is converted into the direct current signal and hence, the terminal acts as a constant voltage source. With this circuit, the energy can be harvested and can be utilized for different purposes.

The circuit comprises of auto stabilizing module that makes it completely independent and hence, no external power source is required to operate the circuit.

OBJECTIVE

A.HARVESTING THE WASTED POWER

The power wasted by the cell tower in transmitting radiations can be harvested to generate descent volts of electricity by means of this circuit. There are 4.5 lac mobile towers in India and each tower transmits power of 20-Watts, continuously. But not all the power is used and hence, most of the power transmitted is wasted. This method helps us to utilize this wasted power in the form of electricity.

B.CONTROLLING THE RADIATIONS-

It's a fact that radiation norms are violated in India, as the operators don't accept the threat caused by the excess of radiations. And because of that biological disorders are found everywhere. It is noticeable that we would never spot a squirrel or a sparrow near or around the cell tower. Rather,

these two species are on the verge of extinction. Also nowadays, the cases of cancers have increased. The amount of radiations can be controlled using this method. Hence, the threat of extinction of sparrows and squirrels and cases of various cancers can be minimized.

C.GETTING A CONSTANT VOLTAGE SOURCE

The method employed here absorbs the FM radiations and as a by-product gives out some volts of electricity. Thus, this voltage source can be freely made available using the circuit. With this, many applications can be run for free. This is again an eco-friendly way to run the electronic applications.

By having array like structure of this circuit, large volts can be generated.

D.CONSERVING ENERGY

Energy conservation is the utmost call of an hour. In other words, researches are constantly done so as to have newer, greener, non-conventional sources of energy.

Conventional sources of energy are easy to use but they cause a lot of pollution. And so, they are posing a great threat to our planet by depleting the ozone layer. The above-mentioned method helps in conserving the energy by using the present radiations in the atmosphere and harvesting the same to get the electricity.

PRIOR ART

The technology available to generate wireless electricity is not in use because of the heavy losses that take place in transmission and reception. It deals with the inductive couplers and the 'TESLA' coils.

Also, the available wireless mobile chargers are not exactly wire free because of the condition, which compels the user to place his cell phone over the charging pad, which is ultimately connected to the power source. This is nothing but inductive coupling, which again incurs losses. By using this technique, we need not to transmit any power, rather, the power wasted in transmitting the mobile radiation, which is not completely utilized is harvested! Also, the areas hit by the excess of radiation and its ill effects can use it to control radiation levels and generate electricity by the same.

TECHNOLOGY USED

Basic components are being used. The list of components includes germanium diodes, electrolytic capacitors, ceramic capacitors and a multiband antenna. Germanium diodes help in forward biasing at merely low voltages; ceramic capacitors are used for radio reception and electrolytic for charge storage. Last but not least, the multiband antenna receives signals in the range of 870-960 MHz (GSM) and 1710-2480 MHz (3G and Wi-Fi).

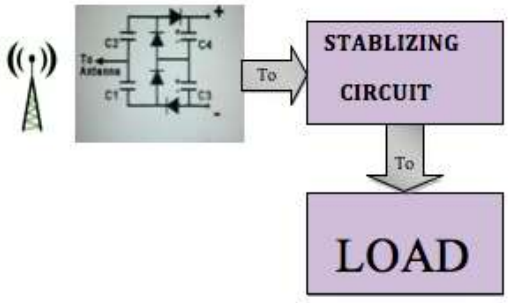

Figure 1 - System block diagram

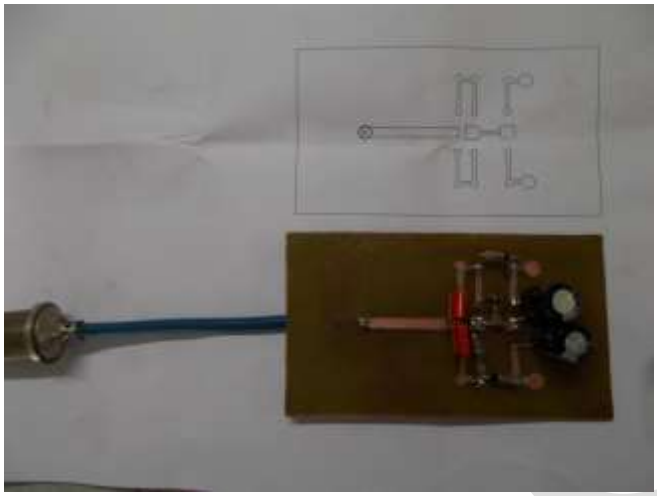

Figure 2 - Rectifier Circuit (1:1 representation)

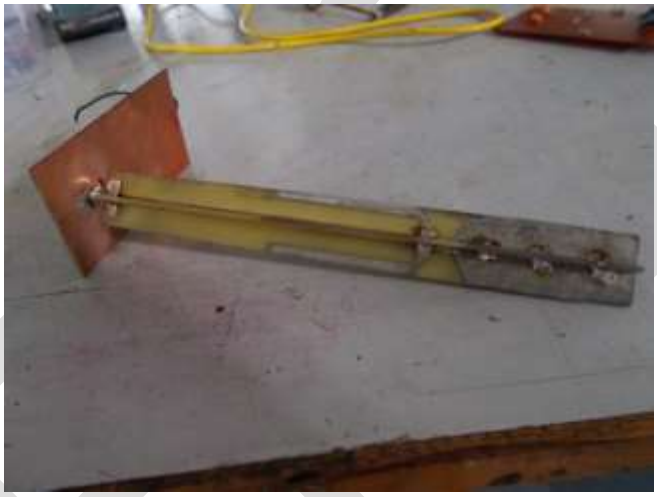

Figure 3 – Antenna mounted circuit

WORKING

The circuit is designed so that the impedance is matched with the designed antenna. Both of their impedances are nearly equal to 1.7 and are properly matched. Broadly, two separate circuits were designed: 1. Cell phone dependent circuit, 2. Independent circuit (with antenna). Now, the working of circuit one is very simple; just have to use the cell phone as the power source and place it very close to the circuit. Now, when the call is made or is received the voltage is developed and the charge can be stored. The voltage developed totally depends upon the cell phone used as the source, since, different phones emit different amount of energies.

THEORETICAL CALCULATION

For Antenna:

At 900MHz;

Reflection coefficient (S_{11}) = {(VSWR-1)/(VSWR+1)}

S_{11} = {(1.6-1)/(1.6+1)} = 0.23

Return Loss (dB) = -20log(S_{11}) = 12.76dB

Mismatch Loss (dB) = 10log(1-S_{11}^2) = -0.0026dB

And at 1.7GHz;

Reflection coefficient (S_{11}) = {(1.7-1)/(1.7+1)}

S_{11} = {(1.7-1)/(1.7+1)} = 0.26

Return Loss (dB) = -20log(S_{11}) = 11.7dB
Mismatch Loss (dB) = 10log(1-S_{11}^2) = -0.304dB

(Refer the output result for the values)

Circuit 1 calculations:
$P_r = P_t \times G_t \times G_r \times (c/(4 \times f \times pi \times R))^2$ …….Friss' Equation.
Where, P_r is the power received by the antenna, P_t is the power transmitted by the antenna, G is the gain, f is the frequency, c is the speed of light and R is the distance between two antennae.

For Antenna:

At 900MHz;

Reflection coefficient (S_{11}) = {(VSWR-1)/(VSWR+1)}

S_{11} = {(1.6-1)/(1.6+1)} = 0.23

Return Loss (dB) = -20log(S_{11}) = 12.76dB

Mismatch Loss (dB) = 10log(1-S_{11}^2) = -0.0026dB

And at 1.7GHz;

Reflection coefficient (S_{11}) = {(1.7-1)/(1.7+1)}

S_{11} = {(1.7-1)/(1.7+1)} = 0.26

Return Loss (dB) = -20log(S_{11}) = 11.7dB
Mismatch Loss (dB) = 10log(1-S_{11}^2) = -0.304dB

(Refer the output result for the values)

Circuit 1 calculations:
$P_r = P_t \times G_t \times G_r \times (c/(4 \times f \times pi \times R))^2$ …….Friss' Equation.
Where, P_r is the power received by the antenna, P_t is the power transmitted by the antenna, G is the gain, f is the frequency, c is the speed of light and R is the distance between two antennae.

So, for P_t = 20 W; G_t = 17dB = 50W; G_r = 2dB = 1.6W
Input Power at 940 MHz = 0.413mW = - 3.8 dBm
Input Power at 1840 MHz = 0.108mW = - 9.7 dBm

And output power calculated practically,
V = 0.7V, I = 0.005mA
Therefore, output power = VI = 3.5 uW = -24.55 dBm

Circuit 2 calculations:

Input Power = 1.8W = 32.5 dB (Cell Phone's output)
Output Power = 10 V x 0.05 mA = 0.5mW = -3.01 dBm

RESULT

Figure 4. POLAR PLOT of the Antenna

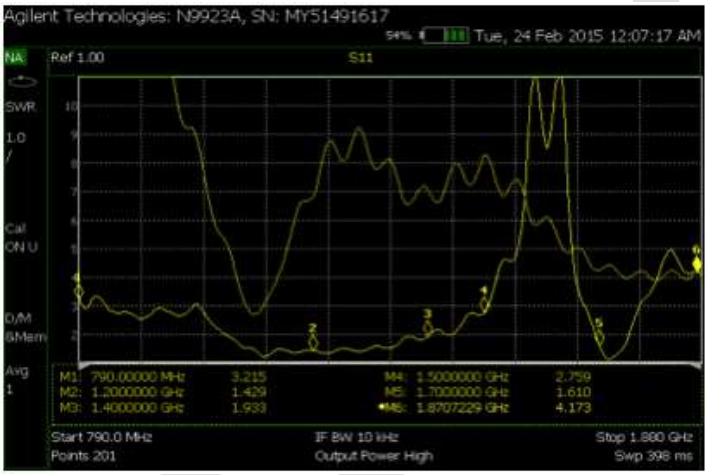

Figure 5. VSWR of the improved Generator circuit

Figure 6. VSWR of the Antenna

Figure 7. Smith CHART of the Antenna

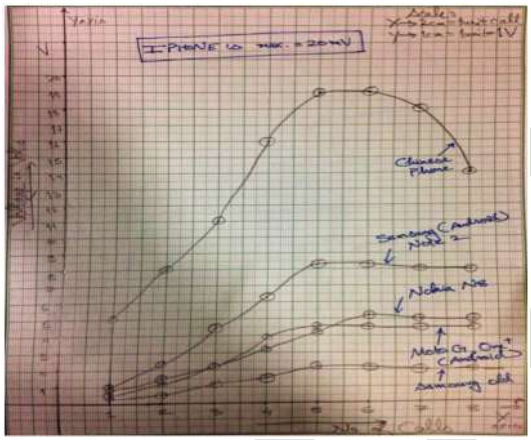

Figure 8. Final Result with the readings

CONCLUSION

Above were the results with and without having specially designed antenna. Now, there is future planning of harvesting the unused Wi-Fi signals, microwave signals, etc. On using this method broadly, the radiations can be controlled. This will help in minimizing the threats of extinction of squirrels, sparrows and human disorders like cancer. Other biological disorders like fruit bearing capacity of the trees and some human related problems can also be minimized. The power wasted by the operators can be harvested and hence, would be conserved to serve as an electricity source to run small devices and to charge mobile phones. Energy would be conserved, as people would opt for free source available to charge mobile phones or to glow couple of LEDs.

Hence, the method mentioned can be successfully used to generate electricity, detect radiation, control radiations and thus, to conserve the energy.

ACKNOWLEDGMENT

The authors wish to thank Dr. Udhav V. Bhosle, Prof. S.D. Patil, Prof. Satish Bhoyar, Dr. Shyam Karode, Prof. Mande, Prof Jayant Mahajan, and other teaching as well as non-teaching staff.

REFERENCES:

[1] •Prof. Girish Kumar, IIT Bombay "Report on Cell Tower Radiation"

[2]Web-journals:

http://www.google.co.in/url?sa=t&rct=j&q=&esrc=s&source=web&cd=2&cad=rja&uact=8&sqi=2&ved=0CCYQFjAB&url=http%3A%2F%2Fwww.cnn.com%2F2011%2FHEALTH%2F05%2F31%2Fwho.cell.phones%2F&ei=HNw6VIvxFdaJuAT1qIL4CA&usg=AFQjCNHBdT3r4ngTTOq92xfIU3C1SKdJUg&sig2=aV1N_uH2iiOMNbpNN9TbGQ

[3]Web-journals:

http://www.google.co.in/url?sa=t&rct=j&q=&esrc=s&source=web&cd=4&cad=rja&uact=8&sqi=2&ved=0CDMQFjAD&url=http%3A%2F%2Fwww.bidocean.com%2Fcellphone.php&ei=HNw6VIvxFdaJuAT1qIL4CA&usg=AFQjCNG1OZaul8Eg42z-

[4]. Nayfeh, O.M J.L. Hoyt, and D.A. Antoniadis. "Strained- Si {1 – x} Ge {x}/Si Band-to-Band Tunneling Transistors: Impact of Tunnel-Junction Germanium Composition and Doping Concentration on Switching Behavior." Electron Devices, IEEE Transactions on 56.10 (2009): 2264-2269. © 2009, IEEE.

[5] Lack of effects of 1439 MHz electromagnetic near field exposure on the blood–brain barrier in immature and young rats, Kuribayashi et al., Bioelectromagnetics, 26(7): 578-588 at http://dx.doi.org/10.1002/bem.20138

International Journal of Engineering Research and General Science Volume 3, Issue 3, Part-2 , May-June, 2015
ISSN 2091-2730

Quality of Service and Scalability in Vehicular Ad Hoc Networks

Harpreet chawla, nitin goyal

Department of computer science engineering , Seth Jai Prakash Mukand Lal Inst. Of Engg. & Tech (JMIT) Radaur
,Harpreetchawla21@gmail.com , 09996859888

Abstract— Vehicular ad hoc networks (VANETs) are expected to support a large spectrum of mobile distributed applications that range from traffic alert dissemination and dynamic route planning to context-aware advertisement and file sharing. Considering the large number of nodes that participate in these networks and their high mobility, The problem still exist about the feasibility of applications that use end-to-end multi-hop communication in Intersection Routing on City Roads when they are executed in Real-Time Vehicular Traffic. The main concern is whether the performance of VANET routing protocols can satisfy the throughput and delay requirements of such applications. From the network perspective, security and scalability are two significant challenges, whereas in a more local context, important questions arise regarding good medium access control (MAC) protocols for IVC, and how to design systems within a DSRC framework. There are essentially two ways to provide QoS for network applications: by resource reservation, and by behavior adaptation, from the application's viewpoint. When QoS is supported then the system behavior can be controlled such that requirements on several performance parameters such as delay jitter and packet loss can be satisfied.

Keywords— Vanet's, RSU, 802.11p, QOS, Throughput, Speed, computer networks

Introduction

VANETs are distributed, self-organizing link webs crafted up from voyaging vehicles, and are consequently delineated by tremendously elevated speed and manipulated degrees of freedom in nodes movement patterns. Such particular features oftentimes make average networking protocols inefficient or unusable in VANETs, and this, joined alongside the huge encounter that the arrangement of VANET technologies could have on the automotive marketplace, explains the producing manipulation in the progress of link protocols that are specific to vehicular networks. The frank believed of VANET is straightforward: seize the extensively adopted and inexpensive wireless innate span web (WLAN) knowledge that links notebook computers to every single supplementary and the Internet, and, alongside an insufficient tweaks, installed on the vehicles. Of sequence, if it were honestly that unambiguous, the alert. VANET scrutiny area should probable not ever have formed. Vehicular environment creates exceptional opportunities, trials, and requirements. If vehicles can undeviatingly converse alongside every single supplementary and alongside groundwork, a jointly new prototype for vehicle protection requests can be created. Even supplementary non-safety requests can rise road and vehicle efficiency. Second, new trials are crafted by elevated vehicle speeds and exceedingly vibrant working environments. Third, new necessities, essentialised by new safety-of-life proposition, contain new outlook for elevated packet transfer rates and low packet latency. Further, client agreement and governmental oversight hold extremely elevated expectations of privacy and security. Even nowadays, vehicles produce and examine colossal numbers of data, even though normally this data is self-collected inside a solitary vehicle. With a VANET, the 'horizon of awareness' for the vehicle or driver drastically grows. The VANET contact can be whichever completed undeviatingly amid vehicles as 'one-hop' contact, or vehicles can retransmit memos, thereby enabling 'multihop' communication. To rise coverage or robustness of contact, relays at the roadside can be deployed. Roadside groundwork can additionally be utilized as a gateway to the Internet and, therefore, data and context data can be amassed, stored and processed 'somewhere', e.g., in Cloud infrastructures. The earth of vehicular request and inter-networking technologies is established on an interdisciplinary power in the cross serving of contact and networking, automotive electronics, road procedure and association, and data and ability provisioning. VANET can consequently be perceived as an vital portion of intelligent transportation arrangements (ITS). Vehicular Ad-Hoc Web (VANET) contact has presently come to be an increasingly accepted scrutiny case in the span of wireless networking as well as the automotive industries. The aim of VANET scrutiny is to develop a vehicular contact arrangement

to enable quick and cost-efficient allocation of data for the benefit of passengers' protection and comfort. VANETs need specific networking methods alongside feasibility and performance.

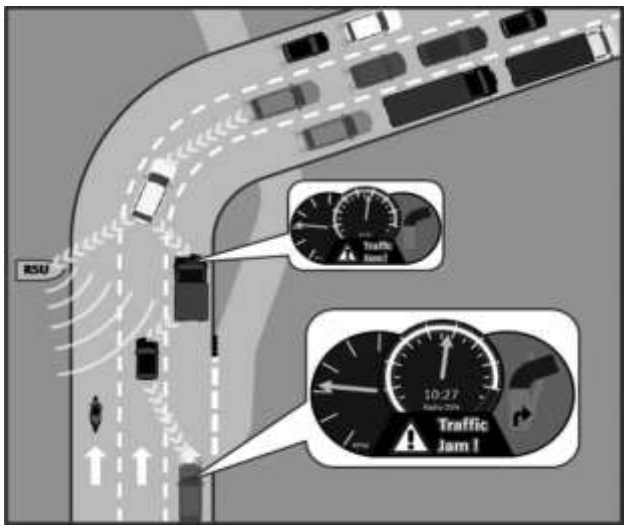

Figure1: By using vehicle-to-vehicle and vehicle-to-roadside communication, accidents can be avoided (e.g., by not colliding with traffic jam) and traffic efficiency can be increased (e.g., by taking alternative router

ii. QOS In Vanets

There are vitally two methods to furnish QoS for web applications: by resource reservation, and by deeds adaptation, from the application's view point. When QoS is upheld subsequent the arrangement deeds can be manipulated such that necessities on countless presentation parameters such as stay jitter and packet conquest can be satisfied. A number of requirements/criteria that can be utilized to difference countless QoS resolutions:Usage of disparate wireless channels for disparate kinds of applications/messages. The physical layer of the wireless technologies utilized by VANET link must to be able to use disparate wireless channels for the varied kinds of vehicular applications. In this method, specific wireless channels can be allocated for the traffic generated. Media Admission Controller (MAC) layer can prop QoS differentiation. The MAC layer of the wireless vision must to be projected in such a method that QoS differentiation is supported. In this method data memos associated alongside TSA (Traffic Protection Applications) will be able to be grasped by the MAC in a disparate method than data memos associated alongside supplementary kinds of applications. Support of an increased end-to-end throughput as accomplished fairness in bandwidth rehearse amid users. The QoS resolutions must to be projected in such a method that the end-to-end throughput associated alongside the TSAs is increased as accomplished a fair bandwidth rehearse amid TSA users. This criterion can be gratified by functionalities that could be endowed by the web, transport or appeal layers upholding the VANET communication

Achieving low latency in grasping emergency warnings QoS resolutions must to be projected in such a method that the latency of emergency notice memos is decreased. This can be accomplished by differentiating amid disparate kinds of TSA messages. TSA memos utilized for emergency warnings must to come to be a higher link and processing priority than supplementary kinds of TSA messages. QoS provisioning oftentimes instructs accord amid host and web, call admission domination, resource reservation, and priority arranging of packets. QoS can be endowed in web across countless methods as in each flow, each link, or each node. In web, the frontier amid the ability provider (network) and the user (host) is not enumerated clearly, therefore making it vital to have larger connection amid the hosts to accomplish QoS. Characteristics of web such as lack of central coordination, mobility of hosts, and minor potential of resources make QoS provisioning extremely demanding. QoS provides flexibility, scalability, efficiency, adaptability, multimedia reusability and maintainability. Agent-based schemes including of stationary or changing agents give countless gains as contrasted alongside standard plans: cut latency, works in heterogeneous nature, less web traffic, encapsulates protocols, flexibility, adaptability, multimedia reusability and maintainability, and facilitates the conception of customised vibrant multimedia infrastructure. Though, mobile agent knowledge is yet in its main period and has precise setbacks that have to be solved

III. IEEE 802.11P

IEEE 802.11p is an authorized correction to the IEEE 802.11 average to add wireless admission in vehicular settings (WAVE), a vehicular contact system. It specifies improvements to 802.11 that supports Intelligent Transportation Arrangements (ITS) applications. This includes data transactions amid high-speed vehicles and vehicles and the roadside groundwork in the licensed ITS group of 5.9 GHz (5.85-5.925 GHz). IEEE 1609 is a higher layer average established on the IEEE 802.11p.

VANETs present a challenging nature for protocol and appeal design due to their low latency and elevated data rate necessities in a elevated mobility environment. The IEEE 1609 working cluster has delineated the main edition of the protocol stack IEEE 802.11p/1609.x protocol families, additionally understood as WAVE (Wireless Admission in a Vehicular Environment). The WAVE protocols are projected for the 5.850- 5.925 GHz cluster, the Dedicated Short Scope Link (DSRC) spectrum cluster in the United States (US), understood as intelligent transportation arrangements wireless skill (ITS-RS).

Figure 2: The set of channels defined in the WAVE trial standard

This 75 MHz cluster is rip into one central manipulation channel (CCH) and six skill channels (SCH) as delineated in Fig.2. An overview of the WAVE protocol families is illustrated in Fig. 2. The IEEE 802.11p average defines the physical (PHY) and medium admission manipulation (MAC) layers instituted on preceding standards for Wireless LANs

(Local Expanse Networks). The IEEE 802.11p uses the enhanced distributed channel admission (EDCA) MAC sub-layer protocol projected instituted on the IEEE 802.11e alongside a slight modifications, as the physical layer is OFDM (Orthogonal Frequency Division Modulation) as utilized in IEEE 802.11a.

Safety demands are tremendously challenging for the design of a MAC protocol in VANETs due to their low latency (less than 100ms) and elevated reliability requirements. Countless evaluations were counseled for the 802.11p MAC protocol recently. Though, the presentation of the 802.11p MAC protocol is exceedingly modified by a slight key parameters, such as the packet size of protection related memo, the memo conception patriotic, the vehicle density, the link scope and etc. A slight of these parameters are not set properly in the present counseled evaluations. Furthermore, as uttered in , this is a momentous concern if BSMs (Basic Protection Messages) are constrained to be dispatched on the CCH across the 50ms CCH interval, as there could be hundreds of mechanisms in a given span and the encounter rate could be tremendously high. A different protection Channel 172 for protection link is additionally proposed. On the supplementary hand, the 50ms CCH interval could be too long and wasted in a low vehicle density environment. The trusted of adapting the intervals of CCH and SCH is counseled in. The CCH interval is cut in order to enhance the SCH abiility, but it is not trusted to range the CCH interval for a elevated vehicle density nature in order to cut the encounter probability. The main aim of this paper is to counsel a simulation instituted evaluation for the 802.11p MAC protocol in words of the protection demands in VANETs. Two inquiries will be addressed in this work: (i) how is the presentation of the IEEE 802.11p MAC protocol in protection demands alongside varied CCH intervals? (ii) how many vehicles can be accommodated in VANET safety applications with various CCH intervals

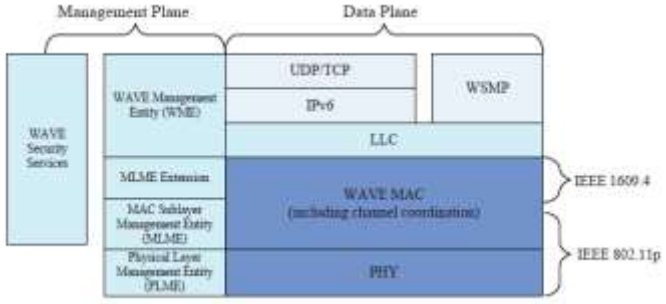

Figure3: The WAVE protocol suite

IV. PRIORITY BASED APPROACH

Figure below motivates the demand for a relevance instituted data dissemination approach. The two vehicles 1 and 2 are inside area wireless scope for merely a short era because of shadowing aftermath provoked by the encircling buildings. Vehicle 2 has countless memos in its memo queue for transmission. As it will not be able to dispatch all memos to vehicle 1 beforehand it leaves its transmission scope, it must to select the most relevant memos and consequently maximize the appeal benefit. In order to do this, it is vital to compute relevance for every single solitary memo and to rearrange the vehicle's memo queue accordingly. As well the grasp transmission, it is additionally probable to use a multi hop connection alongside vehicle 3. Though, this leads to inferior channel utilization and a higher latency.

1. The MDDV method aims at cutting overhead and memo latency by dispatching memos alongside a predefined path. Though, the method cannot differentiate amid memo kinds and it does not assess the relevance of a piece of data as selecting the consecutive memo to be sent.

2. A consecutive method to optimize channel utilization, that uses adaptation of transmission manipulation to cut interference. The scheme endeavors to allocate the manipulated resources in a fair method to enhance the dissemination capabilities. To finish this, the transmission manipulation will be cut to a precise threshold, reliant on the number of alert nodes, that ensures that the medium is not fully utilized. This enables supplementary nodes to admission the channel.

3. In our method, nevertheless, we head for a manipulated unfairness, by setting PRIORITY TO EACH MESSAGE so that resources are allocated according to data relevance. By optimizing the extent to that the innate necessities of all web associates (e.g., data rate) are encountered (utility), a globe utility maximum can be achieved. In the context of our method, the benefit of data is quantified alongside supplementary convoluted intentions that ponder the vehicle's corresponding contexts. By optimizing the medium admission innately additionally the globe design is enhanced, grasping to an finished benefit approaching the optimum. A globe optimization scheme is not feasible in this context, due to the VANET characteristics.

Two fundamental methodologies form the basis of our concept -

- First, the relevance data packets provided to potential recipients in the local neighborhood must be quantified.
- Second, the messages must be prioritized according to the resulting relevance values to maximize the benefit received by all vehicles participating in the network.

The prioritization is performed in two steps.

- First, the most relevant message within the message queue of each vehicle is selected (in-vehicle message selection). Second, the most relevant message among all vehicles that are within mutual radio range is selected for transmission (inter vehicle message selection).

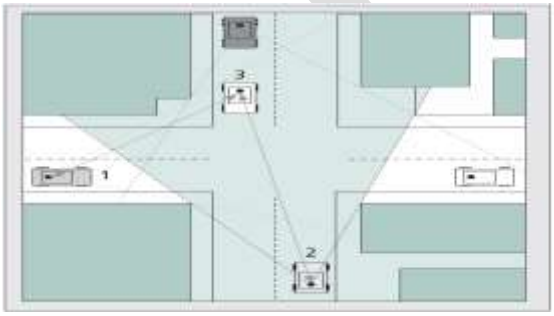

Figure 4: Exemplary vehicle-to-vehicle communication scenario

V. Proposed Work

VEHICULAR ad hoc webs (VANETs) are anticipated to prop a colossal spectrum of mobile distributed requests that scope from traffic alert dissemination and vibrant path arranging to context-aware advertisement and file sharing. Thinking the colossal number of nodes that give in these webs and their elevated mobility, The setback yet continue concerning the feasibility of requests that use end-to-end multi-hop contact in Intersection Routing on Metropolis Roads after they are gave in Real-Time Vehicular Traffic.

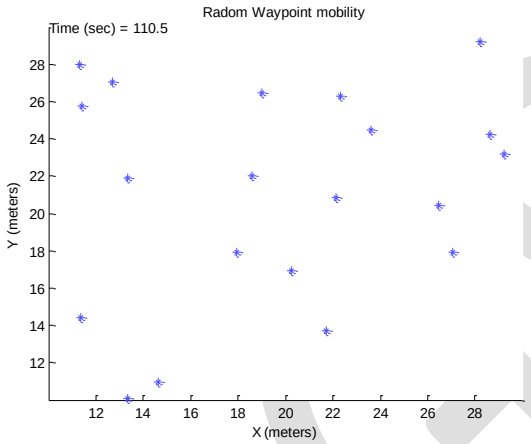

Figure 5: Existing Random Way point model is bad for VANTES

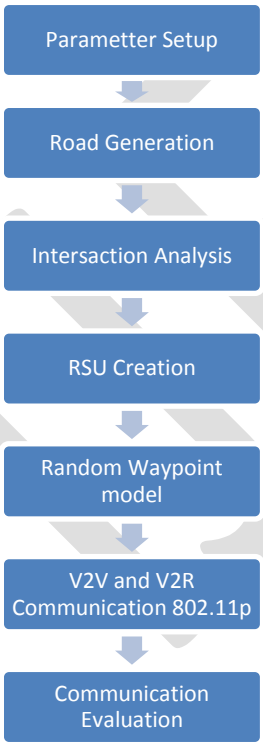

Figure 6: proposed Work Flow

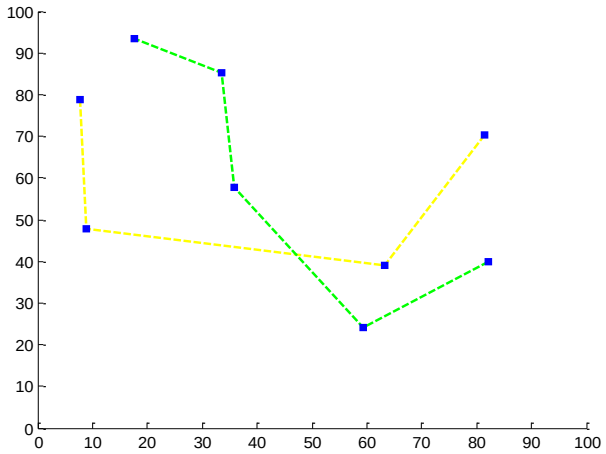

Figure 7: Creation of Two Separate Roads and Simple Car Simula

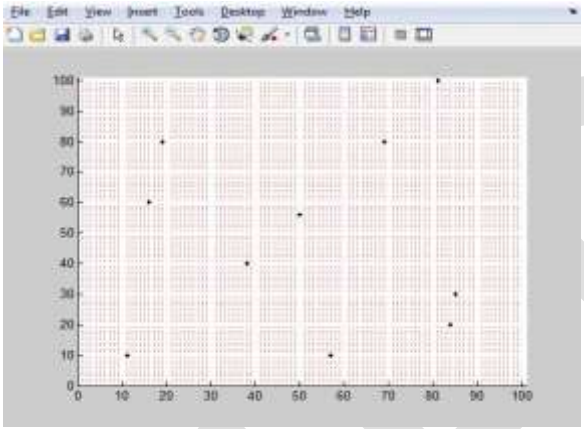

Figure 8: VANTE nodes = 10

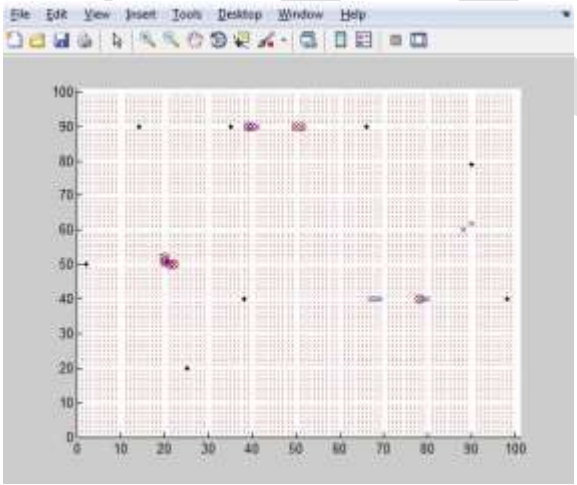

Figure 9: Collisions over the nodes in VANETS

In above Figure we have drawn two separate roads for VANET simulation, in this scenario after the roads have been drawn, two vehicles are used to test the roads. following code has been used for drawing the roads. [Draw Two Separate Roads.m]

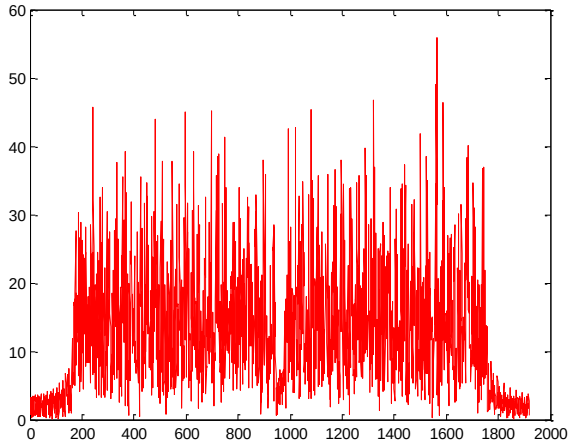

Figure 10: Packet Delivered Durin

VI. RESULTS

The simulator architecture incorporates a previously implemented vehicular traffic simulator VISSIM and two new components: VCOM, used to simulate the inter-vehicle communication on the basis of a statistical model proposed by the authors, and an application module. The simulator has to respond to specific user requirements regarding the functionality (it was aimed to investigate the impact of car-to-x communications on transport efficiency) and the performance (scalability, short response time and ease of use). The relevant characteristics of a VANET simulator are the simulation efficiency and accuracy for large scale VANETs.

VII. CONCLUSION AND FUTURE SCOPE

In VANETS vehicles converse alongside every single solitary supplementary and perhaps alongside a roadside groundwork to furnish a long catalog of demands fluctuating from transit protection to driver assistance and Internet access. In these webs, vision of the real-time locale of nodes is an assumption made by most protocols, algorithms, and applications. But due to elevated worth on road side groundwork it becomes tremendously tough to apply even metropolis expansive VANET circle. The main concern is whether the presentation of VANET routing protocols can gratify the throughput and stay necessities of such applications. Thinking the large number of nodes that give in these webs
and their elevated mobility. This work displays how Priority- instituted link scheme helps comprehend scalability by optimizing the appeal benefit and the bandwidth usage. Data . Worked immaculately below every single conditions and work as the store and onward constituent and cut a lot of above head of puny resource node that not has skill of lot of calculation and storage. A main assisting of the roads are single-lane, bidirectional, and unpaved. Meteorological conditions and topography change across the country. Also, Indian traffic conditions are chaotic, the drivers reckless, and the roads oftentimes in poor repair. In upcoming we will apply VANET intersection instituted Simulation of 802.11p VANET protocol for Indian roads and the road side data will be grabbed from Open Road MAPs

REFERENCES:

[1]. Gainaru, Ana, Ciprian Dobre, and Valentin Cristea. "A realistic mobility model based on social networks for the simulation of VANETs." In Vehicular Technology Conference, 2009. VTC Spring 2009. IEEE 69th, pp. 1-5. IEEE, 2009.
[2]. Karnadi, Feliz K., Zhi Hai Mo, and Kun-chan Lan. "Rapid generation of realistic mobility models for VANET." In Wireless Communications and Networking Conference, 2007. WCNC 2007. IEEE, pp. 2506-2511. IEEE, 2007.
[3]. Krajzewicz, Daniel, Georg Hertkorn, C. Rössel, and P. Wagner. "Sumo (simulation of urban mobility)." In Proc. of the 4th middle east symposium on simulation and modelling, pp. 183-187. 2002.

[4]. Sharma, Manish, and Gurpadam Singh. "Evaluation of proactive, reactive and hybrid ad hoc routing protocol for ieee 802.11 mac and 802.11 dcf in vanet using qualnet." CCSEA, ea DC Wyld, Ed. CS & IT-CSCP (2011): 209Ð220.

[5]. Piorkowski, Michal, Maxim Raya, A. Lezama Lugo, Panagiotis Papadimitratos, Matthias Grossglauser, and J-P. Hubaux. "TraNS: realistic joint traffic and network simulator for VANETs." ACM SIGMOBILE Mobile Computing and Communications Review 12, no. 1 (2008): 31-33.

[6]. Jaap, Sven, Marc Bechler, and Lars Wolf. "Evaluation of routing protocols for vehicular ad hoc networks in typical road traffic scenarios." Proc of the 11th EUNICE Open European Summer School on Networked Applications (2005): 584-602.

[7]. Paul, Bijan, Md Ibrahim, Md Bikas, and Abu Naser. "VANET Routing Protocols: Pros and Cons." arXiv preprint arXiv:1204.1201 (2012).

[8]. Navid Nikaein, Soumya Kanti Datta, Irshad Marecar, and Christian Bonnet. "Application distribution model and related security attacks in VANET." In 2012 International Conference on Graphic and Image Processing, pp. 876808-876808. International Society for Optics and Photonics, 2013.

[9]. Noura Aljeri, Kaouther Abrougui, Mohammed Almulla, and Azzedine Boukerche. "A Performance evaluation of load balancing and QoS-aware gateway discovery protocol for VANETs." In Advanced Information Networking and Applications Workshops (WAINA), 2013 27th International Conference on, pp. 90-94. IEEE, 2013.

[10]. Andrea Baiocchi and Francesca Cuomo. "Infotainment services based on push-mode dissemination in an integrated VANET and 3G architecture." Communications and Networks, Journal of 15, no. 2 (2013): 179-190.

[11]. Abubakar Aminu Mu'azu, Low Tang Jung, Ibrahim A. Lawal, and Peer Azmat Shah. "A QoS approach for cluster-based routing in VANETS using TDMA scheme." In ICT Convergence (ICTC), 2013 International Conference on, pp. 212-217. IEEE, 2013.

[12]. Uday Mane and S. A. Kulkarni. "QoS realization for routing protocol on VANETs using combinatorial optimization." In 2013 Fourth International Conference on Computing, Communications and Networking Technologies (ICCCNT), pp. 1-5. IEEE, 2013.

[13]. Yibo Yang, Hongling Li, and Qiong Huang. "Mobility management in VANET." In Wireless and Optical Communication Conference (WOCC), 2013 22nd, pp. 298-303. IEEE, 2013.

[14]. M. Garai and N. Boudriga. "A novel architecture for qos provision on vanet." High-Capacity Optical Network and Emerging/Enabling Technologies (HONET-CNS 2013), Cyprus (2013).

[15]. Carlos Quadros, Eduardo Cerqueira, Aldri Santos, and Mario Gerla. "A Multi-flow-Driven Mechanism to Support Live Video Streaming on VANETs." In Computer Networks and Distributed Systems (SBRC), 2014 Brazilian Symposium on, pp. 468-476. IEEE, 2014.

[16]. Fan Yang, Zhijian Lin, and Yuliang Tang. "A Traffic Flow Based Clustering Scheme for VANETs." Sensors & Transducers (1726-5479) 180, no. 10 (2014).

[17]. Nardine Basta, Amal El-Nahas, Hans-Peter Grossmann, and Slim Abdennadher. "Geo-social mobility model for VANET simulation." Journal of Mobile Multimedia 10, no. 1&2 (2014): 107-127.

[18]. Yuh-Shyan Chen, Chih-Shun Hsu, and Yi-Guang Siao. "Linear regression-based delay-bounded routing protocols for VANETs." Wireless Communications and Mobile Computing 14, no. 2 (2014): 186-199.

[19]. Kashif Naseer Qureshi and Abdul Hanan Abdullah. "Multiprotocol Label Switching in Vehicular Ad hoc Network for QoS." Information Management & Business Review 6, no. 3 (2014).

[20]. Si-Ho Cha, Min-Woo Ryu, Seok-Joong Kang, and Kuk-Hyun Cho. "Simulation of VANET on Real World Environment." (2014).

[21]. Nabeel Akhtar, S . Coleri Ergen, and Oznur Ozkasap. "Vehicle mobility and communication channel models for realistic and efficient highway VANET simulation." (2014)

[22]. Michael Oche, Rafidah Md Noor, and Ali Jalooli. "Quality of service management for IPTV services support in VANETs: a performance evaluation study." Wireless Networks 21, no. 1 (2015): 315-328

International Journal of Engineering Research and General Science Volume 3, Issue 3, Part-2 , May-June, 2015
ISSN 2091-2730

Comparison of Six Classification Techniques for Post Operative Patient data in the Medicable discipline

Chinky Gera[1], Kirti Joshi[2]

Research Scholar[1], Assistant Professor[2]

Department of Computer Science & Engineering, RIMT-IET, Mandi Gobindgarh, India

chinkygera465.cg@gmail.com[1]

Abstract— Medical databases have accrued prodigious amount of enlightment regarding patients and their medical provision. The salient techniques of medical data mining incorporating post treatment of medicative data, fast, robust mining algorithms and reliability of mining results. The contemplate of this research paper is to provide a review on mining medical dataset, problem formulation and short description of preceding research in mining medical data. The experimental upshot concludes that surface temperature of the patient is not required and shows that while comparing decision table and J48 both has outperformed.

Keywords— Classification techniques; decision table; pre-processing; J48; accuracy; medicable; weka

INTRODUCTION

Data mining is the enactment of involuntary piercing the vast reserve of data to uncover the patterns and trends that progress afar manageable analysis. Data mining is usually to explain and understand the past behavior or to predict future behavior. Data mining plays an important role in healthcare by gathering and arranging the information about various reactions. Data Mining grasps the evident future for the healthcare field to empower the systems to systematically use data and analytics to pinpoint the inefficiencies and leading practices that amend care and rebate costs. Postoperative care is awareness of the potential reactions and complications of procedure. Postoperative care appears from the recovery room and continues throughout the recovery period. Patient's care must be carried out immediately postoperatively in the hospitals. While in a recovery, patient's body temperature, oxygen saturation, blood pressure, etc. will be monitored and when patient's condition seems to be stable moved to the hospital room where post operative care still continues or released to the home based on doctor's decision. The plan of this paper is to predict appropriate classification techniques that underpin the patient's care postoperatively with good accuracy.

The paper is sorted as underneath. In Section II, depicts the problem formulation. Some recent inspection of affiliated work in the medical field of data mining has been presented in Section III. Section IV scans the experiments and results accompanied by the Post Operative Patient dataset which is mined. Finally Section V discloses the conclusion with their future scope.

PROBLEM FORMULATION

There is a need to predict the best algorithm by comparing different classification algorithms. Pre-processing is very important to consider which contains useless attributes in the Post Operative patient dataset. It is necessary to remove those useless attributes to enhance the accuracy in this research paper. This can be run by enacting a respective research of classification algorithms containing 90 instances and 9 attributes including one class attribute. [2]

LITERATURE SURVEY IN THE MEDICAL FIELD

Diverse studies have been catalogued on pursing the machine learning action for the reliability analysis and predictive analysis. In this segment, abundant papers are assessed corresponding to data mining favourable in the medical sphere. The mining of data processes contains different techniques which are doctrinal in the healthcare field. The main aim of this paper is to study the data

mining techniques which are essential for medical data mining, normally to increase the accuracy of dataset.

A survey has been conducted on the current techniques in heart disease prediction by using knowledge discovery of data mining techniques. The mechanisms of predictive data mining on same dataset divulge decision tree outruns and sometime the Bayesian technique possess alike accuracy as of the decision tree and genetic algorithm is used further enhance the accuracy to attain optimal datasets which lessen the real data size helpful in forecasting heart diseases. [4]

Data mining methods and tools are used to produce the information from medical datasets associated with breast cancer disease to lessen time and effort and to aid the specialist to predict prior disease. The model retains 93.467% precise accuracy in testing set and the training set attains 96.8%. [5]

The number of blood donors and the blood group of particular age reveal the data mining model that use actual world data has been collected from EDP department of blood bank centre which uses the J48 algorithm for classification of the donors, help blood bank owner to gather proper decisions rapidly and more precisely. The results exhibit accuracy of 89.9% rate. [6]

Various data mining techniques are utilized to boost accuracy on the breast cancer diagnosis and prognosis. The results display that decision tree is formulated as better predictor having 93.62% of accuracy on the benchmark dataset and on the SEER dataset. [7]

A Hybrid approach is used of CART classifier with feature selection as well as bagging approach is used for analyzing the various datasets related to breast cancer. Training data is tested by using 10- fold cross validation. Bagging method is used to improve the decision tree Experiments performed with the combination of cart classifier, pre-processing and bagging used to enhance the classification accuracy of selected datasets. [1]

K-means method is used for dealing with clustering of medical database. In order to raise the efficiency of mining functions, some pre-processing methods used to seize 81% of accuracy and then by applying the algorithm again 94% accuracy was acquired for data amelioration. After that with current instances (700 records) yields 97% accuracy. [8]

K-Nearest Neighbour achieves higher accuracy of 97.4% in diagnosis of heart disease patients than neural network ensemble. By applying the voting to K-Nearest neighbour could not enhance the accuracy in diagnosis of patients suffering from heart disease. [12]

The comparison of different applications of data mining in healthcare region for releasing the useful information which parade 97.77% of accuracy for the prediction of cancer and success rate of the IVF treatment estimating around 70%. Developing the relevant data mining tools in terms of the human resources and skills lessen the cost and the time. [9]

The conversion of the raw data into useful information and to assist in detecting the patterns to determine the future trends in the medicable environment. The outcome reveals that decision trees are reliable and powerful decision making method imparts high accuracy of classification and helps the specialists to validate and organize the results to test and scan the various new symptoms of diseases which are based on the data. [10]

The main concentration was on the prediction of the unrevealed primary tumors in dataset where multiclass random forest classifier is used for the classification of the multiclass dataset gives higher accuracy as compared to the binary classifiers. For imbalanced dataset, SMOTE method is used for improvement of the results of selected classifier with greater accuracy. [3]

Different classification techniques have been compared equivalent to decision tree, Bayesian classification and concepts correlated with fuzzy. In first step, the outcome unveils that training dataset is better than use 10 cross fold. After that weka tool is utilized where ID3 algorithm is predicted as perfect for this work analysis. [11]

PROGNOSIS OF ALGORITHM: EMPIRICAL RESULTS AND EXPLORATION

This research paper is a formal commence seeks to apply inconsistent classification algorithms of data mining escorted by different statistics. Therefore, with the unveiling of enriched and the strained prediction techniques, there is need for an analyst to originate an algorithm which works best for a particular dataset.

Composed Dataset

For analysis of following data that are in the UCI repository are handed-down: Post-Operative Patient dataset gathered from the University Medical Centre, Institute of Oncology, Ljubljana and Yugoslavia [2]. Dataset include 90 instances having multi-variable data. Information of attributes of patients features are as follows.

- L-CORE: patient's core temperature in C.
- L-SURF: patient's surface temperature in C.
- L-O2: oxygen saturation in %
- L-BP: last measurement of blood pressure
- SURF-STBL: stability of patient's surface temperature
- CORE-STBL: stability of patient's core temperature
- BP-STBL: stability of patient's blood pressure
- COMFORT: patient's perceived comfort at discharge, measured as an integer between 0 and 20.
- Discharge ADM-DECS: discharge decision - Class I: patient sent to Intensive Care Unit,
  - Class S: patient prepared to go home,
  - Class A: patient sent to general hospital floor

Data Pre-processing

- Remove an attribute L-SURF by using unsupervised filter as shown in the Table I column: "After (Total 8 attributes)".
- Remove another attribute SURF-STBL also as shown in the Table I column: "After (Total 7 attributes)".

The surface temperature of the patient is not required and there is no need of more information, so we remove the useless attributes with this the accuracy can be enhanced.

Data Classification

For the enactment of machine learning algorithms, WEKA software is used. The experiments recounted in this research paper were accomplished using libraries from the Weka machine learning environment. Numerous classifiers are used in this paper. The following result shows that after removing the attributes L-SURF and SURF-STBL accuracy can be enhanced. In this paper, Table I shows that decision table achieves 71% of higher accuracy but J48 achieves 70% of same accuracy. It concludes that both decision table and J48 outperformed. Fig. 1 shows the graphical view of the comparison of six different classification algorithms.

ACCURACY COMPARISON OF SIX CLASSIFICATION TECHNIQUES

ALGORITHM	BEFORE (Total 9 attributes)	AFTER (Total 8 attributes)	AFTER (Total 7 attributes)
BayesNet	64%	68%	68%
Logistics	60%	63%	66%
Multilayer Perceptron	53.3%	58.8%	63%
Decision Table	69%	71%	71%
PART	64%	64.4%	67%
J48	70%	70%	70%

Graphical 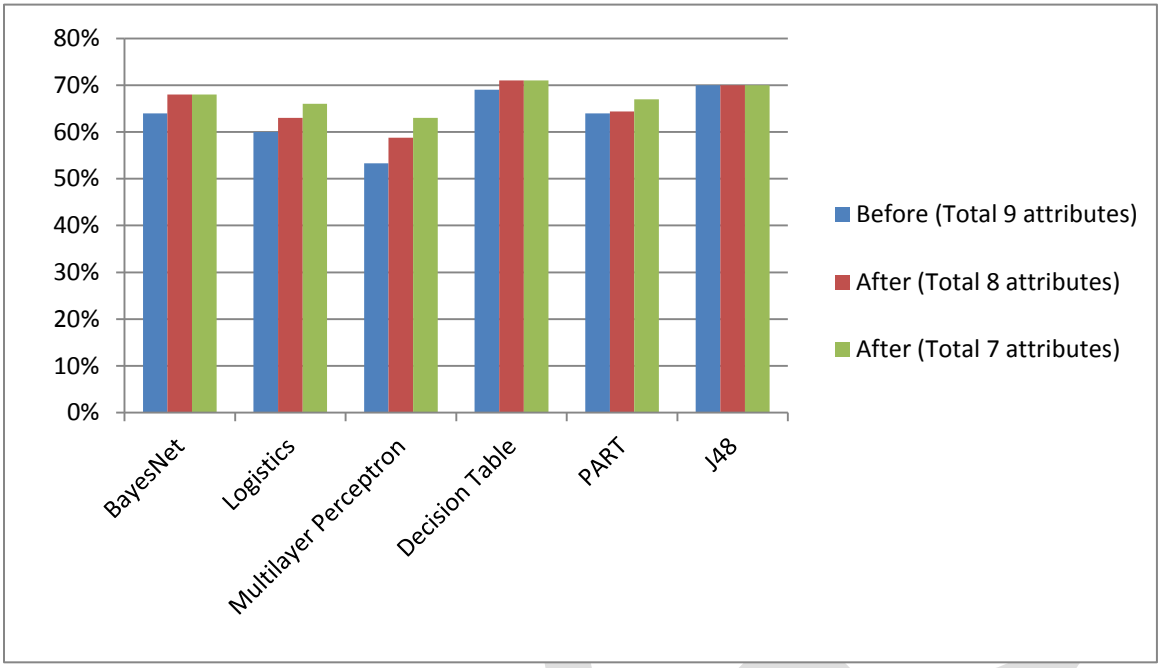

view of

Comparison of different Classification Techniques

ACKNOWLEDGMENT

Foremost, I would like to convey my sincere gratitude to my guide, parents and friends for their continuous support and immense knowledge. I would like to thanks them and wish them all the best in their lives.

CONCLUSION

In this paper the comparison has been performed to forecast the suitable classification algorithm for the post operative patient dataset which shows surface temperature of the patient is not required and it concludes from the experiment that decision tree and J48 outperformed to enhance the accuracy. The idea of the future work is to develop a new class and endorse in scheming medical decision support arrangement with the assist of selected algorithm.

REFERENCES

D. Lavanya and Dr. K. Usha Rani "Ensemble Decision Tree Classifier for Breast Cancer Data" International Journal of Information Technology Convergence and Services (IJITCS) Vol.2, No.1, February 2012.

Dataset collected, [http://tunedit.org/repo/UCI] accessed 2015.

Mehak Naib and Amit Chhabra "Predicting Primary Tumors using Multiclass Classifier Approach of Data Mining" International Journal of Computer Applications (0975 – 8887), Volume 96, No. 8, June 2014.

Jyoti Soni, Ujma Ansari, Dipesh Sharma and Sunita Soni "Predictive Data Mining for Medical Diagnosis: An Overview of Heart Disease Prediction" International Journal of Computer Applications (0975-8887), Vol. 17, No. 8, Mar. 2011.

Samar Al-Qarzaie, Sara Al-Odhaibi, Bedoor Al-Saeed and Dr. Mohammed Al-Hagery "Using the Data Mining Techniques for Breast Cancer Early Prediction".

Arvind Sharma and P. C. Gupta "Predicting the Number of Blood Donors through their Age and Blood Group by using Data Mining Tool" International Journal of Communications and Computer Technologies, Volume 01, No. 6, ISSN Number: 2278-9723, September 2012.

Shweta Kharya "Using Data Mining Techniques for Diagnosis and Prognosis of Cancer Disease" International Journal of Computer Science, Engineering and Information Technology (IJCSEIT), Vol. 2, No. 2, April 2012.

Dr. Bushra M. Hussan "Data Mining based Prediction of Medical data using K-means algorithm" Basrah Journal of Science(A), Vol. 30(1), 46-56, 2012.

M. Durairaj and V. Ranjani "Data Mining Applications in Healthcare Sector: A Study" International Journal of Scientific and Technology Research, Vol. 2, ISSN 2277-8616, Issue 10, October 2013.

Aarti Sharma, Rahul Sharma, Vivek Kr. Sharma and Vishal Shrivatava "Application of Data Mining - A Survey Paper" International Journal of Computer Science and Information Technologies, Vol. 5(2), 2023 – 2025, 2014.

Satya Ranjan Dash and Satchidananda Dehuri "Comparative Study of Different Classification Techniques for Post Operative Patient Dataset" International Journal of Innovative Research in Computer and Communication Engineering, Vol. 1, Issue 5, July 2013.

Mai Shouman, Tim Turner and Rob Stocker "Applying k-Nearest Neighbour in Diagnosing Heart Disease Patients" International Journal of Information and Education Technology, Vol. 2, No. 3, June 2012

International Journal of Engineering Research and General Science Volume 3, Issue 3, Part-2 , May-June, 2015
ISSN 2091-2730

Image Authentication and Forgery Localization

Dinu Innocent, Gopakumar G, Neethu Treesa Jacob

CUSAT university, dinuinnocent@gmail.com, +91 8157044109

Abstract— Robust hashing method is developed for detecting image forgery including removal, insertion, and replacement of objects, and abnormal color modification, and also copy move and spliced forgery, and for locating the forged area. Both global and local features are used in forming the hash sequence. The global features are based on Zernike moments representing luminance and chrominance characteristics of the image as a whole. The local features include position and texture information of salient regions in the image. Secret keys are introduced in feature extraction and hash construction. While being robust against content preserving image processing, the hash is sensitive to malicious tampering and, therefore, applicable to image authentication. The hash of a test image is compared with that of a reference image. When the hash distance is greater than a threshold T1 and less than T2, the received image is judged as a fake. By decomposing the hashes, the type of image forgery and location of forged areas can be determined e.g., replacement of objects or abnormal modification of colors or copy move and spliced forgery. Compared with some other methods using global features or local features alone, the proposed method has better overall performance in major specification, especially the ability of distinguishing regional tampering from content preserving processing.

Keywords— image hashing, Zernike moments, salient region, global and local feature, splicing, Speeded Up Robust Features, Local Binary Pattern,

INTRODUCTION

With the widespread use of image editing software, ensuring credibility of the image contents has become an important issue. Image hashing is a technique that extracts a short sequence from the image to represent its contents, and therefore can be used for image authentication .If the image is maliciously modified, the hash must be changed significantly. Below figure shows the concept of image hashing.

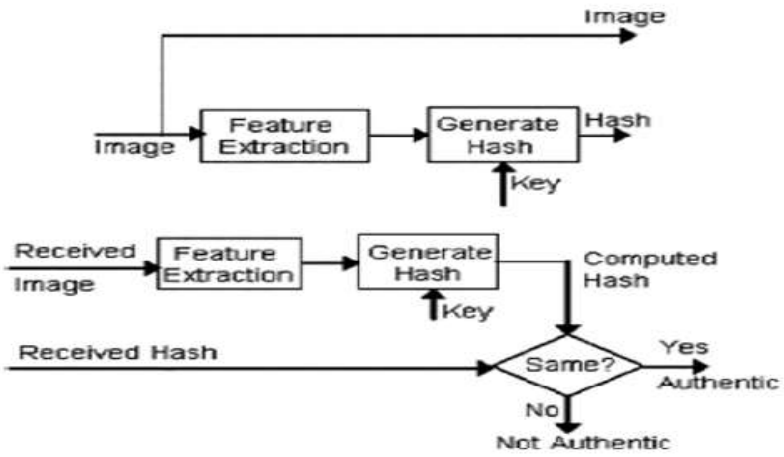

A good image hash should be reasonably short, robust to ordinary image manipulations, and sensitive to tampering. It should also be unique in the sense that different images have significantly different hash values, and secure so that any unauthorized party cannot break the key and coin the hash. To meet all the requirements simultaneously, especially perceptual robustness and sensitivity to tampering, is a challenging task.

So many techniques are introduced with Image Hashing Development. Image hash is developed as a result of feature extraction and the coding of intermediate result. That has become a routine practice in many image hashing methods. Many previous schemes are either based on global [2]-[5] or local [6]-[8] features. Global features are generally short but insensitive to changes of small areas in the image, while local features can reflect regional modifications but usually produce longer hashes.

The proposed method combines the advantages of both global and local features. The objective is to provide a reasonably short image hash with good performance, i.e., being perceptually robust while capable of detecting and locating content forgery. We use Zernike moments of the luminance/chrominance components to reflect the image's global characteristics, and extract local texture features from salient regions in the image to represent contents in the corresponding areas. Distance metrics indicating the degree of similarity between two hashes are defined to measure the hash performance. Two thresholds are used to decide whether a given image is an original/normally-processed or maliciously doctored version of a reference image, or is simply a different image. The method can be used to locate tampered areas and tell the nature of tampering, e.g., replacement of objects or abnormal modification of colors. Compared with some other methods using global features or local features alone, the proposed method has better overall performance in major specifications, especially the ability of distinguishing regional tampering from content preserving processing. The previous scheme [1] only considers forgeries like replacement of objects or abnormal modification of colors addition or removal of object. But the proposed method can found out other two main forgeries such as copy move forgery and spliced attack.

PROPOSED METHOD

The proposed method combines the advantages of both global and local features. The objective is to provide a reasonably short image hash with good performance, i.e., being perceptually robust while capable of detecting and locating content forgery.Here use Zernike moments of the luminance/chrominance components to reflect the image's global characteristics, and extract local texture features from salient regions in the image to represent contents in the corresponding areas. Distance metrics indicating the degree of similarity between two hashes are defined to measure the hash performance. Two thresholds are used to decide whether a given image is an original/normally-processed or maliciously doctored version of a reference image, or is simply a different image. The method can be used to locate tampered areas and tell the nature of tampering, e.g., replacement of objects or abnormal modification of colors. Compared with some other methods using global features or local features alone, the proposed method has better overall performance in major specification, especially the ability of distinguishing regional tampering from content-preserving. The proposed method can found out other two main forgeries such as copy move forgery and spliced attack other than the normal forgeries such as replacement of objects or abnormal modification of colors addition or removal of object.

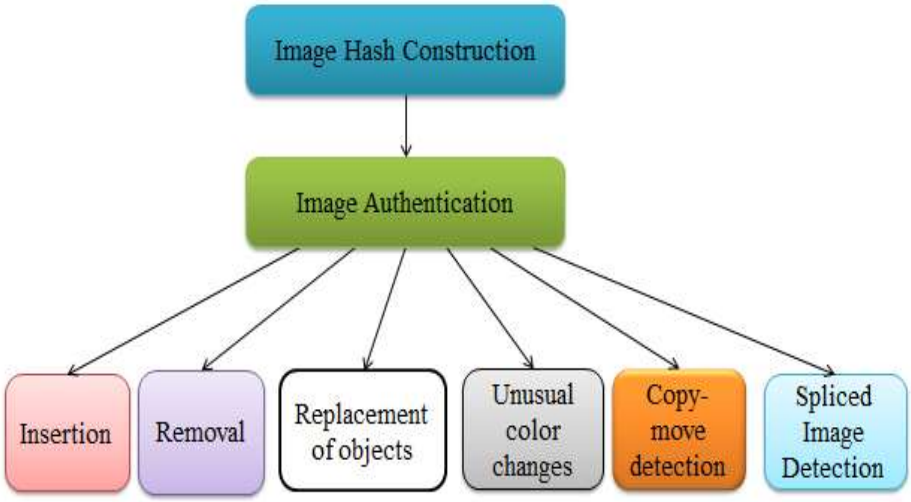

IMAGE HASH CONSTRUCTION

Proposed hashing scheme uses the global and local feature extraction for the construction of image hash for the authentication process.The global vector is based on Zernike moments representing the luminance and chrominance characteristics of the image as a whole. The local features include position and texture information of salient regions in the image.

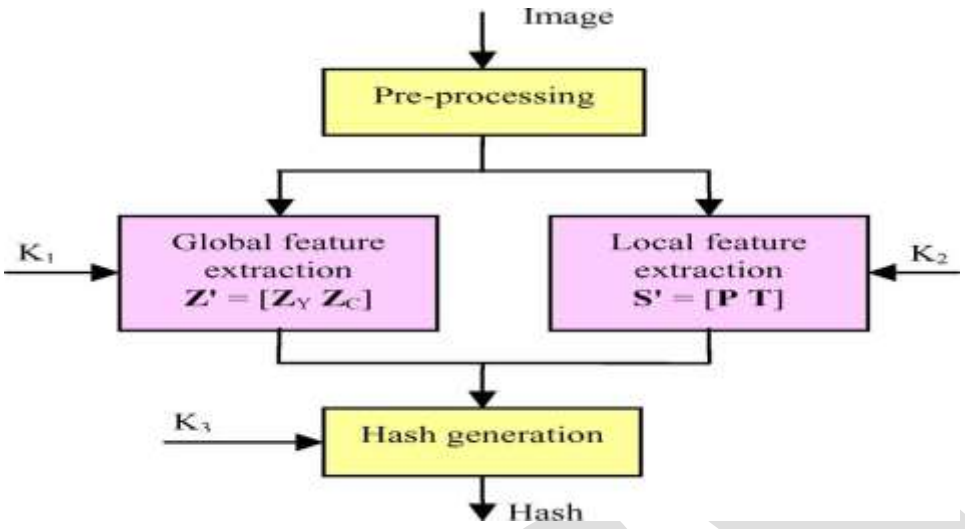

Preprocessing:

The image is first rescaled to a fixed size FxF with bilinear interpolation, and converted from RGB to the YCbCr representation and |Cb-Cr| are used as luminance and chrominance components of the image to generate the hash. The aim of rescaling is to ensure that the generated image hash has a fixed length and the same computation complexity. Small F leads to loss of fine details, while large F results in high computation complexity. Here choose F=256 as an appropriate trade-off.

Global Feature Extraction:

Zernike moments of Y and |Cb-Cr| are calculated.Zernike moments (ZMs) have been used in object recognition and image analysis regardless of variations in position, size and orientation. Basically, the Zernike moments are the extension of the geometric moments by replacing the conventional transform kernel with orthogonal Zernike polynomials.

Zernike moments(ZM)of order n and repetition m of a digital image I(∂,ɵ)can be find out using the below algorithm:

a) Select the values for order n and the repetition m such that, n=0,1..... , 0<=|m|<=n and n-|m| is even.

b) Calculate the Zernike Polynomial of order ”n‟ and repetition “m‟.

$$V_{nm}(\rho, \theta) = R_{nm}(\rho)e^{jm\theta}$$

Where $R_{nm}(\rho)$ are real-valued radial polynomials

$$R_{nm}(\rho) = \sum_{s=0}^{(n-|m|)/2} (-1)^s \frac{(n-s)!}{s!\left(\frac{n+|m|}{2}-s\right)!\left(\frac{n-|m|}{2}-s\right)!}\rho^{n-2s}.$$

Where ρ=length of vector from origin to a pixel, θ=angle between vector and x axis.

c) Multiply the digital image with the Zernike Polynomial.

d) Take the summation over the entire image.

$$Z_{n,m} = \frac{n+1}{\pi} \sum_{(\rho,\theta)\in \text{unit disk}} \sum I(\rho,\theta) V^*_{n,m}(\rho,\theta)$$

Because shape features can be obtained from a small number of low frequency coefficients, the order does not need to be large. This method choose n=5. For n=5, we have 11 Zernike moments, so total 11*2=22 integers. (For luminance and chrominance components) as in the table.

ZERNIKE MOMENTS OF DIFFERENT ORDERS

Order n	Zernike moments	Number of moments
1	$Z_{1,1}$	1
2	$Z_{2,0}$, $Z_{2,2}$	2
3	$Z_{3,1}$, $Z_{3,3}$	2
4	$Z_{4,0}$, $Z_{4,2}$, $Z_{4,4}$	3
5	$Z_{5,1}$, $Z_{5,3}$, $Z_{5,5}$	3

Magnitudes of the Zernike moments are rounded and used to form a global vector, $Z^{'}$=[Zy , Zc] .Each element in is no more than 255.A secret key K1is used to randomly generate a row vector X1with 22 random integers in [0, 255]. The encrypted global vector Z is obtained as Z= [($Z^{'}$+X1) mod 256]

Local Feature Extraction:

The coordinates of top left corner and width/height of each salient region in an image and some texture features are used as the local feature.

A salient region in an image is one that attracts visual attention. According to [11], information in an image can be viewed as a sum of two parts: that of innovation and that of prior knowledge. The former is new and the latter redundant. The information of saliency is obtained when the redundant part is removed. Log spectrum of an image, L (f), is used to represent general information of the image. Because log spectra of different images are similar, there exists redundant information in L (f).

The Salient Region can be detected using the algorithm

a) Calculate the log spectrum of the image, L (f)

b) Find the redundant information exists in the image.

A (f) =h1*L (f) h1=low-pass kernel

c) Obtain the spectral residual by subtracting redundant information from the log spectrum of the image.

B (f) =A (f)-L (f)

d) Calculate the saliency map by inversely Fourier transforming the spectral residual.

Sm(x) =F` (B (f))

e) Determine the salient regions by

O(x) = 1 if S(x) > threshold,

0 otherwise.

Threshold = E(S(x)) × 3, where E(S(x)) is the average intensity of the saliency map.

Fig. 1. Salient region detection: (a) Original image. (b) Saliency map. (c) Salient region. (d) Four rectangles.

K largest salient regions are detected from the luminance image Y. The coordinates of top left corner, and width/height of each circumscribed rectangle are used to form a K element vector P^k, representing the position and size of each salient region. With a larger K, fewer salient regions are missing but will lead to a longer image hash. Also the percentage of images with no more than 7 salient regions is 99.5%.This method choose K=6 as a reasonable trade-off.

Texture Features

Texture is an important feature to human visual perception.There is mainly six texture features relating to visual perception: coarseness, contrast, directionality, line-likeness, regularity and roughness. Here uses coarseness C_1 and contrast C_2 as defined below, plus skewness and kurtosis, to describe the texture properties. Skewness and kurtosis can be obtained by histogram representation.

The algorithm used to find the Coarseness around a pixel is:

a) Select a pixel at (x , y).

b) Averaging the 2k x 2k neighborhood pixels of the above selected pixel.

$$A_k(x,y) = \frac{1}{2^{2k}} \sum_{i=x-2^k}^{x+2^k-1} \sum_{j=y-2^k}^{y+2^k-1} g(i,j), \qquad k = 0, 1, \ldots, 5$$

c) Find the average values of non overlapping neighborhoods on opposite sides of the selected pixel in horizontal and vertical directions.

d) Calculate the difference between the pairs of average values.

$$E_{k,h}(x,y) = |A_k(x + 2^{k-1}, y) - A_k(x - 2^{k-1}, y)|$$
$$E_{k,v}(x,y) = |A_k(x, y + 2^{k-1}) - A_k(x, y - 2^{k-1})|$$

e) Find the size that leads to the highest difference value.

$$S_{\text{opt}}(x,y) = \underset{k=0,\ldots,5;d=h,v}{\arg\max} E_{k,d}(x,y)$$

f) Take average on the highest difference value over a region in order to obtain Coarseness.

Contrast is obtaining the algorithm:

a) Calculate the variance of the gray values of the image.

b) Calculate the fourth order moment of the gray values of the image.

c) Multiply the calculated variance and the fourth-order moment within the region.

$$C_2 = \sigma^2 \mu_4^{-4}$$

So local vector is the combination of position value P (x, y, height, width) and texture features T. position vector P contains 6*4=24 integers also texture feature vector contain 6*4=24 integers, since we consider 6 salient region.So local feature vector contain 48 integers.

S1= [P, T]

S= [(S1+X2) mod 256] where X2 is the row vector generated using a secret key K2.

Hash construction:

The global and salient local vectors are concatenated to form an, intermediate hash H1= [Z, S] scramble H1 based on a key K3 to produce the final hash sequence H.

H= [(H1+X3) mod 256] where X3 is the row vector generated using a secret key K3.

So total our image hash contain 24+24+22=70 integer and is 70*8=560bits long.

IMAGE AUTHENTICATION

In image authentication, the hash of a trusted image H_0 is available and called the reference hash. The hash of a received image to be tested H_1 is extracted using the above method.

a) The hash of a received image to be tested (H_1) is extracted.
H_1= [Z1 P1 T1]

b) Decompose the reference hash (H0) into Global and Local features.
H_0= [Z0 P0 T0]

c) Check if the salient regions found in the test image P1 match those in the trusted image P0.

These two hashes are compared to determine whether the test image has the same contents as the trusted one or has been maliciously tampered, or is simply a different image. Here, two images having the same contents (visual appearance) do not need to have identical pixel values. One of them, or both, may have been modified in normal image processing such as contrast enhancement and lossy compression. In this case, we say the two images are perceptually the same, or similar.

FORGERY CLASSIFICATION

Forgery classification includes classifying the possible forgeries as removal, insertion and replacement of objects, and unusual color changes. For that, Decode H_0 (hash of the test image) and H_1 (hash of the reference image) into components representing global and local features, and find the number of matched salient regions R and the numbers of salient regions in the reference N_0 and test images N_1 then check some conditions which is described below.

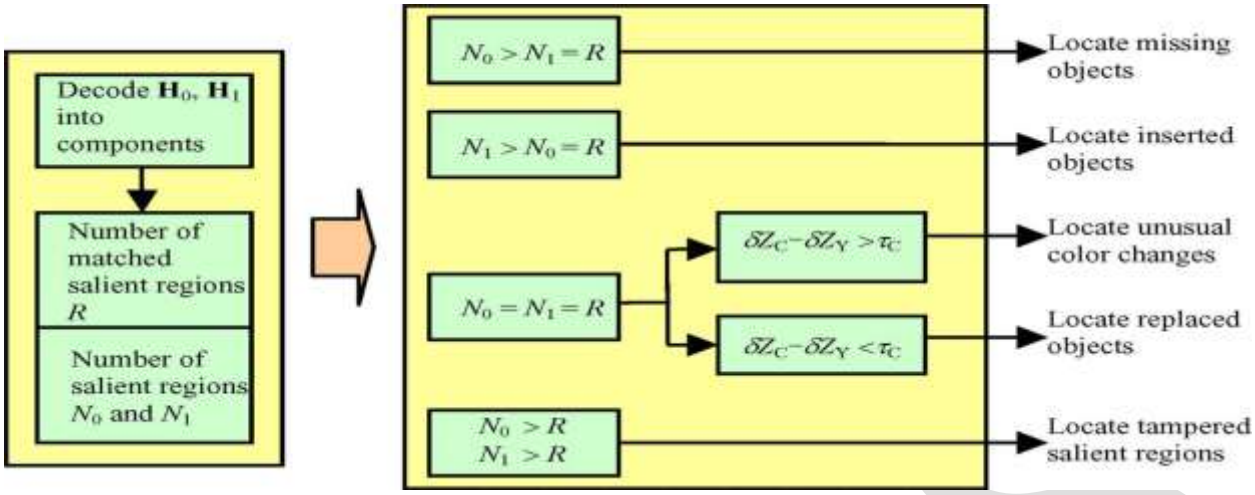

$$\delta Z_C = ||\mathbf{Z}_{C1} - \mathbf{Z}_{C0}||, \quad \delta Z_Y = ||\mathbf{Z}_{Y1} - \mathbf{Z}_{Y0}||$$

The method for finding other two forgeries like copy move and spliced forgery are described below.

COPY MOVE FORGERY

A copy move forgery denotes an image where part of its content has been copied and pasted within the same image. Typical motivations are either to hide an element in the image, or to emphasize particular objects.Here key point-based method is used. In key point-based method, SURF (Speeded Up Robust Features) method is used for feature extraction. Key point-based methods compute their features only on image regions with high entropy, without any image subdivision for feature extraction. Similar features within an image are afterwards matched.

Algorithm for detecting copy move forgery is given below.

A. Pre-Processing:

Here the image is converted from RGB to Gray representation.

B. Feature Extraction:

The features can be extracted by using SURF (Speeded Up Robust Features) method. SURF is the robust local feature detector. Shape feature used to locate and recognition of certain objects, people or faces, object tracking and extraction of points of interest.

C. Matching:

A matching operation is performed among the feature vectors to identify similar local patches in the image. Approximate Nearest Neighbor method is used for feature matching.

D. Filtering:

Filtering schemes are used to reduce the probability of false matches. Neighboring pixels often have similar intensities, which can lead to false forgery detection. The Euclidean distance that can be calculated between each feature vectors. The pairs can be removed if it is less than the particular threshold value T2.

E. Clustering:

The Agglomerative Hierarchical Clustering is used to cluster the forged regions.

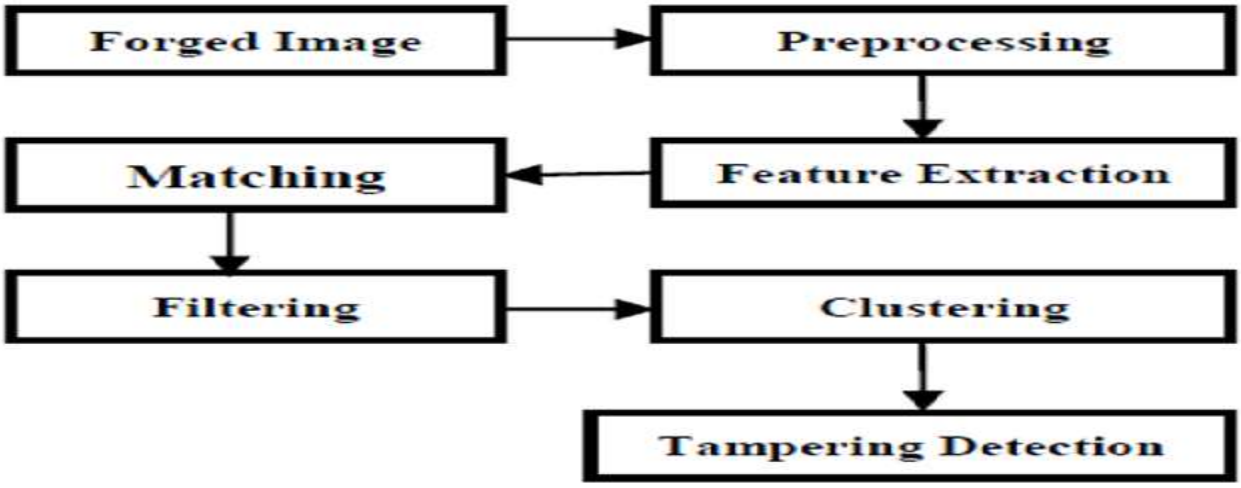

SPLICED FORGERY

Simple joining of fragments of two or more different images leads to the splicing attack.

A. Preprocessing

Input RGB color image is transformed to YCbCr color system. Chrominance component (Cb or Cr) is divided into 16x16 overlapping blocks.

B. Local Binary Pattern (LBP)

LBP is a local operator which discriminates different types of textures and defines a label (LBP code) of each pixel of an image. To compute the LBP code, a 3x3 neighborhood of the pixel is threshold by its intensity value. If the neighbor's pixel value is less than the center, it will hold binary digit '0', otherwise it will hold '1'.The neighbors' binary digits are concatenating to build a binary code. The LBP code is the decimal value of that binary code. Calculated LBP is transformed into frequency domain using 2D DCT. Then standard deviations are calculated of respective frequency coefficients of all blocks and they are used as features.

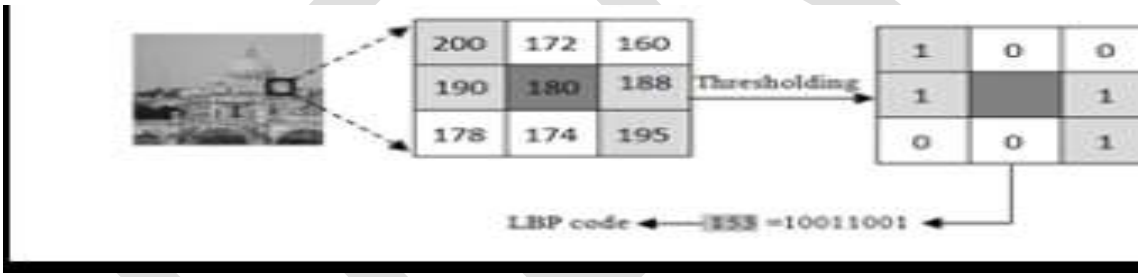

C. Classification

Finally, these features are sent to SVM classifier in order to make the decision about the input image whether it is an authentic or a tampered one.

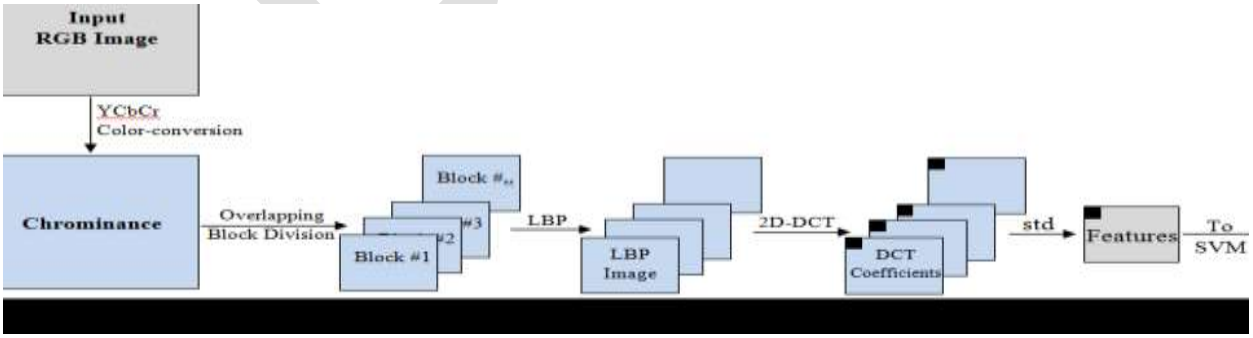

RESULTS

1. Addition of object

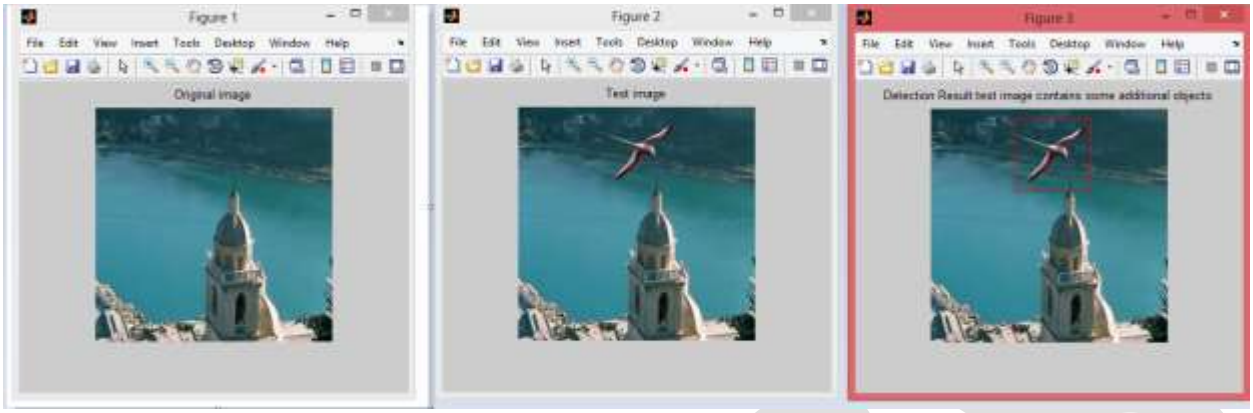

2. Removal of object

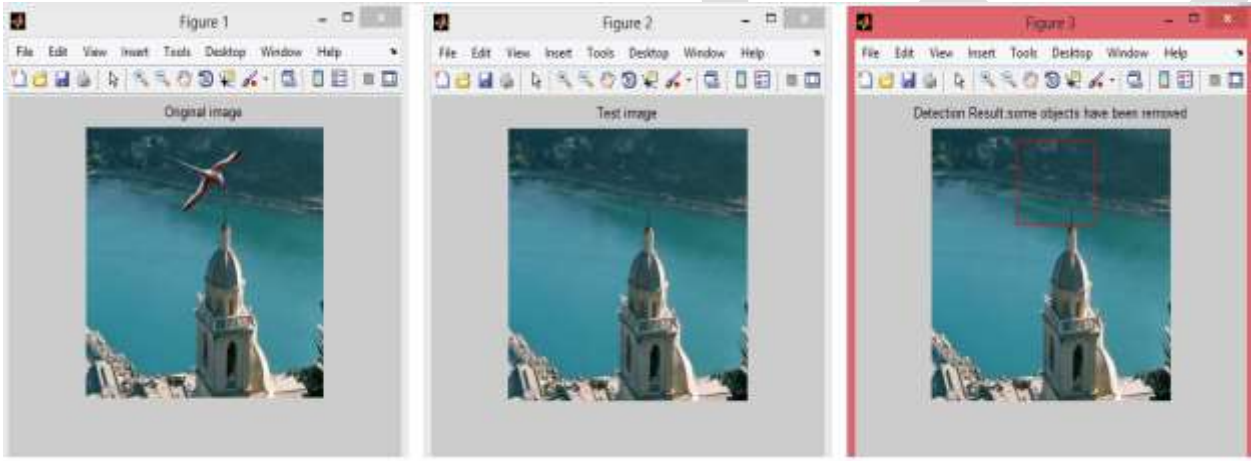

3. Replacement of object

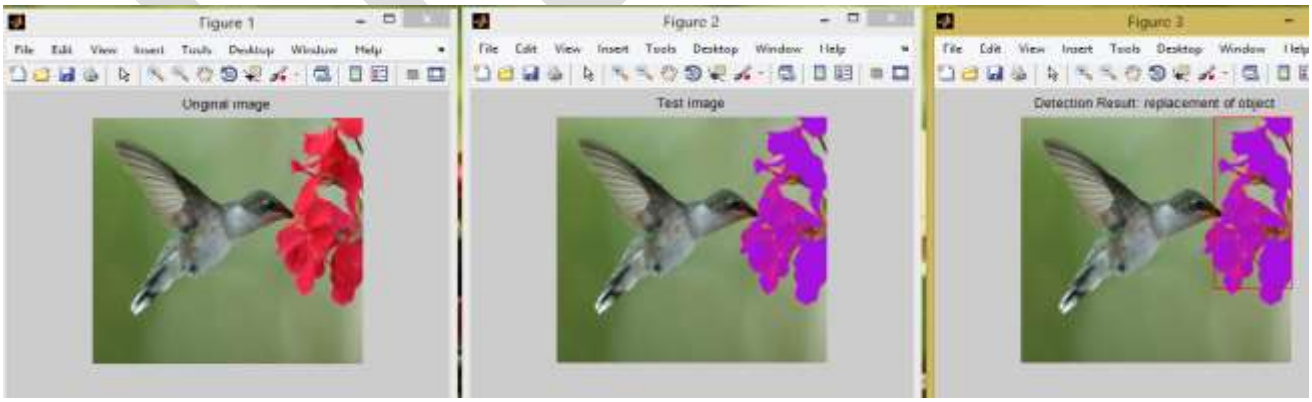

4. Copy move forgery

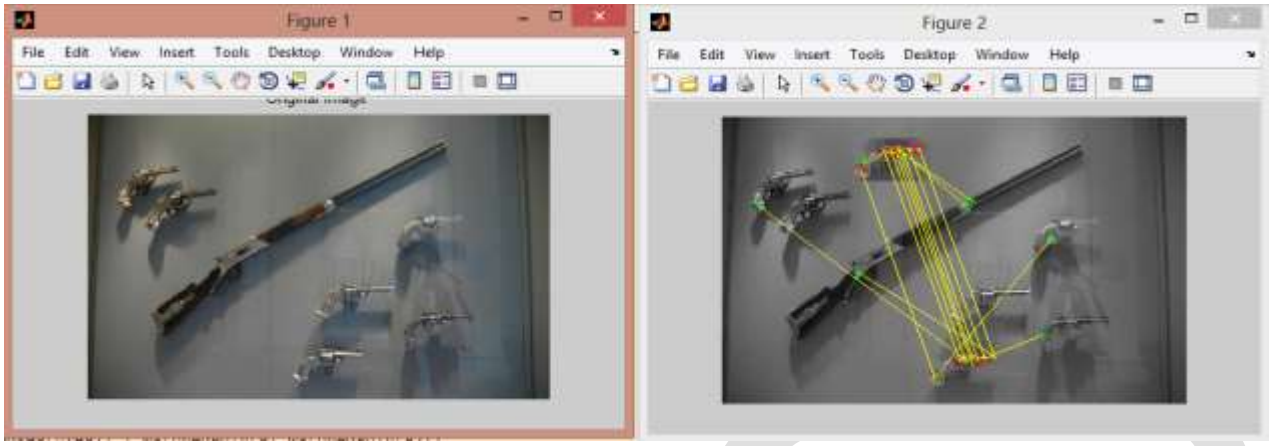

5. Spliced forgery

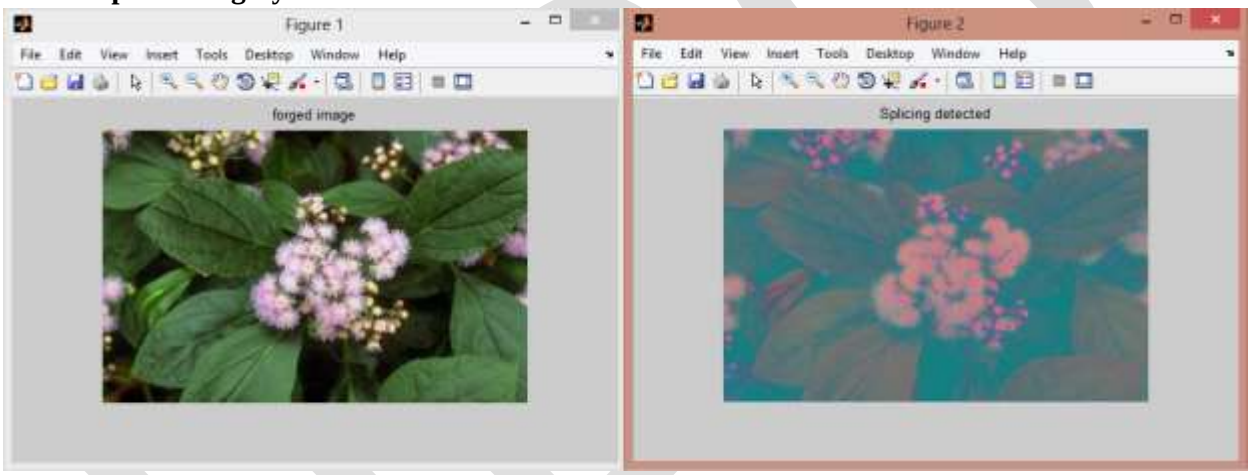

CONCLUSION

In this work, an image hashing method is developed using both global and local features. The global features are based on Zernike moments representing the luminance and chrominance characteristics of the image as a whole. The local features include position and texture information of salient regions in the image.

Hashes produced with the proposed method are robust against common image processing operations including brightness adjustment, scaling, small angle rotation, JPEG coding and noise contamination. Collision probability between hashes of different images is very low. The proposed scheme has a reasonably short hash length.

The method used in this work is aimed at image authentication. The hash can be used to differentiate similar, forged, and different images. At the same time, it can also identify the type of forgery and locate fake regions containing salient contents. In the image authentication, a hash of a test image is generated and compared with a reference hash previously extracted from a trusted image. When the hash distance is greater than the threshold T_1 but less than T2 the received image is judged as a fake. By decomposing the hashes, the nature of image forgery and locations of forged areas can be determined. The previous scheme [1] only considers forgeries like replacement of objects or abnormal modification of colours addition or removal of object. But the proposed method can found out other two main forgeries such as copy move and spliced forgery.

REFERENCES:

[1] Yan Zhao, Shuozhong Wang, Xinpeng Zhang, and Heng Yao, "Robust Hashing for Image Authentication Using Zernike Moments and Local Features" ieee transactions on information forensics and security, vol. 8, no. 1, january 2013

[2] V. Monga, A. Banerjee, and B. L. Evans, "A clustering based approach to perceptual image hashing," IEEE Trans. Inf. Forensics Security, vol. 1, no. 1, pp. 68–79, Mar. 2006.

[3] Xiang, H. J. Kim, and J. Huang, "Histogram-based image hashing scheme robust against geometric deformations," in Proc. ACM Multimedia and Security Workshop, New York, 2007, pp. 121–128.

[4] Tang, S.Wang,X. Zhang, W.Wei, and S. Su, "Robust image hashing for tamper detection using non-negative matrix factorization," J. Ubiquitous Convergence Technol., vol. 2, no. 1, pp. 18–26, May 2008.

[5] A. Swaminathan, Y. Mao, and M. Wu, "Robust and secure image hashing," IEEE Trans. Inf. Forensics Security, vol. 1, no. 2, pp.215–230, Jun. 2006.

[6] K. Fouad and J. Jianmin, "Analysis of the security of perceptual image hashing based on non-negative matrix factorization," IEEE Signal Process. Lett., vol. 17, no. 1, pp. 43–46, Jan. 2010.

[7] W. Lu, A. L. Varna, and M. Wu, "Forensic hash for multimedia information," in Proc. SPIE,Media Forensics and Security II, San Jose, CA, Jan. 2010, 7541.

[8] W. Lu and M.Wu, "Multimedia forensic hash based on visual words," in Proc. IEEE Conf. on Image Processing, Hong Kong, 2010, pp. 989–992.

[9] S. Li, M. C. Lee, and C. M. Pun, "Complex Zernike moments features for shape-based image retrieval," IEEE Trans. Syst., Man, Cybern. A, Syst. Humans, vol. 39, no. 1, pp. 227–237, Jan. 2009.

[10] Z. Chen and S. K. Sun, "A Zernike moment phase based descriptor for local image representation and matching," IEEE Trans Image Process., vol. 19, no. 1, pp. 205–219, Jan. 2010.

[11] X. Hou and L. Zhang, "Saliency detection: A spectral residual approach," in Proc. IEEE Int. Conf. Computer Vision and Pattern Recognition, Minneapolis, MN, 2007, pp. 1–8.

[12] T. Deselaers, D. Keysers, and H. Ney, “Features for image retrieval: A quantitative comparison,” in *Lecture Notes in Computer Science*, 2004, vol. 3175, pp. 228–236, Springer

International Journal of Engineering Research and General Science Volume 3, Issue 3, Part-2 , May-June, 2015
ISSN 2091-2730

Integration of Big Data in Cloud computing environments for enhanced data processing capabilities

Rohit Chandrashekar[1] Maya Kala [2] Dashrath Mane [3]

VES Institute of Technology,

Chembur, Mumbai

[1] rohit28chandrashekar@gmail.com **[2]** maya11kala@gmail.com

[3] dashumane@gmail.com

Abstract— Big data is an evolving term that describes any voluminous amount of structured, semi-structured and unstructured data that has the potential to be mined for information. Big data refers to not only the volume of the data but also the technology used to and processes used to analyze such huge volumes of data into usable information which cannot be performed using traditional database and software technologies.

Cloud computing is an extremely successful paradigm of service oriented computing, and has revolutionized the way computing infrastructure is abstracted and used. Cloud computing eliminates the need to maintain expensive computing hardware, dedicated space, and software.

This paper proposes on how Big Data can be integrated with the elasticity, of cloud computing environment to bring about efficient and cheaper information processing solutions.

Keywords— Big Data, Cloud Computing, Enhanced Data Processing

INTRODUCTION

Cloud Computing is a technology which depends on sharing of computing resources than having local servers or personal devices to handle the applications. In Cloud Computing, the word “Cloud” means “The Internet”, so Cloud Computing means a type of computing in which services are delivered through the Internet. The goal of Cloud Computing is to make use of increasing computing power to execute millions of instructions per second. Cloud Computing uses networks of a large group of servers with specialized connections to distribute data processing among the servers. Instead of installing a software suite for each computer, this technology requires to install a single software in each computer that allows users to log into a Web-based service and which also hosts all the programs required by the user.

There's a significant workload shift, in a cloud computing system. Local computers no longer have to take the entire burden when it comes to running applications. Cloud computing technology is being used to minimize the usage cost of computing resources [4]. The cloud network, consisting of a network of computers, handles the load instead. The cost of software and hardware on the user end decreases. The only thing that must be done at the user's end is to run the cloud interface software to connect to the cloud. Cloud Computing consists of a front end and back end. The front end includes the user's computer and software required to access the cloud network. Back end consists of various computers, servers and database systems that create the cloud. The user can access applications in the cloud network from anywhere by connecting to the cloud using the Internet. Some of the real time applications which use Cloud Computing are Gmail, Google Calendar, Google Docs and Dropbox etc.

Figure1. Benefits of Cloud Computing

Big Data focuses on achieving deep business value from deployment of advanced analytics and trustworthy data at Internet scales. Big Data is at the heart of many cloud services deployments. As private and public cloud deployments become more prevalent, it will be critical for end-user organizations to have a clear understanding of Big Data application requirements, tool capabilities, and best practices for implementation.

Big Data is said to have the following properties:

Volume: Many factors contribute towards increasing Volume streaming data and data collected from sensors etc.,

Variety: Today data comes in all types of formats

Emails, video, audio, transactions etc.,

Velocity: This means how fast the data is being produced and how fast the data needs to be processed to meet the demand.

Variability: Along with the Velocity, the data flows can be highly inconsistent with periodic peaks.

Complexity: Complexity of the data also needs to be considered when the data is coming from multiple sources. The data must be linked, matched, cleansed and transformed into required formats before actual processing.

Big Data and cloud computing are complementary technological paradigms with a core focus on scalability, agility, and on-demand availability. Big Data is an approach for maximizing the linear scalability, deployment and execution flexibility, and cost-effectiveness of analytic data platforms. It relies on such underlying approaches as massively parallel processing, in-database execution, storage optimization, data virtualization, and mixed-workload management. Cloud computing complements Big Data by enabling ubiquitous, convenient, on-demand network access to a shared pool of configurable computing resources that can be rapidly provisioned and released with minimal management effort or service provider interaction.

Big data and cloud computing are both the fastest-moving technologies emerging today. Cloud computing is associated with new paradigm for the provision of computing infrastructure and big data processing method for all kinds of resources. Moreover, some new cloud-based technologies have to be adopted because dealing with big data for concurrent processing is difficult. The current

technologies such as grid and cloud computing have all intended to access large amounts of computing power by aggregating resources and offering a single system view. Among these technologies, cloud computing is becoming a powerful architecture to perform large-scale and complex computing, and has revolutionized the way that computing infrastructure is abstracted and used. In addition, an important aim of these technologies is to deliver computing as a solution for tackling big data, such as large scale, multi-media and high dimensional data sets.

Why Big Data Analytics in Cloud computing:

Cost reduction: Cloud computing offers a cost-effective way to support big data technologies and the advanced analytics applications that can drive business value. Enterprises are looking to unlock data's hidden potential and deliver competitive advantage. Big data environments require clusters of servers to support the tools that process the large volumes, high velocity, and varied formats of big data. IT organizations should look to cloud computing as the structure to save costs with the cloud's pay-per-use model.

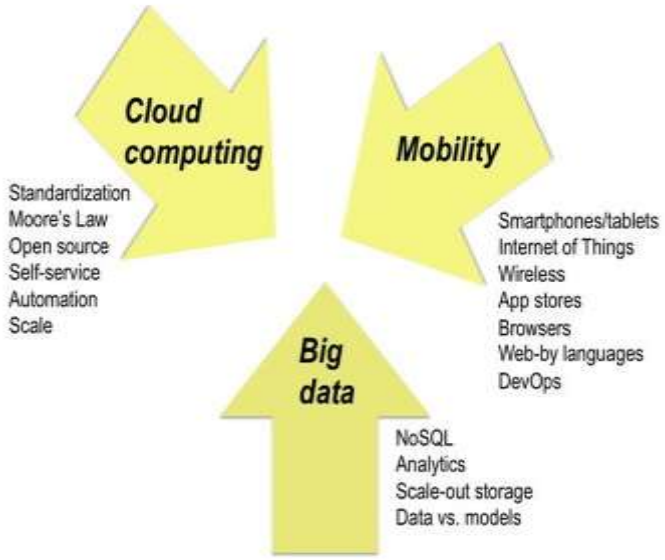

Figure2. Integration of Big Data and Cloud Computing

Reduce overhead: Various components and integration are required for any big data solution implementation. With cloud computing, these components can be automated, reducing complexity and improving the IT team's productivity.

Rapid provisioning/time to market: Provisioning servers in the cloud is as easy as buying something on the Internet. Big data environments can be scaled up or down easily based on the processing requirements. Faster provisioning is important for big data applications because the value of data reduces quickly as time goes by. .

Flexibility/scalability: Big data analysis, especially in the life sciences industry, requires huge compute power for a brief amount of time. For this type of analysis, servers need to be provisioned in minutes. This kind of scalability and flexibility can be achieved in the cloud, replacing huge investments on super computers with simply paying for the computing on an hourly basis.

SYSTEM IMPLEMENTATION

The aim of this paper is to provide a practical reference to help enterprise information technology (IT) and business decision makers of the Finance and Hospital industry as they analyze and consider the implications of big data and cloud computing on their business. The paper includes guidance and strategies, designed to help these decision makers evaluate different requirements from various actors including medical practices, hospitals, capital markets, and finance industry.

Capital Markets:

There are countless opportunities for financial services firms to leverage the benefits of cloud computing by migrating a variety of applications to the cloud. Non-core applications and such business processes as recruiting, billing and organization-wide travel management can—and should—easily move to the cloud. A number of infrastructure operations, such as data center management, data storage and disaster recovery, should also move to a cloud after a thorough evaluation of different vendors offerings and based on the flexibility of cloud vendors in documenting contracts. Although very few firms are currently using cloud computing for their core applications, different hosting architectures provided by IaaS (Infrastructure as a Service) cloud providers and new avenues in the community and hybrid cloud space, will drive more firms to move their core applications to the cloud. In fact, core solutions, such as batch processes running throughout the day, analytics and reporting applications, are perfect candidates.

A few scenarios that would be ideal for a cloud deployment include:

Risk analytics calculation:

Applications that calculate such analytics as cost of trade, current value, yields, Greeks, etc., at the level of a single security, position or portfolio are perfect candidates for a grid-based cloud. A cloud-based grid service can easily scale up or scale down depending on the data load. What's more, the applications can be seamlessly deployed on multiple grid nodes, reducing maintenance overhead. Also, since such applications only run for specific durations, dedicated hardware leads to unutilized CPU cycles, which can be optimized by a grid-based cloud. The whole solution can be implemented on a private cloud where existing computing power can be virtualized and made available as an on- demand service.

Performance attribution:

Performance attribution provides a framework for examining the relative performance of a fund versus its benchmark. It is a methodology that quantifies the success or added value of an investment strategy. Attribution allows investment managers to identify the factors of the investment process that contributed (positively or negatively) to the performance levels highlighted by performance measurement. Hence, these data- intensive processes need access to a huge amount of historical data for correctly calculating metrics. Performance attribution or benchmark rebalancing applications run at specific times of a day, like the analytics calculation processes. As such, these are ideal candidates to be deployed on a cloud, able to optimize the usage of available computing power and the scale-in and scale-out benefits of an existing grid.

Trade matching and reconciliation:

A trade matching process gets trade data from multiple brokers and counterparties and then reconciles it. This process is prone to high volumes during times of peak trading. The solution is to create a hybrid cloud where the reconciliation process can run on a public cloud for scalability and the data can reside on dedicated database servers in a private cloud. The data from multiple brokers and counterparties can be pushed to the public cloud, which can then be streamed to the private cloud. This can also help avoid creating separate connectivity to new partners and maintaining all those connections simultaneously.

Reference data virtualization:

Various types of reference data, such as security master data, positions data, holdings and book data, broker and counterparty data, etc., reside in multiple kinds of data sources. These data sources can be internal databases, file systems or external feeds. When an application needs to access data from many sources, it can be a challenge to devise strategies that connect those data sources and consolidate and aggregate the data within the application for specific needs. The recommended solution is to build a data virtualization layer that seamlessly federates these different data sources and provides different ways to access the single virtual data source. The layer should be flexible enough to mash up different streams of data according to the requirements of a particular application. Similar to the reference data virtualization layer, a transactional or operational data virtualization layer can be created to support risk management, financial analysis and compliance reporting. The goal is to make all data available through centralized data services.

Hospital Industry:

"Patient centricity" has become the key trend in healthcare provisioning and is leading to the steady growth in adoption of electronic medical records (EMR), electronic health records (EHR), personal health records (PHR), and technologies related to integrated care, patient safety, point-of-care access to demographic and clinical information, and clinical decision support. Availability of data, irrespective of the location of the patient and the clinician, has become the key to both patient satisfaction and improved clinical outcomes. Cloud technologies can significantly facilitate this trend.

Some areas where cloud computing can be implemented:

Radiologists: Using Cloud computing, radiology users can efficiently manage multimodality imaging units by using the latest software and hardware without paying huge upfront costs.

Neuroscience: Making brain mapping toolkits more accessible to non-specialist users in virtue of concealing its implementation context as well as rendering local IT infrastructure unnecessary.

Physical therapy: Using Cloud computing, effectiveness of computer-assisted learning (CAL) in physical therapy can be achieved to provide rehabilitation and recovery at a faster rate.

The key stakeholders for the Big Data Analytics Platform at a Hospital or a Medical Research Centre are Physicians / Clinicians, Researchers, Operations and Quality teams – each with their perspective and view of "tangible, measurable value" derived by implementing the platform. The platform leverages some of the finest open source Big Data technologies that include Data Mining / Machine Learning, Advanced Visualisation techniques to help address the opportunities to improve delivery of patient care at the Hospital / Medical Research Centre.

Benefits of implementing a Big Data and Advanced Cloud-based computing system:

Safety and cost effectiveness: Cloud-computing systems require very little in terms of infrastructure, and patients only need access to a Web browser to take part. The essence of cloud computing is a secure, cost-effective way to manage patient information and communication.

More accurate patient information: Cloud-based systems give patients the opportunity to complete their medical history at their convenience, which can eliminate problems that occur from information gathered over the phone.

Ease of use: When selecting a cloud-computing system, choose one that will provide patients with an intuitive interface. If patients can easily work through the system, their information will be more complete and satisfaction greater.

Prediction of 30 Day Readmission Candidates: The opportunity is to identify / predict patients at high risks by the system and thereby enable focused, directed attention to deliver care that would prevent readmissions. An accurate prediction of readmission ensures better, targeted care and interventions to the right patients at the hospital / medical research centre.

Chronic Disease Management: Real-time monitoring of patient data and its map onto advanced algorithm driven predictive models against chronic diseases and patient conditions enables generation of real-time alerts to both caregivers and patients of a deviation from the expected pathway.

Home Health Monitoring: Home health data such as weight, blood pressure, heart rate, respirations, temperature, glucose and other parameters are received, stored, analysed and then pushed to the EHR as discrete data fields. The real-time metrics generated are published as a patient scorecard and predictions around anomalies in patient condition / behaviour is immediately flagged off for relevant intervention to prevent fatalities.

Early Sepsis Detection: Severe sepsis (acute organ dysfunction secondary to infection) and septic shock are major healthcare problems, affecting millions of individuals around the world each year, killing one in four (and often more), and increasing in incidence. The ability to monitor patients in real time to determine the earliest entry point to the sepsis pathway will ensure timely treatment leading to a reduction in mortality and morbidity rates.

Clinical Research: Many pharmacology vendors are starting to tap the cloud to improve research and drug development. The 'explosion of data' from next generation sequencing as well as the growing importance of biologics in the research process is making cloud-based computing "an increasingly important aspect of R&D. Commercial cloud vendors have developed pharma-specific clinical research cloud offerings with the goal of lowering the cost and development of new drugs.

CONCLUSION

This paper described a systematic flow of survey on the big data processing in the context of cloud computing. Cloud computing provides enterprises cost-effective, flexible access to big data's enormous magnitudes of information. Big data on the cloud generates vast amounts of on-demand computing resources that comprehend best practice analytics. Both technologies will continue to evolve and congregate in the future.

REFERENCES:

[1] Changqing Ji, Yu Li, Wenming Qiu, Uchechukwu Awada, Keqiu Li "Big Data Processing in Cloud Computing Environments" 2012 International Symposium on Pervasive Systems, Algorithms and Networks.

[2] Venkata Narasimha Inukollu, Sailaja Arsi and Srinivasa Rao Ravuri "Security Issues Associated With Big Data In Cloud Computing" International Journal of Network Security & Its Applications (IJNSA), Vol.6, No.3, May 2014.

[3] "Deploying Big Data Analytics Applications to the Cloud: Roadmap for Success" 2014 Cloud Standards Customer Council.

[4] "Use of Big Data Technologies in Capital Markets" by Ruchi Verma, Sathyan R Mani INFOSYS.

[5] "Big Data in the Cloud: Converging Technologies" by Intel IT Center.

[6] "Impact of Cloud Computing on Healthcare" 2012 Cloud Standards Customer Council

International Journal of Engineering Research and General Science Volume 3, Issue 3, Part-2 , May-June, 2015
ISSN 2091-2730

Analysis and Design of Doubly Fed Induction Generator for Wind Turbines Using MATLAB

Mrs Aakansha Mercy Steele
Assistant Professor
Department of EX
UIT- RGPV, Bhopal
mercy.steele@yahoo.com

ABSTRACT: This paper presents a grid-connected wind power generation scheme using Doubly Fed Induction Generator (DFIG). This can supply power at constant voltage and constant frequency with the rotor speed varying. This makes it suitable for variable speed wind energy application. The DFIG system consists of wind turbine, asynchronous wound rotor induction generator, inverter and Pulse Width Modulation (PWM) controller. In which the stator is connected directly to the grid and the rotor winding is in interface with rotor converter and grid converter. The use of back-to-back PWM converter in the rotor circuit results in low distortion current, reactive power control and operate at variable speed. Mathematical modelling of the DFIG is done in order to analyze the performance of the systems and they are simulated using MATLAB. The simulation results for the two systems are obtained and hence it shows that the systems can operate at variable speed with low harmonic current distortion. The objective is to track and extract maximum power from the wind energy system and transfer it to the grid or useful work.

Keywords- Doubly Fed Induction Generator, Pulse Width Modulation, Mathematical modelling, Simulation, MATLAB

1. INTRODUCTION

Wind electrical power generation system has many potential benefits from both economical and environmental perspectives. As it is cost–competitive, safe, clean and abundant renewable energy as compared to fossil fuel (Nakra and Benoit, 1988; Z.Xie, et., 2007). The wind electrical power generator transforms mechanical energy into electrical energy. The blades transfer the kinetic energy from the wind into rotational energy in the transmission system and the generator is the next step in the supply of energy from the wind turbine to the electrical grid.

There has been continuous change in the technology like from the fixed speed control system to the variable speed control system. First the Self starting induction generators were used as they require generator to run in motor mode at the start, so they are not self starting **(**Nakra and Benoit, 1988). For this purpose squirrel cage induction generator is used because they are simple, serve the function of self starting, cheap and rugged. But they operate at constant speed and in this system there is no inherent reactive power control method so it requires capacitor banks. Due to capacitor failure use of synchronous generator in Wind Energy Conversion System (WECS) was used (Ammasaigounden. and Subbiah 1988; LeTang and Robert Zavadil, 1993). Which does not requires synchronization with the grid but all the above generator operates at constant speed. So with the advancement in the thyristor converter the turbines can be used to generator power at variable speed. In the control system converter- inverter circuit is use to control the magnitude, phase and frequency. There are different ways to control the inverter and converter output power like fuzzy logic controller, back-to back PWM converter in the rotor circuit of DFIG (M.Hussein, et., 1994; R.S.Pena, et., 1996). DC link chokes were used but they are expensive and required an extra commutation circuit for operating at synchronous speed and this result in the poor performance. It can be improved by the use of chopper but it produces current harmonics to overcome this back draw Pulse Width Modulation (PWM) converter in asynchronous wound rotor induction generator also known

as DFIG is used. It has low distortion of rotor, stator and supply current. It reduces the inverter cost. It can cover a wide operation range from sub synchronous to super synchronous speed operating with the flow in both directions. So maximum energy is capture from the wind and hence enables optimal speed tracking (R.S.Pena, et, 1996; Z.Xie, et., 2007).

2. MATERIAL AND METHOD

In the DFIG the stator is directly connected to the grid and the rotor is connected to the variable frequency converter (PWM) how to change the frequency, phase and magnitude of the rotor current or voltage is the main aim to control the DFIG.

The wind turbine and the doubly-fed induction generator (WTDFIG) are shown in the Fig 1 called the Doubly-Fed Induction Generator System. The AC/DC/AC converter is divided into two components: the rotor-side converter (C_{rotor}) and the grid-side converter (C_{grid}). C_{rotor} and C_{grid} are Voltage-Sourced Converters which consist of forced-commutated power electronic devices (IGBTs) to synthesize an AC voltage from a DC voltage source. The three-phase rotor winding is connected to C_{rotor} by slip rings and brushes and the three-phase stator winding is directly connected to the grid. The power captured by the wind turbine is converted into electrical power by the induction generator and it is transmitted to the grid by the stator and the rotor windings. The pulse width modulation controller system generates the pitch angle command and the voltage command signals for C_{rotor} and C_{grid} respectively in order to control the power of the wind turbine.

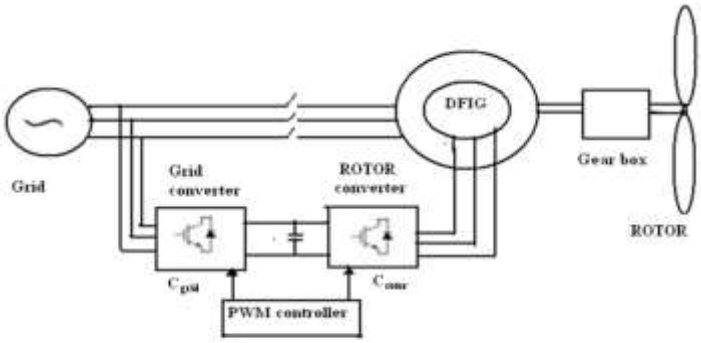

Fig. 1 Doubly-fed induction generator system

3. MATHEMATICAL MODELING OF SYSTEM

Wind energy, doubly fed induction generator, rotor converter, grid converter, all are derived by mathematical model. These mathematical models are used for the simulation purpose. Mathematical modelling of all system is given as follows:

3.1 MAXIMAL POWER POINT TRACKING

The power that can be captured from the wind with a wind energy converter with effective area A_r is given by

$$P_m = \frac{1}{2}\rho C_p(\lambda) A_r v^3 \quad (1)$$

Where $A_r = \pi r_m^2$

$$P_m = \frac{1}{2}\rho C_p(\lambda) \pi r_m^2 v^3 \quad (2)$$

$$\lambda = \frac{r_m \omega}{V}$$

Where,

P_m Turbine mechanical power.

C_p Turbine performance coefficient.

V Wind speed.

ω Turbine angular speed.

ρ Air density.

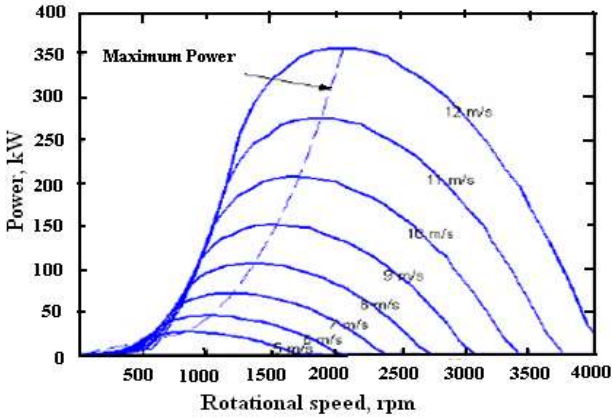

Fig. 2 Relation curve of P_m and n

So we can get the relation curve of mechanical power (P_m) and rotational speed (n) as shown in Fig.2 More energy can be captured from wind by keeping the tip speed ratio to optimal constant. The speed of wind is regulated by controlling the electromagnetic torque .The peak power depends on the turbine characteristic and air density ,the air density may vary considerably over various season, which will not result in optimal tracking of the peak power point under all condition ,there is a considerer able loss in output power energy, in order to restrain the concussion of the system and to improve the tracking, a method of tracking the peak power is proposed which is independent of the turbine parameters and air density (Z.Xie, et., 2007**).**

3.2 **MODELLING OF DFIG**

The following equations are derived for DFIG.

$$u_{sd} = -R_s i_{sd} + \omega_s \psi_{sq} - \frac{d}{dt}\psi_{sd} \quad (3)$$

$$u_{sq} = -R_s i_{sq} - \omega_s \psi_{sd} - \frac{d}{dt}\psi_{sq} \quad (4)$$

$$u_{rd} = R_r i_{rd} - \omega_{s\,l} \psi_{rq} + \frac{d}{dt}\psi_{rd} \quad (5)$$

$$u_{rq} = R_r i_{rq} + \omega_{s\,l} \psi_{rd} + \frac{d}{dt}\psi_{rq} \quad (6)$$

$$\psi_{sd} = L_S i_{sd} - L_m i_{rd} \quad (7)$$

$$\psi_{sq} = L_S i_{sq} - L_m i_{rq} \quad (8)$$

$$\psi_{rd} = L_r i_{rd} - L_m i_{sd} \quad (9)$$

$$\psi_{rq} = L_r i_{rq} - L_m i_{sq} \quad (10)$$

$$T_e = \frac{3}{2} p L_m \left(i_{sd} i_{rq} - i_{sq} i_{rd}\right) \quad (11)$$

Where,

u_{sd} d- axis stator voltage.

u_{sq} q-axis stator voltage.

u_{rd} d-axis rotor voltage.

u_{rq} q-axis rotor voltage.

ψ_{sd} d-axis stator flux linkage.

ψ_{sq}	q-axis stator flux linkage.
ψ_{rd}	d-axis rotor flux linkage.
ψ_{rq}	q-axis rotor flux linkage.
i_{sd}	d-axis stator current.
i_{sq}	q-axis stator current.
i_{rd}	d-axis rotor current.
i_{rq}	q-axis rotor current.
R_s	Stator resistance.
R_r	Rotor resistance.
ω_s	Synchronous angular speed.
ω_{sl}	Slip angular speed.
L_s	Stator self- inductance.
L_r	Rotor self- inductance.
L_m	Mutual inductance.
p	Pole pairs.
T_e	Electrical torque.

3.3 PULSE WIDTH MODULATION

The DC power at the rectifier output is filtered and converted to AC power using the PWM inverter employing double edge sinusoidal modulation (R.S. Pena, et., 1996). PWM signals are used to switch the transistor in the inverter. The output consists of sinusoidal modulated carrier pulses. Both the edges are modulated such that the average voltage difference between any two of the output three phase are sinusoidal.

Mathematically represented by

$$\delta_x = M\sin(\alpha_x)\delta_{max} \qquad (12)$$

Where,

x = 1,2,3,4....., 2r+1

Where,

M Modulation index range from 0 to1

X Edge being considered.

r Ratio of carrier to fundamental frequency in the inverter output.

α_x Angular displacement of the unmodulated edge.

δ_x Maximum displacement of the edge for the chosen frequency ratio r.

4. PROPOSED TECHNIQUE OF DFIG

Fig. 3 shows the schematic diagram of DFIG for step input but the results are also taken for ramp and constant input. The three phase rotor winding of the asynchronous induction is connected to the rotor and the grid converter and the stator is directly connected to the grid. The mechanical torque T_m is given the input for the variable and constant speed. AC -to-DC and then DC- to- AC converter are divided into two components rotor converter and grid converter .They are connected back -to -back by the DC links. PWM generates the pulses for the rotor and the stator converter in order to produce low distortion current, reactive power control and to operate at constant and variable speed.

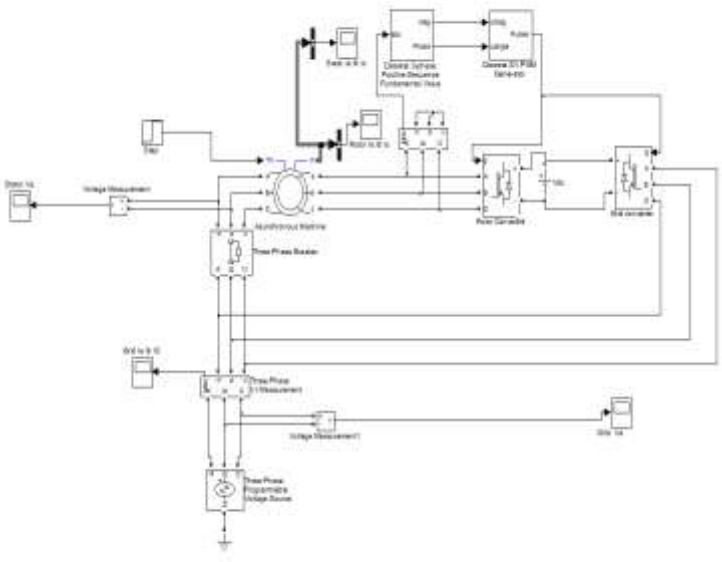

Fig. 3 Schematic diagram of DFIG

5. RESULTS AND DISCUSSIONS

The simulation results of doubly fed induction generator at constant speed and variable speed are shown using MATLAB.

The results have been taken for different mechanical torque of the generator of 160 KW. As the wind speed varies with time so the generator should operate at constant and variable speed. This shows the optimal tracking of power point under all condition by varying the wind speed.

Fig. 4.1a to Fig. 4.5e shows the performance of DFIG. Fig. 4.1a shows the stator current waves. Fig. 4.2b shows the stator voltage waves. Fig. 4.3c shows the grid current waves. Fig. 4.4d shows the grid voltage waves. Fig. 4.5e shows the rotor current waves. For the variable speed the mechanical torque T_m is given by the step at the input the asynchronous induction generator. The step value is from -1 to -4 and step time is 0.01sec. The stator current is 9.9 Amp, stator voltage is 375Volts, grid current is 20 Amp, grid voltage is 350 Volts and rotor current is 7.9Amp.

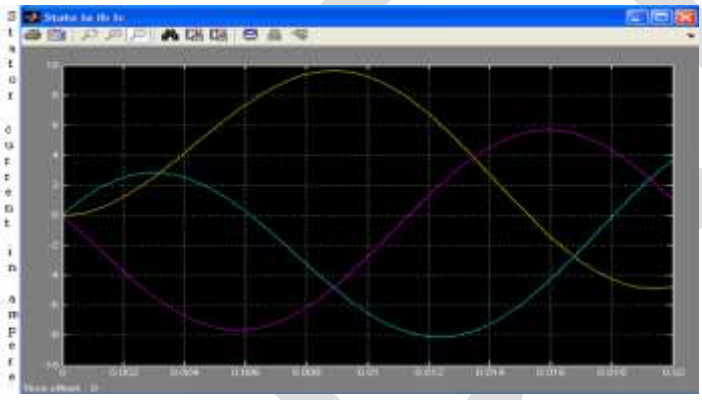

Time in sec

Fig. 4.1a Wave form between stator current wrt time

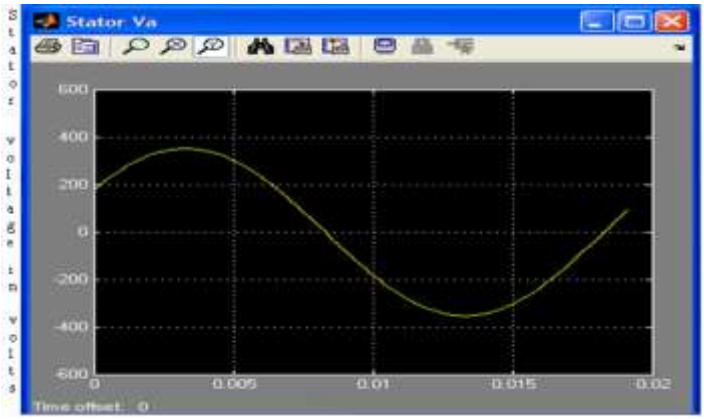

Time in sec

Fig. 4.2b Wave form between stator voltage wrt time

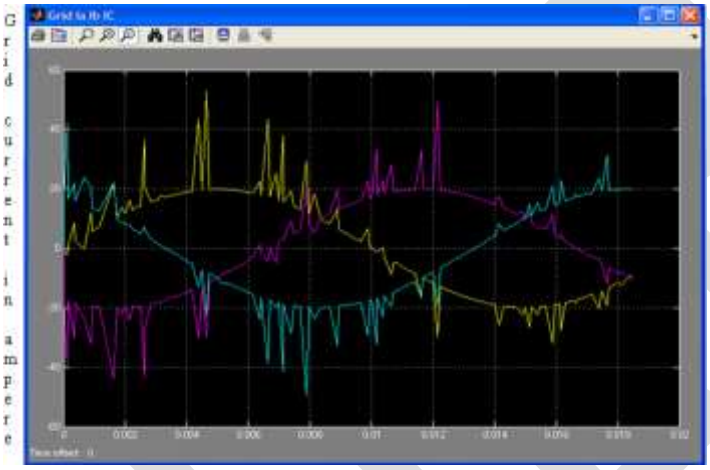

Time in sec

Fig. 4.3c Wave form between grid current wrt time

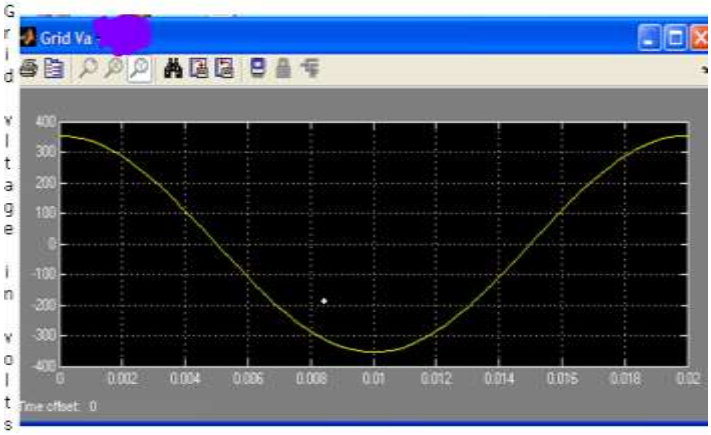

Time in sec

Fig. 4.4d Wave form between grid voltage wrt time

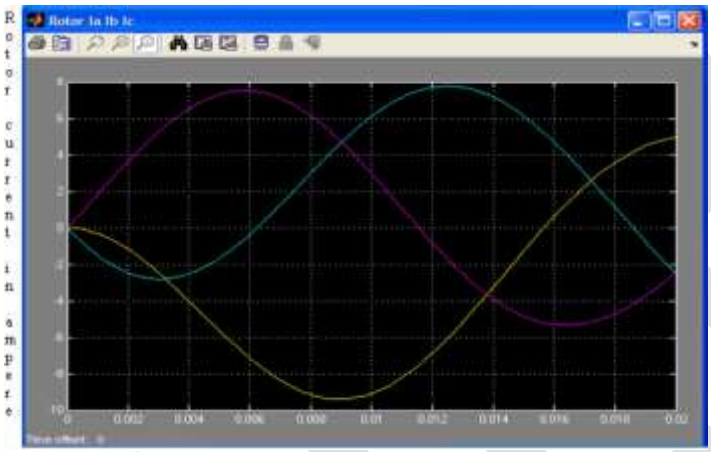

Time in sec

Fig. 4.5e Wave form between rotor current wrt time

Fig. 5.1a to Fig. 5.5e shows the performance of DFIG. Fig. 5.1a shows the stator current waves. Fig. 5.2b shows the stator voltage waves. Fig. 5.3c shows the grid current waves. Fig. 5.4d shows the grid voltage waves. Fig. 5.5e shows the rotor current waves. For the variable speed the mechanical torque T_m is given by the ramp input of the asynchronous induction generator. The ramp value is slope 1, start time 1.5sec and initial output -1. The stator current is 10 Amp, stator voltage is 375Volts, grid current is 12.8 Amp, grid voltage is 350 Volts and rotor current is 7.5Amp.

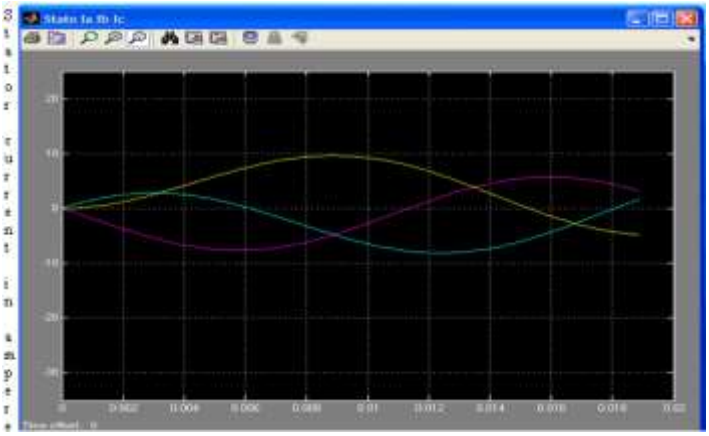

Fig. 5.1a Wave form between stator current wrt time

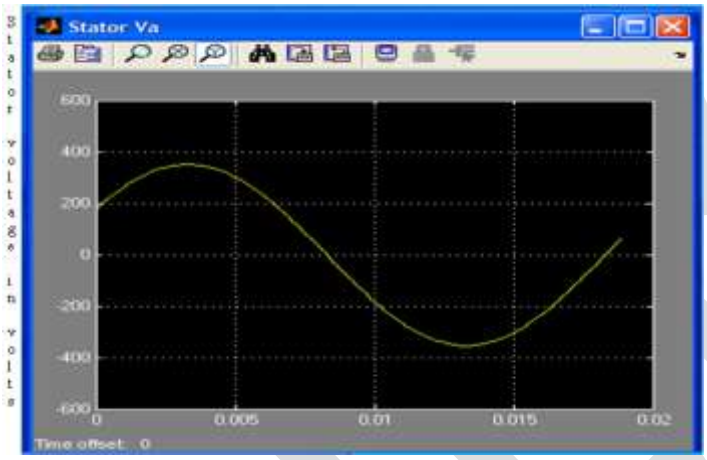

Fig. 5.2a Wave form between stator voltage wrt time

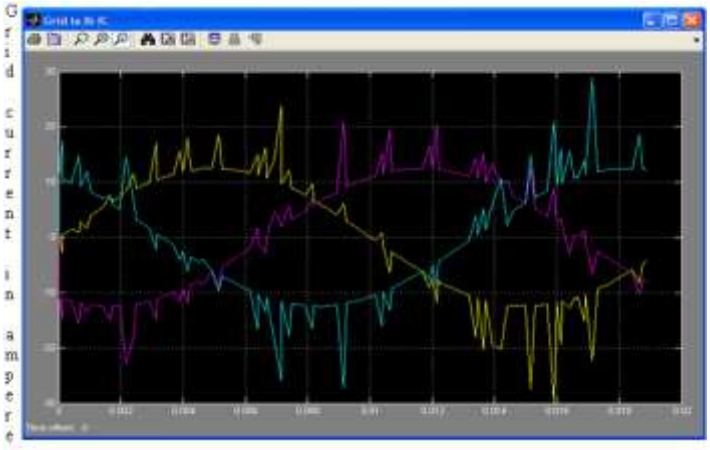

Fig. 5.3c Wave form between grid current wrt time

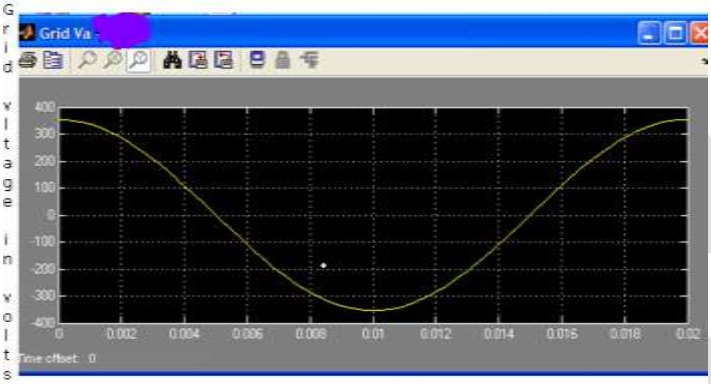

Fig. 5.4d Wave form between grid current wrt time

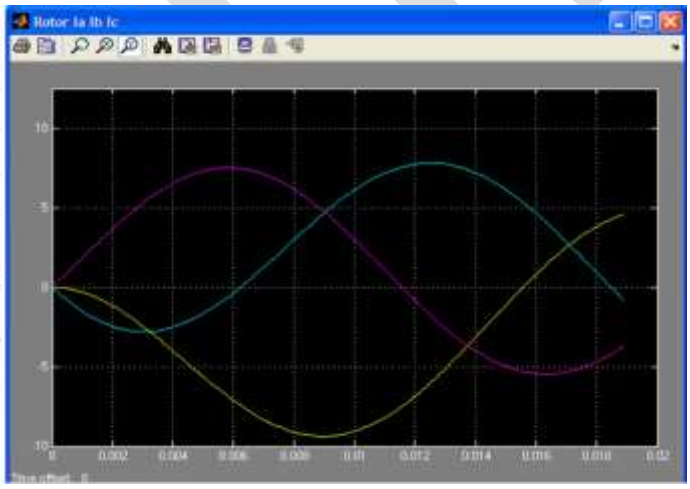

Time in sec

Fig. 5.5e Wave form between rotor current wrt time

Fig. 6.1a to Fig. 6.5e shows the performance of DFIG. Fig. 6.1a shows the stator current waves. Fig. 6.2b shows the stator voltage waves. Fig. 6.3c shows the grid current waves. Fig. 6.4d shows the grid voltage waves. Fig. 6.5e shows the rotor current waves. For the constant speed the mechanical torque T_m is given by the constant at the input of the asynchronous induction generator. The constant value is -1. The stator current is 10 Amp, stator voltage is 375Volts, grid current is 12.8 Amp, grid voltage is 350 Volts and rotor current is 7.5Amp.

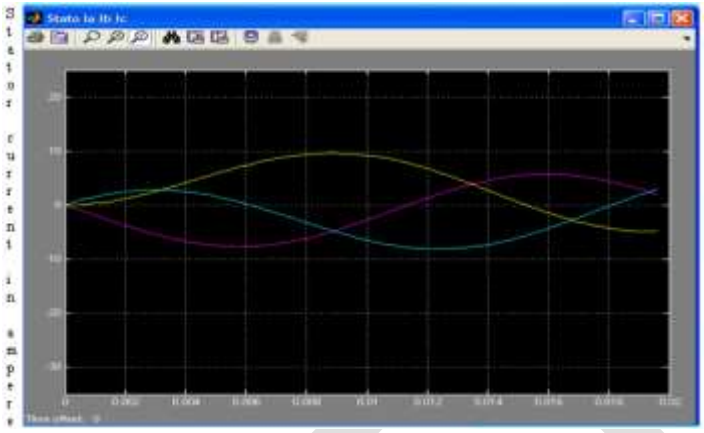

Time in sec

Fig. 6.1a Wave form between stator current wrt time

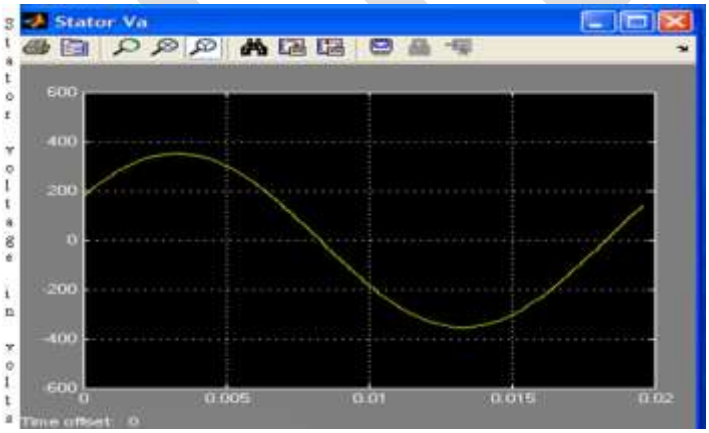

Time in sec

Fig. 6.2bWave form between stator voltage wrt time

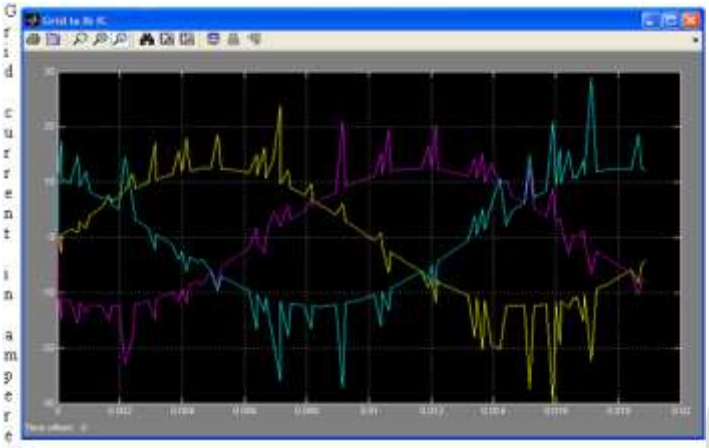

Fig. 6.3c Wave form between grid current wrt time

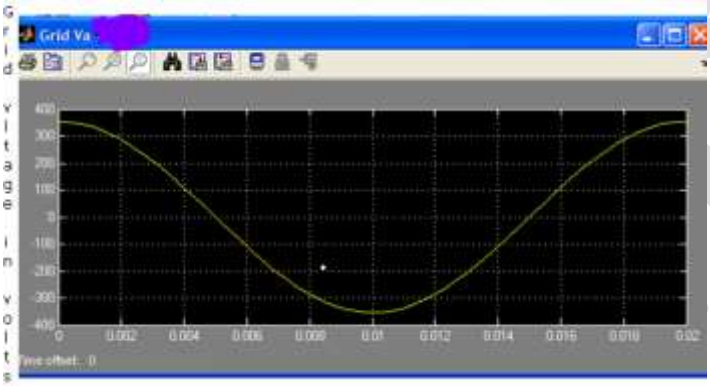

Fig. 6.4d Wave form between grid voltage wrt time

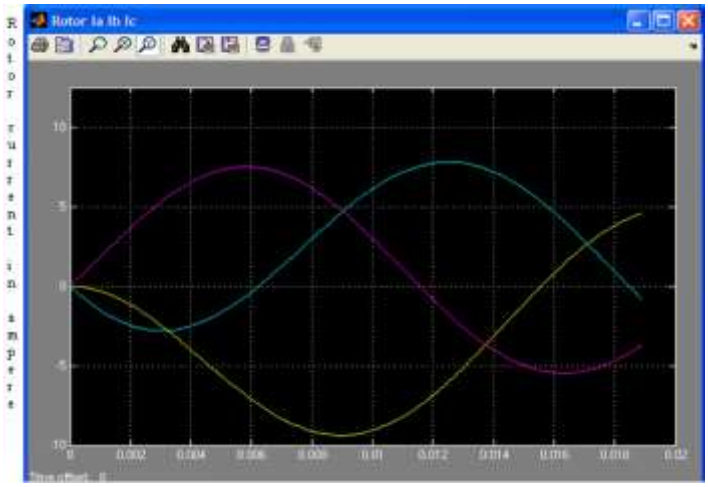

Fig. 6.5e Wave form between rotor current wrt time

In the DFIG system for constant speed and variable speed, the result shows the injection of current harmonics in the grid current but the stator voltage, stator current, grid voltage and the rotor current are all sinusoidal with respect to time. With the use of filter circuit in the DFIG system the current harmonics can be reduced.

CONCLUSION

Mathematical modelling of wind turbine, doubly fed induction generator and controller system is done. In order to find out their performance in DFIG system they are simulated using MATLAB. The simulation results of the system are show that it can operate at variable speed. As the wind speed changes from time to time due to change in temperature and pressure. It rotates the rotor blade of the wind turbine at variable speed. So the wind power can be utilize at variable speed. By the application of power electronics in the DFIG system, this can supply power at constant voltage and constant frequency. While the rotor speeds varies due to variation in the wind speed. This makes it suitable for variable speed wind energy application and hence this is useful in the maximum power tracking. The use of back-to-back PWM converter in the rotor circuit of DFIG allows the bidirectional power flow between the stator and the rotor. This have the advantage of reactive power control and low distortion currents operating at sub and super synchronous speed. The drawback of the DFIG models is that they inject current harmonics in the grid current. However they can be reduced by the implementation of the filter circuit. So further researches are going on to reduce the harmonics by improved PWM schemes and filters. Utilization of wind energy from the offshore wind farms by the selection of reliable, maintenance fee and robust generators.

REFERENCES:

Nakra.H.L. and Benoit Dube (1988). "Slip Power Induction Generator for Large Vertical Axis Wind Turbines", IEEE Transaction on Energy Conversion, Vol.3.

Ammasaigounden.N and Subbiah.M (1988). "Chopper – Controller Wind-Driven Self – Excited Induction Generators", IEEE Transaction on Aerospace and Electronic System, Vol.2.

Cardirci.I and Ermis.M (1992). "Double- Output Induction Generators Operating at Sub synchronous and Super synchronous Speeds: Steady-state Performance Optimisation and Wind-energy Recovery", IEEE proceeding, Vol. 139.

LeTang and Robert Zavadil (1993). "Shunt Capacitor Failures due to Wind farm Induction Generators Self–Excitation Phenomenon", Tennessee USA, IEEE Energy conversion, Vol.8.

Hussein M. Mashaly, Adel M.Sharaf and Ahmed A.EL-Sattar Mohamed Mansour (1994). "A Fuzzy Logic Controller For Wind Energy Utilization", IEEE.

M.Godoy Simoes, Bimal K. Bose and Ronald J. Spiegel (1996). "Design and Performance Evaluation of a Fuzzy Logic Based Variable Speed Wind Speed Wind Generator System", IEEE.

Pena.R , Clare.J.C and Asher.G.M (1996). "A Doubly Fed Induction Generator Using Back-to- Back PWD Converters and its Application to Variable Speed Wind Energy Conversion", IEEE Proc – Electrical Power Appl, Vol.143.

Pena.R, Clare.J.C and Asher.G.M (1996). "A Doubly Fed Induction Generator Using Back-to- Back PWD Converters Supplying an Isolated Load From a Variable Speed Wind Turbine", IEEE Proc – Electrical Power Appl, Vol.143.

Robin M. Hilloowala and Adel M Sharaf (1996). "A Rule– Based Fuzzy Logic Controller for a PWM Inverter in a Stand Alone Wind Energy Conversion Scheme", IEEE Transaction on Industry Application, Vol. 321.

Pena. R.S, Asher.G.M, Clare.J.C and Cardenas.R (1996). "A Constant Frequency Constant Voltage Variable Speed Stand Alone Wound Rotor Induction Generators", England, International conference on Power Generation.

Zhang.I and Wattanasarn.C (1998). "A Matrix Converter Excited Doubly-Fed Induction Machine as a Wind Power Generator", IEEE Conference Publication No.456.

Xie.Z,Zhang.C.W,ZhangX,Yang.S.Y and Cao R.X (2007). "Study on the Rotor Convertor of Doubly Fed Induction Generators Used in Wind Turbine", IEEE.

APPENDIX

Parameters of the DFIG model

Asynchronous (wound rotor) induction generator

Power	P 215Hp(160KW)			Voltage	V 400V
Frequency	f 50Hz				
Speed	N 1487RPM			Stator resistance	R_s 0.01379Ω
Rotor resistance	R_s 0.007728Ω				
Stator self-inductance L_s	0.04755H				
Stator self-inductance L_s					
Rotor self-inductance	L_r	0.04775H			
Mutual inductance	L_m	2.416 H			

International Journal of Engineering Research and General Science Volume 3, Issue 3, Part-2 , May-June, 2015
ISSN 2091-2730

Design and Development of Manure Spreader - A Review

Mr. G.D Yadav[1], Dr. M.S Pawar[2.]
[1,2](Mechanical Engineering Department, Brahmadevdada Mane Institute of Technology, India)

Abstract— Organic manure plays important role to yield productivity of soil. It is good quality source of nitrogen phosphorus and excellent source of calcium and potash. The evenly spreading of manure on farm field is extremely important to achieve better effect. In India traditionally manure has distributed with help of fork and other mechanical device which is very tedious and slow process. The study of existing literature of manure spreader shows there are mainly two types of spreader viz. animal drawn spreader and tractor operated spreader. Performance of available spreader on different parameter has been studied which shows tractor operated spreader gives better result. Study also focus on their limitations of design and source of power supply. There is scope of develop tractor operated spreader attachment which will driven by rear wheel of trailer. By dismantling the attachment we can use trailer for transportation.

Keywords – *Manure, Trailer, Spreader.*

Introduction-Crops need nutrients to grow and develop and they draw these nutrients from the soil. If this withdrawal is not compensated for, the crop yield goes down progressively. This withdrawal is completed through fertilizers and manures to maintain the productivity of the soil and to achieve higher yields. Soil fertilization is carried out by means of organic matter in the form of farmyard manure, liquid manure faces, plants or straw and mineral matters. The manure has to be handled in bulk. So, the problem faced during application of manure differs from that of other fertilizer not only with respect to the rate to be applied per hectare, but also with respect to non-uniformity of the size of the particles. The overall goal for any field receiving manure should be how many gallons or tons of manure should be applied to a known area and to apply the manure as uniformly as possible Organic manure is considered as the eco-friendly bio-fertilizer for the highly polluted modern era. Today's farmer needs machinery which can spread the manure effectively with lest cost with consumes low power.

History-The first successful automated manure spreader was designed by Joseph Kemp in 1875. Manure spreaders began as ground-driven units which could be pulled by a horse or team of horses. At the time of his invention he was living in Waterloo, Canada but thereafter he moved to Newark Valley, NY and formed the J.S. Kemp Manufacturing Co. to manufacture and market his current and subsequent designs. In 1903 he expanded the company to Waterloo, Iowa before selling the design to International Harvester in 1906.

Review of Literature- T P.R Sapkale et.al (2010) [1] test the performance of tractor operated manure spreader. A manure spreader was attached to the 45 HP tractors through the hitch point and test was conducted. The 540+rpm PTO speed was used to operate the rotary blades of manure spreader. The distribution pattern of farm yard manure was uniformly spread over the area and little variation was found. This was due to clods in to manure. It showed that there was saving of 94 per cent in time as compared to traditional method. The field capacity of the manure spreader was also worked out in terms of area coverage per hour. The actual average swath width of manure spreader was found 7.6 m but the effective swath was taken as 7.4 m by considering the overlap uniformity of application and spread pattern. The manure spreader was operated in two different fields. The theoretical field capacity of a tractor operated manure spreader was found to be 1.950 and 2.06 and average actual field capacity of the tractor operated manure spreader was found to be 1.395 and 1.473 at forward speed of 2.438 km/h. The average field efficiency of the tractor operated manure spreader was found to be 71.55 per cent. The field application rate of farm yard manure was observed to be 5.435 and 5.89 t per ha. The cost economics of the manure was analyzed. The cost of spreading with the tractor operated manure spreader was Rs. 247 per ha. The saving in cost and time were 72 and 94 per cent, respectively as compared to conventional method of manual broadcasting.

B. Suthakar et.al (2008) [2], evaluate the field performance of a tractor PTO operated manure spreading attachment to a two wheel trailer and compare it with the traditional method of spreading manure. The machine mainly consists of a manure tub to load the manure, an endless chain conveyor for conveying the manure towards the rear end of the trailer and a hydraulically operated spreader drum to shear off manure. The machine was tested at Research Farms of the Tamil Nadu Agricultural University and at the farmer's fields. It possesses the linear relationship for the forward speed and chain conveyor speed with the application rate. But, the speed of the spreader drum did not influence the application rate of the manure. The desired application rate of the manure (12.202 tonnes/ha) was observed for the forward speed of 2.31 km/hr and the chain conveyor speed of 1.51 m/min with the effective width of 1.20 m and

a time saving of 50-60 % when compared to the conventional method. The spread pattern obtained was a flat top profile, which is acceptable for uniform spreading. It can also be used as a trailer by just shifting a door whenever the trailer is required for transportation.

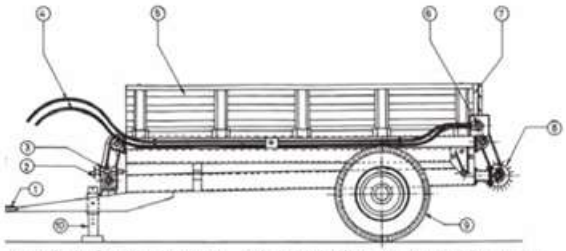

1: Hitch frame, 2: P.T.O. drive coupling, 3: Reduction gear box, 4: Hydraulic hose, 5: Manure tub, 6: Hydraulic motor, 7: Adjustable door, 8: Spreader drum, 9: Pneumatic tyre, 10: Parking stand

Figure 1.Front view of manure spreader

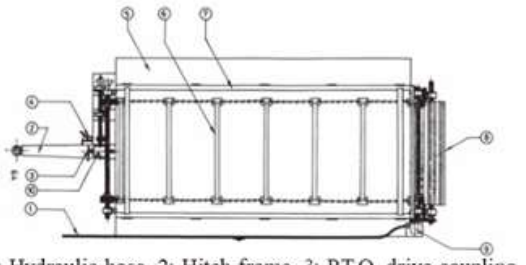

1: Hydraulic hose, 2: Hitch frame, 3: P.T.O. drive coupling, 4: Parking stand, 5: Tractor trailer, 6: Chain conveyor, 7: Manure tub, 8: Spreader, 9: Hydraulic motor, 10: Reduction gear box

Figure 2.Top view of manure spreader

The desired application rate of the manure can be obtained by selecting the suitable combination of the forward speed of operation, chain conveyor speed and the spreader speed. The application rate for the selected combination levels of the variables should meet optimum requirement of manure to be applied over field, which should be around 12 tonnes/ ha. The results of the investigation are summarized and the values are furnished in the It may be seen from the table that the combination of the forward speed of 2.31 km/hr, chain conveyor speed of 1.51 m/min and the any of the speed of spreader drum equals the (12.202 tonnes/ha) optimum requirement of the manure to be applied over the field. Based on analysis of results the following conclusions were made.

The application rate decreased with increase in forward speed of tractor. Minimum (8.13tonnes/ha) and maximum (18.40 tonnes/ha) application rate were observed for the forward speedof 4.00 km/hr and 1.88 km/hr, respectively. The application rate increased with decease in chain conveyor speed. The maximum application rate (13.80 tonnes/ha) was observed for the chain conveyor speed of 1.51 m/min followed by 1.88 m/min (12.437 tonnes/ ha) and 11.219 tonnes/ha), respectively. There was a linear relationship for the forward speed and chain conveyor speed with the application rate manure

Chain conveyor speed, m/min	Spreader speed, m/min	Application rate of manure (tones/ha) at selected levels of forward speed		
		1.88 km/min	2.31 km/min	4.00 km/min
2.26 m/min	25.12 m/min	16.16	10.39	6.93
	37.68 m/min	16.40	9.94	7.22
	47.10 m/min	16.92	10.08	7.06
1.88 m/min	25.12 m/min	18.85	10.59	8.43
	37.68 m/min	17.96	10.86	7.87
	47.10 m/min	18.47	10.74	8.09
1.51 m/min	25.12 m/min	20.11	12.22	9.22
	37.68 m/min	20.41	12.62	8.87
	47.10 m/min	20.25	12.02	9.46

Table 1- Application rate of manure for different combinations

The speed of the spreader drum did not influence the application rate of the manure over the field.

The spread pattern obtained was a flat top profile, which is acceptable form from the point of achieving uniform spreading. The desired application rate of manure (12.202 tonnes/ha) was observed for the forward speed of 2.31 km/hr and the chain conveyor speed of 1.51 m/min. The effective width of the manure for the all the treatments was 1.20 m.

There w as a 50-60 % of time saving with the manure spreading attachment two-wheel trailer when compared to conventional method of manure application. The manure spreading attachment to two-wheel trailer can also be used as a trailer by just Shifting a door whenever the trailer is required for transportation.

R. C. Singh and C. D. Singh (2014) [3] develop animal drawn spreader existing bullock carts which used for transport of manure to the field .it is modified for FYM spreading operation. Keeping all facts in mind an animal drawn FYM spreader is developed for uniform spreading of manure and eliminates the human drudgery involved in spreading of manure in the field. The developed farmyard manure spreader of 480 kg capacity and gave manure application rate of 5 to 10 t/ha for the manure delivery rate of 0.38 to 0.74 kg/s at the operational speed of 2.4 km/h, respectively.

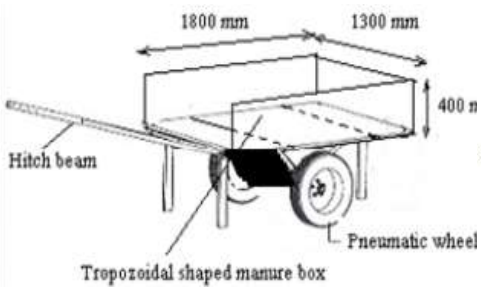

Figure 3-.Schematic view of developed manure spreader

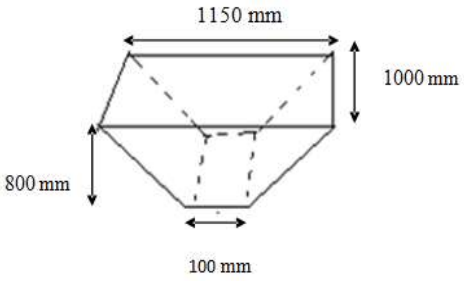

Figure 4.Trapezoidal shaped manure box.

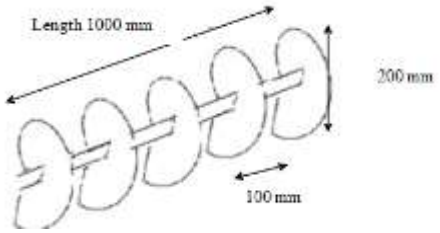

Figure 5. Details of spiral auger used for manure spreading. Spiral auger- disc size: Thickness = 2 mm; Pipe outside dia = 48 mm

Manure delivery rate (kg/min)	Speed, (m/s)	Swath, (m)	Application rate (t/ha)	Field capacity (ha/h)	Field efficiency (%)
23.8	0.68	1.1	5.30	0.19	84
22.4	0.67	1.1	5.06	0.20	83
22.9	0.66	1.1	5.25	0.18	83
Avg. 23.0	0.67	1.1	5.18	019	83

Moisture content = 20% (db).

Table 2 – Field performance on different opening width

Conclusion-Very least work has been done on design of manure spreader. The existing tractor drawn Manure spreader run on hydraulic power. It requires hydraulic motor and gear box. Attachment of spreader gets the power from PTO shaft of tractor. This spreader is heavy and difficult to maintenance. The performance of this spreader on farm field gives effective spreading with low cost and reduction of time, while animal drawn spreader require separate cart which is used only for carrying manure. It require spiral auger which is complex to manufacturing. It is intricate to get evenly spread pattern. The animal drawn spreader is economically efficient but it consume more time as compared to tractor drawn spreader. Review also underlines the need of manure spreader which is easy to operate and design. The Manure tub can be used for transportation after dismantling the spreader.

REFERENCES:

1] *P*.R Sapkale, S.B Mahalle and T.B Bastewad*, "Performance evaluation of tractor operated manure spreader",* International Journal of Agricultural Engineering, Vol. 3 No. 1 (April, 2010): 167-170.

[2] B. Suthakar, K. Kathirvel, R. Manian and D. Manohar Jesudas," Development and Performance Evaluation of Manure Spreading Attachment to Two Wheel Trailer", *agriculture mechanization in Asia, Africa and Latin America , vol. 39 May 2008.*

[3] R.C Singh and C.D Singh "Design and development of animal drawn farmyard manure spreader",*African journal of agricultural reaserch,Vol.9, October 2014.*

[4] Padmavati Manchikanti and Mahashweta sengupta,"Agricultural machinery in india: IPR perspective" ,*Journal of intellectual property right, vol 16,pp 163-169,March 2011*

International Journal of Engineering Research and General Science Volume 3, Issue 3, Part-2 , May-June, 2015
ISSN 2091-2730

Mining TPattern for capture, recognition and visualization in multiparty conversation

Anvita Saxena, Jyoti Chaudhary

Lecturer CSE, MIET Kumaon, Haldwani

anvita21saxena@gmail.com

Abstract— Discovering semantic knowledge is significant for understanding and interpreting how people interact with each other for a discussion. It becomes possible to extract frequent patterns of human interaction based on the captured content of face-to-face meetings by using mining method. Human interactions, such as proposing an idea, giving comments, and expressing a positive opinion, indicate user intention toward a topic or role in a discussion. Tree is used for representing a human interaction flow in a discussion session. Tree-based interaction mining algorithms are designed to analyze the structures of the trees and to extract interaction flow patterns. It can successfully extract several interesting patterns which is useful for the interpretation of human behavior in meeting discussions, such as determining frequent interactions, typical interaction flows, and relationships between different types of interactions.

Keywords— Human interaction, Interaction flow, Interaction Pattern, Meeting, Tree based mining, Decision Tree, Pattern Discovery

INTRODUCTION

Human interaction is the one of the important characteristic for understanding how a human's behavior or human activities under the meeting and determining whether the meeting was well organized or not is the one of the main issues in the meetings [1]. Meetings are an important communication and coordination activity of team where status is discussed, new alternatives are considered, information is presented, details are explained, decisions are made, and new ideas are generated. To understand and interpret human interactions in meetings, we need to discover higher level semantic knowledge about them, such as which interactions often occur in a discussion what interaction flow a discussion usually follows, and what relationships exist among interactions. This knowledge can called as grammar of meeting discussion because it describes important patterns of interaction. We are proposing an idea for a smart meeting system for capturing human interactions and recognizing their types, such as proposing an idea, giving comments, expressing a positive opinion, and requesting information [1]. In this study, we investigate data mining techniques to detect and analyze frequent interaction patterns; we hope to discover various types of new knowledge on interactions. Human interaction flow in a discussion session is represented as tree which is inspired by tree-based mining [2-3].

ANALYSIS OF PROBLEM

It is very important to understand the behavior and activities of a human during interaction. As such, meetings contain a large amount of rich project information that is often not formally documented. Capturing all of this informal meeting information has been a topic of research in several communities over the past decade. The most common way to capture meeting information is through writing the notes. However, it is very difficult task to write the whole content of a meeting.

PROPOSED SYSTEM

We propose a mining tree based method to extract frequent patterns of human interaction based on captured content of face-to-face meetings. The work focuses on discovering higher level knowledge about human interaction. In proposed system T-pattern technique is used to discover hidden time patterns in human behavior [5]. It conducts analysis on human interaction in meetings and addresses the problem of discovering interaction patterns from the perspective of data mining. It extracts simultaneously occurring patterns of primitive actions such as gaze and speech [6]. Discovering patterns of interaction flow from the perspective of tree-based mining [7] rather than using simple statistics of frequency. The main features of the process are user can also provide the idea about the topic. So admin can easily solve the problem based on users needed.

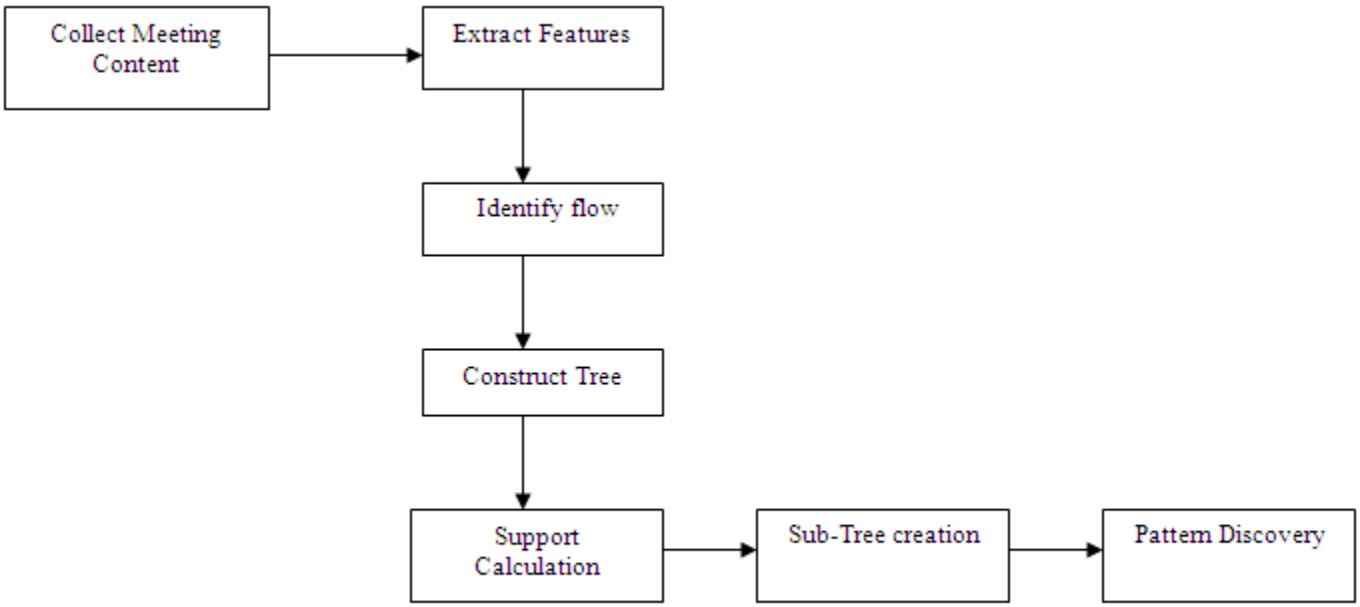

Fig1. Data Flow Diagram

Human Interaction Definition and Recognition

Human interactions in a meeting discussion are defined as social behaviors or communicative actions taken by meeting participants corresponding to the current topic. In meeting discussion human interaction are categorized as; propose, comment, acknowledgement, requestInfo, askOpinion, posOpinion, and negOpinion. The detailed meanings are as follows: propose— a user

Proposes an idea with respect to a topic; comment— a user comments on a proposal, or answers a question; acknowledgement—a user confirms someone else's comment or explanation, e.g., "yeah," "uh huh," and "OK;" requestInfo— a user requests unknown information about a topic; askOpinion- a user asks someone else's opinion about a proposal; posOpinion—a user expresses a positive opinion, i.e., supports a proposal; and negOpinion—a user expresses a negative opinion, i.e., disagrees with a proposal.

Interaction Flow

Based on the interaction defined and recognized, we now describe the notion of interaction flow and its construction. An interaction flow is a list of all interactions in a discussion session with triggering relationship between them. We first give the definition of a session in a meeting discussion.

Definition 1 (Session) A session is a unit of a meeting that begins with a spontaneous interaction and concludes with an interaction that is not followed by any reactive interactions

Pattern Discovery:

Patterns are frequent trees or sub trees in the tree database. TD denotes of Interaction trees.ITD denotes the full set of isomorphic trees to TD.t denotes a tree.tk denotes a sub tree with k nodes, Ck denotes a set of candidates with k nodes. Fk denotes a set of frequent k-sub trees.

Definition 2 (Interaction Tree) :

A tree is used to represent an interaction flow in a session. It is an acyclic connected graph. In which trees are also rooted, directed, and labeled. And they are represented as, L ={PRO,COM,ACK,REQ,ASK,POS,NEG}.

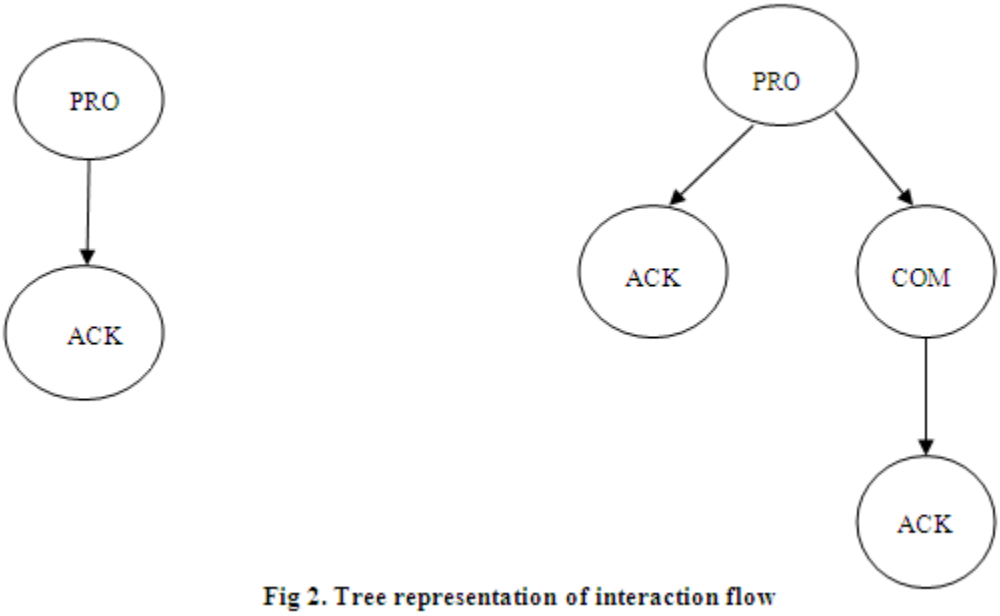

Fig 2. Tree representation of interaction flow

Definition 3 (Tree String Code):

A tree is represented as a string. We represent a tree T by its string encoding, denoted by tsc. It starts with the root, using "-" and " * " to denote parent child and sibling relationships, respectively. If a child has a descendant of its own, a parenthesis is used to separate it and its descendant from the others. According to this definition, trees in Fig. 2 are represented as PRO-ACK, PRO-(ACK-COM)*ACK, respectively.

Definition 4 (Tree Preorder Sequence):

This is a depth-first preorder traversal label sequence of a tree (T), denoted by tps. We use "-" to connect node labels in the sequence. In accordance with Definition 4, the trees in Fig. 2 are represented as PRO-ACK, PRO-ACK-COM-ACK, respectively.

Definition 5 (Isomorphic Tree):

Given two trees, T1 = (V1, E1) and T2 = (V2, E2), if tps(T1) ≠ tps(T2) and through exchanging the places of siblings on T1 or T2 (i.e., commutation processing), tps(T1) = tps(T2), we call T1 and T2 isomorphic trees. The purpose of the isomorphic tree definition is to find the same tree structure by exploiting temporal independence in the original interaction trees. For instance, two trees depicted in Fig. 3 are isomorphic because although their tree preorder sequences are different (PRO-COM-ACK- ACK and PRO-ACK-COM-ACK), through commutation.

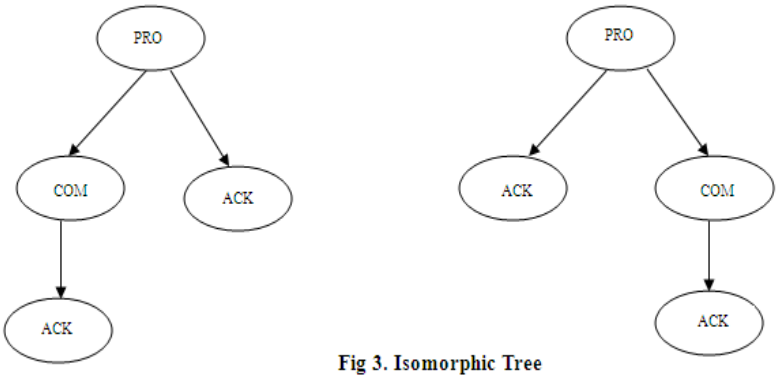

Fig 3. Isomorphic Tree

For the Pattern Discovery, we should have to find the support value.Where, σ denotes a support threshold of minimum support. Support is with given a tree or sub tree T and a data set of trees TD.

$$\text{Support} = \frac{\text{Number of occurrences of T}}{\text{Total no. of trees in TD}}$$

If the value of supp(T) is more than a threshold value Minimum support T is called a frequent tree or frequent sub tree. We have a data set of interaction trees TD. Given a minimum support σ, we would like to find all trees and sub trees that appear at least $\sigma \times |TD|$ times in the data set.

CONCLUSION

We proposed a tree-based mining method for discovering frequent patterns of human interaction in meeting discussions. It determines frequent interactions, typical interaction flows, and relationships between different types of interactions.The mining results would be useful for summarization, indexing, and comparison of meeting records. They also can be used for interpretation of human interaction in meetings .The Human interaction is represented as a Tree. Tree structure is used to capture how the person is interacted in meeting and discovers the interaction flow in meeting. Tree pattern mining and sub tree pattern mining will automatically analyze the structure and extract interaction flow pattern. Interaction flow helps to assume the probability of another type of interaction. The frequent interaction pattern and behavior of the person is determined.

REFERENCES:

[1] Z.W. Yu, Z.Y. Yu, H. Aoyama, M. Ozeki, and Y. Nakamura, "Capture, Recognition, and Visualization of Human SemanticInteractions in Meetings," Proc. Eighth IEEE Int'l Conf Pervasive Computing and Comm. (PerCom '10), pp. 107-115, Mar.-Apr. 2010.
[2] M.J. Zaki, "Efficiently Mining Frequent Tree in a Forest: Algorithms and Applications," IEEE Trans. Knowledge and Data Eng., vol.17, no. 8, pp. 1021-1035, Aug. 2005.
[3] C. Wang, M. Hong, J. Pei, H. Zhou, W. Wang, and B. Shi, "Efficient Pattern Growth Methods for Frequent Tree Pattern mining,"Proc. Pacific Asia Conf. Knowledge Discovery and Data Mining (PAKDD '04), pp. 441- 451, 2004.
[4] Q.Yang and X. Wu, "10 Challenging Problems in Data Mining Research," Int'l J. Information Technology and Decision Making, vol.5, no. 4, pp. 597-604, 2006.
[5] M.S. Magnusson, "Discovering Hidden Time Patterns in Behavior: TPatterns and Their Detection," Behavior Research Methods,Instruments and Computers, vol. 32, no. 1, pp. 93-110, 2000.
[6] K. Otsuka, H. Sawada, and J. Yamato, "Automatic Inference of Cross- Modal Nonverbal Interactions in Multiparty Conversations,"Proc. Int'l Conf. Multimodal Interfaces (ICMI '07), pp. 255- 262, 2007.
[7] S. Junuzovic, R. Hegde, Z. Zhang, P. Chou, Z. Liu, and C. Zhang, "Requirements and Recommendations for an Enhanced MeetingViewing Experience," Proc. ACM Int'l Conf. Multimedia, pp. 539- 548, 2008

International Journal of Engineering Research and General Science Volume 3, Issue 3, Part-2 , May-June, 2015
ISSN 2091-2730

Numerical Studies of Drag reduction on Circular Cylinder With V- Grooves

Munendra C V , Anusha Inamdar, Ranjeeth Kumar

Department of Mechanical Engineering, M. S. Engineering College, Bangalore-562110

munendracv610@gmail.com and 9916389037

Abstract—This work is carried out to investigate the flow structure around a circular cylinder with V- grooves numerically. Drag coefficient and turbulence statistics of wake behind each cylinder were analyzed for Reynolds number based on the cylinder diameter (D = 40mm) in the range $Re_D = 2 \times 10^4$. The V- type grooves reduce the drag coefficient acting on the cylinder by 28.47% at $Re_D = 2 \times 10^4$, compared with that of smooth cylinder at the same Reynolds number. The results were compared with that of a smooth cylinder having the same diameter and the fluid flow characteristics of wake behind the V- grooved cylinder have been analyzed. However, for the case of V- grooved cylinder, the vortices are largely distorted and spread out significantly as they go downstream and the longitudinal grooves seem to shift the location of span wise vortices toward the cylinder, reducing the vortex formation region as compared to the smooth cylinder. The pressure and velocity contours were ensemble averaged to get the spatial distributions of turbulent statistics including turbulent intensities and turbulent kinetic energy. In case of smooth cylinder, large-scale vortices formed behind the cylinder maintain round shape and do not spread out noticeably in the near wake. The sharp peaks of longitudinal V-shaped grooves also suppress the formation of large-scale secondary stream wise vortices and reducing turbulent kinetic energy near-wake region and the secondary vortices are broken into smaller eddies.

Keywords— Circular cylinder, V-Grooves, Drag coefficient, Pressure distribution, Turbulence, velocity vector, stream lines

1. INTRODUCTION

Flow around a circular cylinder was intentionally studied in the past and that returns to its simple geometry as well as the logical structure of the vortices. The studies were led on the one hand by academic interest and on the other hand by practical interest (industrial). In general there are two types to reduce the drag force namely "active control and passive control". The active control methods order the flow by ensuring external energy by means such as the acoustic excitation or the jet blow. The passive control methods order the flow by modifying the shape of the body or by attaching additives devices such as elements of roughness on the body. The active control requires complex mechanics devices which provide the external power to the flow consequently, the passive method is simpler and easier to realize.

Experimental and numerical investigations have showed a reduction in the drag when using longitudinal grooves namely 2 and 6 on the cylinder [1]. The unsteady incompressible flow fields around smooth and grooved circular cylinders have been simulated by solving the Navier-Stokes equations with appropriate boundary conditions. The groove effects are approximated by a "slip" velocity on the cylinder surface, instead of the conventional "non-slip" boundary condition for smooth cylinders, provided that three dimensionality of the whole flow field and interaction between the grooves and fluids near the surface [2]. Flow structure of wake behind a circular cylinder with longitudinal U- grooves has been investigated experimentally using PIV velocity field measurement techniques. The U- grooved cylinder reduces the drag coefficient by about 18.6%, compared with the smooth cylinder at ReD = 1.4 x 105. The drag reduction of the U- grooved cylinder increases with increasing Reynolds number. The vortex formation region behind U- grooved cylinder is smaller than for the smooth cylinder [3]. The incompressible flow around pairs of circular cylinders in tandem arrangements was investigated. The spectral element method is employed to carry out two- and three-dimensional simulations of the flow. The centre-to-centre distance (lcc) of the investigated configurations varies from 1.5 to 8 diameters (D), and results thus obtained are compared to the isolated cylinder case.Covering the transition in the wake the simulations are in the Reynolds number (Re) range from 160 to 320 and this analysis focuses on the small-scale instabilities of vortex shedding, which occurs in the Re range investigated [4]. It is demonstrated that the total groove area has a significant effect on reducing the critical Reynolds number, whether the area is increased through changing the groove shape, width, or depth.Drag reductions may be realized for circular cylinders in cross-flow by using grooves, even at very shallow relative groove depths.A strong correspondence to the minimum drag coefficient is also observed [5]. Studied on viscous flow past two circular cylinders of different diameters is simulated by using a finite element method. The diameter ratio between the small cylinder and the large one is 0.25. The Reynolds number based on the diameter of the

cylinders is 500 for the large cylinder and 125 for the small cylinder & the gap between the small cylinder and the large cylinder ranges from 0.05 to 1.0 times the diameter of the large cylinder. The position angle of the small cylinder relative to the flow direction ranges from 0 to . The effects of the gap ratio between the two cylinders and the position angle of the small cylinder on drag and lift coefficients, pressure distributions around the cylinders, the vortex shedding frequencies from the two cylinders and flow characteristics are investigated [6]. The viability and accuracy of large-eddy simulation (LES) with wall modeling for high Reynolds number complex turbulent flows is investigated by considering the flow around a circular cylinder in the supercritical regime. The results are compared with those obtained from steady and unsteady Reynolds-averaged Navier–Stokes (RANS) solutions and the available experimental data. The LES solutions are shown to be considerably more accurate than the RANS results. The boundary layer separation and reduced drag coefficients consistent with experimental measurements after the drag crisis. The mean pressure distribution is predicted reasonably well at ReD = 5 x 105 and 106 [7]. Flow past cactus-shaped cylinders are performed at Reynolds numbers of 20, 100, and 300. The results are contrasted to those from smooth cylinders at the same Reynolds numbers. The cavities in the cactus-shaped cylinders are seen to reduce the forces acting on them. At Reynolds number of 20, the drag is reduced by 22% due to reduction in the viscous forces. At Reynolds number of 100, the unsteady pressure forces increase, while the unsteady viscous forces acting on the cactus-shaped cylinder decrease. The overall reduction in drag force is about 18%. At Reynolds number of 300, onset of three dimensionality is observed together with significant decrease in pressure and viscous forces. Both the mean and fluctuating forces are found to decrease considerably. The Strouhal number is also found to decrease by about 10%. These reductions in force magnitudes and observed wake instabilities are attributed to the presence of large-scale, quiescent, recirculating flow within the cactus cavities [9]. The flow around a circular cylinder in air stream, a rod was set upstream of the circular cylinder. The diameter of cylinder, D, was 40 mm, and the diameter of rod, d, ranged from 1 to 10 mm. The distance between the axes of the circular cylinder and rod, L, was 50 – 120 mm. The Reynolds number based on D ranged from 1.5 x 104 to 6.2 x 104. Two flow patterns with and without vortex shedding from the rod occurred. The flow pattern changes depending on the rod diameter, its position and the Reynolds number. The optimum conditions of the drag reduction are d/D = 0.25, L/D = 1.75 2.0, in these conditions, vortices do not shed from the rod and the shear layer from the rod reattaches on the front face of the circular cylinder. The reduction of the total drag including the drag of the rod is 63% compared with that of a single cylinder [10]. Reductions in drag and fluctuating forces for a circular cylinder by attaching rings. Cylindrical rings were attached along the span of a cylinder at an interval of several diameters to reduce the drag and fluctuating forces caused by fluid flow. Experiments were performed at Reynolds numbers based on the cylinder diameter d ranging between Red = 3000 for 38 000. The aspect ratio of the cylinder, L/d, was approximately 20. The experimental results revealed that the drag force on the ring-attached cylinder was lower than for the 2D cylinder, even though the projected area was higher. The optimum ring configuration for drag reduction was found to be D/d = 1.3, W/d = 1.0, and P/d = 6 at Red =30 000, where D is the ring diameter, W is the span wise width of the ring, and P is the spanwise pitch of the ring. This configuration reduced the drag force by 15%. The considerable drag reduction was attributed to the formation of separation bubbles on both sides of the ring in the Red > 410 000–20 000 range. This in turn, lead to the narrowing of the wake behind the ring and the pressure recovery at the rear of the ring. The fluctuating lift, which was estimated from the fluctuating surface pressures, was also reduced in this range of Reynolds numbers due to the suppression of vortex shedding.

2. **NUMERICAL STUDY**

The geometry consists of an infinite cylinder mounted horizontally on the side walls where the two ends are fixed (the vibration effects are not considerate here). The downstream length and the upstream length are set at 11.5 of diameter; the origin of the Cartesian coordinate system is located at the centre of the base of the cylinder, the complete geometry is shown in Fig.2.1. The geometry and the boundary conditions remain the same for all tested cylinders.

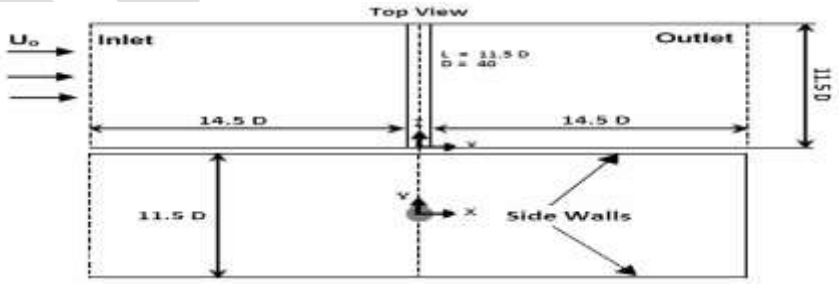

Fig.2.1: Geometry under consideration of infinite cylinder

The geometry carried out numerically corresponds perfectly to the dimensions of the experimental work [1]. In the present study the turbulence models was tested "k – ε standard". The grids have been tested for the case of Re 2×10^4 and AR = 11.5 and that for the smooth cylinders.

2.1 MESHING GEOMETRY OF A SMOOTH CIRCULAR CYLINDER

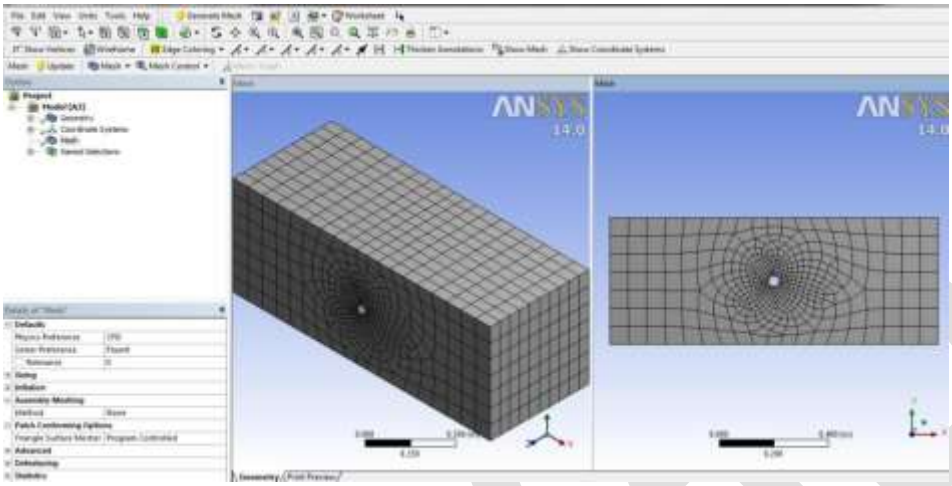

Fig.2.2: Meshing and name selection of meshing for smooth circular cylinder

Fig.2.3: Meshed smooth circular cylinder captured from the rectangular flow domain

ANSYS FLUENT was used for making 3D geometry of smooth surface cylinder with different groove type and angle. For L/D of 11.5 the diameter was taken to be 40mm. Hence the length of the cylinder is 460mm. A rectangular flow domain is taken of height 460mm, width 460mm and length 1200mm. The tested cylinder is placed horizontally at the center of the rectangular flow domain. Coarse mesh for the whole geometry. Then named selection was done for the entire geometry. In this model have been meshed in the ansys14. By this 4010 hexahedra elements and 40 wedges were found as shown in Fig.2.2. Fig.2.3. shows the detailed view of meshed smooth circular cylinder captured from the rectangular flow domain.

2.2 MESHING GEOMETRY OF A CIRCULAR CYLINDER WITH V- GROOVES

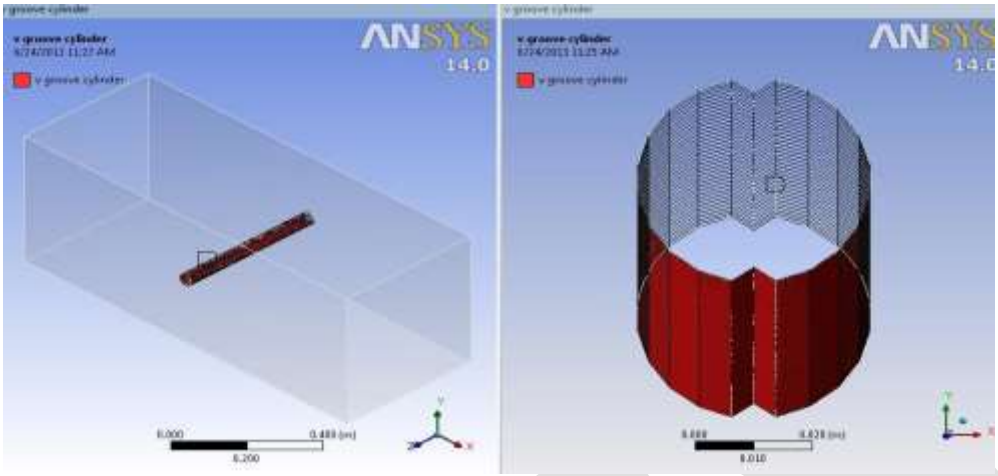

Fig.2.4: Meshed circular cylinder with V-grooves captured from the rectangular fluid flow domain

The modeling and geometrical parameters of circular cylinder with V-grooves remains same as smooth circular cylinder as shown in Fig.2.2. The only modification has been done on the surface of cylinder with V-grooves having 3mm depth and 110^{o} angle as shown in Fig.2.4. The coarse mesh for the whole geometry having 15873 hexahedra elements and 222 wedge elements were obtained.

3. Results and discussion

3.1 NUMERICAL ANALYSIS OF SMOOTH CIRCULAR CYLINDER:

The experimental tests were performed for the following physical parameters for the circular cylinder[1]:

- Reynolds number = 20000 (based on diameter and free-stream velocity).
- Free stream velocity (U_{∞}) = 7.5 m/s.
- Cylinder diameter = 40 mm
- Aspect ratios L/D = 11.5 in this study were investigated.

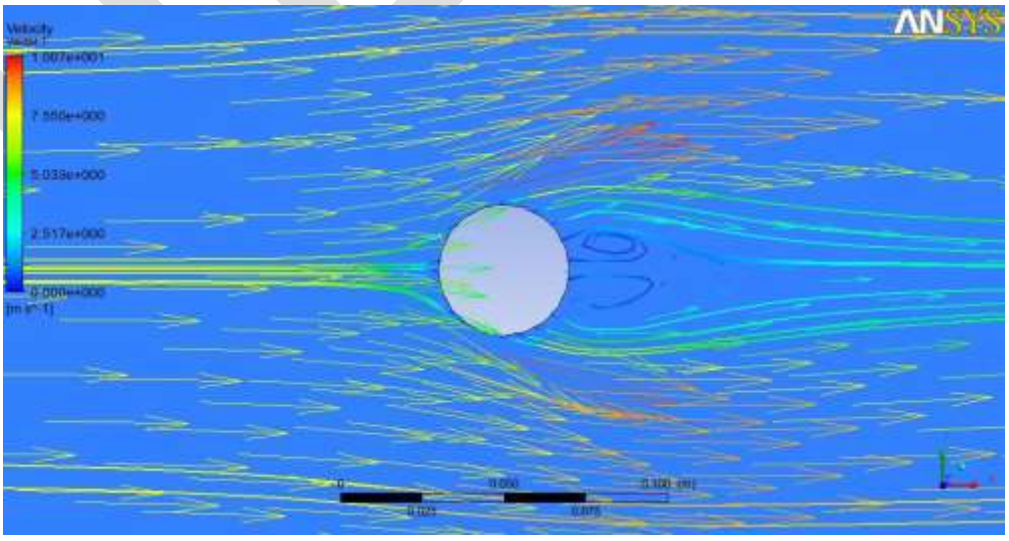

Fig. 3.1: Velocity vectors with stream lines for smooth circular cylinder

At Reynolds = 2×10^4 the flow pattern around the surface as shown in Fig. 3.1, The flow separates takes place in the downstream and a wake zone is formed by two symmetrical standing eddies. This gives rise to a zone of low pressure and the flow in this wake is highly turbulent and consisting of large eddies. High-rate energy dissipation takes place with the result that the pressure in the wake is reduced. A situation is thus created whereby the pressure acting on the front of the body is in excess of that acting on the rear of the body. The force arising from the pressure difference or more generally from the non-uniform pressure distribution on the body. The drag coefficient for the smooth cylinder is nearly constant and has an average value of 1.37. It agrees well with those of previous results measured in the ranges of $2 \times 10^4 < Re_D < 10^5$ nearly well-matched with the total drag coefficients at the same condition within the subcritical regime[1].

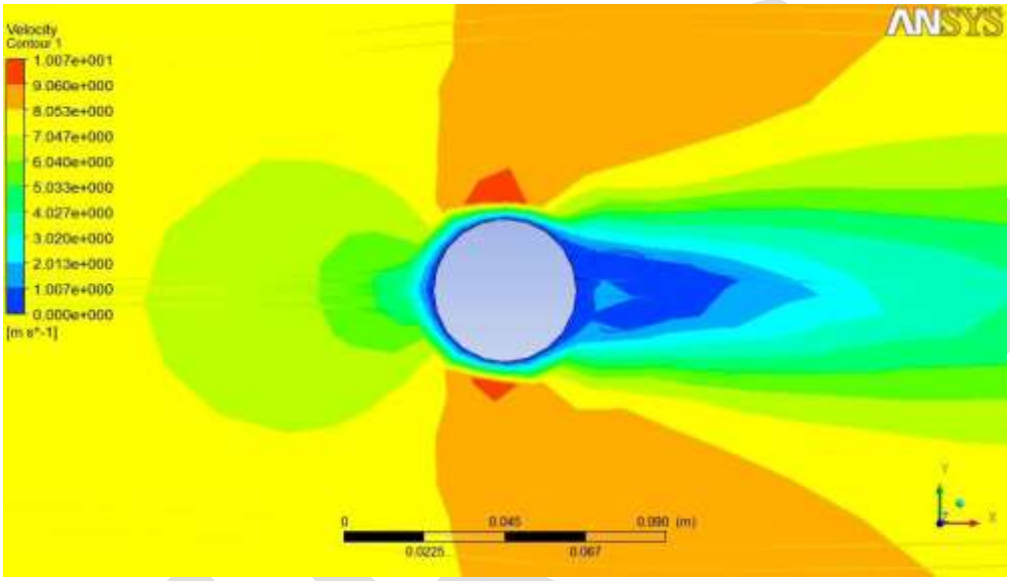

Fig.3.2: Velocity contours for a smooth circular cylinder

Fig.3.2 shows the velocity contours for a smooth circular cylinder. For a given cylinder, it was observed that velocity contours is maximum at top and bottom surface and minimum at back side of the cylinder. Because the velocity flow over the top and bottom is greater than free stream velocity.

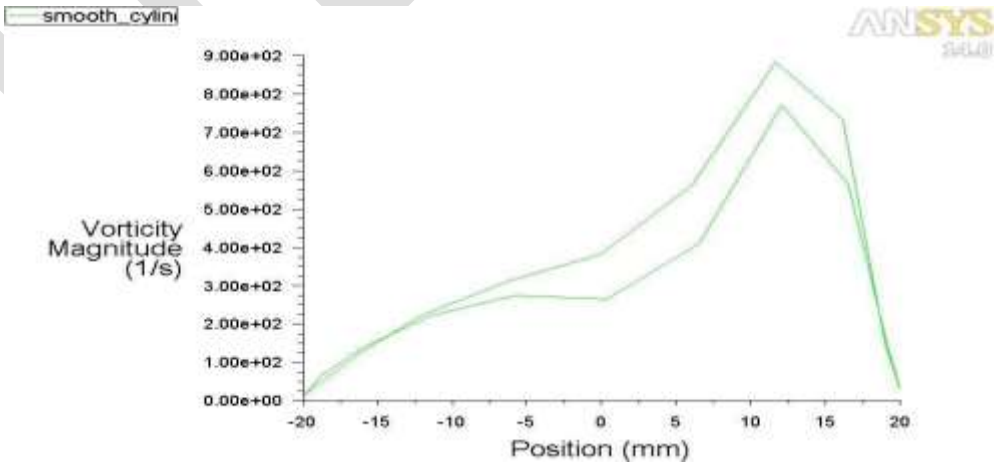

Fig.3.3: Vorticty magnitude v/s position of smooth circular cylinder

Fig.3.3 shows the vorticity magnitude v/s position of the smooth circular cylinder. From the Fig. It was observed that vorticity magnitude increases gradually upto to the sides of the cylinder and it is maximum at the point of wake formation. This gives rise to a wake zone of low pressure and the flow in this wake is highly turbulent and consisting of large eddies. High-rate energy dissipation takes place with the result that the pressure in the wake is reduced.

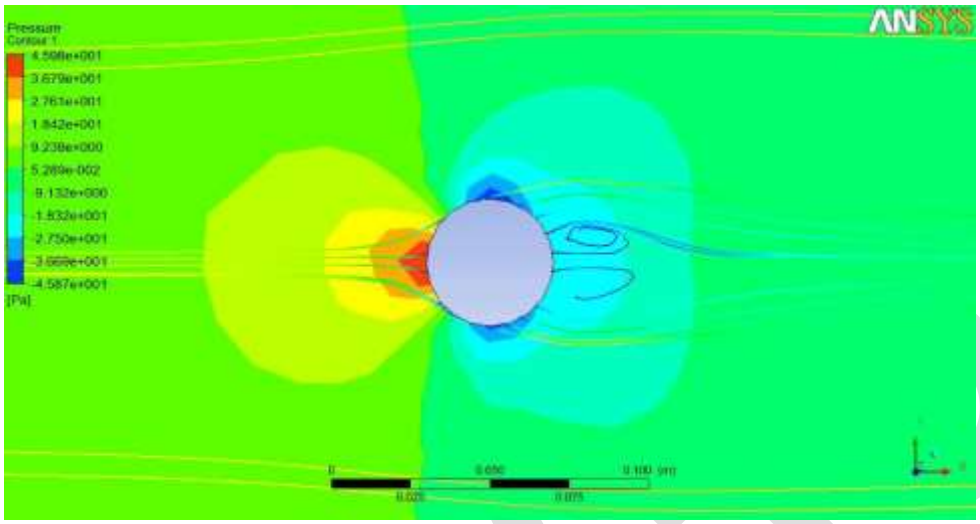

Fig. 3.4: Pressure contours for a smooth circular cylinder.

Fig.3.4 shows the maximum pressure at the front surface and minimum pressure at the back surface of the cylinder. High-rate energy dissipation takes place with the result that the pressure in the wake is reduced. A situation is thus created whereby the pressure acting on the front of the body is in excess of that acting on the rear of the body. The force arising from the pressure difference or more generally from the non-uniform pressure distribution on the body. As a result of pressure difference, drag will increases

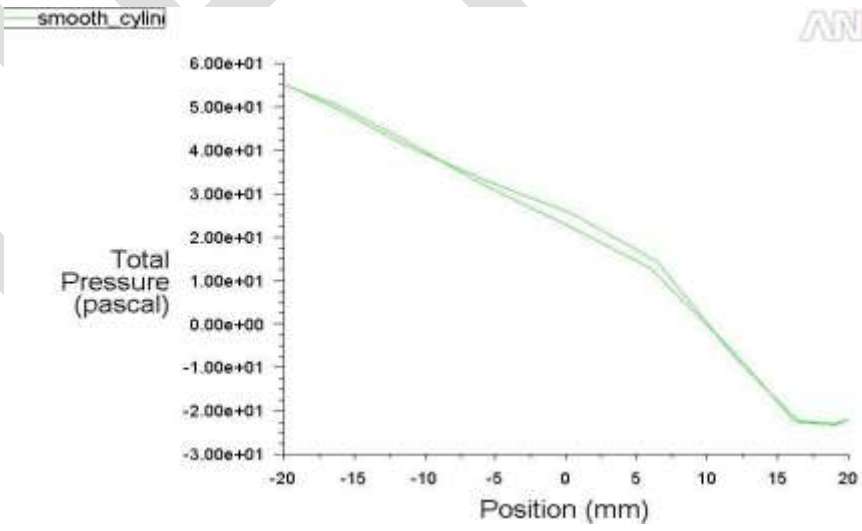

Fig 3.5: Total pressure contours for a smooth circular cylinder

Fig.3.5 shows total pressure curve for the smooth circular cylinder, as velocity increases, the boundary layer breaks away and eddies are formed behind. The drag becomes increasingly due to the pressure up at the front and pressure drop at the back of the cylinder. From the above Fig. it shows that how the total pressure decreases from front to back of the cylinder.

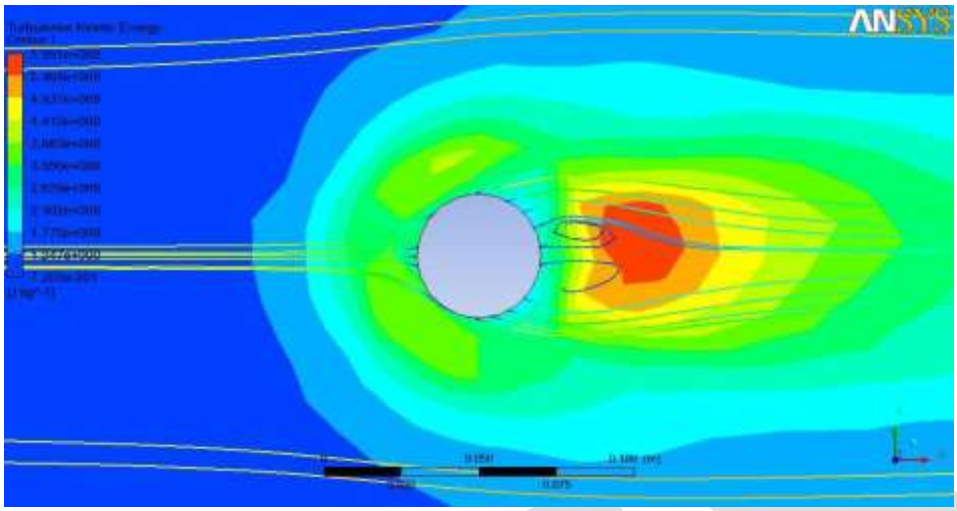

Fig.3.6: Turbulence kinetic energy for a smooth circular cylinder

Fig.3.6 shows that generation of wakes. Normally generation of wake takes place at the back side of the cylinder, turbulence kinetic energy is maximum at wake region and as a result of this smooth cylinder, most vorticity centers are uniformally distributed behind the cylinder. In addition to this, the smooth cylinder has larger number of vorticity at centers

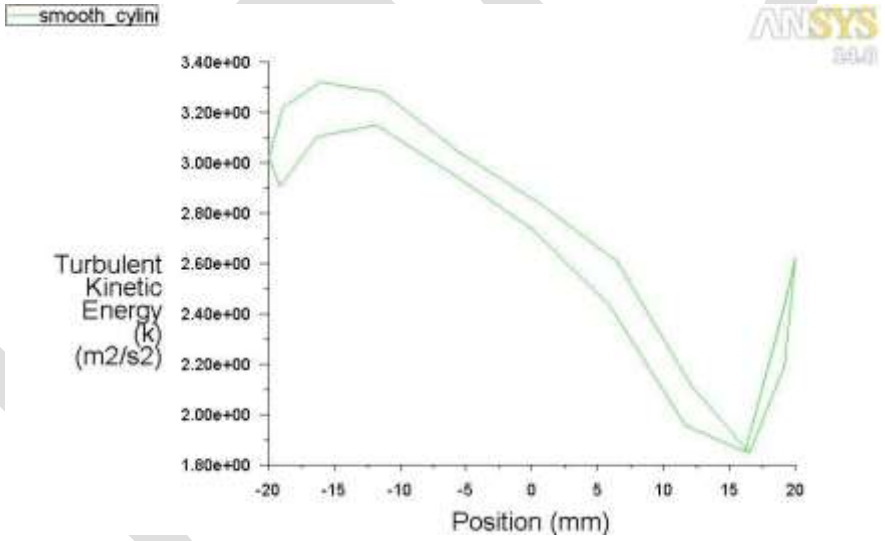

Fig.3.7: Turbulence kinetic energy v/s position of smooth circular cylinder

Fig.3.7 shows that turbulence kinetic energy uniformly decreases upto the point of wake region. After that, the turbulence kinetic energy increase due to the formation wake which results in the increase of drag coefficient.

3.2 NUMERICAL ANALYSIS OF CIRCULAR CYLINDER WITH V-GROOVES:

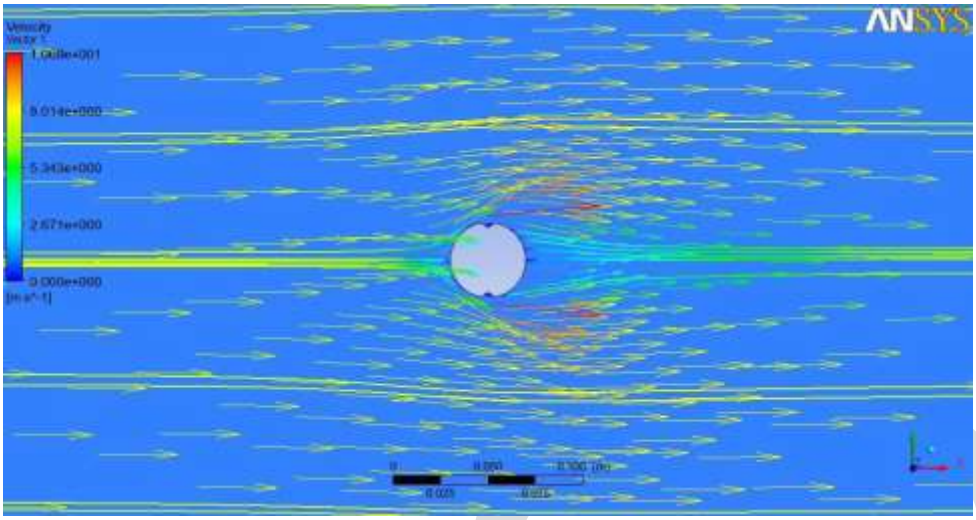

Fig.3.8: Distribution of velocity vectors and stream lines for a cylinder with V- groove

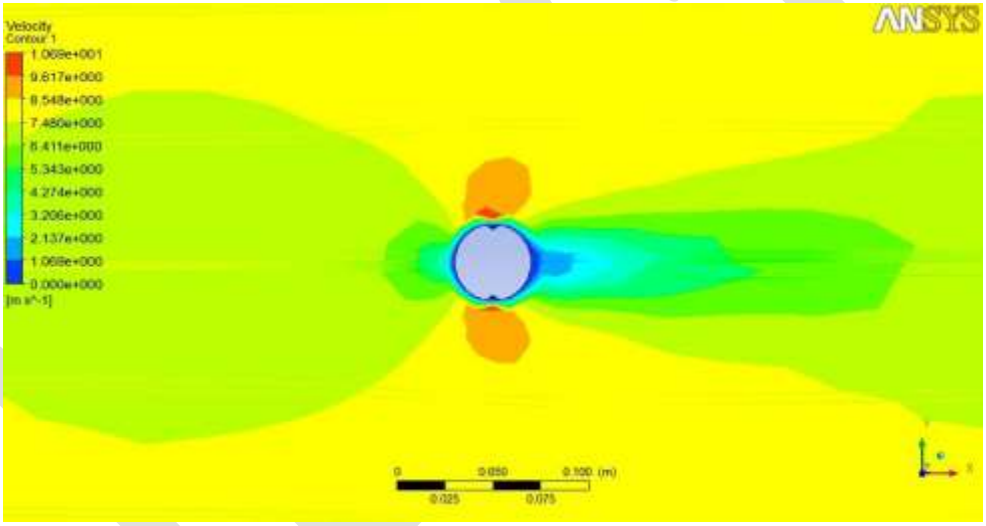

Fig.3.9: Velocity contours for a cylinder with V- groove

It appears that the flow pattern near the surface changes significantly due to the presence of grooves. Figs. 3.8 and 3.9, shows velocity vectors with stream lines and velocity contours. The vector plots indicate the presence of recirculation zones within the V- grooves, although Figs.3.8 and 3.9 contain recirculation zones. This indicates the presence of small-scale flow closer to the surface at high Reynolds numbers. At low Reynolds numbers the grooves create local recirculation zones filled with low momentum quiescent flow. These regions have decreased surface stresses and decreased pressure forces closer to the surface. This mechanism is absent in a smooth cylinder.

V- Grooves geometry for a smooth cylinder it is seen that, the viscous drag and lift forces decrease with increasing Reynolds numbers. At low Reynolds numbers (Re = 20 to 100) the presence of quiescent recirculation zones within the V - grooves lead to lower, which decreases the contribution of viscous forces. As the Reynolds number increases, smaller scales of motion are observed near the surface of V- groove cylinder which lead to higher. Therefore at a given Reynolds number the viscous forces decrease for a V- shaped groove cylinder in comparison to a smooth cylinder. The pressure forces do not change significantly at low Reynolds number. The pressure drag decreases by more than 28% at Re (2×10^4). It is speculated that, it is due to onset of three dimensional effects.

It is speculated that the effect of drag reduction in V- grooves cylinders will be less pronounced at significantly higher Reynolds numbers due to the presence of smaller turbulent length scales. At these high Reynolds numbers, a turbulent flow within the V-grooves will lead to a higher viscous forces near the surface, thereby reducing the effect of drag reduction mechanism. Since this behavior at significantly higher Reynolds numbers is explained based on the understanding at lower Reynolds numbers, the actual drag reduction mechanism might differ. It is therefore seen that the drag reduction is significantly higher at low Reynolds numbers and this grooves effect decreases with increasing Reynolds number.

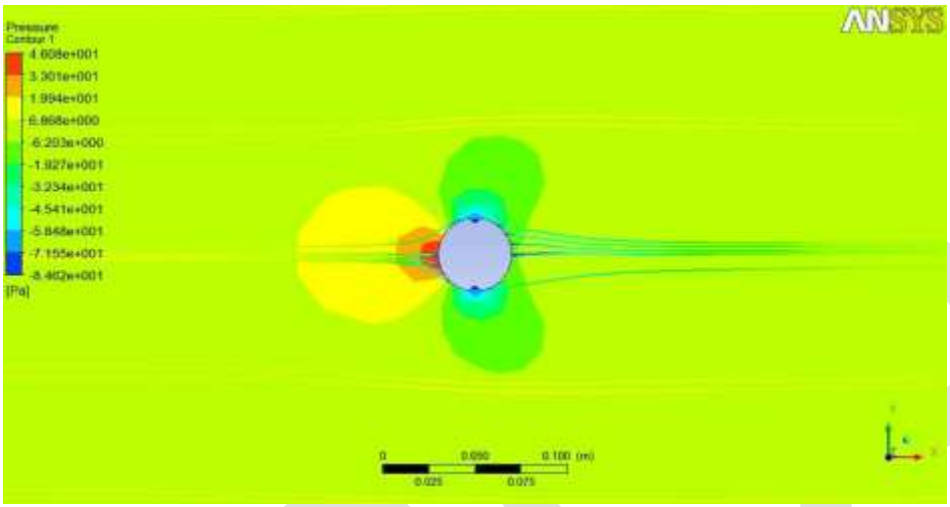

Fig.3.10: Pressure contours for cylinder with V- groove

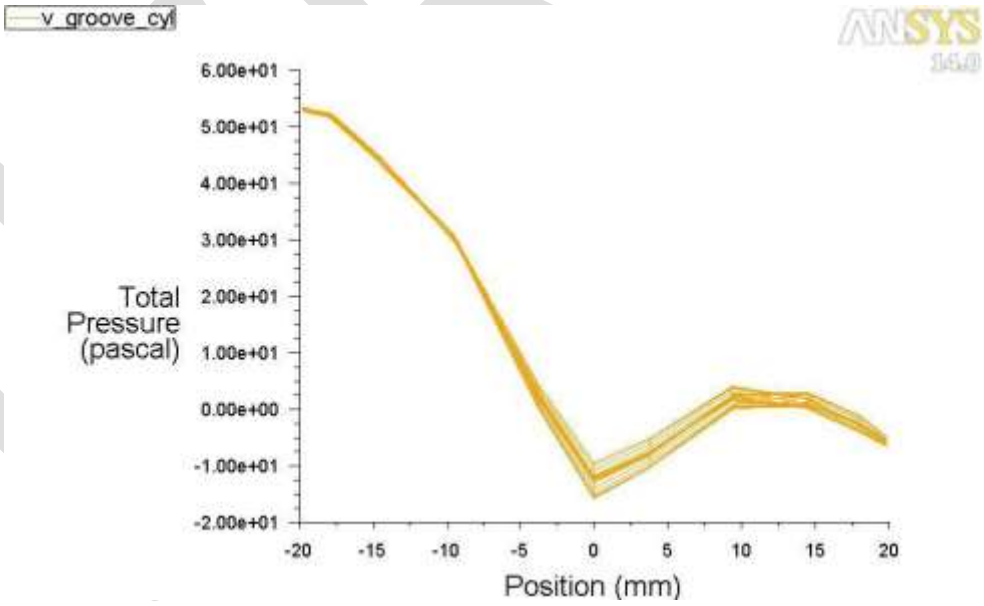

Fig.3.11: Total pressure distribution on cylinder with V – grooves

Pressure distributions at Re = 20000 for the cylinders, shown in Fig.3.10. There is greater pressure recovery for cylinders with cavities than for the smooth and rough cylinders. The cylinders with V- grooves have greater negative pressures on the sides of the cylinder. Pressure recovery appears to increase with increasing groove depth while the negative pressures on the sides of the cylinder appear not to be affected by groove depth. The pressure distribution depends somewhat on the orientation of the groove to the flow. When the groove trough faced the flow static pressures were very similar to those when the wall faced the flow. Conversely, when apex was

facing the flow, static pressures differed from those when the wall or groove trough faced the flow. The largest differences were for pressures on the front and sides of the cylinder. Fig.3.11 shows the total pressure curve for the V - groove cylinder. The pressure gradually decreases upto the position of V - grooves on cylinder surface. Due to this, there is a greater pressure recovery for sides of the cylinder.

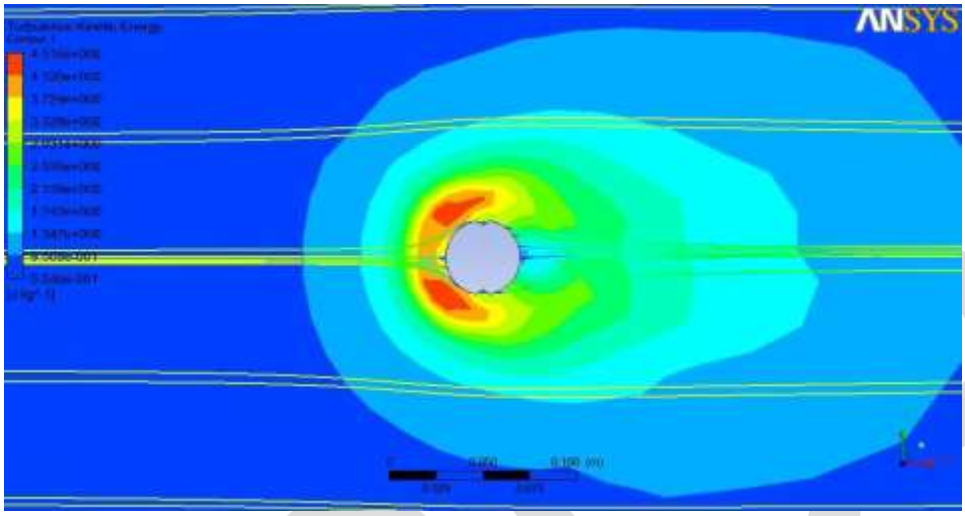

Fig.3.12: Turbulence kinetic energy for cylinder with V- grooves

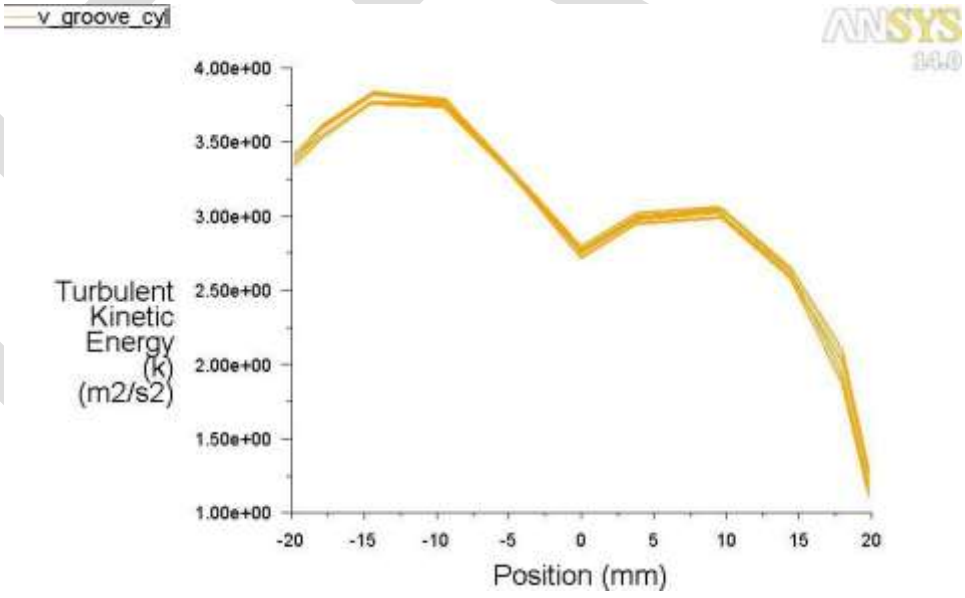

Fig.3.13: Turbulence kinetic energy v/s position of cylinder with V- grooves

Fig.3.12 shows the averaged turbulence kinetic energy distribution, the cylinder has large turbulence kinetic energy and regions of large and small kinetic energy exist together. However, the V - grooved cylinder seems to reduce the turbulence kinetic energy in the near wake. This may be attributed to the fact that formation of secondary vortices is suppressed in the region behind the V- grooved cylinder. The secondary vortices are broken into smaller eddies due to sharp peaks of the longitudinal V- shaped grooves. Fig.3.13

shows the turbulence kinetic energy v/s position of cylinder. The turbulence kinetic energy drops from back side of the V- grooves as there is less vortex formation.

3.3 DRAG COEFFICIENT AND V- GROOVE ANGLE STUDIES OF CYLINDER

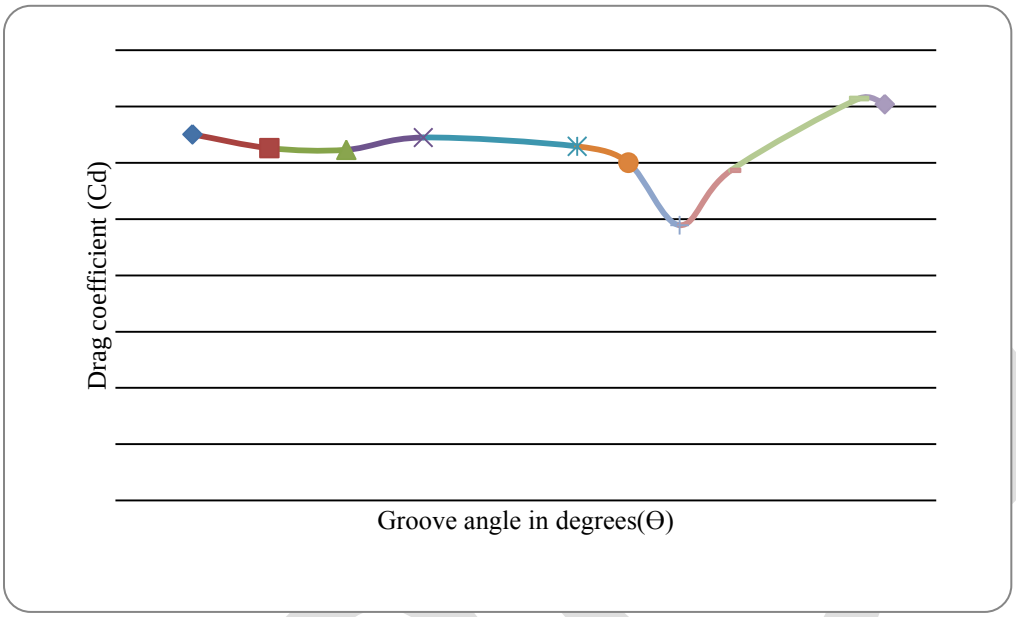

Fig.3.14: V- groove angle versus drag coefficient for cylinder with V- grooves

Fig.3.14 for the study of V – groove angle vary from 15 to 150^o at constant groove depth and Re = 2 × 10^4, The minimum drag coefficient is 0.9781 at an angle of 110^o and 3mm depth and the maximum available drag coefficient is 1.4283 at an angle of 145^o. The values of V – grooves on surface of circular cylinder from the table 3.1.

Table 3.1: Drag coefficient and v- groove angle studies on cylinder with V- groove

Groove angle in degree (Θ)	Groove Depth in mm (h)	Drag force in N (F_D)	Drag coefficient (C_d)
15	3	0.8247	1.3009
30	3	0.7937	1.2520
45	3	0.7899	1.2460
60	3	0.8176	1.2897
90	3	0.7977	1.2583
100	3	0.7609	1.2002
110	3	0.6201	**0.9781**
120	3	0.7436	1.1729
145	3	0.9055	1.4283
150	3	0.8926	1.4080

CALCULATION:

At 110 ^{o} V - groove angle and 3mm depth

From fluent data the properties of fluid, fluid as air given below

$\rho = 1.225\ kg/m^3$, $\mu = 1.7894 \times 10^{-5}$ kg/m-s

Physical parameters:

D = 40mm, L =460mm, S = $D \times L$

Formula for drag coefficient:

$$C_d = \frac{2F_D}{\rho \times U^2 \times S}$$

$$= \frac{2\times 0.6201}{1.225\times 7.5^2 \times 0.04\times 0.46}$$

$$= \frac{1.2402}{1.2679}$$

$$= 0.9781$$

Table 3.2: Drag coefficient and V– grooves depth on cylinder with V-grooves

Angle in degree (Θ)	Groove depth in mm (h)	Drag force in N (F_D)	Drag coefficient (C_d)
110	2	0.7276	1.1477
110	3	0.62008	**0.9781**
110	4	0.6862	1.0824
110	5	0.7264	1.1458

Table3.2 the study of V – groove depth vary from 2 to 5mm at constant groove angle, the numerical results are obtained as shown in the table 3.2. In this study had conclude that the minimum drag coefficient is obtained at an angle 110 ^{o} and 3mm depth, further increases the groove depth, the drag force also increases for this studies.

ACKNOWLEDGMENT

I express my sincere thanks and heartfelt gratitude to my guide, Mr. Kishan Naik for their, inspiration, guidance and support during this project work. I thank my parents & friends for their moral support.

CONCLUSION

The flow structure of wake behind a circular cylinder with longitudinal V-grooves has been investigated numerically using CFD tool techniques.

- The V-grooved cylinder reduces the drag coefficient by about 28.47% at $Re_D = 2\times 10^4$, compared with the smooth cylinder at same Reynolds number.
- The drag reduction of the V- grooved cylinder increases with increasing Reynolds number.
- The vortex formation region behind V- grooved cylinder is smaller than for the smooth cylinder.
- The longitudinal grooves seem to reduce the size of spanwise vortices and shift their location toward the cylinder. The sharp peaks of longitudinal V- shaped grooves also suppress the formation of large-scale secondary streamwise vortices.
- The secondary vortices are broken into smaller eddies, reducing the turbulence kinetic energy in the near-wake region.

REFERENCES:

[1] Ladjedel A.O, Yahiaoui B.T, Adjlout C.L and Imine D.O, " Experimental and Numerical Studies of Drag Reduction on a Circular Cylinder", World Academy of Science, Engineering and Technology 53 2011.

[2] Zhang H.L, and N.W.M. KO, "Numerical Analysis Of Incompressible Flow Over Smooth And Grooved Circular Cylinders", Department of Mechanical Engineering, The University of Hong Kong, Pokfulam Road, Hong Kong, 1995.

[3] Lim H.C, Lee S.J, "PIV Measurements Of Near Wake Behind A U-Grooved Cylinder",Journal Of Fluids And Structures 18 (2003) 119–130.

[4] Carmo B.S, Meneghini J.R, "Numerical Investigation Of The Flow Around Two Circular Cylinders In Tandem", Journal of Fluids and Structures 22 (2006) 979–988.

[5] Steven J. Quintavalla , Alexander J. Angilella, Alexander J. Smits , " Drag Reduction On Grooved Cylinders In The Critical Reynolds Number Regime", Experimental Thermal and Fluid Science 48 (2013) 15–18.

[6] Ming Zhao, Liang Cheng, Bin Teng, Dongfang Liang, "Numerical Simulation Of Viscous Flow Past Two Circular Cylinders Of Different Diameters", Applied Ocean Research 27 (2005) 39–55.

[7] Pietro Catalano, Meng Wang, Gianluca Iaccarino, ParvizMoin, "The Viability And Accuracy Of Large-Eddy Simulation (LES) With Wall Modeling For High Reynolds Number Complex Turbulent Flows Is Investigated By Considering The Flow Around A Circular Cylinder In The Supercritical Regime" International Journal of Heat and Fluid Flow 24 (2003) 463–469.

[8] Braza M, Perrin R, Hoarau Y, "Turbulence Properties In The Cylinder Wake At High Reynolds Numbers", Journal of Fluids and Structures 22 (2006) 757–771.

[9] Pradeep Babu and Krishnan, Mahesh, "Aerodynamic Loads On Cactus Shaped Cylinders At Low Reynolds Numbers", Physics Of Fluids 20, 035112 (2008).

[10] Tsutsui T, Igarashi T, "Drag Reduction Of A Circular Cylinder In An Air-Stream", Journal of Wind Engineering and Industrial Aerodynamics 90 (2002) 527–541.

[11] Sharon Talley and Godfrey Mungal, "Flow Around Cactus-Shaped Cylinders" Center for Turbulence Research Annual Research Briefs 2002.

[12] Fujisawa N, Asano Y, Arakawa C, Hashimoto T, "Computational And Experimental Study On Flow Around A Rotationally Oscillating Circular Cylinder In A Uniform Flow", Journal of Wind Engineering and Industrial Aerodynamics 93 (2005) 137–153

[13] Igbalajobi A, McClean J.F, Sumnern D, Bergstrom D.J, "The Effect Of A Wake Mounted Splitter Plate On The Flow Around A Surface-Mounted Finite-Height Circular Cylinder", Journal of Fluids and Structures 37 (2013) 185–200.

[14] Nakamura H, Igarashi T, "Omnidirectional Reductions In Drag And Fluctuating Forces For A Circular Cylinder By Attaching Rings" Journal of Wind Engineering and Industrial Aerodynamics 96 (2008) 887–899.

[15] Viswanath P.R,"Aircraft Viscous Drag Reduction Using Riblets" Progress in Aerospace Sciences 38 (2002) 571–600.

[16] Shan Huang, "Omcircular Cylinder And Drag Reduction Of A Fixed Circular Cylinder By The Use Of Helical Grooves", Journal of Fluids and Structures 27 (2011) 1124–1133.

[17] Mutschke G, Shatrov V, Gerbeth G, "Cylinder Wake Control By Magnetic Fields In Liquid Metal Flows" Experimental Thermal and Fluid Science 16 (1998) 92-99.

[18] Aswatha Narayana P. A, Seetharamu K. N, "Engineering Fluid Mechanics", text Book, Alpha science international, 2004

International Journal of Engineering Research and General Science Volume 3, Issue 3, Part-2 , May-June, 2015
ISSN 2091-2730

Power Quality Improvement by UPQC in Distribution System

Sneha Bageshwar[1], Dr. D. P. Kothari[2]

[1]M-Tech Student, Department of Electrical Engineering, Waingangā College of Engineering & Management,

Nagpur, Maharashtra, India

snha.bageshwar@gmail.com

[2] as Director – Research in Gaikwad-Patil Group of Institutions, Nagpur, Maharashtra, India

dpkvits@gmail.com

Abstract— The quality of electrical power supply is adversely affected by the use of power electronic based equipment. Power quality problems raised are reduced by using Custom Power Devices (CPD).Unified Power Quality Conditioner (UPQC), is a device which allow the mitigation of voltage and current disturbances that could affect sensitive electrical loads. UPQC is a combination of Series Active Power Filter (APF) that compensates voltage harmonics of the power supply, and Shunt APF that compensates harmonic currents of a non-linear load. This paper presents realization of UPQC using PWM-VSI inverter in MATLAB/Simulink tool. A dqo transformation based PWM controller is used to derive gating pulses for the IGBT switch. Comparison of voltage and current level in different operating condition, along with the level of Total Harmonic Distortion (THD) with and without UPQC and faulted condition.

Keywords— Power Quality, UPQC, APF, THD, dqo transformation, FACTS, Shunt Controller, Series Controller.

INTRODUCTION

In modern power distribution system the use of nonlinear loads is increased. Many non-linear loads like electric arc furnaces, power electronic convertors etc. introduces current and voltage harmonics. Proper functioning of sensitive loads like computers, micro-controllers depend upon the quality of power supplied. Various electrical power quality problems such as voltage sag, swell, harmonics, noise, voltage unbalance, etc are found. For the mitigation of current as well as voltage based distortions, various Custom Power devices can be used. Different CPD such as Dynamic Voltage Regulator (DVR), Distribution Static Compensator (DSTATCOM), and UPQC are also reported for the effective mitigation of voltage sag/swell, while compensation capability of UPQC is better.

The UPQC is a combination of series and shunt active filters connected in cascade via a common DC link capacitor. Both the devices are fired by gating signals. The gate pulses are generated by control technique used. It is the control strategy which decides the efficiency of a particular system. The main purpose of a UPQC is to compensate for supply voltage and current. UPQC can absorb active power or inject active power. The shunt connected converter balance the source currents by injecting negative and zero sequence components and control the power factor by injecting the required reactive current. The series connected converter balance the voltages at the load bus by injecting negative and zero sequence voltages and regulate the magnitude of the load bus voltage by injecting the required active and reactive components.

This paper deals with the effectiveness of UPQC for distribution network with nonlinear load under normal and faulted conditions. The proposed control technique has been evaluated under different load conditions using MATLAB software.

UNIFIED POWER QUALITY CONDITIONER

UPQC is the integration of Series APF and shunt APF, active power filters, connected back-to-back on the dc side, sharing a common DC capacitor. The series component of the UPQC is responsible for mitigation of the supply side disturbances: voltage sags/swells, flicker, voltage unbalance and harmonics. It inserts voltages so as to maintain the load voltages at a desired level; balanced and distortion free. The shunt component is responsible for mitigating the current quality problems caused by the consumer: poor power factor, load harmonic currents, load unbalance etc. It injects currents in the ac system such that the source currents become balanced

sinusoids and in phase with the source voltages. The overall function of UPQC mainly depends on the series and shunt APF controller. The integrated controller of the series and shunt APF of the UPQC to provide the compensating voltage reference V_c and compensating current reference I_c.. The system configuration of a UPQC is shown in the Figure given below.

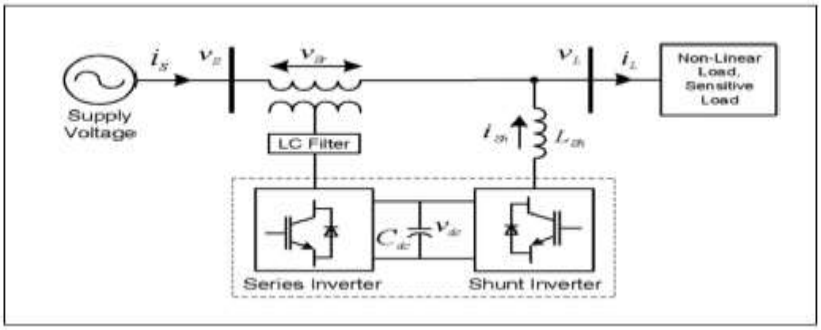

Figure 1. Block Diagram of UPQC

The equivalent circuit of UPQC is shown in the figure 2. An ideal controlled voltage source is connected in series in the circuit and current source is connected in shunt of the circuit so that the circuit works same as that of the UPQC.It is controlled in such a way that the voltage at load bus is always sinusoidal and at desired magnitude. Therefore the voltage injected by series active power filter must be equal to the difference between the supply voltage and the ideal load voltage. Thus the series active power filter acts as controlled voltage source. The function of shunt active power filter is to maintain the dc link voltage at constant level. In addition to this the shunt active power filter provides the VAR required by the load, such that the input power factor will be unity and only fundamental active power will be supplied by the source.

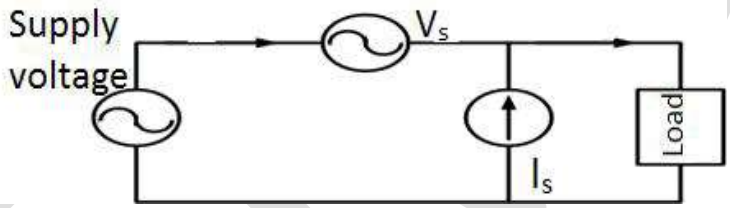

Figure 2. Equivalent Circuit of UPQC

CONTROL STRATEGY OF UPQC

The control strategy proposed here aims to generate reference signals for both shunt and series APFs of the UPQC. The proposed control technique is capable of extracting most of the load current and source voltage distortions. The series APF is controlled to eliminate the supply voltage harmonics; whereas the shunt APF is controlled to the supply current harmonics and negative sequence current. In this paper, d-q frame theory is used to control both series and shunt controller.

A. Description of Implementation of Series Controller

The control strategy of series controller is shown in figure 3, in which voltage from the load and source is converted to its equivalent dq0 components, by using the angles from the discrete three phases PLL. The angles for the calculation are generated by using load voltage. The resultant voltage is then transferred back to the 3 phase component using reverse transformation. The resultant abc component is the fed to the discrete Pulse With Modulation generator (PWM) to produce gate pulses. The dq0 transformation is done by parks transformation. The same formula can be used for current transformation. Inverse parks transformation for the generation of reference signal.

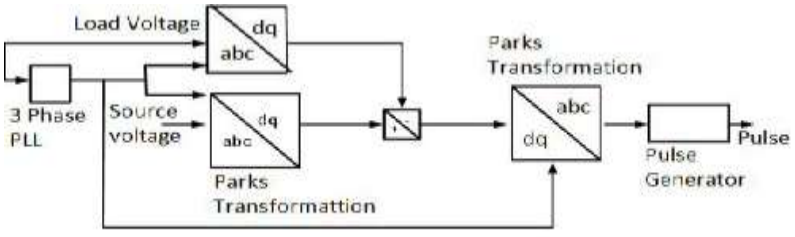

Figure 3. Control Strategy for Series Controller

B. Description of Implementation of Shunt Controller

The control strategy of shunt controller is shown in figure 4. It is same as that for series controller, the difference lies in the fact that input in place of control voltage wave having magnitude of 1 p.u controlled by the angles drawn from the PLL (phase locked loop). Load current is given as input to PLL.The angles for the calculation is generated by using load current using parks transformation equation. Resultant reference signal is fed to PWM generator, which produce gate signal.

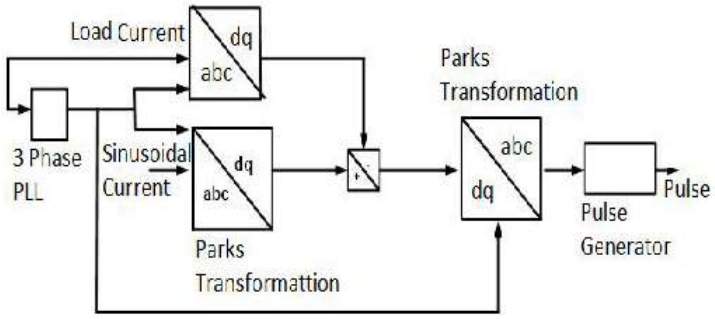

Figure 4. Control Strategy for Shunt Controller

SIMULATION MODEL OF UPQC

In this model, the load is fed from the utility of 200V and 50 Hz as a source. A step up transformer is used to step up the utility voltage of 200V to 440V. A non-linear load is chosen for the purpose of investigation of single line to ground fault and double-line to ground fault. The series and shunt compensator of UPQC is connected through an inductor so that to remove the harmonics from the injected voltage and to remove the distortions in the injected current. Here, two compensators of UPQC works as Dynamic Voltage Restorer (DVR) and Distribution Static Compensator (DSTATCOM), the series compensator works as DVR and the shunt compensator works as DSTATCOM.

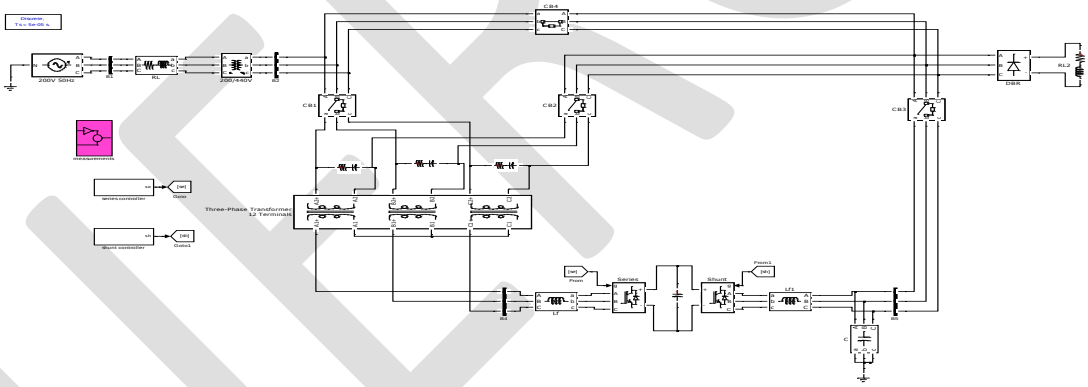

Figure 5. Matlab/Simulink model of UPQC

SIMULATION RESULTS

Based on above proposed model of UPQC, the system is analyzed for normal conditions and fault conditions. Results for simulation without using UPQC are also given for comparison.

A. Simulation results in normal operating conditions

a. Simulation results Without Using UPQC

Model as shown in figure 5, with test parameters is connected to a non-linear load. Load voltage and load current waveforms are shown in figure 6 and 7. Fast Fourier Transform (FFT) analysis is also done to determine the difference in percentage of Total Harmonic Distortion (THD).

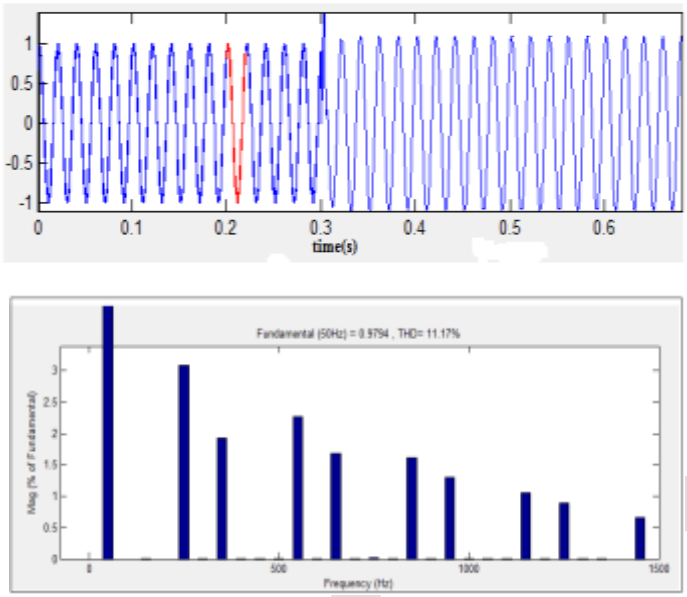

Figure 6. Load Voltage Waveform without UPQC

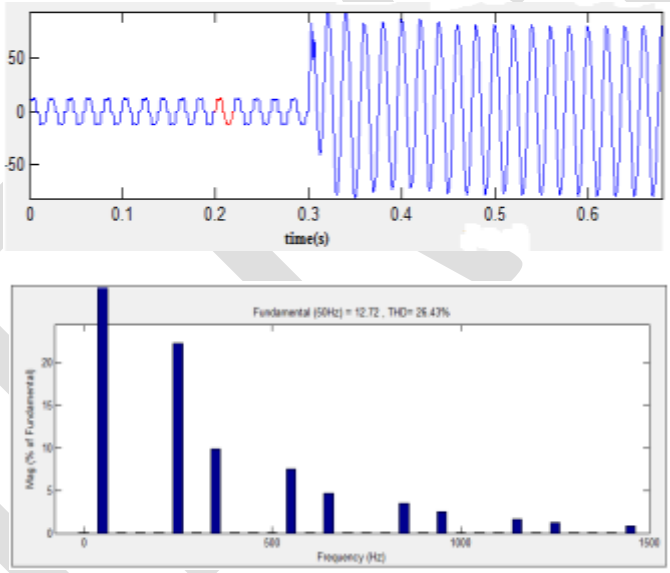

Figure 7. Load Current Waveform without UPQC

Figure 6 and 7 shows the harmonic level with THD.The harmonic level of voltage is 11.17% and the magnitude is 0.9794 p.u and the harmonic level of current is 26.43% and the magnitude level is 12.72 p.u.

b. Simulation results Using UPQC

Load voltage and load current waveforms of test system using UPQC are shown in figure 8 and 9. The harmonic distortion of voltage is reduced to 2.11% and that of current is reduced to 2.92%.

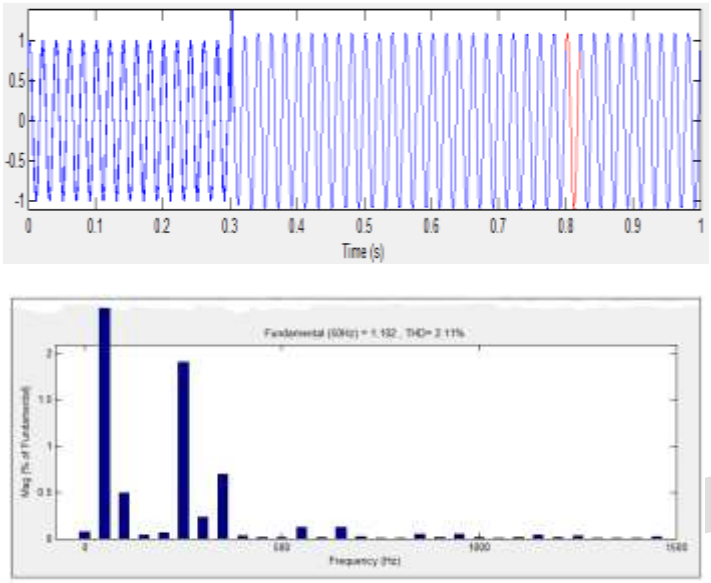

Figure 8. Load Voltage Waveform using UPQC

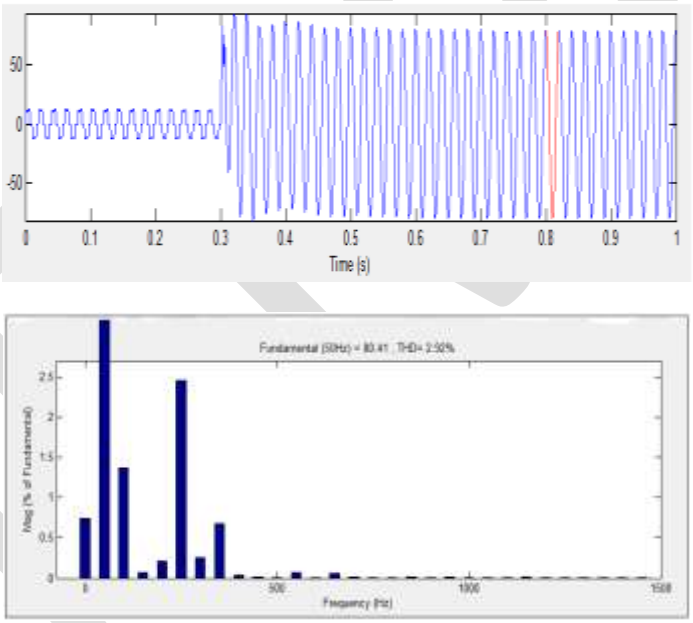

Figure 9. Load Current Waveform using UPQC

The value of total harmonic distortion in both cases signifies the use of UPQC in distribution system.

B. Simulation results in faulted operating conditions

a. Simulation results Without Using UPQC

To check faulted operating condition a single line to ground fault is introduced in the circuit near the load. The fault transition time is chosen between 0.1-0.3 second. It can be seen that voltage level during the transition time is reduced considerably and the current level is increased.

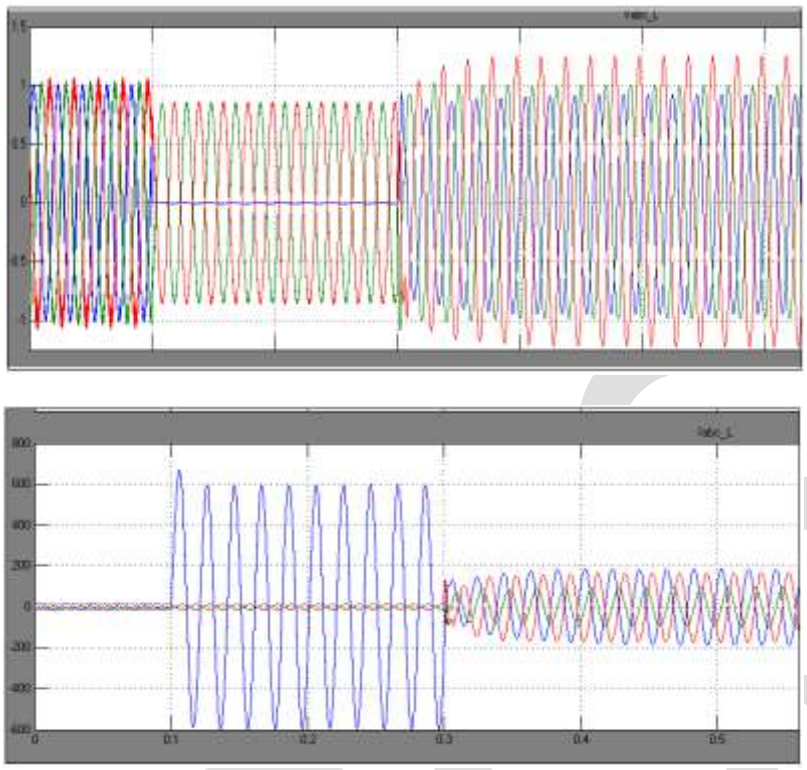

Figure 10. Voltage & Current level during Transition time

At this condition, FFT analysis is done. Figure 11 &12 shows the results for the same.

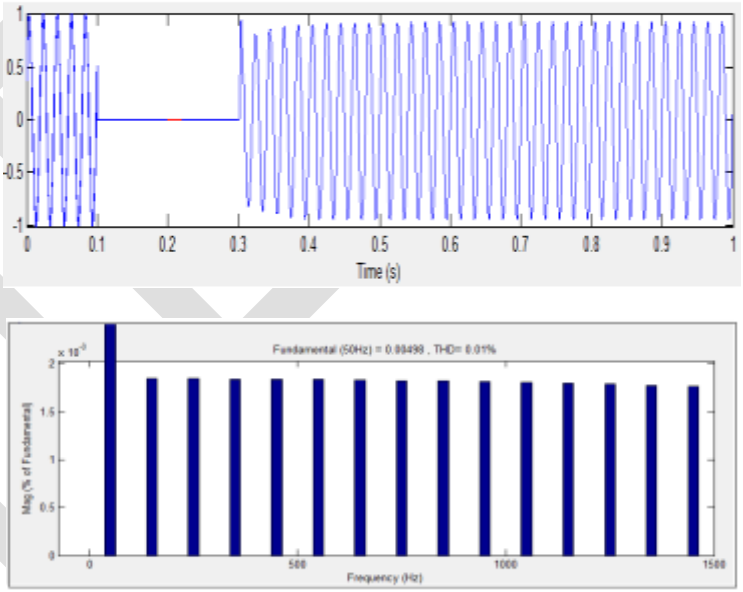

Figure 11. Load Voltage Waveform without UPQC

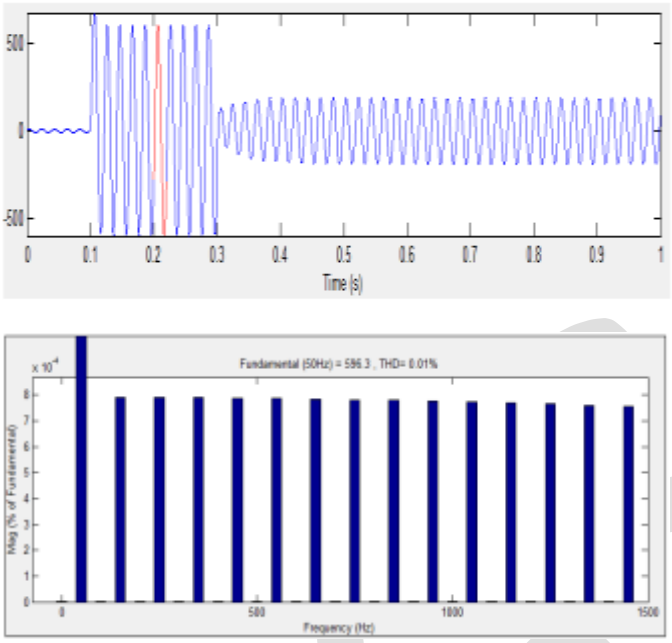

Figure 12. Load Current Waveform without UPQC

b. Simulation results Using UPQC

Wave forms and FFT analysis during UPQC compensation is shown in figure 13 & 14. Voltage and current levels are maintained at permissible limits and the harmonic distortion is considerably reduced below 5%. The harmonic distortions for voltage and current were 1.98% and 1.70% respectively.

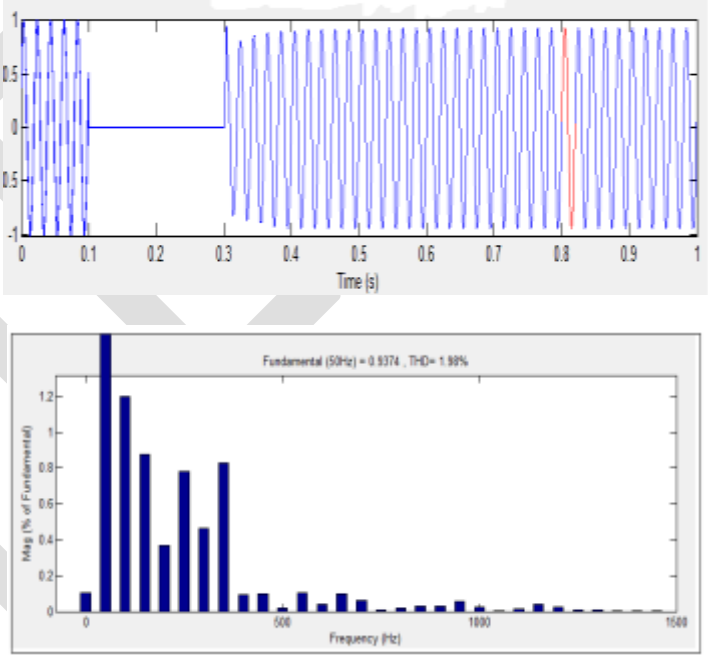

Figure 13. Load Voltage Waveform using UPQC

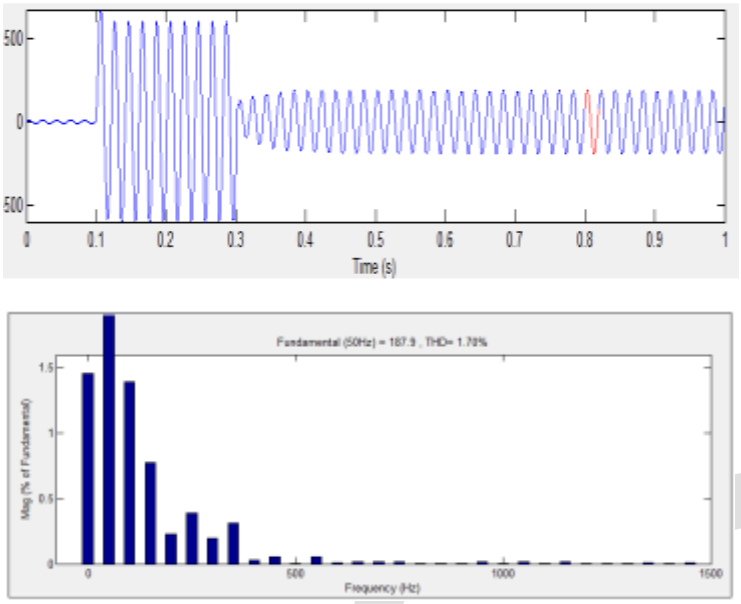

Figure 14. Load Current Waveform using UPQC

Similarly, the waveforms for double line to ground fault can also be observed.

CONCLUSION

In this paper the UPQC is tested under various load condition and single line to ground fault in MATLAB/simulink. It is seen that by designing the model with & without UPQC and analyzing the Fast Fourier transform results, the device is capable to maintain voltage and current in permissible limit and distortion level under 5% of standard.

REFERENCES:

[1] Narain Hingorani & L. Gyugi, "Understanding FACTS, Concepts and Technology of Flexible AC Transmission System", IEEE Press, 2000.

[2] Jos Arrillaga, Neville R. Watson, and S.Chen "Power System Quality Assessment", John Wiley & Sons,2000.

[3] K.R.Padiyar "FACTS Controller in Power Transmission & Distribution". New Age International Publisher, 2007.

[4] I.J.Nagrath and D.P.Kothari "Modern Power System Analysis", McGraw-Hill, New York, 2011.

[5] Hideaki Fujita and Hirofumi Akagi "The Unified Power Quality Conditioner: The Integration of Series-and Shunt-Active Filters", IEEE transactions on power electronics, vol. 13, no. 2, March 1998.

[6] Bhim Singh, Kamal Al-Haddad "A Review of Active Filters for Power Quality Improvement", IEEE transactions on industrial electronics, vol. 46, no. 5, October 1999.

[7] Kolhatkar Y. Y. and Das S. P., "Experimental investigation of a single-phase UPQC with minimum VA loading," IEEE Trans. Power Deliv., vol. 22, no. 1, pp. 373-380, 2007.

[8] Malabika, B., Das, S., Dubey, G. "Investigation on the performance of UPQC-Q for voltage sag mitigation and PQ improvement at a critical load point". IET Generation, Transmission and Distribution, Vol. 2, Issue 3, pp. 414-423. 2008.

[9] Ahmet Teke, Lütfü Saribulut, and Mehmet Tümay "A Novel Reference Signal Generation Method for Power-Quality Improvement of Unified Power-Quality Conditioner", IEEE Transactions On Power Delivery, Vol. 26, No. 4, October 2011.

[10] Khadkikar, V., "Enhancing Electric Power Quality Using UPQC: A Comprehensive Overview", Power Electronics,IEEE Transactions, vol. 27, no. 5, pp. 2284-2297, May 2012.

[11] Yash Pal, A. Swarup and Bhim Singh, "A Novel Control Strategy of Three-phase, Four-wire UPQC for Power Quality Improvement", Journal of Electrical Engineering & Technology Vol. 7, No. 1, pp. 1~8, 2012.

[12] Ankush Malhar and Parag Nijhawan "Improvement of Power Quality of Distribution Network with DTC Drive Using UPQC", International Journal of Emerging Trends in Electrical and Electronics (IJETEE – ISSN: 2320-9569) Vol. 5, Issue. 2, July-2013.

[13] Sumaya Banu, Dr. Sidheswar Prasad, "Study on Three-Phase Four-Wire UPQC device for Power Quality Improvement", IJEDR,Volume 2, Issue 3,2014

International Journal of Engineering Research and General Science Volume 3, Issue 3, Part-2 , May-June, 2015
ISSN 2091-2730

Trends in weight reduction of automobiles "Alu – maximized"

M Sukumar Reddy*, N Nidhin Krishna
B.Tech Scholars, sukumarsybss@gmail.com, nidhin.krishna12@gmail.com, 8130783349

Abstract - Automobiles tend to become heavier as the safety (e.g., collision safety and comfort features) are improved. On the hand, the demand for higher fuel efficiency and lower environmental impact is also rising. The average mass of passenger cars has dramatically increased since the 70's and because vehicle weight directly impacts fuel consumption, light-weighting is necessary more than ever to reduce CO_2 emissions [1]. 100kg mass reduction achieved on a car saves 9 grams of CO_2 per km at the exhaust pipe. Aluminum is the ideal light-weighting material as it allows a weight saving of up to 50% over competing materials in most applications without compromising safety. This paper reports on developments and trends in aluminum alloy sheets for automotive body panels. As a long term vision, an ("Alu-maximised") small family car could be 30-35% lighter after primary and maximum secondary weight savings. [2]

Keywords - Efficiency, Aluminium, Safety.

INTRODUCTION

Automobiles are becoming heavier in order to satisfy requirements [3] such as safety (e.g., collision safety and pedestrian protection), drivability, comfort and larger interior space. Meanwhile, automobiles have to meet more stringent regulations against exhaust emissions, including CO_2 and NO_xemissions [4] , to protect the environment. Transportation is a significant source of CO_2 emissions with individual transportation (cars) producing a major share of it. Among the many measures to reduce CO_2 emissions from cars, technological ones (i.e. the ones that are intrinsic to the car and do not depend on driver behavior) are the most reliable
Light weighting is one of the most effective and directly impacts CO_2 emissions, as 100kg saved on the mass of a car is equivalent to a reduction of 9 grams of CO_2 per kilometer. Various measures are taken to reduce fuel consumption including new power trains involving hybrid systems or advanced diesel engines. Above all, automotive weight reduction is regarded as one of the most effective means for decreasing fuel consumption. So there are numerous light-weighting solutions based on aluminum and aluminum alloys. By the intensive use of safe and cost efficient light-weight aluminum concepts which can be applied with little adaptations across all car models. For car buyers, fuel consumption is seldom the dominant purchasing decision criteria despite its huge impact on operating costs and the well-known environmental consequences.

1. Reducing mass is necessary to reduce Co_2 emissions

Vehicle mas directly impacts fuel consumption.

Weight reduction directly reduces the energy consumption because the energy required to move a vehicle is, except for aerodynamic resistance, directly proportional to its mass.
On average, 100kg mass reduction achieved on a passenger car save:
• 0.35 liter of fuel per 100km.
• 9 grams of CO_2 per km at the car exhaust pipe [5].
When including emissions for fuel production & supply (well-to-wheel), 100kg mass reduction achieved on a passenger car save:
• 10 grams of CO_2 per km.

2. Reducing mass has benefits [6]

2.1 Acceleration: Keeping the car acceleration performance constant, which is generally reflected by the power to weight ratio, saving weight allows downsizing of the power train (engine, transmission, axle, differential etc…) and thus provides additional weight savings. Keeping the power train un-modified, reduced weight increases the power-to- ration and therefore improves acceleration.

2.2 Braking:
Keeping braking power constant, light-weighting shortens braking distance. Keeping the braking performance constant, light-weighting allows downsizing of the brakes, which offers fur their weight saving potential.

2.3. Handling

Road handling is improved by light weighting in many different ways:
• Handling of a lighter car is easier in demanding driving situations.
Reducing body weight lowers the Centre of gravity improving the Car's stability and reducing the risk of roll-over.

2.4 Driving Comfort
Saving weight on unsuspended parts like wheels increases driving comfort.

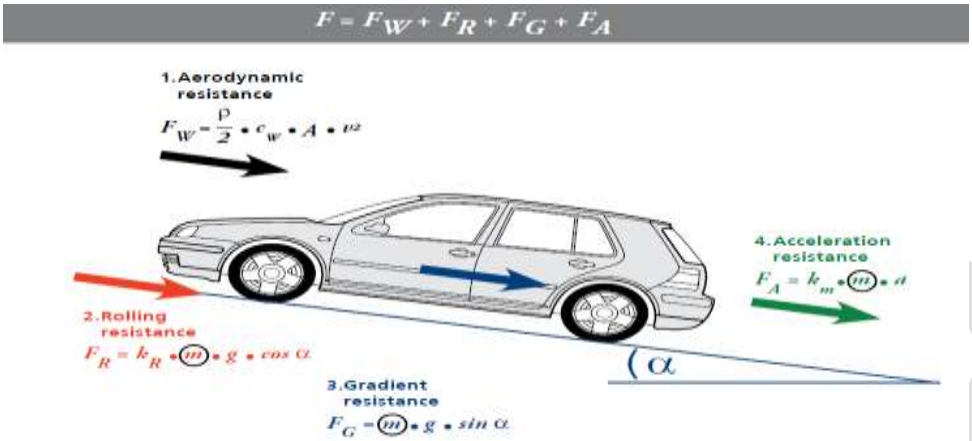

Fig1: Resisting forces [7]

3. Aluminum is the ideal light weighting material. [8] [9]

3.1. Aluminium Properties

With 2,700 kg/m3, the density of aluminum is one third of that of steel. But such a weight reduction is seldom achieved since for a large number of parts, it is necessary to increase the average thickness of aluminum compared to steel to achieve the same part characteristics. The most frequently encountered ratio of thickness in structural applications is approx. 1.5, which means for instance that 0.8 mm steel component can be replaced by a 1.2 mm aluminum component, in this case, the weight reduction is still 50%.
However, the relationship between the material properties and the strength, stiffness and weight of a component is very complex and can be strongly influenced by the part geometry so that there is no absolute rule. In practice, it will be necessary to consider each component individually to determine the actual weight reduction potential. The following section further illustrates this fact. [10]

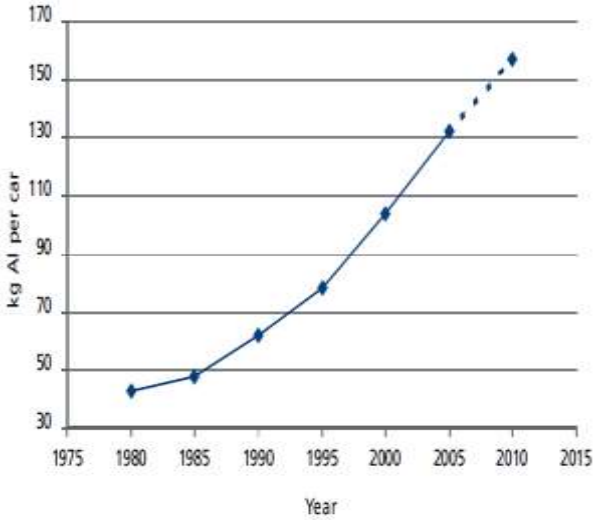

Fig 2: Evolution of aluminum content in European countries

3.2. Primary Weight Savings

Aluminum allows a saving of up to 50% over competing materials in many applications. Typical relative and average absolute weight savings of today's main aluminum applications in mass produced cars are given below

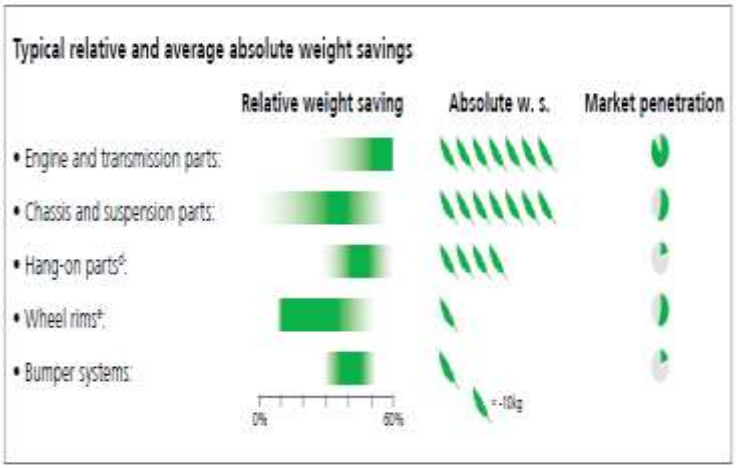

Fig 3: Relative and average weight savings

Keeping a car's performance constant, primary weight savings allow downsizing of other car parts (powertrain, brakes, fuel tank, crash management systems etc…), leading to so called "secondary weight savings". In case the primary weight savings achieved on a defined vehicle are small (i.e. when only little aluminum is used) secondary weight savings are not likely to be achieved by car manufacturers. On the other side, when aluminum is intensively used, secondary weight savings can exceed 50%. For example, in the case of the Audi A2, the intensive use of aluminum allowed direct weight savings of 134kg that allowed 75kg secondary weight savings thanks to drivetrain, motor and chassis downsizing.

3.3. Today's Cars Contain 132kg Of Aluminium

Besides well-known aluminum intensive cars like the Audi A8, which contains about 520kg of aluminum or the Jaguar XJ, many cars contain significant amounts of light metals. A recent study by Knibb, Gormezano & Partners (KGP) in cooperation with the European aluminum Association [11] shows that the amount of aluminum used in new European cars has risen from 50kg in 1990 to 132kg in 2005 and is predicted to grow by another 25kg by 2010. The study is based on the analysis of car models representing a European production volume of 15 million units in 2005.

Key results are summarized below.

Chassis & suspension
• 17 components analyzed
• Highest aluminium application
- Wheels
- Suspension arms
- Steering system
• Aluminum content = 37kg

Drivetrain
• 25 components analyzed
• Highest aluminium application
- Engine block & cylinder head
- Transmission housings
- Radiators

• Aluminum content = 69kg

Car body
• 20 components analyze
• Highest aluminium application
- Bonnets & doors
- Front structure
- Bumper beams
• Aluminum content = 26kg

3.4. Tomorrows Cars Could Easily Be 40kg Lighter [12]

Innovative, safe and cost efficient light-weight aluminum bonnets, wings, doors and bumpers can be found across all car models today. For these parts, switching to aluminum is relatively easy and does not need full re-engineering of the car. Together, their light-weighting potential exceeds 40kg per car. However, penetration in the market is less than 20%. In practice, material substitution is generally connected to a model change where extensive re-design takes place anyway. Mixed material design does not present bigger problems provided appropriate design and manufacturing measures are taken. Thus, the weight saving potential could be even significantly greater.

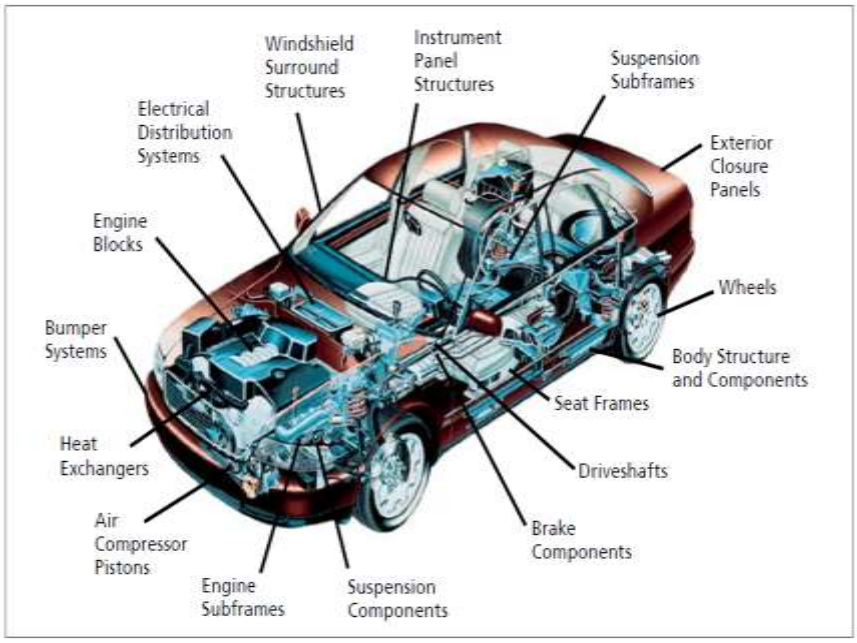

Fig 4: Potential of Aluminium is endless

4. Aluminium is easy to recycle

Aluminum is easy to recycle [13]and saves 95% of the energy necessary to produce primary aluminium. RWTH-Aachen recently analyzed the aluminium recycling process and concluded that 95% of the aluminium contained in end-of life vehicles can be recovered by mechanical processing in modern shredder and non- ferrous metal recovery plants.

The End-of-Life vehicle dismantling and aluminium recycling process [14] is summarized in figure. Aluminium recycling from end-of life vehicles is an established and profitable business and the proceeds from the recycled aluminium are a most important factor in the economy of the car recycling.

4.2 *Aluminium supply*
Aluminium supplies will continue to meet the demand because:

• Current reserves of bauxite, used to produce primary aluminium, will last for many generations
• The amount of aluminium available for recycling is constantly increasing.

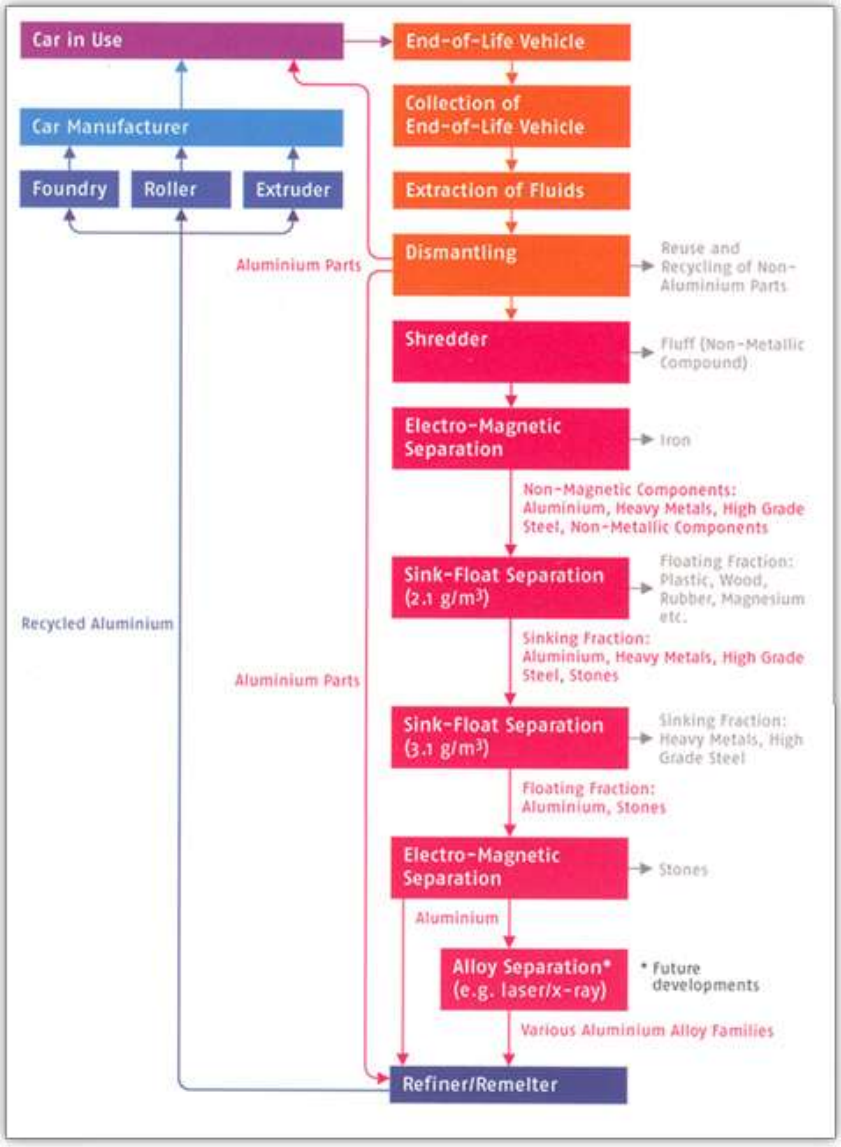

Fig 5: End-of-life vehicle dismantling & recycling process [15]

CONCLUSION

Because the average mass of passenger cars has dramatically increased since the 70's and because vehicle weight directly impacts fuel consumption, light-weighting is necessary more than ever to reduce CO_2 emissions. 100kg mass reduction achieved on a car saves 9 grams of CO_2 per km at the exhaust pipe. Aluminium is the ideal light-weighting material as it allows a weight saving of up to 50% over competing materials in most applications without compromising safety. As a long term vision, an "Alu-maximized" small family car could be 30-35% lighter after primary and maximum secondary weight savings.

The latest trend and new technologies of aluminum sheets have been reviewed with major focus on automotive panels. In the needs for automotive weight reduction, aluminum will continue to be a major candidate for a lighter substitute material.

Functional properties, as well as the weight reduction effect, will be required for aluminum alloys to be used for various automotive parts.

To expand the use of aluminum for automotive panels, forming technologies should be further improved to provide more degree of freedom to automotive design. Tribology is considered to be an area which needs to be pursued to further develop the applications of

aluminum sheets. The formability can be improved by facilitating the material flow in dies by introducing lubricants with low friction coefficients to reduce the cost of aluminum parts for them to be used for various parts of mass produced vehicles. The cost reduction may involve the development of process technologies which simplifies process steps and simultaneously achieve the required quality. Unification and recycling of parts will also be needed.

REFERENCES:

[1] J.G.J. Olivier, G. Janssens-Maenhout, M. Muntan, J.A.H.W Peters, Trends in global CO_2 emissions 2014 report no 1490, dated 16th December 2014.
[2] Japan aluminium association committee: Aluminium, Vol.9, p.150, No46 (2002).
[3] International journal of vehicle performance, Inderscience Publications.
[4] US Environment Protection Agency: Green House gas inventory report 1990-2013.
[5] K. Chiba: Aluminium vol.12, p.75, No61 (2005).
[6] www.autoblog.com/2009/10/29. Weight effects on vehicle efficiency.
[7] https://www.physicsforums.com/threads/forces-acted-on-the-car-when-a-car-moves.623590/
[8] Light weighting of automobiles through aluminium, Aluminium association of India, Conference proceedings at New Delhi, August 2013.
[9] M Saga et al: Proceedings of 87th Conference of the Japan's institute of Light metals, 1994 p.187.
[10] Automotive Trends in Aluminium – The European Perspective, Evolution of aluminium in Europe.
[11] European aluminium report September 2008.
[12] Akoijam: Scope of aluminium in Indian automobiles, IISTE, vol.4, No3 (2012).
[13] Ilgin7, M. A.; Gupta, S. M. Environmentally conscious manufacturing and product recovery (ECMPRO): A review of the state of the art. Journal of Environmental Management. 91, 3(2010), pp. 563-591.
[14] Go, T. F.; Wahab, D. A.; Rahman, M. N. Ab.; Ramli, R.; Azhari, C. H. Disassemblability of end-of-life vehicle: A critical review of evaluation methods. Journal of Cleaner Production. 19, 13(2011), pp. 1536-1546.
[15] Mayyas, A.; Qattawi, A.; Omar, M.; Shan, D. Design for sustainability in automotive industry: A comprehensive review. Renewable & Sustainable Energy Reviews. 16, 4(2012), pp. 1845-1862

International Journal of Engineering Research and General Science Volume 3, Issue 3, Part-2 , May-June, 2015
ISSN 2091-2730

Implementation of CAN protocol for alerting of vehicle accident using GSM and GPS

Krishnaveni.K & Roopa M
Department of Electronics and Communication Engineering

Dayanada Sagar College of Engineering
Bangalore,India
E-mail: krishnaveni.chethan@gmail.com, surajroopa@gmail.com

Abstract— According to records obtained by study conducted by world health organization, lots of the human lives are being lost every year due to vehicular accidents. Many campaigns are being conducted for causing awareness in the public about the frequent disasters occurring due to over speed vehicular movement on the road, but yet the number of injuries and loss of lives are increasing day by day. In order to overcome this situation, a wireless monitoring system along with accelerometer and GPS tracking system with CAN protocol is developed. At the occurrence of the accident, the wireless device will send information in the form of message to predefined phone numbers for immediate medical help. The exact location of the vehicle is traced using GPS tracking system and Google Earth.

Keywords—MEMS (Micro electromechanical sensor), GSM (Global system for mobile), GPS (Global positioning system), LCD (Liquid crystal display), CAN(Controller area network), SPI(Serial peripheral interphase), SMS (Short message service).

.

INTRODUCTION

Now-a-days lots of accident occur on highways due to increasing traffic and rash driving of the vehicle. The accident may be driving the vehicle with insufficient sleep, driving with alcohol intake. In order to decrease the number of vehicular accident many campaigns are being conducted to create public awareness regarding safety measures that are to be kept in mind during driving. In many situations the immediate medical assistance to the victim by healthcare service cannot be provided due to not getting information about the accident in time**.**.This project provides method for detection of the vehicle using GPS and GSM modem along with CAN bus to avoid such incidents.

This paper presents the enhancement and application of driving system for the vehicle to detect the vehicle in case of any accident. An ARM based data acquiring system works without any wire connection. The information about the accident is sent in the form of message using GSM and information can be displayed using LCD installed in the system. The communication method employed in this embedded networking is done by CAN protocol. Additional data for example speed, threshold value of the vehicle can also be extracted. The arrangement consists of GPS tracking system which is used to detect the exact location of the vehicle.

SYSTEM OVERVIEW

Here the system consists of supportive devices such as ARM cortex microcontroller, MEMS accelerometer device , GSM device, and GPS tracking system at the transmitter side**.** The receiver constitutes web server and mobile phones. MEMS is an Micro electro mechanical sensor, which consists of highly sensitive sensor devices used for detecting the inclination of the vehicle in front portion, rear portion, left as well as right directions. Rash driving of the vehicle can be detected with an accelerometer.

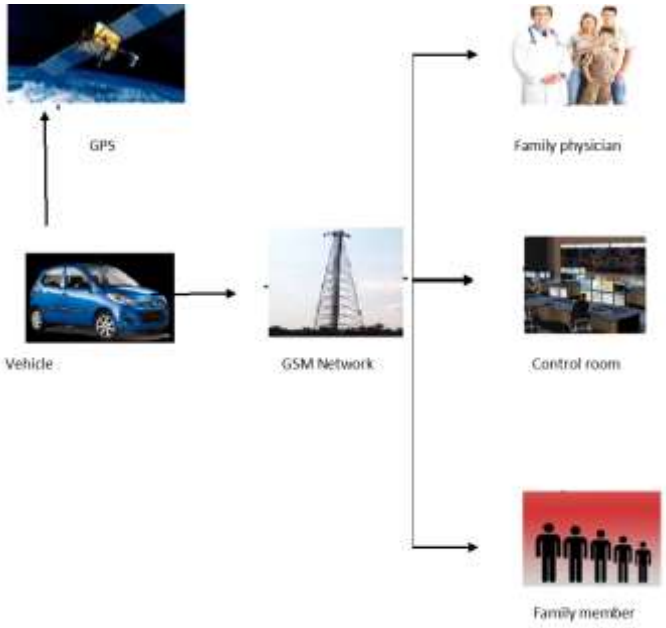

Figure 1: System overview

It can also be used for recording the speed of the vehicle at the time before and after the crash**.** ARM Cortex-M3 are microcontrollers that are used for applications developed for embedded environment has high level of integration and low power consumption features. ARM used is a 32 bit microcontroller that can store and process real-time signals from accelerometer**.** The GPS tracking system provides some of the parameters such as longitude, latitude, speed. Upon occurrence of the accident, the information is sent in the form of message to control room or a rescue team or family person by using GSM for immediate medical help for the injured. At the receiver the web server maintains the database that consists of time, speed, longitude, latitude that are provided wirelessly by GSM.

DESCRIPTION OF CAN

In this paper implementation of CAN communication transmission system in vehicles is being done. The system is capable of sensing obstacles and has speed sensor. The data will be transmitted over CAN bus and will be displayed on LCD. Controller Area Network (CAN) is a serial data communications bus developed by Robert Bosch GmbH in mid-eighties for the German car industry. The CAN protocol is an ISO standard (ISO 11898) for serial data communication. The protocol was developed mainly for automotive applications. CAN has also been found its usage in industrial automation as well as in automotives and mobile machines. The CAN protocol implementation is done using silicon. This makes it likely to combine the error handling and fault confinement feature of CAN with a high transmission speed. The method used for allocating messages to the suitable receivers contributes for making use of the available bandwidth. This requires a simple transmission medium such as a twisted pair of wires.

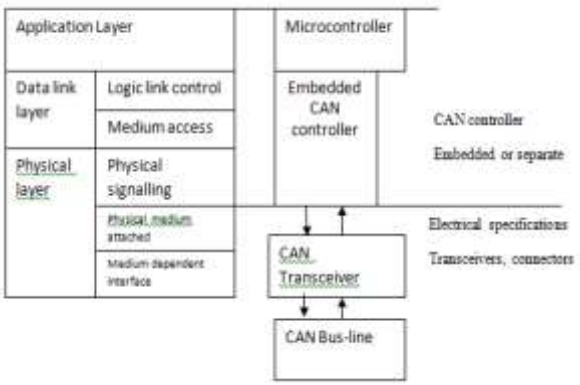

Figure2: Standard layer ISO 11898 architecture

The CAN is a serial communication bus protocol defined in International Standards Organization (ISO). A serial communication bus fundamental use is in data transfer form one point to another point in duplex mode. It was developed as an alternative of complex wiring with two-wire bus for the automotive industry. CAN decreases the electrical interference and noise interference to the signal in the network. CAN introduce an error detection and correction mechanism in the network which is very effective.

CAN bus node:

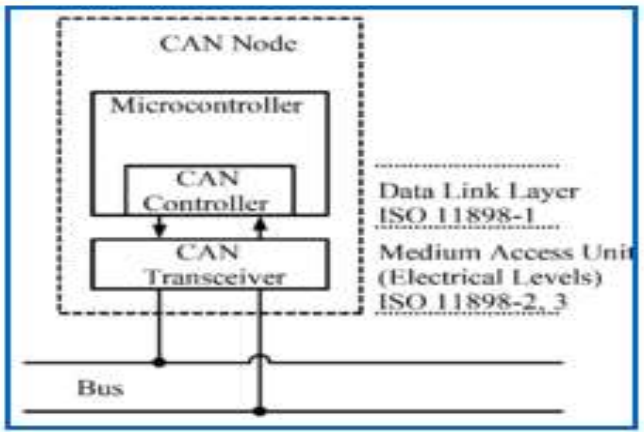

Figure 3: CAN bus node

Central processing unit or host processor consists of the host processor which analyses the meaning of the received messages and what messages is to be transmitted. Sensors, actuators and control devices can be connected to the host processor**.** CAN controller is the vital element of the microcontroller At the receiver the CAN controller stores the received serial bits from the bus until an entire message is available. At the transmitter the host processor sends the transmit message to the CAN controller, which transmits the bits when the bus is free serially onto the bus. Transceiver is defined by ISO 11898-2/3 Medium Access Unit [MAU] standards. At the receiver the conversion from data stream of CAN bus levels to levels that the CAN controller uses is done. Generally it consists of a protective circuitry to protect the CAN controller. At the transmitter, it converts the data stream from the CAN controller to CAN bus levels.

Frame format:

Figure 4: Standard CAN 11 bit identifier

- SOF–It is single dominant start of frame (SOF) bit Message in CAN starts with SOF.
- Identifier-The Standard CAN 11-bit identifier. The priority of the messages can be established using identifier.
- RTR–Remote Transmission Request (RTR)
- IDE–A dominant single identifier extension (IDE) bit. If this bit is enabled it means that a standard CAN identifier is being transmitted without any extension
- r0–Reserved bit
- DLC–The 4-bit data length code (DLC). It consists of number of bytes of data which are supposed to be transmitted.
- Data–Up to 64 bits of application data may be transmitted.
- CRC–The 16-bit (15 bits plus delimiter) cyclic redundancy checks (CRC). It contains the checksum of message
- ACK = Acknowledge bit
- EOF– End-of-frame (EOF) Bit ,
- IFS–This 7-bit interframe space (IFS)

Extended CAN

Figure 5: Extended CAN 29 bit identifier

The Extended CAN message is the same as the Standard message with the addition of:

- SRR–Substitute Remote Request (SRR) bit. It replaces the RTR bit in the standard message
- IDE–A recessive bit in the identifier extension (IDE). It indicates that more identifier bits follow. The 18-bit extension follows IDE.
- r1–Following the RTR and r0 bits, an additional reserve bit has been included ahead of the DLC bit.

The Extended CAN message is the same as the Standard message with the addition of:

- SRR–Substitute Remote Request (SRR) bit. It replaces the RTR bit in the standard message.
- IDE–A recessive bit in the identifier extension (IDE). It indicates that more identifier bits follow. The 18-bit extension follows IDE.
- r1–Following the RTR and r0 bits, an additional reserve bit has been included ahead of the DLC bit.

When the CAN transmits the data, addressing of the stations is not done instead the content of the message will be designated by the identifier. The identifier which is unique throughout the network defines the content along with the priority of the message. This is essential for allocation of the bus when several stations are competing for bus access.

If the CPU of a station requires to send a message to other station it transfers the data to be transmitted to their respective identifiers which is already assigned to the CAN chip. The message thus received is constructed and transmitted by CAN chip. As the bus allocation is done to the CAN chip the data is transmitted to all other stations on the CAN network. After receiving the message by the receiving station an acceptance test is done to check for if the message received is correct or not. If the received information is right than the station does the suitable process otherwise ignores.

CAN broadcast multiple messages in a single instance of time. The USB and Ethernet protocols utilize blocks of data to transfer form one node to another node due to which rate of data transfer is less compared to CAN which does not utilize block of data but attain high signalling rate. In a CAN network, many short messages such as temperature can be broadcasted to the entire network. This provides data consistency and accuracy to each node of the system.

DESIGN IMPLEMENATION

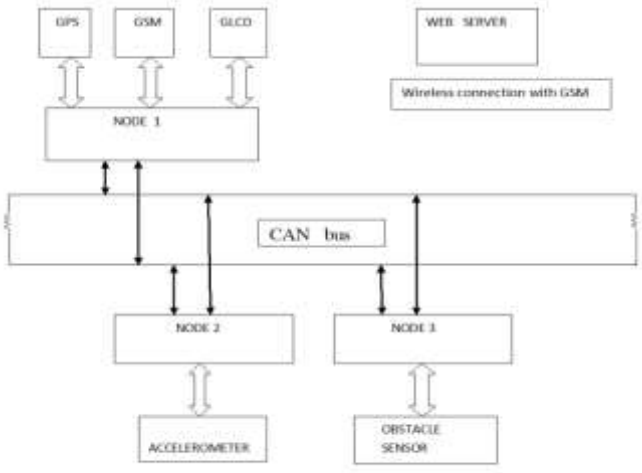

Figure 6: CAN bus system for transmitter section.

The organization contains a master node and two slave nodes. Each node consists of an ARM Cortex M3 LPC1768 processor. The node 1 acts as the main node consisting of GPS, GSM and graphical LCD connected. Node 2 contains MEMS three dimensional accelerometer ADXL362 that measure physical acceleration experienced by an object connected. The interfacing of the MEMS accelerometer to ARM processor is done using SPI. SPI is an serial peripheral interface which is an interface bus frequently used to send data between microcontrollers and small peripherals such as sensors, shift registers. It uses separated clock and data lines along with select line to choose the device. Node 3 consists of ultrasonic obstacle sensor that emits an ultrasonic wave in one direction and would return immediately when it encountered obstacles on the way. The communication technique employed between the nodes is done using **C**AN bus controller. Polysilicon springs suspend the MEMS structure above the substrate such that the body of the sensor can move in the X , Y, and Z axes. Acceleration causes deflection of the proof mass from its centre position. The sensing method has the ability of sensing both dynamic acceleration such as shock or vibration and static acceleration such as inclination or gravity. At any instant of time if there is any static or dynamic changes in the accelerometer detected it is measured. If the measured value is above the threshold value then the signal is send to the main node1. Where at the main node the GSM sends alert message to the predefined numbers and web server. Similarly, whenever the ultrasonic sensor detects the obstacle e within 3 m range it sends signal to the main node. At the main node the graphical LCD displays the message obstacle. The main node transmits the alert message through GSM to the predefined numbers and sends message to the web server instantaneously. The longitude and latitude information is obtained by GPS device. The web server can locate the position of the vehicle by the longitude and latitude data provided by GPS through GMS and by Google Earth application we can get the location of the vehicle.

FLOW OF OPERATION

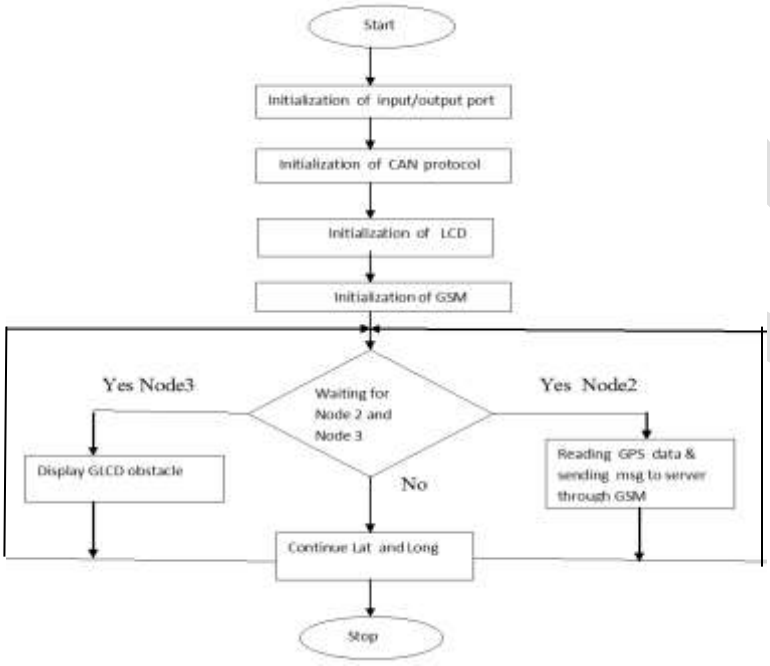

Figure 7: Flowchart for working of main node

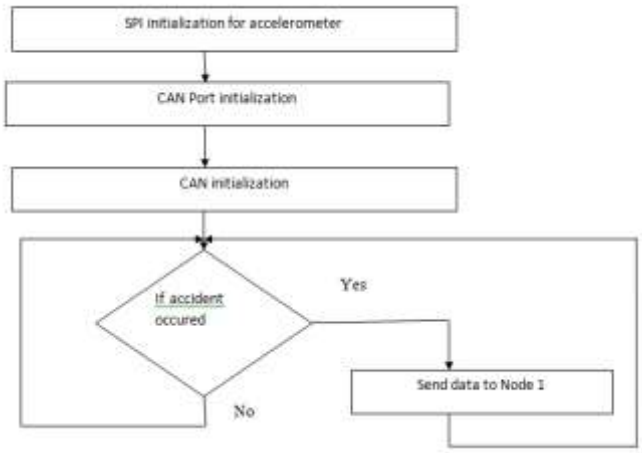

Figure 8: Flowchart of working of Node2(MEMS accelerometer)

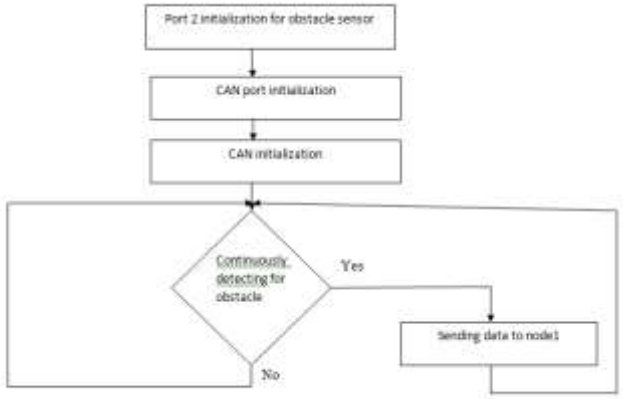

Figure 9: Flowchart of working of Node 3(ultrasonic sensor)

The above flow chart is converted in to embedded C program using µVision IDE from Keil and flash magic tools. The uvision IDE from Keil consists of project management, making use of the facilities, editing the source code, debugging of the program, and complete simulation in a strong setting. The µVision development platform is user friendly and helps to create embedded programs that works earliest. Flash magic is the tool used to program hex code in EEPROM of microcontroller**.** The microcontroller such as Philips and NXP are only supported. It can burn a hex code into those controllers which supports ISP (in system programming) .

EXPERIMENTAL RESULT AND ANALYSIS

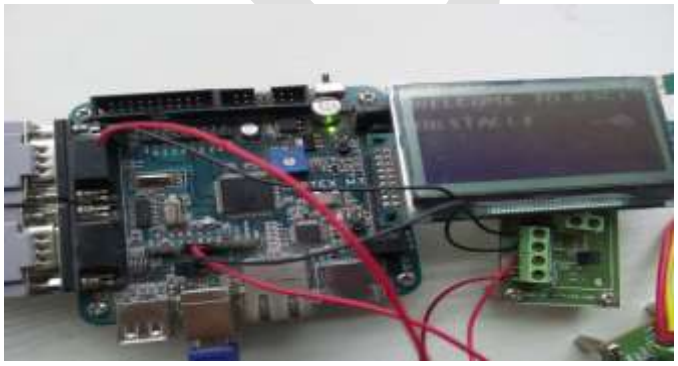

Figure 10: Obstacle detected by ultrasonic sensor

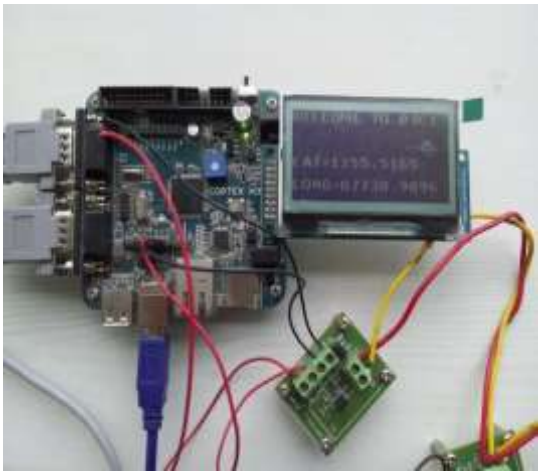

Figure 11: Longitude and latitude data provided by GPS and displayed GLCD

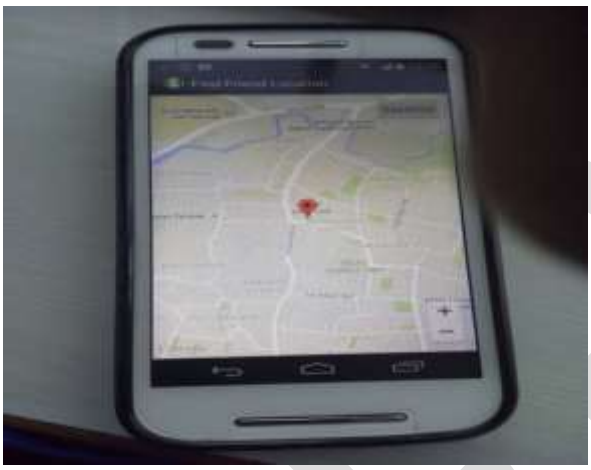

Figure 12: Location identified by predefined number by using message details sent by GSM

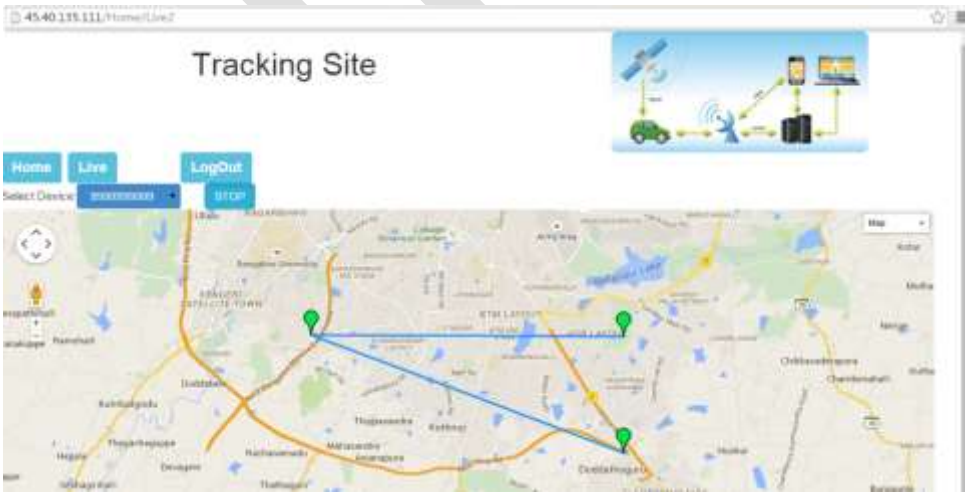

Figure 13: Web server displaying the location using GSM details

The experiments were done for the hardware testing of designed and implemented circuit The results of experiment for the designed circuit were obtained as above. Similarly, GPS module was tested and data transmitted from the GPS to the ARM Cortex M3 with the help of RS 232.ARM Cortex M3 received data serially on its RxD pin and display the same on LCD. At the same time the message was sent to the predefined mobile numbers.

ACKNOWLEDGMENT

I would like to extend a special thank to my guide Mrs Roopa M, Electronics & Communication department for providing valuable suggestions and information for our research work in precious way. I am also grateful to my co-ordinator, Head of the department of Electronics and communication department for their support and guidance.

CONCLUSION

This project consists of embedded system with a combination of CAN bus which is an important criterion of recent technology. ARM cortex M3 is an embedded processor with high performance, low cost, high reliability features which can be used in modern automobile industry applications. The proposed high-speed CAN bus system solves the problem of automotive system applications with ARM as the main controller. The ARM along with CAN provides efficient data transfer applications. This project can be utilized for tracing the vehicle by transport companies and provides information in case of any delay may be due to breakdown or an accident.

REFERENCES:

[1] Benjamin C Kuo, M. Farid Golnaraghi, Automatic Control systems, Eight edition, John wiley & sons., Inc 2003.
[2] J. Fr¨oberg, K. Sandstr¨om, C. Norstr¨om, H. Hansson, J. Axelsson, and B. Villing. A comparative case study of distributed network architectures for different automotive applications. In *Handbook on Information Technology in Industrial Automation*. IEEE Press and CRC Press, 2004.
[3] D.Malan, T.R.F,Fulford-Jones, M.Welsh, S.Moulton, CodeBlue: an ad-hoc sensor network infrastructure for emergency medical care, in: proceedings of the Mobi-Sys 2004 workshop on application of Mobile.
[4] M. Lu, W. Chen, X. Shen, H.C. Lam and J. Liu, "Positioning and tracking construction vehicle in highly dense urban areas and building construction sites," Automation in construction, vol. 16, issue 5.pp.647-656, August 2007.
[5] Stephen Teang Soo Thong, Chua Tien Han and Tharek Abdul Rahman "Intelligent Fleet Management System with Concurrent GPS & GSM Real-Time Positioning Technology", IEEE ,Wireless Communication Centre (WCC), universiti Teknologi Malaysia (UTM), Malaysia in 2007.
[6] Wilfried Voss, A comprehensive guide to controller area network, Copperhill Media Corporation, 2005-2008.
[7] Dae Geun Lee, Se Myoung Jung , Myoung Seob Lim. "System on Chip design of Embedded Controller for Car Black Box". 2007 IEEE Intelligent Vehicles Symposium Istanbul, Turkey, June 13-15, 2007.
[8] Liewei Jiang and Chunxuan Yu. "Design and Implementation of Car Black Box Based on Embedded System". 2010 IEEE DOI 10.1109/iCECE.2010.860.
[9] Thuong Le-Tien, Vu Phung-The "Routing and Tracking System for Mobile Vehicles in Large Area", Fifth IEEE International Symposium on Electronic Design, Test & Applications Dept. of Electrical Electronics Engineering, HCM University of Technology, Vietnam in 2010.
[10] Chulhwa Hong, Truong Le, Kangsuk Chae, and Souhwan Jung. "Evidence Collection from Car Black Boxes using Smartphone's". 2011 IEEE, Annual IEEE Consumer Communications and Networking Conference.
[11] N.Watthanawisuth,T.LomasandA.Tuantranont, "Wireless Black Box Using MEMS Accelerometer and GPS Tracking for Accidental Monitoring of Vehicles", Proceedings of the IEEE-EMBS International Conference on Biomedical and Health Informatics (BHI 2012) Hong Kong and Shenzhen, China, 2-7 Jan 2012.
[12] T. Lomas, A. Tuantranont, "Wireless Black Box Using MEMS Accelerometer & GPS tracking for accidental monitoring of vehicles," Proceedings of the IEEE-EMBS International Conference on Biomedical & Health Informatics, 2-7 Jan 2012, Hong kong, China.
[13] Jing Yang, Student Member, IEEE, Edwin Hou, Senior Member, IEEE, and MengChu Zhou, Fellow, IEEE," Front Sensor and GPS-Based Lateral Control of Automated Vehicles", IEEE Transactions on Intelligent Transportation Systems, Vol. 14, No. 1, March 2013.
[14] http://www.can-cia.org
[15] Automobile Control System using Controller Area Network. International Journal of Computer Applications 67(18):34-38, April 2013

International Journal of Engineering Research and General Science Volume 3, Issue 3, Part-2 , May-June, 2015
ISSN 2091-2730

Hydrochemical Characterization of Coastal Groundwater in Porbandar Region, Gujarat, India

Parul Gupta[1], Anupma Sharma[2], Namita Joshi[1]

[1]Department of Environmental Sciences, Kanya Gurukul Mahavidyalaya, Gurukula Kangri Vishwavidyalaya, Haridwar, India
[2] National Institute of Hydrology, Roorkee, India

Abstract— The hydrochemical data of groundwater samples from a coastal region in Porbandar district, Gujarat, India have been examined using factor analyses to determine the main factors controlling the groundwater chemistry and salinity. A total of seventy groundwater samples were collected from the study area and analysed for pH, EC, Ca^{2+}, Mg^{2+}, Na^{+}, K+, HCO_3^{-}, Cl-, NO_3^{-}, and SO_4^{2-}. Factor analysis has revealed that different hydrogeochemical processes such as saltwater encroachment from sea, saltwater upconing, ion exchange, inherent salinity of rocks / marine sediments, carbonate and silicate weathering of rocks, and leaching of salts/minerals are the key factors regulating the groundwater chemistry of the region.

Keywords— Coastal groundwater, hydrogeochemistry, factor analysis, salinity, total dissolved solids, groundwater quality

INTRODUCTION

Groundwater is a vital resource for communities and ecosystems thriving in the coastal regions. Salinization is the most widespread form of groundwater quality deterioration, especially in the coastal areas, and is represented by the increase of total dissolved solid (TDS) and other related chemical constituents [1,2]. Besides encroachment of saltwater from the sea, the composition of coastal groundwater is influenced by many other processes viz., saltwater upconing, ion exchange, wet and dry deposition of atmospheric salts and water rock interactions. Because of the complexities of the regional hydrogeological conditions and hydro chemical process, advanced techniques are required to interpret observed relationship among different chemical constituents / variables. Hydro chemists have thus applied factor analysis to interpret these relationships and assess controlling factors behind groundwater composition [3-7]. Factor analysis is a technique of quantitative multivariate analysis with the goal of representing the inter-relationship among a set of variables or objects. Factor analysis provides a simple interpretation of a given body of data and affords fundamental description of particular set of variables related to hydro chemical processes beyond strict litho logical controls [8]. Factors are constructed in such a way that they reduce the overall complexity of the data by taking advantage of inherent interdependencies. It is useful for interpreting commonly collected groundwater quality data and relating these data to specify the involved hydrogeologic processes.

STUDY AREA

The study area is a coastal region located in south-western part of the Saurashtra peninsula with its major portion falling in the Porbandar district of Gujarat state in India. It lies between latitudes 21°30’ and 22°0’ N and longitudes 71°22’ and 72°22’E with a geographical area of about 1750 km^2. Porbandar district falls under semi-arid climate zone with annual rainfall of 634 mm. Agriculture is the main occupation of the local population and groundwater is the major resource for irrigating the crops. The geology of the region mainly comprises of milliolitic limestone, clays, laterites and alluvium in the coastal plains, while in the upper inland areas weathered/ hard basalt is present. Groundwater is highly saline near the coast, but it is generally fresh in inland areas. For hydrochemical characterization of groundwater, the study area is divided into four zones based on the distance of the respective zone from the sea coast (Fig. 1): (i) Zone I (region 0-3 km from coast), (ii) Zone II (region 3-6 km from coast), (iii) Zone III (region 6-12 km from coast) (iii) Zone IV (region more than 12 km from coast).

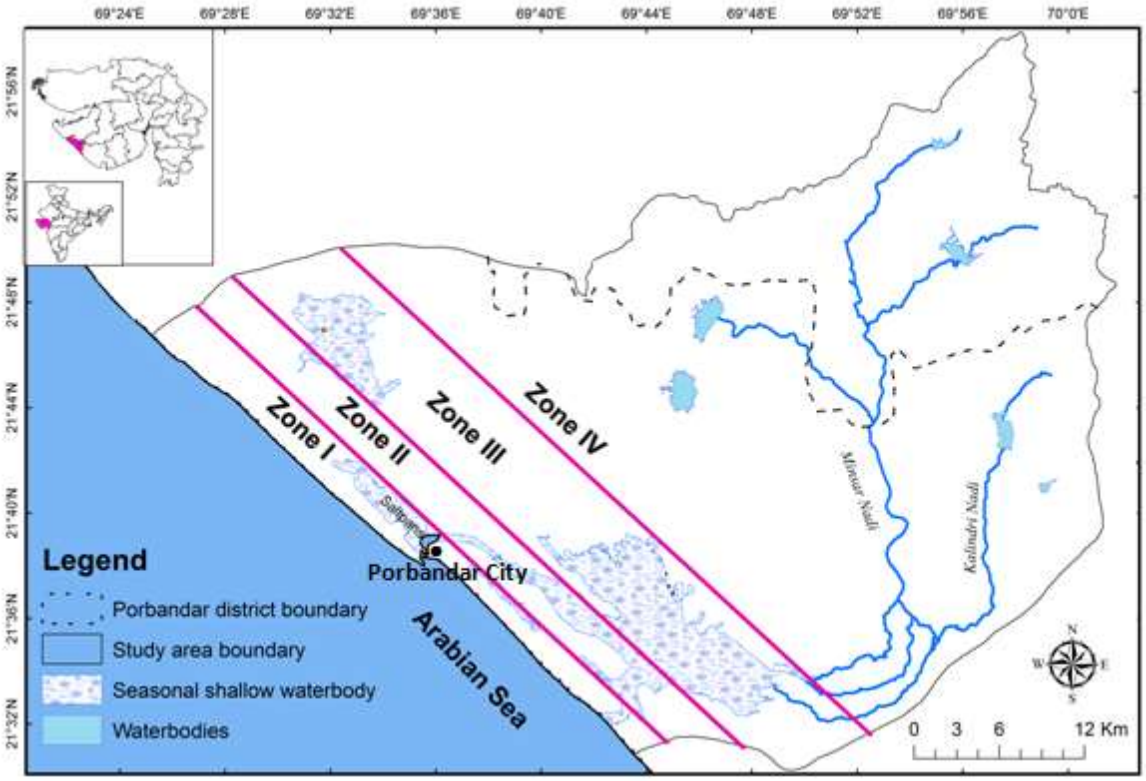

Fig. 1: Location map of study area with zone positions

MATERIAL AND METHODS

A total of 70 groundwater samples were collected during post monsoon period in 2013 from dug wells and piezometers in the study area. The water samples were preserved in polyethylene bottles of 1000 ml. Samples were analyzed in the laboratory for the physico-chemical attributes like pH, Electrical Conductivity (EC), Total Dissolved Solids (TDS), major and minor ions i.e. Calcium (Ca^{2+}), Magnesium (Mg^{2+}), Sodium (Na^{+}), Potassium (K^{+}), Chloride (Cl^{-}), Bicarbonate (HCO_3^{-}), Nitrate (NO_3^{-}), and Sulphate (SO_4^{2-}). These parameters were analyzed using standard methods [9,10]. EC and pH were measured using digital meters immediately after sampling in the field. Ca^{2+}, Mg^{2+}, Cl^{-} and HCO_3^{-} were determined by titration; Na^{+} and K^{+} were measured by flame photometry; NO_3^{-} by colour development with absorption method; SO_4^{2-} by turbidity method; and F^{-} by SPADNS method. The accuracy of the chemical analysis was verified by calculating ion balance errors which were found to be within ± 10%.

In the present study factor analysis is applied to obtain correlations among the hydrochemical constituents of groundwater samples. The general mathematical solution to represent number of factors has been explained as follows [11,12]:

$$Z_{kj} = a_{1j}F_{k1} + a2_jF_{k2\ldots\ldots+}\ a_{mj}F_{km+}\ a_{nj}F_{kn}$$

The a's are factor loadings, coefficients that reflect the importance of each variable j, in the factors represented by the aF terms. Thus, where factor loadings are high, it can be assumed that the variable contributes to that factor. The F's are factor scores. The scores indicate the importance of each factor with respect to each sample k. Z's are original variables in standard form. The sum of the squares of the factor loadings for each variable is the communality and reflects the proportion of the total variability accounted for by the factoring. The sum of squares of factor loadings within each factor before rotation or other manipulation to maximize loadings is the eigen value for that factor. Factor loading is the measure of the degree of closeness between the variables and the factor.

According to Kaiser criterion, the factors with eigen value greater than 1 are selected. The first three highest factors *viz.* Factor 1 (F1), Factor 2 (F2), and Factor 3 (F3) are extracted to carry out the analysis. In order to maximize the variance of the principal axes, the varimax rotation can be applied. The objective of varimax rotation is moving each factor axis to positions so that projections from

each variable on to the factor axes are either near the extremities or near the origin. The largest loading, either positive or negative, suggests the variance of the factor loading of the variables; positive loading indicates that the contribution of the variables increases with the increasing loading in a dimension; and negative loading indicates a decrease [8].

The above methodology was used to identify the source of dissolved ions and the chemical processes which lead to groundwater salinization. Factors were interpreted as different sources of delivering/receiving ions to/from waters. The variables used for factor analysis were pH, Na^+, K^+, Mg^{2+}, Ca^{2+}, HCO_3^-, Cl^-, SO_4^{2-}, NO_3^-, EC and TDS.

RESULTS AND DISCUSSION

The pH of groundwater in the four zones was found to vary in the range 6.70 - 8.46 with an average pH of 7.63. Average value of TDS in Zones I, II, III and IV was found to be 2085.49 mg/L, 2019.04 mg/L, 1584.58 mg/L and 770.41 mg/L, respectively. Thus, the groundwater salinity, in general, decreases as distance from the coast increases.

Concentrations of Cl^-, Na^+, Ca^{2+} and Mg^{2+} were found to generally decrease away from the coast. Ca^{2+} and Mg^{2+} were found to be dominant cations present in groundwater next to Na^+. Similarly, HCO_3^- anion was also present in considerable amounts next to Cl^-. Average values of major cations in Zones I, II, III and IV were found, respectively, as Na^+ : 564.85mg/l, 396.73mg/l and 186.59mg/l; Ca^{2+} : 147.08 mg/l, 252.18 mg/l, 172.61 mg/l and 77.34 mg/l ; Mg^{2+} : 52.64 mg/l, 37.76 mg/l, 31.61 mg/l and 22.72 mg/l. Average values of major anions in Zones I, II , III and IV were found, respectively, as Cl^- : 796.83 mg/l, 767.24 mg/l, 603.67 mg/l and 172.85mg/l; HCO_3^- : 386.91mg/l, 337.21mg/l, 302.34 mg/l and 404.29 mg/l; SO_4^{2-} : 144.67 mg/l, 123.07 mg/l, 170.06 mg/l and 39.54 mg/l; NO_3^- : 8.99 mg/l, 17.73 mg/l, 13.20 mg/l and 9.10 mg/l . As revealed by average values from different zones, these parameters varied in wide ranges across the groundwater samples collected from the area.

Factor analysis was applied to obtain correlations among the hydrochemical constituents of groundwater samples. According to Kaiser criterion, the factors with eigen value greater than 1 were selected. In order to maximize the variance of the principal axes the varimax rotation was applied.

For the purpose of factor analysis, the above four zones (i.e. Zone I, II, III and IV; refer Fig. 1) were regrouped into three zones: Zone A comprising Zone I; Zone B comprising Zone II and III; and Zone C comprising Zone IV. The discussion in the following paragraphs is based on the above three regrouped zones: Zones A, B and C.

For post monsoon season of the year 2013, three factors were identified *viz.* Factor 1 (F1), Factor 2 (F2) and Factor 3 (F3), which control the groundwater chemistry. For factor loadings, high positive loading was defined as greater than 0.75 and moderate loading was defined as 0.5-0.75. Loadings of less than 0.3 were considered insignificant.

The analysis reveals that for Zone A, the three factors (F1, F2 and F3) explain 80.01% of the total variance in post monsoon. Table 1 presents the eigen values, the percentage of variance, the cumulative eigen value and the cumulative percentage of variance associated with each other for Zone A during post monsoon.

In Table 1, F1 has a high positive loading of TDS, EC, Cl^-, Na^+, K^+ and SO_4^{2-} accounting for 40.19% of the total variance in Zone A. The high loading of these ions indicates salinity originating from seawater. F2 explains total variance of 17.30% and has a negative loading of HCO_3^- and NO_3^-. The leaching of salts due to rainfall recharge and irrigation water takes place in monsoon and post monsoon. Therefore, this factor can be related to anthropogenic inputs. F3 explains total variance of 22.52% and has positive loading of Cl^-, Ca^{2+} and Mg^{2+}. The negative loading of pH also contributed to the factor. The positive loading of Cl^-, Ca^{2+} and Mg^{2+} can be attributed to ion exchange process and dissolution of halite salts and calcite minerals in post monsoon. The negative loading of pH may be caused by the biogenic or organic control from marine sediments of the pH value [13,14].

Table 1: Results of factor analysis with varimax rotation for Zone A (2013)

Variable	F1	F2	F3
pH	-0.146	0.338	-0.731
EC	0.864	0.047	0.494
TDS	0.864	0.047	0.494
HCO_3^-	-0.066	-0.711	-0.208
Cl^-	0.827	0.118	0.538
SO_4^{2-}	0.891	-0.106	0.217
NO_3^-	-0.1	-0.851	0.153
Na^+	0.928	0.015	0.309
K^+	0.751	-0.21	-0.222
Ca^{2+}	0.488	0.202	0.681
Mg^{2+}	0.192	0.04	0.807
Cumulative eigen value	5.493	-1.071	2.532
Variability %	40.19	17.3	22.52
Cumulative %	40.19	57.49	80.01

For Zone B, the first three factors explain 77.79% of the total variance in post monsoon season. Table 2 presents the eigen values, the percentage of variance, the cumulative eigen value and the cumulative percentage of variance associated with each other for Zone B during post monsoon.

In Table 2, F1 has a high positive loading of TDS, EC, Cl^-, Na^+, K^+ and SO_4^{2-} accounting for 41.34% of the total variance in Zone B. The relatively low to moderate loading of HCO_3^- also contributes to F1. The high loadings of TDS, EC, Cl^-, Na^+, K^+ and SO_4^{2-} indicate salinization in local areas due to processes such as upconing of saline water due to pumping of groundwater for irrigation on account of dry spells in the monsoon season. The positive values of EC and HCO_3^- concentrations indicate carbonate weathering and silicate weathering. Thus, this factor relates to water rock interaction and salinization. F2 explains the total variance of 21.65 % and associated with high loading of NO_3^- and moderate loading of Ca^{2+} and Mg^{2+}. The positive values of Ca^{2+} and Mg^{2+} concentrations indicate strong carbonate weathering. The high positive loading of NO_3^- indicates leaching of fertilizer due to recharge processes in post monsoon season. Thus, this factor reflects water rock interaction and influence of anthropogenic activities. F3 explains total variance of 14.80% and associated with moderate positive loading of Ca^{2+} and HCO_3^-. High negative pH loading also contributed to factor. The positive values of Ca^{2+} and HCO_3^- concentrations indicate dissolution of calcite minerals. The negative loading of pH may be caused by the biogenic or organic control from marine sediments of the pH value. Thus, this factor reflects water rock interaction.

Table 2: Results of factor analysis with varimax rotation for Zone B (2013)

Variable	F1	F2	F3
pH	-0.008	0.093	-0.922
EC	0.932	0.322	0.106
TDS	0.932	0.322	0.106
HCO_3^-	0.469	-0.478	0.543
Cl^-	0.864	0.417	0.061
SO_4^{2-}	0.724	0.017	0.013
NO_3^-	0.004	0.894	-0.025
Na^+	0.958	-0.1	-0.091
K^+	0.817	-0.213	-0.162
Ca^{2+}	0.213	0.597	0.488
Mg^{2+}	0.211	0.825	0.022
Cumulative Eigen value	6.116	2.696	0.139
Variability %	41.34	21.65	14.8
Cumulative %	41.34	62.99	77.79

For Zone C, the first three factors explain 81.65% of the total variance in post monsoon season. Table 3 presents the eigen values, the percentage of variance, the cumulative eigen value and the cumulative percentage of variance associated with each other for Zone C during post monsoon.

In Table 3, F1 has a high positive loading of TDS, EC, Cl^-, SO_4^{2-}, Ca^{2+} and Mg^{2+} and moderate loading of Na^+. The moderate negative pH loading also contributes to factor. The positive loading of TDS, Cl^-, SO_4^{2-}, Na^+, Ca^{2+} and Mg^{2+} indicate dissolution of halite salts and carbonate and silicate weathering. The factor also reflects salinity in Zone C due to the phenomenon of localized upconing of saline water from deeper depths. F2 explains the total variance of 20.51 % and associated with high loadings of Na^+ and HCO_3^-. The positive loading of Na^+ and HCO_3^- indicate the presence of freshwater which in turn indicates the presence of recharge zone in Zone C that is recharged due to rainfall during monsoon period. F3 explains total variance of 9.90% and associated with high loading of NO_3^-. The high positive loading of NO_3^- reflects widespread use of fertilizers for crop cultivation and indicates presence of leachates from agricultural fertilizers with rainfall recharge occurring in monsoon season in Zone C.

Table 3: Results of factor analysis with varimax rotation for Zone C (2013)

Variable	F1	F2	F3
PH	-0.568	0.099	-0.131
EC	0.949	0.245	0.145
TDS	0.949	0.245	0.145
HCO_3^-	0.201	0.892	0.105
Cl^-	0.946	-0.031	-0.038
SO_4^{2-}	0.947	0.041	0.156
NO_3^-	0.058	0.084	0.979
Na^+	0.669	0.612	0.315
K^+	0.458	-0.354	0.038
Ca^{2+}	0.915	-0.249	-0.041
Mg^{2+}	0.818	0.187	-0.175
Cumulative Eigen value	6.342	1.771	1.498
Variability %	51.24	20.51	9.90
Cumulative %	51.24	71.75	81.65

ACKNOWLEDGMENT

The groundwater samples were collected and analysed under the study carried out at the National Institute of Hydrology, Roorkee, India, in collaboration with Gujarat Water Resources Development Corporation Ltd., Gandhinagar, India. The study was funded by MoWR, GoI, under the World Bank assisted Hydrology Project Phase II.

CONCLUSION

The results indicate that average concentrations of TDS, Na^+, Ca^{2+}, Mg^{2+}, Cl^-, decrease with increasing distance from the sea coast. No significant increasing or decreasing spatial trend is visible in the case of HCO_3^-, which shows higher concentration throughout the region due to presence of calcite minerals. From the factor analysis, it is evident that different hydrogeochemical processes and anthropogenic inputs affect the groundwater quality during post monsoon season, which are as follows: i) saltwater encroachment from sea, ii) localized upconing of saltwater due to pumpage, iii) ion exchange, iv) inherent salinity of rocks / marine sediments v) carbonate and silicate weathering of rocks, and vi) leaching of salts/minerals. Zones of major groundwater recharge exist in the inland area away from the coastal tract, which show presence of freshwater due to groundwater recharge in monsoon season. Overall, it is concluded that the groundwater salinity existing in the coastal area is principally controlled by a combination of factors which modify the concentration of constituent ions in the groundwater.

REFERENCES:

[1] Barlow, P.M., "Ground water in freshwater-saltwater environments of the Atlantic coast", USGS Circular 1262.U.S. Geological Survey, Reston, VA: 133, 2003.

[2] Park, S.C., Yun, S.T., Chae, G.T, Yoo, I.S., Shin, K.S., Heo, C.H. and Lee, S.K., "Regional hydrochemical study on salinization of coastal aquifers, western coastal area of South Korea". Journal of Hydrology, 2005, 313: 182–194.
[3] Morell, L., Gimemnz, E., and Esteller, M.V., "Application of the principal components analysis to the study of salinization of the Castellon Plain (Spain)". The Science of the Total Environment, 1996, 177: 161-171.
[4] Kim, J.H.; Kim, H.R. and Chang, H.W., "Hydrogeochemical characterization of major factors affecting the quality of shallow groundwater in the coastal area at Kimje in South Korea". Geosciences Journal, 2003, 7(4) : .313-322.
[5] Razack, M., and Dazy, J., "Hydrochemical characterization of groundwater mixing in sedimentary and metamorphic reservoirs with combined use of piper's principal and factor analysis", Journal of Hydrology, 1990, 114 : 371–393
[6] Ruiz, F., Gomis, V. and Blasco, P., "Application of factor analysis to the hydrogeochemical study of a coastal aquifer", Journal of Hydrology, 1990, 119 : 169–177
[7] Seyhan E.V., Van de Caried A.A., and Engelen G.B., "Multivariate analysis and interpretation of the hydrochemistry of a dolomite reef aquifer, Northern Italy", Water Resources Research, 1985, 21: 1010–1024
[8] Lawrence, F.W. and Upchurch, B., "Interpretation of recharge areas using geochemical factor analysis". Groundwater, 1982, 20: 681-687.
[9] APHA, "Standard methods for the examination of water and wastewater", 19th ed. Washington, DC: American Public Association, 1995, 1467 pp.
[10] Jain, C.K. and Bhatia, K.K.S., "Physico-chemical analysis of water and wastewater", User's Manual, UM-26, National Institute of Hydrology, Roorkee, 1988.
[11] Davis, J. C., "Statistics and Data Analysis in Geology". John Wiley and Sons, Inc., New York, 1973, 550p.
[12] Klovan, J.E., "R - and Q – mode factor analysis". In R. McCammon (ed.), Concepts in Geostastistics. Springer-Verlag, New York, 1975, 21-69.
[13] Mondal, N.C., Singh, V.S., Saxena, V.K. and Singh, V.P., "Determining the interaction between groundwater and saline water through groundwater major ions chemistry". Journal of Hydrology, 2010, 388: 100–111.
[14] Wen, X., Diao, M., Wang, D. and Gao, M., "Hydrochemical characteristics and salinization processes of groundwater in the shallow aquifer of Eastern Laizhou Bay, China". Hydrological Processes, DOI: 10.1002/hyp.8362, 2011

International Journal of Engineering Research and General Science Volume 3, Issue 3, Part-2 , May-June, 2015
ISSN 2091-2730

Assessment of Characteristics of Urban Area Soil around Bellandur Lake, Bangalore, Karnataka, India

Ramesh. N[1] and Dr. Krishnaiah. S[2]

[1] Department of Civil Engineering, Government Engineering College, K.R.Pet-571 426, Karnataka, India, rameshsreevar@gmail.com

[2] Professor and Registrar, Jawaharlal Nehru Technological University Anantapur, Ananthapuramu – 515 002, (AP), India

Abstract- The main aim in this study is to assess the level of Characteristics of urban area soil focuses on heavy metals parameters around Bellandur Lake. The samples of soil collected at different locations around the Bellandur Lake and one sample at unpolluted area have been analyzed for viz. pH, % CaCO3, Ca, Mg, Cl^-, F, Na, K, SAR, Fe, Cu, Zn, As, Cd, Cr, Hg, Ni and Pb using pH meter, titrimetric method, flame photometric method, spectrophotometric method and atomic absorption spectrophotometer. These values assessed with respect to reference soil taken from unpolluted soil profile. The concentration of all the parameters is high compared to the soil sample taken from unpolluted area. All the parameter values were higher on top layer soil and decreases in subsequent in bottom layer.

Keywords- Soil, Heavy metals, Sewage water, Contamination, Urban Lake, Pollution, Deteriorate

INTRODUCTION

In many developing countries, the expansion of urban centers is of considerable importance for socio- economic growth and this continuously modifies the physical, chemical and biological composition of our living environment. Thus, many people living within these urban centers are often exposed to such unnatural environment since they depend on resources from water, soil and air. Heavy metals are considered as the most important form of pollution of the aquatic environment because of their toxicity and accumulation by marine organisms. Very small amount of certain heavy metals are essential for life and it has been stated that they are more important than vitamins since they cannot be synthesized by living matter. Copper, zinc and chromium, although essential at low levels, are very toxic at higher concentrations. Heavy metals are stable and persistent environmental contaminants since they are not biologically degraded like many organic pollutants; thus, they tend to accumulate, particularly in sediments in association with organic and inorganic matter and involve adsorption, complex formation and chemical combination. Some trace metals are necessary in small amounts for individual metabolic processes, being assimilated by marine organisms. Rapid urbanization and industrialization with improper environmental planning often lead to discharge of industrial and sewage effluents into rivers and lakes. The lakes have a complex and fragile ecosystem, as they do not have self-cleaning ability and therefore, readily accumulate pollutants [1]. Wastewater disposal is becoming a problem in developing countries as large quantities of municipal waste and industrial effluent are being produced due to increased urbanization and industrialization respectively [2]. The problems associated with heavy metals in waste and storm water drainage entering the natural urban aquatic ecosystems have been well documented and studied. Heavy metals are widespread pollutants of great environmental concern as they are non degradable, toxic and persistent with serious ecological ramifications on aquatic ecology. The urban aquatic ecosystems are strongly influenced by long term discharge of untreated domestic and industrial wastewaters, storm water runoff, accidental spills and direct solid waste dumping [3].The contamination of soils directly influences public health, because soils exert a direct impact on human health due to the fact that individuals easily come into contact with them [4].

Soil pollution with heavy metals has become a critical environmental concern due to its potential adverse ecological effects. Heavy metals occur naturally at low concentrations in soils. However, they are considered as soil contaminants due to their widespread occurrence, acute and chronic toxicity. These metals are extremely persistent in the environment. They are non-biodegradable, non thermo-degradable and thus readily accumulate to toxic levels. Since they do not break down, they might affect the biosphere for a long time. It is known that heavy metals form an important polluting group. They have not only toxic and carcinogenic effect but also tend to accumulate in living organisms. Heavy metals are the stable metals or metalloids whose density is greater than 4.5 g/cm^3, namely Pb, Cu, Ni, Cd, Zn, Hg and Cr etc. They are stable and cannot be degraded or destroyed, and therefore they tend to accumulate in soils. There are several sources of heavy metals in the environment: 1) air which contains mining, smelting and refining of fossil fuels, production and use of metallic commercial products and vehicular exhaust, 2) water having domestic sewage, sewage and industrial effluents, thermal power plants and atmospheric fallout and 3) soil like – agricultural and animal wastes, municipal and industrial sewage, coal ashes, fertilizers, discarded manufacture goods and atmospheric fallout [5].

Soil is one of the vital resources on living planet Earth. The comprehensive understanding of temporal variability, physicochemical parameters and affect on the environment is becoming an essential task in soil science and field of environment. In these areas, nutrient loading and physiochemical characteristics adversely affect water bodies and extreme extension causes sever eutrophication.

Inherent soil physicochemical properties influence the behaviour of soil and hence, knowledge of soil property is important. Soil physicochemical properties deteriorate to the change in land use. The waste material discharges from industrial activities causes adverse effects on soil and soil organic matter. The presence of heavy metals and residues from town and industrial wastes has been found to be the causes of pollution in soil. It needs some physicochemical analysis to know the status of this adverse impact on soil quality. Soil pollution usually originates from the industries, chemical fertilizers, use of sewage sludge, city compost and other industrial wastes. The industrial effluents and water drainage from spoil and rubbish heaps either washes direct to nearby fields and entire the local streams, river and ultimately into the soil. Once pollutants enter and are incorporated into the soil, the concentration in soil continuously increasing and accumulating, which is toxic to all forms of life like plant, microorganisms and human being [6].

The present study focuses on with the Characteristics of Urban Area Soil parameters around Bellandur Lake viz. pH, Calcium Carbonate, Calcium, Magnesium, Chloride, Fluoride, Sodium, Potassium, Sodium adsorption ratio, Iron, Copper, Zinc, Arsenic, Cadmium, Chromium, Mercury, Nickel and Lead.

STUDY AREA

Bangalore, the capital of Karnataka, has a history of over 400 years. The origin of Bangalore city can be traced back to 1537 when it was founded by Late Magadi Kempegowda. Bangalore is the principal administrative, cultural, commercial and industrial centre of the state of Karnataka. The city of Bangalore is situated at an altitude of 920 meters above mean sea level. Geographically it is located on 12.95º N latitude and 77.57º E longitude. The population of Bangalore as per the 2001 census was 5,686,844 while it was 163,091 in the beginning of the last century (1901). As per provisional reports of census of India, population of Bangalore in 2011 is 84, 25,970 and is the third densely populated city in India having density of 11,000 per square kilometers. [7]

The earliest history of creation of lakes in and around the city is traced to the founders of Bangalore–the Kempe Gowdas –by damming the natural valley systems by constructing bunds. Most of the lakes and tanks were manmade for purposes of drinking water, irrigation and fishing needs and they have also favorably influenced microclimate of the city. [8]

Bellandur Lake, the largest in Bangalore city spreads across an area of 892 acres. It is located at latitude of 12°58′ N and longitude of 77°35′ E at an altitude of 921 m above mean sea level and has a catchment area of 110.94 sq.miles or 287.33 sqm. The water storing capacity of Bellandur lake is 17.66 million cubic feet, being 3km in length and 2.75km in Width. It is one of the largest man-made lakes in Southeast Asia, located about 20 km from the city towards the south-east of Bangalore city. The tank is a receptor from three chains of tanks. One chain, originates in the north, from Jayamahal, covers the eastern portion and has been referred to as the eastern stream. Another chain originates from the central part of the city, from around the K.R.Market area and covers the central portion and is called the central stream. The other chain, that reaches the tank is through the southwestern region and is called the western stream. Due to urbanization in 1980s, there was breakage of chains of tanks feeding the lake. The breakage in chains, unchecked industrial, residential as well as commercial development, resulted in insufficient rainwater reaching the tank and excess untreated sewerage and effluents laden water flow to the tank. [8]

Figure 1. Satellite view of Bellandur Lake and its surrounding

Satellite view of Bellandur tank and its surrounding shown in Figure 1.Research work has been carried out to study the Characteristics of Urban Area Soil around Bellandur in Bangalore city.

SAMPLING AND ANALYSIS

Soil samples for investigations were collected from six different locations selected around the banks of the Bellandur lake and one location selected at downstream of Bellandur lake, total 14 samples were collected during March 2014. The criterion of selection of sampling points was based upon inflow and outflow regions of the lake. Sampling locations are shown in Figure 2 and 3. At all the sampling locations two samples approximately 1000gm of soil was collected from each site were taken one from the top layer and another at to a depth of over 30cm. Sampling tools were washed and dried with water before the next sample was collected. These soil samples were brought in polythene bags to laboratory for the analysis of characteristics of soil parameters. Soil was collected as per standard procedure given in literature [3, 6].

Soil samples were air dried and then ground in to fine powder using an agate mortar and pestle to pass through a 0.5mm sieve. The powdered samples were stored in polythene covers at room temperature for further analysis of characteristics of soil samples. The soil samples were analyzed for properties using standard analytical methods. All laboratory equipment used for the heavy metal analysis was washed in 3% HNO^3 and rinsed at least twice with distilled water. One gram of each soil sample was placed into a 200 ml flask. Then, 0.2 ml of sulfuric acid, 1 ml of nitric acid and 5 ml of perchloric acid were added. The soil and acid mixture was heated to 180°C for 3 h on a hotplate. After cooling, 1 gram of ammonium chloride and 20 ml of 0.5 N HCl were added. Samples were reheated to 180°C for one hour and evaporated to approximately 10 ml. After cooling, the extracts were filtered into 100 ml plastic bottles through a filter paper and 1 ml of lanthanum chloride was added. The samples were analyzed using pH meter, Titrimetric method, Flame photometric method, Spectrophotometric method and Atomic absorption Spectrophotometer [9, 10, 11, 12].

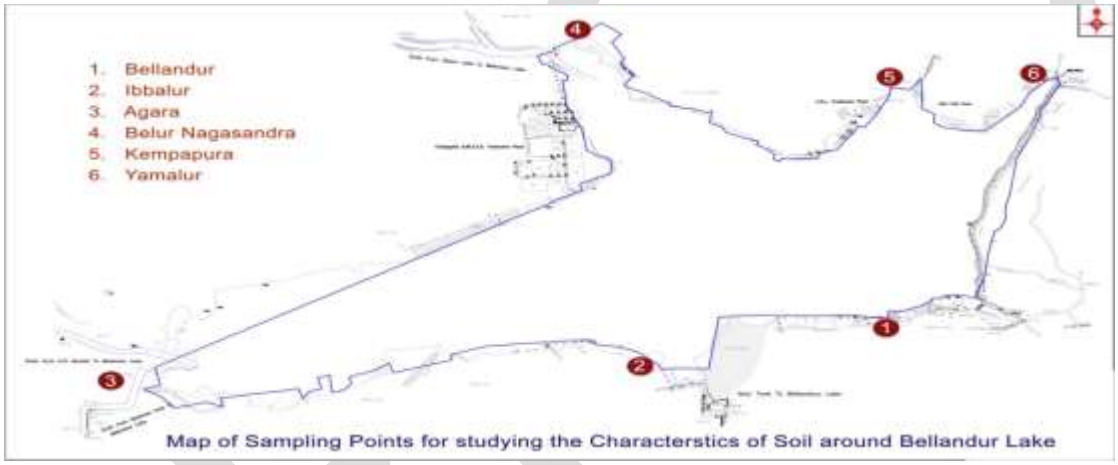

Figure 2. Sampling locations around Bellandur lake

Figure 3. Sampling location of Kadubeesanahalli (S. No.7)

RESULTS AND DISCUSSION

The data analysed for the Soil samples from six different locations around the Bellandur lake namely Bellandur(1), Ibblur(2),

Agara(3), Belur Nagasandra(4), Kempapura(5), Yamalur (6) and one sample from unpolluted soil from Kadubeesanhalli(7) is represented in Table-1 and the different sampling locations is represented in Figure 2 and 3.

The pH value is higher 8.85 at location no.3 and lowest 8.06 at location no.2 decreases with depth at all locations. The % of CaCO3 is higher 15.4 at location no.4 and lowest 5.0 at location no.6 decreases with depth at all locations. Ca value is higher 153.00 mg/kg at location no.5 and lowest 126.20 mg/kg at location no.6 decreases with depth at all locations. Mg value is higher 35.40 mg/kg at location no.4 and lowest 26.30 mg/kg at location no.6 decreases with depth at all locations. Cl^- value is higher 54.30 mg/kg at location no.4 and lowest 35.90 mg/kg at location no.6 decreases with depth at all locations. F is absent at all locations. Na value is higher 30.30 mg/kg at location no.4 and lowest 21.70 mg/kg at location no.6 decreases with depth at all locations. K value is higher 3.10 mg/kg at location no.4 and lowest 2.10 mg/kg at location no.6 decreases with depth at all locations. SAR value is higher 2.90 at location no.3 and lowest 2.40 at location no.6 decreases with depth at all locations. Fe value is higher 1.70 mg/kg at location no.2 and lowest 1.30 mg/kg at location no.1 decreases with depth at all locations. Cu is present at location no. 1 is higher 0.40 mg/kg and lowest 0.08 mg/kg at location no.3 , are decreases with depth and in remaining locations are BDL. Zn is present at location no. 1 is higher 0.90 mg/kg and lowest 0.20 mg/kg at location no.3 , are decreases with depth and in remaining locations are BDL. As, Cd, Cr, Hg, Ni and Pb were found is below detectable limit in all 14 samples. Characteristics of soil were detected higher concentration in the top and decreases in the next 30 cm deep. The concentration of all the metals is high compared to the soil sample taken from unpolluted area is represented in Table-1.]

Table 1. Analytical results of characteristics of soil sample

Parameter	Location	Unit	Bellandur(1)	Ibblur(2)	Agara(3)	Belur Nag asandra(4)	Kempapura(5)	Yamalur (6)	Kadubees anhalli(7)
pH	Top	-	8.23	8.06	8.85	8.18	8.69	8.30	7.86
	30cm deep	-	7.69	7.12	7.41	7.05	7.21	7.54	7.60
%Caco3	Top	%	7.10	7.60	10.00	15.40	9.80	5.00	3.30
	30cm deep	%	5.30	4.90	4.20	5.00	3.70	3.50	3.00
Calcium	Top	mg/kg	135.30	133.90	150.10	176.40	153.0	126.20	110.00
	30cm deep	mg/kg	125.70	127.80	120.40	120.60	118.60	114.50	102.90
Magnesium	Top	mg/kg	27.60	27.00	30.20	35.40	30.60	26.30	21.90
	30cm deep	mg/kg	25.90	25.10	24.50	24.70	23.90	22.80	20.40
Chloride	Top	mg/kg	43.50	44.80	50.60	54.30	50.10	35.90	25.90
	30cm deep	mg/kg	38.20	37.00	30.30	32.50	26.70	28.40	21.30
Fluoride	Top	mg/kg	Ab	Ab	Ab	Ab	Ab	Ab	Ab
	30cm deep	mg/kg	Ab	Ab	Ab	Ab	Ab	Ab	Ab
Sodium	Top	mg/kg	25.60	24.70	28.10	30.30	26.90	21.70	10.20
	30cm deep	mg/kg	22.40	23.00	20.50	21.00	16.60	16.70	8.00
Potassium	Top	mg/kg	2.60	2.50	2.70	3.10	2.70	2.10	1.20
	30cm deep	mg/kg	2.20	2.30	2.00	2.00	1.60	1.40	0.70
SAR	Top	-	2.80	2.70	2.90	2.90	2.80	2.40	1.20
	30cm deep	-	2.50	2.60	2.40	2.40	1.90	2.00	1.00
Iron	Top	mg/kg	1.30	1.70	1.40	1.60	1.50	1.60	2.00
	Bottom	mg/kg	1.20	1.50	1.30	1.50	1.30	1.40	1.80
Copper	Top	mg/kg	0.40	BDL	0.08	BDL	BDL	BDL	BDL
	30cm deep	mg/kg	0.10	BDL	0.06	BDL	BDL	BDL	BDL
Zinc	Top	mg/kg	0.90	BDL	0.20	BDL	BDL	BDL	BDL
	30cm deep	mg/kg	0.70	BDL	BDL	BDL	BDL	BDL	BDL
Arsenic	Top	mg/kg	BDL	BDL	BDL	BDL	BDL	BDL	BDL
	30cm deep	mg/kg	BDL	BDL	BDL	BDL	BDL	BDL	BDL
Cadmium	Top	mg/kg	BDL	BDL	BDL	BDL	BDL	BDL	BDL
	30cm deep	mg/kg	BDL	BDL	BDL	BDL	BDL	BDL	BDL
Chromium	Top	mg/kg	BDL	BDL	BDL	BDL	BDL	BDL	BDL
	30cm deep	mg/kg	BDL	BDL	BDL	BDL	BDL	BDL	BDL

Mercury	Top	mg/kg	BDL	BDL	BDL	BDL	BDL	BDL	BDL
	30cm deep	mg/kg	BDL	BDL	BDL	BDL	BDL	BDL	BDL
Nickel	Top	mg/kg	BDL	BDL	BDL	BDL	BDL	BDL	BDL
	30cm deep	mg/kg	BDL	BDL	BDL	BDL	BDL	BDL	BDL
Lead	Top	mg/kg	BDL	BDL	BDL	BDL	BDL	BDL	BDL
	30cm deep	mg/kg	BDL	BDL	BDL	BDL	BDL	BDL	BDL

Note: BDL - Below Detectable Limit.

The variation in the heavy metal concentration in soil at different locations is due to variation in heavy metal sources and concentration of heavy metals present in polluted water where the water is used continuously for irrigation for several years. The soil pollution also takes place due to atmospheric fall out, emissions from vehicular exhaust, land application of municipal solid waste, sewage sludge, fertilizers, pesticides etc., [13]. Hence the metal concentration is high around the Bellandur lake, compared with unpolluted area of Kadubeesanhalli area.

CONCLUSION

This paper proposes the determination of urban area soil parameters around Bellandur Lake especially concentrated on heavy metals. The study reveals that the irrigation was carried out with polluted water containing variable amount of heavy metal increases the concentration in soil samples. The concentration of all the metals is high compared to the soil samples taken from the unpolluted area. The presence of heavy metals in soil is one of the key components of human exposure to metals through the food chain. The heavy metals can be removed by plants and it is an effective method in cleaning up of contaminated soil. The presence of heavy metals has merit attention especially for developing countries where newly establishing industries and extensive urban growth continue to raise heavy metals in soil.

REFERENCES:

[1] K.G.Pujar, M.I.Kumbar, A.S.Pujar, S.C.Hiremath, U.S.Pujeri and M.S.Yadawe, Studies of Physicochemical and Some Heavy Metals in Soil and Lake Sediments, Online International Interdisciplinary Research Journal, {Bi-Monthly},Volume-IV, Issue-I, Jan-Feb 2014, pp. 169-174.

[2] Chipo Masona, Loveness Mapfaire, Stenly Mapurazi and Revai Makanda, Assessment of Heavy Metal Accumulation in Wastewater Irrigated Soil and Uptake by Maize Plants (Zea Mays L) at Firle Farm in Harare, Journal of Sustainable Development,Vol. 4, No. 6; December 2011,pp. 132-137.

[3] Aboud S. Jumbe and N. Nandini, Heavy Metals Analysis and Sediment Quality Values in Urban Lakes, American Journal of Environmental Sciences, 5 (6), 2009, pp. 678-687.

[4] Mughal Sharif, Yasmin Nergis and M. Afzal Farooq, Soil Contamination from Toxic Elements Irrigated with Mixed Industrial Effluent and its Environmental Impact on the Urban Area of Karachi Pakistan, American-Eurasian J.Agric.& Environ.Sci., 9(5), 2010, pp. 584-591.

[5] Chopra A. K, Chakresh Pathak and G. Prasad, Scenario of heavy metal contamination in agricultural soil and its management, Journal of Applied and Natural Science,1(1), 2009. pp. 99-108.

[6] D. V. Sonawane, S. P. Lawande, V. B. Gaikwad and S. R. Kuchekar, Impact of industrial waste water on soil quality and organic matter around Kurkumbh industrial area Daund, Pune District (MS), Int. J. Chem. Sci., 8(1), 2010. pp. 97-102.

[7] Ramesh. N and Krishnaiah. S, Impact on Bangalore Nisarga due to urbanization: Case study of Bangalore city lakes, Karnataka, India; Midas Touch International Journal of Commerce, Management and Technology, Vol. 2, No. 1, 2014, pp.230-238.

[8] Ramesh. N and Krishnaiah. S, Scenario of Water Bodies (Lakes) In Urban Areas- A case study on Bellandur Lake of Bangalore Metropolitan city, IOSR-JMCE, Vol.7,2013, pp.06-14.

[9] Yoshinori Ikenaka, Shouta M. M. Nakayama, Kaampwe Muzandu, Kennedy Choongo, Hiroki Teraoka, Naoharu Mizuno and Mayumi Ishizuka: Heavy metal contamination of soil and sediment in Zambia; African Journal of Environmental Science and Technology Vol. 4(11), 2010, pp. 729-739.

[10] Neethu Patil, Ananth Nag.B and E.T. Puttaiah: Evaluation of Heavy Metal Accumulation in Soil around Bhadravathi Taluk Shimoga District Karnataka; International Journal of Life Sciences Vol.2. No.3. 2013, Pp. 124-129.

[11] Dr. C.A. Srinivasmurthy, Dr.V.R. Ramakrishna Parama, Dr.T.H. Hanumantharaju and Dr.K. Sudhir; Practical Manual for Hands on Training/ Experiential Learning; University of Agriculture Sciences, GKVK, Bengaluru, 2013.

[12] Jaiswal. P.C: Soil, Plant and Water Analysis; Allahabad Agriculture Institute, Allahabad, India, 2003.

[13] Jayadev and E.T. Puttaih: Heavy metal contamination in soil under the application of polluted sewage water across Vrishabhavathi River; International Journal of Engineering Research and Applications (IJERA) Vol. 2, Issue 6, pp.1666-1671, November- December 2012

International Journal of Engineering Research and General Science Volume 3, Issue 3, Part-2 , May-June, 2015
ISSN 2091-2730

Audio Processing In Car Infotainment Systems

Kavitha. S
Department of Electrical and Electronics,
The National Institute of Engineering,
Mysore, Karnataka, India
Summer Intern, Delphi Automotive Systems Pvt. Ltd.,
Bangalore, India
*Email-id:*kavithasnsd@yahoo.com
Ph. No.: +91-96206-06974

K. V. Nagalakshmi
Associate Professor, Department of Electronics and Communication,
The National Institute of Engineering,
Mysore, Karnataka, India

Abstract— Present day in-car infotainment systems use audio DSP to incorporate many advanced features. The paper briefs about the car radio architecture which is used in high end infotainment systems and explains how the audio mixing takes place in the superposition block of the audio DSP. The paper also explains the audio processing operations like filtering and scaling, which a signal undergoes before it reaches the output of the speakers. It also contains how audio mixing takes place in the superposition block of audio DSP.

Keywords— In-Car Infotainment, audio DSP, superposition block.

INTRODUCTION

Today's car manufacturers are integrating more and more complex multi-media equipment into their vehicles in order to meet the changes in consumers' buying behavior. This collection of firmware equipment installed into automobiles is called In –vehicle Infotainment. The in-vehicle infotainment includes audio and/or audio/visual entertainment, along with automotive navigation systems (SatNav). Present day car radios have features like:

- Tuner sources - FM, AM, XM
- Media Sources like CD/DVD, USB Audio, Picture, Video, SD Card support, iPod, AUX;
- Wireless connectivity: Bluetooth, Phonebook, Internet, Phone app access
- Telematics: GPS, Modem
- Speech Recognition
- Rear-seat entertainment

It also has features like internet radio (Pandora and Stitcher), traffic control radar.

But the DSP (Digital Signal Processor) is the core of the infotainment system. Digital signal processors (DSPs) are being used widely for sound field reproduction. There are various papers published which shows the design of digital audio signal processing circuitry having high fidelity and sound reception ([1] and [2]). Also papers are published which describe different architectures of DSP which is used in car radio ([3] and [4]).

2. ARCHITECTURE

The design to any electronic device is done based on the architecture followed. The overall car infotainment architecture is as shown in Figure 1. This is a layered architecture and can be broadly classified as HMI, Application Interface (API), Middleware and base drivers. The hardware and the OS are at the lowest layer. Software code resides in the middle ware and the application layer. The code is made platform independent so that the programming can be done across platforms [5].

2.1. Car Infotainment Architecture

Figure 2 shows the basic architecture used in present day car radios. The host microcontroller forms the core which is responsible for the flow of signal into and out of the DSP. Present day car radios follow a dual architecture involving: two processors. The processors deals with various features in the car radio like networking, navigation, entertainment, diagnostics, etc. Moreover they also monitor and regulate the power requirements by various components.

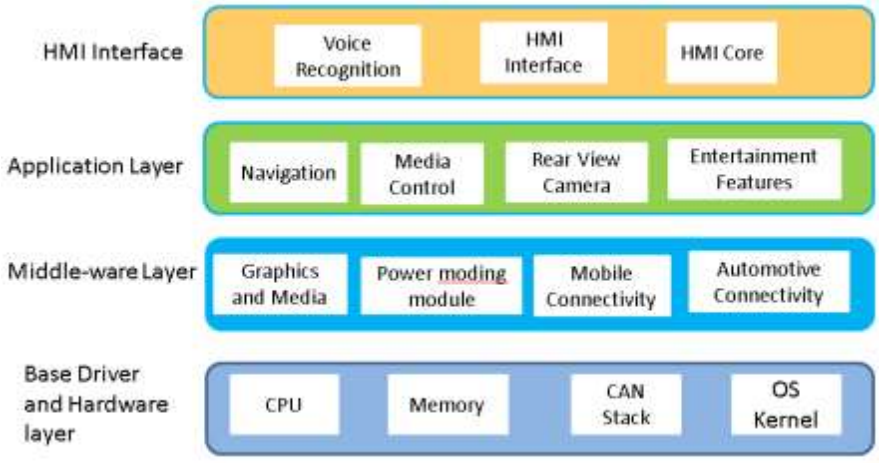

Fig. 1 Car Infotainment Software architecture

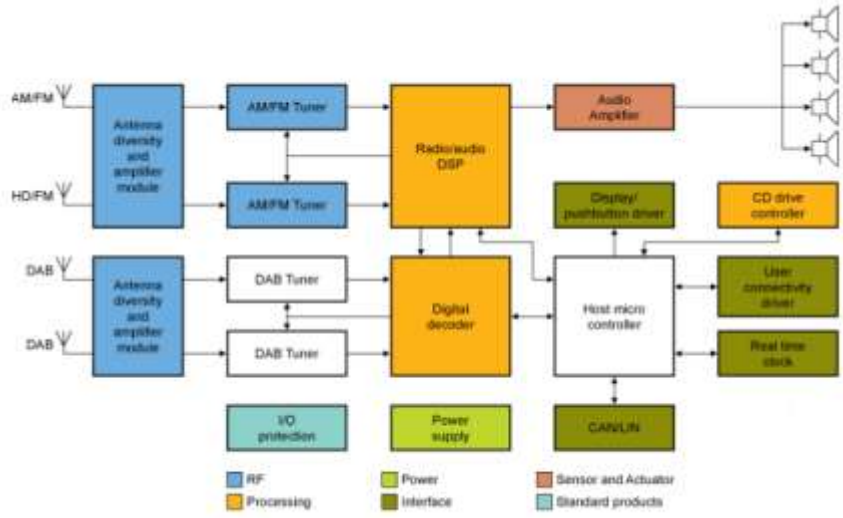

Fig. 2 Car radio Hardware architecture

Additionally there is a CAN (Control Area Network) which is responsible for the communication between the different ECUs (Engine Control Units) in the vehicle. The main audio processing is carried out in the DSP. The DSP can be divided into radio DSP and audio DSP. The output from the DSP is passed to the speakers through the amplifier.

The DSP has the following functional blocks:

2.1.1 Sample Rate Converter (SRC):

Sample rate conversion (SRC) is the process of changing the sampling rate of a data stream from a specific sampling rate (e.g. the input/output hardware rate) to another sampling rate (e.g. the rate at which application samples are processed). With the conversion of communication and software markets, SRC is a prime component in many of today's applications [6]. In most of those applications, a

very high quality sample rate converter is required. Most high quality SRCs employ a digital filter that provides the required quality by up-sampling the data to a very high sampling rate followed by down-sampling to the required output sampling rate.

2.2.2 Radio processing block:

The radio processing block digitizes signal at the tuner interface to digital converter. Additionally, it also performs blind equalization of the FM channel; this results in an outstanding rejection of the adjacent channels and any other interfering signal, even under severe multipath conditions. The DSP of the car radio includes the tuner part, which is responsible the AM/FM reception and signal processing. The signals received undergo demodulation in this block. Frequency translation and filtering of the received signals takes place in this block. DSP based receivers incorporate digital demodulation to replace analog demodulation techniques.

2.2.3 Audio processing block:

The audio processing block takes care of the signal distortion, signal conditioning and equalizations. The audio processing block consists of various filters, noise generators, sine generators, limiters, equalizers, etc. These are explained in the following sections.

3. AUDIO PROCESSING

Following the audio input, the audio data is normally processed by a series of processing blocks programmed. These processing blocks are normally common audio blocks such as IIR (Infinite Impulse Response) filters, volume control, tone control, DRC (Digital Range Compression), loudness, delay, mixers, and many others. As the DSP is fully programmable, the processing that can be done specific to the customer requirements. The DSP programming is done according to the specifications and needs of the customer.

To accomplish the duty of post audio processing, the audio is transferred through the DSP and this audio is transformed in the desired fashion. Audio comes into the DSP via an Input channels. An Input along with a Converter is used to create a Source that is used to transform the audio into a format the DSP can utilize. The Audio travels through the DSP via a Physical Audio Path. This Physical Audio Path is constructed of Components that are used to transform the audio in desired ways. The audio then exits the DSP via an Output.

3.1 Signal flow in Car radio

When a user selects a source in the car radio, the corresponding audio is played through the speakers. The audio for the corresponding source undergoes various stages of processing before reaching the speaker.

Figure 3 shows the flow diagram of a signal in the car radio. The user selects the source from the HMI. The HMI sends the request to the source arbitration block. The main function of this block is to request to the DSP to play the corresponding source. The audio DSP provides the audio path for the corresponding source performs the necessary processing and outputs the signal to the DAC (Digital to Analog Converter). The converted analog signals are then provided to the amplifier. The input to the amplifier will be a low dB signal and finally to the speakers.

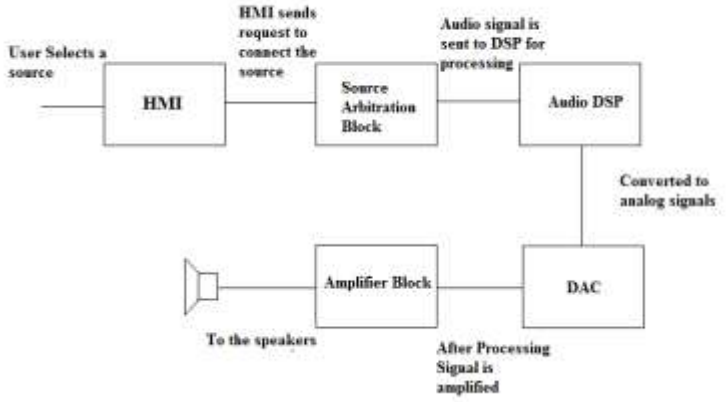

Fig 3. Flow diagram of signal a car radio

3.2 Digital Audio Scaling

In the DSP, the digital audio processing is designed so that noise produced by filter operations is maintained below the smallest signal amplitude of interest. Figure 4 describes the various terminologies used in the audio scaling. This low noise level is achieved by increasing the precision of the signal representation substantially above the number of bits that are absolutely necessary to represent the input signal. These scaling blocks act similar to gain blocks wherein the signals are attenuated at certain levels so that the net output is distortion free.

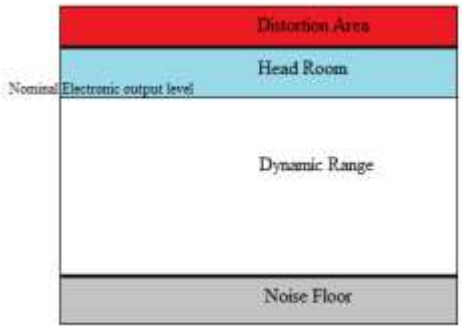

Fig 4: Audio Signal level: Relationship between SNR, Head room and Noise floor.

3.3 Digital Audio Processing in an audio-path

Figure 5 shows how the audio signal is processed in a single audio channel in the audio DSP. The audio signals can be boosted at various levels in a channel path to compensate for the headroom.

Scalar coefficients are used to adjust the volume of the audio passed through the control. Different Scalar coefficients will have different intended purposes. Some are intended for scaling of the audio of an audio path based on which audio application is currently selected. Others are intended for system level volume control. All of these Controls have a minimum and maximum gain property associated with it.

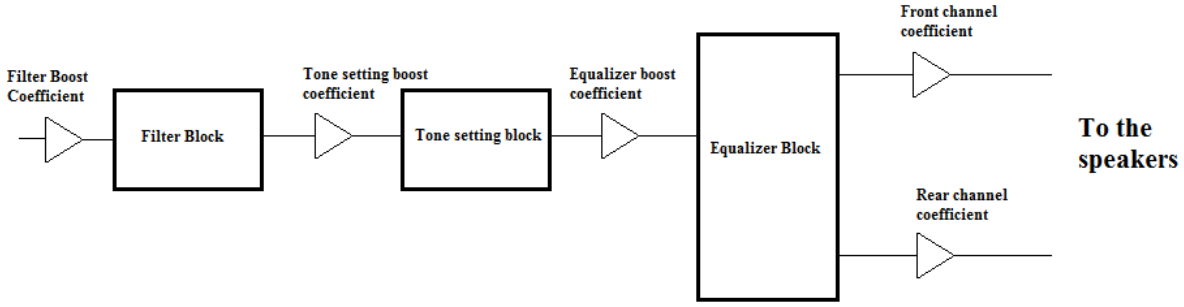

Fig 5. Audio scaling and boost coefficient in an audio path.

3.4 Digital Audio Mixing

When two different applications have to be played on a single channel, the sources have to be mixed. The mixing of sources is achieved by the superposition block. It this block the source signals are added together. The output volume of the sources that are mixed is set according to the customer requirement. For example if a USB/ SD source is playing and navigation prompt comes, the same channel plays both the above sources with varying volume output. This is achieved by the superposition block. Figure 6 shows a block diagram of a superposition block. The superposition block is responsible for the mixing of the audio signals. Appropriate mixing according to the requirement can be achieved by proper software programming.

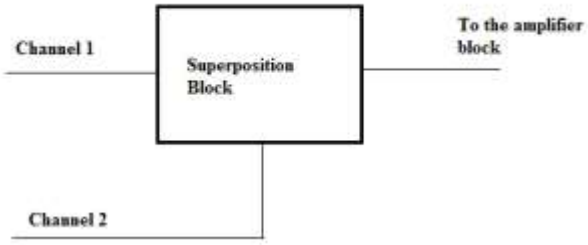

Fig6: Superposition Block in DSP

3.4 Equalizers

In order to alter or control the frequency response characteristics of an audio system, the equalizers are present. An audio equalizer provides more accurate control of tone or frequency than simple bass and treble controls. Equalizers and signal processors are two kinds of devices that allow to fine tune the sound in the vehicle's audio system.

The equalizers are usually present between the amplifier and the head unit. There are various equalizers. The two main equalizers are as follows:

- Graphic Equalizer
- Parametric Equalizer

3.4.1 Graphic Equalizer

These equalizers have fixed bandwidths. The sliders are present for each of the cut off frequencies so. The user can manually change the gain of each of the frequencies to obtain the desired level of attenuation. A graphic equalizer is the simplest type and consists of multiple sliders or controls for boosting or cutting bands or frequencies of sound.

Dynamic adjustment of frequencies of each of the bands can be achieved using the Graphic equalizer. For example, a typical five-band graphic equalizer has sliders for five fixed frequencies: 30Hz (low bass), 100 Hz (mid-bass), 1 kHz (midrange), 10 kHz (upper midrange) and 20 kHz (treble or high-frequency). Each of the bands is made of IIR filter. The equalizer can boost or cut each frequency but each frequency is fixed. With increase in the number of bands better tone control can be achieved.

3.4.2 Parametric Equalizer

A more complex type is the parametric equalizer, which controls more parameters of the sound than a graphic equalizer. A parametric equalizer can control three parameters of each frequency: level (boost or cut), the center or primary frequency and the bandwidth or range of each frequency. However, a parametric equalizer can also control the center frequency.

Some car Audio DSPs have both Graphical and parametric equalizers which help in wider control of audio.

ACKNOWLEDGMENT

I acknowledge Delphi Technical Centre India, Bangalore for the full support and infrastructural assistance for completion of this paper. Also extend thanks to the Head of Department of Electrical and Electronics, Dr. H. V. Saikumar. I also acknowledge Narasimhan Kaulgud, Professor, Department of Electronics and Communication for the valuable inputs to improve this paper.

CONCLUSION

With the present technology, the various features included in the high-end infotainment are discussed. The paper also explains the general architecture followed to manufacture today's car radio systems. The Digital Signal Processor (DSP) forms the core for any car infotainment architecture. All the signal processing is performed in the DSP. A detailed description on the audio processing which occurs in the DSP is provided. The audio signal which is available at the input of the DSP undergoes stages of audio processing. These stages are described in detail. Proposed operations are manual. We can extend it to wireless or Bluetooth.

REFERENCES:

[1] Matsuda, A., Shinada, A., and Morise, K., "Break Through Car Audio with DSP," SAE Technical Paper 910792, 1991, doi:10.4271/910792

[2] Asami, T., Okamoto, M., Mochiyama, Y., and Nakamura, H., "Development of a Practical DSP Car Audio System," SAE Technical Paper 920081, 1992, doi: 10.4271/920081

[3] Tatsuo Ito and Isogai.Y, "Digital Audio Signal Processor: Current Status and future Trends" FujiTsuTenTech.J. No.3, 1993

[4] Edwin J. Tan, Wendi B. Heinzelman,"DSP Architectures: Past, Present and Future", University of Rochester, Rochester, NY 14627

[5] Suresh Marisetty, Durgesh Srivastava, Joel Andrew Hoffmann, An Architecture for in vehicle infotainment system.

R. Nicole, "Title of paper with only first word capitalized," J. Name Stand. Abbrev., in press.

[6] Y. Yorozu, M. Hirano, K. Oka, and Y. Tagawa, "Electron spectroscopy studies on magneto-optical media and plastic substrate interface," IEEE Transl. J. Magn. Japan, vol. 2, pp. 740-741, August 1987 [Digests 9th Annual Conf. Magnetics Japan, p. 301, 1982].

[7] M. Young, The Technical Writer's Handbook. Mill Valley, CA: University Science, 1989.

International Journal of Engineering Research and General Science Volume 3, Issue 3, Part-2 , May-June, 2015
ISSN 2091-2730

Enhancing parameters of MSA for satellite application by using dumb shell oval head DGS technique

Mohit malhotra[1] , Paramjit singh[2]
[1,2]Electronics & Communication Department, [1,2]Punjab technical university
mohitmalhotra469@gmail.com [1], +91-7508803679
paramjit_singh02@yahoo.com [2], +91-9646574568
[1]Student, 2Asstt. Prof
[1,2] GIMET , AMRITSAR , INDIA

Abstract — A novel design of various defective ground structured co-axial feed micro strip rectangular patch antenna resulting to highly enhanced parameters when compared with results of fundamental MSA antenna , is proposed in this paper. Further this low profile antenna dimension can be varied with no trouble to make it perform on different frequency bands. Proposed design in paper resonates at 2.25 GHz and parameters S11, VSWR, input impedance are enhanced by employing DGS technique. Initially the antenna design will be presented and then it is simulated by using ANSOFT HFSS 13.0 [12]and then results will be deeply studied.

Keywords — dumb shell oval head, dgs, HFSS, msa, co-axial feed.

1. INTRODUCTION

As displayed in figure 1, micro strip Patch antenna is formed by sandwiching the dielectric substrate in between radiating patch and ground plane. Gold and silver are primary priorities for constructing the radiating[2]. Further by photo etching this radiating patch along with the feed lines are employed on the dielectric substrate, where the basic radiation of the micro strip patch antennas occurs as result of an occurrence of fringing fields in middle of patch edge and that of the ground plane[1]. Among few MSA shapes the most preferable Micro strip resonant patches are rectangular and circular which are extensively employed in multiple applications. The proposed design operates in between the frequency span of 2GHz - 2.5GHz and is proposed for satellite devotion. After designing it on (FR-4) 2 sided Fiber Reinforced epoxy , the performing characteristic parameters like the S11, VSWR, and input impedance were taken from the HFSS 13.0and then further these parameters of the fundamental MSA is enhanced by employing the dumb shell oval head defective ground structure technique in this paper.

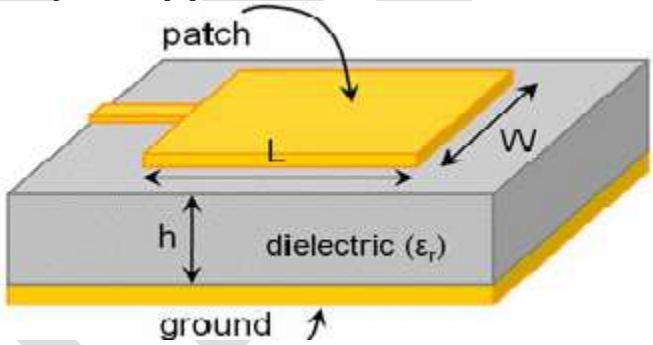

FIGURE 1 – Micro strip patch antenna

1.1 OVERVIEW OF DGS TECHNIQUE

DGS is a technique which intrude the shield distribution of current in the ground plane due to defect in the ground which is cascaded periodic or may be non-periodic carved configuration defect in the ground of a planar transmission line[3]. Like line capacitance and inductance, there are many transmission line characteristics which will get change due to this intrusion[5]. Any proper designed DGS and carved on right coordinates will be highly beneficial in rising an effective capacitance and inductance. Among numerous shapes of DGS , in this paper a dumb shell oval head dgs is used. To construct this DGS shape , the two circular shapes along with a rectangle sandwiched in between them which joins the two circles are united and this constructs the complete structure of dgs, as shown in figure 2

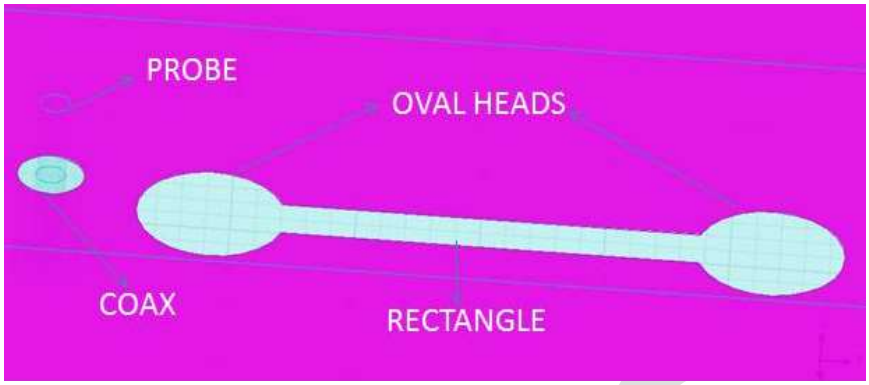

FIGURE 2 – Dumb shell oval head dgs on HFSS 13.0

1.2 ANTENNA DESIGN

The design of coaxial fed micro strip rectangular patch antenna and dumb shell oval head defective ground structured coaxial fed micro strip rectangular patch antenna are displayed in Figure 3(a) and 3(b) which are operating on single band WLAN application. An excitation of an antenna is implemented by coaxial feed line which is intended for characteristic impedance of 50 ohm. It is carved upon a substrate which has thickness of a 1.6mm , it has relative permittivity of 4.4 and at last having a loss tangent of 0.0009. The table 1 which is written below mentions proposed design without DGS dimensions:

VARIABLE	***VALUE***
Patch width	**40.57mm**
Patch length	**31.43mm**
Patch height	**1.6mm**
Ground width	**50.32mm**
Ground length	**41.19mm**
Interior Feed center radius	**0.3mm**
Exterior Feed center radius	**0.675mm**

Table 1 Dimensions of the co-axial fed rectangular patch antenna without dgs for 2.25 GHz frequency

The feeding of the designed antenna is done by co-axial cable which experiences the 50 ohms of characteristic impedance. The material used in order to make outer conductor is substrate material and for inner conductor, PEC material is used. An outer conductor runs from bottom to top of ground where inner conductor runs from the top of the patch to the bottom of ground. The feed point of the design without DGS is (30.5, 16.66) and the feed point of the design with that of DGS is (31, 16.35). The brilliant 47.1626 ohms of an impedance matching has been obtained as accurate impedance matching every time yields the brilliant results. Positioning measurements of shapes and design of proposed DGS antenna are described in table 2:

VARIABLE	***VALUE***
Patch width	**40.57mm**
Patch length	**31.43mm**
Patch height	**1.6mm**
Ground width	**50.32mm**
Ground length	**41.19mm**
Interior Feed center radius	**0.3mm**
Exterior Feed center radius	**0.675mm**
Radius of DGS ovals slot on the ground	**1.2mm**
Length & breath of DGS rectangle slot on the ground	**8.4mm , -1mm**

Table 2 Dimensions of the DGS MSA operating at 2.25 GHz Frequencies.

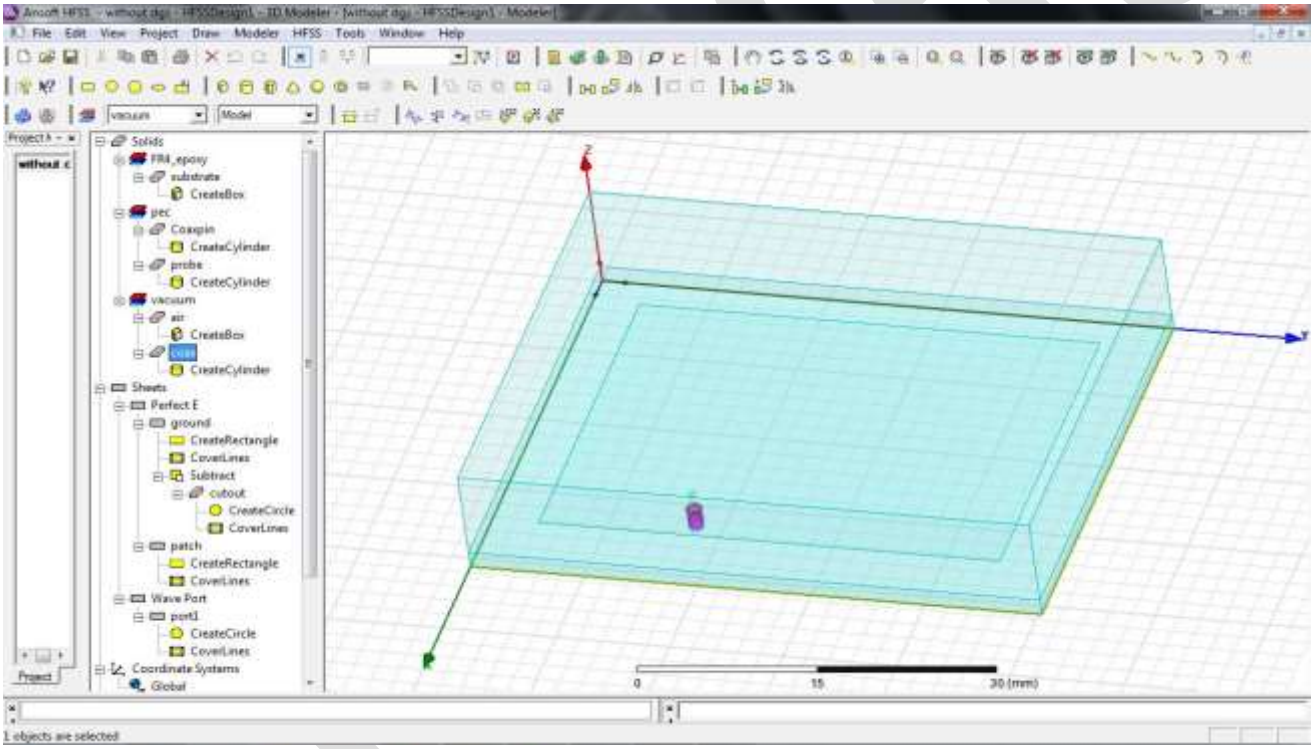

FIGURE 3(A) MSA without DGS on HFSS 13.0 operating at 2.25 ghz

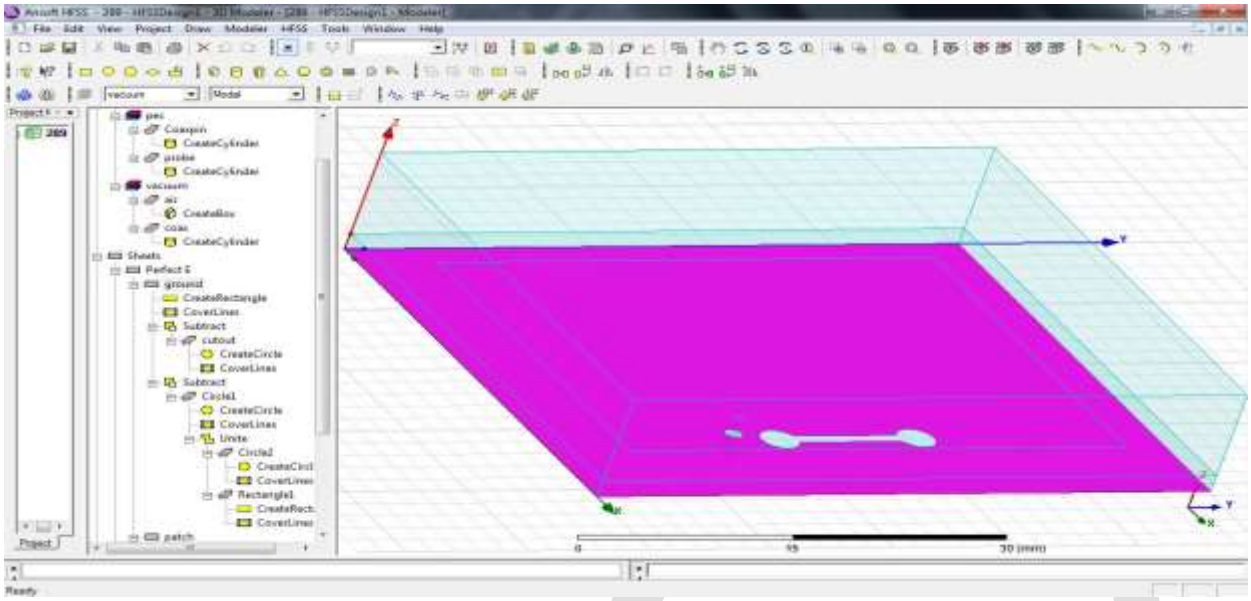

FIGURE 3(b) Proposed design on HFSS 13.0 of MSA with dumb shell oval head shape DGS

2. SIMULATIONS AND RESULTS

The results of both above described antennas generated through the aid of HFSS 13.0 and parameters like S11, directivity, impedance & voltage standing wave ratio are simulated below:

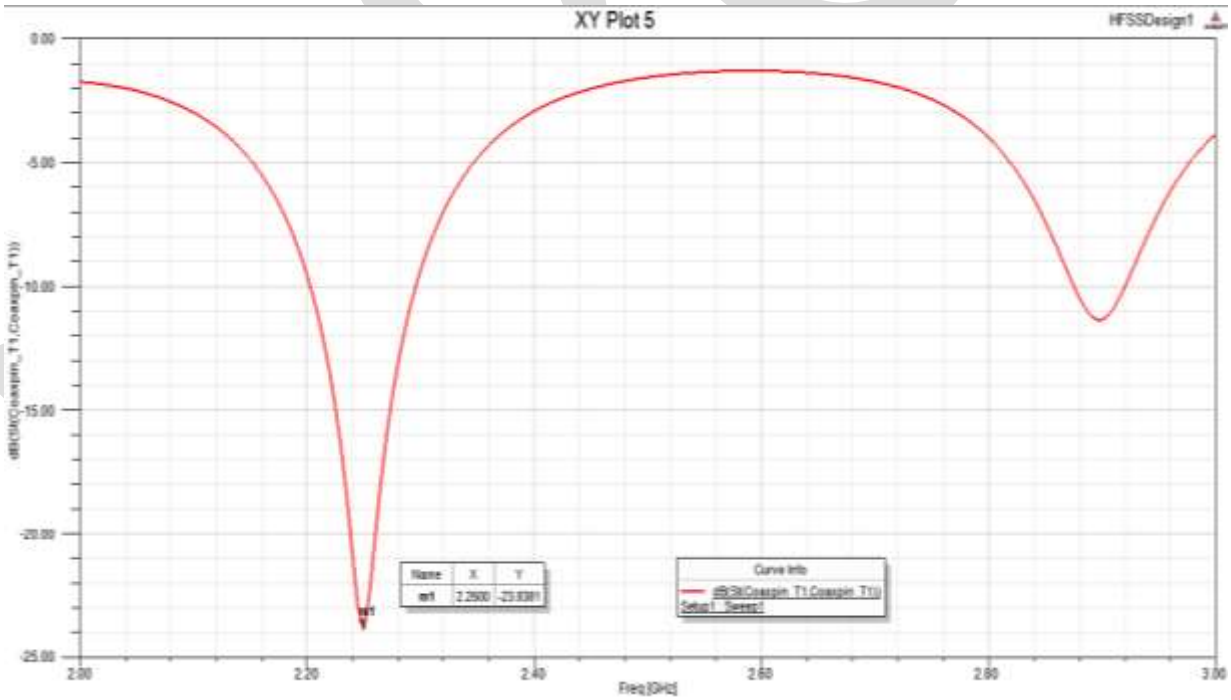

Figure 4 Simulated S11 on HFSS 13.0 of MSA without DGS operating at 2.25 GHz

The return loss S11 resulted by design without DGS is -23.8 which very close to -24 which is brilliant result while operating upon 2.25 GHz that is appropriate for Wireless Local Area Network and results the bandwidth of nearly 90 MHz. The WAN standards are - 2.2 - 2.483 GHz for IEEE 802.11 b/g and to calculate the bandwidth, the lower frequency is subtracted at -10 dB from upper bandwidth. Proposed design with DGS provides impedance of 44.8 ohms representing that antenna is approximately matched and the loss of power is very minimum. Here is represented the result of designed antenna:

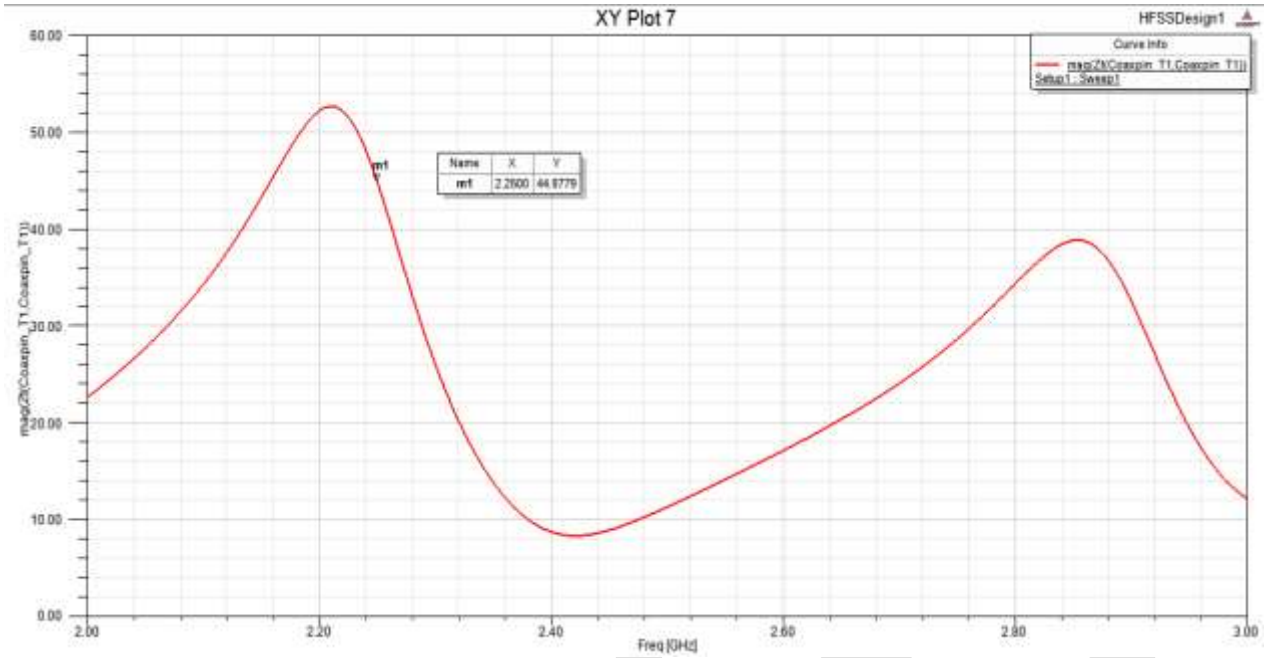

FIGURE 5 Simulated impedance on HFSS 13.0 of MSA without DGS operating at 2.25 GHz

The proposed design without DGS results out VSWR of 1.1374 in operating upon 2.25 GHz

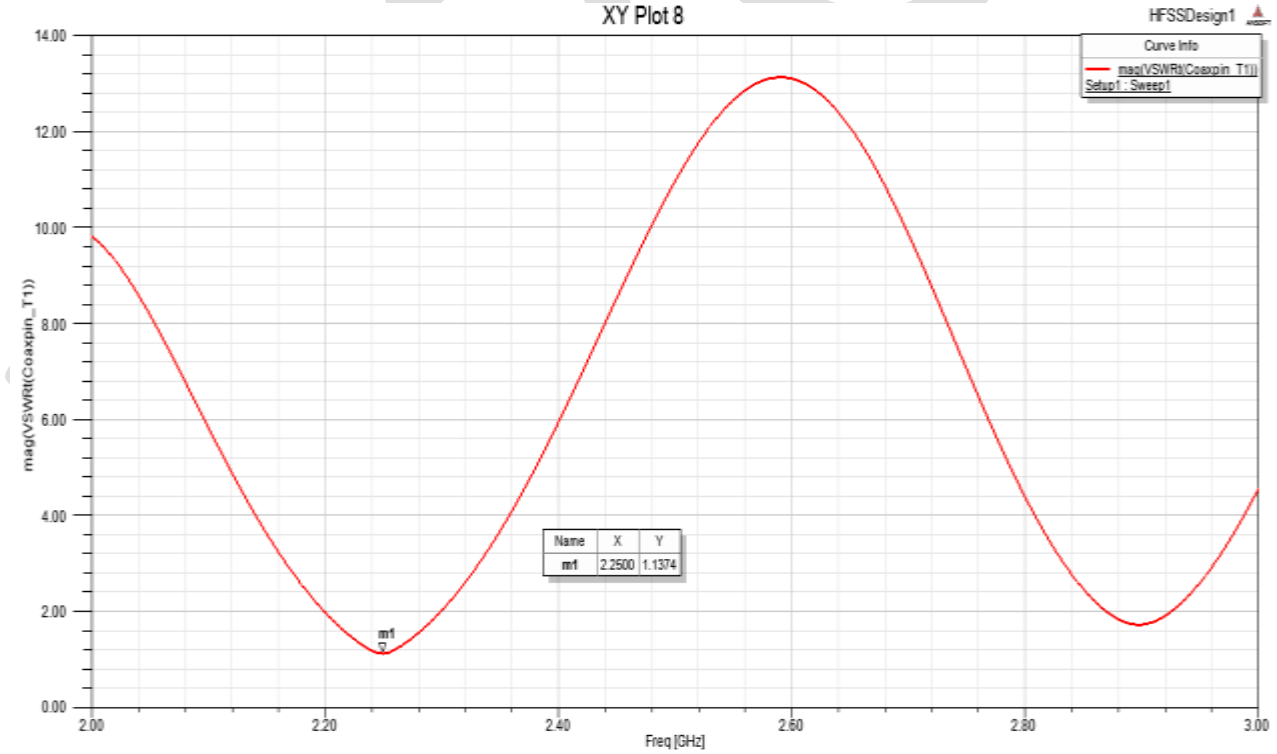

FIGURE 6 Result of VSWR of MSA without DGS at 2.25 GHz on HFSS 13.0

The summarization of results generated above by HFSS 13.0 in the form of table 3 as below:

Parameters	**Values**
Operating frequency	2.25Ghz
Return loss	-23.8381
Impedance	44.8779
VSWR	1.1374
Bandwidth	90

Table 3 Summary of results of designed antenna without DGS at 2.25 GHz frequency on HFSS 13.0.

2.1 SIMULATION RESULT FOR DUMB SHELL OVAL HEAD SHAPE

The design dumb shell oval head defective ground structured co-axial feed micro strip rectangular patch antenna results out the S11 return loss of -29.5415 dB shown below which is far better than previous design.

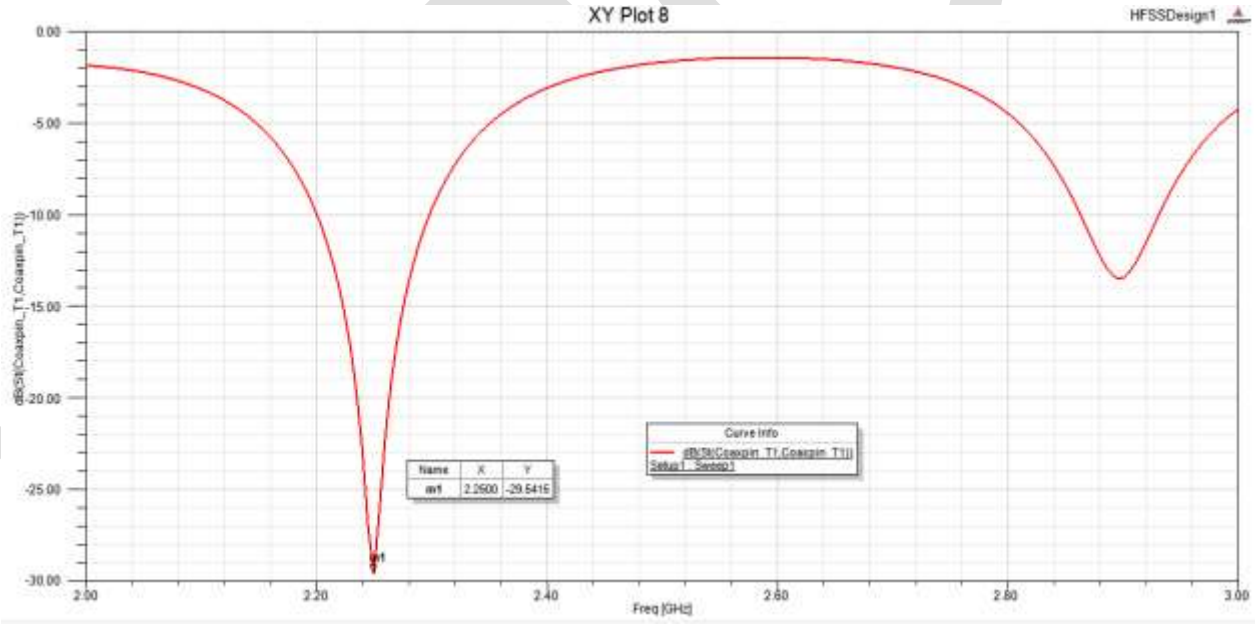

Figure 7 Simulated S11 of MSA with DGS operating upon 2.25 GHz on HFSS 13.0.

The design dumb shell oval head defective ground structured co-axial feed micro strip rectangular patch antenna results out an impedance of 47.1626 ohms which is satisfactory. The result is displayed below.

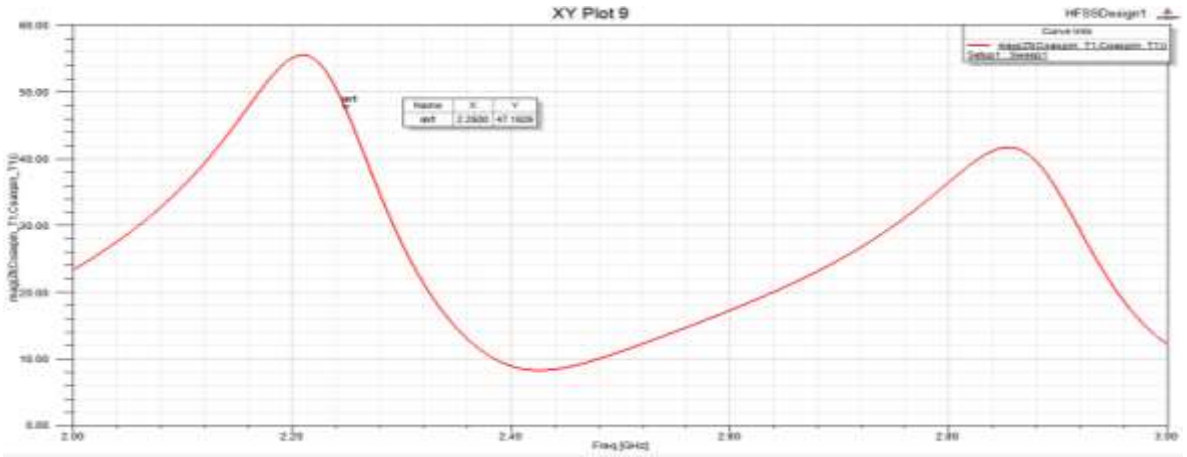

Figure 8 Simulated impedance of MSA with DGS operating at 2.25 GHz on HFSS 13.0

The DGS MSA results out VSWR of 1.0690 operating upon 2.25GHz which is nearly expected and result is displayed below:

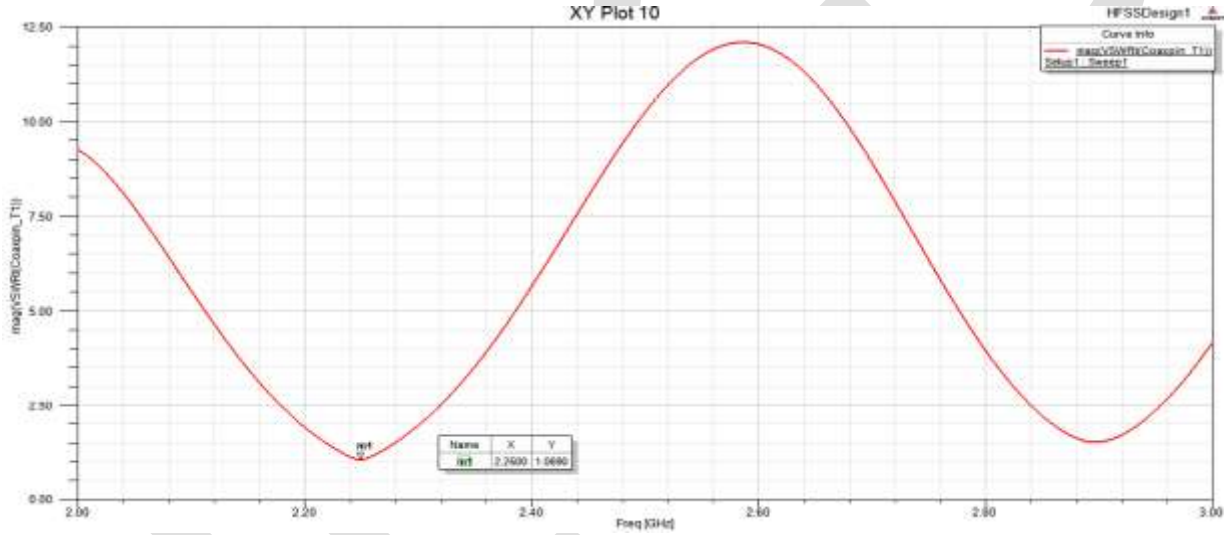

Figure 9 Simulated VSWR of DGS MSA operating at 2.25 GHz on HFSS 13.0

The summarization of results generated above by HFSS 13.0 in the form of table 4 as below:

Parameters	**Values**
Operating frequency	2.25Ghz
Return loss	-29.5415
Impedance	47.1626
VSWR	1.0690
Bandwidth	90

Table 4 Summary of results of Designed Antenna with DGS at 2.25 GHz frequency.

3. CONCLUSION

This paper represents the designs of two antennas of co-axial feed micro strip rectangular patch antenna , with and without dumb shell oval head DGS technique , operating in between frequency spectrum of 2GHz−2.5 GHz. it is also simulationly proven that the design results out a bandwidth of nearly 4% which will always provide stable radiation pattern in between the allotted frequency range. In the center frequency the proposed design exhibit excellent impedance match of nearly 50 ohms. as proved above the enhancement of parameter by employing the dumb shell oval head DGS technique and further the comparison of both with and without DGS technique is displayed below. Which at last proves that dumb shell oval head DGS enhances an overall efficiency of co-axial feed micro strip rectangular patch antenna.

Parameters	**Without DGS MSA Values**	**With DGS MSA Values**
Operating frequency	2.25Ghz	2.25Ghz
Return loss	-23.8381	-29.5415
Impedance	44.8779	47.1626
VSWR	1.1374	1.0690
Bandwidth	90	90

Table 5 Comparison of results of with and without DGS technique in MSA operating upon 2.25 GHz

As it is clear that for numerous applications this design is acceptable as proved that S11 , VSWR are minimum in dumb shell oval head shape of DGS antenna and is also proven that there is enhanced line impedance when it is brought in comparison with other simple antenna (without DGS). This all will practically results into an excellent communication.

REFERENCES:

[1] Balanis, C.A., "Antenna Theory Analysis and Design", 3rd Edition. New Jersey, John Wiley and Sons, 2005.
[2] Theodore S. Rappaport, "Wireless Communication and Practice", Second Edition, 2002.
[3] Lee, H. F., and W. Chen, "Advances in Microstrip and Printed Antennas", New York, John Wiley & Sons, 1997
[4] SunilKumar Vats1, and Hitanshu Saluja, International Journal of Engineering Research and General Science Volume 2, Issue 4, June-July, 2014 ISSN 2091-2730
[5] J. P. Geng, J. J. Li, R. H. Jin, S. Ye, X. L. Liang and M. Z. Li, "The Development of Curved Microstrip Antenna with Defected Ground Structure" Progress In Electromagnetic Research,PIER, vol. 98, pp 53-73, 2009.
[6] JaswinderKaur and Rajesh Khanna, "Co-axial Fed Rectangular Microstrip Patch Antenna for 5.2 GHz WLAN Application", Universal Journal of Electrical and Electronic Engineering 1(3):94-98, 2013.
[7] Alak majumder , "rectangular microstrip patch antenna using coaxial probe feeding technique to operate in s-band" international journal of engineering trends and technology (ijett) - volume4issue4- april 2013
[8] phani kumar tvb, abhinay kumar reddy s, aditya k,nagaraju a , "co-axial fed microstrip rectangular patch antenna design for bluetooth application" international journal of research in engineering and technology , eissn: 2319-1163 | pissn: 2321-7308
[9] MANDAL, A. DEPT. OF ECE, GURU NANAK INST. OF TECHNOL., KOLKATA, INDIA GHOSAL, A. ; MAJUMDAR, A. ; GHOSH, A. ; DAS, A. ; DAS, S.K. "ANALYSIS OF FEEDING TECHNIQUES OF RECTANGULAR MICROSTRIP ANTENNA " PUBLISHED IN: SIGNAL PROCESSING, COMMUNICATION AND COMPUTING (ICSPCC), 2012 IEEE INTERNATIONAL CONFERENCE ON 978-1-4673-2192-1
[10] BASILIO, LORENA I. ; COLL. OF BUS. ADM., HOUSTON UNIV., TX, USA ; KHAYAT, M.A. ; WILLIAMS, J.T. ; LONG, S.A. "THE DEPENDENCE OF THE INPUT IMPEDANCE ON FEED POSITION OF PROBE AND MICROSTRIP LINE-FED PATCH ANTENNAS" ANTENNAS AND PROPAGATION, IEEE TRANSACTIONS ON (VOLUME:49 , ISSUE: 1).
[11] Garima Sanyal1, Kirti Vyas2 , PW fed Circular Microstrip Patch Antenna with Defected Ground Structure , Volume 2, No.4, July – August 2013 , International Journal of Microwaves Applications.
[12] HFSS 13.0v pdf , "http://www0.egr.uh.edu/courses/ece/ECE6351-5317/SectionJackson/5113/HFSS%20waveguide%20combiner.pdf"

International Journal of Engineering Research and General Science Volume 3, Issue 3, Part-2 , May-June, 2015
ISSN 2091-2730

Utilizing Big Data, Cognitive Computing and Big Data Testing to deduce optimized result based decisions

Dashrath Mane[1] (Asst.Prof), Swapna Salian[2] (Student) MCA

[1] Vivekanand Education Society of Information Technology, Mumbai

dashumane@gmail.com

[2] Vivekanand Education Society of Information Technology, Mumbai

salianswap@gmail.com

Abstract— This paper enlists the possibilities of combining three different aspects and trying to get the best out of them. It derives the various advantages that these technologies have as individual entities and the probability that they can proliferate better if put together to use. We will assess how Big Data, Cognitive Computing and Big Data Testing have their own strengths in general. We will later deduce how we can possibly exploit their pros. In today's world data plays a very key role in everyday decision making. The cons of these technologies can be mitigated if they work in harmony. The results derived from such a combination would be better in accuracy, efficiency and quality.

Keywords— Big Data, Cognitive Computing, Big Data Testing, Watson, Internet of Things, Jeopardy Quiz show, Big Data Architecture

Introduction- Background and Motivation

In today's world volumes of unstructured information is growing at an enormous rate. Big Data as we call it is increasing in leaps and bounds. This data if put to proper use could help us harness the best results. If not utilized to its optimal capability, it remains just another chunk of useless data. We really need better technologies to make sense of it and make better decisions. The data that is processed needs to be accurate for it to be of any use. This is when Big Data Testing aspect comes into picture. The data that we are working on first needs to be the right data for us to even begin with. We're seeing a new era of computing starting with tabulating era, then to the programmable computer era and now cognitive computing systems which expand the boundaries of human cognate to become smarter with use and have much more natural interaction between the human and the computer. In the area of artificial intelligence there are a lot of amazing ideas but computational capabilities just weren't ready for them. Watson suddenly makes some of these crazy ideas possible.

At the Core, we're trying to leverage knowledge the way humans record and communicate it in natural human language, in particular text. It's initial introduction to the world was as a competitor on the Jeopardy Quiz Show. In healthcare space we are approaching it as a support tool to expand the physicians' cognitive boundaries by giving them deeper access to much larger volumes of information. The history associated with the patient, the journal articles, clinical results, best practices, guidelines etc. That volume of content is doubling every 5 years. Physicians have precious little time to keep up with everything. A system like Watson can leverage the computer's ability to deal with huge volumes of data, understand the knowledge that's contained within this data. Apply it to the problem that the physician is trying to solve, give them different alternatives to consider and in particular the underlying evidence that supports those alternatives. That basic problem solving pattern applies to a wide variety of industries. Any area where you have complex problems that you are trying to solve, where adapting the computer technology to work better with the way humans want to work so that its more natural relationship between the human and the computer.

IBM's CEO and CHAIRMAN Ginni Rometty has called the coming times a new era in Computing, a new era in cognitive computing, a new era in cognitive systems. The phrase new era signifies not an incremental or a tactical shift, it signifies a fundamental, strategic and technological shift. In terms of the technology and what we do with it. Cognitive computing draws inspiration from the brain and yet respects the technological engineering constraints of the society. The amalgamation of Big Data, Cognitive Computing and Big

Data testing in turn will allow us to witness a new generation of computer and a new generation of services and solutions to make the work better.

Problem Definition

The main problem with usage of Big Data lies in the fact that there is no defined way that the data would be related to one another. Big data encompasses related, unrelated, structured and unstructured data as well. The task of bringing the hidden diamond from a coal mine with nothing but a sliver of light is huge. Since, the data that we have at hand is in it's rawest form in the beginning, the major part of the hurdle is how to bring it or process it in a form where it could be helpful to us in making decisions.

The data that we have could be from various sources. The sources could be reliable ones or unreliable ones. Irrespective of it's source the process that we use to modify the data into information should be powerful enough to differentiate between data that needs to be used and the data that doesn't make any quality input. This is something that is achieved using some form of validating and verifying. A filter of sorts which helps you segregate the required data from the whole collection of data that you have.

One of the ideas is to get computers to interact with us the way we want to interact with one another instead of us sitting down and programming a computer someplace, then this notion of computers that deal with images the way we do or being able to visualize what we do in a way which isn't a spreadsheet, it isn't a bar chart, its really visual its really the way humans interact with the world. I think that will transform how we do a lot of what we do in the business world as well as in our private lives. This isn't something that is achieved using simple processing strategies.

Understanding Big Data[1]

Big data is a broad term for data sets so large or complex that traditional data processing applications are inadequate. Challenges include analysis, capture, data curation, search, sharing, storage, transfer, visualization, and information privacy. The term often refers simply to the use of predictive analytics or other certain advanced methods to extract value from data, and seldom to a particular size of data set. Accuracy in big data may lead to more confident decision making. And better decisions can mean greater operational efficiency, cost reductions and reduced risk.

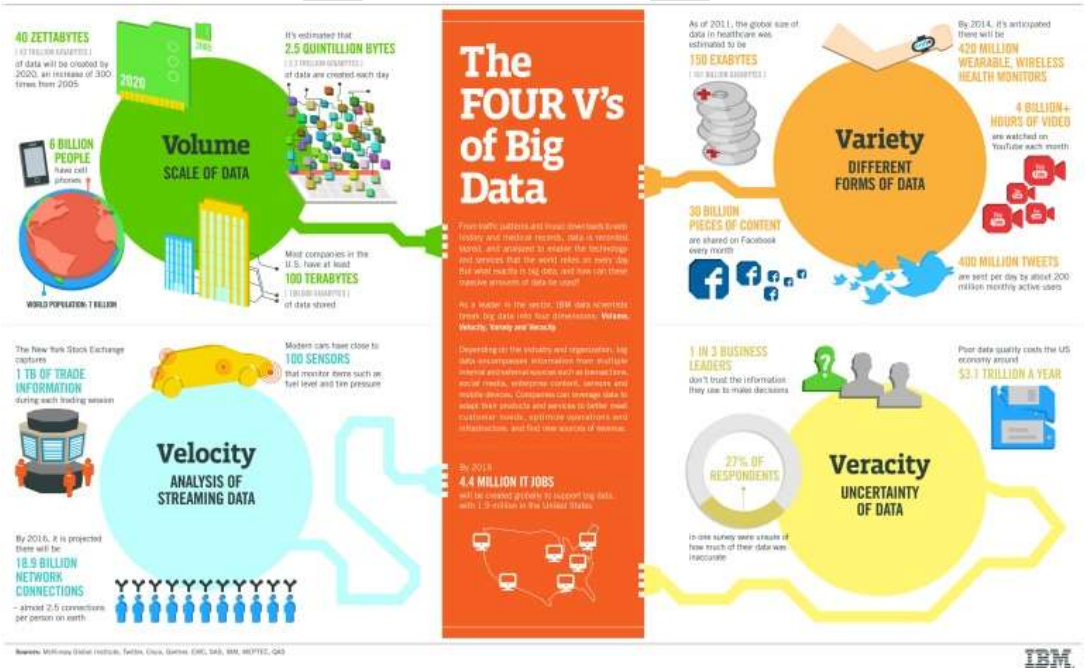

Figure 1. The four V's of Big Data[3]

Understanding Cognitive Computing

Cognitive computing is its simplest form the way we get computers to behave and think and interact the way humans do. If a computer can experience it's environment then by definition it can act upon it to improve it and that is a unique capability compared to what we have today.

I)Touch
We will be able to touch through our phone or computer systems.

How can we use technology to make us more aware. How can we use technology to make touch come to life. Within the next five years the phone will be such a ubiquitous part of our everyday experience of understanding our world that we will be able to completely understand the sensation of touch through our phone. The phone will be able to help you feel fabric. You will be able to share the texture of a basket woven by a woman in a remote village halfway across the globe. So if you think about buying a shirt online we can use different technology like vibration. The aim is to be able to manage vibration through an understood lexicon of texture. To be able to use vibration to translate linen versus silk and how heavy or rough is the texture of the vibration as you stroke your finger across your device screen. The device becomes just as intuitive as we understand touch in any other form today.

II)Sight
Computers will be able to not only look at images but understand them.

In cognitive computing, systems are basically taught to understand photos by being given examples and it basically learns the patterns that matter. So it's basically the computer that is learning to make this discrimination. It is learning what boundaries are. It is learning what matters most. It could be for a beach scene where the color is more important or where for another kind of scene like the downtown city scene perhaps it's edge information is something that is crucial.
Pictures and videos have a lot of use in safety and security application. So when an event may occur it may be a severe storm where people can acquire photos today and share those in real time and then this can be useful for raising alerts. It can also help in guiding emergency personnel. It can be very useful for sharing experiences that others can benefit from. In the future the computer will be enormously powerful in the fields like medicine. We can consider one case of dermatology and skin cancer where often it's too late when a patient may show up and already there might be a melanoma. A computer then can start to look for patterns and situations where sometimes there is something that may have a pre-cancerous and a good indicator that something is likely to happen. Computers are great tool and cognitive computing they will understand contents in a way that will go beyond human capacity.

III)Hearing
Computers will hear what matters.

During the period of having a first born child in the house the parents often get frustrated as they often don't understand what the baby wants or what is the reason behind the baby's cries. In five years we expect such an application which in situation when a baby starts to talk to us, the system will be able to understand and interpret to the parents what the baby wants. It would be able to let the parents or the doctors what the baby wants to convey. Cognitive computing when we talk about applications means that it tries to imitate how our brain works. It creates a much better system that has much better results. As an example the big problem during mud slides and flooding situations can have a solution wherein sensors are located in nearby regions to hear the sound and alert the emergency squad in case if any tremors of mountains is heard. This is an example of how hearing sensors can prevent catastrophes too.

IV)Taste
Computer systems will know what a person likes to eat better than him.

The way humans taste things, the way they perceive flavors is very chemical in nature. When we have something on our tongue and we notice and we understand the flavor by how their chemicals react with our neuro system. In the future the computer will be able to access large depositories of data that tell us about the chemical components and structure of various ingredients. It will be able to tell us about what humans really perceive in terms of flavors and then be creative and be able to put together different recipes. So what is to be done is figuring out what is good for humans and develop machines that can actually help us achieve that. So what we would be looking at is having a future where the new designed recipes that taste good to humans so people will be willing to eat it and is at the same time is healthy for them too. If we go to a school we see that children miss their nutritional needs when they start nit picking from their given lunchboxes. The aim in such a situation is to make recipes that are flavorful and at the same time are meeting the nutritional benefits required for their health and growth. In the future you might have a web application that does not only

consider your personalized medical characteristics but also your personalized tastes. To take an example of a diabetic who isn't allowed to eat much sugar can be in the future be able to eat recipe modeled in a way that satisfies his sweet tooth.

V)Smell
Computers will have a sense of smell.

If you smell a good wine it is a very interesting scientific question to actually understand what it is that you smell with your nose. A cognitive computing system will try to do similar things as your brain. It will try to combine the information of the smell with all the other information. In future it is considered that doctors will be able to diagnose a whole set of diseases based on your smell. An area which will be emerging will be in house care wherein smelling diseases remotely and then communicating to the doctor will be one of the techniques which will promise to reduce cost in the house care sector. For example your phone would know where you are, it could smell things around you, may be your breath and in turn your phone might know you have a cold before you do.

Understanding Big Data Testing[2]

Harvesting relevant information from big data is an imperative for enterprises seeking to optimize strategic business decision-making. Opportunities that were traditionally unavailable are now a reality, with new and more revealing insights extracted from sources such as social media and devices that constitute the Internet of Things. Consequently, emerging technologies are enabling organizations to gain valuable business insights from data that is growing exponentially in volume, velocity, variation of data formats and complexity. Leading industry analysts forecast the big data market to reach U.S.$25 billion by 2015. As a consequence, organizations will require newer data integration platforms, fueling demand for QA processes that service new platforms, leading to the necessity of big data testing.

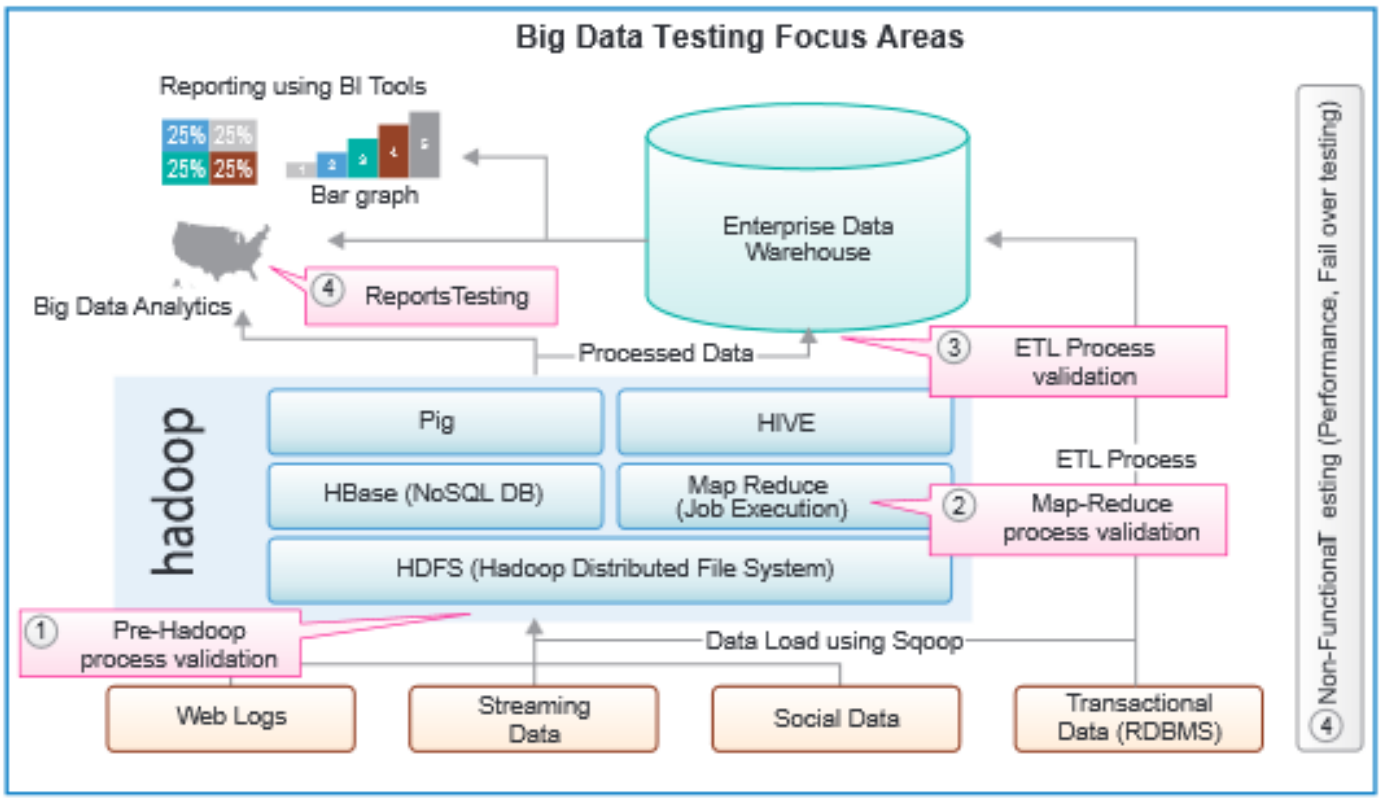

Figure 2. Big Data Architecture with Testing phases[4]

Proposed System

The proposed system basically instigates the usage of Big Data, Cognitive Computing and Big Data Testing so as to get the results in a better manner.

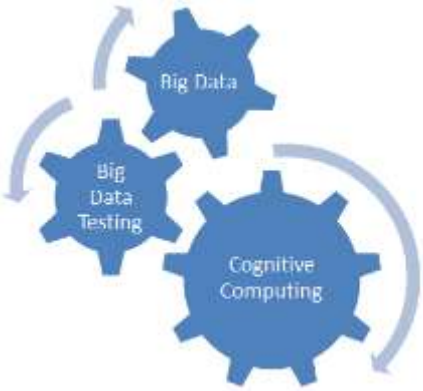

Figure 3. Correlation of Big Data, Big Data testing and Cognitive Computing

The companies that deal with consumers need to come up with better strategies than they make today if they intend on retaining their consumer base. The fickle nature of a consumer can't be stopped. Thus, companies need to understand their consumers better.

The role of Cognitive Computing is to help systems think in a similar fashion as humans. Big data allows us to bring together all such information that are rallied through from the consumers. Similarly, to call that data legit, there needs to be some procedure followed to ensure the integrity of the data. This can be done using Big Data Testing.

When you look at what human brain can do, it's really amazing the way we can reason about things and think very deeply about things. But where we start to run into a wall is when we are faced with leveraging huge volumes of data, so looking through tones of documents, millions of books for instance is almost impossible for the human brain but in order to push the boundaries of human cognition we want to provide access to all that data so I think one of the 1st challenge or task of these cognitive systems along with Big Data and Big Data Testing is to facilitate or enable human cognition beyond these barriers and it's exactly what this proposed system is all about. In fact it's about providing efficient access to huge volumes of literature, unstructured information and text, digesting it, evaluating it and providing efficient access for the humans to that information to help that human cognitive process.

With all due respect to current technology the computers today are just large calculators. They calculate very fast lots and lots of data but they really don't think.

In today's world we always provide imperfect answers because we don't have all the information. What this proposed systems allows us to do is to be able to collect that information from what is seen, from what is heard, from what is felt, from what is tasted an so on to provide a more accurate answer to the problem at hand.

ACKNOWLEDGMENT

I would like to thank my supervisor Mr. Dashrath Mane for his continuous support in my project and his willingness to bring his breadth of experience to this project. I would like to thank my lecturers and colleagues in VESIT, MCA program for the great learning experiences and interaction we shared which helped me in my project to a great extent.

CONCLUSION

The essence of this proposed system is to think of the difference between the way that most computers work now and the way that most sophisticated computers on the planet work and those computers are the things that we all carry around in our heads along with you know mammals and all the other little animals that run around and do these amazing feats. In real time taking in their

environment, understanding, making decisions very fluidly and responding and how often have you looked at a computer while its little hourglass is spinning and it does the wrong thing. So we bring about the ability to bring a level of fluidity and appropriation to the way that we interact with computing. We put out effort into making computers actually more like biological systems, whether or not they've brains. Where they actually have that fluidity where they respond and react appropriately. So you feel like you're dealing with another living thing and not a machine.

Thus, they would act as much more that systems that are just another calculator like machine. It would actually help us come up with decisions that make a difference. Implementing all these 3 discussed facets of technology would not just strengthen the kind of information brought at the end of a Big Data Analysis process but would also one day go many steps ahead by coming up with corporate decisions that can be drawn using it.

REFERENCES:

[1] "Big Data," https://en.wikipedia.org/wiki/Big_data , para. 1, June. 9, 2015. [Online]. [Accessed: Feb. 11, 2015].
[2] Sushmitha Geddam "Building a Robust Big Data QA Ecosystem to Mitigate Data Integrity Challenges", October 2014, Cognizant 20-20 insights.
[3] "The four V's of Big Data," http://www.ibmbigdatahub.com/sites/default/files/infographic_file/4-Vs-of-big-data.jpg [Online]. [Accessed: Feb. 11, 2015].
[4] "Big Data Testing Focus areas", http://4.bp.blogspot.com/-iWRDYGUjLXY/UqeRExSygtI/AAAAAAAACuc/Fk04CxxIwgc/s1600/hadoop-qa.png, [Accessed: Mar. 12, 2015].
[5] Perspectives on Cognitive Computing and Applications", October-December 2010, http://www.ucalgary.ca/icic/files/icic/17-IJSSCI-2403-CoP.pdf
[6] By Dharmendra S. Modha, Rajagopal Ananthanarayanan, Steven K. Esser, Anthony Ndirango, Anthony J. Sherbondy, Raghavendra Singh, "Cognitive Computing", http://cacm.acm.org/magazines/2011/8/114944-cognitive-computing/fulltext
[7] Alex Knapp, "How IBM's Cognitive Computer Works", http://www.forbes.com/sites/alexknapp/2011/08/26/how-ibms-cognitive-computer-works/
[8] Steve K. Esser, Alexander Andreopoulos, Rathinakumar Appuswamy, Pallab Datta, Davis Barch, Arnon Amir, John Arthur, Andrew Cassidy, Myron Flickner, Paul Merolla, Shyamal Chandra§, Nicola Basilico†, Stefano Carpin,†, Tom Zimmerman, Frank Zee§, Rodrigo Alvarez-Icaza, Jeffrey A. Kusnitz, Theodore M. Wong, William P. Risk, Emmett McQuinn, Tapan K. Nayak‡, Raghavendra Singh‡, and Dharmendra S. Modha IBM Research - Almaden, San Jose, CA 95120 ‡IBM Research - India †UC Merced, Merced, CA 95343, "Cognitive Computing Systems: Algorithms and Applications for Networks of Neurosynaptic Cores"
[9] Arnon Amir, Pallab Datta, William P. Risk, Andrew S. Cassidy, Jeffrey A. Kusnitz, Steve K. Esser, Alexander Andreopoulos, Theodore M. Wong, Myron Flickner, Rodrigo Alvarez-Icaza, Emmett McQuinn, Ben Shaw, Norm Pass, and Dharmendra S. Modha IBM Research - Almaden, San Jose, CA 95120, "Cognitive Computing Programming Paradigm: A Corelet Language for Composing Networks of Neurosynaptic Cores"
[10] Jean-Pierre Dijcks, "Oracle: Big Data for the Enterprise", June 2013, Oracle Corporation World Headquarters 500 Oracle Parkway Redwood Shores, CA 94065 U.S.A
[11] Bill, Hamilton, "Big Data is the Future of Healthcare", September 2014, Cognizant 20-20 insights.
[12] Sushmitha Geddam, "Strengthening the Quality of Big Data Implementations", February 2015, Cognizant 20-20 insights

International Journal of Engineering Research and General Science Volume 3, Issue 3, Part-2 , May-June, 2015
ISSN 2091-2730

Implementation of offline signature verification based on LBP and LDP techniques on Beagle Board XM

Dibin C Mathew1 , Prof. Nagachandra2

1. P.G.Scholar ECE Dept. Dayananda Sagar College of Engineering Bangaluru, INDIA dibincmathew@yahoo.com

2. Professor ECE dept. Dayananda Sagar College of Engineering Bangaluru, INDIA

Abstract-The main objective is to design and implement offline signature verification based on LBP and LDP technique on BegalBoard-XP hardware using OpenCV software. This will help you to know the efficiency of the algorithm on a processor. To design efficient algorithm for offline signature verification. To improve performance parameters like FAR, FRR, TSR. Implementation of the algorithm using Begalboard.In off–line signature recognition we are having the signature template coming from an imaging device, hence we have only static characteristic of the signatures. The person need not be present at the time of verification. Hence off-line signature verification is convenient in various situations like document verification, banking transactions etc.

Keywords-LBP,LDP,FAR,FRR,TSR.

I.INTRODUCTION

Recoginizing a person using Biometrics is more secure and reliable means for person identification.Since biometrics are the characteristic feature of every human being it will be impossible or an uphill task for miscreant person for hacking the biometric system.Since biometric traits are natural and god given they will be the permanent source of identification for every human being in the world.Recognition through biometrics is a way of determining identity of every person considering his natural characteristics of a person.Hence biometric serves as a very useful tool in present day world for our day to day activities. Identifying every human being through their personal characteristics and attributes uniquely is very important for smooth function of the society.The set of characteristics associated with the person helps individually in his unique identification in this vast society.People used to generally used to identify the person by physically seeing each other or through the help of listening his/her voice through the communication system such as mobile/telephone. A biometric framework determines one or more physical or behavioral qualities,including fingerprint, print of palm, image of face, retina,odour to confirm his/her identity. These qualities can be called by distinctive terms, for example, characteristics, pointers, identifiers, or modalities.The different traits considered in a biometric system considered with respect to a person were shown in the figure 1.

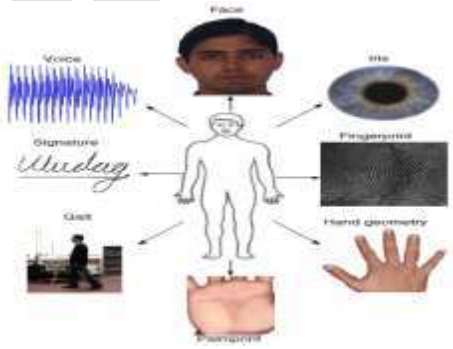

Figure 1:- Different Biometrical traits considered for Person recognition

handwritten signature checking has been widely mulled over & actualized. Its numerous applications incorporate charge card approval, managing an account security frameworks and so on , handwritten signature confirmation can be classified into two sorts.

1. Online verification.

2. Off–line verification.

Online check needs a stylus and an electronic tablet joined with a PC to snatch dynamic mark data. In On–line approach we can gain more data about the signature which incorporates the dynamic properties of signatures. We can remove data about the pace of pen, weight , quickening and strokes and also the static qualities of signatures.This is all that much precise in light of the fact that the dynamic components are extremely hard to copy, yet the framework requires co-operation of client and complex equipment framework. Digitizer tablets or weight delicate pads are utilized to sweep signature alterably. Off–line check, manages signature data which is in a static format.In off–line signature acknowledgment we are having the signature layout originating from an gadget which catches the picture, subsequently we get just static normal characteristics of the signature.At the time of check, the individual ought to be on location. Henceforth offline signature verification is helpful in different circumstances like archive confirmation, saving bank exchanges and so on. As we have a constrained arrangement of components for check reason, offlinesignature acknowledgment frameworks should be composed precisely to accomplish the wanted precision.

II. RELATED WORKS

Earlier they used Robust Off-line Signature Verification taking into account Global Features for irregular and talented manufactured marks. The model concentrates the components which are preprocessed by standardization, diminishing and binirisation.The highlight extraction system incorporates global features, for example, most extreme flat histogram, viewpoint proportion, greatest vertical histogram, level and vertical focus of mark and signature zone.But larger efficiency could not be achieved by this method,so in order to overcome this an alternative method is proposed.that is offline signature confirmation plan taking into account 60 component points acquired from the signaturess geometric focus and contrasts them and the effectively prepared companent points. Highlight focuses are characterized in view of measurable parameters like fluctuation and mean. The above plan separate between two sorts of forged and original signatures. The technique deals with talented and irregular frauds. The point of this work is to decrease the two fundamental parameters called False Acceptance Rate (FAR) and False Rejection Rate (FRR) ordinarily utilized as a part of any signature check plan. At last similar examination has been made with standard existing plans.

III. PROPOSED METHODOLOGY

In this, the signature identification is used to recognize a person. The signature samples are preprocessed and features are extracted using Local Binary Pattern and Local Directional Pattern techniques. The block diagram of proposed model is given in Figure 2 Here both LBP and LDP features are compared and both should match the original signature. The GPDS300 signature database is considered. Signatures are extracted from users on a white sheet at various periods depending upon his intrest level and pressure levels and are scanned to get pictures of 96 dpi resolution in png format to build a database. Test Signature Preprocessing LBP/LDP features Feature Vector Signature Database Preprocessing LBP/LDP features Feature Vector Euclidean Distance Match/Mismatch

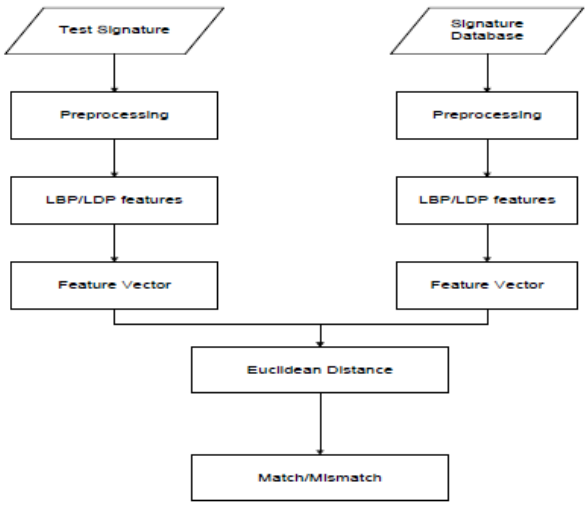

Figure 2:-Block diagram of the proposed Model for LBP/LDP

3.3.1LOCAL BINARY PATTERN: The Local Binary Pattern (LBP) highlight is characterized as measure of grey level composition in a nearby neighborhood. The essential characterstic of the LBP administrator is its invulnerability against varieties in monotonic grey level . Additionally similarly essential is its effortlessness included in processing. LBP administrator fundamentally portrays the neighbourhood of a pixel. Each ILBP(x, y) code is carried out as given: the eight encompassing pixels are binarized considering as threshold the middle grey level worth I(x, y), creating a binary 1 if the neighbor is more higher than or equivalent to the threshold ; else it delivers a binary 0. The eight binary number are indicated by 8-bit number which are stored in ILBP(x, y), it ought to be in the scope of 0 to 255

$$I_{LBP}(x,y) = \sum_{n=0}^{7} s(I_N(n) - I(x,y)) \cdot 2^n,$$

where $s(l) = \begin{cases} 1 & l \geq 0 \\ 0 & l < 0 \end{cases}$ the unit step function

Eg of LBP operator

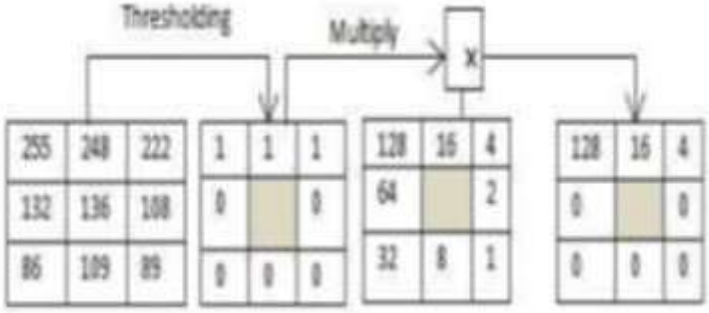

In this case I (x,y) =136.IN(n) = {89,108,222,109,248,86,135,255 }, IN(n) > I(x,y) =1 or else 0.so we get the set as {0,0,1,0,1,0,0,1}, so ILBP(x,y)=4+16+128=148. LBP could also be further used to rotation invariant operator and generalized gray level operator. The main drawback of LBP is it gets easily affected by noise and dependency on pen. Everyone must write using the same pen since LBP is more capable to acquire the distribution of personal ink when all signers use the same pen. But when the personal ink distribution involves variations of pen, in such a cases the efficient algorithm could be LDP.

3.3.2 LOCAL DIRECTIONAL PATTERN: This feature converts the input image I(x, y) to ILDP(x, y), $2 \leq y \leq M-1$, $2 \leq x \leq N-1$, Where the edge response is represented by ILBP(x,y) . accordingly determines edge response values in 8 different directions for I (x, y) using masks which is referred as Kirch in all possible eight angular directions.

KIRCH COMPASS MASKS

Here we characterize the mask by taking a solitary mask and pivoting it to eight conceivable compass directions: North, West, South, East, northwest, northeast,southeast,southwest .The masks are characterized as : The edge reaction is the most extreme value found by convolution of every mask with the picture. The heading is given by mask that creates the crest size.

$$M_0=\begin{bmatrix}-3 & -3 & -3\\ -3 & 0 & 5\\ -3 & 5 & 5\end{bmatrix} \quad M_1=\begin{bmatrix}-3 & -3 & -3\\ 5 & 0 & -3\\ 5 & 5 & -3\end{bmatrix} \quad M_2=\begin{bmatrix}-3 & -3 & -3\\ -3 & 0 & -3\\ 5 & 5 & 5\end{bmatrix} \quad M_3=\begin{bmatrix}5 & -3 & -3\\ 5 & 0 & -3\\ 5 & -3 & -3\end{bmatrix}$$

$$M_4=\begin{bmatrix}5 & 5 & -3\\ 5 & 0 & -3\\ -3 & -3 & -3\end{bmatrix} \quad M_5=\begin{bmatrix}5 & 5 & 5\\ -3 & 0 & -3\\ -3 & -3 & -3\end{bmatrix} \quad M_6=\begin{bmatrix}-3 & 5 & 5\\ -3 & 0 & 5\\ -3 & -3 & -3\end{bmatrix} \quad M_7=\begin{bmatrix}-3 & -3 & 5\\ -3 & 0 & 5\\ -3 & -3 & 5\end{bmatrix}$$

$$m_l = \sum_{i=0}^{2}\sum_{j=0}^{2} I(x-1+i, y-1+j)\cdot M_l(i,j).$$

$$0 \le l \le 7$$

peak output values in each particular orientation is determined by The existence of edges and corners and their directions. ILDP(x, y) gives the k most required orientations. As a result, the top k magnitude values |m| are assigned to 1 and the rest of values are reset to 0. The obtained binary value is indicated by an 8-bit code word. In the given example k=3, so the LDP feature is obtained as shown below:

$$I_{LDP}(x,y) = \sum_{l=0}^{7} s\left(|m_l| - m_{l,3}\right)\cdot 2^n$$

E.g. I(x, y) = 136,m0 = M0(0, 0) I(x-1,y-1).+ M0(1, 0) I(x, y-1).+ xM0(2, 0) I(x, y-1).+ M0(0, 1) I(x- 1,y).+ M0(1, 1) I(x, y).+ M0(2, 1) I(x+1, y).+ M0(0, 2) I(x-1,y+1).+ M0(1, 2) I(x,y+1).+ M0(2, 2) I(x+1,y+1). here m is the third largest value of the sequence.{|m0|, |m1|, |m2|, …, |m7| when the values are equal, which means there are several values same as ml,3, the most significant bit is set to 1.

Kirch Mask	M_7	M_6	M_5	M_4	M_3	M_2	M_1	M_0
m_l value	-385	877	2053	1333	37	-1131	-1465	-1283
Rank	7	6	1	3	8	5	2	4
Code bit	0	0	1	1	0	0	1	0
LDP code	50							

calculation of the LDP code $I_{LDP}(x, y)$: I(x, y) =136.

$\{|m_l|, 0<=k<=7 = \{1283, 1465, 1131, 37, 1333, 2053, 877, 385\}$

$m_{l,3}=1333, |m_l| > m_{l,3} = \{0, 0, 1, 1, 0, 0, 1, 0\}$

So $I_{LDP}(x, y)$ = 2+16+32 = 50

3.3.3 COMBINATION OF LBP AND LDP LBP features of pattern are obtained and given as input to Local Directional Pattern proposed in 3.3.4 and features are extracted, using these extracted features Euclidean Distance is calculated for match/mismatch of signature. Combination of LBP and LDP takes the advantage of both intensity information and directional edge response. IV RESULTS The performance parameters like FAR, FRR, EER, TSR are calculated using the Euclidean distances between the final feature coefficients of the test and database signatures. The database is created by considering 10 persons from GPDS 300 with five genuine signatures per person, i.e., fifty signatures are available in the database. In the test section genuine signatures are considered to compute FRR and TSR. The forged signatures are considered in the test section to compute FAR. The values of FAR, FRR and TSR for ten persons are tabulated in table. As threshold value increases FAR and TSR increases, whereas FRR decreases. Threshold FRR FAR TSR 0.520000 1.000000 0.000000 0.000000 0.530000 0.800000 0.000000 20.000000 0.690000 0.700000 0.200000 30.000000 0.710000 0.400000 0.200000 50.000000 0.810000 0.200000 0.600000 60.000000 0.830000 0.000000 0.600000 60.000000

Threshold	FRR	FAR	TSR
0.520000	1.000000	0.000000	0.000000
0.530000	0.800000	0.000000	20.000000
0.690000	0.700000	0.200000	30.000000
0.710000	0.400000	0.200000	50.000000
0.810000	0.200000	0.600000	60.000000
0.830000	0.000000	0.600000	60.000000

Table 1:- FAR, FRR, TSR for different thresholds calculated for 10 persons using LBP technique.

Threshold	FRR	FAR	TSR
0.440000	1.000000	0.000000	0.000000
0.460000	0.800000	0.000000	20.000000
0.600000	0.700000	0.000000	30.000000
0.640000	0.600000	0.200000	40.000000
0.660000	0.400000	0.200000	50.00000
0.700000	0.300000	0.300000	60.000000
0.720000	0.200000	0.400000	70.000000
0.770000	0.100000	0.400000	80.000000
0.810000	0.000000	0.900000	80.000000

Table 2:- FAR, FRR, TSR for different thresholds calculated for 10 persons using LDP technique.

Threshold	FRR	FAR	TSR
0.420000	1.000000	0.000000	0.000000
0.430000	0.900000	0.000000	10.000000
0.460000	0.800000	0.000000	20.000000
0.540000	0.700000	0.000000	30.000000
0.640000	0.300000	0.200000	60.000000
0.680000	0.200000	0.300000	70.000000
0.730000	0.100000	0.500000	80.000000
0.790000	0.000000	1.000000	90.000000

Table 3:- FAR, FRR, TSR for different thresholds calculated for 10 persons using combination of LBP and LDP

V. CONCLUSION AND FUTURE WORK

An Off-line Signature Verification System (OSVS) has been described is developed using a feature set comprising the Local Binary Patters and Local Directional Patterns features of the image. The Local Binary Patter will differentiate the genuine and forged signatures of different persons using intensity values whereas the Local Directional Patterns features will differentiate the genuine and forged signature of the person using directional response (edge detection). And their combination is used to overcome the limitation of the both the technique to verify the signature. The results have been tabulated and have been shown that it combination of both gives better EER and TSR when compared to the LBP and LDP technique. In future the results are expected to be further improved with the use of neural networks or SVM (Support Vector Machines), PCA (Principal Component Analysis) in the place of Euclidean distance classifier.

REFERENCES:

[1] Ramachandra A.C, Rao, J.S, Raja, K.B. andVenugopla, K.R "Robust Offline Signature Verification Based On Global Features" IEEE International conference on Advanced computing ,pp. 1173 – 1178.

[2] Ms.PallaviPatil and Ms.ArchanaPatil "Offline Signature Recognition Using Global Features", International Journal of Emerging Technology and Advanced Engineering, Volume 3, Issue 1, pp. 408 – 411, January 2013.

[3] SamanehGhandali and Mohsen EbrahimiMoghaddam, "Off-line Persian Signature Identification and Verification Based on ImageRegistration and Fusion," Journal of Multimedia, Vol. 4, No. 3, pp.137-144, June 2009.

[4] Jing Wen, BinFang, Y.Y.Tang and TaiPing Zhang "Model-based signature verification with rotation invariant features", Pattern Recognition 42, Elsevier, pp.1458 – 1466 : 2009.

[5] Debasish Jena, BanshidaharMajhi, and Sanjay Kumar Jena, "Improved Off-line Signature Verification Scheme using FeaturePoint Extraction Method," Journal of Computer Science, pp. 111-116, 2008. Threshold FRR FAR TSR 0.440000 1.000000 0.000000 0.000000 0.460000 0.800000 0.000000 20.000000 0.600000 0.700000 0.000000 30.000000 0.640000 0.600000 0.200000 40.000000 0.660000 0.400000 0.200000 50.00000 0.700000 0.300000 0.300000 60.000000 0.720000 0.200000 0.400000 70.000000 0.770000 0.100000 0.400000 80.000000 0.810000 0.000000 0.900000 80.000000

[6] Vahid, Manal Khalil ,Malekian AlirezaAghaeiMahdieRezaeian and Mahmood Alian "Rapid Off-line Signature Verification Based on Signature Envelope and Adaptive Density Partitioning", First Iranian Conference onPattern Recognition and Image Analysis (PRIA), pp. 1 – 6 : 2013.

[7] Vaibhav Shah, UmangSanghavi and Udit Shah "Off-line Signature Verification UsingCurve Fitting Algorithm with Neural Networks" International Conference onAdvances in Technology and Engineering (ICATE), pp. 1 – 5 : 2013.

[8] Suhail M. Odeh and Manal Khalil "Off-line signature verification and recognition: NeuralNetwork Approach" International Symposium on Innovations in Intelligent Systems and Applications (INISTA), pp. 34 – 38 : 2011.

[9] EfstathiosHadjidemetriou, Michael D. Grossberg andShree K. Nayar "Multiresolution Histograms andTheir Use for Recognition" IEEE TRANSACTIONS ON PATTERN ANALYSIS AND MACHINE INTELLIGENCE, VOL. 26, NO. 7, pp. 831-847 : July 2004

[10] M. TaylanDas andL.CananDulger "Signature verification (SV) toolbox: Application of PSO-NN" Engineering Applications of Artificial Intelligence 22, pp.688–694 : 2009

International Journal of Engineering Research and General Science Volume 3, Issue 3, Part-2 , May-June, 2015
ISSN 2091-2730

THE APPLICATION OF VEDIC MATHEMATICS FOR HIGH SPEED MULTIPLIER IN FIR FILTER DESIGN

Kavita.H.Dharmannavar[1], Mrs.Dharmambal.[2]
[1] M.Tech, 4th Sem, Department of Electronics and Communication, NH College of Engineering.
[2]Senior Assist. Prof., Department of Electronics and Communication, NH college Engineering Marathalli,
Kavitahd.1992@gmail.com[1],dharmambal62@gmail.com[2]
Bangalore, India.

Abstract— The application of high speed multiplication plays vital role in the Digital Signal Processors. The method of implementation of High speed multiplier is of great concern. The modern multipliers process a drawback of speed in their multiplier design. The mode of multiplication operation takes more time as the the number of implicates increases. Thus designing a processor for High speed multiplication is of great concern. Finite Impulse Response filters normally called as a convolution filter includes a multiplier in it. Both FIR and IIR filters can be designed using the Vedic method. For the fast computation of signals Vedic Mathematics is used. Urdhwa Tiryagyam is one sutra among 16 sutras. It increase the speed compared to conventional method. The time comparison is done between Vedic method and conventional method in MATLAB Domain. The computation time taken by Vedic method is compared with the inbuilt function MATLAB. Later, the computation time is implemented by using Graphical User Interface (GUI).GUI is a tool in Matlab and it acts as a mode of interaction between the user and the system. The results show that the Urdhwa Tiryagbyam sutra reduces the execution time as compared to the inbuilt function of MATLAB.

Keywords— FIR, IIR, GUI, DSP, Urdhawa Tiryagyam, Vedic multiplier, Frequency sampling, FIR windows.

I.INTRODUCTION

Multipliers are basic building blocks of any processor design and normally we called as heart of DSPs. Modern multipliers speed of computation decreases as the inputs increase. There are many multipliers available today like Combinational multiplier, array multiplier, serial and parallel multiplier and many more. Thus building high speed multipliers for processor design is done using Vedic. In DSPs, Filtering is normally used and is applied to many applications like speech processing etc. Digital Signal Processing operations like convolution, Fast Fourier Transform, DFT calculation. Frequency sampling etc method is being used in many applications.

Filtering is a method which is used for removing unwanted signal frequencies by being sensitive to the wanted signal frequencies. Digital audio or video when it is transmitted through the communication channel, noisy is added to the original signal. So,at receiver side filtering is must in order to get original one. Basically, filters are Classified into 4 types depending upon the pass band and stopbands.FIR and IIR(Infinite Impulse Response Filter) are two types of filter designed in this paper. And computation time is compared (convolution and Urdhwa Tiryagbyam).Urdhwa Tiryagbyam is a method which reduces the computation time in processors. The method of computation of conventional and Vedic Urdhwa Tiryagbyam is same. In this paper, the computation time taken by both the methods are compared and implemented in GUI.

This paper is organized into VII parts. Part I spreads light over introduction, Part II explains about the ancient Vedic mathematics, III describes about FIR and IIR filter types and windows, IV shows the method of computation using Urdhwa Tiryagbyam method, V shows the Design Approach, VI proposed method, VII shows Results Analysis and VIII provides Conclusion and Future scope of the project.

II. VEDIC MATHEMATICS

Vedic mathematics is an ancient Indian mathematics discovered by ancient sages of India. It was rediscovered by Jagadguru shankaracharya Bharathi Krishna Teerthji maharaja (1884-1960) in the year 1965.Swaiji called the use of Vedic mathematics is as mental calculation. Vedic mathematics consists 16 sutras (formulae) and 16 Upa sutras (sub formulae), these sutras cannot be finding in Atharva Veda. These sutras were derived from Atharva Veda discovered by ancient sages of India. Vedic mathematics is a unique system of computation based on simple rules and basic principles. By using which we can able to solve complicated mathematical calculations within few seconds. These formulae proposed in Vedic math deals with many modern mathematical terms like arithmetic, trigonometry, geometry (plane or co-ordinate), calculus, factorization and many more mathematical terms. The Vedic methods builds simple rules based on natural principles and are derived from Atharva Veda. This field seems to be very interesting and gives us effective computation algorithm by using which we can solve mathematical equations of various branches in engineering such as computing. Image processing, Speech processing, Digital Signal Processing etc.

The word' vedic ' has been taken from the Sanskrit word 'veda', it means a bunch of knowledge or collection of all knowledge[1].Vedic mathematics is a logical tool and deals with several simple as well as complex mathematical operations. Because

of these marvelous, phenomenal characteristics, it has already crossed the boundaries of India and has became a leading research topic in foreign countries. Advantages of Vedic method is listed in brief below

1) Reduces the complexity of solving the equation
2) Allows a person to solve complex equation within 5 seconds
3) Avoids finger counting and scratch
4) Helps to solve equations 10-15 times faster.

As Vedic Math consists of 16 Sutras and 16 upa sutras and these are used to solve equations relating to any branch of engineering are enlisted below the brief description of each sutra alphabetically [1].

1) (Anurupye) Shunyamanyat – If one is in ratio, the other is zero.
2) Chalana-Kalanabyham – Differences and Similarities.
3) Ekadhikina Purvena – By one more than the previous one.
4) Ekanyunena Purvena – By one less than the previous one.
5) Gunakasamuchyah – The factors of the sum is equal to the sum of the factors.
6) Gunitasamuchyah – The product of the sum is equal to the sum of the product.
7) Nikhilam Navatashcaramam Dashatah – All from 9 and last from 10.
8) Parvarya yojayet – Transpose and adjust.
9) Puranapuranabhyam – By the completion or no completion.
10) Sankalana- vyavakalanabhyam – By addition and by subtraction.
11) Shesanyankena Charamena – The remainders by the last digit.
12) Shunyam Saamyasamuccaye – When the sum is the same that sum is zero.
13) Sopaantyadvayamantyam – The ultimate and twice the penultimate.
14) Urdhava-tiryagbhyam – Vertically and crosswise.
15) Vyashtisamanstih – Part and Whole.
16) Yaavadunam – Whatever the extent of its deficiency.

The Sub Sutras are

1) Anurupyena
2) Shishyate Sheshsamjnah
3) Adyamadye Nantyamantyena
4) Kevalaih Saptakam Gunyat
5) Vestanam
6) Yavadunam Tavadunam
7) Yavadunam Tavadunikutya Vargankach Yojayet
8) Antyayordhshakepi
9) Antyatoreva
10) Samucchayagunitah
11) Lopanasthapanabhyam
12) Vilokanam
13) Gunitasamucchyah Samucchayagunitah.

Using these above enlisted sutras and upa sutras we can be able to solve complicated mathematical equations relating to any branch of engineering.

Vedic multiplier:

Multiplier with the use of Vedic multiplication is called as vedic multiplier. The method applied here is Urdhwa Tiryagyam method. A simple block diagram below shows the 8×8 multiplier.

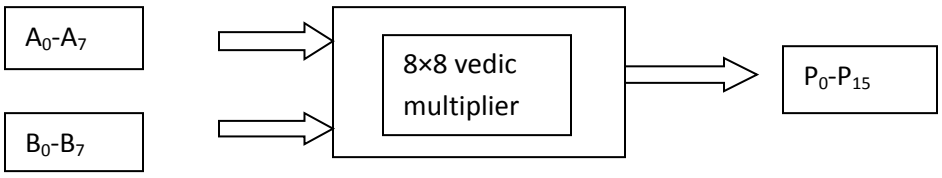

Figure 1.8×8 Vedic multiplier

III .FIR AND IIR FILTER DESIGN:

Finite impulse response filters are also called as convolution filter. These filters are used in the DSPs.IIR and FIR are types of digital filter.

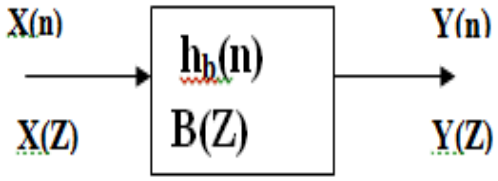

(a)

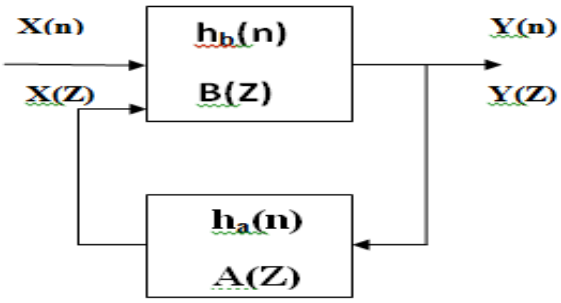

(b)

Figure 2. (a)FIR filter and (b) IIR filter

FIR filter has finite impulse response and linear in nature. Whereas IIR are not linear in nature and phase linearity is not maintained. As shown in diagram (a) shows an FIR filter which does not have any feedback connection in the system design and (b) IIR filter has feed beck connection. Because of this system design FIR filters are more advantages than IIR in systems where phase linearity is maintained. There are many methods of designing both FIR and IIR filters. In this paper, an FIR filter design using window is shown. Windows like Hamming, Gaussian, Triangular, Rectangular, Kaiser, FIR filters are designed. In IIR Butterworth, Chebyshev Type-1 and Type-2 is shown in GUI.

IV.URDHWA TIRYAGBYAM

Urdhwa Tiryagbyam is one sutra among 16 sutras published by Swamiji Maharaja. This word is a Sanskrit word taken from 'veda', which means 'Vertical and Crosswise' [2].This sutra explains about a algorithm which can be applied to any cases of multiplication. Urdhwa Tiryangyam algorithm deals with the even numbered sequence and results in giving odd number of sequences. One more name given to this algorithm is Array multiplication. This method involves calculation of partial products with the concurrent operation of multiplication and addition. The multiplication operation which is used in FIR filter design is used by using Urdhwa Tiryagbyam method. This sutra can be applied to the generalization of N×N multiplication. The figure 3 shows the mode of multiplication for 8×8 bits.

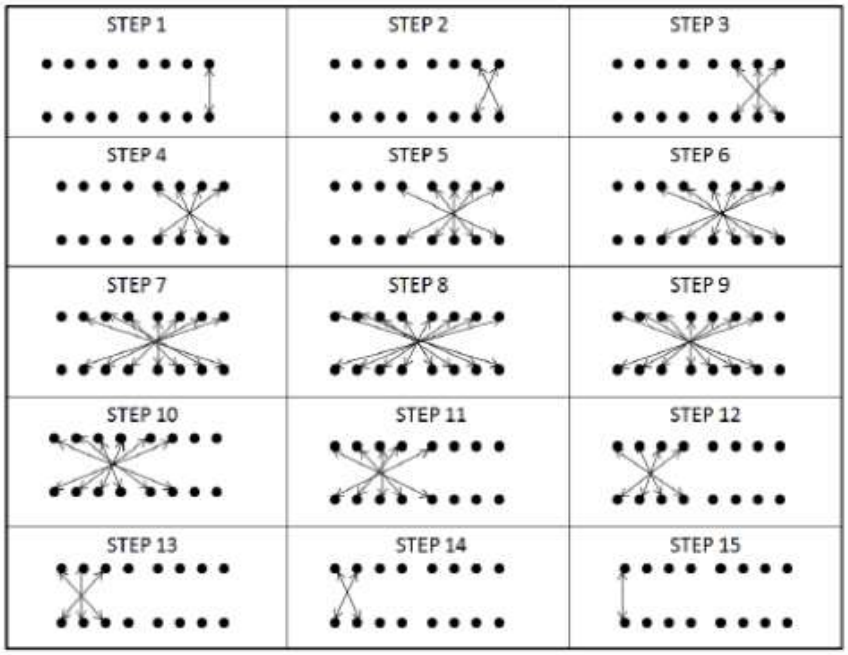

Figure 3.Urdhwa Tiryagbyam algorithm

V. FILTER DESIGN APPROACH

Using linear convolution operation the Direct form realization of FIR filter can be analyzed easily.FIR filter design approach is given below in figure 4.

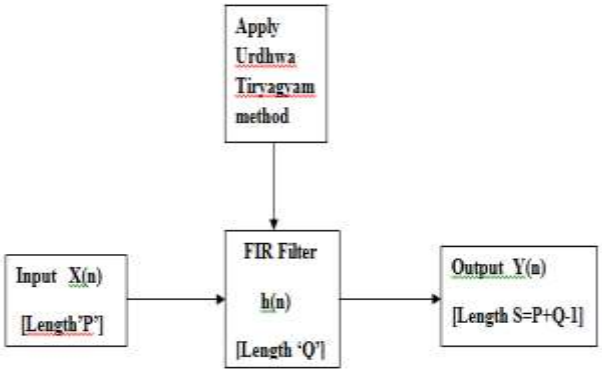

Figure 4 FIR filter

Let x(n)=Input sequence having length'P'

h(n)=Impulse response of filter having length 'Q'.

x(n)={0,1,2,3,…….,P-1}

h(n)={0,1,2,3,…….,Q-1}

The linear convolution of x(n) and h(n) produces the output sequence y(n).The length of y(n) is given by

$$L=P+Q-1 \quad (1)$$

If the number of sequence in x(n) and h(n) is less then by applying zero padding algorithm we made their sum equal to L.This means in order to get the exact output equal to L,we need to increase the length of x(n) by P points and length of h(n) by Q points.

In FIR filter,both the sequences x(n) and h(n) are finite length sequences and hence the resulting sequence would be finite length sequence.The convolution of x(n) and h(n) is given by

$$y(n) = \sum_{k=0}^{Q-1} h(k)x(n-k) \tag{2}$$

Figure 5 shows the diagram of direct form structure of FIR filter.The direct form structure based on the equation 2 is shown in figure5.By expanding that equation we get

$$y[n] = b_0x[n] + b_1x[n-1] + b_2x[n-2] + b_3x[n-3] \tag{3}$$

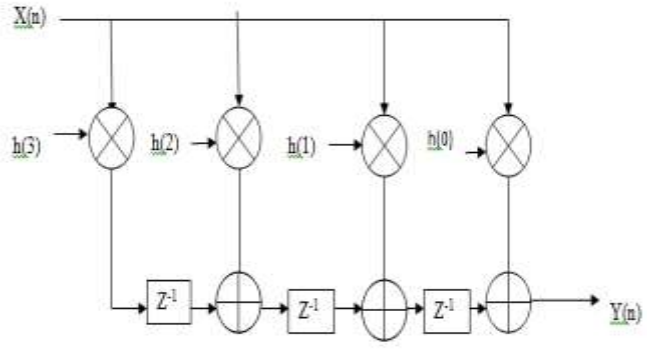

Figure 5. Direct form realization of FIR filter

The other name given to the direct form is the canonical structure since the order of the filter defines the number of delay elements. And the number of delay elements is equal to the order of the difference equation. Of a digital filter. This structure has 'Q-1' additions and 'Q' multiplications.

VI.PROPOSED METHOD

Output sequence y(n) of an FIR filter depends on the input sequence x(n) and impulse response h(n).The design methodology used in this paper is illustrated by figure 3.

Let us take a filter of order 4

Input sequence x(n)={x(0),x(1),x(2),x(3)}

Filter coefficient h(n)={h(0),h(1),h(2),h(3)}

The length of input sequence is x(n)=P=4

Therefore L=4+4+-1=7

By using Urdwa Tirygyam method,

y(0)=x(0)*h(0) (4)

y(1)=x(0)*h(1)+x(1)*h(0) (5)

y(2)=x(0)*h(2)+x(1)*h(1)+x(2)*h(0) (6)

$$y(3)=x(0)h(3)+x(1)*h(2)+x(2)h(1)+x(3)h(0) \quad (7)$$

$$y(4)=x(1)h(3)+x(2)h(2)+x(3)h(1) \quad (8)$$

$$y(5)=x(2)*h(3)+x(3)*h(2) \quad (9)$$

$$y(6)=x(3)*h(3) \quad (10)$$

VII. RESULT ANALYSIS

A Graphical User Interface (GUI), an inbuilt MATLAB function is used to show the computation time taken by both conventional and Vedic method is shown. A GUI builds the interaction between a user and the system, it helps the user to interact with the system through graphical icons.GUI is easy way to manipulate information and present data. The main aim of GUI is to increase the efficiency of computation and ease of use for the logical design of a stored program, Different technologies and devices uses GUI to provide a platform for the user to interact with the software for the tasks of producing information. In this paper, the computation using GUI is divided into 2 section. Section 1 explains deals with FIR filter and section 2 deals with IIR filter.

Section 1:FIR filter

For 36 order FIR filter with input as unit step signal

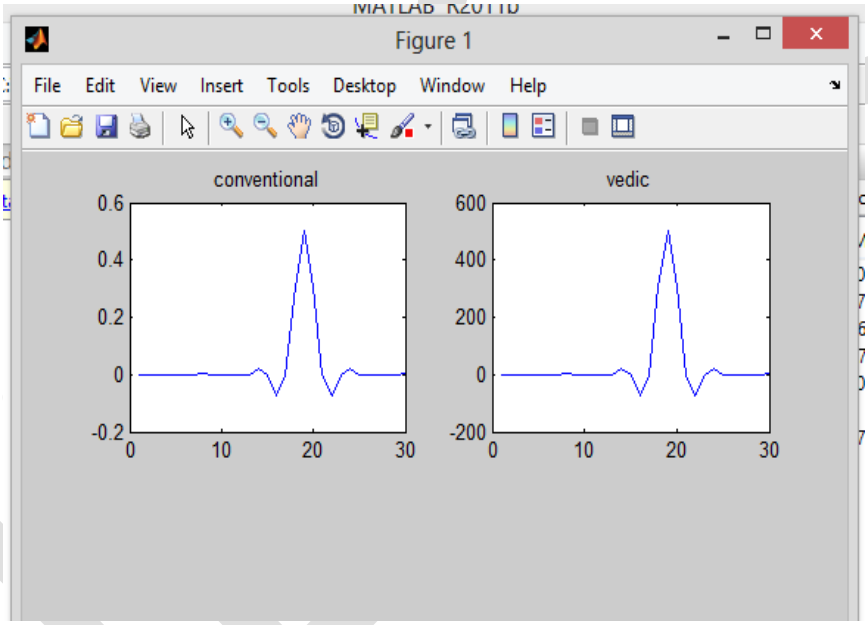

Figure 6.Output Response of FIR filter-36 order low pass Triangular window

Table 1.conventional versus Vedic time in LPF

S. No	FIR window	Vedic method	Conventional method
1	Flat top	2.057273s	0.045232s
2	Gaussian	0.371102s	0.0483s
3	Triangular	0.36913s	0.057355s
4	Kaiser	0.377437s	0.0483s
5	Hamming	0.836380s	0.0483s
6	Rectangular	3.587520s	0.045119s

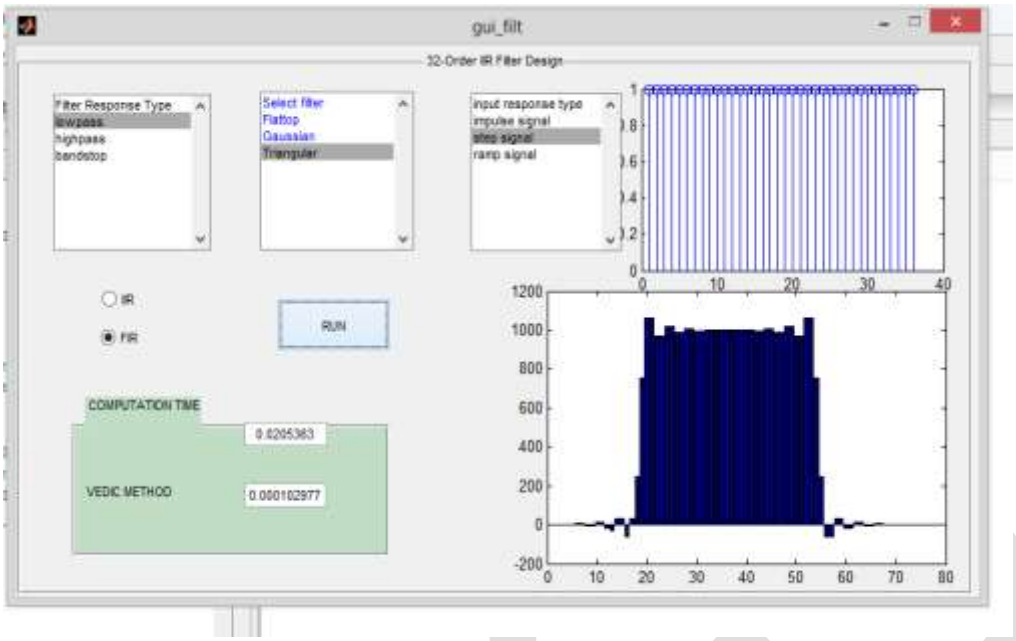

Figure 7.GUI for FIR filter for Triangular window

The above GUI is shown for FIR filter for Triangular window.The Y-axis shows the time consumed for the execution of sequences and the above graph in GUI shows the input and below one shows the Output of an FIR filter.

Section 2:IIR filter

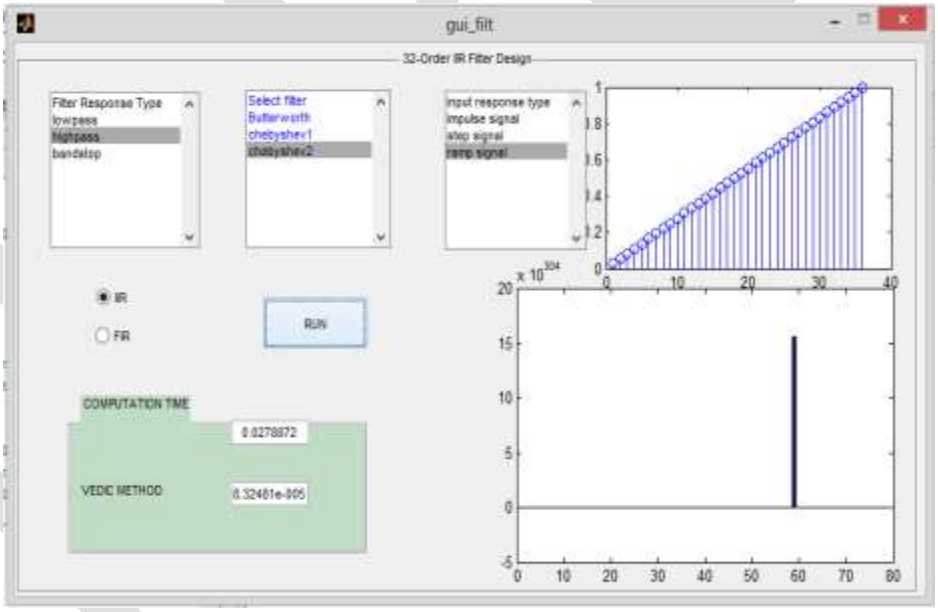

Figure 7 GUI filter for IIR Chebyshev filter Type-2

The above shown result for IIR filter is executed in the same way as for other butterworth,chebyshev filter type-1 filters for unit step,ramp,impulse etc.

VII.CONCLUSION

The implementation of IIR and FIR is done using Matlab. A window based FIR filter design is implemented by the use of Urdhwa Tiryakbyam multiplication Vedic sutra in Graphical user interface window. The computation time is calculated for Triangular, Rectangular, Hamming, Kaiser, Gaussian and flat top windows are calculated. By seeing the result we come to know that the execution time taken by Vedic method using Urdhwa Tiryakbyam is less compared to conventional method. These Vedic formulae are

much more efficient compared to conventional one. An IIR filter based on Vedic method computation is done and shown in GUI same like FIR for Butterworth, Chebyshev Type 1 and Chebyshev Type 2 filters. The computation time is compared for Frequency sampling method of design of filters. Thus FIR filter and IIR filter based on vedic method consuming less average execution time compared to inbuilt MATLAB function. This means the execution time taken by Urdhwa Tiryagbyam method is reduced.

Future works for filter design using Urdhwa Tiryagbyam method can be used to improve filtering technique used in Image processing, Stenography, Network security, for moving actions average like in finance business and in many more signal processing field. And also can be used for calculating Fast Fourier Transforms and Inverse fast Fourier Transforms (IFFT)..As a future scope the Vedic sutra can be applied to other filter design techniques like LMS (Least Mean Square), Frequency Domain sampling methods. And can be compared the execution time of Urdhwa Tiryakbyam method with other Vedic sutras like Nikhilam Navatashcaramam Dashatah etc.

REFERENCES:

1]Tushar Shukla,Prabhat Kumar Shukla,Harish Prabhakar,"High speed multiplier for FIR filter design using window",2014

International conference on Signal processing and integrated networks.

2] S.Koushighan, K.Hariharan and V.Vaithiyanathan,"Design of an optimized High speed multiplier using Vedic mathematics", contemporary Engineering Sciences, vol.7, 2014 no.9, 443-448

3] Jagadguru Swami Bharathi Krishna Tirthaji,"vedic mathematics or sixteen simple sutras from the Vedas", Motilal Banarasidas, Varnasi, IndiA-1992

4]Padma Kunthe,Ankit Sharma,sameena Zafar,"32-order IIR filter design using vedic mathematics",International Journal of Artificial Intelligence and mechatronics,volume2,issues 5,ISSn 2320-5121

5] M.Bharathi,D.leela Rani,"A novel approach for High speed convolution of finite and infinite length sequences using vedic mathematics ",International journal of research in Engineering and technology,eISSN :2319-1163/pISSN 2321-7308.

6] Shivkumar, Shridhar KP, Poornima M and Sanjay H,"Implementation of multiplier using vedic algorithm", International journal of Innovative technology and exploring Engineering vol.2 may 2013, PP, 219-223

7] Yogita banasal, Charu madhu, Pradeep kaur,"High speed vedic multiplier designs", proceedings of 2014 RAECSUIET, Punjab University Chandigarh, 06-08-2014

8] Honey Durga Tiwari, Ganzorig Gankhuyag, chan mo kim,Yong Beom Cho, "multiplier design based on ancient Indian vedic mathematics",978-1-4244-2599@2008 IEEE,2008 International SOC design conference.

9] Vaijyanth Kunchagi, Lingangouda kulkarni,Subhash Kulkarni,"High speed and area efficient vedic multiplier ",IEEE conference on devices, circuits and systems,march 2012

10] S.siddamal, R.M.Banakar, S.S soakar,"High speed signed multiplier for digital signal processing application",IEEE International conference on signal processing computing and control, march 2012

11] Emi Retna and Isbella"Study paper on test case generation for GUI based testing", international Journal of software engineering and applications,vol3,Jan 2012

International Journal of Engineering Research and General Science Volume 3, Issue 3, Part-2 , May-June, 2015
ISSN 2091-2730

A Novel Approach For Web Pre-fetching and caching

Varun Kumar[1] Ms.Nidhi Seth[2]
[1]Research Scholar [2]Assistant Professor
[1 2] Department of Computer Science & Engineering [1,2]JMIT, Radaur, Haryana, India
varunsaini727@gmail.com er.nidhi25@gmail.com

Abstract- Due to the fast development of internet services and a huge amount of network traffic web caching and prefetching are the most popular techniques that play a key role in improving the Web performance by keeping web url that are likely to be visited in the near future closer to the client. Web caching technique work integrated or independently with the web prefetching. The Web caching and prefetching techniques are complement each other since the web caching exploits the temporal locality for predicting revisiting requested url, while the web prefetching utilizes the spatial locality for predicting next related web object of the requested Web url. In this paper proposed work represent the working of a novel approach for web caching and prefetching.This technique enhance the performance with help of using user priority approach. In this paper explain how the response time of hit taken from the user cache is less as compare to the data taken directly from the log file.In this approach cache size and which replacement policy is used for replacement in cache play an important role .For this in this paper explain the comparision of three replacement technique – LRU,FIFO,LFU on basis of hit rate on cache .For improving the performance and response time in web caching and prefetching technique use the best replacement policy after comparision .In this paper also explain enhance the performance of caching and prefetching using user based approach and analyze the prefetching hit ratio b/w priority and user based approach in which clustering used.

Keywords— Web Caching, Web pre-fetching, Response Time, Proxy server, replacement policy, Hit,clustering

Introduction

Web caching is a well-known strategy for improving the performance of Web- based system by keeping Web objects that are likely to be used in the near future in location close to user. The Web caching mechanisms are applied at three levels: client level, proxy level and original server level[5,6] . Significantly, proxy servers play the key roles between users and web sites in lessening of the response time of user requests and saving of network bandwidth.Thus, for achieving better response time, an efficient caching technique can be built in a proxy server

Web caching is a well-known strategy for improving the performance of Web- based system by keeping Web objects that are likely to be used in the near future in location close to user. The Web caching mechanisms are applied at three levels: client level, proxy level and original server level[5,6] . Significantly, proxy servers play the key roles between users and web sites in lessening of the response time of user requests and saving of network bandwidth.Thus, for achieving better response time, an efficient caching technique can be built in a proxy server

The cache replacement is the core or heart of the web caching; consquently, the design of efficient cache replacement algorithms is crucial for caching mechanism achievement. so, cache replacement algorithms are also called web caching algorithms[7]. Because of limited space of cache, an intutive mechanism is required to manage the Web cache content properly. The conventional caching policies are not efficient in the Web caching since they consider just one factor and ignore other factors that have impact on the efficiency of the Web caching . In these caching policies, most popular objects get the most requests, while a large segment of objects, which are stored in the cache, are never requested again. This is called cache pollution problem. Therefore, many Web cache replacement policies have been proposed attempting to get good performance. Hence, the difficulty in determining which ideal web objects will re-accessed is still a big challenge faced by the existing Web caching techniques. In other words, what Web objects should be cached and what Web objects should be replaced to make the best use of available cache space, better hit rates, decrease network traffic, and reduce loads on the original server[3,4] .

Unfortunately, the cache hit ratio is not improved much with caching schemes. despite with a cache of infinite size, the hit ratio are still limited only at the range from 40% to about 50%, regardless of the caching scheme [8,9,10]. This is because most people browse and explore the new web pages trying to find new information. In order to improve the hit ratio of cache, Web pre-fetching technique is integrated with web caching to overcome these limitations

Web prefetching is fetching web pages in advance by proxy server/client before a request is send by a client/proxy server. The major advantage of using web prefetching is reduced latency. When a client makes a request for web object, rather than sending request to the web server, it may be fetched from a pre-fetch area. The main factor for selecting a web prefetching algorithm is that its ability to predict the web object to be pre-fetched in order to reduce latency. Web prefetching exploits the spatial locality of web pages, ie. pages that are linked with current page will be accessed with higher probability than other pages. Web prefetching can be implemented in a web environment as between clients and web server, between proxy server and web server and between clients and proxy server [11]. If it is implemented between web server and client , it is helpful in decreasing user perceived latency, but the problem is that it will increases network traffic. If it is implemented between web server and proxy server, can reduce the bandwidth usage by prefetching only a specific number of hyper links. If it is implemented between clients and proxy server, the proxy starts feeds pre-fetched web objects from its cache to the clients so there won't be extra internet traffic.

Web Pre-Fetching Techniques

(i) Domain Top

In Domain Top approach for web prefetching, combination of knowledge of most popular domains andmost popular documents is done by proxy server. In this approach proxy is responsible for calculating the most popular domains and most popular documents in those domains, and then prepares a rank list for prefetching.

(ii) Top 10 Approach

Evangelos P. Markatos et al. proposes a top 10 approach to prefetching on the web, in which the server calculates the list of most popular documents. This approach is easy to implement in client server architecture. It considers frequency of access for predicting the web object, not the client characteristics on the web.

(iii) A Keyword based semantic prefetching approach in internet news services

This proposes a key word based semantic pre-fetching, in which prediction of future requests are based on semantic preferences of past retrieved web documents. This technique is applied to internet news service; it finds out semantic preferences by analyzing keywords in URL anchor text of previously accessed documents in different news categories.The semantic representation is represented in an open self learning capable model which collects the knowledge about the client preferences. Client future request predictions are based on this knowledge. The pre-fetched documents are stored in internal cache. When client makes a request the web document is fetched from cache if it is available otherwise it fetches self learning.

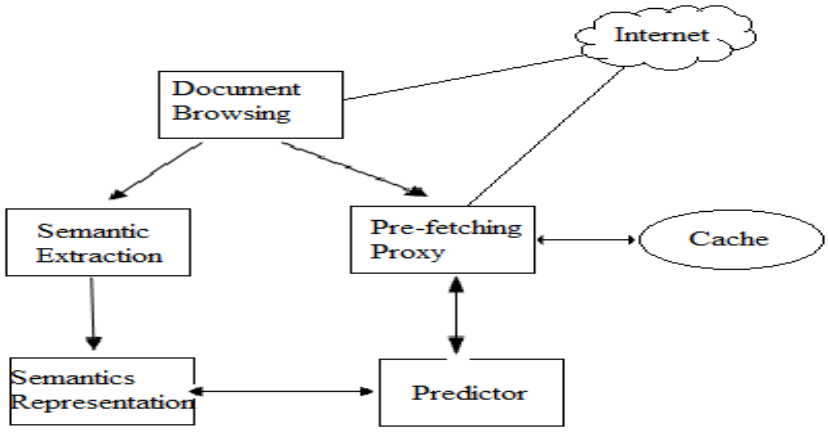

Fig (a) semantic prefetching approach

(iv) Dynamic web prefetching

In dynamic web pre-fetching technique [12], each user can keep a list of sites to access immediately called user's preference list. The preference list is stored in proxy server's database. Intelligent agents are used for parsing the web page, monitoring the bandwidth usage and maintaining hash table, preference list and cache consistency. It controls the

web traffic by reducing pre-fetching at heavy traffic and increasing pre-fetching at light traffic. Thus it reduces the idle time of the existing network and makes the traffic almost constant. A hash table is maintained for storing theist of accessed URLs and itsweight information [12], [13]. Depending upon the bandwidth usage and weights in the hash table, the prediction engine decides the number of URLs to be pre-fetched and gives the list to pre-fetch engine for pre-fetching the predicted web pages. After prefetching, the proxy server keeps the pre-fetched web pages in a separate area called pre-fetch area.

(v) Link Pre-fetching

A web page provides a set of pre-fetching hints to the browser and after the browserfinishes loading the page, it starts pre-fetching specified documents and stores them in its cache. When the user visits one of the pre-fetched documents, it can be served up quickly out of thebrowser's cache. Fisher et. Al proposed a server drive approach for ink prefetching [14].In thisapproach browser follows special directives from the web server or proxy server that instructs itto pre-fetch specific documents. This mechanism allows servers to control the contents to be perfectedby the browser. The browser looks for either HTML <link> tag or an HTTP Link: headerTag to pre-fetch the subsequent links. The Link: header can also be specified within the HTMLdocument itself by using a HTML <meta>tag[16].When the browser is idle, it observes thesehints and queues up each unique request to be pre-fetched.

(vi) Adaptive pre-fetching Scheme

Adaptive pre-fetch scheme are developed to adapt user's browsing history and habits [15]. Jiangand et al. proposed an adaptive pre-fetch scheme, in which the number of files to be pre-fetcheddepends on user access history and network conditions . This scheme consists of two modules: prediction module and threshold module. The prediction module updates the history and computesthe access probability of each file. Files whose access probabilities greater than or equal to thepre-fetch threshold are onlypre-fetched. Chen and et. al[7] proposed an adaptive pre- fetchscheme, in which dynamically adjust the pre¬fetch aggressiveness in web servers and uses athreshold to adjust the aggressiveness of pre¬fetching. Fagni and et. al[proposed usesanapproach for boosting the performance of search engine by exploiting the spatial and temporallocality present in the stream of processed queries.They do not consider real semantics of document, however. As semantic prefetching we understand prefetching based on preferences of past retrieved documents in semantics, rather than on the chronological relationships between URL accesses. Semantically based prefetching tries to extract a semantic description of a document and asks server to provide pages with similar semantics, with the same so called "semantic locality". Based on the document semantics, this approach is capable of prefetching documents whose URLs have neverbeen accessed

Related work

(i) A Survey of Web Caching and Prefetching"(Waleed Ali , Siti Mariyam Shamsuddin, and Abdul Samad Ismail)(2011)
Web caching and prefetching are the most popular techniques that play a key role in improving the Web performance by keeping web objects that are likely to be visited in the near future closer to the client. Web caching can work independently or integrated with the web prefetching. The Web caching and prefetching can complement each other since the web caching exploits the temporal locality for predicting revisiting requested objects, while the web prefetching utilizes the spatial locality for predicting next related web objects of the requested Web objects. This paper reviews principles and some existing web caching and prefetching approaches. The conventional and intelligent web caching techniques are investigated and discussed. Moreover, Web prefetching techniques are summarized and classified with comparison limitations of these approaches. This paper also presents and discusses some studies that take into consideration impact of integrating both web caching and web prefetching together.

(ii) A Survey On Web Pre-Fetching and Web Caching Techniques in a Mobile Environment"(Greeshma G. Vijayan1 and Jayasudha J. S.) (2012)
As the Internet continues to grow in size and popularity, web traffic and network bottlenecks are major issues in the network world. The continued increase in demand for objects on the Internet causes severe overloading in many sites and network links. Many users have no patience in waiting more than few seconds for downloading a web page. Web traffic reduction techniques are necessary for accessing the web sites efficiently with the facility of existing network. Web pre-fetching techniques and web caching reduces the web latency that we face on the internet today. This paper describes about the various prefetching and caching techniques, how they

predict the web object to be pre-fetched and what are the issues challenges involved when these techniques are applied to a mobile environment

(iii) Survey on Improving the Performance of Web by Evaluation of Web Prefetching and Caching Algorithms" (Arun Pasrija) (2013)

Web caching and prefetching have been studied in the past separately. In this paper, present an integrated architecture for Web object caching and prefetching. Our goal is to design a prefetching system that can work with an existing Web caching system in a seamless manner. In this integrated architecture, a certain amount of caching space is reserved for prefetching. To empower the prefetching engine, a Web-object prediction model is built by mining the frequent paths from past Web log data.We show that the integrated architecture improves the performance over Web caching alone, and present our analysis on the tradeoff between the reduced latency and the potential increase in network load.

(iv) Survey of Recent Web Prefetching Techniques" (Sonia Setia, Dr. Jyoti, Dr. Neelam Duhan) (2013)

Web caching and web prefetching are the two major areas of research focused at reducing the user perceived latency. Both if used well can greatly help in reducing this latency as web caching helps in exploiting temporal latency while web prefetching helps in exploiting spatial latency. However if prefetched pages are not visited by the users in their future accesses, they can increase the network traffic and overload the web server. This paper aims at surveying various research papers who have worked in this direction.

(v) Study of Web Pre-Fetching With Web Caching Based On Machine Learning Technique " (K R Baskaran, Dr. C.Kalarasan, A Sasi Nachimuthu) (2013)

High bandwidth utilization, reduced load on the origin server, high access speed are possible by combining Web caching and pre-fetching techniques. Pre-fetching is the process of fetching few Web pages in advance which will be assumed to be needed by the user in near future and those pages are cached in the memory. Lots of work has been reported for caching and pre-fetching of Web pages in the literature. In this paper, pre-fetching using clustering technique is combined with SVM (Support Vector Machine) - LFU algorithm, a machine learning technique for Web proxy caching .By using real dataset it will be shown that the SVM technique will be better than clustering based prefetching technique using caching policy like LFU considering bandwidth utilization and access latency

(vi) Hybrid Approach for Performance of Web Page Response through Web Usage Mining ” (Ravinder Singh,Bhumika garg) (2014)

In this paper present the web caching and prefetching together using Dynamic technique into Domain Top approach. . Optimized top domain approach will consist of preference list along with the rank list. In this approach proxy is responsible for calculating the most popular domains and most popular documents in those domains, and then prepares a rank list for pre-fetching. In Dynamic web pre-fetching technique, each user can keep a list of sites to access immediately called user's preference list.

PROBLEM DEFINITION

Caching is an significant technique for enhancing the performance of web based applications with help of web caching techniques. Web caching provides great features like traffic reduction, less load on servers, user-end retrieval delays by replicating popular content on proxy caches that are strategically placed within the network. Web pre-fetching schemes have also been widely discussed where web pages and web objects are pre-fetched into the proxy server cache. In our research we will work on integration of web caching and web pre-fetching approach to improve the performance of proxy server’s cache. In Domain Top approach for web pre-fetching, combination of knowledge of most popular domains and most popular documents is done by proxy server. In Dynamic web pre-fetching technique, each user can keep a list of sites to access immediately called user’s preference list. In recent research concept of preference list from Dynamic technique into Domain Top approach is used but there is no graphical representation about performance and there is not mentioned about which replacement policy used in this technique. The main focus of the research is to improve accuracy in caching and prefetching technique. Our research is started with information fetching of pre-fetching and caching techniques. The major targets and objectives for our research is given as below:

- Develop an significant technique for optimizing the web caching and web pre-fetching processes with user based new technique in which we use clustering .
- Enhance the performance of existing technique using priority concept and using the best replacement policy.
- .Analyze FIFO,LRU,LFU replacement policy on the basis of hit rate on cache using various size of cache.
- .Analyze the existing prefetching approach and user based prefetching technique on the basis of hit rate . .
- For find loopholes and issues in new approach and to highlight the benefits for new approach.

Proposed Work

(i). WEB LOG FILE

A **log file** is a recording of everything that goes in and out of a particular server.Web user visits many web sites time to time and spent random quantity of time among various visits.To deal with the user browsing behavior, we should analyze the proxy server log file. In fussy,

the web proxy access log is an in order file with one user access data per line. Web proxy log files make available information about actions performed by a user from the moment the user logs.

(ii). Extraction & preprocessing

In extraction phase web log file is extacted which maintain the all record of the users. In our proposed work during preprocessing phase we carried out the cleaning task to filter out all the unwanted entries from the proxy log data.suppose in log file it contain the link http://www.sscnwr.org/notice_down_file/Advt.%20No.%20ER2015%20English%20Version-FINAL%20FOR%20ADVT.pdf. So after the preprocessing we get only " www.sscnwr.org"

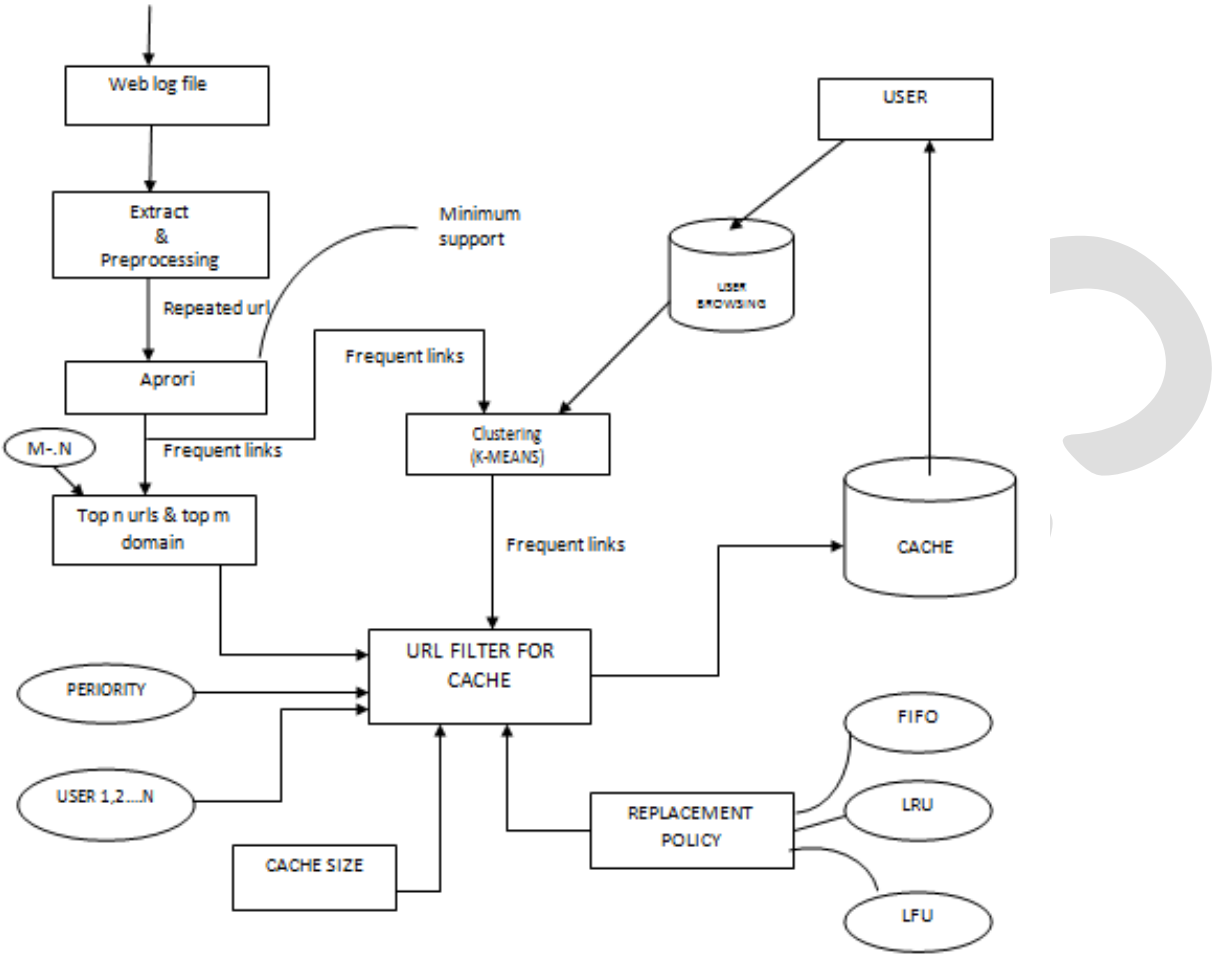

Fig.(b) Proposed work flow chart

(iii). Aprori After the preprocessing step we get all type of domain which are accessed by user.After this we use Aprori for getting unique url and their frequency how many time they used by user.with help of this we get the frequent links In this algorithm we will use the minimum support.minimum support is the confidence level which we decide p% and the term that appears less than p% will be remove and the more combination is applied to take the proper frequent set of the given data.after this we get top m url of top n domain.

(iv). Clustering:

To cluster users we use the KMeans clustering which is used to gather different users into clusters on the basis of their usage behavior and searching pattern. The *K-Means* is the simplest clustering algorithm widely used for web proxy server .The algorithm is used to cluster users data based onattributes into *K* clusters. Each cluster has its center (known as centroid) at point *Cj*. The centroid is calculated from mean distance of all records in the cluster [26]. In this study, we make an assumption that users in the same cluster should have same surfing habits and patterns. Users surfing habits can be determined by several factors such as the time of day of their access, and their most frequently visited websites. In our proposed work we apply this on user browsing history and frequent link which we get after aprori .

(v). URL Filter

url filter work for cache.it's working is that how the url arrange or which url contain by the cache suppose cache size is 20 and our url is 50 then its work is that after filtering we get those url for cache which are more relevant and used in future by user .For filtering we used priority concept,diff-2 replacement policy,user based approach with help of clustering.

Replacement policy The cache replacement is the core or heart of the web caching; consquently, the design of efficient cache replacement algorithms is crucial for caching mechanism achievement. so, cache replacement algorithms are also called web caching algorithm.there are following replacement policy is used in our proposed work and there comparision

a. LFU-least frequent used
b. LRU-least recently used
c. FIFO-first in first out

Priority concept without priority most frequent url is displayed on cache if we use the priority concept in this the one of the users is having highest priority other will have less priority.suppose there are n user and suppose One of the user has highest priority than other.suppose cache size is 20 and in this already 19 url placed if all the user browse the diff url at same time then url which have highest priority is added on cache.

User base concept

in this url displayed on cache on the basis of user . with this concept url in cache accrding to the user.in this approach we use the clustering on user browsing history and frequent link which we get after aprori.in this url in cache according to the user .in our proposed work there is 1,2,3……10 user .with this concept we see the top 5,10,15,20 frequent link on cache according to user1,2……..10.in this if we want to cache maintain top 15 url of user 5 then it show the top 15 url of user 5.it increase the hit ratio . if we want to cache maintain top 5 url of user 3 then it show the top 5 url of user 3.this is user based approach .it maintain the cache according to user interest.

RESULT ANALYSIS

In this section, result analysis has discussed on the basis of experimental work in which we have tested .with help of our experimental work we draw two graph

1. In our work we used three replacement policy for cache i.e FIFO ,LRU,LFU and compare each of them on the basis of hit rate at different -2 cache size.

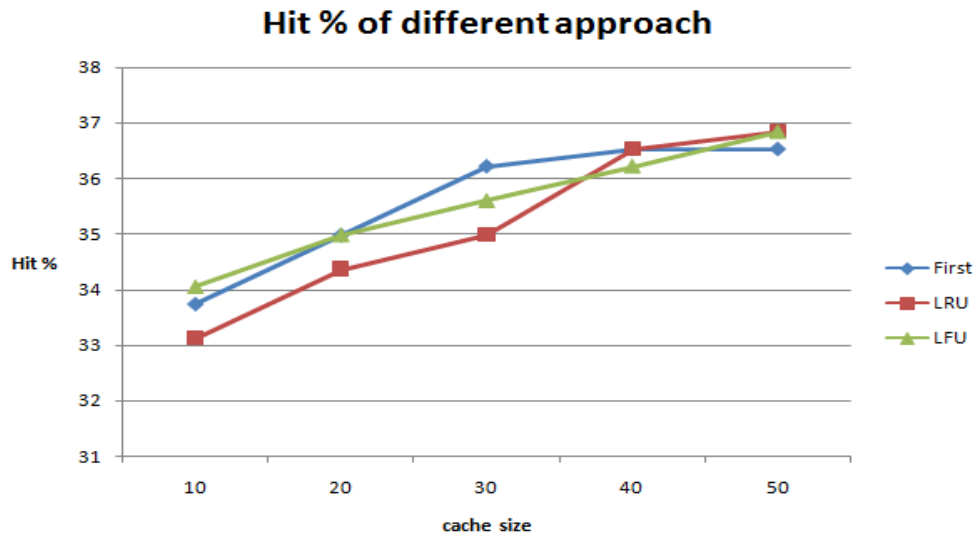

Fig c Hit ratio comparison between FIFO,LRU & LFU with prefetching

Fig. shows effect of hit ratio on different values of cache size used in all the cases FIFO,LRU and LFU. In all the cases, as the cache size increases, the hit % also increases accordingly. But from the Fig. it is clear that when the size of cache is small than LFU approach works better than LRU & FIFO.But if the cache size is large then LRU approach works better than LRU & FIFO.After a certain size of cache the result is same for FIFO.so it show if we use small size cache then we should use LFU or if we use large size cache then we use LRU replacement policy.

2) with help of our experimental work we compare the existing system and our proposed sysem on the basisiof hit ratio at different -2 size cache.

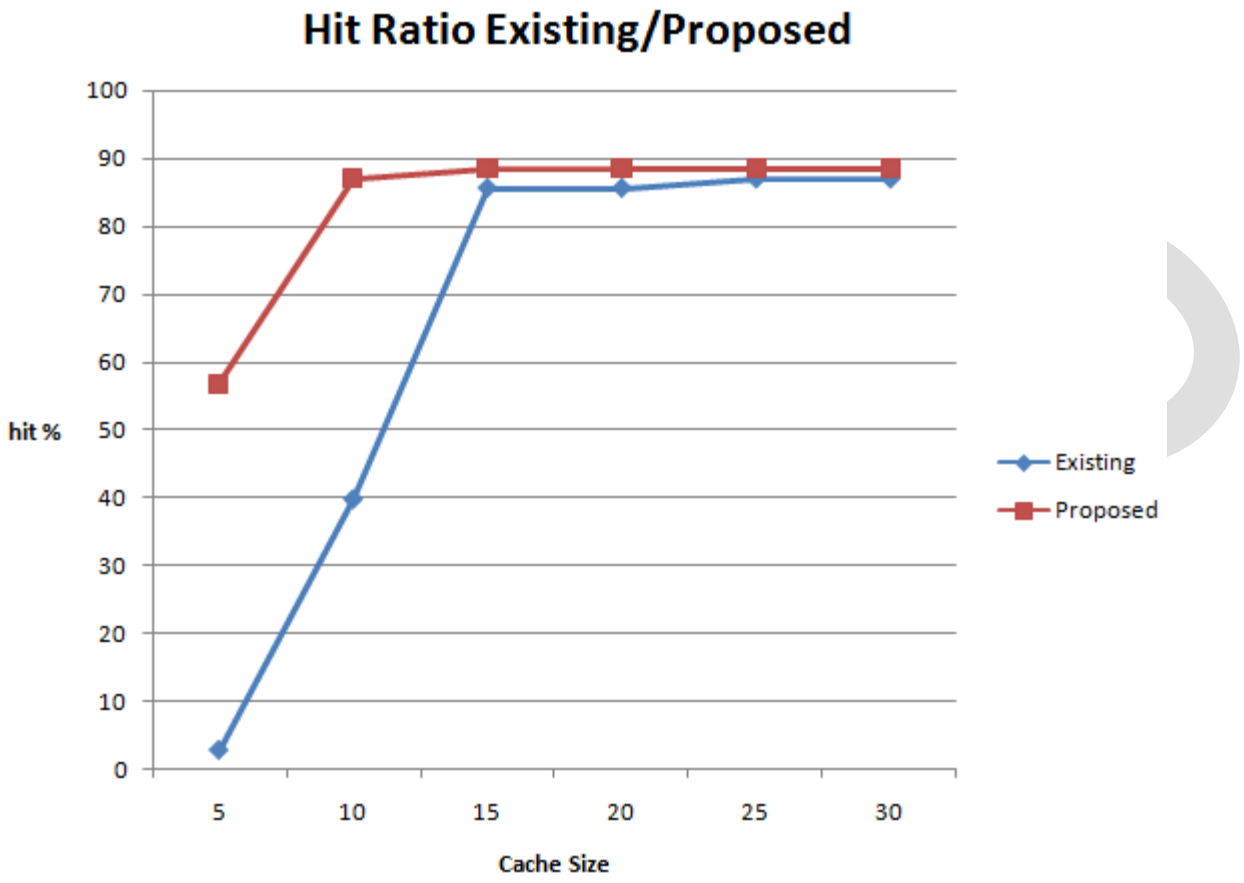

Fig (d) Hit ratio comparison between existing and proposed system

Fig. shows effect of hit ratio on different values of cache size used in both the cases existing(top 10 domain +dynamic approach) and proposed(user based using clustering) system. In both the cases, as the cache size increases, the hit ratio % also increases accordingly. But from the Fig. it is clear that our approach works better than existing approach

CONCLUSION AND FUTURE WORK

In this paper, we have proposed a system for prediction of web requests of users and accordingly,prefetching the content from the server. The dataset is used for the experimental work which has collected from the user history. The proposed framework improves performance of web proxy server using user based approach for caching and prefetching scheme which is clear in the result section. By using this proposed framework hit ratio is improved as shown in result section. In this paper also compare replacement policy.Designing of proxy server and implementation of the proposed framework are under the future scope.To find other technique which help in increase the hit ratio and improve performance uder future scope.

Acknowledgement

I would express my deep sense of regard to our Head of Department Mr. Vivek Sharma and to Mrs. Nidhi Seth, AP CSE Department for regular inputs and for constantly guiding. I am obliged to the staff members of CSE department, JMIT for the valuable information provided by them as and when necessary

REFERENCES:

[1]. Toufiq Hossain Kazi, Wenying Feng and Gongzhu Hu "Web Object Prefetching: Approaches and a New Algorithm", IEEE 2010, pp 115-120.

[2]. J. B. Patil and B. V. Pawar, "Improving Performance on WWW using Intelligent Predictive Caching for Web Proxy Servers," IJCSI International Journal of Computer Science Issues, Vol. 8, Issue 1, January 2011.

[3]. C. Kumar and J.B. Norris, "A new approach for a proxy-level Web caching mechanism", *Decision Support Systems, Elsevier*, 46(1), (2008), pp.52-60.

[4]. R. Chiang, P. B. Goes, and Z. Zhang, "Periodic cache replacement policy for dynamic content at application server", *Decision Support Systems, Elsevier*, 43 (2), (2007), pp. 336- 348.

[5]. H.T. Chen, *Pre-fetching and Re-fetching in Web caching systems: Algorithms and Simulation*, Master Thesis, TRENT UNIVESITY, Peterborough, Ontario, Canada(2008).

[6]. T.Chen, "Obtaining the optimal cache document replacement policy for the caching system of an EC Website", *European Journal of Operational Research.181(* 2),(2007), pp. 828. Amsterdam.

[7]. Koskela, J. Heikkonen, ,and K. Kaski, (2003). "Web cache optimization with nonlinear model using object feature", *Computer Networks journal, elsevier* , 43(6), (2003), pp. 805-817

[8]. H.k. Lee, B.S. An, and E.J. Kim, "Adaptive Prefetching Scheme Using Web Log Mining in Cluster-Based Web Systems", *2009 IEEE International Conference on Web Services (ICWS)*, (2009), pp.903-910.

[9]. L. Jianhui, X. Tianshu, Y. Chao. "Research on WEB Cache Prediction Recommend Mechanism Based on Usage Pattern", *First International Workshop on Knowledge Discovery and Data Mining(WKDD)*, (2008), pp.473-476.

[10]. Abhari, S. P. Dandamudi, and S. Majumdar , "Web Object-Based Storage Management in Proxy Caches", *Future Generation Computer Systems Journal* , 22(1-2), (2006). pp. 16-33.

[11]. *Seung Won Shin, Byeong Hag Seong & Daeyeon Park, (2000)"Improving World-Wide- Web Performance Using Domain-Top Approach to Prefetching", Fourth International Conference on High- Performance Computing in the Asia-Pacific Region vol. 2, pp. 738-746.*

[12]. Sandhaya Gawade and Hitesh Gupta, "Review of algorithms for prefetching and caching" 2012 IJARCCE

[13]. [13]HeunKi Lee, Baik Song an, and Eun Jung Kim, "AdaptivePrefetching Scheme Using Web Log MininginCluster-basedWeb", InternationalConference on Web Services, IEEE, 2009, pp. 903-910.

[14]. Wenying Feng and Hua Chen ,"A Matrix Algorithm for Web Cache Prefetching", International Conference IEEE/ACIS, 2007, pp. 788-794

[15]. J. B. Patil and B. V. Pawar, "Improving Performance on WWW using Intelligent Predictive Caching for Web Proxy Servers," IJCSI International Journal of Computer Science Issues, Vol. 8, Issue 1, January 2011

[16].]MukeshDawar, Charanjit Singh, "A Review on Web CachingTechniques",International Journal of Advanced Research inComputer Science and Software Engineering, ISSN: 2277 128X,Volume 4, Issue 3, March 2014

[17]. B.lalithadevi, A.Merry Ida, W.AncyBreen "A new Approach for improving world wide web techniques in data mining".IJARCSSE,2013.

[18]. Suvarnatemgire, poonam Gupta, "Review on web prefetchingtechniques", IJTEEE,2013

[19]. Anuradha,kiran jain, "Survey on an Integrated Approach for Web Pre-Fetching and Caching," Vol. 2, Issue 02, 2014 | ISSN (online): 2321-0613

[20]. Bhumika garg,Ravinder singh , "Hybrid Approach for Performance of Web Page Response through Web Usage Mining " Vol. 4, Issue 07, july 2014 | ISSN (online): 2277-128X

International Journal of Engineering Research and General Science Volume 3, Issue 3, Part-2 , May-June, 2015
ISSN 2091-2730

Reverse Engineering of Telecom Towers

M. D. Kevadkar [1], Sai Praveen. S [2], Siddhesh Deorukhkar [3]

[1] HOD Civil Department, UCOER, PUNE, INDIA.
mdkevadkar@gmail.com
[2, 3] Students, BE Civil Engineering, UCOER, PUNE, INDIA.
spsuraparaju@gmail.com
Mob: - +91 8446753232

Abstract— The Indian Telecom industries have witnessed a tremendous growth in network services and data utilization from the last few years which have resulted in installation of large number of towers to increase the coverage area and network consistency. But the construction of new towers takes long time and needs huge initial capital investment. The time delay during construction of new towers and installation of new antennas causes a great interruption for customers in their network services. To avoid these congestions the existing towers should be utilized to their full capacities instead of constructing new towers. The geometrical details of the existing towers can be availed using the mapped data done by the tower climbers and this process of climbing the tower, measuring the dimensions of members and mapping that data is called Reverse Engineering.

In this present study, a case study of 3-Legged Triangular Ground Based Tower of elevation 280 ft (85.344m)has done and the tower is analyzed for the newly proposed and installed LTE antennas loads by removing the old GSM/CDMA antennas and checked whether the tower can safely carry the newly proposed loads or not. The analysis has been done using TIA-222-G standard and brief data regarding analysis and results obtained has mentioned below.

Keywords— Reverse Engineering, 3-Legged Steel Lattice Tower, Gust Effect Factor, Tele-Density, Tower mapping, Ground Based Triangular tower, Optimal Design

INTRODUCTION

Reverse Engineering – The need of the hour in Telecom Industry:

The Indian telecom industry has witnessed significant growth in subscriber base over the last decade, with increasing network coverage and a competition-induced decline in tariffs playing facilitators. The growth story and the potential have also served to attract newer players in the industry, with the result that the intensity of competition has kept increasing, forcing the Telecom Operators (TELCOs) to look for cost-cutting measures. One such measure has been the hive-off of telecom tower related operations into separate companies to allow for greater operating efficiencies and tower sharing. The attractiveness of the telecom tower industry, given the aggressive network rollout plans of the TELCOs, has led to the entry of several companies in the fray.

Telecom tower companies with a relatively large portfolio of towers offer certain clear advantages to Telcos, including rapid rollout over a large area, and tenancy driven discounts. Further, large tower companies can access capital markets better to fund growth. These advantages make it somewhat difficult for the smaller tower companies to grow; thereby paving the path for consolidation in the industry. The exponential growth in the telecom industry resulted in the huge demand for telecom carriers. As a result of this the telecom carriers are experiencing huge demand from customers to provide network coverage along with quality service. In order to meet this huge demand the telecom carriers have two options:

A. To build the new Tower sites

i. To build a new cell site (GBT) it costs about 25 Lacs and for a new rooftop site it costs around 15 Lacs. This is a huge capital investment and please note that India has very least revenue per call rates, this is becoming a challenge for TELCOs as the Return-On-Investment (ROI) period becomes too long. Also the telecom carriers have issues with the funding. Because of these reasons the TELCOs do not want to spend huge capital expenditure for new cell sites unless it is inevitable.

ii. New Site takes longer time to build & commission. Since Telecom is a fast paced industry any delay may cause huge loss in the revenue for the investors.

B. To utilize the existing towers for its full capacity.

There are thousands of towers which were built by the telecom carriers decades ago. That time these towers were built for stringent condition considering the future expansion. However these towers are not utilized to its full capacity which may be instant revenue generators for the TELCOs. However there are many challenges that the TELCOs face utilizing the existing tower. Many times the

site information, structural drawings are unavailable. In such cases, the Reverse Engineering process has to be carried out in order to get the missing information, analyze the tower and check whether the tower can withstand the existing and additional loading.

BACKGROUND

Communication has grown to be an essential infrastructure for socio-economic development in an increasingly knowledge intensive world. The reach of telecom services to all parts of the country is integral to development of an innovative and technologically driven society. Studies have shown that there is a positive correlation between the penetration of Internet and Mobile Services on the growth of GDP of a country. As a result of the measures taken by the Government over the years, the Indian Telecom Sector has grown exponentially and has become the second largest network in the world, next to China.

Tele-density:

Tele-density, which denotes the number of telephones per 100 population, is an indicator of telecom penetration in the country. Tele-density in the country, which was 73.32% as on 1st April, 2013, increased to 75.23% at the end of March 2014. The rural Tele-density increased from 41.05% to 44.01% during this period urban Tele-density, however, registered a decline from 146.64% to 145.46% during this period. The chart below indicates the trend in Tele-density over the years.

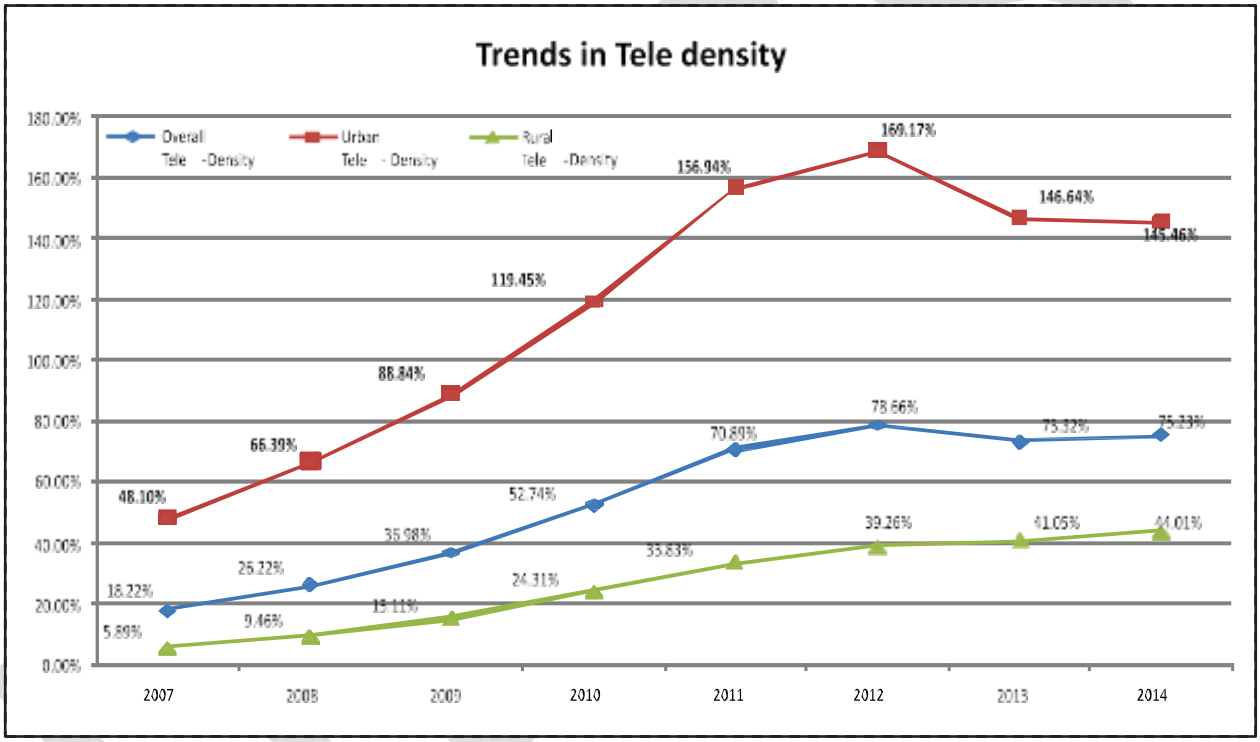

Growth Indicators / Key Statistics:

Indian telecom network is the second largest in the world after China. Following are the recent growth indicators/statistics/trends

- **Tele-density**: Overall Tele-density in the country is 75.23%. Urban Tele-density is 145.46%, whereas rural Tele-density is 44.01%.
- **Telephony**: The country has 933.02 million telephone connections. The number of telephony connection increased from 898.02 million in the beginning of the financial year to 933.02 million at the end of March 2014.
- Wireless Connections: 904.52 million-96.95%.of the total Telephones
- **Fixed / Wireline Connections:** 28.5 million-3.05 %.of the total Telephones
- The share of private sector in total telephones is 87.13%.
- Number of Broadband connections is 60.87 million

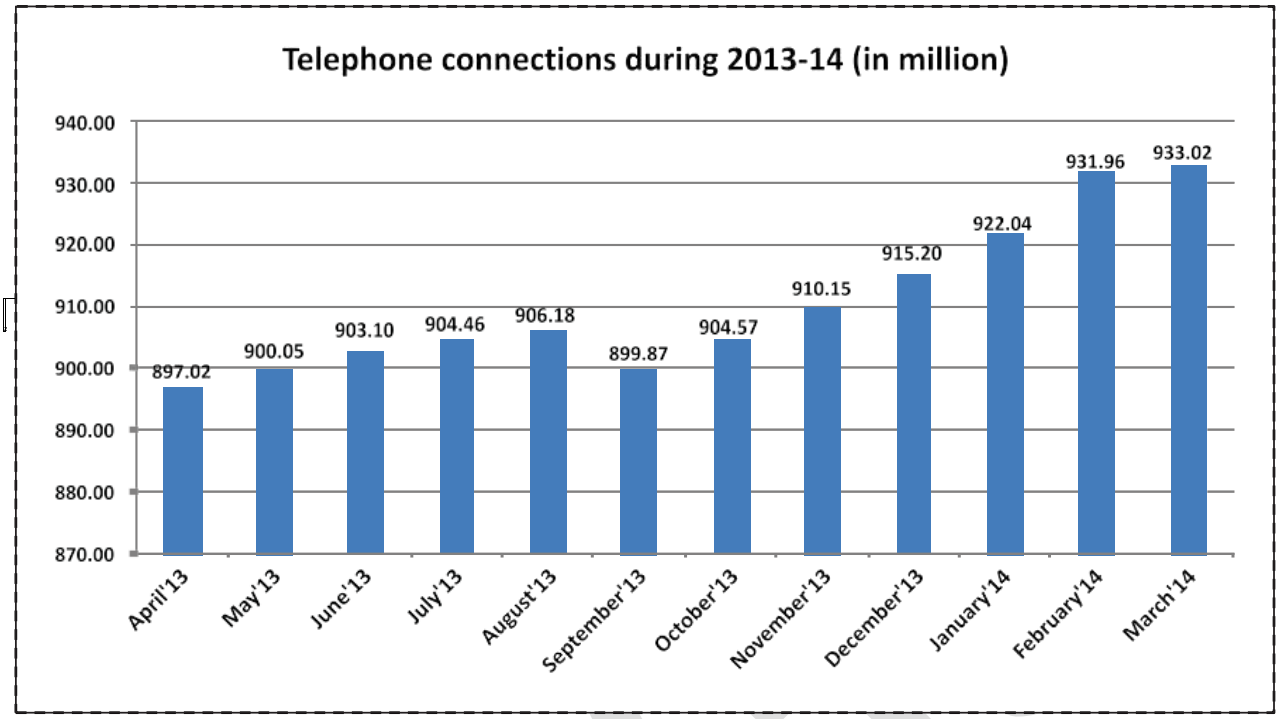

MODELLING OF TOWER:-

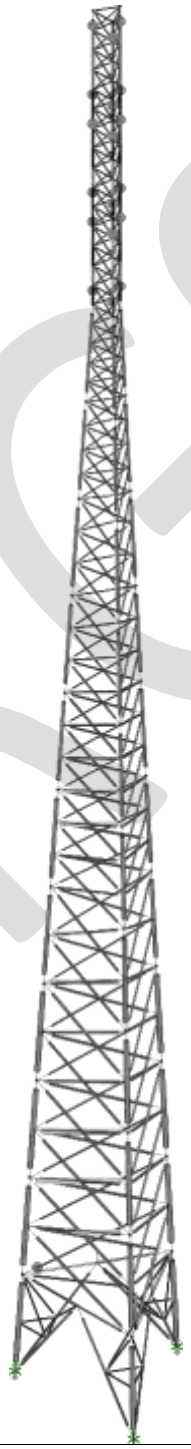

	RENDERED VIEW OF	DWG NO: 01
	280’ SELF SUPORTING TOWER	REV NO: 00
		Mar 24, 2015 at 3:29PM

ANALYSIS:-

Basic Tower Details:

· Type of Tower- Simply Supported 3-Legged Triangular
· Location- Wyandotte County, Kansas, USA
· Elevation- 280 ft (85.344m)
· Face Width at top- 4.67 ft (1.423 m)
· Base width- 27.75 ft (8.458 m)
· Basic Wind Speed- 90 mph (40.23 m/s)
· Structure Class II.
· Exposure Category C
· Topographic Category 1

The Tower has 14 panels each having section height 20ft. The Wind load on each section is calculated separately using TIA-222-G standard and it is assumed to act at Centre of Gravity (CG) of that section. The Wind Load acting on CG is divided into nodal loads for analysis purpose to get force on each member.

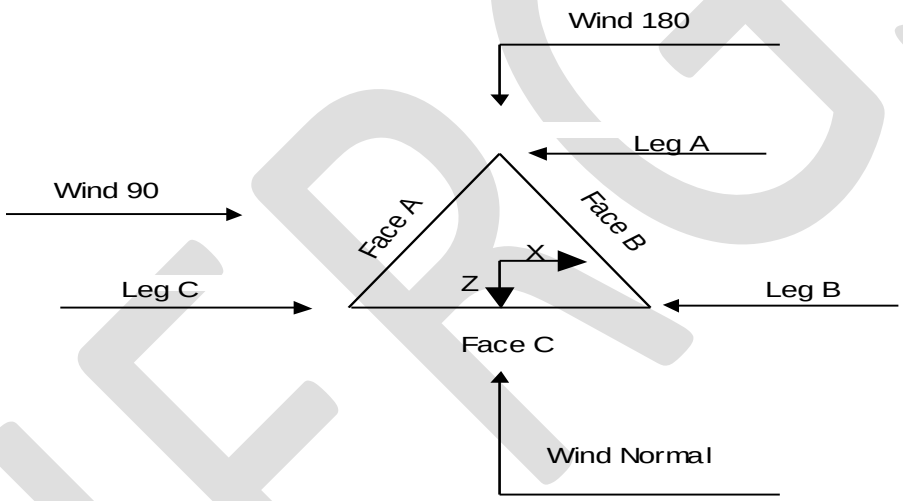

Triangular Tower

Tower Input Data

Tower Section	*Tower Elevation (ft)*	*Section Width (ft)*	*Section Length (ft)*	*Diagonal Spacing (ft)*	*Bracing Type*
T1	280.00-260.00	4.67	20.00	4.00	X Brace
T2	260.00-240.00	4.67	20.00	4.00	X Brace

Tower Section	*Tower Elevation (ft)*	*Section Width (ft)*	*Section Length (ft)*	*Diagonal Spacing (ft)*	*Bracing Type*
T3	240.00-220.00	4.67	20.00	4.00	X Brace
T4	220.00-200.00	4.67	20.00	4.00	X Brace
T5	200.00-180.00	6.76	20.00	5.00	X Brace
T6	180.00-160.00	8.86	20.00	6.67	X Brace
T7	160.00-140.00	10.96	20.00	6.67	X Brace
T8	140.00-120.00	13.06	20.00	6.67	X Brace
T9	120.00-100.00	15.16	20.00	6.67	X Brace
T10	100.00-80.00	17.26	20.00	10.00	X Brace
T11	80.00-60.00	19.36	20.00	10.00	X Brace
T12	60.00-40.00	21.45	20.00	10.00	X Brace
T13	40.00-20.00	23.55	20.00	10.00	X Brace
T14	20.00-0.00	25.65	20.00	20.00	K1 Down

Section capacity table

Section No.	*Elevation (ft)*	*Component Type*	*Size (inch)*	*Developed stress P (K)*	*Allowable stress $øP_{allow}$ (K)*	*% Capacity*	*Pass or Fail*
T1	280 - 260	Leg	P2x.154	-3.17	36.84	8.6	Pass
		Diagonal	L1 1/2x1 1/2x1/8	-0.55	5.51	10.1	Pass
		Top Girt	L1 1/2x1 1/2x1/8	-0.02	2.48	0.9	Pass
T2	260 - 240	Leg	P2x.154	-12.95	36.84	35.2	Pass
		Diagonal	L1 1/2x1 1/2x1/8	-1.38	5.51	25.1	Pass
T3	240 - 220	Leg	P2.5x.276	-56.06	83.25	67.3	Pass
		Diagonal	L1 1/2x1 1/2x1/8	-4.37	5.59	78.2	Pass

Section No.	***Elevation (ft)***	***Component Type***	***Size (inch)***	***Developed stress P (K)***	***Allowable stress $øP_{allow}$ (K)***	***% Capacity***	***Pass or Fail***
T4	220 - 200	Leg	P3x.3	-81.80	119.06	68.7	Pass
		Diagonal	L1 1/2x1 1/2x1/8	-2.16	3.44	62.6	Pass
T5	200 - 180	Leg	P3.5x.318	-100.57	141.80	70.9	Pass
		Diagonal	L1 3/4x1 3/4x1/8	-2.50	3.27	76.6	Pass
T6	180 - 160	Leg	P4x.337	-118.00	159.90	73.8	Pass
		Diagonal	L2x2x3/16	-3.11	4.46	69.7	Pass
T7	160 - 140	Leg	P5x.375	-136.61	239.38	57.1	Pass
		Diagonal	L2 1/2x2 1/2x3/16	-3.60	6.85	52.6	Pass
T8	140 - 120	Leg	P5x.375	-155.88	239.38	65.1	Pass
		Diagonal	L3x3x3/16	-4.27	9.35	45.7	Pass
T9	120 - 100	Leg	P6x.432	-176.44	343.09	51.4	Pass
		Diagonal	L3x3x3/16	-4.87	7.53	64.7	Pass
T10	100 - 80	Leg	P6x.432	-195.67	303.73	64.4	Pass
		Diagonal	L3x3x1/4	-5.85	6.98	83.8	Pass
T11	80 - 60	Leg	P8x.322	-216.78	334.41	64.8	Pass
		Diagonal	L3 1/2x3 1/2x1/4	-6.53	9.67	67.5	Pass
T12	60 - 40	Leg	P8x.322	-238.75	334.41	71.4	Pass
		Diagonal	L4x4x3/8	-7.44	17.98	41.4	Pass
T13	40 – 20	Leg	P8x.5	-261.67	505.53	51.8	Pass
		Diagonal	L4x4x3/8	-8.16	15.48	52.7	Pass
T14	20 – 0	Leg	P8x.5	-267.96	505.53	53.0	Pass
		Diagonal	P2.5x.276	-13.46	20.37	66.1	Pass

Section No.	***Elevation (ft)***	***Component Type***	***Size (inch)***	***Developed stress P (K)***	***Allowable stress $øP_{allow}$ (K)***	***% Capacity***	***Pass or Fail***
		Horizontal	P2.5x.203	-7.27	6.86	106.0	Fail ✗
		Redund.Horz 1 Bracing	P1.5x.145	-4.65	12.65	36.7	Pass
		Redund.Diag 1 Bracing	P1.5x.145	-4.21	4.09	102.8	Fail ✗
		Redund. Hip 1 Bracing	P1.5x.145	-0.03	11.59	0.3	Pass
		Redund. Hip Diagonal Bracing	P1.5x.145	-0.06	2.11	2.8	Pass
						Summary	
					Leg (T6)	73.8	Pass
					Diagonal (T10)	83.8	Pass
					Horizontal (T14)	**106.0**	**Fail ✗**
					Top Girt (T1)	0.9	Pass
					RedundHorz 1 Bracing (T14)	36.7	Pass
					RedundDiag 1 Bracing (T14)	**102.8**	**Fail ✗**
					Redund Hip 1 Bracing (T14)	0.3	Pass
					Redund Hip Diagonal Bracing (T14)	2.8	Pass
					RATING =	**106.0**	**Fail ✗**

RESULTS:-

From the above Section Capacity table, it is evident that the all the members of the tower are passing for the proposed LTE load and other loads, except two members i.e.

- T14-Horizontal member **Pipe P2.5x.203overstressed with 106.0%**
- T14-Redundant diagonal-1 bracing **Pipe P1.5x.145overstressed with 102.8%**

It is recommended to replace these members with the higher sections, in order to bring the stresses to the acceptable limit (below 100%). Since the overstress is marginal, we can increase the member thickness, without changing the overall diameter. As a result of this, there will not be any change on the tower loading as the exposed area remains the same. We just need to re-run the analysis / design in order to check the modified stress ratios of these members.

CASE STUDY I: OPTIMAL DESIGN OF LATTICE TOWERS MADE UP OF SOLID ROUND STEEL BARS [9]

The rational design of lattice steel towers made up of solid round steel bars affected by the static load are discussed.

Peterson, 1993

A large portion of such construction works are towers of a low and medium height. Lattice towers are portable, can be installed on roofs of buildings. Those towers are used for telecommunication facilities and other construction purposes as well. The behaviour and calculations of typical steel towers structures are broadly analyzed in numerous studies.

Smith, 2007

The efficiency of lattice steel tower is determined by their relatively simpler construction, low production and assembling cost. Wind pressure is considered as the predominant loading on tower structures. Therefore, Chords and Bracing members in towers most often are of round cross section.

Jasim, Galeb, 1998, 2002

The designing practice often makes the use of so called multivariate analysis in order to reduce the mass of structures. The mass or volume of steel in tower structures is selected as main criterion of quality while solving optimization problem.

Conclusions:

The tower under consideration gives the calculation of optimal values of tower width and inclination of bracing members, considering the towers height, steel grade and wind load intensity.

Tower's optimal width varies between (1/17)H and (1/55)H. The increase in the towers height also causes an increase in values of tower's optimal width. Higher wind load intensity demands for the increased spacing between chords.

As strength of the Steel increases, optimal width of the tower decreases. The optimal inclination of bracing members in a tower of round solid bar is virtually independent of towers height and wind load intensity. Its average value is 35 degrees

CASE STUDY II: - INFLUENCE OF MODELING IN THE RESPONSE OF STEEL LATTICE MOBILE TOWER UNDER WIND LOADING [10]

The tower under consideration in this case is Guyed Tower for radio antenna by finite element method in ANSYS using three different structural idealization of the model.

Sullins Eric James

Used ERI Tower software for wind and ice effects concluded that diagonal bracing tends to control the ability of the tower to withstand wind and ice loading.

Wind Load and Analysis of Lattice Towers

For assessing Dynamic Response of the towers, Indian code of standard and most of other countries worldwide recommends the use of GFM (Gust Factor Method) or GEFM (Gust Effectiveness Factor Method).

IS: 875 (Part 3) gives wind load on structure on a strip area A_e at a height z is,

$$F_z = C_f \times A_e \times P_z \times G$$

Where, C_f = Force co-efficient of the Structure

A_e = Effective Frontal Area considered for the structure at height z

P_z = Design Pressure at height z due to hourly mean wind obtained as $0.6v_z^2$

G = Gust factor

Above notations are as per IS: 875 (Part3)

There are three models adopted in this study and are discussed below:

a) Model-1 or Rigid Space Frame model in which members are considered as rigid jointed members.
b) Model-2 or Space Truss Model in which members are considered to be hanged permitting in plane rotation.

c) Model-3 or Combined or Hybrid models in which main leg members were rigid jointed and bracings are considered to be hinged.

Result:

Rigid frame model gives the least displacements exhibited by the truss model.

Conclusions:

The wind analysis results showed that irrespective of tower height, modelling strategy does not significantly affect the displacement pattern, particularly maximum lateral displacement at the top of the tower. Truss model, in general, reflects the lower bound on stresses, irrespective of height, due to dominance of the axial stresses. The bending components normal to the plane of the element are of lower order.

CASE STUDY III: WIND ANALYSIS OF MICROWAVE ANTENNA TOWERS [11]

The Telecommunication towers are triangular and square in plan, made up of standard angles and connected together by means of bolts and nuts.

The analysis of microwave antenna towers with Static and Gust Factor methods. The comparison is made between the towers with angle and square hollow sections. The displacement at the top of the tower is considered as the main parameter. The analysis is also done for different configuration by removing one member as present in the regular tower at lower panels.

Gomathianayagam, S, June 2000

Triangular towers attract lesser wind loads compared with square towers. But they are used only for smaller heights due to difficulties in joint detailing and fabrication using angle sections.

The use of tubular joints greatly improved the aesthetic qualities of the structural tube members provided a wide range of applications for a triangular cross section are used for truss members, the range of different standard shapes and sizes produced is much lesser than wide flange shapes and availability of some standard shapes is still limited.

N. Prasad Rao, September 2001

In order to reduce the unsupported length and to increase their buckling strength, the main legs and the bracing members are laterally supported at the intervals in between their end nodes using secondary bracings or redundant. These secondary bracings increase the buckling strength of the main compression members. K and X bracings with secondary bracings were commonly used in microwave towers.

For optimization of telecom towers, limiting the displacements and stresses to allowable limits optimizes the weight using different sections.

J.D. Holmes, 1994

The need to design a lattice tower considering resonant dynamic response to wind loads arises when their natural frequencies are low enough to be excited by the turbulence in the natural wind.

Abraham August 2005

The structural loads produced by wind gusts depend on size, natural frequency and damping of the structure in addition to the inherent wind turbulence. One of the approaches used for evaluating the dynamic response of lattice towers is the Gust Facto Method.

Conclusions:

The analysis of microwave antenna tower with different sections and configuration are done for wind loads. The following conclusions may be drawn from above analytical results. Square hollow sections can be used more effectively in leg members in comparison with the angle sections in regular tower under Static method and GFM. Square hollow sections used in bracings along with the leg members do not show much reduction of displacement compared to tower with square hollow sections used in leg members under Static method and GFM.

X and M bracing in square hollow sections for legs and bracings at the lower first panel shows a maximum reduction of displacement in the comparison with the tower with square hollow sections for legs and bracings in the lower second, lower first and second panel with different configuration in both static and GFM

ACKNOWLEDGMENT

We would like to thank our mentor Er. SESHENDRA KUMAR KURICHETI, Engineering Manager, Telecom Division, Pune for giving an opportunity to work on a case study of Telecom project which helped us to understand the areas of improvement technically and professionally. And also thankful to Prof. M.D.KEVADKAR, Head of Civil Engineering Department, for reviewing the manuscript and the valuable comments and suggestions he offered during the preparation of this paper.

CONCLUSION

The modified stress ratios which are obtained after structural modifications are tabulated below:

Section	Existing Member	Over Stress Ratio	Modified Member	New Stress Ratio
T14-Horizontal	Pipe P2.5x.203 (Grade 50 ksi)	106%	Pipe P2.5x.276	84.3%
T14- Redundant diagonal-1	Pipe P1.5x.145 (Grade 36 ksi)	102.8%	Pipe P1.5x.20	81.5%

DISCUSSION:

The main aim of the paper is to introduce the new methodological approach for the optimum utilization of existing towers and to use the existing towers to their full capacities. This can be checked and achieved by removing and adding additional proposed loads (Updated Antennas, Feedlines, Climbing ladders etc). The experiences obtained by different researchers in their studies of analysis and design of towers have been approached by three case studies that have been indicated above. Based on the observations discussed in these case studies the authors would like to draw the following conclusions:

1. The tower under consideration gives the calculation of optimal values of tower width and inclination of bracing members, considering the towers height, steel grade and wind load intensity.
2. As strength of the Steel increases, optimal width of the tower decreases. The optimal inclination of bracing members in a tower of round solid bar is virtually independent of towers height and wind load intensity. Its average value is 35 degrees.
3. The wind analysis results showed that irrespective of tower height, modeling strategy does not significantly affect the displacement pattern, particularly maximum lateral displacement at the top of the tower.
4. Truss model, in general, reflects the lower bound on stresses, irrespective of height, due to dominance of the axial stresses.
5. The bending components normal to the plane of the element are of lower order
6. Square hollow sections used in bracings along with the leg members do not show much reduction of displacement compared to tower with square hollow sections used in leg members under Static method and GFM

REFERENCES:

[1] TIA-222-G- Structural Standard for Antenna Supporting Structures and Antennas
[2] https:// www.google.co.in/
[3] https:// www.trai.gov.in/
[4] Singer's Engineering Mechanics (Statistics and Dynamics) (Third Edition) (SI units) (K. Vijaya Kumar Reddy, J. Suresh Kumar) (BS publications)
[5] Strength of Materials, (S.Ramamrutham and R.Narayan), Dhanpat Rai Publications
[6] Analysis of Structures Vol-2, (Theory, Design & Details of structures), (Prof. V. N. Vazirani, Dr. M. M. Ratwani, Dr. S.K. Duggal), (Khanna Publications)
[7] Design of Steel Structures, (Ram Chandra), (Standard book house Delhi6)
[8] Foundation Engineering, (P.C. Varghese) (PHI learning private limited New Delhi)
[9] Optimal Design of Lattice Towers made up of Solid Round Steel bars (Donatas Jatulis, Algirda Juozapaitis, Povilas Vainiunas)
[10] Influence of Modelling in the Responce of Steel Lattice Mobile Tower under Wind Loading (Richa Bhatt, A.D. Pandey, Vipul Prakash), Department of Civil Engineering, Indian Institute of Technology, Roorkee, India
[11] Wind Analysis of Microwave Antenna Towers, (Siddhesha. H, Lecturer, Department of Civil Engineering, S.I.T. Tumkur, Karnataka, India).
[12] Influence of Telecommunication Tower on the Response of Host Structure, Vikaskumar Pandey, N.G.Gore, P.J.Salunke, V.G.Sayagavi MGM's College of Engineering & Technology, Mumbai, Maharashtra

International Journal of Engineering Research and General Science Volume 3, Issue 3, Part-2 , May-June, 2015
ISSN 2091-2730

Effect of Quarry Dust and Fly Ash Mix on strength properties of M40 grade Concrete

Anjali H Jamale[1], Urmila R Kawade[2]

P.G.Student[1], Dept. of Civil Engg, P.D.V.V.P. College of Engineering, Ahmednagar, M.H., India, anjalidahatonde26@gmail.com,
Assosiate Professor[2], Dept. of Civil Engg, P.D.V.V.P. College of Engineering, Ahmednagar, M.H., India, urmilaanagar@gmail.com
Contact- 9420002271

Abstract— this paper presents the variation in the strength of concrete when replacing sand by quarry dust and also effect of inclusion of Fly Ash with the addition Quarry Dust. Slump cone test, carried out on fresh concrete to check the workability while compressive strength, flexural strength, split tensile strength was carried out on hardened concrete. The reduction in the sources of natural sand and the requirement for reduction in the cost of concrete production has resulted in the increased need to identify substitute material to sand as fine aggregates in the production of concretes. In such a situation the Quarry dust can be an economic alternative to the river sand. The study analyses the effect on strength characteristics by various % of quarry dust as a replacement of natural sand in M40 grade concrete and also the combination of various % of quarry dust and Fly ash as a replacement of natural sand and cement in M40 grade concrete. Natural sand is replaced by quarry dust with 0%, 15%, 35%, 55%, and 75% and in combination Natural sand is replaced by quarry dust with 0%, 15%, 35%, 55%, 75% & Cement replaced by fly ash with 0%, 5%, 10%, 15% and 20%. Compressive strength, split tensile strength, and flexural strength were conducted according to Indian standard code procedure. The effect of % of Quarry dust and fly ash in cement concrete is studied in detailed. Test results for each variation are tabulated and discussed in details and some important conclusions are made.

Keywords— Natural Sand, Quarry Dust, Fly Ash, Workability, Compressive strength, Split tensile strength, Flexural strength.

INTRODUCTION

Basic Ingredients of Conventional concrete are cement, sand and aggregate. Natural sand derived from river banks is mostly used as fine aggregate. Common river sand is expensive due to the excessive cost of transportation from natural sources. Also large-scale depletion of these sources creates environmental problems [1]. The reduction in the sources of natural sand and the requirement for reduction in the cost of concrete production has resulted in the increased need to identify substitute material to sand as fine aggregates in the production of concretes. In such a situation the dust can be an economic alternative to the river sand. Fly Ash which is a waste material can be used as filler material and helps reduce total voids content in concrete. The decrease in early Strength by the addition of fly ash is compensated by addition of quarry dust also decrease in workability of concrete due to addition of Quarry dust can be improved by addition of Fly ash[2]

MATERIALS USED & METHODOLOGY

A. *Cement:*

An ordinary Portland cement (opc 53 grade) was used.

B. *Fly Ash*

Class F fly ash was used

C. Natural sand

Natural river sand passing through 4.75 mm was used as fine aggregate and was tested following Is: 383-1970. The sand conformed to zone II

D. Aggregate

The aggregates were selected based on the limitation of IS 881 and 882 and the aggregate was 20 mm and 12.5 mm crushed granite. In the proportion of 60:40 percentage

E. *Quarry Dust*

Quarry dust is collected from local stone crushing units of Ahmednagar, Maharashtra. The physical properties of Quarry dust obtained by testing the sample as per IS standard

F. *Water*

Potable tap water available in lab was used for casting and curing of concrete

G. *Admixture*

Commercially available super plasticizer is used

The physical properties of natural, coarse aggregate and quarry dust are mentioned in Table no I

TABLE NO I: PHYSICAL PROPERTY OF AGGREGATES

SR. NO	PROPERTY	RESULT FOR SAND	RESULT FOR QUARRY DUST	RESULT FOR COARSE AGGREGATE
1	Particle Shape	Round	Flaky	Flaky
2	Fineness Modulus	3.177	2.23	2.65
3	Specific Gravity	2.67	2.97	3.39
4	Bulk density	1793 Kg/m3	1893 Kg/m^3	1603 Kg/ mm^3
5	Surface moisture	Nil	Nil	Nil
6	Crushing value	-	-	15.9%
7	Impact value	-	-	6.67%

h. *Mix Proportioning:*

The mix design is done according to the IS design method
M 40 Grade concrete having mix proportion 1:1.707:3.62 was used with 0.4 W/ C ratios

h. Concrete Mixes

In this study, the early age properties of fresh concrete and mechanical performance and tensile strength of hardened concrete were examined. All tests were conducted using the following sample groups:

1. Conventional concrete,
2. Sand is replaced by Quarry dust with 15%, 35%, 55% and 75%.
3. Replacement of sand by Quarry dust and cement by Fly Ash together for various % that is (15%QD+5%FA, 35%QD+10%FA, 55%QD +15%FA and 75%QD +20% FA).
3. Each of the above samples was tested for compressive strength, split tensile strength and workability tests.

The compressive, split tensile strength and flexural strength test on hardened concrete were performed on Universal testing machine. Concrete cubes of size 150×150×150mm were cast. Total 81 cubes were casted for determination of compressive strength. Compressive strength of concrete cubes was tested at 3 days, 7 days and 28 days. Total 27 concrete cylinders were casted for determination of split tensile strength and tests were taken at 28 days. Total 27 beam specimens were casted to determine flexural strength and the beam specimens were tested at 28 days.

RESULTS & DISCUSSION

A. Workability:

Various mixes of freshly mixed concrete were tested for workability by slump value. It was observed that, the workability decreases with increase in Quarry dust content in the mix. The mix with cement as the only binder, the workability was medium. As per the table below it shows that there is in increase in workability with the inclusion of Fly ash

TABLE NO II: WORKABILITY OF CONCRETE MIX

SR. NO.	QUARRY DUST CONTENT	FLY ASH CONTENT	SLUMP OF CONCRETE
1.	0%	0%	95mm
2	15%	0%	89mm
3	35%	0%	78mm
4	55%	0%	67mm
5	75%	0%	55mm
6	15%	5%	93mm
7	35%	10%	86mm
8	55%	15%	78mm
9	75%	20%	70mm

B. compressive strength:

Various mixes of concrete were tested for compressive test. Max compressive strength value at 28th day is obtained at 15% replacement of sand by QD is 45.18 Mpa. Compressive strength with 35% replacement of sand by quarry dust is 43.97 Mpa nearly equal to the compressive strength of CC which is 44.05 Mpa. And for the combination of Quarry Dust and Fly Ash, max compressive strength obtained at 15% QD and 5% FA is 44.78 Mpa.

TABLE. NO III: 3, 7, 28 DAYS COMPRESSIVE STRENGTH OF CONCRETE MIX

SR. NO.	SAND REPLACEMENT BY QUARRY DUST	CEMENT REPLACEMENT BY FLY ASH CONTENT	3DAYS COMPRESSIVE STRENGTH (N/MM^2)	7DAYS COMPRESSIVE STRENGTH (N/MM^2)	28DAYS COMPRESSIVE STRENGTH (N/MM^2))
1	0%	0%	24.78	34.39	44.05
2	15%	0%	25.85	35.05	45.18
3	35%	0%	29.91	35.39	43.97
4	55%	0%	25.44	33.31	40.91
5	75%	0%	23.61	31.13	39.32
6	15%	5%	22.47	32.26	44.78
7	35%	10%	20.14	31.36	42.93
8	55%	15%	20.37	30.46	39.64
9	75%	20%	19.84	29.27	38.22

TABLE NO IV: COMPARISION OF 28 DAYS COMPRESSIVE STRENGTH OF THE CUBES CASTED FOR CC & VARIOUS REPLACEMENT % OF QD AND COMBINATION OF QD AND FA.

SR. NO.	REPLACEMENT OF SAND BY Q.D. (%)	COMPRESSIVE STRENGTH OF 28 DAYS (MPA)	REPLACEMENT OF SAND BY Q D.AND CEMENT BY FA (%)	COMPRESSIVE STRENGTH OF28 DAYS (MPA)
1	0%	44.05	0%	44.05
2	15%	45.18	15%QD5%FA	44.78
3	35%	43.97	35%QD10%FA	42.93
4	55%	40.91	55%QD15%FA	39.64
5	75%	39.32	75%QD20%FA	38.22

Fig no 1 present the 3, 7, 28 days compressive strength for various proportions of mixes. 3 days and 7 days compressive strength is max for 35% QD and 28 days compressive strength is max for 15% QD content from the fig it is also observed that with the addition of fly ash or increase in % of FA causes decease in compressive strength

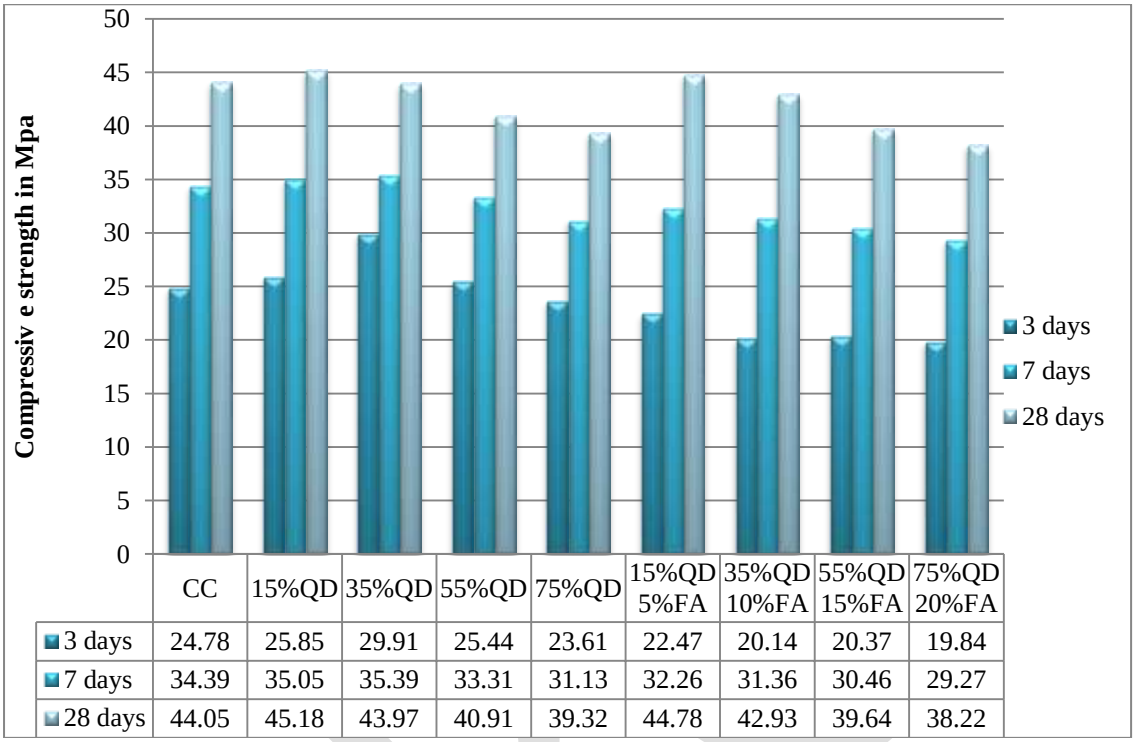

	CC	15%QD	35%QD	55%QD	75%QD	15%QD 5%FA	35%QD 10%FA	55%QD 15%FA	75%QD 20%FA
3 days	24.78	25.85	29.91	25.44	23.61	22.47	20.14	20.37	19.84
7 days	34.39	35.05	35.39	33.31	31.13	32.26	31.36	30.46	29.27
28 days	44.05	45.18	43.97	40.91	39.32	44.78	42.93	39.64	38.22

CC-Conventional concrete, QD- Quarry Dust, FA- Fly Ash

Fig no 1: 3, 7, 28 days compressive strength of the cubes casted for CC, various % of QD and combination of QD and FA.

Fig. 2 shows the comparison of 28 days compressive strength for various proportion which indicate that as the Quarry dust content increases compressive strength decreases still the compressive strength of 15%QD and combination of (15%QD & 5%FA) content is max as compare to conventional concrete

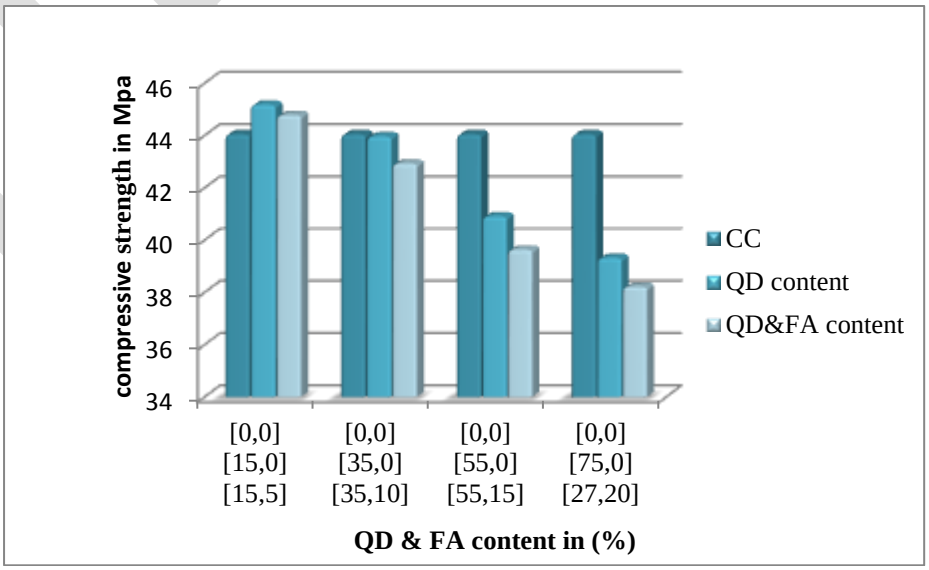

CC-Conventional concrete, QD- Quarry Dust, FA- Fly Ash

Fig NO 2: Comparison of 28 days compressive strength of the cubes casted for CC Various % of QD and Combination of QD and FA.

C Split tensile strength:

Various mixes of concrete were tested for compressive test. It was observed that, the workability decreases with increase in

TABLE NO V: COMPARISON OF 28 DAYS SPLIT TENSILE STRENGTH OF THE CUBES CASTED FOR CC AND VARIOUS % OF QD .AND COMBINATION OF QD AND FA

SR. NO.	REPLACEMENT OF SAND BY Q.D. (%)	SPLIT TENSILE STRENGTH OF CC (MPA)	REPLACEMENT OF SAND AND CEMENT BY Q.D AND FA (%)	SPLIT TENSILE STRENGTH (MPA)
1	0%	4.24	0%	4.24
2	15%	5.35	15%QD5%FA	4.71
3	35%	4.74	35%QD10%FA	4.48
4	55%	4.60	55%QD15%FA	4.43
5	75%	4.38	75%QD20%FA	4.24

Fig.3 shows the comparison of 28 days split tensile strength for various proportion which indicate that as the Quarry dust content increases Split tensile strength decreases still the split tensile strength of up to 75%QD and combination of (55%QD &15%FA) content is max as compare to conventional concrete

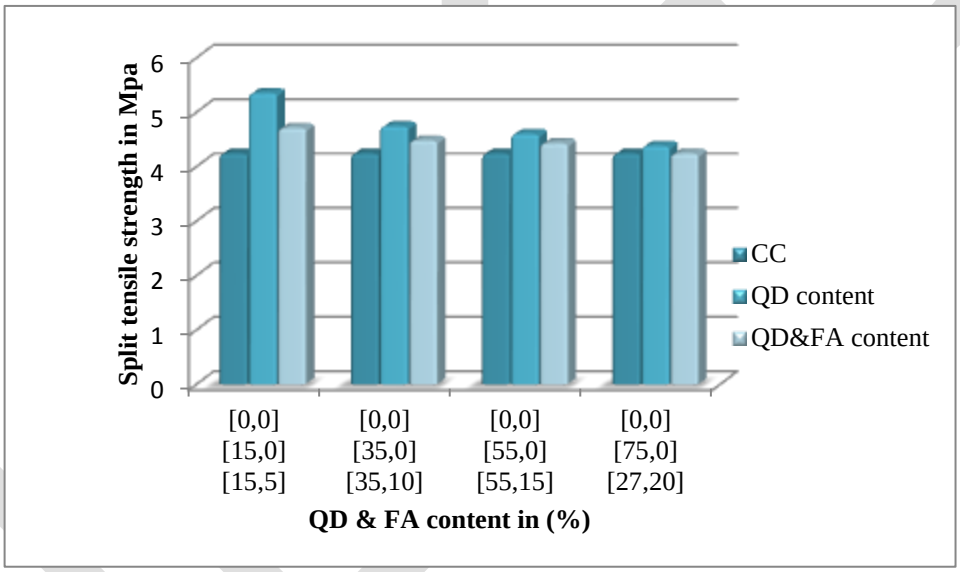

CC-Conventional concrete, QD- Quarry Dust, FA- Fly Ash

Fig. no 3: 28 days Split tensile strength of the cubes casted for CC and Various % of QD and FA.

D Flexural strength:

Various mixes of concrete were tested for compressive test. It was observed that, the workability decreases with increase in

TABLE NO VI: COMPARISON OF 28 DAYS FLEXURAL STRENGTH OF THE CUBES CASTED FOR CC AND VARIOUS % OF QD. AND COMBINATION OF QD AND FA

SR. NO.	REPLACEMENT OF SAND BY Q.D. (%)	FLEXXURAL STRENGTH OF CC (MPA)	REPLACEMENT OF SAND AND CEMENT BY Q.D AND FA (%)	FLEXURE TEST RESULT (MPA)
1	0%	5.52	0%	5.52
2	15%	6.25	15%QD5%FA	5.63
3	35%	5.65	35%QD10%FA	5.58
4	55%	5.48	55%QD15%FA	5.40
5	75%	5.18	75%QD20%FA	4.93

Fig.4: shows the comparison of 28 days Flexural strength for various proportion which indicate that as the Quarry dust content increases Flexural strength decreases still the Flexural strength up to 35% QD and combination of (35% QD &10% FA) content is max as compare to conventional concrete

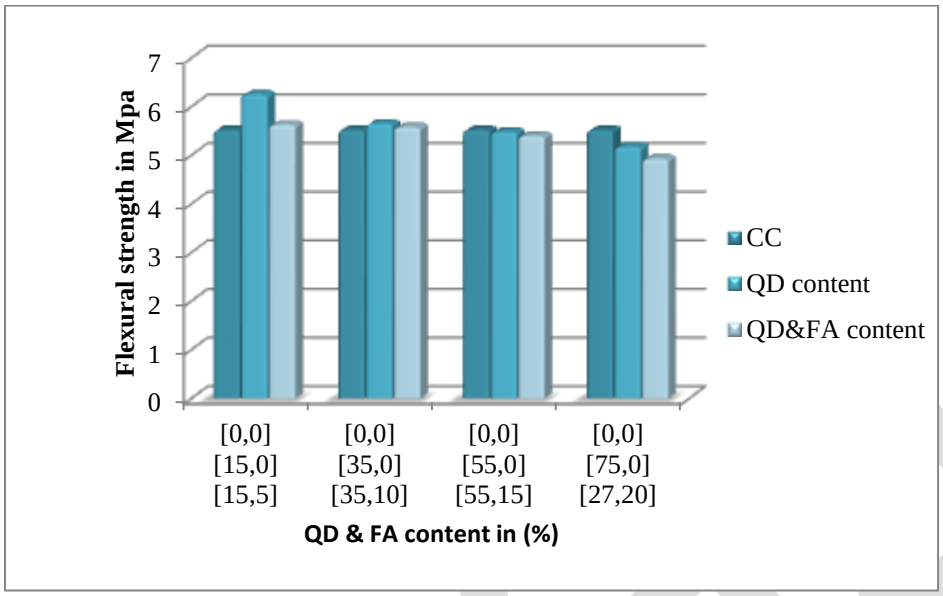

QD- Quarry Dust, FA- Fly Ash, CC- conventional concrete

Fig. no 4: 28 days Flexural strength of the cubes casted for CC and Various % of QD and FA

CONCLUSION

- As the sand is not available or use of sand creates environmental problems need to find alternative material. Quarry dust is a waste material from stone crusher plant as per physical properties of Quarry dust, it is a suitable substitute for sand at very low cost.
- QD and FA are the waste material so as per the environmental impact view use of waste material is helpful to maintain effective sustainable development
- From the above result it is concluded that use of QD causes decrease in workability but addition of fly ash is useful to improve workability and also loss in early strength due to fly ash can be improved by the use of QD. So it is beneficial to use both materials together.
- Optimum percentage of QD for max values for various strength in cement concrete is 15%. Even though sand can be replaced up to 35% quarry dust
- Optimum percentage of combination of QD and FA for max values of various strength in concrete is 15% QD and 5%FA.
- For the split tensile strength result up to75%QD shows greater strength than CC As compare to all characteristics strengths max replacement of QD can be possible to achieve split tensile strength when it is compared with CC
- Hence as per the results obtained, it can be suggested that use of quarry dust as a replacement for sand will be beneficial.

REFERENCES:

[1] R. Ilangovana, N. Mahendrana, and K. Nagamanib , "Strenght and Durability Properties of Concrete Containing Quarry Dust as Fine Aggregate", ARPN Journal of Engineering and Applied Sciences VOL. 3, NO. 5, OCTOBER 2008, ISSN 1819-6608

[2] A Krishnamoorthi, and G.Mohankumar, "Properties Of Green concrete Mix by Concurrent Mix of Fly Ash and Quarry Dust", IOSR Journal of Engineering (IOSRJEN) Vol. 3 Issue 8 (Augaust. 2013).V3 PP 48- 54

[3] Robert Bakker, Edwin Keijsers, and Hans van der Beak "Alternative Concepts and Technologies for Beneficial Utilization of Rice Straw" Wageningen UR Food & Biobased Research ,Number Food & Biobased Research number 1176 ,ISBN-number 978-90-8585-755-6,December 31st, 2009

[4] Chandana Sukesh, Katakam Bala Krishna, P.Sri Lakshmi Sai Teja, S.Kanakambara Rao., "Partial Replacement of Sand with Quarry Dust in Concrete", International Journal of Innovative Technology and Exploring Engineering (IJITEE) ISSN: 2278-3075, Volume-2, Issue-6, May 2013

[5] Lohani T. K. Etal, "Optimum utilization of Quarry dust as partial replacement of sand in concrete" Int. Journal of Applied Science and Engineering Research. Vol. 1 No 2, 2012(IJASER) ISSN2277- 9442

[6] Dr P. B. Sakthivel, C.Ramya, M Raj, "An Innovative Method of Replacing River Sand by Quarry Dust Waste in Concrete for sustainability", International Journal of Scientific & Engineering Research Volume 4, Issue 5, May-2013, ISSN 2229-5518

[7] Anitha selva sofia S.D., Gayathri R., SwathiG.,"Prince arulraj G., ,Experimental Investigation on Quarry Dust Concrete with Chemical Admixure". International Journal of Latest Research in Science and Technology Volume 2,Issue 2 :Page No.91-94, March - April (2013), ISSN (Online):2278-5299

[8] Prof M Devi, prof V. Rajkumar, Dr K. Kanan, "Inhibitive Effect of Organic Inhibitors in Concrete Containing Quarry Dust as Fine Aggregate", International Journal of Advances in Engineering Sciences Vol.2, Issue 1, Jan, 2012

[9] Er. Lakhan Nagpal, Arvind Dewangan, Er Sandeep Dhiman, Er. Sumit Kumar, "Evaluation of Strength Characteristics of Conrete Using Crushed Stone Dust as Fine Aggregate", International Journal of Innovative Technology and Exploring Engineering (IJITEE) ISSN: 2278-3075, Volume-2 Issue-6, May 2013

[10] Sudhir S.Kapgate And S.R.Satone, "Effect of Quarry Dust as Partial replacement of sand in Concrete" Indian Streams Research Journal Volume 3, Issue. 5, June. 2013 ISSN:-2230-7850

[11] A. Sivakumar and Prakash M., "Characteristic studies on the mechanical properties of quarry dust addition in conventional concrete," Journal of Civil Engineering and Construction Technology Vol. 2(10), pp. 218-235, October 2011 ISSN 2141-2634 ©2011 Academic Journals

[12] Dr. M Devi, "Significance of Fibres in Enhancing Strength and Corrosion Resistance of Fly Ash Blended Quarry Dust Concrete", International Conference on Biological, Civil and Environmental Engineering (BCEE-2014) March 17-18, 2014 Dubai (UAE)

[13] Manguru G.n., Karugu C.K.,Oyawa,W.O., Abuodha S.O. and Mulu P.U.," Partial Replacement of Natural River Sand with Crushed Rock Sand in Concrete Production", Research, Vol. 1, No. 2, 2012

[14] IS 2386: Part 3: "Methods of Test for Aggregates for Concrete" Part 3, 1963.

[15] IS 4031: Part 4: "Methods for physical test for hydraulic cements", Bureau of Indian standards, New Delhi, 1988.

[16] IS 516:1959, "Method of Test for Strength of Concrete", Reaffirmed 2004, Bureau of Indian standards, New Delhi

International Journal of Engineering Research and General Science Volume 3, Issue 3, Part-2 , May-June, 2015
ISSN 2091-2730

ARM- Based Pesticide Spraying Robot

Snehal M. Deshmukh
Electronics -VLSI
BVDUCOE
PUNE, INDIA
deshmukhsnehal05@rediffmail.com

Dr.S.R.Gengaje
Head and Professor
Dept' of Electronics
WIT COE
SOLAPUR, INDIA
srgengaje@rediffmail.com

ABSTRACT- In agriculture robots are deployed for agricultural purposes. The main use of robots in agriculture is for harvesting , Fruit picking , driverless tractor or sprayer are design to supersede human labor. Main aim is to avoid manual spraying of pesticides at actual farm. It will achieve by replacing human by a robot, through transmission of video of crop to central station. Then central station will control movements of the robot and spraying of the pesticides, using processor in real time. This will reduce the excessive use of pesticide for plant.

KEYWORDS-- Robotics, Agro-technology, Agricultural terms, Mechanical assembly, ARM-LPC2148, Pesticide

I. INTRODUCTION

The main businesses of Indian people is agriculture and the economy of the nation is decided by agriculture .The agriculture production is being stimulated by various environmental parameters like temperature, rain and other weather parameters in factors such as quality and quantity that are beyond control. The productivity of the crop is affected by other major biological parameters such as pests, disease and these parameters can be controlled by human beings for improvising the production of crop.

The purpose of agricultural robotics is not only to apply robotics technologies on the field of agriculture but withal to utilize the agricultural challenges to develop incipient techniques and systems. Robots are taking over more and more functions from humans where precision and repeatability in routine tasks are needed and where human workers are exposed to peril. One such task is cultivation of crops in fields and greenhouses where human operators still manually perform most operations on the crop albeit they are often highly perpetual and sometime even perilous.

Autonomous mobile robots and their systems are relegated as a component of the Precision Agriculture, which aims to optimize agricultural field management fixating on the enhancement of crop cognizance, environmental auspice and economics Researches on utilizing autonomous mobile robots for sundry tasks in greenhouse environment are being performed for over several decades, but only recent advances in embedded control systems, optical plant apperception and localization methods sanctioned develop individual robots and cooperative robot systems (colonies of robots) yare for in-field tasks. Wherewith topics such as design of grippers, sprayers, weed control and other plant harvesting and of the area under surveillance can be captured with camera.

II. PROPOSED SYSTEM

This paper introduces implementation of a robot for agricultural predicated, here robot perpetually scan the crop. Wireless Camera mounted on robot which take the video of the crops and send video to the central station. The person seated in the central station is deciding the action of robot. When the utilizer found that the crop is defected then it will give command to robot and according to that robot's kineticism will done and it will spray the pesticides over the crop. This transmission will do by RF transceiver.

III. ROBOTICS

A robot is a programmable machine which does certain tasks .we can be reprogrammed as per utilizer requisite. Fundamentally it is an electromechanical system.

Agricultural robotics: this technology uses sundry automation techniques in bio-systems such as agriculture, forestry and fisheries.

Different types of robots:

Autonomous robots: these robots work entirely under the control of computer program. Sundry sensors are habituated to amass the data about their circumventions.

Tele-controlled robots: these robots work under the guidance of either computer programs or humans. [6].

Remote-controlled robots can be controlled by users with a controller such as joystick, TV remote or other hand-held contrivance.

Robots used in Agriculture field:

- **Demeter (for harvesting):** it is a robot utilized for cutting crops. It looks akin to a mundane harvester, but it drive itself without any human supervision.[6].
- **Weed controller**: it does the task of weed abstracting.[6].
- **Forester Robot:** it is a particular type of robot utilized for cutting up of wood.[6].
- **Fruit picking robot:** The fruit picking robots need to pick ripe fruit without damaging the branches or leaves of the tree. The robots must be able to access all areas of the tree being harvested. The robot can distinguish between fruit and leaves by utilizing video image capturing.[6].

IV. BLOCK DIAGRAM

The main objective of this paper is to develop "Pesticide spraying robot using ARM- LPC2148", which helps to avoid manual spraying in farm. This will help to minimize the excessive pests over the crop in an agricultural field. The proposed system work can be divided into two units- One Robot section and other is Central Station.

Robot section: The robot module consists of ARM-LPC2148, spraying machine, motor driver IC, DC motors, Zigbee and wireless camera.

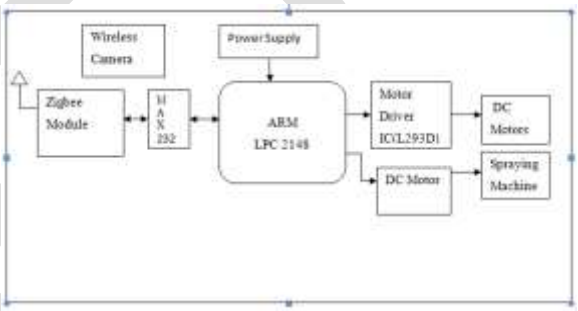

Fig. IV .1 Robot section block diagram

Robot continuously monitors the field of farm and sends the video to central station by camera. Camera will consistently capture the video and send it to central station using Zigbee. Robot consists of different module such as ARM LPC2148, RF transceiver-Zigbee, DC motors. LPC2148 will control the angle of rotation of DC Motors to position the cannon aiming at the intruding object. At last cannon will get fired. DC motor which used for moving the robot left, right, forward, backward direction. The speed of the Motor is controlled by the help of relay. The motor is used here to rotate the wheels. Actually a set of 2 DC motors are require to move in different directions.

Central Station: This section includes PC, Zigbee Module.

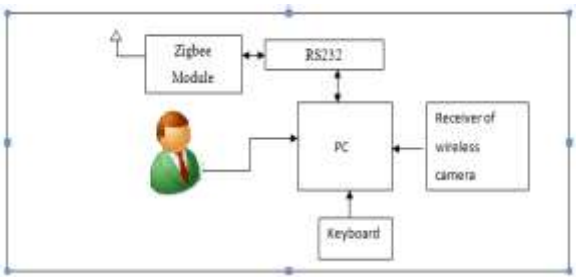

Fig. IV.2 Central station block diagram

As the central station gets the image input from camera, it will start next process. Person whose is setting in central station will continuously monitor the video on PC. If the image shows the leaf is affected by disease, person will send commands to robot. This will be received by robot through wireless module on it. ARM LPC2148 is programmed in such a way that, if it receives commands, it will move accordingly and spray the pesticide on affected part of leaf. If the image will not show any diseased part, it will move forward and not spray the pesticide. Process continues until the triggering of image capture is in process.

ARM LPC 2148: The LPC2148 micro-controllers are based on a 32/16 bit ARM7TDMI-S CPU core. They have real-time emulation and embedded trace support; it has flash memory of 512 kB. A 128-bit wide memory interface and unique accelerator architecture enable 32-bit code execution at the maximum clock rate.

Zigbee:

Zigbee standard is IEEE 802.14.5. This standard provide both physical and medium access control layer for low rate wireless sensor network. The Physical layer three frequency band with different data rates 2,450MHZ, 915MHZ, 868MHZ. Zigbee support both physical and application layer. Zigbee used in low data rate application that require high battery power and secure system. Zigbee range is up to 300meter and rate of data transmission and reception is around 225kbps. Application of Zigbee is in wireless light switches, traffic management system. Other application in agriculture and food demand. It is used for RF transceiver purpose.

DC Motors: It is used for robot movement and for spraying action.

Wireless camera: It captures the crop video and sends it to the central station.

Spraying Machine: It is used for spraying pesticide.

V. RESULTS

Fig. V.1. Assembly of system

Fig. V. 2. GUI of Robot Movement

Fig. V.3 . video captured by wireless camera

VI. CONCLUSION

These system most commonly used for agriculture application to reduce the man power. It is possible to implement the real time system by using ARM LPC2148. The system has the advantage of high speed, high quality and processing precision and low cost.

The future scope of this system will be design the system by using smartness of robot.

As per area of the farm increase the capacity of the pesticide's tank.

REFERENCES:

[1] Tao Liu, Bin Zhang, Jixing Jia,"Electromagnetic navigation system design of the green house spraying robot" ,IEEE(2014).

[2]. Gholap Dipak Dattatraya1, More Vaibhav Mhatardev, Lokhande Manojkumar Shrihari, Prof. Joshi S.G "Robotic Agriculture Machine", International Journal of Innovative Research in Science, Engineering and Technology, Volume 3, Special Issue 4, April 2014.

[3]. Sajjad Yaghoubi,Negar Ali Akbarzadeh, Shadi Sadeghi Bazargani, Sama Sadeghi Bazargani, Marjan Bamizan,Maryan Irani AS1 ," Autonomous Robots for Agricultural tasks and farm assignment and future trends in Agro Robots", IJMME-IJENS Vol.13 No.03(2013).

[4]. K. Prema, N.Senthil Kumar, S.S.Dash ,Sudhakar Chowdary, 'Online control of remote operated agricultural Robot using Fuzzy Processor and Virtual Instrumentation",IEEE(2012).

[5]. John Billingsley,"Agricultural Robotics ", IEEE Robotics & Automation Magazine (2009).

[6]. Agricultural Robots Presentation by Hamayal Wajid Lodhi Aleena Ahmed Khan Maria Aziz

[7]. Alireza Rafiq1, Davood kalantari2*, Hamid Mashhadimeyghani3," **Construction and development of an automatic sprayer for greenhouse",** CIGR Journal, June 2014.

[8]. Julián Sánchez-Hermosilla1, Francisco Rodríguez2, Ramón González2,

José Luís Guzmán2 and Manuel Berenguel2

," A mechatronic description of an autonomous mobile robot for agricultural tasks in greenhouses".

[9]. P.D.P.R.Harsh Vardhan1, S.Dheepak2, P.T.Aditya3, Sanjivi Arul4,"
DEVELOPMENT OF AUTOMATED AERIAL PESTICIDE SPRAYER",IJRET, April 2014.

[10]. Philip J. Sammons, Tomonari Furukawa and Andrew Bulgin," Autonomous Pesticide Spraying Robot for use in a Greenhouse",September 2005.

[11]. Autonomous Agricultural Robot: towards robust autonomy,by Martin Holm Pedersen

Jens Lund Jensen.

[12]. Sun Ming,Li Minzan. Agricultural Robot(II).Beijing:China Agriculture University Press,2009

International Journal of Engineering Research and General Science Volume 3, Issue 3, Part-2 , May-June, 2015
ISSN 2091-2730

Analysis and Optimization of parameters for casting ductile iron pipes

Mr. Karan Thacker, Prof. Himanshu Joshi, Prof. N.J. Patel

P.G. Scholar, HJD-ITR Kera-Kutch;Karan.thacker1988@yahoo.com; 9428684039

Abstract—Ductile iron Pipes are casted by Horizontal centrifugal process in which liquid iron is filled through an open channel into a fast rotating mould that is slightly tilted. The mould is water cooled from outside. In order to distribute the metal, the spinning mould including its cooling system is shifted axially in a controlled movement. The quality of ductile iron pipe largely depends on microstructure as well as mechanical properties like Ferrite %, Carbide %, Elongation % and Hardness. These can be improved by analyze and optimize the process parameters during the casting process. In this research paper, Design of Experiment (DOE) based Taguchi Method is used to analyze and optimize the parameters like Pouring molten metal Temperature, Inoculation Quantity and inlet cooling water flow rate. By using Taguchi Method L16 orthogonal array is generated in MINITAB 17 and responses are analyzed by experimental work at different levels of factors. From S/N ratio the best combination of parameters are analyzed by which the predicted Taguchi result is generated. The confirmation experimental test is done and predicted result is compared with actual results. Also the Significance of factors and interactions of parameters are analyzed by Analysis of variance (ANOVA). By performing all this an attempt has made to analyze and optimize the parameters to improve the pipe quality and its life by supplying optimized resources.

Keywords— Ductile iron pipes, Centrifugal casting , Mechanical properties, Microstructure, analysis and optimization of processing parameters, Design of Experiments(DOE), Taguchi Method, Analysis of Variance(ANOVA).

INTRODUCTION

1.1 Ductile iron

Ductile Iron also referred to as **"Nodular Iron"** or Spheroid graphite iron was patented in 1948.After a decade of intensive development work in the 1950's, ductile iron had a Phenomenal increase in the use as an engineering material during the 1960's, and the rapid Increase in commercial application continues today. The word ductile comes from the Latin "ducere" which means pliable and that means malleable. In static calculations, pipes in ductile iron are therefore considered as having piable properties or being flexible pipes. An unusual combination of properties is obtained in ductile iron because the graphite occurs as spheroids rather than as graphite flakes as in grey iron. This mode of solidification is obtained by adding a very small, but specific amount of Mg & Ce or both to molten iron of proper composition are added Mg reacts with S or O in the melt or molten iron and the way the graphite is formed. Control procedures have been developed to make the processing of ductile iron dependable.

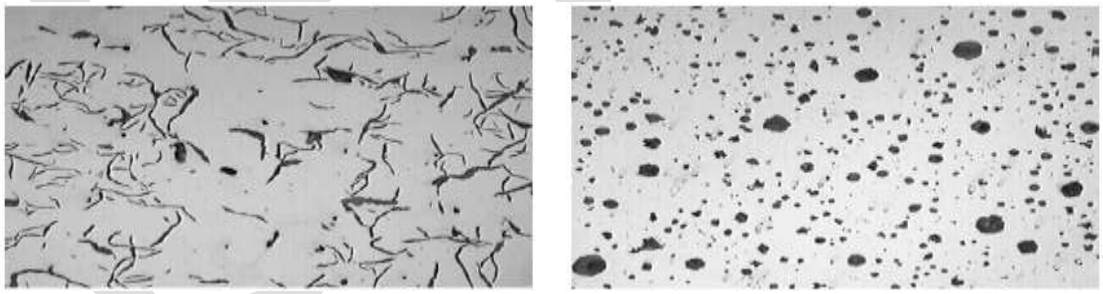

Figure 1.1: Comparison of microstructure of gray cast iron pipes and ductile iron pipes

Engineering applications of cast iron have been traditionally based upon gray (Flake graphite) irons providing a range of tensile strengths between about 150 N/mm^2 and 400 N/mm^2 with recommended design stresses in tensile applications of 0.25*tensile strength. Despite their limited strength gray irons provided very useful combinations of properties, which have ensured there wide continuing use. In fact gray irons still account for nearly 70 % of all iron castings produced. In contrast ductile irons have tensile strengths ranging from 350 to 1500 N/mm^2 with good elongation and high toughness.

1.2 Evolution of ductile iron pipes

In 1918 centrifugal casting process which revolutionised pipe production is introduced. The use of centrifugal force of rotating mould eliminated need for centre core and water-cooled metal mould permitted repetitively casting at high production rate.

With the advances in metallurgy, melting controls, chemical composition and spectrometer laboratories gray iron pipe progressively improved and its strength increased when discovery of ductile iron was announced. Some pipe producers suggest no need for it, since gray iron had served well and was stronger that other competitive pipe materials. At the start some companies experimented with ductile iron and some trial orders were produced for special applications and evaluations. The experiments were very much favourable.

After successful trials, number of experiments was done on ductile iron pipes for various improvements regarding the properties, thickness, pressure analysis, weights etc. These tests verify the superior quality of ductile iron pipe which permitted reduction in thickness, reduction in cost etc. Thus ductile iron pipe replace the grey cast iron pipes and its demand progressively increased.

1.3 Ductile iron pipes

Ductile iron pipe have been produced since 1951. It is spheroidal graphite formation which makes extreme malleability and stretching ability possible with ductile iron pipes. With the improvement in metallurgy of cast iron, the condition is met for the use of ductile iron pipe systems in nearly all areas of urban piping infrastructure.

Ductile iron pipes are made of ductile iron commonly used for water transmission and distribution. Ductile iron pipes are the direct development of cast iron pipes which were used in earlier years for water transmission. The Ductile iron used to manufacture the ductile iron pipe is characterized by spheroidal or nodular nature of graphite within it. Chemically Ductile iron pipe is same as gray cast iron pipe but the main difference between both of them is in gray cast iron pipe the graphite is present in the form of graphite flakes while in ductile iron pipe the graphite is present in the form of nodules which give it the tensile strength 350 N/mm^2 to 1500 N/mm^2 rather than 150 N/mm^2 to 400 N/mm^2 of the gray cast iron pipe with good elongation and High Toughness. Also the cast iron or gray cast iron pipes are brittle because of the lack of Ductility. [4]

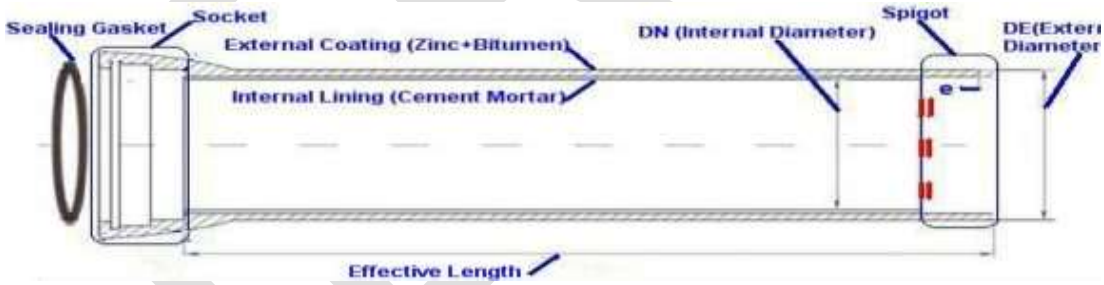

Figure 1.2: Cross section of ductile iron pipe [2]

Ductile iron pipe with its elements is shown in Figure 1.5. There are mainly three sections of ductile iron pipe:

1. Socket

Socket is the one of the end of ductile iron pipe. It is generally known as the front portion of the pipe. It is thicker portion of the pipe which is casted by providing sand-core. Core is made of silica. The core is arranged at the front portion of the centrifugal casting machine and the socket is casted during the centrifugal casting. Sand Core is made as per the dimensions requirement of the socket. Generally the time for solidification of socket is more compare to other sections of pipe.

2. Barrel

It is the main body-section of the ductile iron pipe. It is comparatively thin section compare to socket and spigot. During casting process solidification of this section occur speedily. It the long section and covers majority of the portion of the ductile iron pipe. The thickness of the as well as the diameter of the pipe is described by this section of the pipe.

3. Spigot

Spigot is the second end of ductile iron pipe which is casted lastly during the casting process. It is the smaller section of the pipe which solidifies lastly during the centrifugal casting process. During the installation process of ductile iron pipe network for application each Spigot is jointed with socket section.

Generally, Standard length of ductile iron pipe should be kept from 4.0 meter to 6.0 meters. When the installation of ductile iron pipe is done, they are placed in series. So that number of pipes can be easily arranged and maintenance of pipe, in case, can be done easily. The diameter of pipe also varies from 80mm to 1000mm. Also the weight of the pipes varies as per the diameter and class. Now a day's also the pipe with 1200mm diameter can be made as the requirement arises. In India as per the requirement of customers for different purposes, ductile iron pipe is mainly classified into two categories. This classification is on the based on thickness and weight of the pipe. It is classified as K7 and K9 type of pipes. Between them K7 is thinner than K9. K7 type of pipe is used for generally low pressurised fluid where K9 is used for High pressurised fluid for transportation purpose.

1.4 Centrifugal casting

Centrifugal casting is one of the largest casting branches in the casting industry, accounting for 15% of the total casting output of the world in terms of tonnage. The technique uses the centrifugal force generated by a rotating cylindrical mould to throw molten metal against a mould wall to form the desired shape. Therefore, a centrifugal casting machine must be able to spin a mould, receive molten metal, and let the metal solidify and cool in the mould in a carefully controlled manner. All metals that can be cast by static casting can be cast by the centrifugal casting process, including carbon and alloy steels, high-alloy corrosion- and heat-resistant steels, gray iron, ductile and nodular iron, high-alloy irons, stainless steels, nickel steels, aluminium alloys, copper alloys, magnesium alloys, nickel- and cobalt-base alloys, and titanium alloys. Non-metals can also be cast by centrifugal casting, including ceramics, glasses, plastics, and virtually any material that can be made into liquid or pourable slurries. The centrifugal technique is used primarily for the production of hollow components, but centrifugal casting is used to create solid parts. The centrifugal casting process is generally preferred for producing a superior-quality tubular or cylindrical casting, because the process is economical with regard to casting yield, cleaning room cost, and mould cost. The centrifugal force causes high pressures to develop in the metal, and it contributes to the feeding of the metal, with separation from non-metallic inclusions and evolved gases. Centrifugal casting machines are categorized into three basic types based on the direction of the spinning axis: horizontal, vertical, or inclined. Centrifugal casting processes also have three types:

1. True centrifugal casting (horizontal, vertical, or inclined)
2. Semi-centrifugal (centrifugal mould) casting
3. Centrifuge mould (centrifugal die) casting

Horizontal centrifugal casting is mainly used to cast pieces with a high length-to-diameter ratio or with a uniform internal diameter. Products include pipe, tubes, bushings, cylinder sleeves (liners), and cylindrical or tubular castings that are simple in shape. When metal is poured into the horizontally rotating mould, considerable slip occurs between the metal and the mould such that the metal does not move as fast as the rotating mould. To overcome this inertia, the metal must be accelerated to reach the mould rotation speed. When metal is poured into the horizontally rotating mould, considerable slip occurs between the metal and the mould such that the metal does not move as fast as the rotating mould. To overcome this inertia, the metal must be accelerated to reach the mould rotation speed. [6]

1.5 Manufacturing process of ductile iron pipe

Ductile iron foundries usually melt their iron in cupola or blast furnace from recycled material pig iron. Coke, oil or natural gas is the fuel used here for melting the iron ore which is the solid raw material for casting process. Crystallisation of the carbon dissolved in liquid iron in the form of graphite nodules is achieved by the addition of magnesium into the molten metal. These days ductile iron pipes are manufactured exclusively by means of centrifugal casting process, where the centrifugal forces produce the pipe wall. The rapid cooling applied in ductile iron pipe production by the means of heat treatment of pipes is necessary in order to give them a ductile microstructure. Also the lining and protective coating is the part of

production process. Throughout the entire production process there is defined control system of controls and tests to guarantee the specified properties of the product. [2]

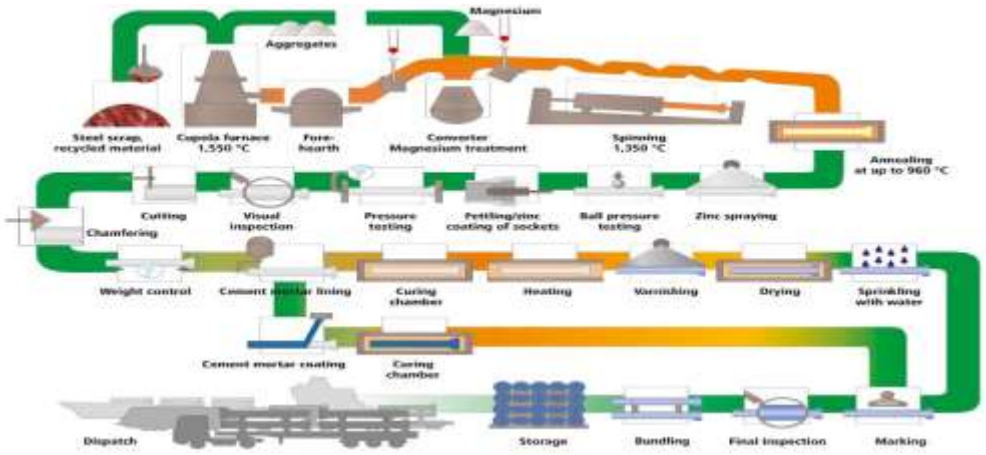

Figure 1.3: Process of manufacturing the ductile iron pipes

1.6 Effect of inlet cooling water flow rate

In ductile pipe casting machines, a measured amount of molten metal is poured into an elongated generally cylindrical metal mould progressively from one end to the other while the mould is being rotated about its longitudinal axis at a rate to evenly distribute and retain the molten metal over the interior wall of the mould.

During pouring of the molten iron and for a predetermined time thereafter, the external wall of the mould is cooled to prevent damage to the mould and to extract heat of fusion from the molten metal. This cooling is accomplished either by directing a spray or multiple streams of water onto the external surface of the mould or by submerging the mould in a cooling water bath. In either case, the mould must be cooled uniformly to avoid damage to the pipe being cast and to prevent excessive distortion of the mould.

Centrifugal castings should be cooled unidirectional from outside to inside. Any two-way solidification will increase the chance of shrinkage porosity and machining allowance, which should be avoided or minimized in thick-wall castings. Cooling rate can affect the microstructure, casting hardness, circumferential and axial cracks, machine productivity, as well as mould life. In most cases, the early cooling rate of the castings is mainly controlled by the coating thickness, coating texture, coating materials, as well as mould thickness and mould materials; however, the later cooling rate is mainly controlled by water cooling (unless the mould is not cooled by water). Water-cooling methods include water submerge, water-jet spray, and water sleeve. Ductile iron pipe production uses all three water-cooling methods For example the middle section of a long tube mould usually needs more water for cooling.

1.7 Effect of metal pouring temperature

Before casting process of ductile iron pipe, liquid metal is poured into the Hopper from the ladle. This liquid metal should be at the required higher temperature that the fluidity of the metal can be maintained during the casting process. During the pouring process metal temperature should be high enough that can dissolve the inoculation and thoroughly mixed. The overall response to inoculation is dependent on melt condition- the poring temperature.

The grain size of inoculation varies from 0.2 to 6.0 mm depends on quantity and temperature of metal. The grain structure of centrifugal castings is concerned; the pour temperature or the variable spinning speed plays a much more important role in obtaining the equated grains than the water-cooling rate or mould temperature.

1.8 Effect of Inoculation

Inoculation is small amount of material which is added into the molten metal stream during the pouring process. Inoculation mainly contains silica of about 45-75 % and some amount of calcium and aluminium as per the application required. There are various types of inoculants which are used in casting process. Among them Zircobar is used for casting ductile iron pipes.

Zircobar is used for following purposes:

- Increases nodule counts and hence better mechanical properties.
- Consistent microstructure and mechanical properties.
- Uniform properties in varying section thickness
- Chill removal

Zircobar contains 60-70 % silica and 3-5 % Mn and Zr. This inoculation provides the better microstructure and mechanical properties in ductile iron pipes. As the result, tensile strength, elongation hardness and machine-ability become more uniform from one section to another section in the same casting

1.9 Effect of carbide in structure

Ductile iron castings are more prone to contain carbides than flake-graphite castings of similar section and size and carbon and silicon contents. This occurs partly because the spherodizing process generally involves the addition of magnesium and/or cerium, which are both elements to promote the formation of eutectic carbide; and partly because the sequence of solidification produced by the growth of nodular graphite tend to promote under-cooling during solidification to temperatures at which white iron structure as likely to form. Carbides in ductile irons can occur in three forms:

Eutectic carbide (or chill) results mainly from the rapid solidification and is most prevalent in corners and thin sections. Inadequate inoculation, low carbon and in particular low silicon and the presence of carbide promoting elements increases the likelihood of carbides being present in the structure. Inverse chill, which has fine acicular form, occurs at or near the heat centre of a casting section. The geometry of the casting and method of running the casting are important variables and the problem is often only solved by re-positioning or altering the size of in gates to change the pattern of solidification of casting.

The presence of carbide in ductile iron is undesirable for a number of reasons:

- It increases the tendency to form shrinkage porosity and thus increases the feeding requirements during casting.
- It increases the risk of cracking during knockout and fettling.
- It decreases the ductility of the iron.
- It drastically reduces the impact resistance.
- It increases hardness and reduces machinability.
- It requires heat treatment to 900-920^{o}C to remove the carbide.

1.10 Effect of Elongation

Elongation is defined as the permanent increase in length, expressed as a percentage of a specified gage length marked in a tensile test bar, which is produced when the bar is tested to failure. Elongation is used widely as the primary indication of tensile ductility and is included in many Ductile Iron specifications. Although shown as the uniform elongation in figure 4.4, elongation also includes the localized deformation that occurs prior to fracture. However, because the localized deformation occurs in a very limited part of the gage length, its contribution to the total elongation of a correctly proportioned bar is very small. Brittle materials such as Gray Iron can fail in tension without any significant elongation, but ferrite Ductile Irons can exhibit elongation of over 10 %

1.11 Effect of Hardness

The hardness of Ductile Iron is usually and best measured by the Brinell test, in which a 10 mm diameter hardened steel or tungsten carbide ball is pressed into a flat surface of the work piece. Hardness is expressed as a Brinell Indentation Diameter (BID) or a Brinell Hardness Number (BHN). Hardness may also be described as BHN/3000 to indicate the force applied to the ball is 3000 kg, the normal value for ferrous materials. The sizes of the Brinell indentation, and its related volume of plastic deformation, are large relative to the scale of the microstructure and as a result an average hardness is obtained which exhibits good reproducibility for similar microstructures. Brinell hardness is included in many Ductile Iron specifications. Brinell hardness should be used for production control and as an auxiliary property test.

1.12 Literature review

Study about the defects, their causes and remedies in casting process showed the root causes of casting defects which helped to quality department of different industries for finding roots and remedies of different defects. Different research papers were studied and casting defects, causes and their remedies were listed. [7]

Variation in tensile properties and fracture properties for ductile cast iron by experiments and numerical analysis was studied. By fractrographic analysis it was possible to establish a relation between elongation at fracture and size of slag defects. Relative contribution to the loss of ductility, size of slag defects, perlitic contents, nodularity and changing graphite were demonstrated by deterministic models. [8]

Solidification rate greatly affect on the microstructure, quality and mechanical property. The rotational speed effect the solidification of liquid metal during the centrifugal casting process. It was found that setting 800 RPM. Of die in centrifugal casting machine the metal poured was directly lifted and rapid solidification took place and finer grain size can be achieved compare to 400 and 600 RPM of the die which improved the microstructure of casting. This helped to achieve the best quality pipe. [9]

The design of easy locking and un-locking arrangement by using electromagnet lock plate to avoid the excess metal fly-out was found. The productivity also increased by using the electromagnetic plate which minimizes dwell time. [10]

Investigation about the effect of electromagnetic force on the centrifugal force in centrifugal casting was done. It was found that under 0.15T electromagnetic field intensity both absolute pressure of metal flow to mould wall and metal flow velocity on same location had some differences between electromagnetic centrifugal casting and centrifugal casting. [11]

This paper talks about the Using the Taguchi method in centrifugal casting of 5500 alloys which specifies that number of experiments can be minimized by using orthogonal array and optimum set of parameters can be analyzed. Also the significance of the parameters on the result can be checked [14]

Also the discussion about the effect of mould wall thickness on the rate of solidification of centrifugal casting was investigated. Result of this paper was as mould thickness increases, due to chilling effect solidification time decreased. Rapid solidification showed well distributed fine grains and slow solidification showed coarse grains. [18]

This paper talks about the Taguchi method in the optimization of injection moulding parameters for manufacturing products. Parameters can be analyzed and optimized by Taguchi method also the predicted results can be verified by confirmation test.[20]

Discussion about modes and causes of gray cast iron pipes failures was investigated. Various failure causes were found. Also the causes of remedies were predicted as per the failure modes. Also it was observed that failure was always unexpected and produces emergencies which were mostly shown in medium and large diameter pipes. [24]

1.13 Problem Definition

Ductile iron pipes are most widely used for transportation of drinking and sewerage water. So it is the prime responsibility of the Industries to make the defect-less ductile iron pipe for smooth and continuous transportation of water. If the quality of pipe is not maintained properly it will affect the service and life of the pipe. Also the rejections level increases due to poor control of parameters which can affect the quality of the pipe. Quality of the ductile iron pipe largely depends on the microstructure as well as the mechanical properties of the pipe. During the casting process of ductile iron pipe if the parameters like pouring metal temperature, inoculation quantity and inlet water flow rate are analyzed and optimized properly, a better quality pipe can be manufactured.

Analysis and optimization of parameters for casting ductile iron pipe is the study about the analysis and optimization of parameters like pouring metal temperature, inoculation quantity and inlet cooling water flow rate by which a better quality pipe with improved microstructure and enhanced mechanical properties can be produced. In this study how the grouping of different parameters like temperature range, inoculation quantity and inlet water flow rate will affect on the microstructure (ferrite % and carbide %) and mechanical properties (Elongation %, and Hardness) are analyzed and optimized by Design of Experiment Method. Taguchi based L16 orthogonal array was used for experimental purpose and analysis was carried out by using Minitab 17 software. Also the ANOVA method is used to analyze the variance, significance of factors and interactions on microstructure and mechanical properties.

This method will be beneficial because it will reduce many shop-floor trials. Also the result can be achieved within minimum time period. Resources can be effectively saved by using this method and optimized parameters can be implemented.

Experimental Set-up

2.1 Introduction

Research on the centrifugal casting can be done for various sizes (DN 100 to 1000 mm) and classes (K9 & K7) of ductile iron pipe but here ductile iron pipes of **DN 450 K9** are considered for experimental analysis. The **DISP** plant of **JINDAL SAW LTD.** was producing casting of these pipes during the time of dissertation work hence this size and class of the pipe was selected for convenience.

2.2 Experimental Set-up

Figure 2.1: Experimental Set-up

As shown in figure 2.1, centrifugal casting machine is casting ductile iron pipe of DN 450 K9. The mould of DN 450 pipe is inserted inside the CCM. Surrounding that mould rollers at 120^0 are employed to provide the rotation motion of the mould during the casting process. Runners are aligned properly before casting the pipe. Hopper is filled with liquid metal by pouring ladle and the pyrometer is used to measure the pouring metal temperature. The rail-track is provided to move casting machine the casting machine longitudinally. Inlet and outlet cooling water pipes are provided to cool the mould and solidify the pipe on the casing of the centrifugal casting. By using PLC (programmable logic control) most of the parameters can be adjusted as per the requirement from operator's Desk.

Table 2.1 Specification of parameters of centrifugal casting machine

Pipe Size (in mm)	**Traverse Down Time** (in Seconds)		**Hopper Up-time** (in Seconds)		**Motor RPM (Reference)**		**Minimum Mould RPM**
DN	**Min.**	**Max.**	**Min.**	**Max.**	**Min.**	**Max.**	
100	14	18	45	75	800	950	700
150	15	20	45	75	800	900	650
200	16	20	45	75	800	850	525
250	17	21	45	75	800	925	425
300	17	21	45	75	750	900	375
350	18	22	45	75	700	850	300
400	18	22	45	75	700	850	300
450	19	25	35	65	550	750	225
500	20	26	35	65	500	700	200
600	22	28	50	80	500	700	200
700	23	29	30	50	500	700	175
750	24	30	30	50	550	750	150
800	25	31	30	50	550	750	140
900	26	32	30	50	700	900	125
1000	27	33	35	55	700	900	125

2.3 Experimental procedure

In the experimental procedure, first the diameter and class of the pipe is selected by using PLC from Operator's Desk. All the other fixed parameters are set which would not vary during the experiments. Liquid metal as per the required quantity which depends on the size and class of the pipe was filled into the hopper. The temperature of the Poring liquid metal is measured by pyrometer.

Figure: 2.2 Temperature measurements by pyrometer

Now the CCM was moved longitudinally to the hopper end by operating. Mould was rotated at full RPM before starting throe casting process. Hopper is tilted as per the require amount from where the liquid metal gets inside the open section of runner and from runner to the socket end of the rotating mould. Inoculation is added by inoculants pipe on the metal stream by controlling the flow rate of inoculation from operator's desk. Cooling water is continuously supplied from inlet cooling water pipe to the surrounding of the rotating.

Figure: 2.3 casting of pipe

After casting the pipe it was passing through the annealing furnace for heat treatment process. In this section the speed of annealing is maintained constant that it will not affect the quality of the pipe. After heat treatment a part of the pipe is analyzed from different equipments like microscope, Brinell hardness machine for examine the microstructure as well as the mechanical properties of the pipe.

2.4 Experimental Results

Table 2.2: Analysis of Microstructure from orthogonal array

Exp. No.	Pouring Temp. (^{0}C)	Inoculation quantity (%)	Inlet water flow rate (m^3/Hr)	Ferrite (%)	Carbide (%)
1	1280-1310	0.15	100	85	13
2	1280-1310	0.20	120	90	10
3	1280-1310	0.25	140	92	8
4	1280-1310	0.30	160	94	6
5	1310-1340	0.15	120	89	11
6	1310-1340	0.20	100	92	8
7	1310-1340	0.25	160	94	6
8	1310-1340	0.30	140	96	4
9	1340-1370	0.15	140	90	10
10	1340-1370	0.20	160	94	6
11	1340-1370	0.25	100	96	4
12	1340-1370	0.30	120	98	2
13	1370-1400	0.15	160	85	13
14	1370-1400	0.20	140	90	10
15	1370-1400	0.25	120	94	6
16	1370-1400	0.30	100	96	4

Table 2.3 Analysis of Mechanical Properties from orthogonal array

Exp. No.	Pouring Temp. (^{0}C)	Inoculation quantity (%)	Inlet water flow rate (m^3/Hr)	Elongation (%)	Hardness (BHN)
1	1280-1310	0.15	100	7	205
2	1280-1310	0.20	120	10	195
3	1280-1310	0.25	140	11	197
4	1280-1310	0.30	160	12	194
5	1310-1340	0.15	120	8	200
6	1310-1340	0.20	100	11	197
7	1310-1340	0.25	160	14	190
8	1310-1340	0.30	140	10	195
9	1340-1370	0.15	140	12	195
10	1340-1370	0.20	160	14	190
11	1340-1370	0.25	100	16	180
12	1340-1370	0.30	120	7	185
13	1370-1400	0.15	160	10	205
14	1370-1400	0.20	140	14	195
15	1370-1400	0.25	120	12	190
16	1370-1400	0.30	100	14	180

RESULT AND DISCUSSION

3.1 Analysis of Performance for Microstructure

3.1.1 Analysis of Ferrite %

Table 3.1: Response Table for Means of Ferrite %

Level	Poring Temperature	Inoculation Quantity	Inlet water flow rate
1	90.25	87.25	92.25
2	92.75	91.05	92.75
3	94.50	94.0	92.00
4	91.25	96.0	91.75
Delta	4.25	8.75	1.00
Rank	2	1	3

Table 3.1 represents that the mean value is maximum (94.50) for 1340-1370 Pouring temperature and Minimum (90.25) for 1280-1310 Pouring temperature. The mean value is maximum (96.0) for 0.30 % inoculation quantity of pipe weight and minimum (87.25) for 0.15 %. The Mean value is maximum (92.75) for 120 m^3/Hr water flow rate while Minimum (91.75) for 160 m^3/Hr. It also represents Delta value by Maximum and minimum mean differences and rank them. So it can be said that the effect of inoculation quantity is Maximum and effect of inlet water flow rate is minimum on the Ferrite %. Figure 7.1 represents the Main effects plot for means of ferrite % by Taguchi method

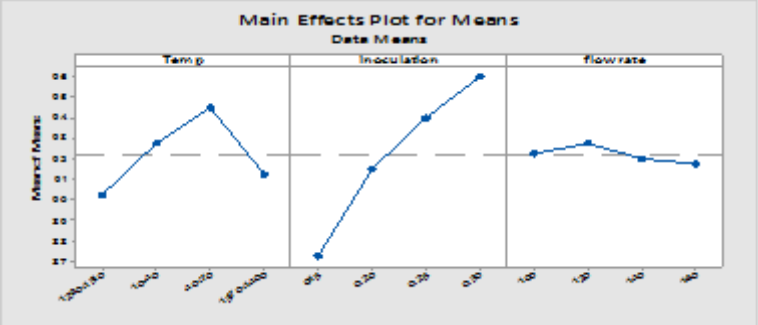

Figure 3.1 Main Effect plots for Means of Ferrite %

Table 3.2: Means of Responses Table for S/N ratio of Ferrite %

Level	Poring Temperature	Inoculation Quantity	Inlet water flow rate
1	39.09	38.80	39.28
2	39.33	39.22	39.33
3	39.05	39.45	39.26
4	39.44	39.64	39.24
Delta	0.39	0.84	0.09
Rank	2	1	3

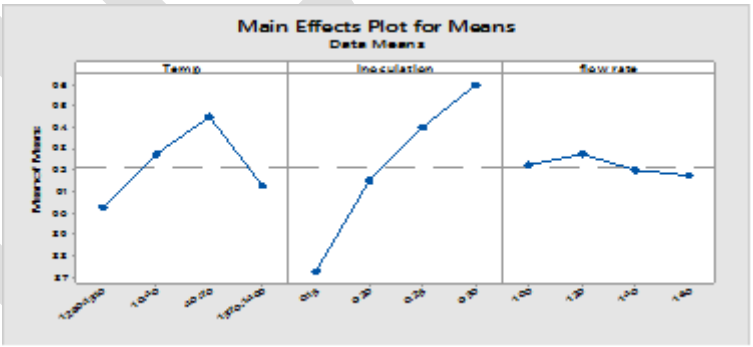

Figure 3.2 Main Effect plots for S/N ratio of Ferrite %

Response curve analysis is aimed at determining influential parameter and their optimum set of control parameters. Figure 3.2 shows the response at each factor level. The S/N ration for different performance were calculated at each factor level and the average effect were determine by taking total

of each factor level and divided by the number of data points in the total. The greater difference between S/N ratios, the parametric influence will be much. The parameter level having the highest S/N ratio corresponds to the sets of parameters indicates highest performance.

The term optimum setting is reflects only optimum combination of parameters defined by this experiment. Optimum setting is determined by choosing the level with highest S/N ratio. The response curve for S/N ratio, the highest S/N ratio was observed at **1340-1370 ^{0}C** Pouring temperature, **0.30%** of pipe weight inoculation quantity and **120 m^{3}/Hr** water flow rate, which optimum parameters is setting for highest ferrite %.

Table 3.3 Factor levels for predicted ferrite %

Pouring Temperature (0C)	Inoculation Quantity (%)	Water flow rate (m3/Hr)
1340-1370	0.30	120

Table 3.4 Predicted result for Ferrite %

Ferrite %	S/N Ratio
98.87	39.91

Using optimum set of parameters, which was achieved by Minitab software for Taguchi method, the result was obtained by experiment is compared with predicated value of software for highest ferrite %

Table 3.5 Experimental result for Ferrite %

Pouring Temperature (^{0}C)	Inoculation Quantity (%)	Water flow rate (m^{3}/Hr)	Ferrite %
1340-1370	0.30	120	98

Experiment has done for above set of parameters, which gives performance given in table 7.7 Ferrite is **98%** and experimental results is nearer to our predicted value **98.87 %.** From Taguchi method and experimental investigation it has been concluded that **1340-1370 °C** pouring temperature, **0.30 %** inoculation quantity and **120 m³/Hr** inlet water flow rate gives highest Ferrite %

3.1.2 Analysis of Carbide %

Table 3.6: Response Table for Means of Carbide %

Level	Poring Temperature	Inoculation Quantity	Inlet water flow rate

1	9.25	11.75	7.30
2	7.25	8.5	7.25
3	5.50	6	8.00
4	8.25	4	7.75
Delta	3.75	7.75	0.75
Rank	2	1	3

Table 3.6 represents that the mean value is maximum (9.25) for 1280-1310 Pouring temperature and Minimum (5.50) for 1340-1370 Pouring temperature. The mean value is maximum (11.75) for 0.15 % inoculation quantity of pipe weight and minimum (4) for 0.30 %. The Mean value is maximum (8.00) for 140 m^3/Hr water flow rate while Minimum (7.25) for 120 m^3/Hr. It also represents Delta value by Maximum and minimum mean differences and rank them. So it can be said that the effect of inoculation quantity is Maximum and effect of inlet water flow rate is minimum on the carbide%. Figure 7.3 represents the Main effects plot for means of carbide % by Taguchi method.

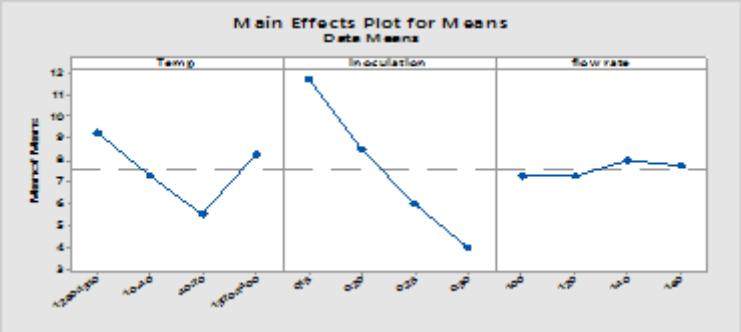

Figure 3.3 Main Effect plots for Means of Carbide %

Table 3.7: Response Table for S/N ratio of Carbide %

Level	Poring Temperature	Inoculation Quantity	Inlet water flow rate
1	-18.98	-21.35	-16.11
2	-16.62	-18.41	-15.60
3	-13.41	-15.31	-17.53

4	-17.47	-11.42	-17.24
Delta	5.57	9.93	1.92
Rank	2	1	3

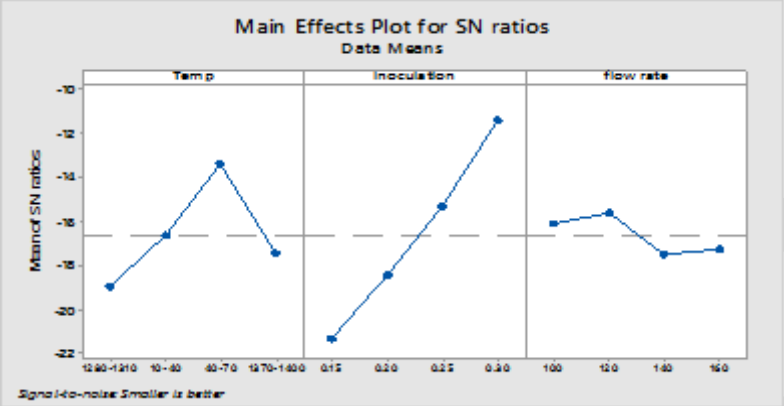

Figure3.4 Main Effect plots for S/N ratio of carbide %

Response curve analysis is aimed at determining influential parameter and their optimum set of control parameters. Figure 3.4 shows the response at each factor level. The S/N ration for different performance were calculated at each factor level and the average effect were determine by taking total of each factor level and divided by the number of data points in the total. The greater difference between S/N ratios, the parametric influence will be much. The parameter level having the highest S/N ratio corresponds to the sets of parameters indicates highest performance.

The term optimum setting is reflects only optimum combination of parameters defined by this experiment. Optimum setting is determined by choosing the level with highest S/N ratio. The response curve for S/N ratio, the highest S/N ratio was observed at 1340-1370 ^{0}C Pouring temperature, 0.30% of pipe weight inoculation quantity and 120 m^3/Hr water flow rate, which optimum parameters is setting for highest Carbide %.

Table 3.8 Factor levels for predicted of Carbide %

Pouring Temperature (^{0}C)	**Inoculation Quantity (%)**	**Water flow rate (m^3/Hr)**
1340-1370	0.30	120

Table 3.9 Predicted result for Carbide %

Carbide %	**S/N Ratio**
1.65	-7.18

Using optimum set of parameters, which was achieved by Minitab software for Taguchi method, the result was obtained by experiment is compared with predicated value of software for Lowest Carbide %

Table 3.10 Experimental result for Carbide %

Pouring Temperature (^{0}C)	Inoculation Quantity (%)	Water flow rate (m^3/Hr)	Carbide %
1340-1370	0.30	120	2.0

Experiment has done for above set of parameters, which gives performance given in table 7.12 Carbide is **2.0 %** and experimental results is nearer to our predicted value **1.65 %**. From Taguchi method and experimental investigation it has been concluded that **1340-1370 °C** pouring temperature, **0.30 %** inoculation quantity and **120 m³/Hr** inlet water flow rate gives Lowest Carbide %

3.2 Analysis of Performance for Mechanical Properties

3.2.1 Analysis of Elongation %

Table 3.11: Response Table for Means of Elongation %

Level	Poring Temperature	Inoculation Quantity	Inlet water flow rate
1	10.00	9.25	12.0
2	10.75	12.25	9.25
3	12.25	13.25	11.75
4	12.50	10.75	12.50
Delta	2.5	4.0	3.25
Rank	3	1	2

Table 3.11 represents that the mean value is maximum (12.50) for 1370-1400 Pouring temperature and Minimum (10.00) for 1280-1310 Pouring temperature. The mean value is maximum (13.25) for 0.25 % inoculation quantity of pipe weight and minimum (9.25) for 0.15 %. The Mean value is maximum (12.50) for 160 m^3/Hr water flow rate while Minimum (9.25) for 120 m^3/Hr. It also represents Delta value by Maximum and minimum mean differences and rank them. So it can be said that the effect of inoculation quantity is Maximum and effect of pouring temperature is minimum on the Elongation %. Figure 7.5 represents the Main effects plot for means of Elongation % by Taguchi method.

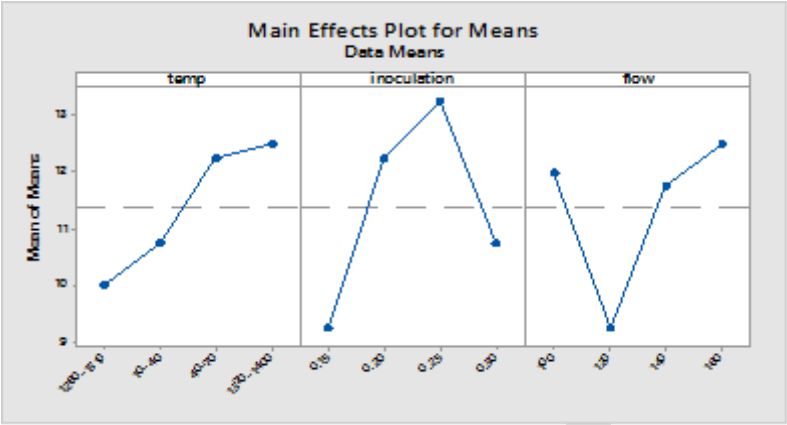

Figure 3.5 Main Effect plots for Means of Elongation %

Table 3.12: Response Table for S/N ratio of Elongation %

Level	Poring Temperature	Inoculation Quantity	Inlet water flow rate
1	19.83	19.14	21.18
2	20.45	21.67	19.14
3	21.37	22.35	21.33
4	21.86	20.35	21.86
Delta	2.03	3.22	2.72
Rank	2	1	3

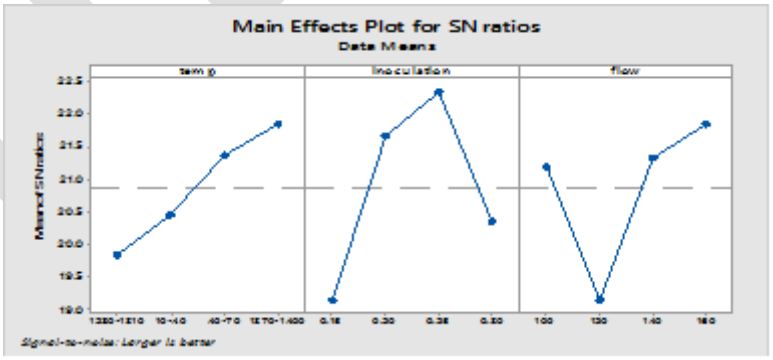

Figure 3.6 Main Effect plots for S/N ratio of Elongation %

Response curve analysis is aimed at determining influential parameter and their optimum set of control parameters. Figure 3.6 shows the response at each factor level. The S/N ration for different performance were calculated at each factor level and the average effect were determine by taking total

of each factor level and divided by the number of data points in the total. The greater difference between S/N ratios, the parametric influence will be much. The parameter level having the highest S/N ratio corresponds to the sets of parameters indicates highest performance.

The term optimum setting is reflects only optimum combination of parameters defined by this experiment. Optimum setting is determined by choosing the level with highest S/N ratio. The response curve for S/N ratio, the highest S/N ratio was observed at 1370-1400 0C Pouring temperature, 0.25% of pipe weight inoculation quantity and 160 m3/Hr water flow rate, which optimum parameters is setting for highest Elongation %.

Table 3.13 Factor levels for predicted of Elongation %

Pouring Temperature (^{0}C)	Inoculation Quantity (%)	Water flow rate (m^3/Hr)
1370-1400	0.25	160

Table 3.14 Predicted result for Elongation %

Elongation %	S/N Ratio
15.5	24.31

Using optimum set of parameters, which was achieved by Minitab software for Taguchi method, the result was obtained by experiment is compared with predicated value of software for highest Elongation %

Table 3.15 Experimental result for Elongation %

Pouring Temperature (^{0}C)	Inoculation Quantity (%)	Water flow rate (m^3/Hr)	Elongation %
1370-1400	0.25	160	15

Experiment has done for above set of parameters, which gives performance given in Table 3.15 Elongation is **15%** and experimental results is nearer to our predicted value **15.5 %.** From Taguchi method and experimental investigation it has been concluded that **1370-1400 °C** pouring temperature, **0.25 %** inoculation quantity and **160 m³/Hr** inlet water flow rate gives highest Elongation %

3.2.2 Analysis of Hardness (BHN)

Table 3.16: Response Table for Means of Hardness

Level	Poring Temperature	Inoculation Quantity	Inlet water flow rate
1	197.8	201.3	190.5

2	195.5	194.3	192.5
3	187.5	189.3	195.5
4	192.5	188.5	194.8
Delta	10.3	12.8	5.0
Rank	2	1	3

Table 3.16 represents that the mean value is maximum (197.8) for 1280-1310 Pouring temperature and Minimum (187.5) for 1340-1370 Pouring temperature. The mean value is maximum (201.3) for 0.15 % inoculation quantity of pipe weight and minimum (188.5) for 0.30 % inoculation. The Mean value is maximum (195.5) for 140 m^3/Hr water flow rate while Minimum (190.5) for 100 m^3/Hr. It also represents Delta value by Maximum and minimum mean differences and rank them. So it can be said that the effect of inoculation quantity is Maximum and effect of Water flow rate is minimum on the Hardness. Figure 7.11 represents the Main effects plot for means of Hardness by Taguchi method.

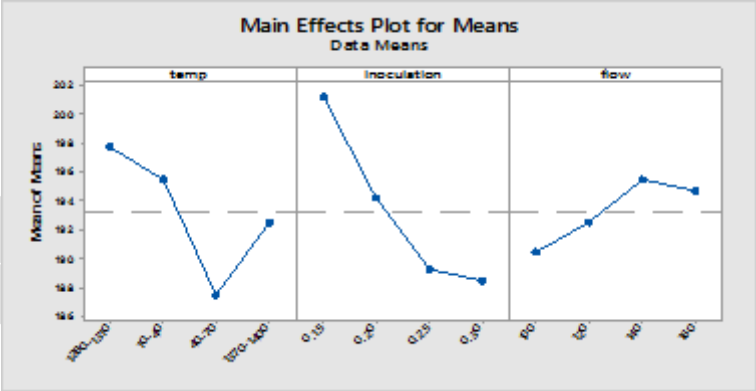

Figure 3.7 Main Effect plots for Means of Hardness

Table 3.17: Response Table for S/N ratio of Hardness

Level	Poring Temperature	Inoculation Quantity	Inlet water flow rate
1	-45.92	-46.07	-45.58
2	-45.82	-45.77	-45.68
3	-45.46	-45.54	-45.82
4	-46.68	-45.50	-45.79

Delta	0.46	0.57	0.24
Rank	2	1	3

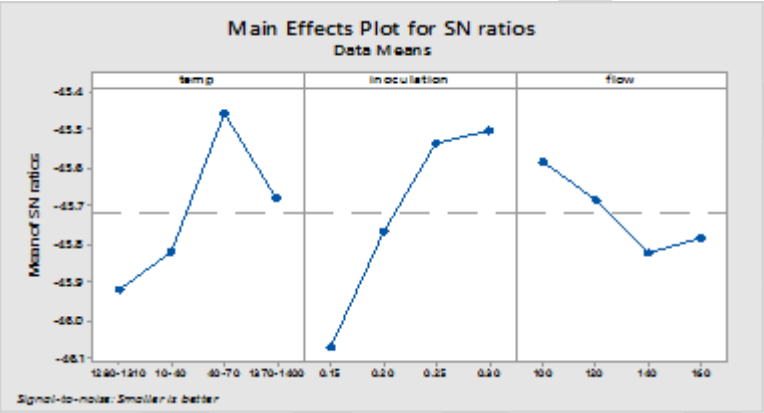

Figure 3.8 Main Effect plots for S/N ratio of Hardness

Response curve analysis is aimed at determining influential parameter and their optimum set of control parameters. Figure 3.8 shows the response at each factor level. The S/N ration for different performance were calculated at each factor level and the average effect were determine by taking total of each factor level and divided by the number of data points in the total. The greater difference between S/N ratios, the parametric influence will be much. The parameter level having the highest S/N ratio corresponds to the sets of parameters indicates highest performance.

The term optimum setting is reflects only optimum combination of parameters defined by this experiment. Optimum setting is determined by choosing the level with highest S/N ratio. The response curve for S/N ratio, the highest S/N ratio was observed at **1340-1370^{0}C** Pouring temperature, **0.30%** of pipe weight inoculation quantity and **100 m^3/Hr** water flow rate, which optimum parameters is setting for Lowest Hardness.

Table 3.18 Factor levels for predicted of Hardness

Pouring Temperature (^{0}C)	**Inoculation Quantity (%)**	**Water flow rate (m^3/Hr)**
1340-1370	0.30	100

Table 3.19 Predicted result for Hardness

Hardness (BHN)	**S/N Ratio**

179.875	-45.10

Using optimum set of parameters, which was achieved by Minitab software for Taguchi method, the result was obtained by experiment is compared with predicated value of software for Lowest Hardness

Table 3.20 Experimental result for Hardness

Pouring Temperature (^{0}C)	**Inoculation Quantity (%)**	**Water flow rate (m^3/Hr)**	**Hardness (BHN)**
1340-1370	0.30	100	180

Experiment has done for above set of parameters, which gives performance given in table 7.22 Hardness is **180 BHN** and experimental results is nearer to our predicted value **79.875** From Taguchi method and experimental investigation it has been concluded that **1340-1370 °C** pouring temperature, **0.30 %** inoculation quantity and **100 m³/Hr** inlet water flow rate gives Lowest Hardness

3.3 ANOVA Results for microstructure

Since as already stated ANOVA help us to identify which parameter is important for us after literature review following ANOVA table is obtained for Ferrite % and Carbide %. **Minitab 17** software is used for statistical calculation purpose

Table 3.21 ANOVA Results for Ferrite %

Parameters	**DF**	**Adj SS**	**Adj MS**	**F Value**	**P Value**
Regression	7	207.86	29.694	22.45	0.000
Pouring Temperature(°C)	1	10.64	10.635	8.04	0.022
Inoculation (%)	1	10.85	10.850	8.20	0.021
Water flow rate (m³/Hr)	1	12.98	12.979	9.81	0.014
Temperature*Inoculation	1	10.48	10.477	7.92	0.023
Temperature*Flow Rate	1	12.80	12.804	9.68	0.014
Inoculation*Flow Rate	1	12022	12.217	9.24	0.016
Temp.*Inoculation*Flow rate	1	12.02	12.021	9.09	0.017
Error	8	10.58	1.323		
Total	15	218.44			

Table 3.21 shows the Analysis of Variance (ANOVA) by Regression method for Ferrite % response. ANOVA table shows the amount of variation in response data. The important information can be obtained here is the P- value which shows the significance level of the individual as well as interactive parameters. P value less than 0.0500 indicate model terms are significant. P- Value for regression 0.000 indicating that regression model is significant. The co-efficient of determination indicates the goodness of the fit for the model, so the percentage value of this regression model is **95.15 %** which indicates the highly significance of the model.

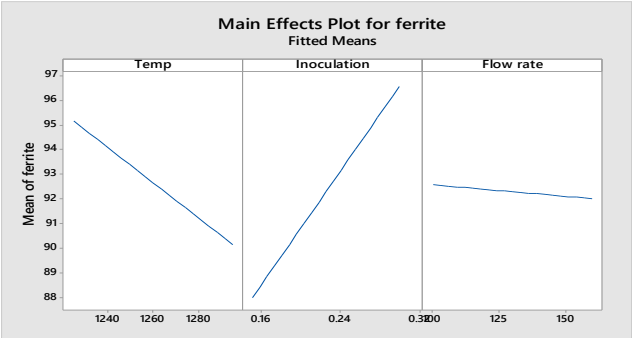

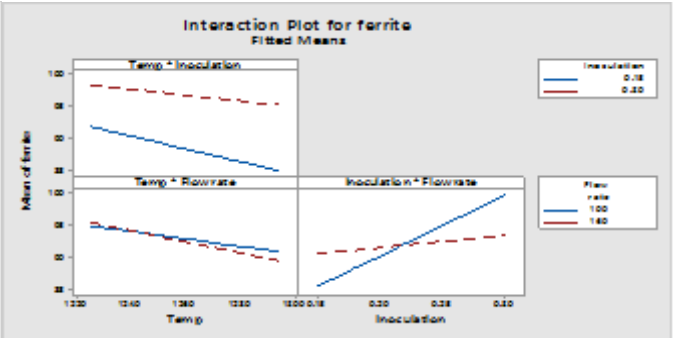

Figure 3.9: Analysis of Main Effect on Ferrite % **Figure3.10: Analysis of Interaction Effect on Ferrite %**

Main effect plot is most useful when we have select more variables. We can compare the change in level means to see which categorical variable influence the Response the most. A main effect is present when mean of the responses changes at different levels of variable. By comparing the graph shows that **Ferrite %** is higher at 1240° C Temperature, 0.30 % inoculation quantity and 100 m³/Hr water flow rate. The Magnitude of the main effect for **inoculation quantity** is higher than other variable.

In interaction effect if the lines are parallel than there is no interaction between factors. If the greater the lines depart from being parallel, the greater the strength of interaction. Factorial plots do not use the data from the worksheet instead Minitab estimates the fitted means based on a stored model. In the interaction graph the Temperature and inoculation, neither of both panels interact with each-other, while in Temperature and flow rate and inoculation and flow rate both of these interactions indicates that variables interact with each other.

Table 3.22 ANOVA Results for Carbide %

Parameters	DF	Adj SS	Adj MS	F Value	P Value
Regression	7	163.614	23.373	43.25	0.000
Pouring Temperature(°C)	1	10.604	10.604	19.62	0.002
Inoculation (%)	1	10.895	10.894	20.16	0.002
Water flow rate (m³/Hr)	1	11.862	11.8619	21.95	0.002
Temperature*Inoculation	1	10.555	10.5550	19.53	0.002
Temperature*Flow Rate	1	11.699	11.6991	21.65	0.002
Inoculation*Flow Rate	1	11.396	11.3958	21.09	0.002
Temp.*Inoculation*Flow rate	1	11.212	11.2125	20.75	0.002
Error	8	4.324	0.5404		
Total	15	167.938			

Table 3.22 shows the Analysis of Variance (ANOVA) by Regression method for Carbide % response. The important information can be obtained here is the P- value which shows the significance level of the individual as well as interactive parameters. P value less than 0.0500 indicate model terms are significant. P- Value for regression 0.000 indicating that regression model is significant. The co-efficient of determination indicates the goodness of the fit for the model, so the percentage value of this regression model is **97.43 %** which indicates the highly significance of the model.

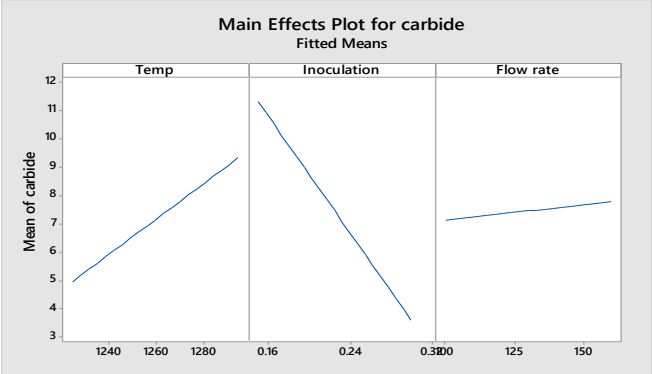

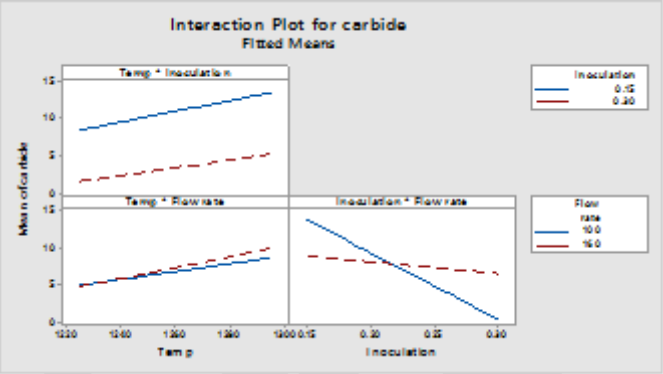

Figure 3.11: Analysis of Main Effect on Carbide % **Figure 3.12: Analysis of Interaction Effect of on Carbide %**

Main effect plot is most useful when we have select more variables. We can compare the change in level means to see which categorical variable influence the Response the most. A main effect is present when mean of the responses changes at different levels of variable. By comparing the graph shows that **Carbide %** is lower at 1240° C Temperature, 0.16 % inoculation quantity and 150 m^3/Hr water flow rate. The Magnitude of the main effect for **inoculation quantity** is higher than other variable.

In interaction Effect if the lines are parallel than there is no interaction between factors. If the greater the lines depart from being parallel, the greater the strength of interaction. Factorial plots do not use the data from the worksheet instead Minitab estimates the fitted means based on a stored model. In the interaction graph the Temperature and inoculation, neither of both panels interact with each-other, while in Temperature and flow rate and inoculation and flow rate both of these interactions indicates that variables interact with each other.

3.4 ANOVA Results for Mechanical properties

ANOVA help us to identify which parameter is important for us after literature review following ANOVA table is obtained for Hardness and Carbide %. Minitab 17 software is used for statistical calculation purpose.

Table 3.23 ANOVA Results for Hardness

Parameters	DF	Adj SS	Adj MS	F Value	P Value
Regression	7	672.36	96.05	5.45	0.015
Pouring Temperature(°C)	1	52.96	52.96	3.00	0.121
Inoculation (%)	1	25.79	25.79	1.46	0.261
Water flow rate (m^3/Hr)	1	74.44	74.44	4.22	0.049
Temperature*Inoculation	1	23.63	23.63	1.34	0.280
Temperature*Flow Rate	1	75.60	75.60	4.32	0.048

Inoculation*Flow Rate	1	40.87	40.87	2.32	0.166
Temp.*Inoculation*Flow rate	1	38.52	0.178	2.18	0.178
Error	8	141.08	17.63		
Total	15	813.44			

Table 3.23 shows the Analysis of Variance (ANOVA) by Regression method for Hardness response. The important information can be obtained here is the P- value which shows the significance level of the individual as well as interactive parameters. P value less than 0.0500 indicate model terms are significant. P- Value for regression 0.015 indicating that regression model is significant. The co-efficient of determination indicates the goodness of the fit for the model, so the percentage value of this regression model is **82.65%** which indicates the highly significance of the model.

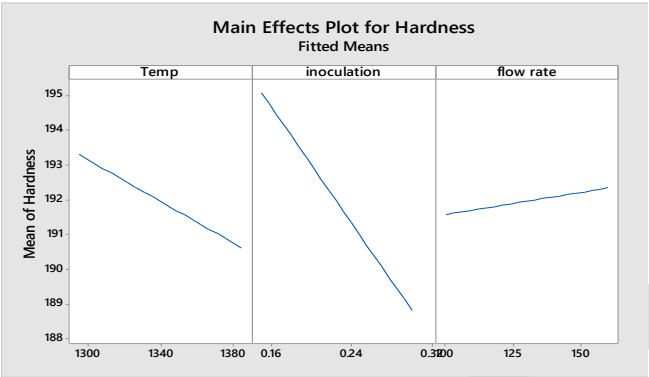

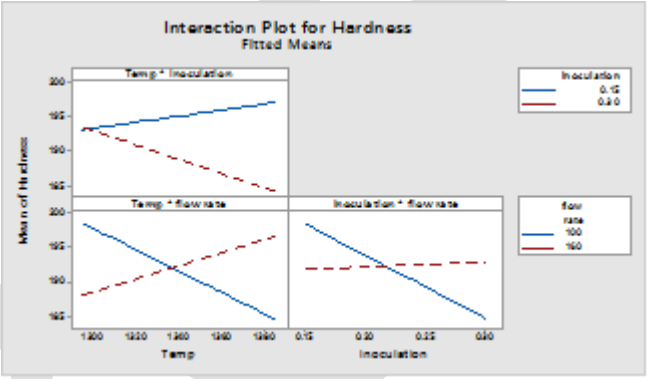

Figure 3.13: Analysis of Main Effect on Hardness **Figure 3.14: Analysis of Interaction Effect of on Hardness**

Main effect plot is most useful when we have select more variables. We can compare the change in level means to see which categorical variable influence the Response the most. A main effect is present when mean of the responses changes at different levels of variable. By comparing the graph shows that **Hardness** is lower at 1300° C Temperature, 0.16 % inoculation quantity and 150 m³/Hr water flow rate. The Magnitude of the main effect for **inoculation quantity** is higher than other variable.

In interaction Effect if the lines are parallel than there is no interaction between factors. If the greater the lines depart from being parallel, the greater the strength of interaction. Factorial plots do not use the data from the worksheet instead Minitab estimates the fitted means based on a stored model. In the interaction graph the Temperature and inoculation, Temperature and flow rate and inoculation and flow rate all of these interactions indicate that variables interact with each other.

Table 3.24 ANOVA Results for Elongation %

Parameters	DF	Adj SS	Adj MS	F Value	P Value
Regression	7	46.538	6.648	0.90	0.550
Pouring Temperature(°C)	1	9.950	9.950	1.34	0.280
Inoculation (%)	1	2.675	2.675	0.36	0.564
Water flow rate (m³/Hr)	1	8.389	8.389	1.13	0.318

Temperature*Inoculation	1	2.687	2.687	0.36	0.563
Temperature*Flow Rate	1	8.328	8.318	1.13	0.320
Inoculation*Flow Rate	1	2.111	2.111	0.29	0.608
Temp.*Inoculation*Flow rate	1	2.083	2.083	0.28	0.310
Error	8	59.212	7.402		
Total	15	105.750			

Table 3.24 shows the Analysis of Variance (ANOVA) by Regression method for Hardness response. The important information can be obtained here is the P- value which shows the significance level of the individual as well as interactive parameters. P value less than 0.0500 indicate model terms are significant. P- Value for regression 0.550 indicating that regression model is insignificant. The co-efficient of determination indicates the goodness of the fit for the model, so the percentage value of this regression model is **44.00%** which indicates the insignificance of the model.

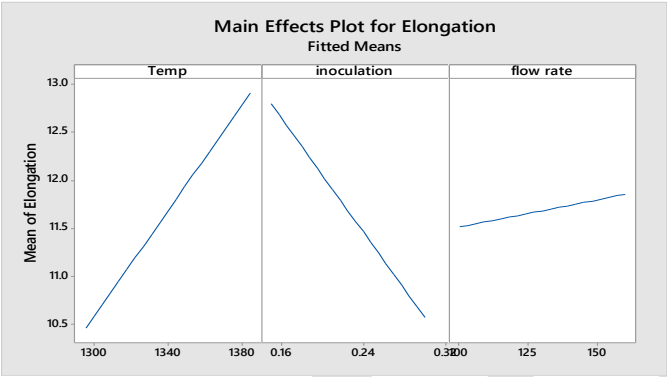

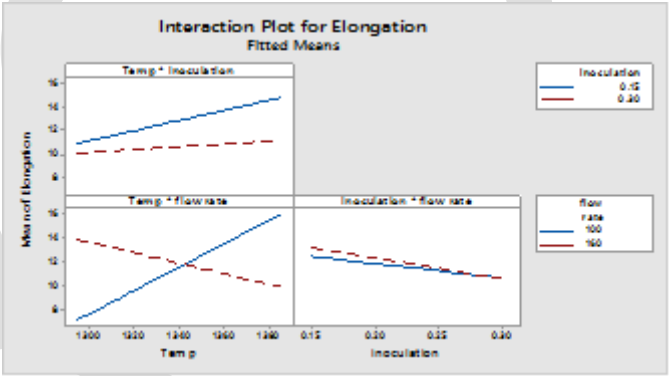

Figure 3.15: Analysis of Main Effect on Elongation % **Figure 3.16: Analysis of Interaction Effect of on Elongation**

Main effect plot is most useful when we have select more variables. We can compare the change in level means to see which categorical variable influence the Response the most. A main effect is present when mean of the responses changes at different levels of variable. By comparing the graph shows that **Elongation %** is higher at 1380° C Temperature, 0.16 % inoculation quantity and 150 m³/Hr water flow rate. The Magnitude of the main effect for **Pouring Temperature** is higher than other variable.

In interaction plots if the lines are parallel than there is no interaction between factors. If the greater the lines depart from being parallel, the greater the strength of interaction. Factorial plots do not use the data from the worksheet instead Minitab estimates the fitted means based on a stored model. In the interaction graph the Temperature and inoculation, neither of both variable clearly interact with each other while in Temperature and flow rate and inoculation and flow rate both of these interactions indicates that variables interact with each other.

ACKNOWLEDGMENT

I would like to thank to my respected guides **Mr. Hemanshu Joshi,** Department of Mechanical Engineering, HJD institute of technical educations and research, kera-kutch & **Mr. Shankar Rao,** Manager of production Department, Jindal Saw Ltd, Mundra-kutch. I would like to thank **Mr. M. RAJA**, General Manager, Jindal saw Ltd, for his co-operation and support.

I would also like to thank **Mr. N.J. Patel**, Head of the Mechanical Engineering department who has always been ready to offer help at any time, in spite of having his busy schedule. I am thankful to all the faculty members of Mechanical Engineering Department and all my friends who have directly or indirectly helped me during this dissertation work.

I would like to thank my best friends and colleagues for their great support in dissertation work as well as in social life. Without them the research work would not complete successfully.

The final thanks must to go to my parents who have provided me with every opportunity and encouragement from the life years. I could not and would never wish for more.

CONCLUSION

The aim of this Research is to investigate the effect of Process Parameters like Pouring Temperature, Inoculation quantity and Inlet water flow rate on the Quality (Microstructure and Mechanical properties) of the Ductile iron Pipe and to find the Optimum Combination of Parameters which give the Best Performance at that Condition. The Conclusions derived from the Experimental investigation, Taguchi Method and Analysis of Variance (ANOVA) are:

- At 1340-1370 °C Pouring Temperature, 0.30 % Inoculation and 120 m³/Hr Cooling water flow rate the highest ferrite % (Which is the major Part of Microstructure properties in ductile iron pipe) can be obtained. At given set of parameters highest Taguchi Predicted ferrite % are 98.87 % which is very nearer to the experimental result of 98.00%

- At 1340-1370 °C Pouring Temperature, 0.30 % Inoculation and 120 m³/Hr Cooling water flow rate the Lowest Carbide % can be obtained. At given set of parameters the Lowest Taguchi Predicted Carbide % is 1.65 % which is very nearer to the experimental result of 2.0 %

- At 1370-1400 °C Pouring Temperature, 0.25 % Inoculation and 160 m³/Hr Cooling water flow rate the Highest Elongation % can be obtained. At given set of parameters the highest Taguchi Predicted Elongation % is 15.50 % which is very nearer to the experimental result of 15.0 %

- At 1340-1370 °C Pouring Temperature, 0.30 % Inoculation and 100 m³/Hr Cooling water flow rate the Lowest Hardness can be obtained. At given set of parameters the Lowest Taguchi Predicted Hardness is 179.87 BHN which is very nearer to the experimental result of 180.0 BHN

- By using Analysis of Variance in regression (As the Responses Vary Polynomialy) the Significance of the Factors as well as the interactions of factors are analyzed and the most Significant parameter Or interaction can be find out.

- ANOVA Results for Ferrite % Shows that all the factors as well as interactions are largely significance as their P-values are less than α level.

- ANOVA Results for Carbide % Shows that all the factors as well as interactions are largely significance as their P-values are less than α level.

- ANOVA Results for Hardness(BHN) Shows that all the factors as well as interactions are largely significance as their P-values are less than α level.

REFERENCES:

[1] [1] M. Jagdishwar, “Casing Feeder Design Optimization based on feed path and temperature analysis”,2012

[2] [2] Guss –Rohrsysteme, Griesheim,"Ductile iron pipe system", European association for Ductile iron pipe systems, 2004

[3] [3] Anita Bisht, "Effect of Heat treatment procedures on microstructure and Mechanical Properties of Nodular iron", 2009

[4] [4] Charles W. Mooney, Jr. Dies, "The best of Ductile iron news", 2001, IL 60016-8399

[5] [5] Courtesy of Jindal saw Ltd.

[6] [6] Sufei Wei, Steve Lampman, "Centrifugal casting", ASM Handbook, Volume 15: Casting, 2008, P 667-673

[7] [7] Rajesh Rajkhole, J.G. Khan,"Defects, causes and their Remidies in casting process", volume 2, 2014, E-ISSN: 2321-9637

[8] [8] Bishnu Prasad Mahto, "Characterization of Ductile iron Through Fractographic study", 2014

[9] [9] Madhusudan, Narendranath, G C Kumar, "properties of centrifugal casting at different rotational speeds of the die", International Journal of Engineering Technology and advanced Engineering Vol. 3, January 2013 ISSN 2250-2459

[10] [10] Jitendra khare "Design and Development of Locking arrangement for centrifugal casting machine",2013, international journal of pure and applied research in engineering and technology, ISSN: 2319-507X

[11] [11] Minghu yunan, Leilei cao, Yaozeng Xu, Xuding Song,"Numerical Simulation on effects of Electromagnetic force on centrifugal casting process of high speed steel roll", Modelling and numerical simulation of material Science,2013

[12] [12] Yuwen Xuan-Xuan, Chen Ling, Han Yi-jie, " Numerical Simulation of Casting Filling Process Based on FLUENT", international conference on future Electrical power and Energy system, 2012, 1864-1871

[13] [13] Madhusudan, Narendra Nath S., G C Mohan, "Experimental Study on Cooling Rate of centrifugal casting based on Grain Size", International journal Scientific and engineering Research, Volume 3, Issue 1, January-2012 1 ISSN 2229-5518

[14] [14] P. Shailesh," Experimental investigation on centrifugal casting of 5500 alloy", Science Research and essays, vol. 79(44), ISSN 1992-2248, 12 November, 2012

[15]

[16]

[17] [15] Nan Nan Song, Shi Ping Wu, Xiu Homg Kang, Dian Zhong Li1, " Hydraulic experiments of mould filling Process in Horizontal centrifugal Casting, Advanced Materials Research Vols. 154-155, 2011, pp 314-320

[18] [16] Vivek Singh,"Analysis of process parameters of plasma arc cutting using Design of experiments", NIT Rourlela, 2011.

[19] [17] R. Arbi Jeshvaghani, M. Shaminian, M. jaberzadeh, "Enhancement of Wear Resistance of ductile iron surface by stellite 6" , material and design 32,2011, 2028-2033

[20] [18] Madhusudan, Narendranath, Mohankumar G C 2, Mukunda P G, "Effect of Mould wall Thickness on rate of Solidification of centrifugal casting" , International Journal of Engineering Science and Technology, Vol. 2, 2010, 6092-6096

[21] [19] Shamanian, S.M.R. Mousavi Abarghouie,S.R. Mousavi Pour, "Effect of surface alloying on microstructure and wear behavior of ductile iron", Department of Materials Engineering, Isfahan University of Technology, Isfahan 84156-83111, Iran

[22] [20] S. Kamaruddin, Zahid Khan,S.H. foong,"Application of Taguchi Method in the Optimization of injection Moulding parameters for Manufacturing Products from Plastic Blend", IACSIT, Vol. 2, ISSN: 1793-8263, December 2010

[23] [21] Cai Qizhou, Wei Bokang, "Recent Development of ductile cast iron production technology in china", 2008, 02-0082-10

[24] [22] Karl-Fredrik Nillson, darina Blagoeva, Pietro Moretto, " An Experimental and numerical analysis to correlate variation in ductility to defects and microstructure in ductile cast iron components", engineering fracture mechanics 73, 2006, 1133-1157

[25] [23] S. Konoplyuk T. Abe, T. Uchimonto T. Takagi, M. Kurosawa," Characterization of ductile cast iron by eddy current method, Institute of Fluid Science, Tohoku University, Katahira 2-1-1, NDT&E International 38 (2005) 623–626

[26] [24] J.M. Makar, R. Desnoyears,S. E. McDonald, "Failure Modes and Mechanism in gray cast iron pipe", National Research Council Canada,2001, NRCC-44218

[27] [25] Ugur Sen, Saduman Sen, Fevzi Yilmaz, " An Evaluation of some Properties borides deposited on boronized ductile iron", Journal of Materials Processing Technology 148 (2004) 1–7

[28] [26] R. Zagorski, J. Oelezino, " Pouring of Mould during Centrifugal casting process of high speed steel roll", Modeling and Numerical Simulation of Material Science,2014

[29] [27] Uday A. Dabade, Rahul C. Bhedasgaonkar, "Casting Defect analysis using Design of Experiments and Computer Aided Casting Simulation Technique", CIRP Conference on Manufacturing Systems, 2013, 616- 621

[30] [28] Courtesy of Kastwel Foundries, Ahmedabad

[29] Susanta Kumar Swain; Sudipta Sen, "Effect of Chemistry and Poring Variables on the Mechanical Properties of Thin-wall Ductile iron Casting", NIT-Rourkela

International Journal of Engineering Research and General Science Volume 3, Issue 3, Part-2 , May-June, 2015
ISSN 2091-2730

Optimization and Analysis of Dry Turning of EN-8 Steel for Surface Roughness

Sudhir B Desai[a], Sunil J Raykar[b]*,Dayanand N Deomore[c]

[a] Yashwantrao Chavan School of Rural Development, Shivaji University,Kolhapur,416004,India.

[a]Assistant Director/Assistant Professor,Sbd.ycsrd@unishivaji.ac.in, 9673748181

[b,c]D Y Patil College of Engineering and Technology,Kolhapur,416006,India.

Abstract- Dry machining has gained a lot of importance in at the moment in manufacturing industries because possibilities of health hazards due to use of coolants while machining. Many industries are now using dry environment whenever it suitable during machining of various metal alloys. This paper presents a detailed analysis and optimization of surface roughness in dry turning of EN-8 which is widely used material for general-purpose axles, shafts, gears, bolts and studs. ANOVA is used for studying influence of various cutting parameters on surface roughness. For optimization Taguchi methodology is used. The optimized parameters are selected on basis for smaller is better signal to noise ratio criterion. During the analysis it is found that feed is the most significant parameter while dry turning of EN-8 steel. The optimized parameters are 180 m/min of speed, 0.2 mm/rev. feed and 1 mm depth of ct which gives surface roughness value of 1.21 µm.

Keywords: DryMachining, SurfaceRoughness, TaguchiMethodology, Turning, Analysis, Optimisation, EN-8

1.INTRODUCTION

Dry machining is a practice in which no coolant is used while cutting process. Coolants in many machining processes are used because of their capability to assist to improve the surface finish. But In the past years the cost of cutting fluids has risen from just 3% of the overall cost of the machining process, to that of more than 15% of a production shop's cost. In several countries 'spent' cutting fluids have been re-classified as either 'toxic-' , or 'hazardous-waste' ,moreover, if they have been found to have machined certain alloyed and exotic material workpieces, they are under even harsher disposal regulations [1]. Health professional around the world has pointed out numerous health hazards due to long term exposure of lubricants and coolants [2]. Recently dry and near dry cutting conditions are more popular developments in machining because of concern about coolant costs and environmental problems from large quantity cutting fluid applications [3].Due the latest advancement in manufacturing and cutting technology many of metal alloys can be cut without or very less use of coolant.

Numerous parts are machined to produce explicit surface characteristics because they have features such as bearing, locking, or gasketing surfaces which necessitate a consistent surface finish. In many applications, particularly finishing operations, the surface finish requirement restricts the range of tool geometries and feed rates which can be used. Furthermore, since the machined surface finish becomes rougher and less consistent as the tool wears, stringent finish requirements may also limit tool life and thus strongly influence machining productivity and tooling costs[4].Raykar et al.[5] investigated dry machining of EN-8 steel using regression models their analysis showed that feed has greatest influence on surface finish. They also found very less difference between surface roughness values obtained dry machining and machining with coolant therefore recommended use of dry machining conditions when situation is favorable. Asilturk et al. [6] reported significant effect of feed rate on the surface topology parameters Ra and Rz while optimization of cutting parameters to minimize surface roughness during turning of hardened AISI 4140 steel (51 HRC) with coated

carbide tools. Diniz and Micaroni [7] reported increases in surface roughness with increase in feed while dry maching but for wet cutting this increase roughness was greater than for dry cutting.Asiltürk and Neseli [8] presented a combined approach of Taguchi method and the RSM for optimization of CNC turning parameters. They found feed rate is the most significant factor on the work piece surface roughness (Ra and Rz) with the percent contribution of 85.5% in bringing down the average roughness values.

2. Details of Experiment

2.1 Experimental Set up

The experimental studies were carried out on a CNC turning center. All the experiments were conducted under dry cutting conditions Work pieces of EN-8 steel were used with size of 40mm in length and 40 mm in diameter. The turning length was 30mm which also permit holding of workpiece with a length 5mm. The cutting insert was TNMG 06 04 04 M3 for the insert tool holder used was MTLNR 25 25 M 06 W. The experiments were carried out on 27 specimens for every experimental run a fresh insert side was used for making suitable analysis and comparison. The surface roughness was measured using a Mitutoyo SJ-201 sampling length of 0.8mm. Fig. 1 shows the specimens. After every turning operation specimen were cleaned and surface roughness was measured with a suitable clamping arrangement. The surface roughness was measured at three points on the specimen and average of there was taken as final roughness value.

Fig.1 Machined Workpieces and Workpiece with cutting tool during machining

2.2 Design of Experiment

Taguchi methodology is used for design of experiment. Speed, feed and depth of cut are the three process parameters are selected for this investigation. The levels these parameters are selected on basis of some trial experiment and from tool manufacture's catalogue. Each parameter is kept at three levels high low and medium. Therefore experiment consists of three factors at three levels. For this purpose L_{27} Taguchi array is used to design the experiment. The three process parameters with their levels are shown in Table 1.Table 2 indicates details L_{27} array with actual values of all process parameters and the measured value of surface roughness parameter R_a after experiment.

Table 1 Process Parameters and Their Levels

Levels	Process Parameters		
	Speed 'V' (m/min.)	Feed 'f' (mm/rev.)	Depth of Cut 'd' (mm)
Low	125.60	0.2	0.2
Medium	150.72	0.25	0.4
High	175.84	0.3	0.6

Table 2.Taguchi L27 array with Process parameters, Surface roughness and Signal to Noise Ratio for Surface Roughness

EN	Speed 'V' (m/min.)	Feed 'f' (mm/rev.)	Depth of Cut 'd' (mm)	Surface Roughness 'Ra' (µm)	SNR for Roughness 'db'
1	125.6	0.2	0.2	4.1527	-12.3666
2	125.6	0.2	0.4	3.884	-11.7856
3	125.6	0.2	0.6	4.322	-12.7137
4	125.6	0.25	0.2	7.0147	-16.9202
5	125.6	0.25	0.4	5.8123	-15.287
6	125.6	0.25	0.6	6.1787	-15.8179
7	125.6	0.3	0.2	8.5757	-18.6654
8	125.6	0.3	0.4	8.384	-18.469
9	125.6	0.3	0.6	9.3137	-19.3824
10	150.72	0.2	0.2	3.7507	-11.4822
11	150.72	0.2	0.4	3.87	-11.7542
12	150.72	0.2	0.6	4.131	-12.3211
13	150.72	0.25	0.2	5.7883	-15.251
14	150.72	0.25	0.4	6.408	-16.1345
15	150.72	0.25	0.6	5.7337	-15.1687
16	150.72	0.3	0.2	8.0542	-18.1204
17	150.72	0.3	0.4	8.377	-18.4618
18	150.72	0.3	0.6	8.7917	-18.8815
19	**175.84**	**0.2**	**0.2**	**3.6503**	**-11.2466**
20	175.84	0.2	0.4	3.8543	-11.7189
21	175.84	0.2	0.6	3.85	-11.7092
22	175.84	0.25	0.2	6.015	-15.5847
23	175.84	0.25	0.4	5.986	-15.5427
24	175.84	0.25	0.6	5.9207	-15.4475
25	175.84	0.3	0.2	9.0097	-19.0942
26	175.84	0.3	0.4	8.811	-18.9005
27	175.84	0.3	0.6	9.0937	-19.1748

3 Analysis of Results

Analysis of the experimental data obtained through Taguchi experimental design was carried out using MINITAB 16. Analysis of variance (ANOVA) and analysis of means (AOM) were performed to determine the influence of process parameters on the surface roughness. The statistical significance of process parameters were evaluated by corresponding P values. When P-value is less than 0.05 (or 95% confidence) the parameter is said to statistically significant on the surface roughness. Main effects plot were used in conjunction with ANOVA to visualize the effect of the process parameters on surface roughness.

Table 3. Analysis of Variance for Roughness (µm), using Adjusted SS for Tests

Source	**DF**	**Seq SS**	**Adj SS**	**Adj MS**	**F**	**P**
Speed 'V' (m/min)	2	0.416	0.416	0.208	1.79	0.193
Feed ' f' (mm/rev)	2	102.784	102.784	51.392	442.46	0.000
DoC 'd'(mm)	2	0.220	0.220	0.110	0.95	0.405
Error	20	2.323	2.323	0.116		
Total	26	105.742				
S = 0.340807 R-Sq = 97.80% R-Sq(adj) = 97.14%						

From ANOVA table and AOM plot shown in Figure 2 it is clear that feed is the most significant parameter which affects the surface roughness at 95% confidence with P value of 0.000 which is less than 0.05.This trend follows the general machining system. Because surface roughness is directly proportional to feed rate used during the machining. During the investigation it is found that surface roughness increases with increases with increase in feed from 0.2 to 0.25 and also from 0.25 to 0.3.The other two parameters that is speed and depth of cut do have a significant effect on surface roughness. Surface roughness marginally decreases with increase in speed from 125.8 to 150.72 but thereafter it slightly increases when speed increase to 175.84.When depth of cut changes from 0.2 to 0.4 surface roughness remains unchanged but a slight increase in surface roughness is noticed when depth up further increase to 0.6 mm.

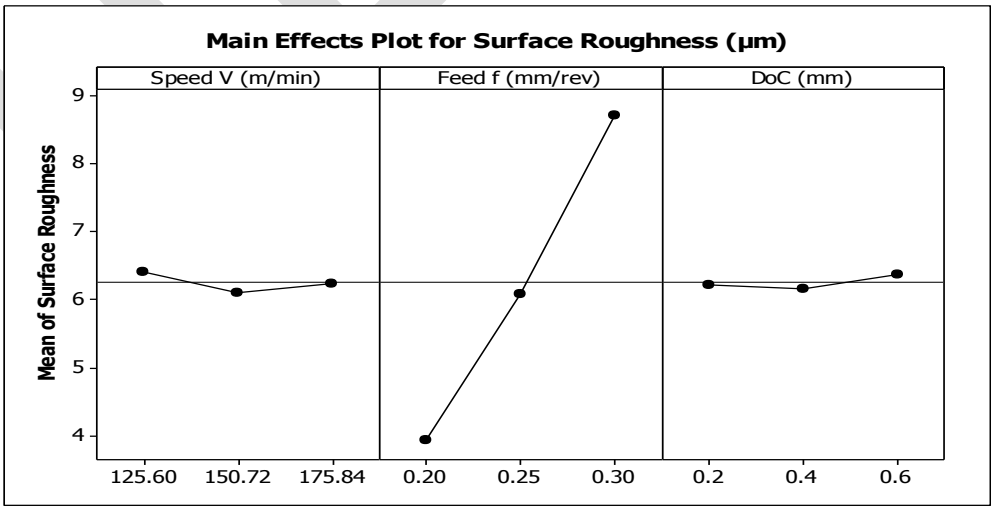

Figure 2 Main Effect Plot for Surface Roughness

For optimization Taguchi methodology is used. The optimized process parameters are selected on basis for smaller is better signal to noise ratio criterion because for any maching process smaller values of roughness are preferred. From signal to noise ratio shown in Table 2 it is clear that optimum combination of process parameter for dry turning of EN-8 are 175.84 m/min speed, 0.2 mm/rev feed and 0.2 mm depth of cut. At these process parameters the signal to noise ratio is -11.2466 and surface roughness is 3.6503 µm.

4 Conclusions

Optimization and analysis of dry turning of EN-8 steel is presented in this investigation. Taguchi methodology and ANOVA techniques are used for optimization and analysis purpose. Based on analysis following conclusions can be drawn.

- Feed has greatest influence on surface roughness. Feed affects the surface roughness at 95% confidence with P value of 0.000 for the parameters under investigation.
- The Cutting Speed and depth of cut do not show significant effect on surface roughness fro parameters under study.
- The optimized parameters for dry turning of EN-8 steel for this investigation are 175.84 m/min speed, 0.2 mm/rev feed and 0.2 mm depth of cut. At these process parameters the signal to noise ratio is -11.2466 and surface roughness is 3.6503 µm.

REFERENCES:

[1] Graham T. Smith,Cutting Tool Technology-Industrial Handbook,Springer-Verlag London Limited 2008,pp 425.
[2] Geoffrey Boothroyd and Winston A Knight, Fundamentals of Machining and Machine tools, Tayor & Francis Group,2006,pp189-90.
[3] Edward Trent, Machining and Machine tools technology, Elsevier,2006, pp189-90.
[4] Stephenson David A.; Agapiou John S.,Metal Cutting Theory and Practice Manufacturing,Engineering and Materials Processing ; 49, CRC Press,1997,pp 629.
[5] Sunil J Raykar, D.M. D'Addona, Davorin Kramar, Analysis of Surface Topology in Dry Machining of EN-8 Steel,Proceedings of 3rd International Conference on Materials Processing and Characterisation (ICMPC 2014), Procedia Materials Science 6 (2014) 931 – 938
[6] Ilhan Asilturk, Harun Akkus, Determining the effect of cutting parameters on surface roughness in hard turning using the Taguchi method, Measurement 44 (2011) 1697–1704.
[7] Anselmo Eduardo Diniz, Ricardo Micaroni, Cutting conditions for finish turning process aiming: the use of dry cutting, International Journal of Machine Tools & Manufacture 42 (2002) 899–904.
[8] Ilhan Asiltürk, Süleyman Neseli, Multi response optimisation of CNC turning parameters via Taguchi method based response surface analysis Measurement 45 (2012) 785–794. [10] J Paulo Davim, A note on determination of optimal cutting conditions for surface finish obtained in turning using design of experiments, Journal of Materials Processing Technology 116 (2001) 305-308

International Journal of Engineering Research and General Science Volume 3, Issue 3, Part-2 , May-June, 2015
ISSN 2091-2730

IP Core Design of Task Scheduler to Support Out-of-Order Execution in an MPSoC Environment

Ruchika Bamnote, Priya M. RavaleNerkar

PG Student [VLSI & Embedded Systems], Dept. of ETC, DYPCOE Akurdi, Pune, Maharashtra

ruchikabamnote@gmail.com, 8412824480

Abstract—In this paper the design of an IP core of Multiprocessor System-on-Chip (MPSoC) in the context of microarchitecture of the Scheduling Processor targeted for multicore systems is explored. This scheduling processor schedules the tasks i.e. units of computation in parallel for execution on different processors and IP cores. As this model is dealing with Out-of-Order (OoO) execution, the data dependencies like Read-after-Write (RAW), Write-after-Read (WAR) and Write-after-Write (WAW) imposes the challenging constraints on the direct use of techniques like register renaming and dynamic scheduling at instruction level. The scoreboarding algorithm with parameter renaming technique at task level analyzes the data dependencies in order to solve the stalling problem occurring in OoO execution. Thus the scheduler schedules different tasks in OoO manner. The model for the same has been verified by using resulting timing diagram. The results demonstrate that the model can largely release the burden on programmers as well as uncover the task level parallelism (TLP).

Keywords—Multiprocessor System-on-Chip, Out-of-Order execution, scoreboarding algorithm, register renaming, data dependencies, stalling, task scheduling.

INTRODUCTION

Multiprocessor system on chip has been seen in main stream since last few years [1]. Companies like Xilinx and Altera have prime focus of research on this emerging area. The development of MPSoC begins from the multi-core central processing unit. It is a platform that contains multiple processing elements with specific functionalities which are usually heterogeneous. However, due to its heterogeneous instruction set architectures, software tool chains and programming interfaces, it has presented many challenges to efficient designing and implementation of rapid prototype for diverse applications.

The most promising future processor architectures are considered as the combination of reconfigurable computing and multi-core technologies [1]. However, there are some critical issues like computational capabilities, scalability, programmability, flexibility, power consumption and so on, which are becoming increasingly important. Such raising demands have resulted into the outgrowth of FPGA based MPSoC composed of a variety of heterogeneous computational units. Whereas, OoO execution is a paradigm used in most high-performance microprocessors to make use of instruction cycles that would otherwise be wasted by delay. In this paradigm, a processor executes instructions in out-of-order as soon as the input data is available, instead of their original order in a program. As it allows execution with less waiting time, the performance definitely improves. Also the process technology has improved and per units more transistors can be fitted in the same die area, hence adding new features to the system becomes effectively easy. Thus dynamic scheduling can easily be implemented to build cost effective system.

In basic pipelining the system uses in-order instruction issue technique due to which if an instruction stalls rest all instructions are stalled. In contrast to this, the OoO execution has capability to schedule the ready instructions independently. Therefore to solve the stalling problem OoO execution technique is used for multi-cycle task execution, as this study focuses on multi-cycle task execution. Dynamic scheduling is a useful scheduling technique for multi-cycle instructions systems. Scoreboarding and Tomasulo are two such effective methods for dynamic scheduling, out of which this study implements scoreboarding algorithm for OoO parallel execution of task scheduling. Thus an IP core of task scheduler intending to solve the data dependencies during OoO execution using dynamic scheduling is developed in MPSoC environment.

RELATED STUDY

Rigorous research is being done on MPSoC regarding the critical issues like computational capabilities, programmability, flexibility, scalability and power consumption. By using parallel programming paradigm the computational capabilities can be achieved. Such parallel task execution models have been studied for parallel computing machines during the past decades. Initially, many task based parallel programming models were popular like Cilk [2] to enhance ILP to TLP. Mostly it was focused on symmetric multiprocessor but it was unable to support fully automatic parallelization. So the programmers have to handle the task scheduling and mapping

schemes manually. Some of them focused on the utilization of reconfigurable FPGA platform and integration of acceleration engines, such as Chimaera [3], Platune [4] and MOLEN [5].

Also models like Wave Scalar [6] combined both static and dynamic dataflow analysis in order to exploit more parallelism. Later on with the tremendous advancements in chip integration, to solve the programming wall problem, MPSoC programming models such as StarSs [7] [8], Oscar [9] and CellSs [10] are taken into consideration. These models implicitly schedule work and data, thereby saving the efforts of programmer by explicitly managing parallelism. These models share conceptual similarities with the out-of-order superscalar pipelines, such as dataflow scheduling and dynamic data dependency analysis. The traditional algorithms, such as Scoreboarding and Tomasulo, can dynamically schedule the instructions for OoO execution and explore ILP with multiple arithmetic units.

Task Superscalar pipeline is an abstraction of out-of-order superscalar pipelines which can use processors as function units. It dynamically identifies task-level parallelism, detects intertask data dependencies, and executes the tasks out-of-order [11]. An object-based dataflow execution with data dependencies analysis method achieve even more dataflow-like execution and exploit higher degrees of concurrency. Using this model the parallel execution of statically-sequential programs is achieved. In a dataflow fashion, it dynamically parallelizes the execution of suitably-written sequential programs on multiple processing cores [12]. OoOJava is a compiler-assisted approach that uses developer annotations along with the static analysis to provide an easy-to-use deterministic parallel programming model. This method is based on task annotations that instruct the compiler to consider a code block for OoO execution [13].

MP-Tomasulo is a dependency-aware automatic parallel task execution engine for sequential programs. It detects and eliminates WAW and WAR inter-task dependencies in the dataflow execution by applying the instruction-level Tomasulo algorithm to the MPSoC environment. So this system operates tasks in OoO on heterogeneous units but it has the overhead of scheduling which could be reduced [14]. In order to reduce these overheads, Task-scoreboarding was developed. It is a data hazards detection engine for OoO task execution. It considers IP cores and processors as function units and treats tasks as abstract instructions. It can analyze intertask data dependencies at runtime and issues tasks to heterogeneous function units automatically with parameter renaming techniques [15].

PROPOSED DESIGN

The OoO task scheduler proposed here is intended to provide the high speed execution by solving the stalling problem in OoO execution due to data dependency at TLP. The proposed work, execution flow for it and the algorithm implementation is discussed in this section.

A. Proposed work

The distinctive heterogeneous MPSoC hardware consists of multiple processors and a variety of heterogeneous IP cores for dedicated applications to extract the task level parallelism. Accountable components of such systems are computing processors, hardware IP cores, scheduling processor, interconnect modules, memory and peripherals. This paper is going to focus on the scheduling processor part, because handling immense number of tasks is a very critical job. This proposed design is a parallel task execution model for the fast execution of such system at TLP. It supports out of order execution along with register renaming mechanism by dynamically scheduling the tasks.

The proposed block diagram for IP core implementation of task scheduler to support OoO execution in an MPSoC environment is shown in Fig. 1. The block diagram consists of two computing processors and three IP cores interfaced with the scheduling processor which uses scoreboarding algorithm for dynamic scheduling. Scoreboarding can provide a light-weight task hazards detection engine for OoO execution, its architecture is simple, which brings smaller scheduling overheads and for TLP, WAW and WAR data dependency do not encounter as much as at instruction level [15]. Therefore here scoreboarding algorithm is preferred instead of Tomasulo.

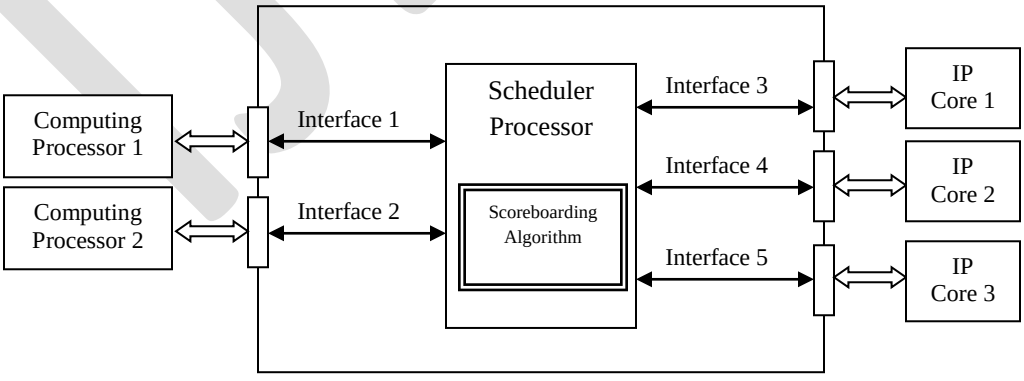

Fig. 1 Block diagram for IP core design of task scheduler to support OoO execution

B. Microarchitecture of scheduler processor

The microarchitecture of scheduler processor is shown in Fig. 2. The scheduler processor fetches the task-instructions from the register file which represents invocation of a task. It decodes each task-instruction and then schedules it to the computing processors

and IP cores where the corresponding task is executed. Each task specifies its outputs and inputs to and from the registers in register file. After issuing the task-instruction, register is renamed by using register renaming technique. In this system a merged type rename buffer is used. A merged type feature is only a Register File that contains both the renaming (in-process) registers and architectural (retired) registers [16]. After renaming, the updated values are dispatched to the OoO execution unit. The task scheduler has its own scoreboard memory. The physical register file used here is of load-store type architecture. The tasks are then executed parallelly in the computing processors and IP cores. Then the result is written back in the register file and alternatively scoreboard memory gets updated.

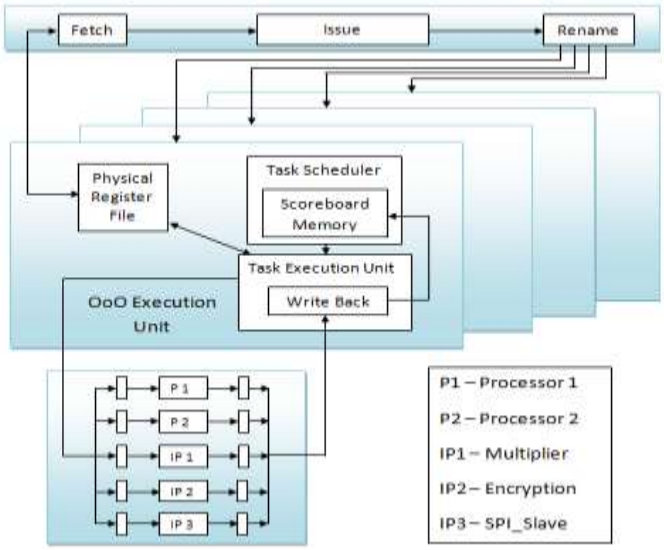

Fig. 2: Scheduler processor microarchitecture

C. Execution flow for OoO scheduling

The task sequence is issued and executed through seven stages: fetch, issue, rename, read operand, task partition, execute and write result. From these fetch, issue and rename are in-order stages. Whereas, read operand, task partition and execution stage are out-of-order stages. At last the result is again writing back in in-order. All these stages are similar to the instruction level pipelining, in addition to that register renaming stage is included as stage 3. Each task undergoes through these seven stages as shown in Table 1. The seven stages of execution flow are as follows:

1) *Fetch* – initially the instruction is fetched from the physical register file. Then it is decoded for further execution.
2) *Issue* – after decoding, the scoreboard issues the instruction to the functional unit (FU) and updates its internal data structure if a FU for instruction is free and no other active instruction has same destination register. After confirming that no other active FU wants to write its result into the destination register, WAW- Hazards are avoided. The instruction issue is stalled in the case of a WAW-Hazard or a busy FU.
3) *Rename* – this technique is used for dependency decoding. It assigns a unique storage location with each write-reference to a register.
4) *Read operand* – the scoreboard monitors the availability of the source operands. If no earlier issued active instruction is going to write the register, then that source operand is available and as soon as it gets available the instruction can proceed. In this way it resolves all RAW-Hazards dynamically and allows instructions to execute out of order.
5) *Task partition* – after finishing read operand stage, availability of function unit check is done and then goes for execution.
6) *Execute* – the required FU starts the execution of the instruction. As soon as the result is ready, it informs the scoreboard that it has completed the execution. If another instruction is waiting on the same result, it can be forwarded to the stalled FU.
7) *Write result* – the write back of the instruction is stalled on the existence of a WAR-Hazard until the source operand is read by the dependent instruction which is a preceding instruction in the order of issue.

TABLE 1 PROCESSING FLOW OF SCOREBOARDING

Task status	Wait until	Bookkeeping
Fetch		Fetch the data from register file

Issue	Not Busy [FU] and not Results [D]	Busy [FU] ←yes; Op [FU]←op; F_i [FU] ←D; F_j [FU] ←S1; F_k [FU] ←S2; Q_j←Result [S1]; Q_k←Result [S2]; R_j←not Q_j; R_k←not Q_k; Result [D] ←FU
Rename	Task issued	Rename with new register from register file
Read Operand	R_j and R_k	R_j ←No; R_k←No;
Task Partition	! ∀ Busy [FU]	Select the FU and replace table entries
Execute	Function unit done	Distribute tasks to function units
Write Result	∀f((F_j [f]≠F_i [FU] or R_j [f] = No) & (F_k [f] ≠F_i [FU] or R_k [f] =No)	∀f(if Q_j [f]=FU then R_j [f] ←Yes); ∀f(if Q_k [f]=FU then R_k [f] ←Yes); Result [F_i [FU]] ←0; Busy [FU] ←No

D. Algorithm implementation

Scheduling is very useful for the multi-cycle instructions, because when instructions are multi-cycled then only the scheduling will work more efficiently; otherwise, single cycle instructions does not need the scheduling. The scoreboard algorithm maintains three status tables to control the execution of the instructions:

- *Instruction Status*: Indicates the existing status of stages for each instruction being executed.
- *Functional Unit Status*: Indicates state of each functional unit. The function unit status is listed in Table 2. Each function unit maintains 9 fields in the table:
  1. Busy: Indicates whether the unit is being used or not
  2. Op: Operation to be performed in the unit (e.g. MULT, DIV, LOAD, ADD)
  3. F_i: Destination register
  4. F_j,F_k: Source-register numbers
  5. Q_j,Q_k: Functional units that will produce the source registers F_j, F_k
  6. R_j,R_k: Flags that indicates when F_j, F_k are ready
- *Register Status*: Indicates which function unit will write results into it for each register.

TABLE 2 Function unit status table

Name	Function Unit Status							
	Busy	F_i	F_j	F_k	Q_j	Q_k	R_j	R_k
Load								

Multiplier								
AES_ENC								
SPI_slave								

RESULT

In order to solve the problem of stalling, the task scheduler is designed and developed in this research that supports OoO execution in an MPSoC environment. Five processing units are interfaced to the scheduler with two computing processors and three IP cores. The IP cores interfaced here are AES encryption, SPI slave and multiplier and computing processors are of RISC architecture. The task scheduler is designed in ModelSim software using Verilog language. As technology independent modeling is developed, it can be used as an IP core in any system for OoO execution and hazards detection.

Here four tasks are considered for the algorithm implementation as shown in Table 2. The experimental results are taken under four situations: no hazards, RAW, WAW and WAR. Task execution time and task scale, these two parameters are considered for performance evaluation. The task execution time denotes the entire execution time for different types of data hazards. Whereas, task scale is nothing but the total amount of different tasks or number of loop iterations.

The task scale is considered up to 1046 for result analysis. From the analysis it is found that this model is able to solve 25 % and 50 % RAW, WAW and WAR hazards and 100 % WAR hazards as shown in Fig. 3. Also from the RTL level simulation it is found that the model is able to solve the WAW and WAR dependencies at task level which has been avoided in case of ILP.

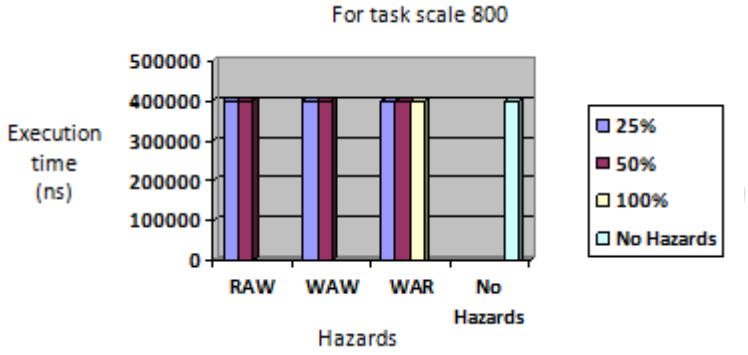

Figure 3: Result analysis for hazard detection

CONCLUSION

In this paper, a synthesizable IP core of task scheduler is designed in an MPSoC environment. The stalling problem in OoO execution is solved using dynamic scheduling scoreboard algorithm for TLP. The algorithm considers the abstract instructions as tasks and; processor and IP cores as function units. The model analyzes the inter-task data dependencies at runtime and after solving dependencies, it issues the tasks to function units. The experimental result shows that the designed IP core can support the OoO execution with data dependency resolution at TLP. It also resolves the WAW and WAR dependencies which are not possible at ILP. This designed IP core can be used in SoCs to support OoO execution for task scheduling. The work can be extended with the implementation of algorithm for superscalar processors.

REFERENCES:

[1] S. Borkar, and A.A. Chien, The future of microprocessors. Communications of ACM, 54(5): 67-77, 2011
[2] Robert D Blumofe, Christopher F Joerg, Bradley C Kuszmaul, Charles E Leiserson, Keith H Randall, and Yuli Zhou. Cilk: An efficient multithreaded runtime system. Journal of parallel and distributed computing, 37(1):55-69, 1996.
[3] Scott Hauck, Thomas W Fry, Matthew M Hosler, and Jeffrey P Kao. The Chimaera reconfigurable functional unit. IEEE Transactions on Very Large Scale Integration (VLSI) Systems, 12(2):206-217, 2004
[4] Tony Givargis and Frank Vahid. Platune: a tuning framework for system-on-a-chip platforms. IEEE Transactions on Computer-Aided Design of Integrated Circuits and Systems, 21(11):1317-1327, 2002
[5] Georgi Kuzmanov, Georgi Gaydadjiev, and Stamatis Vassiliadis. The Molen processor prototype. 12th Annual IEEE Symposium on Field-Programmable Custom Computing Machines, 296-299, 2004
[6] Steven Swanson, Ken Michelson, Andrew Schwerin, and Mark Oskin. Wavescalar. Proceedings of the 36th annual IEEE/ACM International Symposium on Microarchitecture, 291-302, 2003
[7] Dallou, Tamer, and Ben Juurlink. Nexus++: A Hardware Task Manager for the StarSs Programming Model, 2011
[8] Josep M. Perez, Rosa M. Badia and Jesus Labarta. A Dependency-Aware Task-Based Programming Environment for Multi-Core Architectures. Cluster Computing, 2008 IEEE International Conference on. IEEE. 142-151, 2008

[9] A. Hayashi, Y. Wada, T. Watanabe, et al. Parallelizing compiler framework and API for power reduction and software productivity of real-time heterogeneous multicores. in Proceedings of the 23rd international conference on Languages and compilers for parallel computing. Houston, TX: Springer-Verlag. 2010

[10] Bellens, Pieter, Josep M. Perez, Rosa M. Badia, and Jesus Labarta. CellSs: a programming model for the Cell BE architecture. In *SC 2006 Conference, Proceedings of the ACM/IEEE*, pp. 5-5. IEEE, 2006

[11] Yoav Etsion, Felipe Cabarcas, Alejandro Rico, Alex Ramirez, Rosa M Badia, Eduard Ayguade. Task superscalar: An out-of-order task pipeline. 43rd Annual IEEE/ACM International Symposium on Microarchitecture (MICRO), 89-100, 2010

[12] Gagan Gupta and Gurindar S Sohi. Dataow execution of sequential imperative programs on multicore architectures. Proceedings of the 44th Annual IEEE/ACM International Symposium on Microarchitecture, 59-70, 2011

[13] James Christopher Jenista and Brian Charles Demsky. OoOJava: Software out-of-order execution. ACM SIGPLAN Notices, 46(8):57-68, 2011

[14] Chao Wang, Xi Li, Junneng Zhang, Xuehai Zhou, and Xiaoning Nie. MP-Tomasulo: A dependency-aware automatic parallel execution engine for sequential programs. ACM Transactions on Architecture and Code Optimization (TACO), 10(2):1-9, 2013

[15] C. Wang, X. Li, J. Zhang, P. Chen, Y. Chen, X. Zhou, and R. Cheung. Architecture support for task out-of-order execution in MPSoCs. IEEE Transactions on Computers, 1-14, 2014

[16] D. Capalija, & T. S. Abdelrahman, Microarchitecture of a coarse-grain out-of-order superscalar processor. Parallel and Distributed Systems, IEEE Transactions on, *24*(2), 392-405, 2013

International Journal of Engineering Research and General Science Volume 3, Issue 3, Part-2 , May-June, 2015
ISSN 2091-2730

Impact of Various Symptoms of Carpal Tunnel Syndrome in Vehicle and Axle Assembly Line in Industry

Md Sarfaraz Alam[1], Ahsan Moazzam[2], M.A.Akhtar[3], Manoj Kumar[4],

Department of Mechanical Engineering, Sant Longowal Institute of Engineering and Technology, India

E-mail: sarfaraz8665@gmail.com, ahsansliet10@gmail.com

Abstract— For localized vibration exposure of the hand and arm to occur, the hand must grip a vibrating object. The effects of vibration in hand intensive work, along with factors, such as forceful and repeated exertion and certain postures. Vibration has been cited as a factor tendon disorders such as Carpal Tunnel Syndrome (CTS) and tendinitis. Vibration may increase the risk of chronic tendon and nerve disorders by increasing the force exerted in repetitive manual tasks. In this study, the survey has been conducted on 69 vehicles assembly line (vibrating unit) workers and 69 axle assembly line (non-vibrating unit) workers. The study was conducted by questionnaire, physical examination, exposure evaluation, medical inspection, interviews and job observation.

Keywords— Vehicle assembly line, axle assembly line, CTS, hand-arm vibration, tendinitis, vibration

INTRODUCTION

CARPAL TUNNEL SYNDROME (CTS)

CTS is a condition in which tendons or ligaments in the wrist become enlarged. The main (median) nerve of the hand and its branches enter the hand through a narrow Passageway (Carpal tunnel) formed by wrist bones (Carpal bones) and the tough membrane that holds the bones together (transverse carpal ligament). The median nerve supplies sensation to the thumb, index finger, middle finger and in most people to part of the ring finger. Because this passageway is rigid, inflammation, swelling, or increase fluid retention may compress the nerve (Nerve entrapment), causing pain and numbness in the fingers (particularly the index, middle, and thumb) and eventually serious hand weakness.

SYMPTOMS OF CTS

The typical symptoms of CTS are tingling of the thumb and of the index, middle and ring fingers and night pain. The pain awakens the patient, but is often relieved by shaking, hanging, or massaging the hand. Pain may involve not only in the hand, but also the arm and the shoulder. Numbness and loss of manual dexterity occur in more advanced cases. Weakness of the hand also occurs, causing difficulty with pinch and grasp. The victim may drop objects or be unable to use keys or count change with the affected hand. The skin may dry because of reduced sweating.

Some of the main important of symptoms are as follows:

- Wrist pain
- Hand pain
- Weakness
- Grasping
- Tingling
- Numbness

VEHICLE ASSEMBLY LINE

In Automobile manufacturing industry job are done through multiple manual and semi-automatic operations. It is found to have a considerable difference in the way of doing the job at several work stations. The various components used in a four wheeler vehicle assembly line are follows:

i. **Sub- assembly suspension front and rear**: In this operation, the suspension is assembled with front and rear axles. It is made up of four huge and five-axis machining that are made from 7075 forgings specific alloy having weight around 313 kg. The operation is performed on a conveyor line in the company. Repetitive use of both hands is involved in the process. The operators engaged in this operation are eight.

ii. **Attach hoses flexible to rear axle brake pipe**: In this process, the hoses flexible are attached in to rear axle brake pipe. The brake hose is an integral part of the braking system and used to transmit brake fluid under hydraulic pressure from the brake pipe to the calipers. They are manufactured from reinforced rubber. It is performed on a moving conveyor, while assembly is done by air nut runner. Both hands are involved in the operation. The operators engaged in this operation are six.

iii. **Attach ALSV, DDU and tight sensing valve**: In this operation, ALSV, DDU are attached with sensing valve. Automatic load sensing valve (ALSV) is developed which can be used in air brake system in commercial vehicles. The dry distributing unit (DDU) dries moist compressed air through a desiccant bed. It maintains system pressure within a required range. The DDU is used in the circuit of an air brake system of an automobile. Repetitive use of right hand is involved in process. Operators engaged in this operation are five.

iv. **Attach stay Intercooler**: In this operation attach stay intercooler, the intercooler are fitted on the stay intercooler. It is made up of mild steel. The operation is performed on a moving conveyor vehicle assembly line. This operation involves lifting and holding the profile with finger extremities/hands. The operators engaged in this operation are eight.

v. **Attach 3 way joint hydraulic brake and brake pipe**: In this operation 3 way joint hydraulic brakes and brakes pipe is attached. 3 ways joint are manufactured from copper and copper-nickel. The brake pipe is a rigid pipe usually made of steel, and carries pressurized brake fluid from the master cylinder to the brake hoses. Steel or copper brake pipes from the main network of pipes supplying brake fluid to all the brake components. Repetitive use of both hands is involved in process. The operators engaged in this operation are five.

AXLE ASSEMBLY LINE

An axle is a central shaft for a rotating wheel or gear. On wheeled vehicles, the axle may be fixed to the wheels, rotating with them, or fixed to the vehicle, with the wheels rotating around the axle. Axles are integral component of most practical wheeled vehicles. In a live-axle suspension system, the axles serve to transmit driving torque to the wheel, as well as to maintain the position of the wheels relative to each other and to the vehicle body. For the analysis potential CTS symptoms amongst worker, worker engaged in axle manufacturing unit operation of XYZ manufacturing industry were involved in the study. The various components of the axle manufacturing and their function are as follows:

i. **Fitting of retainer**: In this operation, retainer is fitted in the axle shaft. It is a made up of steel, zinc plate. Retainer plates are a critical part in the retainment of any bolt in axle. The operation is performed on a work station. Repetitive use of right hand is involved in process. The numbers of operators engaged in this operation are six.
ii. **Fitting of oil seal**: In this operation, oil seal fitted is pushed with the help of a riveting machine. It is made up of rubber, Nitrile Buna-N 70, Silicone, fluoride rubber. Median nerve related muscles are fatigued in this operation involving thumb, index and middle finger extremities.
iii. **Fitting of gasket**: This operation function is very similar to oil seal but it is performed on a similar kind of special purpose machine, so that enforcement of oil seal joint to ensuring the leakage of hydraulic oil and air in the chamber. Both hands are involved in the operation. Operators engaged in this operation are nine.
iv. **Fitting of ball bearing**: In this operation, ball bearing is fitted in the axle shaft. A bearing in which the parts are separated by a ring of small freely rotating metal balls which reduce friction. It is the made up of steel or stainless steel. This operation involves lifting and holding the profile with finger extremities/hands. Operators engaged in this operation are eleven.
v. **Fitting of circlip**: In this process, Circlips are a type of retaining ring. They are typically made from carbon steel, stainless steel or beryllium copper. Median nerve related muscles are fatigued in this operation involving thumb, index and middle finger extremities.

EXPERIMENTATION

FISHER'S EXACT TEST

It is used to check statistical significance by 2 × 2 contingency tables. In present study Fisher's exact test has been done to check significance for all the symptoms obtained in collected data for vehicle assembly line and axle assembly line workers for their comparison. Notations a, b, c and d are assigned to cells for Fisher's exact test and the grand total is assigned the notation 'n' and are presented below in Table 1.

Table 1.: A 2 × 2 contingency table set-up used for Fisher's exact test

Description	Vehicle Assembly Line	Axle Assembly line	Total
Symptom present (test positive)	a	b	a+b
Symptom present (test positive)	c	d	c+d
Total	a + c	b + d	a+b+c+d = n

The test is done on categorical data that result from classifying situation in two different ways. The probability value from the test is computed by the hyper geometric distribution as following (Montgomery, 2005)

$$P = \frac{\binom{a+b}{a}\binom{c+d}{c}}{\binom{n}{a+c}} = \frac{(a+b)!(c+d)!(a+c)!(b+d)!}{a!b!c!d!n!}$$

Where, the number of observations obtained for analysis is small (sample size ≤ 30).

ANALYSIS USING FISHER'S EXACT TEST

Hand arm vibration (HAV) exposed workers often experience tingling and numbness in their fingers. These symptoms can be intermittent or have a short duration if caused by the vibrations per sec. Patients can easily interpret symptoms differently or may have another definition for the symptom, which may confuse the picture of how common the HAVS is (Edlund, 2014). Symptoms related to CTS are numbness, tingling, difficulty in grasping, weakness, hand pain, wrist pain, positive Tinel's and Phalen's sign. These symptoms amongst vibrating and non-vibrating unit workers with their percentage of occurrence are obtained from the collected data and significance are checked for the symptoms as shown in Tables 2, 3, 4, 5, 6, 7, 8, 9, 10.

Table 2.: Survey based CTS symptoms data for Numbness

Symptoms	Vehicle Assembly Line	Axle Assembly line	Total
Numbness	21	9	30
No Numbness	48	60	108
Total	69	69	138

Table 3.: Survey based CTS symptoms data for Tingling

Symptoms	Vehicle Assembly Line	Axle Assembly line	Total
Tingling	26	11	37
No Tingling	43	58	101
Total	69	69	138

Table 4.: Survey based CTS symptoms in Difficulty data for Grasping

Symptoms	Vehicle Assembly Line	Axle Assembly line	Total
Grasping	22	10	32
No Grasping	47	59	106
Total	69	69	138

Table 5.: Survey based CTS symptoms data for weakness

Symptoms	Vehicle Assembly Line	Axle Assembly line	Total
weakness	24	19	43
No weakness	45	50	95
Total	69	69	138

Table 6.: Survey based CTS symptoms data for hand pain

Symptoms	Vehicle Assembly Line	Axle Assembly line	Total
Hand pain	28	16	44
No Hand pain	41	53	94
Total	69	69	138

Table 7.: Survey based CTS symptoms data for wrist pain

Symptoms	Vehicle Assembly Line	Axle Assembly line	Total
Wrist pain	20	09	29
No Wrist pain	49	60	109
Total	69	69	138

Table 8.: Survey based CTS symptoms data for Phalen's Test

Symptoms	Vehicle Assembly Line	Axle Assembly line	Total
Phalen's sign	27	14	41
No phalen's sign	42	55	97

Total	69	69	138

Table 9.: Survey based CTS symptoms data for Tinel's Test

Symptoms	Vehicle Assembly Line	Axle Assembly line	Total
Tinel's sign	31	18	49
No Tinel's sign	38	51	89
Total	69	69	138

Table 10.: Comparing of CTS symptoms Vehicle assembly line and Axle Assembly line

Symptoms	% of CTS symptoms in Vehicle Assembly Line	% of CTS symptoms in Axle Assembly line	p-value	Significance
Numbness	30.43	13.04	0.0222	($p<0.05$)
Tingling	37.68	15.94	0.0067	($p<0.05$)
Difficulty in grasping	31.88	14.49	0.0256	($p<0.05$)
Weakness	34.78	27.53	0.4625	Not significant
Hand pain	40.57	23.18	0.0439	($p<0.05$)
Wrist pain	28.98	13.04	0.0355	($p<0.05$)
Phalen's Sign	39.13	20.28	0.0248	($p<0.05$)
Tinel's sign	44.92	26.08	0.0323	($p<0.05$)

P-values are calculated through Fisher's exact test to find out the significant values of potential CTS sufferers. A parameter is significant if $0.01 < p < 0.05$, highly significant if $p < 0.01$ and not significant if $p \geq 0.05$.
From the above Table 10, it is observed that percentage of workers having all CTS symptoms i.e. numbness, tingling, difficulty in grasping, weakness, hand pain, wrist pain Phalen's sign and Tinel's sign is more in vibrating unit as compared to non-vibrating unit. Calculated p-value shows that there is a significant difference in the percentage of workers having symptoms except weakness (p-value = 0.4625). So weakness cannot be correlated to CTS in present study. As p-value is found to be minimum for tingling (p-value = 0.0067) it is the most significant CTS symptom related to CTS.

ANALYSIS USING CORRELATION

Data from health surveillance in vehicle assembly line and axle assembly line workers is classified according to potential CTS symptoms. To study the correlation between vehicle and axle assembly line for potential CTS symptoms, a hypothesis is assumed that the use of vibration tool does not affect potential CTS symptoms.

Table 11.: Vibrating and non-vibrating unit workers based potential symptom data for Correlation analysis

	Num-bness	**Tingling**	**Difficulty in grasping**	**Hand pain**	**Wrist pain**	**Phalen's Sign**	**Tinel's Sign**
No. of workers with symptom in Vehicle Assembly line (X)	21	26	22	20	20	27	31
No. of workers with symptom in Axle Assembly line (Y)	9	11	10	14	9	14	18

The values of ΣX^2, ΣY^2 and $\Sigma X.Y$ are calculated from survey based potential CTS symptoms data from the equation to get the correlation coefficient (r).

Table 12.: Calculated corresponding values of dependent and independent variables

X	Y	X^2	Y^2	X.Y
21	9	441	81	189
26	11	676	121	286
22	10	484	100	220
20	14	400	196	280
20	9	400	81	180
27	14	729	196	378
31	18	961	324	558
ΣX=167	ΣY=85	ΣX^2=4091	ΣY^2=1099	Σ XY=2091

$$r\ (\text{correlation coefficient}) = \frac{\sum x.y}{\sqrt{(\sum x^2 . \sum y^2)}} = \frac{2091}{\sqrt{(4091 x 1099)}} = 0.986$$

Significance t-test value is obtained by putting correlation coefficient (r) in equation

$$t = r\sqrt{N-2}/\sqrt{1-r^2}$$

$$t = 0.986\sqrt{7-2}/\sqrt{1-(0.986)^2} = 13.222$$

Standard value of significance t-test for degree of freedom 5, at 5% level is equal to 2.015. Since calculated value of t-test (13.201) is more than standard value (2.015), so the alternative hypothesis is rejected. It concludes that CTS symptoms are affected by use of vibration tool.

RESULT AND CONCLUSION

From Fisher's exact test, it is observed that percentage of workers having all CTS symptoms i.e. numbness, tingling, difficulty in grasping, weakness, hand pain, wrist pain, Phalen's sign and Tinel's sign is more in vehicle assembly line as compared to axle assembly line.

Calculated p-value shows that there is a significant difference in the percentage of workers having symptoms except weakness. As p-value is found to be minimum for tingling, it is the most significant CTS symptom related to CTS.

By correlation, it is observed that standard value of significance t-test for degree of freedom 5, at 5% level is equal to 2.015. Since calculated value of t-test is more than standard value, so the alternative hypothesis is rejected. It concludes that CTS symptoms are affected by use of vibration tool.

REFERENCES:

[1] Ainsa Ignacio, Gonzalez David, Lizaranzu Miguel, Bernad Carlos, "Experimental evaluation of uncertainty in handearm vibration measurements" International Journal of Industrial Ergonomics, (2011); 41: 167-179.

[2] Astrom Charlotte, Rehn Borje, Lundstro mb Ronnie, Nilssonc Tohr, Burstromd Lage, Sundelin Gunnevi, "Hand-arm vibration syndrome (HAVS) and musculoskeletal symptoms in the neck and the upper limbs in professional drivers of terrain vehicles - A cross sectional study" Applied Ergonomics, (2006); 31: 793–799.

[3] Atroshi I, Gummesson C, Johnson R, Ornstein E, Ranstam J, Rosen . "Prevalence of carpal tunnel syndrome in a general population" JAMA (1999); 281(2): 153-8.

[4] Babski-Reeves Kari L., Crumtpon-Young Lesia L. "Comparisons of measures for quantifying repetition in predicting carpal tunnel syndrome" International Journal of Industrial Ergonomics (2002), 30: 1–6

[5] Barcenilla A, March LM, Chen JS, Sambrook PN "Carpal tunnel syndrome and its relationship to occupation: a meta-analysis" Rheumatology (Oxford) (2012), 51:250–261.

[6] Barnhart Scott, MD, MPH, Demers A Paul, MS, Miller Mary, ARNP, MN, Longstreth WT, Jr, MD, MPH, Rosenstock Linda, MD, MPH. "Carpal tunnel syndrome among ski manufacturing workers", Scand J Work Environ Health (1991);17:46-52.
[7] Bianchi G, Frolov K, Oledzki A. "Man under Vibration: Suffering and Protection", Bridger RS. "An Introduction to Ergonomics". New York, USA: McG Hill. Elsevier (1981).
[8] Burt Susan, Deddens A James, Crombie Ken, Jin Yan, Wurzelbacher Steve, Ramsey Jessica, "A prospective study of carpal tunnel syndrome: workplace and individual risk factors" Burt S, et al. Occup Environ Med (2013); 0:1–7.
[9] Cartwright MS, Walker FO, Blocker JN, Schulz MR, Arcury TA, Gzywacz JR, Mora D, Chen H, Marín AJ, Quandt SA "The Prevalence of Carpal Tunnel Syndrome in Latino Poultry Processing Workers and Other Latino Manual Workers" J Occup Environ Med. 2012 February; 54(2): 198–201.
[10] Cederlund Ragnhild, Isacsson Ake, Lundborg Goran, "Hand Function in Workers with Hand-Arm Vibration Syndrome" J HAND THER (1999); 12:16-24.
[11] Cherniack M., Brammer A. J., Lundstrom R., Morse F., Neely G., Nilsson T.,Peterson D., Toppila E., Warren N., Diva U., Croteau M., Dussetschleger J. "Theeffect of different warming methods on sensory nerve conduction velocity in shipyard workers occupationally exposed to hand–arm vibration" Int Arch Occup Environ Health (2008);8: 1045–1058.
[12] Chung MK, Lee I and Yeo YS. "Physiological workload evaluation of screw driving tasks in automobile assembly jobs". International Journal of Industrial Ergonomics, (2001); 28: 181-188.
[13] Clark BD, Barr AE, Safadi FF, Beitman L, Al-Shatti T, Amin M, Gaughan JP, Barbe MF. "Median Nerve Trauma in a Rat Model of Work-Related Musculoskeletal Disorder". Journal of Neurotrauma (2003); 20: 681-695.
[14] Dahlin B Lars, Sanden Helena, Dahlin Erik, Zimmerman Malin, Thomsen Niels and Bjorkman Anders, "Low myelinated nerve-fibre density may lead to symptoms associated with nerve entrapment in vibration-induced neuropathy" Journal of Occupational Medicine and Toxicology (2014), 9:7
[15] Dale AM, Harris-Adamson C, Rempel D, Gerr F, Hegmann K, Silverstein B, Burt S, Garg A, Kapellusch J, Merlino L, Thiese MS, Eisen EA, Evanoff B, "Prevalence and incidence of carpal tunnel syndrome in US working populations: pooled analysis of six prospective studies" Scand J Work Environ Health (2013);39(5):495-505

International Journal of Engineering Research and General Science Volume 3, Issue 3, Part-2 , May-June, 2015
ISSN 2091-2730

Measuring Code Quality to Improve Specification Mining

Roshan Deshmukh, Prof.Umesh Kulkarni

KVCT's ARMIET, roshan982@gmail.com

Abstract— Every software Industry requires the quality of code. Formal specifications are mathematically based techniques whose purposes are to help with the implementation of systems and software. They are used to describe a system, to analyze its behavior, and to aid in its design by verifying key properties of interest through rigorous and effective reasoning tools. These specifications are formal in the sense that they have syntax, their semantics fall within one domain, and they are able to be used to infer useful information. Formal specifications can help with program testing, optimization, refactoring. However, they are difficult to write manually, and automatic mining techniques suffer from 90–99% false positive rates. To address this problem, we propose to augment a temporal-property miner by incorporating code quality metrics. We measure code quality by extracting additional information from the software engineering process, and using information from code that is more likely to be correct as well as code that is less likely to be correct.

Keywords— Specification mining, machine learning, software engineering, code metrics, program understanding

INTRODUCTION

Incorrect and buggy behavior in deployed software costs up to $70 billion each year in the US [7]. Thus debugging, testing, maintaining, optimizing, refactoring, and documenting software, while time-consuming, remain critically important.

Such maintenance is reported to consume up to 90% of the total cost of software projects .A key maintenance concern is incomplete documentation up to 60% of maintenance time is spent studying existing software(e.g.,[8]). Human processes and especially tool support for finding and fixing errors in deployed software often require formal specifications of correct program behavior(e.g.,[9]); it is difficult to repair a coding error without a clear notion of what "correct" program behavior entails. Unfortunately, while low-level program annotations are becoming more and more prevalent, comprehensive formal specifications remain rare.

Many large, preexisting software projects are not yet formally specified. Formal program specifications are difficult for humans to construct .and incorrect specifications are difficult for humans to debug and modify. Accordingly, researchers have developed techniques to automatically infer specifications from program source code or execution traces [2]. These techniques typically produce specifications in the form of finite state machines that describe legal sequences of program behaviors.

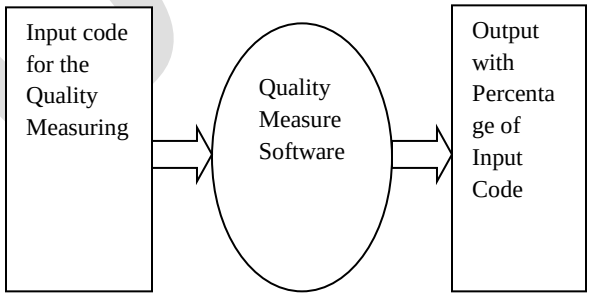

Fig.1.Block Diagram

LITERATURE SURVEY

API-based and Information Theoretic Metrics for Measuring the Quality of Software Modularization [10]. This system is developed using Object oriented software system. Create a set design principles for code modularization and produce set of metrics. Modularization quality is calculated using metrics such as structural, architectural and notions. There are three contributions such as coupling, cohesion and complexity metrics to modularize the software. This metrics seek to characterize a body of software according to the enunciated principles. Provide two types of experiments to validate the metrics.

Whaley *et al.* propose a static miner [1] that produces a single multi-state specification for library code. The JIST[2] miner refines Whaley *et al.*'s static approach by using techniques from software model checking to rule out infeasible paths. Gabel and Su [3] extend Perracotta using BDDs, and show both that two-state mining is NP-complete and some specifications cannot be created by composing two-state specifications. Lo *et al.* use learned temporal properties, such as those mined in this article, to *steer* the learning of finite state machine behavior models [4].Shoham *et al.* [5] mine by using abstract interpretation, where the abstract values are specifications

MINING CHARACTERISTICS

This section shows the underlying concepts of mining techniques and their limitations which encourage the researchers to step into incorporating code quality metrics. Specification mining techniques produces specifications but still they have high false positive rates. The Comparison between most of these approaches is provided in the Table 1.

In WN miner [6] the specification mining was motivated by the observations of run-time error handling mistakes. In other approaches examining such mistakes, the code frequently violates simple API specifications in exceptional situations. Despite the proliferation of specification-mining research, there is not much report on issues pertaining to the quality of specification miners. This technique is same as that of Engler et al. but is based on assumptions about run time errors, chooses candidate event pairs differently, presents significantly fewer candidate specifications and ranks presented candidates differently.

In a normal Table1.A Comparison study execution, events „a' and „b' may be separated by other events and difficult to discern as a pair. After an error has occurred, however, the cleanup code is usually much less cluttered and contains only operations required for correctness. The candidate specifications are filtered using varied criteria such as exceptional control flow, one error, data path etc.

This highlights the practical importance of the algorithmic assumptions, in particular the use of exceptional control flow. It can serve as a requirement for acceptance. It can even assist inspections by helping to target effort at parts of a program that may need improvement. Though this miner select specifications from software artifacts and finds per-program specifications for error detection, it does not have profound results in bug finding.

Strauss, ECC and WN technique were all good at yielding specifications that found bugs. The WN technique found all bugs reported by other techniques on these benchmarks and did so with the fewest false positives.

QUALITY METRICS

Code metrics like LOC and Cyclomatic Complexity examines the internal complexity of a procedure whereas this structure metrics examines the relationship between a section of code and the rest of the system. Process oriented metrics are used through the different phases of the software life cycle. Measurement on quality should concentrate on the early phases in the life cycle to improve the quality of software and decrease of development and maintenance costs. Defects must be tracked to the release origin which is the portion of the code that contains the defects and at what release the portion was added, changed, or enhanced.

When calculating the defect rate of the entire product, all defects are used; when calculating the defect rate for the new and changed code, only defects of the release origin of the new and changed code are included. On the one hand, the process quality metrics simply means tracking defect arrival during formal machine testing for some organizations. On the other hand, some software organizations with well-established software metrics programs cover various parameters in each phase of the development cycle.

Miners	Characteristics	Comment
Engler et al.	Use two state temporal properties.	High false positive rates
Whaley et al.	Produces Single multi state specification	Human intervention
Strauss	focuses on machine learning to learn a Single specification from traces	Use of single specification is not sufficient
JIST	Refines Whaley et al. technique to mainly disregard infeasible paths	Handles only simple subset of Java
WN miner	Selecting specifications from software artifacts	Does not have profound results in finding bugs
Claire	Use measurements of trustworthiness of source code to mine specifications	Does not give adequate results over precision.

ACKNOWLEDGMENT

I would like to express my sincere gratitude towards my guide Prof.Umesh Kulkarni for the help, guidance an encouragement in the development of this methodology. They supported me with scientific guidance, advice and encouragement, and were always helpful and enthusiastic and this inspired me in my work. I have benefitted from numerous discussions with guide and other colleagues.

CONCLUSION

Formal specifications have a variety of applications including testing, maintenance, optimization, refactoring, documentation, and program repair. However, such specifications are difficult for human programmers to produce and verify manually, and existing

automatic specification miners that discover two-state temporal properties have prohibitively high false positive rates. The goal of this survey is to support the study on the legacy of generating specifications to the new automatic techniques. It helps to get an insight into this dynamic field of study in Specification Mining. Since the object orientation is emerging in all kinds of applications, it is also welcome in the specification mining process. It is mentioned to be dynamic, as these approaches are under development and it steps higher everyday to achieve efficiency in capturing specifications.

REFERENCES:

[1]J. Whaley, M. C. Martin, and M. S. Lam, "Automatic extraction of object-oriented component interfaces," in ISSTA, 2002.

[2]R.Alur, P.Cerny, P.Madhusudan, and W. Nam, "Synthesis of interface specifications for Java classes," in POPL, 2005.

[3]M. Gabel and Z. Su, "Symbolic mining of temporal specifications, "in ICSE, 2008, pp. 51–60.

[4]D. Lo, L. Mariani, and M. Pezz`e, "Automatic Steering of Behavioral Model Inference," in FSE. ACM, 2009, pp. 345–354.

[5]S. Shoham, E. Yahav, S. Fink, and M. Pistoia, "Static specification mining using automata-based abstractions," in *International* Symposium on Software Testing and *Analysis*, 2007, pp. 174–184.

[6]W. Weimer and G.C. Necula, "Mining Temporal Specifications for Error Detection," Proc. Int'l Conf. Tools and Algorithms for the Construction and Analysis of Systems, pp. 461-476, 2005.

[7]National Institute of Standards and Technology, "The economic impacts of inadequate infrastructure for software testing," Tech. Rep. 02-3, May 2002.

[8]S. L. Pfleeger, Software Engineering: Theory and Practice. Upper Saddle River, NJ, USA: Prentice Hall PTR, 2001.

[9]D. Malayeri and J. Aldrich, "Practical exception specifications."In Advanced Topics in Exception Handling Techniques, 2006, pp. 200–220.

[10]Sarkar, S.; Kak, A.C.; Rama, G.M. "Metrics for Measuring the Quality of Modularization of Large-Scale Object-Oriented Software", Software Engineering, IEEE Transactions on, on page(s): 700 - 720 Volume: 34, Issue: 5, Sept.-Oct. 2008

International Journal of Engineering Research and General Science Volume 3, Issue 3, Part-2 , May-June, 2015
ISSN 2091-2730

Patient-Centric Secure Sharing of Personal Health Records in Cloud Storage

Prajakta Solapurkar,Girish Potdar

Department of Computer Engineering, Pune Institute of Computer Technology, Pune, Maharashtra, India

Email-praj.solapurkar112@gmail.com

Abstract— In a modern healthcare environment, personal health record(PHR) owners are willing to store and share electronic medical records via the cloud because of its ubiquity and on-demand self service. Secure and efficient data sharing scheme enable patients to have full control over their PHRs and at the same time provide confidentiality and authenticity of personal health data. Selective data sharing requires different documents to be encrypted with different keys, which implies, patients to distribute to users a large number of keys and the authorized users have to securely store the received keys. The need for secure storage, communication and efficient key management renders the approach impractical. The current work focuses on reducing key management overhead by generating a single aggregate key, but does not provide, how it can satisfy the principles of efficient data sharing. So, we propose a scheme to achieve: confidentiality of personal health data, authenticity of personal health data, patient-centric fine-grained access control and revocation of access control using key-aggregate cryptosystem. Experimental results show that the proposed scheme reduces key-size and key management overhead.

Keywords— Key-aggregate Cryptosystem, Personal Health Records, Secure Sharing, Cloud Storage, Data sharing, Access Control, Security.

INTRODUCTION

With the increasing popularity of electronic health records, personal health records (PHR) that include personal and medical information, insurance details, etc. have become increasingly important. Cloud computing has emerged as a promising solution for providing ubiquitous, convenient, and on-demand accesses to large amounts of data. Hence it is considered as an attractive option by many patients to store and share their health records and hence remove the geographical dependence between health care provider and patient. However, PHRs may contain sensitive data like patients' personal contact information, laboratory test reports, X-rays and so on. Due to data outsourcing, patients do not have full control privileges over the data which increases security and privacy risks.

To ensure data privacy and access control, PHR owners choose to encrypt their data before uploading it on the cloud and hence the data remains secure against the cloud providers and other malicious users. Suppose that patients want to share their PHRs with different data users, there are two ways to achieve this under traditional encryption scheme:

- Data owner (patient) encrypts all categories of personal health records with a single encryption key (symmetric key cryptosystem) and gives the data users like doctors, nurses the corresponding secret key directly.
- Data owner (patient) encrypts different categories of personal health records with different keys and sends the corresponding secret keys to data users like doctors, nurses, relatives etc.

Here, the first method is inappropriate since it also provides access to unauthorized categories of PHR. The second method is inefficient as the number of keys will be equal to the number of file categories. In practice, transferring these secret keys requires a secure communication channel, and storing of these keys requires an expensive secure storage. Therefore, the best solution for the above problem is that the data owner encrypts different categories of PHR with different public-keys, but is sent to data users like doctors, nurses etc. a single key for decryption. Small key-size is desired since the secure communication and storage is required. So to reduce key management overhead (key-size, key transfer, key storage) of data owner a concept of a key aggregate cryptosystem is used [1].

But secure and efficient data sharing scheme also enables a data owner to have full control over their PHRs.Many recent studies [3-5] discuss on how patients apply the encrypted-once and decrypted-many-times encryption technique to their PHR data using Attribute-Based Encryption (ABE) [8-10] or proxy re-encryption schemes [11-12]. But, if the access structure is too complicated, then ABE is insufficient for providing patients with full control over their data [2]. It is therefore necessary to explore how patients set up

access privileges for fine-grained access control of their PHR data, i.e., PHR data categories should be accessible only to those users who possess the corresponding decryption keys and the set of decryption keys should be kept confidential from others with the minimum key management overhead. Our proposed solution employs the concept of a key-aggregate cryptosystem and successfully resolves the problem of data access control in a health care setting.

LITERATURE SURVEY

Several recent studies have focused on the issue of secure sharing of electronic health records in the cloud.

Chen *et al.* [4] proposed an EHR solution, relying mainly on smart cards and RSA that enables patients to store their medical records on hybrid clouds. In this approach, patients' medical records are stored in two types of cloud: the hospital's private cloud and the public cloud. The authors discussed two usage cases. The first is that of the medical records being accessed by the owner of the data, *i.e.*, the doctor who created the records. They can directly access the records from their private cloud or from the public cloud. The second case is that of the medical records being accessed by other hospitals, who must seek permission from the data owner before they can access the records. The authors also provide a solution for emergency situations. However, the shortcoming of this approach is that data owners, *i.e.*, doctors have access control for the medical records and their computing load is heavy.

Leng *et al.* [5] proposed a solution that allows patients to specify a policy to support fine-grained access control. They primarily utilized Conditional Proxy Re-Encryption to enforce sticky policies and provided users with write privileges for PHRs. When users finish writing data to their PHRs, they sign the modified PHRs. However, users sign the PHRs using the signature key of the PHR owner and it is therefore difficult to correctly verify who signed the PHRs.

Kuo et al. [2] proposed a scheme for patient-centric access control over PHR data. The proposed scheme ensures the following security properties: (1) confidentiality of health data, (2) integrity of health data, (3) authenticity of health data, (4) patient-centric fine-grained access control, and revocation of access control using symmetric key cryptosystem and proxy re-encryption (PRE) scheme. But the main drawback of this scheme is, each file category is encrypted with distinct secret key so whenever a data user (e.g. Doctor or nurse) wants to update PHR categories, patient have to provide the corresponding secret keys. Besides this, the scheme is based on proxy re-encryption scheme which requires data owners to have too much trust on the proxy that it only converts cipher texts according to his instruction. A PRE scheme allows data owners to delegate to the proxy the ability to convert the cipher texts encrypted under his public key into ones for data users. Hence it is desired that proxy doesn't reside in the storage server. This increases communication overhead since every decryption requires separate interaction with the proxy.

Chu et al.[1] proposed a new public key cryptosystem which can aggregate any set of secret keys to generate a single compact aggregate key encompassing the power of all the keys being aggregated. But the work did not focus on how it can help patients to have fine grained access control and revocation of access control and at the same time ensuring confidentiality, authentication and integrity of their PHRs.

So in this paper, we redesign the scheme in [2] for patient-centric access control over PHR data belonging to the patient using the concept of a key-aggregate cryptosystem. Our solution ensures the following security properties: (1) confidentiality of personal health data, (2) integrity of personal health data, (3) authenticity of personal health data, (4) patient-centric fine-grained access control, and (5) revocation of access control.

PROPOSED SCHEME

A. Access control policy for PHR data

In the architecture of the proposed scheme, PHR data are divided into different categories and arranged in hierarchy as shown in Fig 1. PHR data may include several medical records like dental records, medical records and other categories like personal information, insurance policy information etc.

PHR owners specify policies for their PHR data to grant access privileges to each user. A policy may contain the following details:

(1) Role: users who are permitted to access the data, for example, the doctor, nurse, or insurance broker.
(2) Category of PHR data: Personal Information, Laboratory Test Reports, Medical History, etc.
(3) Permission: includes read, write, and even print.

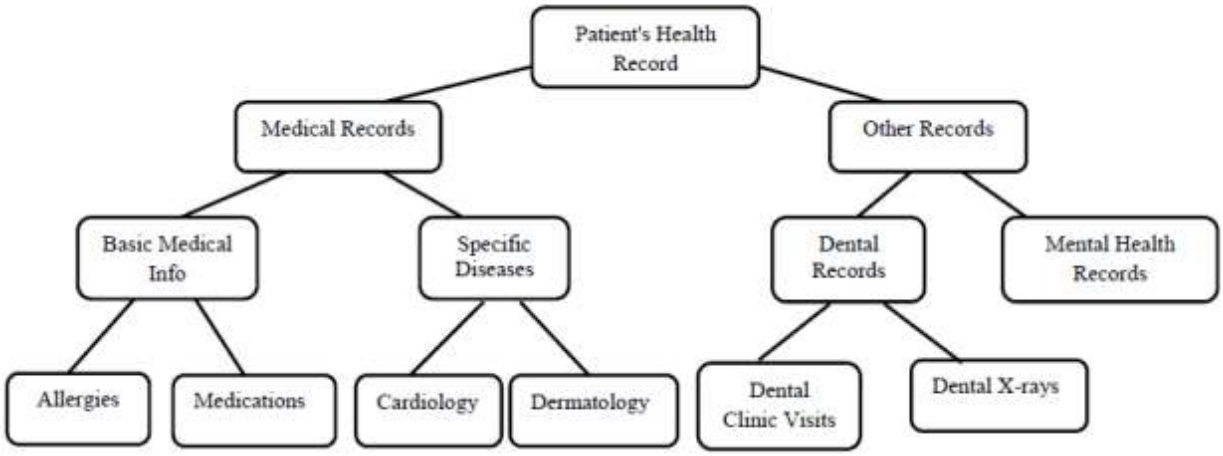

Figure 1. A hierarchical personal health record

B. Construction of Proposed Scheme

The architecture of proposed scheme consists of three roles PHR owners (patients), PHR users (doctors, nurses, insurance policy brokers etc.) and cloud server. The framework of the proposed scheme is shown in the Fig.2.It is as follows:

a) Setup (1^k, n):
This algorithm is executed by the patient to set up an account on an untrusted server. On input of security level parameter (k) which can be high, medium or low and the number of cipher text classes n (i.e., class index should be an integer between 1 and n), it outputs the public system parameter param which is set of public keys p_1, p_2...p_n.

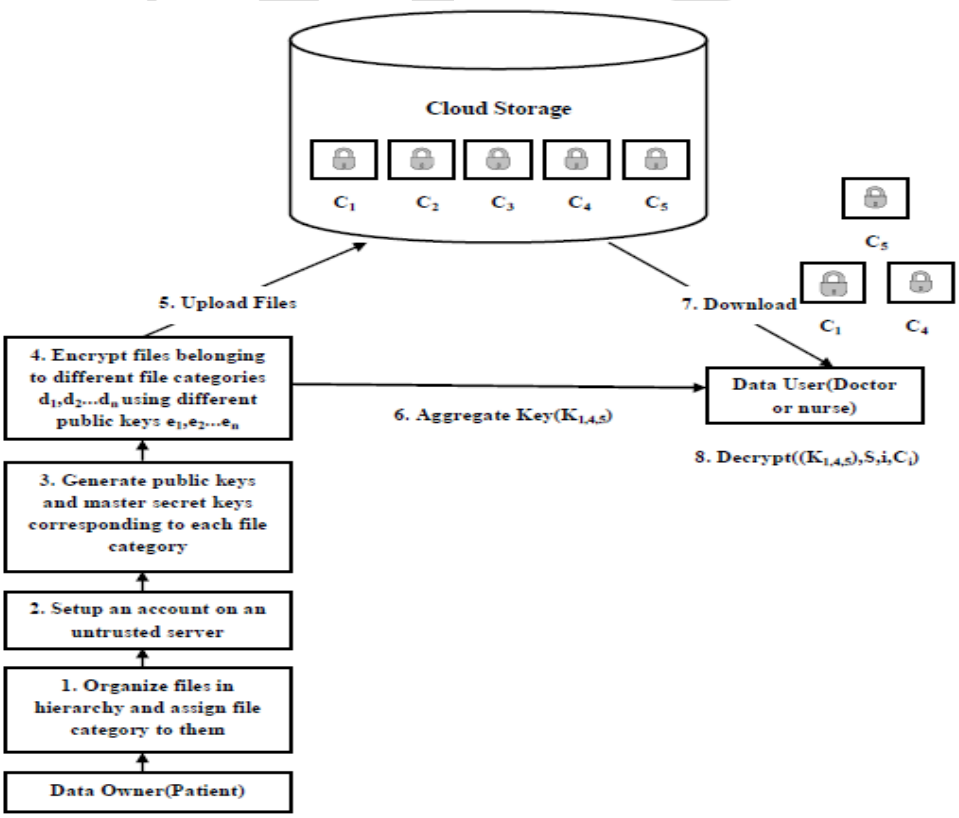

Figure 2. Framework of Proposed System

b) Key Generation (pk, msk):
This algorithm is executed by the patient to randomly generate a public/master-secret key pair (pk, msk).

c) Encrypt (pk, i, d):
This algorithm is executed by anyone who wants to encrypt data. On input a public-key pk, an index i denoting the PHR category, and a document d, it outputs a ciphertext C.

d) Extract (msk, r, S):
This algorithm is executed by the patient for delegating the decrypting power for a certain set of ciphertext classes to a delegatee. On providing input of the master secret key msk, an access right r and a set S of indices corresponding to different classes, it outputs the aggregate key for set S denoted by KS.

e) Decrypt (KS, S, i, C):
This algorithm is executed by a data user who received an aggregate key KS generated by Extract. On input KS, the set S, an index i denoting the file category the ciphertext C belongs to, and C, it outputs the decrypted result, if $C \in S$.

SOLUTION ANALYSIS

A. Confidentiality of Personal Health Data:

Before uploading a health record i, it is encrypted using the product of $(pk)_i$ and (msk)i. The master secret key is kept secret. When patient generates an aggregate key which is the product of master secret keys, data user or an interceptor cannot obtain each multiplier from the product. Hence, even pk_i component of the encryption key is publicly available, other component msk_i is hidden hence confidentiality of personal health data is ensured.

B. Authenticity of Personal Health Data:

In our proposed scheme owner of the PHR generates an aggregate key. At the time of decryption,an aggregate key successfully decrypts the authorized set of cipher text. This verifies the authenticity of personal health data.

C. Patient-centric fine-grained access control:

In our scheme, the PHR owner generates a value representing a particular access right when generating the aggregate key. The PHR owner can therefore control access privileges for every user.

D. Revocation of access control:

If the PHR owner wishes to revoke some users in a certain category, then they need only to replace the aggregate key K_s with K_{s1}. The small aggregate key size minimizes the communication overhead for transferring the new key. Revocation therefore, is easily achieved.

EXPERIMENTAL WORK AND RESULTS

A. Platform and Technology

The experimental setup in our proposed system will be configuration of OpenStack, an open source cloud platform using DevStack module.

Platform and technology used are:

a) O.S: Ubuntu 12.04
b) Database: OpenStack MySQL
c) Web Server: Apache
d) Network: OpenStack Nova
e) Hypervisor: KVM
f) Language: Java
g) Browser: Mozilla Firefox, Google Chrome etc.

B. Datasets

We conducted experimental evaluation of the proposed system on the basis of performance parameters mentioned in subsection C on a real world dataset [14].We selected the records and arranged them into a hierarchical tree structure with different heights as per the requirements of different patients.

C. Performance Parameters

Performance is the accomplishment of a given task measured against preset known standards of accuracy, completeness, cost, and speed [13]. Following is the list of parameters that we are going to evaluate:

a) Key-assignment Ratio (Ratio of number of keys granted to total number of keys granted in traditional (one-to-one) approach and proposed approach.
b) Amount of compression with respect to key size.

D. Results

Section (C) identifies performance parameters of our proposed system. We have implemented the parameters and their results are as follows: Table I. Shows compression with respect to the number of keys granted in our proposed system to the total number of keys generated as per cipher text classes (Key Assignment Ratio) and compression with respect to the key size.

Total Number of Cipher Text Classes	511 records			
Delegation Ratio	Compression ratio (no. of keys granted)	Existing Scheme [2] Key-Size in bytes	Proposed Scheme Key-Size in bytes	Compression achieved in bytes
0.1	0.66	3366	969	2397
0.2	0.71	6732	1938	4794
0.3	0.75	10098	2907	7191
0.4	0.80	13464	3876	9588
0.5	0.88	16896	4864	12032
0.6	0.90	20262	5833	14429
0.7	0.91	23628	6802	16826
0.8	0.92	26994	7771	19223
0.9	0.93	30360	8740	21620
1	0.97	33726	9109	24617

TABLE I. Compression for Different Delegation Ratios and Cipher Text Classes

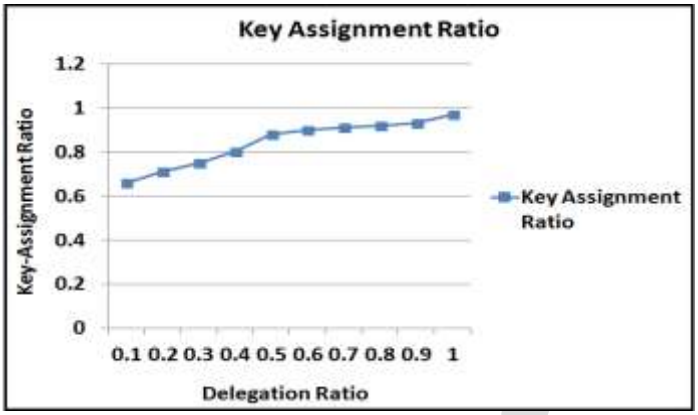

Figure 3. Key Assignment Ratio

Fig. 3 illustrates the relationship between Key Assignment Ratio and Delegation Ratio. The X-axis represents delegation ratio and Y-axis represents Key assignment Ratio (Ratio of number of keys granted to total number of keys granted in traditional(one-to-one approach). We observe that the high compression ratio can be achieved when the delegation ratio is 1.

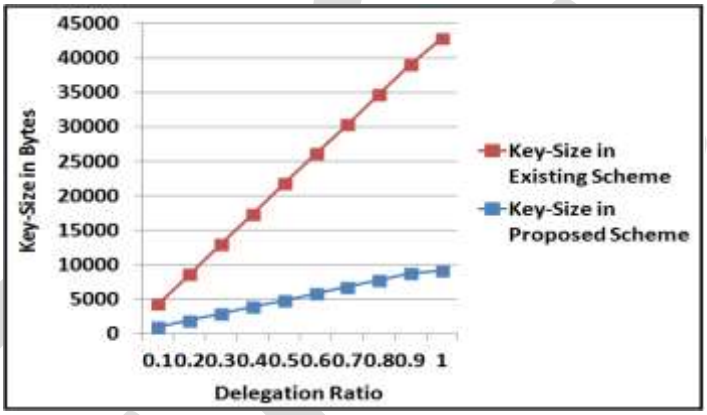

Figure 4. Key Size in Different Approaches

Fig. 4 illustrates the key-size for different approaches in the case of 511 records. The X-axis represents delegation ratio and the Y-axis represents key-size in bytes for different approaches.

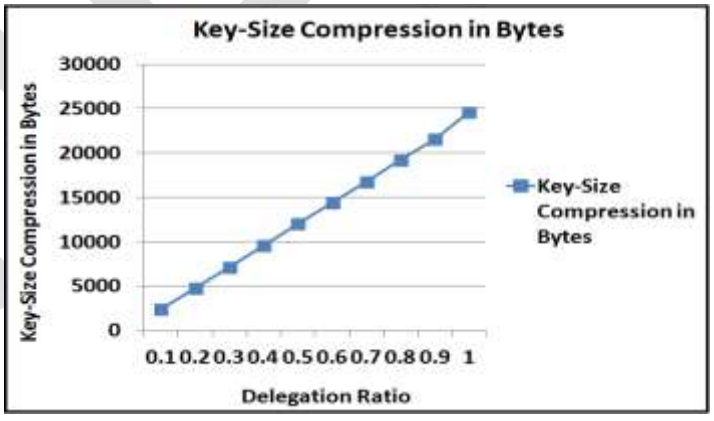

Figure 5. Compression in Key Size in Bytes

Fig. 5 illustrates the relationship between Compression in Key Size and Delegation Ratio. We observe that as delegation ratio increases and approaches to 1 (i.e. Entire PHR can be accessed by delegating single root key) the amount of key-size compression increases.

CONCLUSION

With the increasing popularity of modern healthcare systems based on cloud storage, how to protect PHRs stored in the cloud is a central question. Cryptographic techniques are getting more versatile and often involve multiple keys for a single application which increases the key management overhead. In this article, we consider how to generate a single compact aggregate key, but encompassing the power of all keys being aggregated and generate compressed secret keys in public-key cryptosystem. We also discuss how the confidentiality, and authentication of PHRs can be achieved using a key aggregate cryptosystem. This system also enables a patient to exercise complete control over their PHRs and perform revocation of access rights.

REFERENCES:

[1] C. Chu, S. Chow, and W. Tzeng, "Key-Aggregate Cryptosystem for Scalable Data Sharing in Cloud Storage", IEEE Transactions on Parallel and Distributed Systems, 2014, 25 (2): 468- 477.

[2] Kuo-Hsuan Huang, En-Chi Chang, and Shao-Jui Wang, "A Patient-Centric Access Control Scheme for Personal Health Records in the Cloud", Fourth International Conference on Networking and Distributed Computing, 2014.

[3] Dixit, G. N. "Patient Centric Frame Work For Data Access Control Using Key Management In Cloud Server", International Journal of Engineering, *2* (4), 2013.

[4] Chen, Y. Y., Lu, J. C., & Jan, J. K. "A secure EHR system based on hybrid clouds," Journal of medical systems, 36 (5), 3375-3384, 2012.

[5] Leng, C., Yu, H., Wang, J., & Huang, J. "Securing Personal Health Records in the Cloud by Enforcing Sticky Policies," TELKOMNIKA Indonesian Journal of Electrical Engineering, 11 (4), 2200-2208, 2013.

[6] J. Benaloh, M. Chase, E. Horvitz, and K. Lauter, "Patient Controlled Encryption: Ensuring Privacy of Electronic Medical Records", Proc. ACM Workshop Cloud Computing Security (CCSW 09), pp. 103-114, 2009.

[7] Chen Danwei, Chen Linling, Fan Xiaowei, He Liwen, Pan Su, and Hu Ruoxiang "Securing Patient-Centric Personal Health Records Sharing System in Cloud Computing", China Communications, Supplement No.1, 2014.

[8] Ming Li, Shucheng Yu, and Yao Zheng, "Scalable and Secure Sharing of Personal Health Records in Cloud Computing Using Attribute-Based Encryption", IEEE Transactions on Parallel and Distributed Systems, 24(1), pp. 131-143, 2013.

[9] V. Goyal, O. Pandey, A. Sahai, and B. Waters, "Attribute-Based Encryption for Fine-Grained Access Control of Encrypted Data", Proc. 13th ACM Conf. Computer and Comm. Security (CCS 06), pp. 89-98, 2006.

[10] M. Chase, and S.S.M. Chow, "Improving Privacy and Security in Multi-Authority Attribute-Based Encryption", Proc. ACM Conf. Computer and Comm. Security, pp. 121-130. 2009.

[11] R. Canetti, and S. Hohenberger, "Chosen-Ciphertext Secure Proxy Re- Encryption", Proc. 14th ACM Conf. Computer and Comm.Security (CCS 07), pp. 185-194, 2007.

[12] S.S.M. Chow, J. Weng, Y. Yang, and R.H. Deng, "Efficient Unidirectional Proxy Re-encryption", Proc. Progress in Cryptology AFRICACRYPT, vol. 6055, pp. 316-332, 2010.

[13] Mell, Timothy Grance, "The NIST Definition of Cloud Computing", NIST Special Publication 800-1145, Sept. 2011.

[14] https://catalog.data.gov/dataset/va-personal-health-record-non identifiable-data

International Journal of Engineering Research and General Science Volume 3, Issue 3, Part-2 , May-June, 2015
ISSN 2091-2730

NSCT domain image fusion, denoising & K-means clustering for SAR image change detection

Yamuna J. [1], *Arathy C. Haran* [2]

[1,2,] Department of Electronics and Communications Engineering, [1] P. G. student, [2] Faculty of Electronics and Communication Engineering, Mar Baselios College of Engineering and Technology, Trivandrum, India.

yamunamohan93@gmail.com[1] , arathychv1@gmail.com[2] .

Abstract— The change detection in SAR (synthetic aperture radar) images mainly aims to obtain a reliable change map. The existing method based on log ratio difference image and k-means clustering gives fair results. Efficiency of the change map can be increased in two ways: 1) by increasing the efficiency of the difference image by using a fused difference obtained by fusing log-ratio and gauss log ratio difference images. 2) by means of using an improved fusion technique such as NSCT. An unsupervised change detection of multi-temporal SAR images combining image fusion and denoising using NSCT (Non Sub-sampled Contourlet Transform) and clustering approach is proposed. Difference image is obtained by fusing log-ratio and gauss log ratio image. NSCT is used to fuse the difference images, reduce the effect of noise and feature map construction. The final change map is obtained by clustering the feature vector into two classes: changed and unchanged class. The combination of image fusion, NSCT noise reduction and the feature clustering is expected to give a better change map than the existing techniques.

Keywords— DWT, NSCT, NSSC, ground truth, Donohov threshold, SSIM, fmi, k-means clustering.

1.INTRODUCTION

Change detection aims for obtaining a reliable change map of the multitemporal images over the same geographical area to get the information about the changed and unchanged areas. Multitemporal images are the images obtained over the same geographical area at different time [1]. The process of change detection involves mainly two steps: 1) generating a difference image and 2) clustering the features to obtain the final change map. The satellite image change detection is a very difficult process due to the presence of speckle noise. Speckle noise is a noise which inherently present in the radar [2]. And the noise is multiplicative in nature so it is very difficult to process and denoise the image. In order to get a reliable change map difference image via two operators, image fusion, NSCT [3] and k- means clustering techniques are incorporating as part of this work. So the change map will be more accurate and is more close to the ground truth of the actual dataset. Ground truth is the actual change map of the multitemporal dataset.

The major techniques used are: difference image operators, image fusion using DWT, NSCT (Non Subsampled Contourlet Transform) and k-means clustering. The first step for satellite image change detection is the generation of difference image. The difference image obtained through a single operator does not provide satisfactory result due to the presence of speckle noise. So instead of using a single operator here two operators such as log ratio and gauss log ratio operators are used to produce the initial difference image. Then the difference images obtained via two operators are combined using image fusion technique via DWT (Discrete Wavelet Transform). The image fusion technique improves the spatial information by retaining the relevant pixel information that contains the change [3]. The features are extracted from the fused difference image through NSCT operator. The obtained NSSC [4] (Non Subsampled Contourlet Coefficients) is then denoised using Donohov threshold [4], which reduces the effect of speckle noise.

The application of change detection involves remote sensing, terrain change identification, hazard detection *etc*. The main objective of this paper is to obtain a reliable change map and which is obtained by increasing the efficiency of the difference image and by increasing the efficiency of the change map. Image fusion and NSCT techniques are also used to improve the efficiency. The image fusion technique combines the most desirable characters of the difference images and the NSCT extracts the features from the fused difference image and do the denoising process as well. NSCT is the non subsampled version of contourlet transform, having the features such as shift invariance, good localization, directionality, multi resolution *etc*. The shift invariance and denoising capability makes the NSCT more advantageous than contourlet transform. This makes NSCT to capture the geometric details, object information and edge information very well even if the effect of noise is more. The output of NSCT processed image is then clustered to get the final change map. The reliability of the proposed method are analyzed using the ground truth of the dataset. The ground truth represents the true information regarding the geographical area that has been considered. The techniques make the changed portion more homogeneous.

2. PROPOSED METHOD

2.1 Problem formulation

The existing method associated with the satellite image change detection suffers the effect of speckle noise. In addition to presence of speckle noise the effect of sensor noise, illumination variation, non uniform attenuation or atmospheric absorption causes an unreliable change map. Speckle noise is a noise which inherently present in the radar itself occurred due to the backward reflections from the object. And this noise is multiplicative in nature causing an unreliable change detection process for the multi temporal image dataset. Speckle noise is a noise which inherently present in the radar itself occurred due to the backward reflections from the object. And this noise is multiplicative in nature causing an unreliable change detection process for the multi temporal image dataset.

2.2 Method

Initially, two multi temporal images, {X1, X_2} are considered and the difference images are obtained via two operators such as log ratio and gauss log ratio operator. Log ratio difference image find outs the log difference associated with the input dataset and the gauss log ratio operator find out the log of the image and then multiply it with a Gaussian low pass filter so that the effect of multiplicative speckle noise can be reduced. These two operators helps to obtain the initial change image and also it convert the multiplicative nature of the speckle noise in to an addictive one. Then the two difference images are combined using efficient image fusion K-means clustering K means is an unsupervised clustering method to partition the difference image into two classes: changed and unchanged, so the obtained fused difference image retains the most desirable features associated with the difference image with less spectral distortion and complexity. The two fusion results are undergone with same procedure such as NSCT denoising and k-means clustering operation. And the two methods are compared finally, The features such as coefficients associated with changes are obtained through NSCT decomposition for two levels. Denoising operation is also performed using NSCT since the effect of speckle noise is dominant even after the image fusion operation. NSCT (Non Sub sampled Contourlet Transform) is the shift invariant feature of contourlet transform having good frequency characteristics and is built upon iterated non separable filter bank to obtain shift invariance. The denoised NSCT coefficients are then clustered using suitable clustering approach such as k-means clustering to obtain the final change map. So that the final change map for the input can be obtained and the approach is less complex.

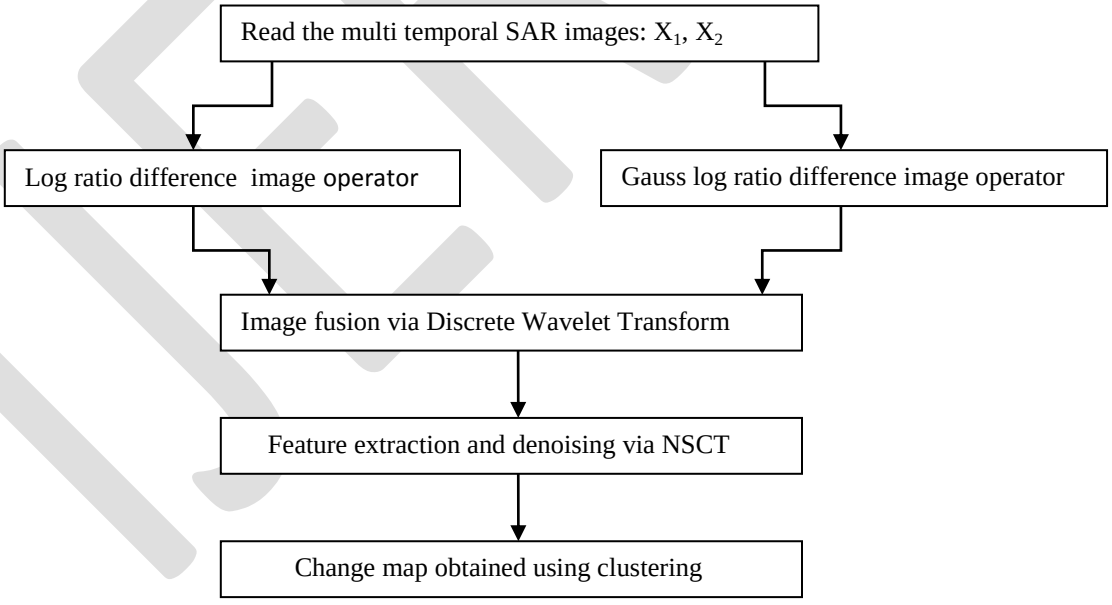

FIGURE 1: PROPOSED METHOD

3. DIFFERENCE IMAGES

The initial difference image is generated using ratio operators such as log ratio and Gauss log ratio difference image operator. These two difference image finds the major change associated with the multi temporal input images. The difference images are produced via

two operators such as log ratio and Gauss log operator so that these two difference images can be fused to obtain an efficient difference image.

3.1 Log ratio difference image

The log ratio difference images for the multi temporal images X_1 and X_2 are obtained using the formulae

$$X_L = |\log X_2 - \log X_1| \tag{1}$$

Log ratio difference image is a simple difference image operator which calculates the log difference between images. The log operation causes the conversion of multiplicative noise in to an addictive one. The log-ratio operator enhances the low-intensity pixels and deteriorates the high intensity pixels; as a result the categorization of the pixels into the changed and the unchanged classes is made more symmetrical. Also the background of the log-ratio image is flat. But the drawback in using the log-ratio operator is that, the information about the changed areas gained from the log-ratio image is not in accordance with real change trends, since the log-operator deteriorates the high intensity pixels.

3.2 Gauss log ratio difference image operator

Inorder to enhance the real change trend as well as suppress the unchanged portions in the difference image and preserve the homogeneity of the changed portions, the Gauss-log ratio operator is used. Gauss log ratio difference image considers the intensities of local patches. Where $X_1'(i, j)$ and $X_2'(i, j)$ are two patches centered at points (i, j) and using this the gauss log ratio operator is calculated as follows

$$X_{1r}(i,j) = \log\big(X_1'(i,j)\big) * G \tag{2}$$

$$X_{2r}(i,j) = \log\big(X_2'(i,j)\big) * G \tag{3}$$

Here G is a rotationally symmetric Gaussian low pass filter with a standard deviation of 0.5, defined as

$$G = \begin{bmatrix} 0.0113 & 0.0838 & 0.0113 \\ 0.0838 & 0.6193 & 0.0838 \\ 0.0113 & 0.0838 & 0.0113 \end{bmatrix}$$

And the difference image is obtained as

$$X_r(i,j) = \sum_{m=-1}^{1} \sum_{n=-1}^{1} \big| X_{1r}(i+m, j+n) \quad - X_{2r}(i+m, j+n) \big| \tag{4}$$

Here G matrix is used to maintain the integrity of the subsequent clustering algorithm.

4. IMAGE FUSION

Image fusion is used to fuse the difference image obtained via log ratio difference image and gauss log ratio difference image operator, so that we can make use of full information of both operators. Image fusion combines the difference image output so that it retains the desirable characteristics of the input image as well as increases the efficiency of the difference image. The basic steps are:

1. Load the images.
2. Merge the two images using Daubenchies wavelet decomposition for 2 levels.

4.1 Image fusion using DWT

The image fusion using DWT is considered because of it is spatially good with less computational complexity. DWT increases the quality and also overcomes the correlation between adjacent scale image information and fully reflects local variation of the original image. The DWT fusion is an earlier method and it lacks shift invariance and have problem of aliasing. So in this paper a recent method such as NSCT is used for fusion as well as for denoising the images, and also NSCT method is compared with the DWT fusion method to analyze the results.

4.2 Image fusion using NSCT

NSCT has the characteristics of multi resolution, localization, directionality, anisotropy, and shift-invariant. It can sufficiently capture the geometrical details of the image and keep the object information and the edge well. Gauss log-ratio operator and mean ratio operator is used to transform multiplicative noise into additive one. In order to make the change map possess more complete edge and contour, it is feasible to use NSCT. NSCT is the nonsubsampled version of contourlet transform (CT) and is having features such as multiresolution, localization, directionality, shift invariance etc. The process of image fusion using is shown in figure 2. The procedure for image fusion using NSCT is similar to DWT fusion and the difference is that, the two level decomposition is performed using NSCT as shown in figure 3 and the use of special NSCT filters for fusing high and low frequencies. For that initially the log ratio and gauss log ratio images are considered. The low frequency bands accurately represents the changed regions from both the log and gauss log ratio image, average operation is done in the low frequency band .For the high frequency band the rule of minimum local energy of the coefficients is chosen, and finally the weighted average is applied on coefficients to get the final fused image.

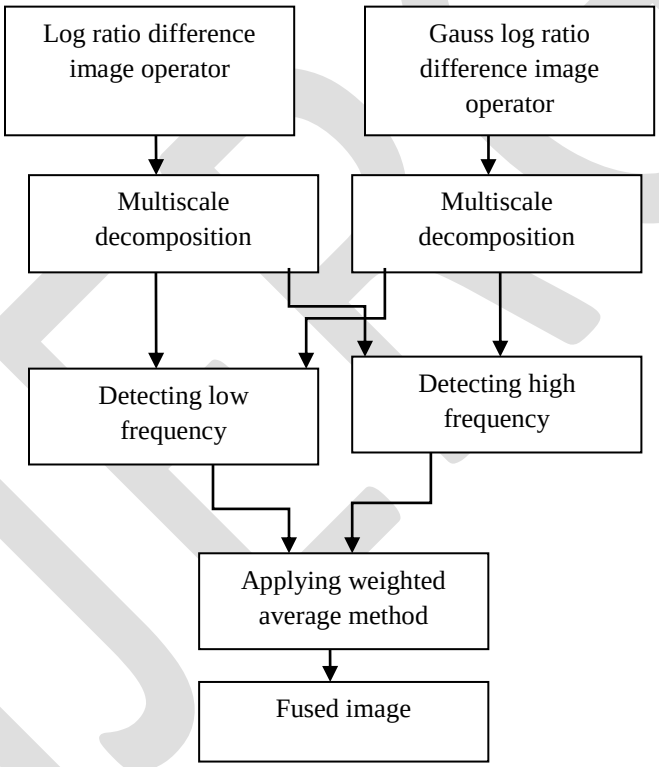

Figure 2: Image fusion using DWT

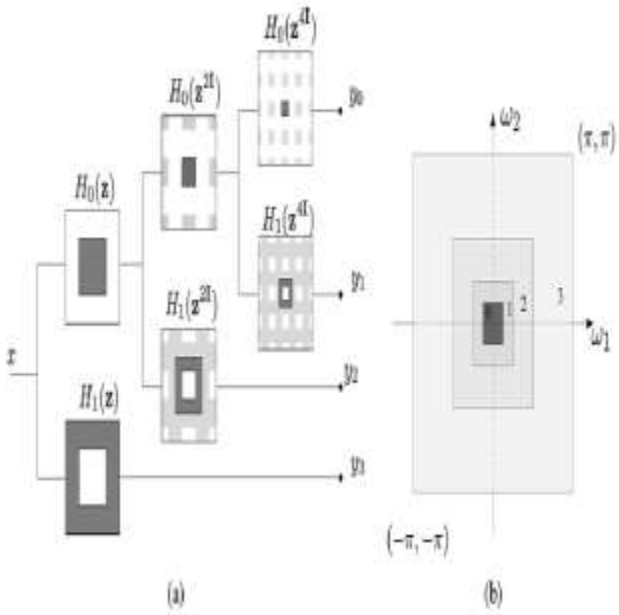

Figure 3: NSCT decomposition (a) 3 stage pyramid decomposition of NSCT. (b) Subbands on the 2-D frequency plane.

5. DENOISING USING NSCT

To reduce the noise of the fused difference image. The main steps are described as follows.

1. Subband images in the different scales and different directions are obtained after the decomposition of the fused difference image, which have the same size as the fused one. The subband images consist of low frequency subbands and high frequency subbands.

2. The coefficients in low-frequency subbands remain unchanged and ones of high-frequency directional subbands at the different scales are suppressed with Donohov threshold.

Donohov threshold is defined as

$$\lambda = \sigma\sqrt{2\log N} \qquad (5)$$

Where σ represents noise standard deviation and denotes the sample size. σ is generally unknown, so estimation method is used to determine σ. It is defined as $\sigma = Y_j / 0.6745$, where Y_j denotes the value of coefficient which lies in the intermediate position according to the order of amplitude of high-frequency coefficients of at scale j. When the high-frequency coefficients are larger than the threshold, the coefficients remain unchanged. Otherwise, the coefficients are set to zero. Finally, the denoised difference image X_d is obtained by using inverse NSCT transform. The following figure represents the NSCT decomposition and sub band frame. The lighter gray regions in the figure denote the aliasing caused by upsampling.

6. K-MEANS CLUSTERING

The purpose to process the difference image is to discriminate changed area from unchanged area. The difference image obtained by image fusion is sorted out into changed and unchanged area using kernel k-means clustering algorithm. In order to improve the accuracy of the binary change map, the data samples obtained by fusing the log-ratio and gauss log-ratio images are projected to a higher dimensional feature space, in which a linear algorithm can be applied to separate the changed and unchanged pixels. K-means clustering algorithm is applied on the data samples of the fused image in order to perform non-linear clustering. The techniques allows linear evaluation of data in higher dimensional feature space, which results in nonlinear clustering of data samples present in the input

space. The higher dimensional feature space is generated by distance measurement applied on the image obtained by fusing the log-ratio and gauss log ratio difference image. Clustering is a nonlinear feature extraction technique. Input is a matrix of similarities, which should be positive semi-definite and symmetric. If two or three features need to be extract use it as a non-linear dimensionality reduction method, otherwise it becomes a nonlinear clustering method. The clustering based on k-means clustering, which is very simple and computationally efficient. The following flow chart represents the k-means clustering algorithm. The NSCT coefficients are extracted from fused image and minimum distance is calculated and coefficients are classified accordingly to generate the change map.

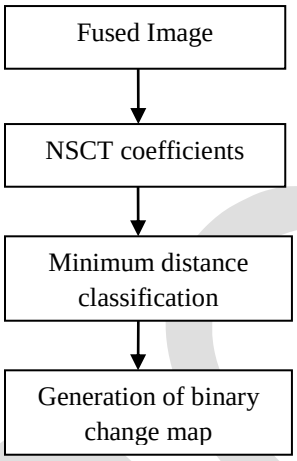

Figure 4: Flow chart for k-means clustering

7. EXPERIMENTAL RESULTS

7.1 Description of the Dataset

The dataset is a portion (512x512 pixels) of two images taken by European Remote Sensing 2 satellite SAR sensor above the region in the vicinity of the city of Bern, Switzerland during April and May, 1999 correspondingly. During this period the river Aare flooded wholly the cities of Thun and Bern, and hence the Aare valley was selected as the test site.

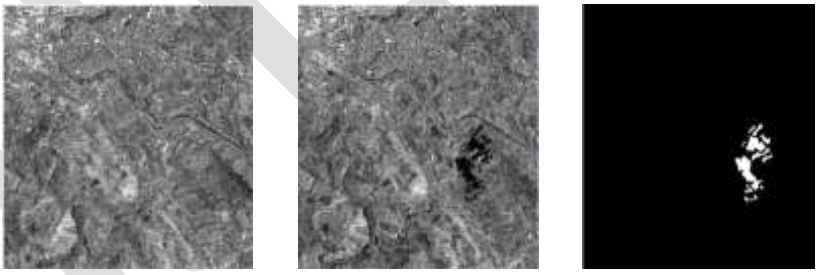

(a) (b) (c)

Figure 5: Multitemporal images for the city of Bern :(a) April, 1999 (b) May, 1999(c) ground truth.

In order to validate the accuracy of the proposed approach quantitatively, the results obtained has been compared with the ground truth for the Bern area. This ground truth was obtained through past information and photo analysis.

7.2 Experimental Results

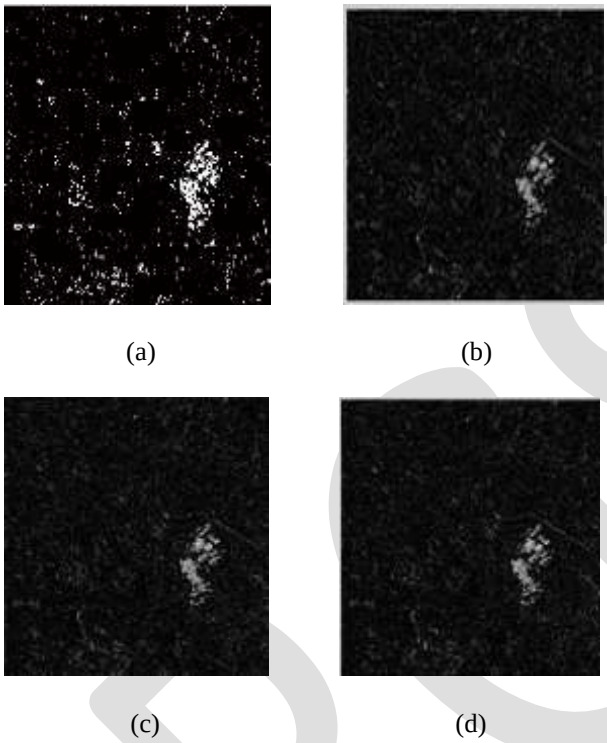

(a) (b)

(c) (d)

Figure 6: (a) Log ratio difference image (b) gauss log ratio difference image (c) DWT fused image (d) NSCT fused image.

Initially the multi temporal satellite images are loaded and difference images are obtained via log ratio and gauss log ratio operator. The results are shown in figure 6, and then these two images are combined to get the fused image. The fused images are constructed using NSCT. The previous DWT (Discrete Wavelet Transform) technique of fusion is also done to compare results of both the methods. After fusion the images are decomposed using NSCT. The coefficients are extracted using this approach and denoising using Donohov threshold is also performed for the efficient reduction of speckle noise. The denoised NSCT coefficients are shown in figure7. Then the NSCT coefficients are reconstructed and are then subjected for K- means clustering to obtain final change map.

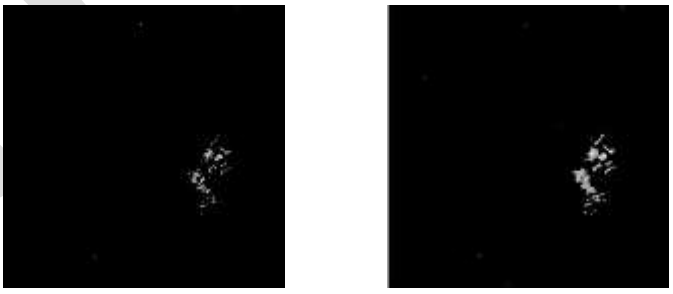

(a) (b)

Figure 7: Image obtained after (a) DWT fusion (b) NSCT fusion

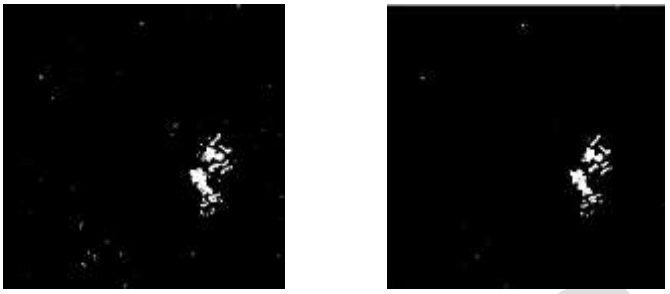

(a) (b)

Figure 8: (a) Change map obtained for 7.a (b) change map obtained for 7.b, using k-means clustering.

Table 1: Result analysis using parameters of the obtained output with ground truth

Parameters	For DWT fusion	For NSCT fusion
Mean	0.3642	0.4574
Standard Deviation	0.2163	0.1746
PSNR (dB)	18.9797	29.6073
Entropy	5.856	7.5362
Structural similarity index(SSIM)	0.9325	0.9545
Feature Mutual Information (fmi)	0.7562	0.8862

Table 1 shows the quantitative analysis of the obtained results. From the table it is clear that the NSCT method of fusion improves the change detection process with an improved PSNR of 29.6073dB and SSIM as 0.9539. Also other quantitative parameters such as mean, variance, entropy, structural and feature mutual information (fmi) are also measured to compare the results. The NSCT method of fusion gives good results with the ground truth data.

8. CONCLUSION

This work mainly focuses on the multi temporal SAR image's change detection and aims for a reliable change map. The techniques for the proposed work involve the techniques such as: difference image operator, image fusion, NSCT (Non Sub-sampled Contourlet Transform) and feature clustering. Efficiency of the change map can be increased by fusing the difference image and by using an advanced clustering algorithm. The concept of change detection of SAR data is likely to extend to the medical field, since the medical field contains a wide variety of applications in medical diagnosis.

ACKNOWLEDGMENT

The authors acknowledge the support of the Mar Baselios College of Engineering and Technology in this paper.

REFERENCES:

[1]. R.C. Gonzales, R.E. Woods and S.L. Eddins, "*Digital Image Processsing using MATLAB*", Pearson prentice Hall, Upper saddle River: New Jersy, 2004.

[2]. R. J. Radke, S. Andra, O. Al-Kofahi, and B. Roysam, "*Image change detection algorithms: A systematic survey*," IEEE Trans. Image Process., vol. 14, no. 3, pp. 294–307, Mar. 2005.

[3]. Qiang Sun, Yong Gao *etal, "Unsupervised Change Detection in Multitemporal SAR Images via NSCT-domain Feature Clustering",* IEEE Geoscience and remote sensing letters, Vol.18, No.4,July 2013.

[4]. Biao Hou,Qian Wei, Yaoguo Zheng, and Shuang Wang, "*Unsupervised -Change Detection in SAR Image Based on Gauss-Log Ratio Image Fusion and Compressed Projection*", IEEE journal for selected topics in Applied Earth Observations and remote sensing,Vol.18, May 2014.

[5]. F. Bujor, E. Trouvé, L. Valet, J. M. Nicolas, and J. P. Rudant, "*Application of log-cumulants to the detection of spatiotemporal discontinuities in multitemporal SAR images*," IEEE Trans. Geosci. Remote Sens., vol. 42, no. 10, pp. 2073–2084, Oct. 2004.

[6]. T. Celik, "*Change detection in satellite images using a genetic algorithm approach*," IEEE Geosci. Remote Sens. Lett., vol. 7, no. 2, pp. 386–390, Apr. 2010.

[7]. X. R. Zhang, Z. M. Li, B. Hou, and L. C. Jiao, "*Spectral clustering based unsupervised change detection in SAR images*," in Proc. Int. Geosci. Remote Sens. Symp. (IGARSS), Vancouver, BC, Canada, Jul. 2011, vol. 3, pp. 712–715.

[8]. X. H. Zhang, L. Wang, and L. C. Jiao, "*An unsupervised change detection based on clustering combined with multiscale and region growing*," in Proc. Int. Workshop Multi-Platform/Multi-Sensor Remote Sens. Mapp. (M2RSM), 2011, pp. 1–4.

[9]. Leyuan Fang, Shutao Li and Jianwen Hu, *"Multi temporal Image change Detection with Compressed Sparse Reprsentation",* 18th IEEE International Conference on Image Processing, 2011

International Journal of Engineering Research and General Science Volume 3, Issue 3, Part-2 , May-June, 2015
ISSN 2091-2730

Characterisation of Particulate Epoxy Composites for Mechanical Behaviour

Sumangala G Patil , Anilkumar K, Srinivasa Chari. V, Puneeth K R

Department of Mechanical Engineering,MSEC,Bangalore-562110

Sumagala.patil2901@gmail.com and 7411562639

Abstract— over the last century, polymers have emerged as one of the most indispensible components used in everyday life, epoxy or poly- epoxide being one such example. Until recently, synthetic filler materials have been the preffered choice for reinforcement of epoxy to improve its toughness. However, natural filler and fiber materials are emerging as suitable alternatives to synthetic materials for reinforcing polymers such as epoxy due to their environment friendliness, high abundance, renewability and cost effectiveness.

Several research efforts have been put to study the effectiveness of natural fiber based materials on the mechanical behavior of epoxy composites, focusing mainly on fibers and their weight percent's within the composites.

The present experimental study aims at investigating mechanical behavior of walnut shell powder reinforced epoxy composites. Composites bearing 10, 20, 30 and 40% weight fraction of walnut shell powder where made using hand layup method. The fabricated composite samples are prepared according to the ASTM standards for flexural testing. Three-point bending testy is carried samples and results are presented. Analytical results and experiment results are compared and they found to be very close agreement.

Keywords— Composite, Epoxy resin, Particulate, Polymer, Matrix, FEA, SEM (Scanning Electron Microscopic) & PMC (Polymer Matrix Composites).

INTRODUCTION

The development of mankind is defined in terms of advances in materials: the Stone Age, the Bronze Age, and the Iron Age. Today the development of any country is decided based on the amount of steel and concrete used. The Industrial Revolution was to a large extend made possible by advances in the use of materials in industrial equipments [1]. In the continued quest for improved performance, materials which may be specified by various criteria including less weight, more strength and lower cost, currently used materials frequently reach the limit of their usefulness [2]. In the last half century, the growth of materials technology has been explosive, and its impact on our daily lives, pervasive. In last few decades the developments in materials technology is fuelled mainly by composite material [1]. Thus material engineers and scientists are always striving to produce either improved traditional materials or completely new materials. Composites are an example of the latter category. They are developed as mixture of two distinct physical constituents and perform better than either of the constituents in its individual existence. The concept of composites is not very new. Bricks made from mud reinforced with straw, which are used in ancient civilizations, could be named composite. Also the naturally occurring materials like bone and wood are composites. But presently the same concept is used to develop man-made composite materials that perform well at a reduced weight/cost [2].

1.1 Definition of composites

A composite material is a materials system composed of a mixture or combination of two or more macro constituents differing in form and/or material composition and that are essentially insoluble in each other [3].

Composite materials represent nothing but a giant step in the ever constant endeavor of optimization in materials [4].

A structural composite is a material system consisting of two or more phases on macroscopic scale, whose mechanical performance and properties are designed to the superior to those of the constituent materials acting independently. One of the phase is usually discontinuous, stiffer, and stronger and is called reinforcement, where as a less stiff and weaker phase is continues and is called matrix (Figure 1.1). sometimes, because of chemical interactions or other processing effects, an additional phase, called interphase, exists between the reinforcement and matrix [6].

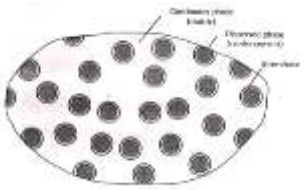

Figure 1.1 Phases of composite materials

1.2 Classification of composites

Two phase composite materials are classified into three broad categories depending on the type, geometry, and orientation of the reinforcement phase, as illustrated in the chart of Figure

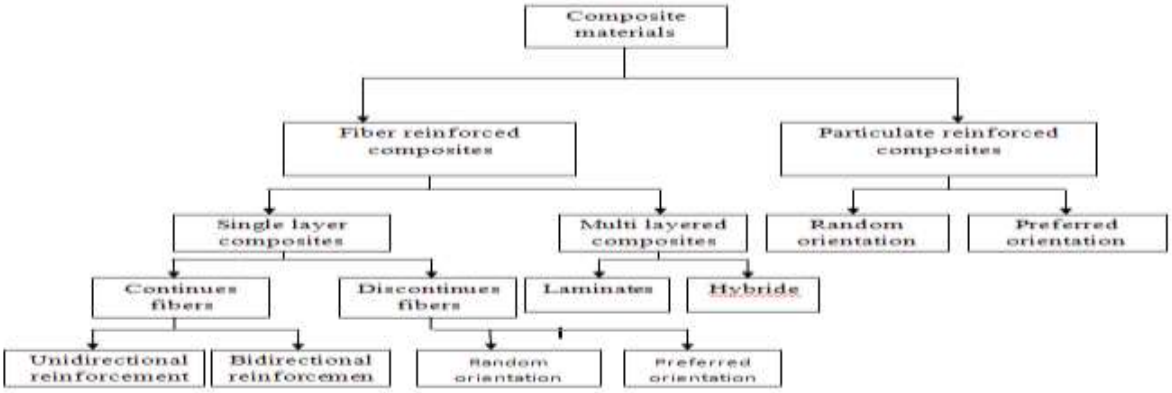

Fig 1.2 Classification of composite materials

4. Materials, Processing and Testing Methods

This chapter describes specification and properties of materials used as filler and matrix. This chapter covers the methods adopted for processing composites with varying content of the filler. In the present work walnut shell powder is used as the filler with Lapox L-12 epoxy resin as a matrix system and K-6 hardener .This chapter also covers the testing methods followed and the procedure of testing.

4.1 Materials

4.1.1Filler

Use of inorganic fillers in composites is increasing. Fillers not only reduce the cost of composites, but also frequently impart performance improvements that might not otherwise be achieved by the reinforcement and resin ingredients alone. Fillers can improve mechanical properties including fire and smoke performance by reducing organic content in composite laminates. Also, filled resins shrink less than unfilled resins, thereby improving the dimensional control of molded parts. Important properties, including water resistance, weathering, surface smoothness, stiffness, dimensional stability and temperature resistance, can all be improved through the proper use of fillers.

The thermosetting resin segment of the composite industry has taken advantage of the properties of fillers for many years. More recently, the thermoplastic industry has begun to make widespread use of inorganic fillers. Breakthroughs in chemical treatment of fillers that can provide higher filler loadings and improved laminate performance are accelerating this trend.

Figure 4.1 Walnut Shells

Figure 4.2 Walnut shell Powder

4.1.2 Filler Types

There are a number of inorganic filler materials that can be used with composites including:

Calcium carbonate is the most widely used inorganic filler. It is available at low cost in a variety of particle sizes and treatments from well-established regional suppliers, especially for composite applications. Most common grades of calcium carbonate filler are derived from limestone or marble and very common in automobile parts.

Kaolin (hydrous aluminum silicate) is the second most commonly used filler. It is known throughout the industry by its more common material name, clay. Mined clays are processed either by air flotation or by water washing to remove impurities and to classify the product for use in composites. A wide range of particle sizes is available.

Alumina trihydrate is frequently used when improved fire/smoke performance is required. When exposed to high temperature, this filler gives off water (hydration), thereby reducing the flame spread and development of smoke. Composite plumbing fixture applications such as bathtubs, shower stalls and related building products often contain alumina trihydrate for this purpose.

Calcium sulfate is a major flame/smoke retarding filler used by the tub/shower industry. It has fewer waters of hydration, and water is released at a lower temperature. This mineral filler offers a low cost flame/smoke retarding filler.

Other commonly used fillers include:

Mica
Feldspar
Wollastonite
Silica
Talc
Glass microspheres
Flake glass
Milled glass fibers
Other microsphere product

4.1.3 Using Fillers in Composites

When used in composite laminates, inorganic fillers can account for 40 to 65% by weight. They perform a function similar to silica fume in concrete. In comparison to resins and reinforcements, fillers are the least expensive of the major ingredients. These materials are nevertheless very important in establishing the performance of the composite laminate for the following reasons:

Fillers reduce the shrinkage of the composites part.
Fillers influences the fire resistance of laminates.
Fillers lower compound cost by diluting more expensive resin and may reduce the amount of reinforcement required.
Fillers can influence the mechanical strengths of composites.
Fillers serve to transfer stresses between the primary structural components of the laminate (i.e., resin and reinforcement), thereby improving mechanical and physical

Uniformity of the laminate can be enhanced by the effective use of fillers. Fillers help maintain fiber-loading uniformity by carrying reinforcing fibers along with the flow as resin is moved on the mold during compression molding.

Crack resistance and crack prevention properties are improved with filled resin systems. This is particularly true in sharp corners and resin-rich areas where smaller particles in the filler help to reinforce the resin in these regions.

The combination of small and medium filler particles helps control compound rheology at elevated temperatures and pressures, thereby helping to ensure that compression molded parts are uniform.

Low-density fillers are used extensively in marine putty and the transportation industry. They offer the lowest cost of filled systems, without the increases of weight that affect the performance of the final product.

The Walnut shell powder is used as a filler material in this work.

4.1.2 Matrix system:

The matrix system consists of a medium viscosity epoxy resin (LAPOX L-12) and a room temperature curing polyamine hardener (K-6) supplied by Yuje marketing, Malleswaram, Bangalore. Epoxy resin was selected as the material for the matrix system because of its wide application, good mechanical properties, excellent corrosion resistance and ease of processing. Some details including density of the constituents of the matrix system are listed in Table 4.1.

Lapox L–12: is a liquid, unmodified epoxy resin of medium viscosity which can be used with various hardeners for making glass fiber reinforced composites. The choice of hardener depends on the processing method to be used and on the properties required of the cured composite.

Hardener K–6: is a low viscosity room –temperature curing liquid hardener. It is commonly employed for hand layup applications. Being rather reactive, it gives a short pot-life and rapid cure at normal ambient temperatures. Details of constituent

properties as supplied by manufacturer are presented in Table [4.1].

Constituent	Trade name	Chemical name	Epoxide equivalent	Density (kg/m^3)	Supplier
Resin	LAPOX L-12	Diglycidyl Ether of bisphenol A (DGEBA)	182-192	1162	Yuje Marketing Bangalore
Hardener	K-6	Tri ethylene Tetra amine (TETA)	--	954	Yuje Marketing Bangalore

Table 4.1 Details of constituent properties as supplied by manufacturer

4.2 Moulds Used for Testing PRC's

4.2.1 Flexural Test

A mould of size 85 mm X 85 mm X 30mm (Figure 4.1) was prepared of mild steel for preparing compression samples. Mould cons of a base plate, frame that could be dismantled to facilitate easy removal of casting after the curing. All the surfaces of the mould w coated with wax. All the inner surfaces of mould, coming in contact with surfaces of composite to be cast are smeared with unifo coating of wax in order to facilitate the release of the cast slab.

Figure 4.3 Bending Sample mould

4.3 Processing

4.3.1 Particulate Reinforced Epoxy Composite:

Walnut shell powder is reinforced by mechanically mixing measured quantities of walnut shell powder in epoxy resin. The mixture is stirred using mechanical mixture until a slurry of uniform viscosity is obtained. K6 hardener in 12% by volume of resin was added to epoxy in the container with gentle stirring to minimize the formation of air bubbles. The slurry is cast in mild steel mould and allowed to cure at room temperature for about 24 hours, after which cast sample is withdrawn and trimmed to required shape.

The samples were made by considering different percentages of walnut shell powder by the weight fraction of the epoxy i.e. 10%, 20%, 30% and 40%.

Figures 4.4 Bending samples used for testing.

4.3.2 Post curing of samples:

All the samples are post cured at about 75`c for 3hrs in an oven. The samples are cured below 75'c because above 75'c the epoxy resin present in the samples starts melting. Then the samples are cut into ASTM standard using hacksaw.

"Archimedes principle states that the buoyant force on an object is going to be equal to the weight of the fluid displaced by the object or the density of the fluid multiplied by the submerged volume times the gravitational constant".

The density of the specimen is determined by keeping the cantilever beam as shown in Figure 4.4 over the weighing balance and then suspending the sample in air by means of thread, on the notch provided. An electronic weighing balance was used to determine the

weight of the sample. The weight of the cantilever beam and the thread is initially set to zero by using the tare option of the weighing balance.

The weight of the sample is determined in air and then the sample is dipped in water, to determine its weight in water as shown in Figure 4.5. Then the density of the sample is determined by using the formula given below.

$$\rho = \frac{W_a}{W_a - W_w} \quad (4.1)$$

Where; ρ = density of the composite material (g/cm^3)
W_a = weight of sample in air ($g/cm^{3)}$
W_w = weight of sample ($g/cm^{3)}$

Figure 4.6 Sample weighed in

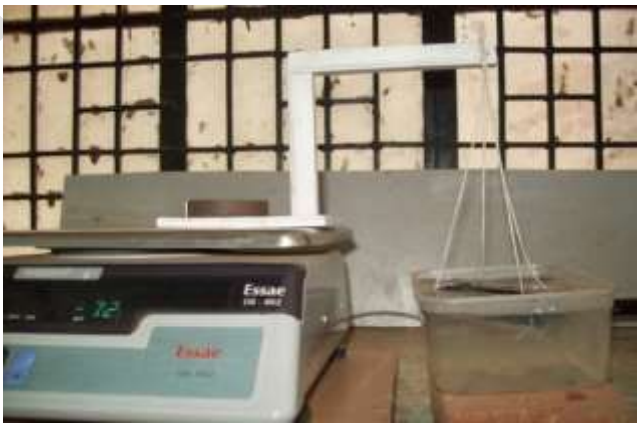

Figure 4.7 Sample weighed in distilled water

4.4.2 Mechanical Test

4.4.2.1 Bending Test

The bending test is used for studying the properties are flexural modulus, strength and maximum mid span deflection.
Testing is done on 15kN digitally controlled servo hydraulic test system equipped with load cell, stroke transducer. It is computer controlled for setting test assignments, acquiring data online and with provision to store the test results on computer media. Load cell has capacity to measure the load up to 15kN. Stroke has capacity to measure the displacement up to 60mm.

The testing machine setup is showed in below Fig 4.6. 3 point bending setup is showed in Fig 4.7.

Figure 4.8 Bending setup

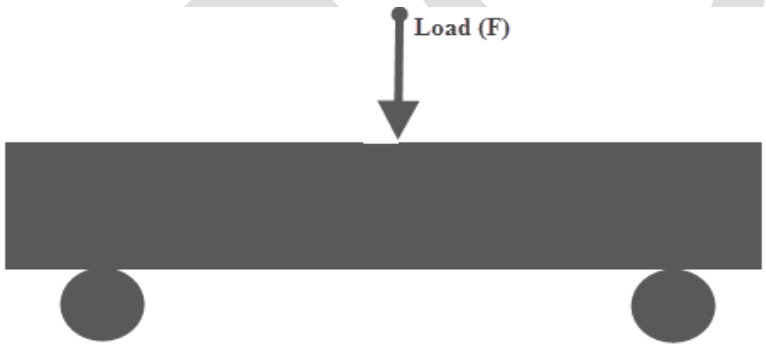

Figure 4.9Sample loading for 3 point bending test

5. Results and discussion

The experimental study presented in this chapter gives the results of both physical testing methods i.e density of all samples, and also the mechanical testing methods.

5.1.1 Physical Testing

Physical testing consists of density.

Density Test of bending

The density of all samples was calculated using the equation (4.1):
The following table 5.1 shows the densities of all PRC's

Table 5.1 Densities of all Bending PRC samples

Density test of Samples					
Serial Number	**Sample Coding**	**Weight in Air (gm)**	**Weight in Water (gm)**	**Density (gms/cc)**	**Average**
1	**10% - 1**	3.55	0.51	1.1666	1.16834
2	10% - 2	3.73	0.53	1.1774	
3	10% - 3	3.35	0.49	1.18456	
4	10% - 4	3.78	0.56	1.20066	
5	10% - 5	3.59	0.53	1.20192	
6	10% - 6	3.44	0.47	1.19808	
7	10% - 7	Broken Samples			
8	10% - 8				
9	**20% -1**	3.59	0.54	1.16776	1.18633
10	20% - 2	3.75	0.53	1.16562	
11	20% - 3	3.88	0.62	1.17132	
12	20% - 4	3.64	0.60	1.17391	
13	20% - 5	3.76	0.58	1.17320	
14	20% - 6	3.70	0.60	1.15224	
15	20% - 7	3.76	0.62	1.19745	
16	20% - 8	3.60	0.57	1.18811	
17	**30% - 1**	3.50	0.50	1.16666	1.19177
18	30% - 2	3.45	0.52	1.17741	
19	30% - 3	3.53	0.55	1.18456	
20	30% - 4	3.59	0.60	1.20066	
21	30% - 5	3.75	0.63	1.20192	
22	30% - 6	3.75	0.62	1.19808	
23	30% - 7	3.80	0.63	1.19873	
24	30% - 8	3.92	0.67	1.20615	
25	**40% - 1**	4.16	0.69	1.19873	1.20240
26	40% - 2	3.93	0.67	1.20552	
27	40% - 3	3.26	0.57	1.21189	
28	40% - 4	3.81	0.65	1.20569	
29	40% - 5	3.88	0.63	1.19384	
30	40% - 6	4.27	0.70	1.9607	
31	40% - 7	4.22	0.71	1.20227	
32	40% - 8	4.23	0.72	1.20512	

From the above tables (Table 5.1), and Figure 5.1 is clearly observed that with increase in weight fraction of filler density increases. Obvious reason for this could be, influences the weight of the products.

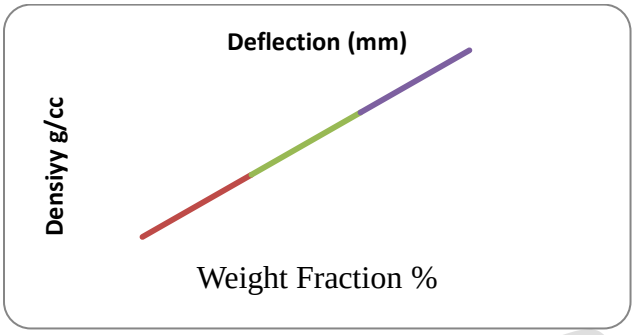

Figure 5.1 Densities of PRC Samples

5.1.2 Mechanical

Bending Test

The stress-deformation curves obtained from the flexural testing of PRCs. Below figures show that all types of PRCs fail in the brittle fracture mode at the end of the linear region in their stress-deformation curves. The failure starts at the tensile side of the specimen, in-line with the central loading anvil, and grooves towards the compressive side. Hence, the deformation and fracture behavior are governed by the tensile properties of these specimens. Figure 5.13 shows the fracture pattern of four different configuration specimens, which are selected randomly.

Table5.2 Flexural property of 10% reinforced composite

Specimen identifier	modulus MPa	sec mod MPa	flex strngth MPa	deflection %	thickness mm	spec width mm
10% -1	2320	2510	47.9	1.9	3.1	12.4
10% -2	2280	2410	47.4	1.9	3.1	12.4
10% -3	3020	3140	59.4	1.9	3.1	12.3
10% -4	3410	3520	50.0	1.4	3.1	12.2
10% -5	3170	3420	38.9	1.1	3.1	12.3
10% -6	1040	2140	48.8	2.2	3.1	12.2
10% -7	2990	3260	49.6	1.5	3.1	12.4
10% -8	2900	3170	50.5	1.6	3.2	12.6

The Table 5.2 represents the flexural property of 10% weight fraction of particulate reinforced composites.

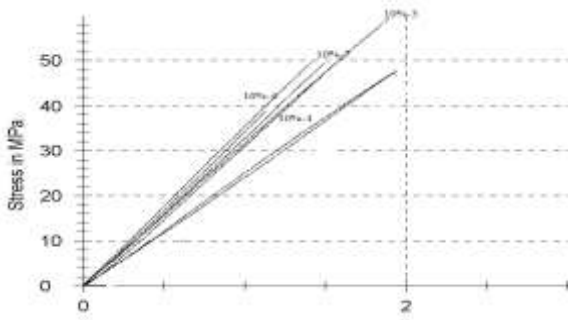

Figure5.2 Stress v/s Deflection in for curve 10% PRC from the experiment

The above Figure5.2 represents the stress v/s deflection curve for 10% weight fraction of PRCs; these results are obtained from 3-point bending test.

Table 5.3 Statistical table for 10% weight fraction of PRCs

Series n = 8	modulus MPa	sec mod MPa	flex strngth MPa	deflection %	thickness mm	spec width mm
$\bar{x}$	2640	2950	49.1	1.7	3.113	12.35
s	755	516	5.57	0.35	0.03536	0.1309
ν	28.58	17.52	11.36	20.75	1.14	1.06

Table 5.3 shows the statistical representation of 10% weight fraction of PRCs.

Note: $\bar{x}$ = arithmetic mean of the set of observation
n = number of observation
s = estimated standard deviation
ν= value of single of single observation

Table5.4 Flexural property of 20% reinforced composite

Specimen identifier	modulus MPa	sec mod MPa	flex strngth MPa	deflection %	thickness mm	spec width mm
20% -1	2200	2350	35.7	1.5	3.1	12.1
20% -2	3220	3400	44.7	1.3	3.1	12.4
20% -3	-20.4	1380	39.9	2.6	3.1	12.3
20% -4	2500	2870	40.8	1.4	3.2	12.4
20% -5	2470	2680	42.4	1.6	3.2	12.4
20% -6	1970	2110	26.5	1.2	3.3	11.82

The Table 5.8 represents the flexural property of a 40% weight fraction of particulate reinforced composites.

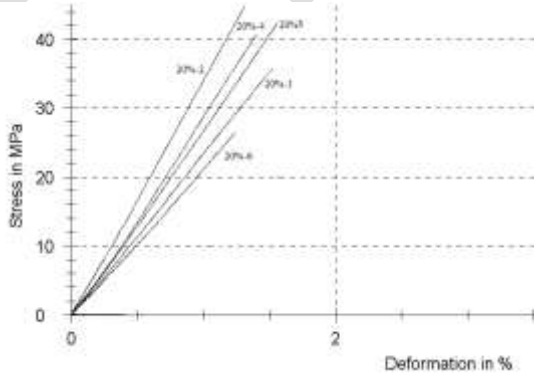

Figure5.3 Stress v/s Deflection in for 20% PRC from the experimental

The above Figure5.3 represents the stress v/s deflection curve for 20% weight fraction of PRCs; these results are obtained from 3-point bending test.

Table 5.5 Statistical table for 20% weight fraction of PRCs

Series n = 6	modulus MPa	sec mod MPa	flex strngth MPa	deflection %	thickness mm	spec width mm
$\bar{x}$	2060	2460	38.3	1.6	3.167	12.24
s	1100	691	6.52	0.49	0.08165	0.2351
ν	-	28.06	17.02	30.55	2.58	1.92

Table 5.5 shows the statistical representation of 20% weight fraction of PRCs

Table5.6 Flexural property of 30% reinforced composite

Specimen identifier	modulus MPa	sec mod MPa	flex strngth MPa	deflection %	thickness mm	spec width mm
30% -1	3230	3560	39.8	1.1	3.14	12.3
30% -2	2490	2640	27.1	1.0	3.44	12.55
30% -3	2550	2730	38.1	1.4	3.25	12.3
30% -4	2970	3250	38.2	1.2	3.12	12.3
30% -5	2830	3050	39.4	1.3	3.1	12.31
30% -6	3230	3410	49.0	1.4	3.04	12.4
30% -7	3060	3480	39.6	1.1	3.12	12.35
30% -8	3070	3270	46.6	1.4	3.12	11.9

Table 5.6 shows that the flexural property for the 30% weight fraction of particulate reinforced composites.

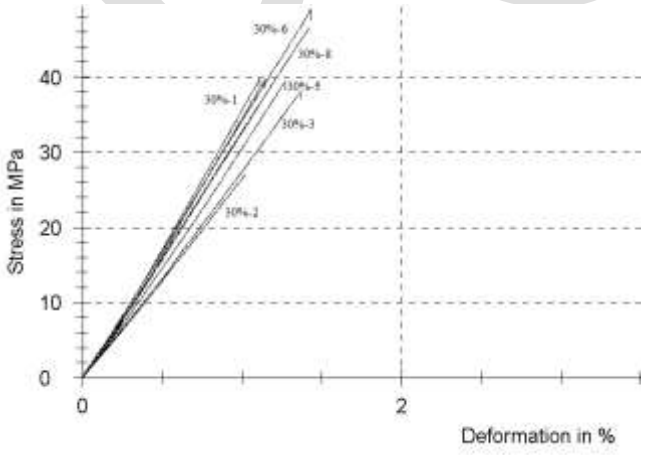

Figure5.4 Stress v/s Deflection curve for 30% PRC from the experimental

The above Figure5.4 represents the stress v/s deflection curve for 40% weight fraction of PRCs; these results are obtained from 3-point bending test.

Table 5.7 Statistical table for 30% weight fraction of PRCs

Series n = 8	modulus MPa	sec mod MPa	flex strngth MPa	deflection %	thickness mm	spec width mm
$\bar{x}$	2930	3170	39.7	1.2	3.166	12.3
s	285	341	6.53	0.15	0.125	0.1833
ν	9.72	10.74	16.44	12.42	3.95	1.49

Table 5.7 shows the statistical representation of 30% weight fraction of PRCs.

Table5.8 Flexural property of 40% reinforced composite

Specimen identifier	modulus MPa	sec mod MPa	flex strngth MPa	deflection %	thickness mm	spec width mm
40% -1	3310	-	26.9	0.78	3.15	13.08
40% -2	3090	-	24.3	0.74	3.22	12.44
40% -3	3240	3430	45.2	1.3	3.31	10.39
40% -4	3170	3330	40.5	1.2	3.25	12.42
40% -5	3120	3190	46.3	1.5	3.3	11.75
40% -6	3010	3250	48.4	1.5	3.35	13.15
40 % -7	3210	3460	42.9	1.2	3.32	12.9
40% -8	3310	3490	53.3	1.5	3.28	13.08

The Table 5.8 represents the flexural property of a 40% weight fraction of particulate reinforced composites.

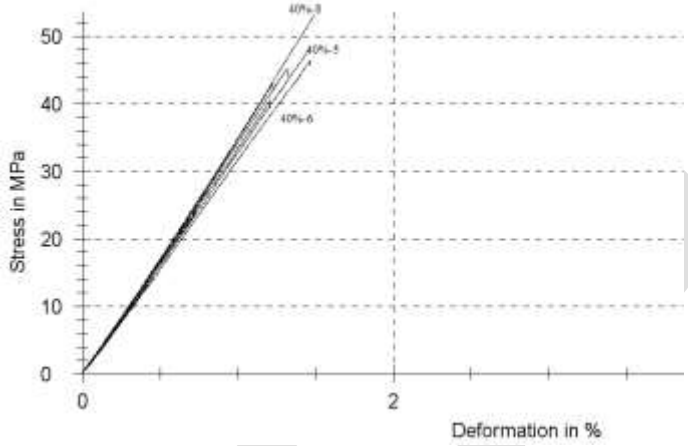

Figure5.5 Stress v/s Deflection curve for 40% PRC from the experimental

The Figure 5.5 shows the stress v/s deformation curve for the 40% weight fraction of PRCs, which is obtained from the 3- point bending experiment.

Table 5.9 Statistical table for 40% weight fraction of PRCs

Series n = 8	modulus MPa	sec mod MPa	flex strngth MPa	deflection %	thickness mm	spec width mm
$\bar{x}$	3180	3360	41.0	1.2	3.273	12.4
s	106	120	10.2	0.30	0.06409	0.9413
ν	3.34	3.57	24.97	24.77	1.96	7.59

The above Table 5.9 shows that the statistical representation of the 40% weight fraction of the particulate reinforced composites.

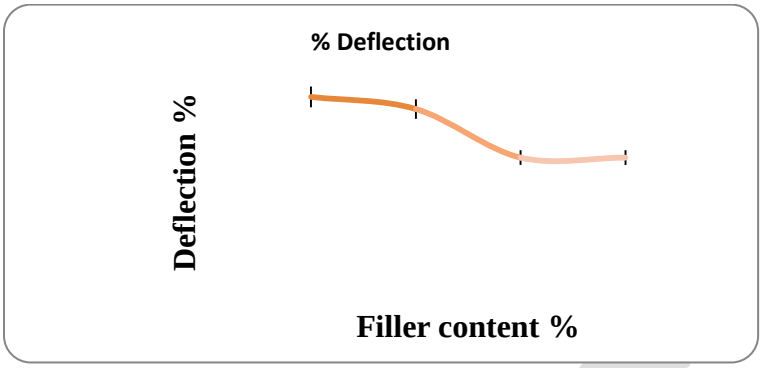

Figure 5.6 Deflection vs. weight fraction of particulate reinforced composite

Figure 5.6 shows the crack pattern of the samples for different weight fraction of walnut shell powder, it is clear that in all the cases of samples of pure composites which are randomly selected the crack has initiated near the mid-span of the specimen and propagated vertically.

5.2 Analytical Approach

The load–displacement data is used in calculating the flexural modulus and strength of bending samples. The flexural modulus and flexural strength are calculated by using Equation 5.1.

Mid span deflection (*D*) of PRC bending sample is calculated by the following equation [18].

$$D = \frac{rL^2}{6d} \qquad (5.1)$$

Where 'r' is the strain and 'L' is the span length'd' is depth of beam. The mid span deflection obtained from analytical calculation is presented in table 5.2 to 5.5.

Table 5.10 MOM approach for 10% PRCs

Load (N)	15.76	31.52	47.28	63.04	78.08	94.56
Deflection mm	0.4451	0.8902	1.3354	1.7805	2.2056	2.6708

Table 5.11 MOM for 20% PRCs approach

Load (N)	15.88	31.77	47.67	63.56	78.08
Deflection mm	0.4172	0.8347	1.2525	1.6700	1.8786

Table 5.12 MOM approach for 30% PRCs

Load (N)	15.27	30.55	45.87	61.16	74.92
Deflection mm	0.4382	0.8768	1.3165	1.7554	2.1503

Table 5.13 MOM approach for 40% PRCs

Load (N)	15.76	31.52	47.28	63.04	78.08	94.56
Deflection mm	0.4451	0.8902	1.3354	1.7805	2.2056	2.6708

Table 5.10 to 5.13 shows the results of theoretical calculation which is calculated by using Equation 5.1

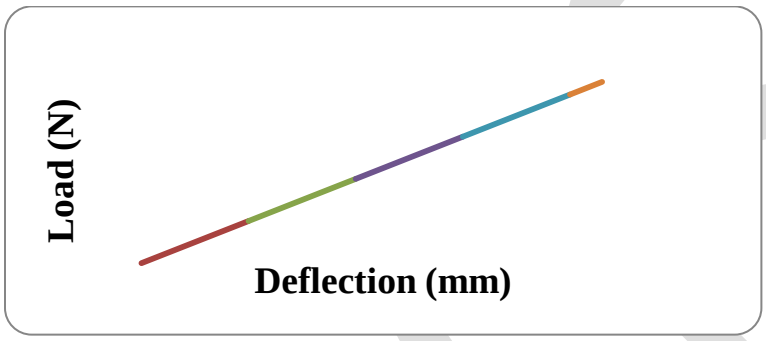

Figure 5.7 Load v/s Deflection curve from MOM approach

Figure 5.7 shows load v/s deflection curve which is obtained from the theoretical calculation using the equation 5.1. The graph shows that the deflection increases with increase the load.

ACKNOWLEDGMENT

I express my sincere thanks and heartfelt gratitude to my guide, Dr. M. R. Doddamani for their, inspiration, guidance and support during this project work. I thank my parents & friends for their moral support. I thank the God for hearing my prayers & I seek his blessings for all my future endeavors.

CONCLUSION

The present work deals with the preparation of characterization of waste walnut shell powder reinforced epoxy composite. The successful fabrication of a new class of epoxy based composites reinforced with walnut shell powder. In this work, flexural properties of walnut shell powder reinforced composites are analyzed under three-point bending test. Experimental results on these composites show that the specific modulus of these lightweight composite is higher. The composite flexural modulus can be effectively tailored by varying the weight fraction. On the other hand, the flexural strength is primarily influenced by the resin content of the composite. It is found that the composite strength decreases as the inclusion weight fraction increases. The flexural strength of the composite is found to be maximum with 40% weight fraction of walnut shell powder.

REFERENCES:

[1] Autar K. Kaw, Mechanics Of Composite Materials, CRC press, 2nd Edition, 2006

[2] F. L. Matthews and R.D. Rawlings, Engineering and Science,

[3] M. M. Schwartz, Composite Materials Handbook

[4] K. K. Chawla, Composites Materials Science & Engineering, 2nd Edition 1998

[5] POP.P. Adrian, Manufacturing processes and applications of composite materials BEJINARU MIHOC Gheorghe, Volume 9 (19) 2010, NR2

[6] Composite materials: by Daniel

[7] Incremental damage theory of particulate-reinforced composites with a ductile inter phase: Hui Yang, Puhui Chen, Yunpeng Jiang c, Keiichiro Tohgo.

[8] G. Tagliavia, M. Porfiri, N. Gupta, Analysis of flexural properties of hollow-particle filled composites, Composites: Part B 41 (2010) 86–93

[9] A. Aruniit, J. Kers and K. Tall Influence of filler proportion on mechanical and physical properties of particulate composite**,** *Agronomy Research* Bio system Engineering Special Issue 1, 23-29, 2011

[10] Gabriele Tagliavia, Maurizio Porfiri, Nikhil Gupta, Influence of moisture absorption on flexural properties of syntactic foams, Composites: Part B 43 (2012) 115–123

[11] A. Arias, P. Forquin, R. Zaera, C. Navarro, Relationship between static bending and compressive behaviour of particle-reinforced cement composites, Composites: Part B 39 (2008) 1205–1215

[12] M.T. Kim, K.Y. Rhee, S.J. Park, D. Hui, Effects of silane-modified carbon nanotubes on flexural and fracture behaviors of carbon nanotube-modified epoxy/basalt composites, Composites: Part B 43 (2012) 2298–2302

[13] Nihad Dukhan, Nassif Rayess, James Hadley, Characterization of aluminum foam–polypropylene interpenetrating phase composites: Flexural test results, Mechanics of Materials 42 (2010) 134–141

[14] Bernd Wetzela, Frank Haupert a, Ming Qiu Zhang, Epoxy nanocomposites with high mechanical and tribological performance, Composites Science and Technology 63 (2003) 2055–2067

[15] Arijit Das, Bhabani K. Satapathy, Structural, thermal, mechanical and dynamic mechanical properties of cenosphere filled polypropylene composites, Materials and Design 32 (2011) 1477–1484

[16] Aleksandar Todic, Blagoje Nedeljkovic, Dejan Cikara , Ivica Ristovic, Particulate basalt–polymer composites characteristics investigation, Materials and Design 32 (2011) 1677–1683

[17] Alok Satapathy, Amar Patnaik, Manoj Kumar Pradhan, A study on processing, characterization and erosion behavior of fish (Labeo-rohita) scale filled epoxy matrix composites, Materials and Design 30 (2009) 2359–2371

[18] Hui Yang, Puhui Chen, Yunpeng Jiang , Keiichiro Tohgo[18], Incremental damage theory of particulate-reinforced composites with a ductile interphase, Composite Structures 93 (2011) 2655–2662

[19] W.L. Azoti, Y. Koutsawa, N. Bonfoh, P. Lipinski, S. Belouettar, On the capability of micromechanics models to capture the auxetic behavior of fibers/particles reinforced composite materials, Composite Structures 94 (2011) 156–165

[20] ASTM 790-03, Standard test methods for Flexural properties of Unreinforced and Reinforced Plastics and Electrical Insulating Materials. ASTM International, PA, USA.

[21] ASTM Help manual

International Journal of Engineering Research and General Science Volume 3, Issue 3, Part-2 , May-June, 2015
ISSN 2091-2730

COMPARISON OF STACKING AND boost SVM METHOD FOR KDD DATASET

NilufarZaman D.P. Gaikwad

AISSMS College of Engineering , Pune

nilufar.zaman@mescoepune.org dp.g@rediffmail.com

Abstract: The method of combining classifier can be done in various ways of which the most competent of them are Stacking and Voting method. Stacking is a way of combining multiple generalizers one after another where the output of the first classifier is considered as an input to the next one, whereas Voting method works on the principle of best result oriented generalizers. In this paper the author have used a large dataset i.e. KDD which helps in anomaly detection methods. In this paper the author has explained the paramount of Voting method over stacking method in the combination algorithm named as boostSVM for the above mentioned specified dataset. The classifiers used are Support Vector Machine (SVM) and AdaBoost where the AdaBoost algorithm boosts SVM to debase the error rates. SVM is mainly chosen as it provides a global maxima instead of local minima's. ROC curves are also being used to justify the results as it helps in evaluating the performance efficviently.

Keywords: Stacking, Voting, ROC, SVM, AdaBoost, prediction rules, hyperplane, support vectors, boostSVM.

I. INTRODUCTION

In this paper the author has used the classification methodology to find anomalies for the KDD dataset. In the dataset used in this paper two classes are being contemplated i.e. normal and anomaly. Classification is mainly used to determine whether a particular attribute belongs to normal or anomaly class i.e. if S= attribute

N= normal class &

A= anomaly class Then we need to find whether

$S \in N$ or $S \in A$

Here we will be comparing two methodologies for KDD dataset which are stacking and boostSVM method. Stacking is the method which combines various classifiers, step by step to increase its efficiency where the output of the first classifier is taken as an input to second classifier. In the voting method winner survive strategy is used in which the classifier with maximum accuracy or minimum error is selected as the output classifier and the accuracy level of the same is considered to be the final output. For the stacking and boostSVM method two classifiers are used which are SVM and AdaBoost. Boosting technique is used to create a highly accurate prediction rule by combining various weak prediction rules. It boosts other algorithm to provide more accurate results by reducing the error rates. In this paper AdaBoost[1] is used to boost SVM which as a result reduces the error rate shown in the results below. Support Vector Machine is used for classification of object depending on the number of divulge classes. It stratify the object by drawing hyperplane to discriminate the various classes. The data points that lie closest to the decision surface are called the support vectors. Normally we divide the data into two types, linear and nonlinear. Linear data are the data which can be easily separable by drawing a boundary in between whereas non linear are datasets which are in a slapdash format and cannot be separated by a single hyperplane. SVM deals with both the data types i.e. for linear data it uses LibSVM while for nonlinear data it uses kernel functions. Kernel functions help in the transformation that maps the original data to the new space. The main reason behind using SVM as a base classifier is that it gives a global maxima instead of multiple local minima's. The dataset used here is the KDD99 dataset which helps in intrusion detection and it is based on 1998 DARPA initiative. Intrusion detection helps in detecting the security issue signs by monitoring the events that occur in computer systems. It includes the procedure of identifying the set of malicious actions that modus vivendi the information resources. Normally for intrusion detection Systems we have two approaches : misuse detection and anomaly detection. Misuse detection basically works by pattern detection i.e.it matches the pattern between the captured network and attack signatures[2][3]. As soon as it detects any malicious

thing it immediately raise a trepidation. The main advantage of it is that it detects the familiar attacks easily, but faces problems for unknown errors. While anomaly detection works by behavioral identification[3][4]. It searches for the behavior that doesn't come seems normal and it establishes a model for all users and components in a network. If any aberration is being observed immediately a trepidation is being raised. The main advantage of this is that it doesn't require any known attacks to detect the anomaly, but it mainly finds problem in deciding what constitutes the attack and may give high false positive rate.[2][3][4] There are two classes involved in this dataset which are normal class and the anomaly class which includes four types:

a. DoS: In Denial of Service statutory users is being prevented by the assailant from using a service.

b. R2L: In Remote to Local assailant tries to gain access over the victim's machine.

c. U2R: In User to Root assailant have local access to a victims machine but tries to gain super user prerogative.

d. Probe: Here the assailant tries to get information about the target host.

II. STACKING:

Stacking is the method which uses the combination of generalizers rather than choosing any of the results with certain conditions. It is the method that takes the output guesses of generalizers as an input component in new space and then again generalizing it in the new space.

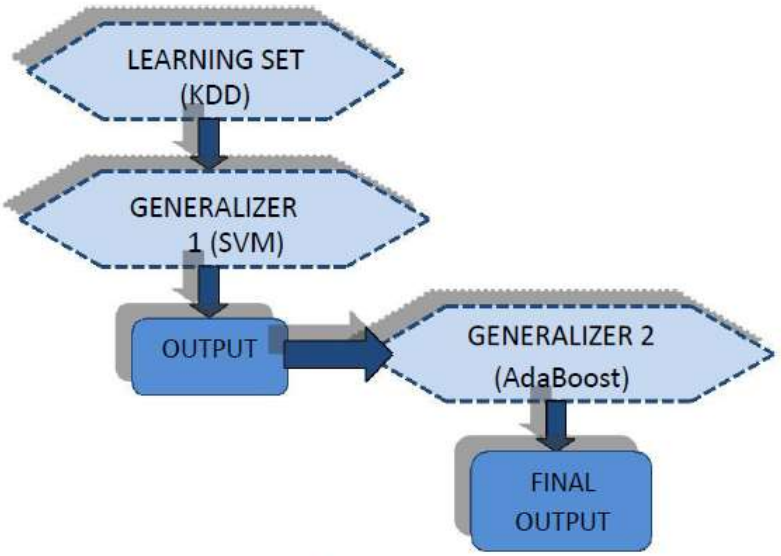

Fig1: Stacking

For Stacking method we first divide the whole dataset into n number of partitions. For all n partitions we again take two sets for each partition. Usually we consider both the sets to be disjoint. Suppose we have Sij where i denotes the number of partitions and j denotes the two disjoint sets. Stacking basically consists of two stages: Stage 1: Base learner, which learns from a dataset by using various models. A new dataset is being created by combining the outputs of the various models and the instance of that dataset is used for the prediction purpose. Stage 2: Stacking Model Learner takes the new dataset created by base learner and use it to obtain the final output.[5] For example, here the author has stacked AdaBoost with Support Vector Machine (SVM) to find the accuracy level of the dataset in the anomaly detection procedure. Here the AdaBoost is used as stage 1 classifier i.e. the base classifier whose output can be used as an input variable to SVM which is our stage 2 classifier i.e. the Stacking Model Learner. The Stacking Model Learner tries to learn from the data obtained from stage 1 and the ways of combining the predictions obtained from various models to achieve best accuracy level.[6] Though we know that AdaBoost method helps in boosting any algorithm to decrease the error rate or to increase the accuracy level, but for stacking method with KDD database , AdaBoost could neither increase the accuracy of SVM nor could decrease the error rate which is being clearly shown in the results whereas when we have used voting method for combining them we could find better results.

III. boostSVM

There are various approaches to combine classifiers at various levels:

a. Combiner approach: In this approach the main focus is on the way of combining the classifier results. The logic of the combiner decides the performance of the system.

b. Base Classifier approach: The base classifier design model for the ensemble is partly specified with bagging and boosting models but for combining the classifiers the logic used is not allied with any base classifiers.

c. Feature Level: At this level different feature subset is used is used for the classifiers. The dataset is divided here so that each classifier can get training over its own dataset. d. Manipulate output labels: The outputs received by the classifier can be manipulated by using error correcting codes (ECOC). There are more approaches of interest which includes miscellany classifier ensembles and also include certain clustering ensembles also. In this paper the author has used the fusion of label outputs. The logic of combining outputs depends on the information of individual classifiers. There are basically three types of classifier outputs:

1. The Abstract level: The classifier produces a class label which belongs to a feature space and each classifier output defines a vector(S) which can be mathematically written as: If Ci is the classifier, Li is the class label and F gives the feature space then Li ∈ F where i=1,2,.....m If S defines the vector, then the m classifier outputs define the vector as S=[S1,S2.....Sm] n ∈ Fm At this level, we didn't find any information about the guessed level nor are any alternative suggested which is the reason for calling this level as the ubiquitous one.

2. The Rank level: It is mainly used for large number of class labels. At this level the output of each classifier belongs to the feature space which is the probable reason of providing the correct labels. [8,9] Ci ∈ F

3. The Measurement level: Here each classifier produces a- dimensional vector [D] which provides output between 0 and 1.

D= [Ci,1, Ci,2,.....Ci,a] ^{m}

In this paper the combine classifier model is known as boostSVM which uses SVM as the base classifier and AdaBoost is used here to boost the classifier SVM which helps in mainly reducing the error rate and if possible increases the accuracy. LEARNING SET (KDD) GENERALIZER 1 GENERALIZER 2 (AdaBoost) (SVM) COMBINER (boostSVM) FINAL OUTPUT

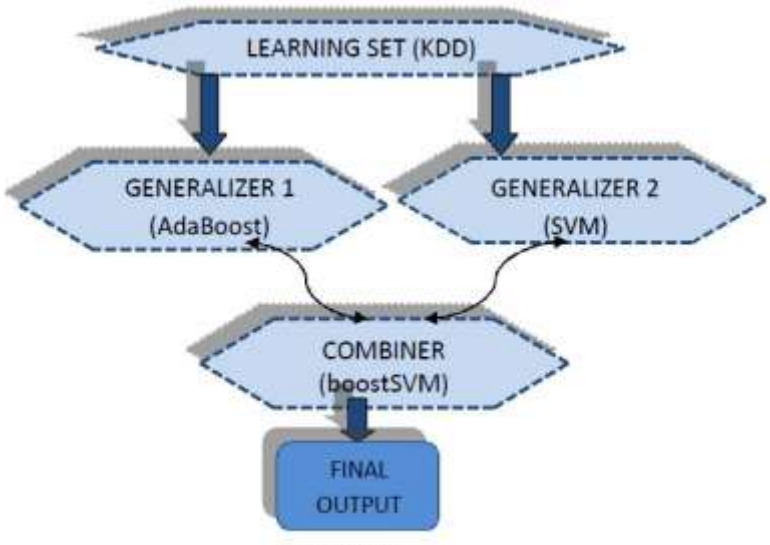

Fig2: boostSVM

Here we have introduced the majority vote technique which basically considers the classifier having more accuracy level but considering the average of probabilities. The Average of probabilities returns the mean of a probability distribution for the base classifiers. It considers the classifier which reduces the error more which is being clearly shown in the results.

IV. RESULTS

There are various ways of testing the dataset but the main aim is to train the classifier as much as possible and provide the maximum amount of data for testing but we also need to be careful about overtraining classifier. We may overtrain the classifier by providing the same dataset for testing and training. Suppose is the dataset of size C x a where

C = number of objects and contain a- dimensional feature vectors. Thus the various ways of making the best use of can be summarised as follows:

1. R-method: This Re-substitution method considers the same dataset for testing and training. Though this gives very good results but this is the condition which overtrain the classifier. This gives biased results so for understanding the classifier more we should ignore this method.

2. S-method: The splitting method or Hold out method splits the dataset into two parts and uses one part for training and one part for testing.

3. Random-method: This method overcomes the disadvantage of R-method by precipitating a random set which will be used for testing the classifier. This method helps in understanding the classifier more than its previous version. Though R-method may give more accuracy level but it gives biased predictions. This biasness is being minimized by the Random-method.

4. CV-method: Lastly we have the Cross Validation which is another technique for estimating performance. Suppose we have a dataset of size "P" which is divided into "K" subsets. Now from this K subset we use one for testing and the remaining "K-1" for training and we repeat the procedure till we reach the last subset.

In this paper cross validation method is being used to find the accuracy level of boostSVM as it helps the classifier to estimate the performance properly. The CV-method used here is 2-folded, i.e. the dataset is divided into two subsets i.e. set1 and set2 . Initially set 1 is used for training and set 2 is used for testing and for next step continues by taking set2 as training set and set1 as testing set. In this paper the error rate and the accuracy level are being checked.[14][15] The error rate is being determined by comparing the error by the classifier and the error by the labelled data

i.e. Error (C) = EC/EL

Where EC = misclassification by classifier (C) and

EL = misclassification of the labelled data

After finding the error the accuracy level is being determined by

Accuracy = 1 - Error (C)

The results for boostSVM compared with AdaBoost, SVM ans Stacking method is shown below: Classifier Correctly Classified ROC Relative absolute Root relative squared [CC] (%) error [RAE] (%) error [RRSE] (%) AdaBoost 94.3355 .9878 15.94 39.0935 SVM 94.0219 .936 12.0113 49.0128 Stacking 53.386 .5 100 100 boostSVM 94.0219 .995 13.9756 35.9053

Classifier	Correctly Classified [CC] (%)	ROC	Relative absolute error [RAE] (%)	Root relative squared error [RRSE] (%)
AdaBoost	94.3355	.9878	15.94	39.0935
SVM	94.0219	.936	12.0113	49.0128
Stacking	53.386	.5	100	100
boostSVM	94.0219	.995	13.9756	35.9053

Table 1: Accuracy and error for boostSVM

The graphical representation of the above result is shown below:

100 50 RRSE CC RAE 0 ROC ROC CC RAE RRSE

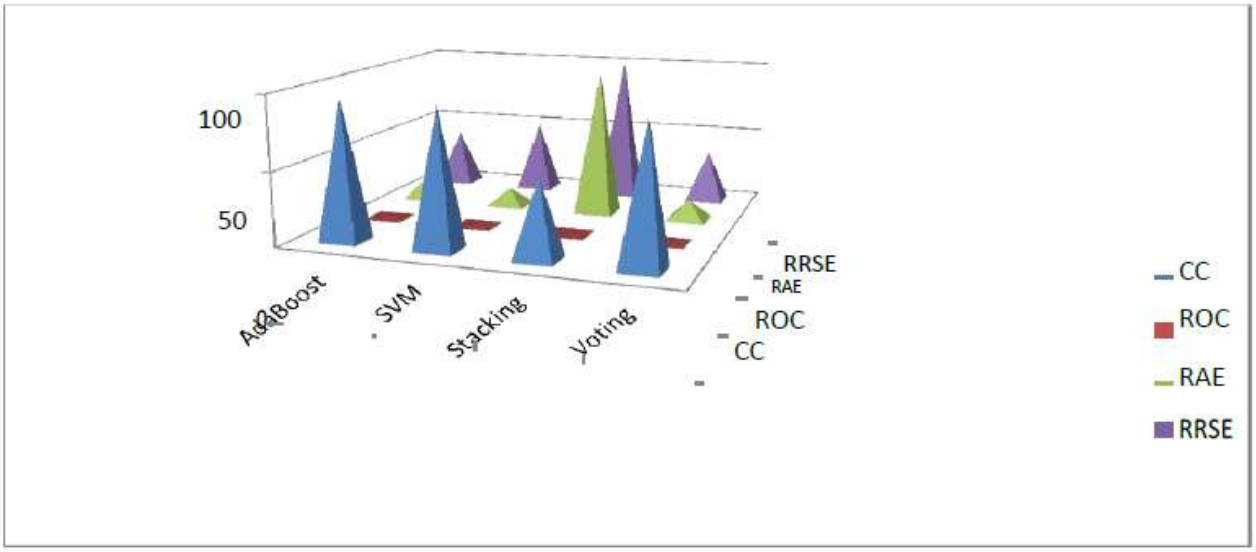

Fig 3: The graphical representation of the results

The ROC curves for verifying the result are shown below:

Fig 8: ROC for anomaly class for Stacking

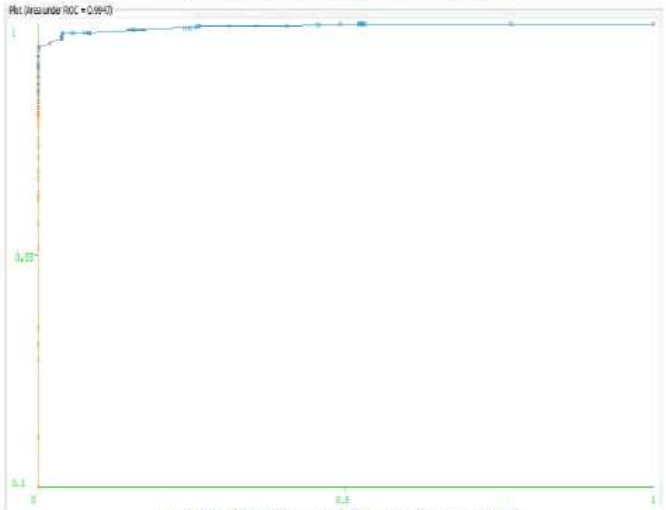

Fig 9: ROC for normal class for Stacking

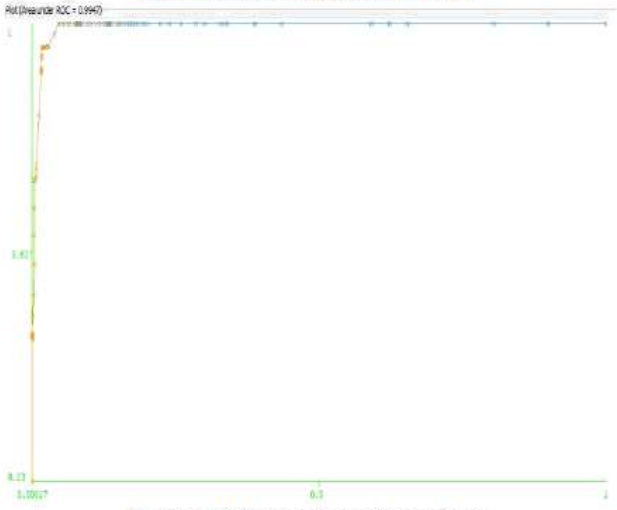

Fig 10: ROC for anomaly class for boostSVM

Fig 11: ROC for normal class for boostSVM

The ROC (Receiver Operating Characteristics) or AUC (Area under the curve) shown above is the statistical attributes which helps in determining the active compounds in the dataset. The X-axis here helps in plotting the false positive rate whereas Y-axis quadrate to the true positive rate. The color in the ROC curves represents the threshold value and the compounds which exceeds the current threshold value is considered to be active. For a particular attribute if correct prediction is being made, then that attributes is prophesied as active one. The true positive values mentioned above can be identified using confusion matrix which helps in anticipating the performance of the algorithms. The confusion matrix consists of four quadrants which includes true positive, true negative, false positive and false negative. The true positive section is the most secure one as it correctly identified the object. Secondly, true negative is the portion which of negative cases which are classified correctly. Thirdly , false positive are the negative classes which are incorrectly classified. Finally, false negative positive cases which is incorrectly classified and it is the most dangerous one. Thus the accuracy can be increased by correctly classified objects or we can say if more values are there in positive diagonal then it is the more efficient classifier. False Negative(FN) False Positive(FP)

Fig 12: Efficiency of the classifier increases diagonally for the confusion matrix.

The confusion matrices for our results are shown below:

1. ***AdaBoost Confusion Matrix:***

a (normal)	b (anomaly)
12919(TP)	530 (FN)
897 (FP)	10846(TN)

2. ***SVM Confusion Matrix:***

a (normal)	b (anomaly)
13442 (TP)	7 (FN)
1499 (FP)	10244 (TN)

3. ***Stacking method Confusion Matrix:***

a (normal)	b (anomaly)
11743 (TP)	0 (FN)
13449 (FP)	0 (TN)

4. ***boostSVM Confusion Matrix:***

a (normal)	b (anomaly)
13442 (TP)	7 (FN)
1499 (FP)	10244 (TN)

V. CONCLUSION

Thus the result clearly shows that though both Stacking and boostSVM methods are the coherent method for combining classifiers for getting better results but for KDD dataset which can be considered as a big data as it contains a huge amount of information, boostSVM gives a much more better accuracy level than stacking method. The base classifier used in this paper is the SVM which is being boosted by AdaBoost . There are variegated reasons for selecting SVM which includes its way of avoiding overfitting problems. Secondly it doesn't contain local minima which increases its efficiency. Thirdly, it can deal with non-linear data also with the help of kernel functions. Lastly, it provides conjecture for the test error conditions. Though for nonlinear data it is being said that selecting kernel may become a difficult task but if we observe the objective function for logistic

regression it can be seen that in comparison for dealing with non-linear data, this difficult task is worth. The SVM for KDD dataset increases the area under the curve or the ROC to the maximum, i.e. 0.995 which is greater than both individually SVM and Adaboost. ROC is the statistical characteristics which easily help in identifying the instances correctly classified and our result which shows ROC for boostSVM is 0.995 which clearly indicates that it can very advantageously increases the viewing components.

REFERENCES:

[1] Freund, Y., Schapire, R.E.: A Decision-Theoritic Generalization of on-line Learning andan Application to Boosting. (1995)

[2] Panda, M., Patra, M.R.: Ensemble of Classifiers for Detecting Network Intrusion. In: InternationalConference on Advances in Computing, Communication and Control(ICAC3'09), pp. 510-515. (2009)

[3]Garcia-Teodoro,P., Diaz-Verdejo,J., Macia-Fernandez,G., Vazquez,E.: Anomaly-basednetwork intrusion detection: Techniques, systems and challenges.Computer & Security,Volume 28, Issues 1-2, pp. 18-28. (2009)

[4]Davis, J.J., Clark, A.J.: Data preprocessing for anomaly based network intrusion detection:A review. Computer & Security, Volume 30, Issues 6-7, pp 353-375. (2011)

[5] Graczyk, M., Lasota, T., Trawiński, B., Trawiński, K.: Comparison of Bagging, Boostingand Stacking Ensembles Applied to Real Estate Appraisal. In: ACIIDS'10 Proceedings ofthe Second international conference on Intelligent information and database systems: PartII Proceeding. Springer-Verlag Berlin, Heidelberg. (2010)

[6] Zhou, Z.-H.: Ensemble Learning, Encyclopedia of Biometrics, Volume 1, pp. 270-273,Berlin, Springer, ISBN: 978-0-387-73002-8 (2009)

[7] L. Xu, A. Krzyzak, and C. Y. Suen. Methods of combining multiple classifiers and their application to handwriting recognition. IEEE Transactions on Systems, Man, and Cybernetics, 22:418–435, 1992.

[8] T. K. Ho, J. J. Hull, and S. N. Srihari. Decision combination in multiple classifier systems. IEEE Transactions on Pattern Analysis and Machine Intelligence, 16:66–75, 1994.

[9] J. D. Tubbs and W. O. Alltop. Measures of confidence associated with combining classification rules. IEEE Transactions on Systems, Man, and Cybernetics, 21:690–692, 1991.

[10] W. H. E. Day. Consensus methods as tools for data analysis. In H. H. Bock, editor, Classification and Related Methods for Data Analysis, Elsevier Science Publishers B.V. (North Holland), 1988, pp. 317–324.

[11] R. Battiti and A. M. Colla. Democracy in neural nets: Voting schemes for classification. Neural Networks, 7:691–707, 1994.

[12] L. Lam and A. Krzyzak. A theoretical analysis of the application of majority voting to pattern recognition. In 12th International Conference on Pattern Recognition, Jerusalem, Israel, 1994, pp. 418–420.

[13] L. Lam and C. Y. Suen. Application of majority voting to pattern recognition: An analysis of its behaviour and performance. IEEE Transactions on Systems, Man, and Cybernetics, 27(5):553–568, 199

[14] Ludmila I. Kuncheva (2004). Combining Pattern Classifiers: Methods and Algorithms. John Wiley and Sons, Inc..

[15] J. Kittler, M. Hatef, Robert P.W. Duin, J. Matas (1998). On combining classifiers. IEEE Transactions on Pattern Analysis and Machine Intelligence. 20(3):226-239.

[16] David H. Wolpert (1992). Stacked generalization. Neural Networks. 5:241-259

[17] Yasser EL-Manzalawy (2005). WLSVM. URL http://www.cs.iastate.edu/~yasser/wlsvm/.

[18] Chih-Chung Chang, Chih-Jen Lin (2001). LIBSVM - A Library for Support Vector Machines. URL http://www.csie.ntu.edu.tw/~cjlin/libsvm/.

[19] Yoav Freund, Robert E. Schapire: Experiments with a new boosting algorithm. In: Thirteenth International Conference on Machine Learning, San Francisco, 148-156, 1996.

[20] Mohammad Khubeb and Shams Naahid, Analysis of KDD CUP '99 Dataset using Clustering based Mining, International Journal of Database Theory and Application, 6(5), 2013, 23-34.

[21] Mahbod Tavallaee,Ebrahim Bagheri,Wei Lu and Ali .A.Ghorbani, A Detailed Analysis of the KDD CUP '99 Dataset, Proc.of 200 9 IEEE Symposium on Computational Intelligence in Security and Defense Applications,978-1-4244-3764-1/09

International Journal of Engineering Research and General Science Volume 3, Issue 3, Part-2 , May-June, 2015
ISSN 2091-2730

Characterization of Painting Materials of Presage of Angel Gabriel to the Priest Zechariah Icon

Gomaa Abdel-Maksoud[a], Yousry M. Issa[b,*], Mina Magdy[c]

[a]Conservation Department, Faculty of Archeology, Cairo University, Giza, Egypt.

[b]Chemistry Department, Faculty of Science, Cairo University, Giza, Egypt.

[c]National Museum of Egyptian Civilization, Cairo, Egypt.

E-mail: gomaaabdelmaksoud@yahoo.com (G. Abdel-Maksoud)

yousrymi@yahoo.com (Y. M. Issa)

minamagdy_2000@yahoo.com (M. Magdy)

Abstract- The aim of study is identification, determination, and assessment of the painting materials of Coptic icon, presage of angel Gabriel to the priest Zechariah. Different analytical techniques were applied for characterization of the icon materials. The results revealed that the rigid support was *Tamarix* hardwood, the flexible support was linen fibers, the ground materials was gypsum. The pigments were vermilion, kermes carmine red and ultramarine blue, the binder was egg yolk, and the varnish was mastic resin. The chemical analyses showed the stability of icon materials with surrounding environment, in addition to the impact of metal salts result in decreasing of the free amino acids of egg yolk binder and cracking the paint film.

Keywords: Icon; characterization; OM; ATR-FTIR; FESEM-EDX; AAA.

1. INTRODUCTION

Application of analytical chemistry in archaeology can refer to the term "archaeological chemistry" and has benefit aspects in conservation, restoration of the artworks. It provides valuable information about the materials used in artworks such as the nature of materials and the processes that used to make and change them [1].

The "Coptic" word refers to the Egyptian Christians artworks [2]. The "Icon" word describes a religious image and it is associated with the painting of the Orthodox Churches [3]. The painting of icon is composed of four layers (support layer, ground layer, paint layer "pigments and binder", and varnish layer) [4]. Characterization of the icon materials will give information about the state of icon and the effect of the aging and environmental conditions. There are many factors that make the process of identifying the icon layers is difficult such as the use of small quantity of the sample and the lack of sample purity.

The chemical compositions of icon materials are very complex so analytical methods with high spatial resolution will be used. Light microscope (OM) is used to identify the fibers. In addition to that, it can be used for identification of the fiber group.

Fibers have a characteristic appearance in the cross-sectional view. Attenuated total reflection-Fourier transform infrared spectroscopy (ATR-FTIR) is used for determination the chemical structure of painting materials. Field emission scanning electron microscope (FESEM) is used to provide information about the surface texture such as fine cracking and the nature of relationship between the pigment and the binding medium at the surface. Energy dispersive spectroscopy (EDS) is used to characterize the elemental chemical composition. Amino acid analyzer (AAA) is used to detect the free amino acids of proteinaceous binder. The metal ions in the pigments can form complexes with some amino acids leading to change the amount of free amino acid measured [5].

Icon of presage of angel Gabriel to the priest Zechariah has been hold (Fig. 1) in *Church of* Saint Mercurius in south of Cairo. The church dates back to 6th century. The icon is believed to have been drawn by Yuhanna Al-Armani and dates back to 18th century.

Fig. 1. Icon of Presage of Angel Gabriel to the Priest Zechariah.

Angel Gabriel stands left to the altar. Angel Gabriel presages the priest Zechariah with birth of his son "John the Baptist". The priest Zechariah wears sticharion with red color at the upper part and white color at the lower part, blue-color tailasan with brown cap on his head. The priest Zechariah also holds thurible in his left hand and there is golden halo around his head. Angel Gabriel has two white wings, upper brown wear and lower green wear. The altar has white appearance and alternate tiles of blue-white color. The icon shows deterioration at the lower right part. Five samples were carefully extracted from deteriorated parts including: wood support, canvas fibers, light red color "deteriorated part of the outer frame", dark red color "deteriorated part of the inner frame", and violet Color "deteriorated part of the floor tiles".

2. EXPERIMENTAL

2.1. Samples

Five samples were taken from the damaged parts of the icon and analyzed by different techniques. The samples were wood specimen, canvas fibers, light red color, dark red color, and violet color.

Six reference materials were assembled and analyzed by ATR-FTIR method for comparison with the historical samples. The reference samples includes: ground (gypsum), chalk (filler), binder (egg yolk), pigments (vermilion, artificial ultramarine blue), and varnish (mastic resin) materials. Egg yolk sample also analyzed by amino acid analyzer to be compared with the historical sample.

2.2. Instruments

Leica motorized optical microscope system attached with a digital Camera Leica ICC50 HD (Leica DM750, Wetzlar, Germany) was used for identification of the canvas fibers and wood specimen.

The samples were analyzed by Vertex 70 FTIR spectrometer (Bruker Optics, Billerica Inc., Massachusetts, USA) equipped with a diamond ATR and DLaTGS detector. The spectral range was from 400-4000 cm^{-1} and resolution was 4 cm^{-1}, with 16 scans.

Field emission scanning electron microscope (Quanta FEG-250, FEI company, Hillsboro, OR, USA) equipped with EDX unit (Energy Dispersive X-ray Spectrophotometer, EDAX Apollo SDD, Mahwah, New Jersey) was performed to study the samples. The samples were examined in low-vacuum mode at an accelerating voltage 20 kV, resolution of 1 nm, and magnification 14× up to1,000,000×.

LC 3000 amino acid analyzer (Eppendorf, Hamburg, Germany) was used for analysis of the proteinaceous binder. The chromatographic separation was performed on a cation exchange column BTC 2410-4 µm, 125×4 mm and lithium citrate buffer system. The device is controlled by WinLC combined with EZChrom data software.

3. RESULTS AND DISCUSSION

The study by OM, ATR-FTIR, FESEM, and EDS analyses reveals that the rigid support is hardwood and the flexible support is linen fibers and the ground material is a mixture of gypsum, lead white, the binder is egg yolk and the varnish is mastic resin.

Optical microscope demonstrates that cross-section of wood (Fig. 2) belongs to the hardwood, *Tamarix* species (*Tamarix aphylla*). It is characterized with diffuse-semi ring pores, cluster pores, thin-thickness fibers (¼ lumen), multi-seriate rays (5-20 cells), heterocellular rays, and abundant crystals in rays [6-8].

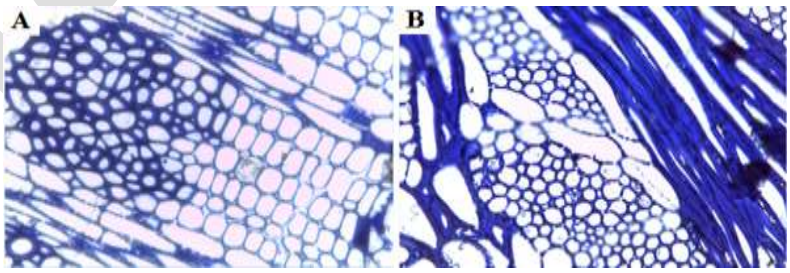

Fig. 2. Cross-section of Wood.

(A) Transverse Section (B) Longitudinal Section

Canvas fibers (Fig. 3) are examined by optical microscope. It is linen fibers characterized with nodes and cross cracks along the fibers [9].

Fig. 3. Fibers of Canvas.

ATR-FTIR spectra of the reference samples (Table 1) give characteristic bands that will be compared to the bands of historical samples (Table 2).

Gypsum is characterized with ATR-FTIR bands at 3536-3283 cm^{-1} υ(O-H), 1644-1620 cm^{-1} δ(O-H), 1140-1102 cm^{-1} υ(SO_4^{-2}), and 672-657 cm^{-1} δ(SO_4^{-2}) [10-12]. EDS microanalysis (Table 3) detects Ca, S, and O elements which are characteristic of gypsum [13].

Table 1. Characteristic Infrared Bands of the Reference Samples.

Material	Band (cm^{-1}), (Assignment)
Gypsum	3606, 3551 υ(O-H), 1110, 1087, 1007 υ(SO_4^{-2}), 658 δ(SO_4^{-2})
Chalk	1396 υ(CO_3^{-2}), 872, 712 δ(CO_3^{-2})
Vermilion	643 υ(Hg-S)
Artificial Ultramarine Blue	1120, 991, 948 υ(Si-O-Si)
Egg Yolk	3282 υ(N-H), 2923, 2853 υ(C-H), 1744, 1633 υ(C=O), 1541, 669 δ(N-H), 1541 υ(C-N), 1458, 1416, 1378 δ(C-H)
Mastic Resin	2930, 2868 υ(C-H), 1704 υ(C=O), 1453, 1377 δ(C-H), 1181, 1109, 1080, 1045, 1028, 1010, 987, 973, 945, 922 υ(C-O)

Table 2. Characteristic Infrared Bands of Paint Colors of Presage of Angel Gabriel to the Priest Zechariah.

Color	Bands (cm^{-1}) in IR Spectra	Material
Light Red	3394, 3283, 1642, 1622, 1102, 672	Gypsum
	635	Vermilion
	3394, 3283, 2919, 2850, 1642, 1622, 1537, 1392, 672	Egg Yolk
	3394, 3283, 2919, 2850, 1642, 1622, 1392, 1102, 1051	Mastic Resin

Dark Red	3390, 3287, 1644, 1140, 657	Gypsum
	3390, 3287, 2981, 2951, 1727, 1537, 1445, 1235	Kermes Carmine Red
	3390, 3287, 2981, 2951, 2852, 1727, 1644, 1537, 1445, 1384, 657	Egg Yolk
	3390, 3287, 2981, 2951, 2852, 1727, 1644, 1445, 1384, 1235, 1140, 1096, 1031	Mastic Resin
Violet	3536, 3400, 1620, 1116	Gypsum
	1409, 872	Chalk
	3536, 3400, 1075, 872	Ultramarine Blue
	3536, 3400, 2921, 1737, 1243	Kermes Carmine Red
	3400, 2921, 1737, 1620, 1409	Egg Yolk
	3536, 3400, 2921, 1737, 1620, 1409, 1243, 1186, 1116, 1075, 984	Mastic Resin

Egg yolk shows characteristic bands at 3400-3283 cm^{-1} υ(N-H), 2981-2850 cm^{-1} υ(C-H), 1737-1620 cm^{-1} υ(C=O), 1537, (672-657) cm^{-1} δ(N-H), 1537 cm^{-1} υ(C-N), and 1445-1384 cm^{-1} δ(C-H) [14-17].

Mastic resin is proved by appearance of ATR-FTIR bands (Table 2) at 3536-3283 cm^{-1} υ(O-H), 2981-2850 cm^{-1} υ(C-H), 1737-1642 cm^{-1} υ(C=O), 1644-1622 cm^{-1} υ(C-C), 1445-1384 cm^{-1} δ(C-H), and 1392-984 cm^{-1} υ(C-O) [18-20].

FESEM micrographs (Fig. 4) show the topography of paint surface and state the paint film of historical samples.

All samples taken from different positions (colors) produce the same behavior regarding the support, ground, binder and varnish material.

Table 3. EDS Microanalysis and Elemental Composition (Atomic Percentage) of Each Color of Historical Sample.

Element	Light Red	Dark Red	Violet
C K	44.99	60.06	27.40
O K	20.01	26.94	39.10
Na K	1.19	0.83	-
Mg K	-	0.55	0.38
Al K	0.98	1.03	1.81
Ca K	1.29	1.14	2.35
Si K	1.79	1.29	0.51
S K	14.31	1.07	9.53
Cl K	0.13	0.23	1.09
K K	-	0.47	-
P K	0.76	0.80	-
Fe K	0.75	0.40	0.82
Hg L	13.79	-	-

Sn L	-	4.81	-
Mn K	-	0.10	0.14
Co K	-	0.11	0.23
Zn K	-	0.18	4.32
Ti K	-	-	5.76
Ba L	-	-	5.87
As K	-	-	0.70

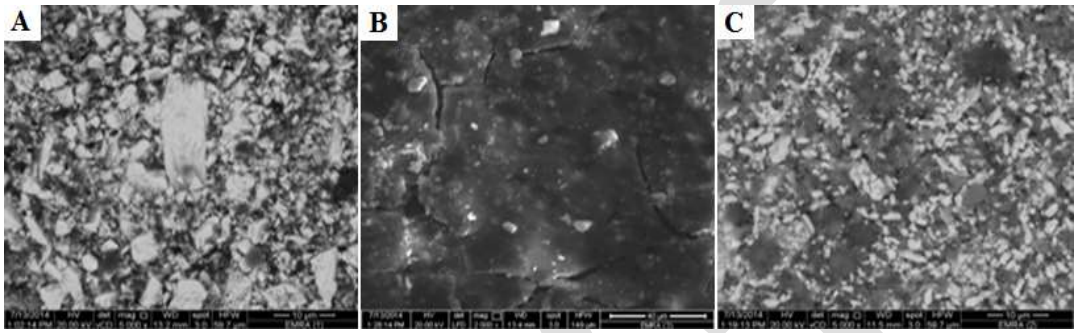

Fig. 4. FESEM Micrograph of Historical Samples: (A) Light Red Color; (B) Dark Red Color; (C) Violet Color.

3.1. Light Red Color

EDS microanalysis (Table 4) detects Hg, S elements that are characteristic for vermilion pigment [21-23]. FESEM micrograph (Fig. 4) shows aggregation of particles of the pigment. ATR-FTIR spectra (Fig. 5) manifest bands at 635 cm^{-1} that refer to vermilion pigment [24,25]. Mercury ions can form complexes with egg yolk protein and this assumption is confirmed by amino acid analysis (Table 4). The results obtained show that content of some amino acids of light red color are reduced (aspartic acid, threonine, serine, valine, leucine, phenylalanine, histidine, lysine, and methionine) or zeroed (tyrosine) as a result of oxidation process in which the mercury cations can form complexes with egg yolk binder [17,26,27].

Table 4. Relative Concentration of Amino Acids of Light Red Color and Reference Sample.

Amino Acid	Light Red Color	Reference Sample
Aspartic Acid	4.60	5.06
Threonine	1.62	3.38
Serine	3.50	5.10
Glutamic Acid	40.69	39.44
Proline	4.79	2.05
Alanine	15.89	7.97
Valine	2.79	4.28
Leucine	3.47	7.57

Phenylalanine	5.55	6.43
Histidine	2.10	2.45
Arginine	10.19	7.65
Lysine	3.91	4.90
Methionine	0.27	0.98
Isoleucine	0.62	-
Tyrosine	-	2.74

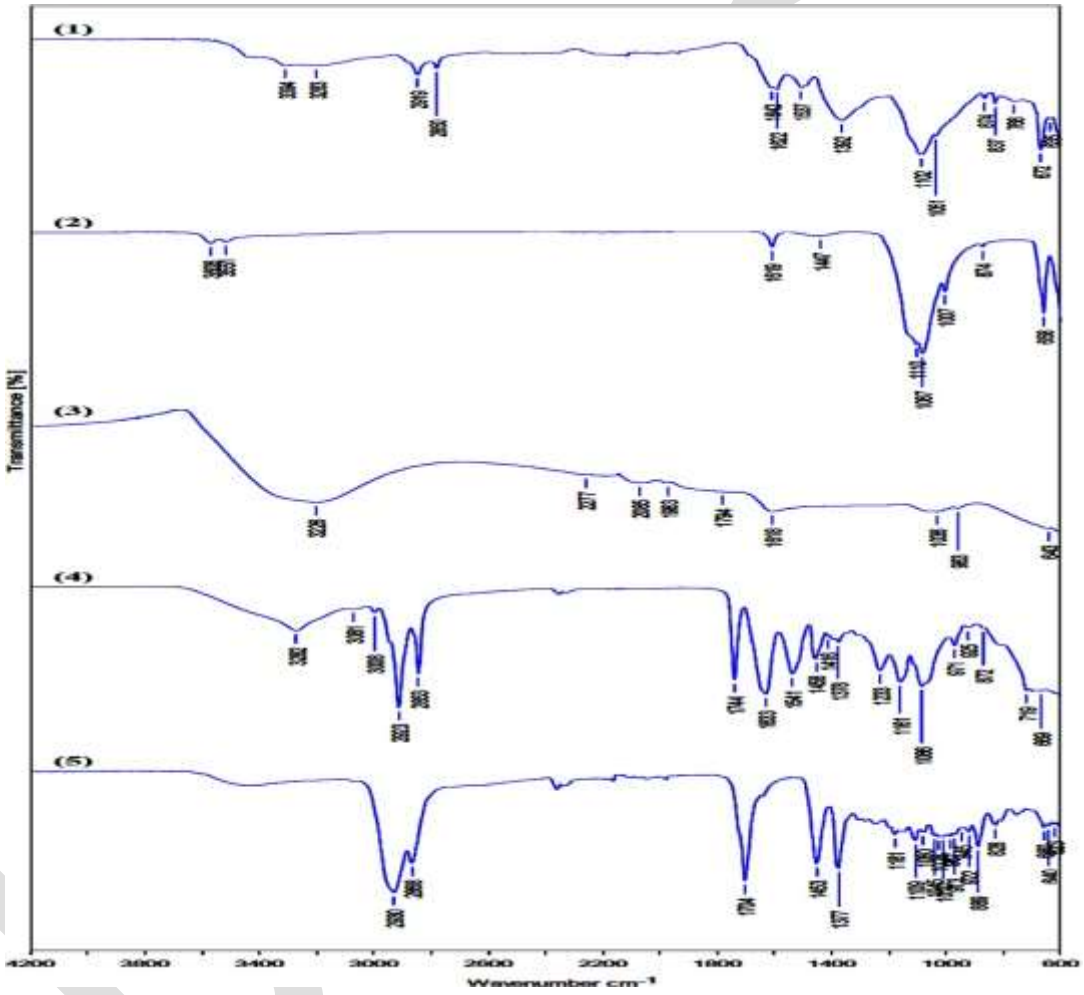

Fig. 5. ATR-FTIR Spectra of: (1) Historical Sample "Light Red Color"; (2) Gypsum; (3) Vermilion Red; (4) Egg Yolk; (5) Mastic Resin.

3.2. Dark Red Color

ATR-FTIR spectra (Fig. 6) exhibit characteristic bands at 3390, 3287 cm^{-1} υ(O-H), 2981, 2951 cm^{-1} υ(C-H), 1727 cm^{-1} $\upsilon(C=O)_{Carboxylic\ acid}$, 1537, 1445 cm^{-1} $\upsilon(C=C)_{Aromatic}$, 1235 cm^{-1} υ(C-O) that refer to kermes carmine red [12,28]. EDS microanalysis (Table 3) detects high amount of Sn element as tin oxide mordant for the organic dye. FESEM micrograph (Fig. 4) shows black

appearance indicating their organic composition and cracking of the paint film due to the presence of tin oxide can promote the oxidation process.

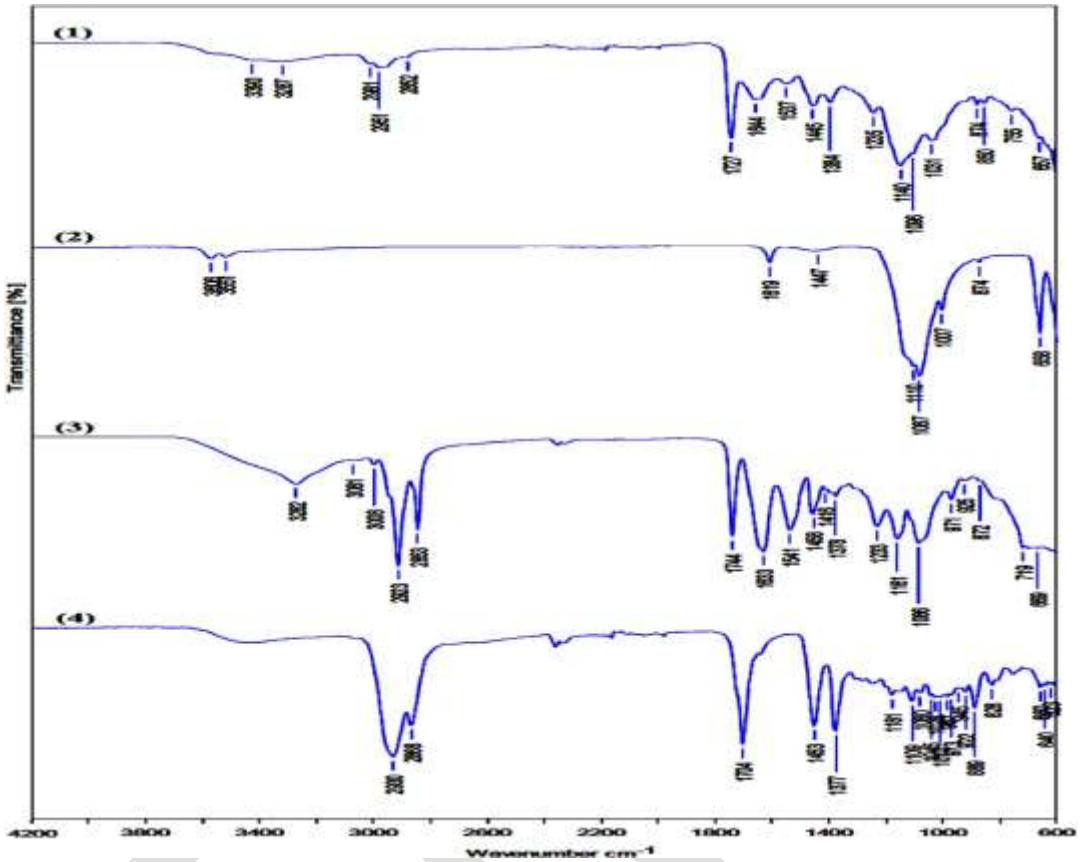

Fig. 6. FTIR Spectra of: (1) Historical Sample "Dark Red Color"; (2) Gypsum; (3) Egg Yolk; (4) Mastic Resin.

3.3. Violet Color

Violet color may result from mixing the natural ultramarine blue and kermes carmine red pigment. ATR-FTIR spectra (Fig. 7) show characteristic bands at 3536, 3400 cm^{-1} υ(O-H), and 1075, 872 cm^{-1} υ(Si-O-Si), υ(Si-O-Al) that refer to a*luminosilicate* of natural ultramarine pigment [29] and bands at 3536, 340 cm^{-1} υ(O-H), 2921 cm^{-1} υ(C-H), 1737 $\upsilon(C=O)_{Carboxylic\ acid}$, and 1243 cm^{-1} υ(C-O) refer to kermes carmine red [12,28]. Appearance of chalk (Fig. 7) with characteristic ATR-FTIR bands at 1409, 872, and 712 cm^{-1} as carrier for kermes carmine pigment [10,11,30]. FESEM micrograph (Fig. 4) shows distribution of large particles of ultramarine and black appearance of kermes pigment. EDS microanalysis (Table 3) detects of Ca, Al, S, Si and Mg elements of ultramarine pigment [29,30]. The cations (Ca, Al) can catalyze the oxidation process of proteinaceous binder and this appears obviously with bands of oxalate 1620 cm^{-1} with broad band at 1409 cm^{-1} [30,31].

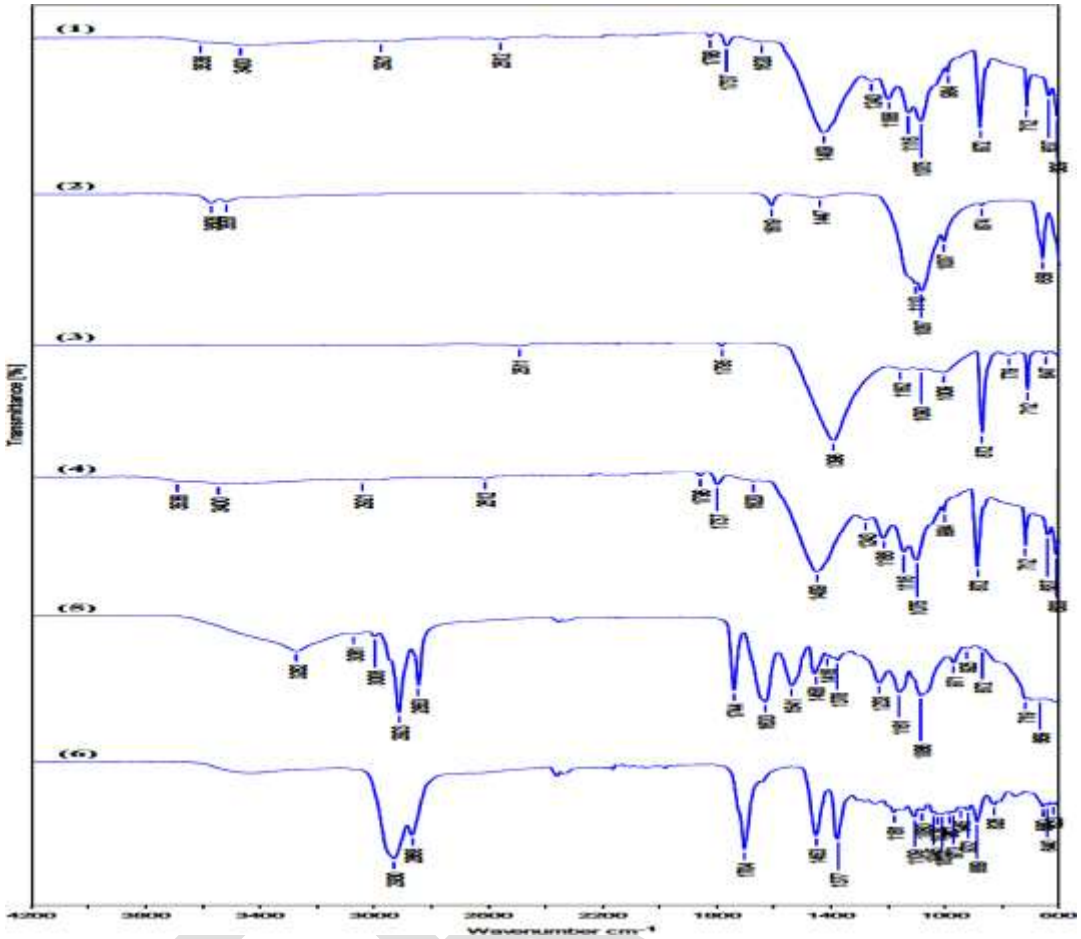

Fig. 7. ATR-FTIR Spectra of: (1) Historical Sample "Violet Color"; (2) Gypsum; (3) Chalk; (4) Artificial Ultramarine Blue; (5) Egg Yolk; (6) Mastic Resin.

ACKNOWLEDGMENT

The authors would like to thank Dr. Wadea Malek (Ministry of Antiquities, Egypt) for his help during collection of the samples. The authors also are grateful to Dr. Rim Hamdy (Botany Department, Faculty of Science, Cairo University, Egypt) for identification of the wood specimen.

CONCLUSION

Combination of OM, FTIR, FESEM-EDX, and AAA was used to give information about the identity of icon materials. The obtained results show that *Tamarix* hardwood was used as rigid support and linen fibers as flexible support and gypsum as ground and vermilion, kermes carmine red, and ultramarine blue as pigments and egg yolk as binder and mastic resin as varnish materials. The good state of icon layers attributes to stability of the pigments with environment conditions and permanence of the colors. Taking into consideration the impact of metal salts toward the organic compounds, it may lead to degradation of the organic molecules and decreasing the content of amino acids, and cracking of the paint film.

REFERENCES:

[1] Z. Goffer, "*Archaeological Chemistry", 2nd Edn.*, John Wiley, England, 2007.

[2] Z. Skalova and G. Gabra, "Icons of the Nile Valley Egyptian", 1st Edn., International Publishing Company-Longman, Cairo, Egypt, 2003.

[3] V. Losskey and L. Ouspensky, "The Meaning of Icons", 2nd Edn., St Vladimir's Seminary Press, New York, 1983.

[4] W. S. Taft and J. W. Mayer, "The Science of Paintings", 1st Edn., Springer-Verlag, New York, USA, 2000.

[5] B. H. Stuart, "Analytical Techniques in Materials Conservation", 1st Edn., John Wiley, England, 2007.

[6] V. Dorge and F. C. Howlett, "*Painted Wood: History and Conservation", 1st Edn., J. Paul Getty Trust, Los Angeles, USA, 1998.*

[7] M. Van der Veen, "The Exploitation of Plant Resources in Ancient Africa", 1st Edn., Springer, New York, USA, 1996.

[8] N.M. Waly, Wood Anatomical Characters of the Egyptian *Tamarix* L. Species and Its Taxonomic Significance, Taeckholmia, 1999, 19, 115-125.

[9] M. Humphries, "Fabric Reference", 4th Edn., Prentice Hall, New Jersey, USA, 2008.

[10] M.T. D. Carbó, V. P. Martínez, J.V. G. Adelantado, F. B. Reig, and M.C.M. M. Moreno, Fourier Transform Infrared Spectroscopy and the Analytical Study of Sculptures and Wall Decoration, J. Mol. Struct., 1997, 410-411, 559-563.

[11] C. Genestar and C. Pons, Earth Pigments in Painting: Characterisation and Differentiation by Means of FTIR Spectroscopy and SEM-EDS Microanalysis, Anal. Bioanal. Chem., 2005, 382, 269-274.

[12] D. Kovala-Demertzi, L. Papathanasis, R. Mazzeo, M. A. Demertzis, E. A. Varellac, and S. Prati, Pigment Identification in A Greek Icon by Optical Microscopy and Infrared Microspectroscopy, J. Cult. Herit., 2012, 13, 107-113.

[13] J. A. Stratis, C. Makarona, D. Lazidou, E. G. Sánchez, A. Koutsoudis, M. Pamplona, R. Pauswein, G. Pavlidis, S. Simon, and N. Tsirliganis, Enhancing the Examination Workflow for Byzantine Icons: Implementation of Information Technology Tools in A traditional Context, J. Cult. Herit., 2012, 15, 85-91.

[14] R. Mazzeo, S. Prati, M. Quaranta, E. Joseph, E. Kendix, and M. Galeotti, Attenuated Total Reflection Micro FTIR Characterisation of Pigment–binder Interaction in Reconstructed Paint Films, Anal. Bioanal. Chem., 2008, 392, 65-76.

[15] R. J. Meilunas, J. G. Bentsen, and A. Steinberg, Analysis of Aged Paint Binders by FTIR Spectroscopy, IIC-Int. Inst. Conserv., 1990, 35, 33-51.

[16] V. Ganitis, E. Pavlidou, F. Zorba, K.M. Paraskevopoulos, and D. Bikiaris, A post-Byzantine Icon of St. Nicholas Painted on A leather Support. Microanalysis and Characterisation of Technique, J. Cult. Herit., 2004, 5, 349-360.

[17] K. A. Dooley, S. Lomax, J. G. Zeibel, C. Miliani, P. Ricciardi, A. Hoenigswald, M. Loewb, and J. K. Delaney, Mapping of Egg Yolk and Animal Skin Glue Paint Binders in Early Renaissance Paintings Using Near Infrared Reflectance Imaging Spectroscopy, Analyst, 2013, 138, 4838-4848.

[18] M. R. Derrick, D. Stulik, and J. M. Landry, "Infrared Spectroscopy in Conservation Science", *1st Edn.*, J. Paul Getty Trust, Los Angeles, USA, 1999.

[19] C. *Azémard*, C. Vieillescazes, and M. *Ménager*, Effect of Photodegradation on the Identification of Natural Varnishes by FT-IR Spectroscopy, Microchem. J., 2014, 112, 137-149.

[20] S. Prati, G. Sciutto, R. Mazzeo, C. Torri, and D. Fabbri, Application of ATR-far-infrared Spectroscopy to the Analysis of Natural Resins, Anal. Bioanal. Chem., 2011, 399, 3081-3091.

[21] M.L. Franquelo, A. Duran, L.K. Herrera, M.C. Jimenez de Haro, and J.L. Perez-Rodriguez, Comparison Between Micro-Raman and Micro-FTIR Spectroscopy Techniques for the Characterization of Pigments from Southern Spain Cultural Heritage, J. Mol. Struct., 2009, 924-926, 404-412.

[22] M.L. Franquelo, A. Duran, J. Castaing, D. Arquillo, and J.L. Perez-Rodriguez, XRF, μ-XRD and μ-Spectroscopic Techniques for Revealing the Composition and Structure of Paint Layers on Polychrome Sculptures After Multiple Restorations, Talanta, 2012, 89, 462-469.

[23] T. D. Chaplin, R. J.H. Clark, and M. *Martinón-Torres*, A combined Raman Microscopy, XRF and SEM–EDX Study of Three Valuable Objects – A large Painted Leather Screen and Two Illuminated Title Pages in 17th Century Books of Ordinances of the Worshipful Company of Barbers, London, J. Mol. Struct., 2010, 976, 350-359.

[24] S. Vahur, A. Teearu, and I. Leito, ATR-FT-IR Spectroscopy in the Region of 550–230 cm^{-1} for Identification of Inorganic Pigments, Spectrochim. Acta, Part A, 2010, 75, 1061-1072.

[25] S. Vahur, U. Knuutinen, and I. Leito, ATR-FT-IR Spectroscopy in the Region of 500–230 cm^{-1} for Identification of Inorganic Red Pigments, Spectrochim. Acta, Part A, 2009, 73, 764-771.

[26] L. Valianou, S. Wei, M. S. Mubarak, H. Farmakalidis, E. Rosenberg, S. Stassinopoulos, and I. Karapanagiotis, Identification of Organic Materials in Icons of the Cretan School of Iconography, J. Archaeol. Sci., 2011, 38, 246-254.

[27] C. Duce, L. Ghezzi, M. Onor, I. Bonaduce, M. P. Colombini, M. R. *Tiné*, and E. Bramanti, Physico-chemical Characterization of Protein–pigment Interactions in Tempera Paint Reconstructions: Casein/Cinnabar and Albumin/Cinnabar, Anal. Bioanal. Chem., 2012, 402, 2183–2193.

[28] P. L. Lang, C. D. Keefer, J. C. Juenemann, K. V. Tran, S. M. Peters, N. M. Huth, and A. G. Joyaux, The Infrared Microspectroscopic and Energy Dispersive X-ray Analysis of Paints Removed from A painted, Medieval Sculpture of Saint Wolfgang, Microchem. J., 2003, 74, 33-46.

[29] S. Bruni, F. Cariati, F. Casadio, and L. Toniolo, Spectrochemical Characterization by Micro-FTIR Spectroscopy of Blue Pigments in Different Polychrome Works of Art, Vib. Spectro., 1999, 20, 15-25.

[30] D. Ajò, U. Casellato, E. Fiorin, and P.A.Vigato, Ciro Ferri's frescoes: a Study of Painting Materials and Technique by SEM-EDS Microscopy, X-ray Diffraction, Micro FT-IR and Photoluminescence Spectroscopy, J. Cult. Herit., 2004, 5, 333-348.

[31] C. Miliani, B. Doherty, A. Daveri, A. Loesch, H. Ulbricht, B.G. Brunetti, and A. Sgamellotti, In Situ Non-invasive Investigation on the Painting Techniques of Early Meissen Stoneware, Spectrochim. Acta A, 2009, 73, 587-592

International Journal of Engineering Research and General Science Volume 3, Issue 3, Part-2 , May-June, 2015
ISSN 2091-2730

PRIVACY PROTECTION FOR VIDEO, IMAGE, TEXT TRANSMISSION

1. Ms. Shraddha Bhatte ,
Student, Department of Computer Engineering, Shree L. R. Tiwari College of Engineering, Mumbai University, Thane, Maharashtra, 401107, India ,shraddhabhatte@yahoo.com

2. Dr. J. W. Bakal
Principal, Shivajirao S. Jondhale College of Engineering, Mumbai University, Thane, Maharashtra,421204, India ,bakaljw@gmail.com,

3. Mrs.Madhuri Gedam
Assistant Professor, Department of Computer Engineering, Shree L. R. Tiwari College of Engineering, Mumbai University, Thane, Maharashtra, 401107, India

Abstract— The issue of personal privacy is increasingly becoming prominent with the widespread use of large media (video, image, text) transmission systems. While the deployment of media transmission systems is justified by the perception of insecurity due to terrorist threats and high criminality rate, the rightful fear of privacy invasion is turning into a significant concern. In this project, we attempt to reconcile on the one hand the need for media transmission systems and on the other hand the concern of privacy protection.

Keywords—**Privacy protection ,multimedia data,H.264/AVC algorithm ,Compression ,Encryption Scrambling**,**SHA-1.**

INTRODUCTION

Media (Video/Text/Image) transmission systems are becoming ubiquitous. They are widely deployed in many strategic places such as airports, banks, public transportation or busy city centre. While people usually appreciate the sense of increased security brought by media transmission system, they often fear the loss of privacy which comes along.

In this project we are going to focus on three forms on media transmission i.e. VEDIO, IMAGE, and TEXT. A great many algorithms of video encryption have been proposed nowadays with the necessity of data rights management, especially the selective video encryption algorithms, which ensure the security of the information and meanwhile reduce the data to encrypt. The residue data, intra-prediction modes, inter-prediction modes and motion vectors are key elements that are usually partially or completely selected to encrypt to keep the security.

In this project, a new encryption algorithm that encrypts different elements according to different intra-prediction or inter-prediction modes for the H.264 /AVC standard is proposed. This novel algorithm keeps format appliance and has little impact on compression. Most importantly, it has flexible security levels with different applications.

AES/DES is the latest text compression standard which provides a higher compression gain as compared to earlier standards.

MOTIVATION

Multimedia information, such as graphics, images, audio and video, have been widely used in VOD, video conference, video surveillance system and so forth. The wide-spread use of these systems put forward corresponding demands on transmission security and copyright protection of the Multimedia information.

Encoded Multimedia information are often of large quantity, special coding structure, and demand real-time processing. These characteristics bring forward new requirements for encryption systems, namely: security, preservation of Multimedia information format, real time processing, maintenance of compress ratio, and robustness to transmission errors, etc

PROBLEM STATEMENT

Information, such as graphics, images, text and video, have been widely used in VOD, video conference, video surveillance system and so forth. The wide-spread use of these systems put forward corresponding demands on transmission security and copyright protection of the video information**.**

|Information hiding techniques have recently become important in a number of application areas. Digital audio, video, and pictures are increasingly furnished with distinguishing but imperceptible marks, which may contain a hidden copyright notice or serial number or even help to prevent unauthorised copying directly.

It is often thought that communications may be secured by encrypting the traffic, but this has rarely been adequate in practice, So the study of communications security includes not just encryption but also traffic security, whose essence lies in hiding information.

In this project, we intend to provide a solution to the problem arising due to loss of privacy as a result of increase in media (video/image/text) surveillance systems. Scrambling can be used to solve this problem.

The scope of H.264 can be explained as, H.264 offers greater flexibility in terms of compression options and transmission support. Similarly and AES/DES offers greater flexibility in terms of compression options and transmission support for text respectively. An encoder can select from a wide variety of compression tools, making it suitable for applications ranging from low-bit rate, low-delay mobile transmission through high definition consumer TV to professional technology production. The standard provides integrated support for transmission or storage, including a pocketsize compressed format and features that help to minimize the effect of transmission errors.

These standards has been adopted for an increasing range of applications, including:

- High Definition DVDs (Blu-Ray)
- High Definition TV broadcasting in Europe
- Apple products including iTunes video downloads, iPod video and MacOS
- NATO and US DoD video applications
- Mobile TV broadcasting
- Many mobile services

EXISTING SYSTEM

The issue of personal privacy is increasingly becoming prominent with the widespread use of large video, image, text transmission systems. While the deployment of video surveillance systems is justified by the perception of insecurity due to terrorist threats and high criminality rate, the rightful fear of privacy invasion is turning into a significant concern.

Previous works addressing the topic of privacy protection have previously reported. The system in [1] is based on an object-based representation of the scene. Basically, an altered rendering of the video is produced where some objects are masked out depending on the user authorizations, preventing the transmission of privacy-sensitive objects.

In [2], wavelet-domain and code stream-domain conditional access control techniques are proposed for JPEG 2000 to scramble code-blocks corresponding to Regions of Interest (ROI) containing for instance people or faces.

In[3] , it is extended to a region-based transform-domain scrambling method applicable to Motion JPEG 2000 or MPEG-4. More

Specifically,[4] AC transform coefficients corresponding to ROI are scrambled by pseudo-randomly inverting their signs, concealing any privacy-sensitive data. Similarly, encryption is used to conceal faces in. A secret encryption key is required in order to invert the process, thus guaranteeing privacy protection.

It is often thought that media transmissions may be secured by encrypting the traffic, but this has rarely been adequate in practice. So the study of communications security includes not just encryption but also traffic security, whose essence lies in hiding information**.**

PROPOSED SYSTEM

Information hiding techniques have recently become important in a number of application areas. It is often thought that communications may be secured by encrypting the traffic, but this has rarely been adequate in practice.

This paper concentrated on methods for hiding messages rather than for enciphering them.

DESIGN FLOW OF PROJECT

The main aim of project is privacy protection of multimedia transmission .here focus is mainly on video, image and text. Security to media (video, image ,text) transmission will give in three layers

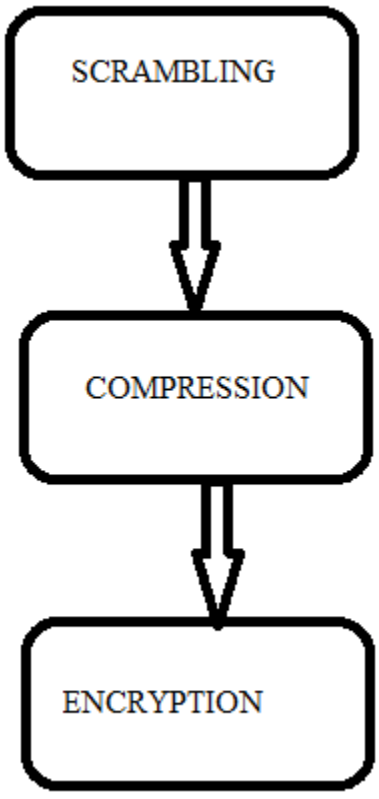

Figure [1] Basic flow diagram of proposed system

Design Details:

According to literature survey most of the existing systems used one layer of protection that is either scrambling or compression otherwise only encryption but as per the recent market need only one layer protection for maintain privacy of the media (video ,image ,text) transfer is not sufficient.

Also it is important to maintain all basic parameters like bandwidth, compression ratio, PSNR ratio, speed of transmission, quality of product after transmission, and total cast of transmission adequate.

In proposed system H.264/AVC algorithm is use for scrambling and compression of video, image.

Encryption is done using SHA-1 and AES/DES algorithms

H.264 algorithm:

H.264 can mean different things from different viewpoints. It is an industry Standard; it defines a format for compressed video data; it provides a set of tools that can be used in a variety of ways to compress and communicate visual information; it is a stage in an evolving series of standardized methods for video compression **[5]**

H.264/AVC standard:

H.264/MPEG-4 AVC is a block-oriented motion-compensation-based video compression standard developed by the ITU-T Video Coding Experts Group (VCEG) together with the ISO/IEC JTC1 Moving Picture Experts Group (MPEG). The project partnership effort is known as the Joint Video Team (JVT). The ITU-T

A valuable content scrambling approach is a raising issue as protecting contents copyright is important. Image and video scrambling is well employed, and its general way is to hide unwanted information and disclose un interpretable image and video. There have been many methods regarding image and video scrambling

The proposed approach scrambles ROI while leaving the background intact, with the resulting scrambled stream still complying with the standard syntax. System use two scrambling approaches. The first one pseudo-randomly inverts the sign of AC transform coefficients of blocks belonging to ROI similarly. The second one applies a pseudo-random permutation of the AC transform coefficients in blocks corresponding to ROI.

Compression:

Compression is the act or process of compacting data into a smaller number of bits. Video compression (video coding) is the process of converting digital video into a format suitable for transmission or storage, whilst typically reducing the number of bits. 'Raw' or uncompressed digital video typically requires a large bitrate, approximately 216Mbits for 1 second of uncompressed Standard Definition video.[7]

Compression involves a complementary pair of systems, a compressor (encoder) and a decompressor (decoder). The encoder converts the source data into a compressed form occupying a reduced number of bits, prior to transmission or storage, and the decoder converts the compressed form back into a representation of the original video data. The encoder/decoder pair is often described as a CODEC (enCOder/DECoder)

In H.264/AVC this is carried out by applying a transform to the residual samples and quantizing the results. The transform converts the samples into another domain in which they are represented by transform coefficients. The coefficients are quantized to remove insignificant values, leaving a small number of significant coefficients that provide a more compact representation of the residual frame.

The output of the spatial model is a set of quantized transform coefficients. The parameters of the prediction model, i.e. intra prediction mode(s) or inter prediction mode(s) and motion vectors, and the spatial model, i.e. coefficients, are compressed by the entropy encoder.

Encryption:

Advanced Encryption Standard (AES)

Advanced Encryption Standard (AES) algorithm not only for security but also for great speed. Both hardware and software implementation are faster still. New encryption standard recommended by NIST to replace DES. Encrypts data blocks of 128 bits in 10, 12 and 14 round depending on key size . It can be implemented on various platforms especially in small devices. It is carefully tested for many security applications.

SHA1:

SHA1 stands for "Secure Hashing Algorithm". It is a hashing algorithm designed by the United States National Security Agency and published by NIST. It is the improvement upon the original SHA0 and was first published in 1995 [6,10]. SHA1 is currently the most widely used SHA hash function. It is currently used in a wide variety of applications, including TLS, SSL, SSH and PGP SHA1 outputs a 160-bit digest of any sized file or input. It uses a 512 bit block size and has a maximum message size of 2^{64} -1 bits.

The key string which is taken from the user is converted into a hash using SHA-1 algorithm. The first 128 bits of this hash generated is used as our key for AES encryption process.

CONCLUSION

In this paper, we have detailed our motivation for selecting the "Privacy protection for video, image, text transmission" project and literature survey for the same. We have discussed the various algorithms and methods for information hiding, scrambling and compression and AES/DES. On basis of the technical papers that we have studied, it's been concluded that all the proposed algorithms help effectively to protect privacy of data transmission. In fact, combination of those algorithms provides a simplicity and best protection to your end.

ACKNOWLEDGMENTS

I owe a deep gratitude towards my honourable guide, Dr J. W. Bakal. He rendered his valuable guidance with a touch of inspiration and motivation. I would like to thank Prof .Madhuri Gedam, my co-guide who extended every facility and helped me for completing this paper. I would also like to thank my principal, Dr. S. Ram Reddy for his moral support

REFERENCES:

[1] Thomas St¨utz and Andreas Uhl,, "A Survey of H.264 AVC/SVC Encryption', Technical Report,2013

[2]Frederic Dufaux and Touradj Ebrahimi,"Scrambling for privacy protection in video surveillance systems". IEEE Transactions , 2008

[3] Gwanggil Jeon "Block Shuffling Approach for Contents Protection", ' International Journal of Security and Its Applications , 2014

[4] Thomas Wiegand, Gary J. Sullivan, Gisle Bjøntegaard, ,Ajay Luthr, "Overview of the H.264/AVC Video CodingStandard",IEEETRANSACTIONS,2003

[5] "Fabien A.P. Petitcolas, Ross J. Anderson, and Markus G. Kuhn "Information hiding-a survey IEEE , 1999

[6] Qiuhua Wang, Xingjun Wang , "A New Selective Video Encryption Algorithm for the H.264 Standard", **IEEE,2014**

[7] Fabien A. P. Petitcolas, Ross J. Anderson and Markus G. Kuhn . "Information Hiding|A Survey", *IEEE*,1999.

[8] D. Chaum"Untraceable electronic mail, return addresses and digital pseudonyms.",*Communications of the A.C.M.*,1981.

[9] Frederic Dufaux and Touradj Ebrahimi,"H.264/AVC VIDEO SCRAMBLING FOR PRIVACY PROTECTION", IEEE, 2008

[10] A.W. Senior, S. Pankanti, A. Hampapur, L. Brown, Y.-L. Tian, and A Ekin,. "Blinkering Surveillance: Enabling Video Privacy through Computer Vision", IBM, 2003.

[11] F. Dufaux, and T. Ebrahimi "Video Surveillance using JPEG 2000", , SPIE ,2004.

[12] F. Dufaux and T. Ebrahimi , "Scrambling for Video Surveillance with Privacy", IEEE, 2006

[13] T.E. Boult ,"PICO: Privacy through Invertible Cryptographic Obscuration", IEEE, Nov. 2

International Journal of Engineering Research and general science is an open access peer review publication which is established for publishing the latest trends in engineering and give priority to quality papers which emphasis on basic and important concept through which there would be remarkable contribution to the research arena and also publish the genuine research work in the field of science, engineering and technologies

International Journal Of Engineering Research and General Science
ISSN 2091 - 2730